

**Parametric Study of the Influence of Operating Conditions,  
Atomiser Geometry and Fluid Viscosity on Effervescent  
Atomisation**

Thesis submitted for the  
Degree of Doctor of Philosophy  
of the University of Wales Cardiff

by  
Dancho Danchev Konstantinov  
(MEng AMIMechE)

April 2012

## Abstract

---

This thesis investigates effervescent atomisation, a liquid fuel atomisation technique with wide industrial applications, and one which offers several important advantages over conventional atomiser types. An “inside-out” type atomiser rated at 2MW equivalent power (based on mass flow rate) was designed and tested using a state-of-the-art 2-D Phase Doppler Anemometry (PDA) system which allowed for simultaneous real-time droplet size and velocity data to be obtained. High quality data was achieved, with data rates up to 10 kHz and validation rates over 90% in 2-D PDA coincident mode in the high density sprays. Droplet diameters up to 600  $\mu\text{m}$  could be measured.

The parameters investigated included operating parameters (air-to-liquid by mass ratio, pressure drop across the nozzle), geometric parameters (exit orifice diameter, nozzle length-to-diameter ratio, mixing chamber diameter, mixing length and air injection geometry) and fluid viscosity. The parameter ranges investigated included 1.83-11.11% air-to-liquid by mass ratio, 4.64-7.05 barG pressure drop across the nozzle, 2-2.8mm exit orifice diameter, 60-136 mm mixing length, 20-30 mm mixing chamber diameter, 0.5-2 nozzle length-to-diameter ratio and  $1-18 \times 10^{-6} \text{ m/s}^2$  kinematic viscosity. In addition 3 air injector geometries were studied which allowed the influence of air injector hole radial symmetry and aerating hole diameter to be determined.

Water and air were used as the operating fluid and assist-medium, respectively, for the operating parameter and geometric parameter tests. However, the use of water-glycerol mixtures in the fluid viscosity tests allowed the viscosity of the operating fluid to be controlled. Altering the fluid viscosity allowed the production of a range of simulated fuels (that will encompass Bio-Fuels).

The effervescent atomiser designed was compared to an industrial type Y-Jet atomiser frequently used in steam-assisted boiler combustion applications. It was found that the Y-Jet atomiser performed slightly better than an effervescent atomiser without any optimisation, but that improvements in effervescent atomiser performance were possible once atomiser geometry had been fully optimised. Comparisons were also made with the droplet SMD, coefficient of discharge and spray angle predicted by correlations from the literature (obtained using earlier versions of the hardware or alternative sampling techniques). These were found to provide poor agreement with the present experimental data. Finally, global spray SMD correlations were developed; these were shown to agree well with the present experimental data.

# Acknowledgements

---

I would like to take this opportunity to thank Dr. Richard Marsh and Professor Phil Bowen for presenting me with the opportunity to undertake this study. I am especially grateful to Dr. Richard Marsh for his continual guidance and support.

Special thanks are due to Dr. Peter Kay for his assistance, particularly with the PDA system.

I am grateful to Dr. Andrew Crayford for his help during the experimental set-up and to Steve Morris for use of the GTRC facilities throughout my preliminary tests.

I would like to thank Malcolm Seabourne, Paul Malpas, Steve Mead and the remaining workshop technicians for their help in the construction and maintenance of the experimental facilities, and for their assistance with all things practical.

My thanks also go to Stork Thermeq B.V. for the financial support generously provided; I am especially grateful to Dr. Marco Derksen and Sjoerd Dijkstra for their considerable input throughout this study.

Finally, I would like to express my sincere gratitude to my parents and family for their support and for the encouragement to pursue this course of study.

## **Declaration**

This work has not previously been accepted in substance for any degree and is not being concurrently submitted in candidature for any degree.

Signed..... (candidate)

Date.....

## **Statement 1**

This thesis is being submitted in partial fulfilment of the requirements for the degree of PhD.

Signed..... (candidate)

Date.....

## **Statement 2**

This thesis is the result of my own independent work/investigation, except where otherwise stated. Other sources are acknowledged by footnotes giving explicit references.

Signed..... (candidate)

Date.....

## **Statement 3**

I hereby give consent for my thesis, if accepted, to be available for photocopying and for inter-library loan, and for the title and summary to be made available to outside organisations.

Signed..... (candidate)

Date.....

# Nomenclature

## Roman Characters

Symbol	Definition	Units
$A_a$	Total Area of Aerator Air Injection Holes	$m^2$
$A^*$	Discharge Orifice Area	$m^2$
$C_d$	Coefficient of Discharge	-
$C_{dW}$	Coefficient of Discharge with Water as Working Fluid	-
$D_b$	Gas Bubble Diameter	m
$D_o / d_o / D^*$	Exit Orifice Diameter	m
$D_{32}$	Sauter Mean Diameter	m
$d_a$	Aerator Air Injection Hole Diameter	m
$d_c$	Mixing Chamber Diameter	m
$d_L$	Spray Ligament Diameter	m
$d_{av,lig}$	Average Ligament Diameter	m
$D_{10\%}$	Diameter such that 10% of the spray mass is in smaller droplets	m
$D_{90\%}$	Diameter such that 90% of the spray mass is in smaller droplets	m
$D_{50\%}$	Diameter such that 50% of the spray mass is in smaller droplets	m
$E$	Gas Entrainment Rate	kg/s
$E_b$	Gas Bubble Energy	J/kg and J
$f_d$	Doppler Frequency	$s^{-1}$
$G$	Gas Mass Flux	kg/cm <sup>2</sup> hr
$j_g$	Superficial Gas Velocity	m/s
$K$	Consistency Index	-
$k$	Ratio of Specific Heats	-
$L_o$	Length of Exit Orifice	m

<b>Symbol</b>	<b>Definition</b>	<b>Units</b>
$m_L$	Liquid Mass Flow Rate	kg/s
$n$	Flow Behaviour Index	-
$n_{rel}$	Relative Refractive Index	-
$p_A$	Supplied Air Pressure	N/m <sup>2</sup>
$p_C$	Mixing Chamber Pressure	N/m <sup>2</sup>
$p_{inj}$	Fluid Injection Pressure	N/m <sup>2</sup>
$\Delta P$	Mixing Chamber/Ambient Air Pressure Differential	N/m <sup>2</sup>
$p_{amb}$	Ambient Pressure	N/m <sup>2</sup>
$Q_A$	Volumetric Air Flow Rate	m <sup>3</sup> /s
$Q_L$	Volumetric Liquid Flow Rate	m <sup>3</sup> /s
$R$	Universal Gas Constant	J/molK
$sr$	Gas-Liquid Phase Slip Ratio	-
$U$	Fluid Velocity	m/s
$U_a$	Air Velocity	m/s
$U_L$	Liquid Velocity	m/s
$U_{av,rel}$	Average Relative Velocity	m/s
$V_g$	Gas Volume	m <sup>3</sup>
$V_l$	Liquid Volume	m <sup>3</sup>
$v_1$	Specific Volume	m <sup>3</sup> /kg
$C_1, C_2, C_3,$ $a, b, c, C'$	Dimensionless Empirical Constants	-

## Greek Characters

Symbol	Definition	Units
$\alpha$	Gas Volume Void Fraction	-
$\gamma$	Ratio of Specific Heats	-
$\varepsilon$	Nozzle Efficiency	-
$\zeta_{opt}$	Critical Instability Wavenumber	-
$\theta$	Mixing Chamber Contraction Angle	degree
$\theta_s$	Spray Cone Angle	degree
$\Phi$	Phase Difference	radian
$\lambda$	$(\rho_G / \rho_A)(\rho_L / \rho_W)^{0.5}$	-
$\mu_L$	Liquid Dynamic Viscosity	kg/ms
$\eta$	Liquid Kinematic Viscosity	m <sup>2</sup> /s
$\pi$	Ambient to Atomiser Mixing Chamber Pressure Ratio	-
$\rho_A$	Air Density	kg/m <sup>3</sup>
$\rho_{AP}$	Air Density in Plenum/Mixing Chamber	kg/m <sup>3</sup>
$\rho_f$	Fluid Phase Density	kg/m <sup>3</sup>
$\rho_g$	Gas Phase Density	kg/m <sup>3</sup>
$\rho_L$	Liquid Density	kg/m <sup>3</sup>
$\sigma$	Surface Tension	kg/s <sup>2</sup>
$\psi$	$(\sigma_L / \sigma_W)^{-1}(\mu_L / \mu_W)^{1.3}(\rho_L / \rho_W)^{-2.3}$	-

## Acronyms

---

Symbol	Definition	Units
ALR	Air to Liquid Ratio by Mass	-
AMD	Arithmetic Mean Diameter	m
EA	Effervescent Atomisation	-
MMD	Mass Median Diameter (=D <sub>50%</sub> )	m
PDA	Phase Doppler Anemometry	-
SMD	Sauter Mean Diameter (=D <sub>32</sub> )	m

## Dimensionless Parameters

---

Symbol	Definition	
Oh	Ohnesorge Number	$Oh = \frac{\mu_l}{\sqrt{\rho\sigma d}}$
Re	Reynolds Number	$Re = \frac{\rho U d}{\mu}$
We	Weber Number	$We = \frac{\rho U^2 d}{\sigma}$



# Contents

---

Chapter 1 : Introduction .....	1
1.1 Motivation.....	1
1.2 Liquid Fuel Atomisation .....	2
1.3 Aims and Objectives of Thesis .....	4
1.4 Thesis Layout.....	5
Chapter 2 : Literature Review .....	6
2.1 Effervescent Atomisation – Background .....	6
2.2 Jet Atomisation Theory.....	10
2.2.1 Mechanical Jet Disintegration .....	10
2.2.2 Jet Break-up Length .....	12
2.2.3 Jet Velocity Profile .....	12
2.2.4 Droplet Primary Break-up .....	13
2.2.5 Droplet Secondary Break-up.....	13
2.3 Effervescent Atomiser Internal Flow .....	14
2.4 Atomiser Geometry .....	19
2.4.1 Aerator geometry (size, arrangement of holes).....	19
2.4.2 Mixing Chamber Characteristics .....	21
2.4.3 Exit Orifice Geometry.....	24
2.4.4 Number of Exit Orifices.....	25
2.5 Parameters Influencing Spray Quality .....	25
2.5.1 Air to Liquid Ratio .....	26
2.5.2 Pressure Drop across Nozzle .....	30
2.5.3 Viscosity .....	31
2.5.4 Surface Tension .....	32
2.5.5 Fuel Type (Newtonian and Non-Newtonian Fluids).....	33
2.5.6 Molecular Weight of Atomising Gas.....	34
2.6 Effervescent Atomiser Spray Characteristics.....	35
2.6.1 Sauter Mean Diameter (SMD) .....	35
2.6.2 Spray Cone Angle .....	41
2.6.3 Velocity Profile.....	42
2.6.4 Gas Entrainment.....	43
2.6.5 Spray Unsteadiness .....	43
2.7 Further Correlations Related to Effervescent Atomisation .....	44

2.8 Summary.....	47
Chapter 3 : Experimental Methods.....	76
3.1 Effervescent Atomiser Design .....	76
3.2 Effervescent Atomiser Testing Facilities .....	80
3.3 Phase Doppler Anemometry – Theory of Operation .....	84
3.4 PDA System Used.....	91
3.5 PDA Set-up .....	93
3.6 PDA Data Collection.....	94
3.7 PDA Post-Processing .....	97
3.8 Experimental Errors.....	101
3.8.1 Systematic Measurement Errors.....	101
3.8.2 Operating parameter Fluctuations .....	102
3.8.3 Limited Sample Sizes .....	102
3.8.4 Other Errors.....	103
3.9 Summary.....	104
Chapter 4 : Comparison with Industrial Y-Jet Atomiser .....	105
4.1 Operating Conditions.....	105
4.2 PDA Sampling.....	105
4.3 PDA Spray Droplet Data.....	106
Chapter 5 : Results – Operating Parameters .....	111
5.1 Test Phase No.1 – Air-to-Liquid-by-Mass Ratio (ALR).....	111
5.1.1 Preliminary Investigations.....	111
5.1.2 Assumptions.....	113
5.1.3 Spray Characteristics and Results .....	115
5.1.4 Nozzle Coefficient of Discharge.....	115
5.1.5 Mode of Liquid Break-up at Nozzle .....	116
5.1.6 Spray Half-Angle .....	118
5.1.7 Spray Droplet Size Distribution by Number.....	119
5.1.8 Spray Droplet Size Distribution by Mass.....	120
5.1.9 Choice of PDA Settings .....	122
5.1.10 Spray Average Cumulative Droplet Size Distributions .....	123
5.1.11 Validated Local Data Rates .....	124
5.1.12 Local Droplet Velocity.....	126
5.1.13 Inferred Local Gas and Relative Velocity .....	128
5.1.14 Local Droplet AMD and SMD.....	131
5.1.15 Local Droplet Size Consistency .....	133
5.1.16 The Importance of Measurement Location.....	136

5.1.17	Droplet Secondary Break-up.....	136
5.1.18	Spray Development in the Downstream Direction.....	138
5.1.19	Droplet SMD Correlations from the Literature .....	141
5.1.20	Effect of ALR on Global Spray SMD for Experimental Data .....	142
5.1.21	Discussion of PDA Findings.....	145
5.2	Test Phase No.2 – Pressure Drop across Nozzle, $\Delta P$ .....	146
5.2.1	Preliminary Investigations.....	146
5.2.2	Spray Characteristics and Results.....	147
5.2.3	Nozzle Coefficient of Discharge.....	148
5.2.4	Mode of Liquid Break-up at Nozzle .....	149
5.2.5	Spray Half-Angle .....	149
5.2.6	Spray Droplet Size Distribution by Number.....	151
5.2.7	Spray Droplet Size Distribution by Mass .....	151
5.2.8	Spray Average Cumulative Droplet Size Distributions .....	152
5.2.9	Validated Local Data Rates .....	153
5.2.10	Local Droplet Velocity.....	154
5.2.11	Inferred Local Gas and Relative Velocity .....	155
5.2.12	Local Droplet AMD and SMD.....	156
5.2.13	Local Droplet Size Consistency .....	157
5.2.14	Droplet Secondary Break-up.....	158
5.2.15	Spray Development in the Downstream Direction.....	159
5.2.16	Droplet SMD Correlations from the Literature for EA .....	161
5.2.17	Effect of $\Delta P$ on Global Spray droplet SMD for Experimental Data .....	162
Chapter 6	: Results – Atomiser Geometry.....	135
6.1	Test Phase No.3 – Exit Orifice Diameter, $D_o$ .....	135
6.1.1	Preliminary Investigations.....	135
6.1.2	Spray Characteristics and Results.....	137
6.1.3	Nozzle Coefficient of Discharge.....	138
6.1.4	Mode of Liquid Break-up at Nozzle .....	138
6.1.5	Spray Half-Angle .....	139
6.1.6	Spray Droplet Size Distribution by Number.....	140
6.1.7	Spray Droplet Size Distribution by Mass .....	140
6.1.8	Spray Average Cumulative Droplet Size Distributions .....	141
6.1.9	Validated Local Data Rates .....	142
6.1.10	Local Average Droplet Velocity.....	143
6.1.11	Inferred Local Gas and Relative Velocity .....	143
6.1.12	Local Droplet AMD and SMD.....	143

6.1.13	Local Droplet Size Consistency .....	144
6.1.14	Droplet Secondary Break-up.....	145
6.1.15	Spray Development in the Downstream Direction.....	145
6.1.16	Droplet SMD Correlations from the Literature .....	147
6.1.17	Effect of $D_o$ on Global Spray Droplet SMD for Experimental Data .....	148
6.2	Test Phase No.4 – Mixing Chamber Length, $L_{MC}$ .....	150
6.2.1	Preliminary Investigations.....	150
6.2.2	Spray Characteristics and Results.....	152
6.2.3	Spray Droplet Size Distribution by Mass .....	152
6.2.4	Spray Average Cumulative Droplet Size Distributions .....	153
6.3	Test Phase No.5 – Mixing Chamber Diameter, $D_{MC}$ .....	154
6.3.1	Preliminary Investigations.....	154
6.3.2	Spray Characteristics and Results.....	155
6.3.3	Nozzle Coefficient of Discharge.....	156
6.3.4	Spray Half-Angle .....	157
6.3.5	Spray Droplet Size Distribution by Number.....	158
6.3.6	Spray Droplet Size Distribution by Mass .....	158
6.3.7	Spray Average Cumulative Droplet Size Distributions .....	159
6.3.8	Validated Local Data Rates .....	160
6.3.9	Local Droplet Velocity.....	161
6.3.10	Inferred Local Gas and Relative Velocity .....	162
6.3.11	Local Droplet AMD and SMD.....	162
6.3.12	Local Droplet Size Consistency .....	163
6.3.13	Droplet Secondary Break-up.....	164
6.3.14	Spray Development in the Downstream Direction.....	164
6.3.15	Droplet SMD Correlations from the Literature .....	166
6.3.16	Effect of $D_{MC}$ on Global Spray Droplet SMD for Experimental Data.....	166
6.4	Test Phase No.6 – Exit Orifice Length-to-Diameter Ratio, $L_o/D_o$ .....	168
6.4.1	Preliminary Investigations.....	168
6.4.2	Spray Characteristics and Results.....	169
6.4.3	Nozzle Coefficient of Discharge.....	170
6.4.4	Spray Half-Angle .....	170
6.4.5	Spray Droplet Size Distribution by Number.....	171
6.4.6	Spray Droplet Size Distribution by Mass .....	172
6.4.7	Spray Average Cumulative Droplet Size Distributions .....	173
6.4.8	Validated Local Data Rates .....	173
6.4.9	Local Droplet Velocity.....	174

6.4.10	Inferred Local Gas and Relative Velocity .....	175
6.4.11	Local Droplet AMD and SMD.....	175
6.4.12	Local Droplet Size Consistency .....	176
6.4.13	Droplet Secondary Break-up.....	177
6.4.14	Spray Development in the Downstream Direction.....	177
6.4.15	Droplet SMD Correlations from the Literature .....	179
6.4.16	Effect of $L_0/D_0$ on Global Spray Droplet SMD for Experimental Data...	180
6.5	Test Phase No.7 – Aerator Geometry.....	181
6.5.1	Preliminary Investigations.....	181
6.5.2	Spray Characteristics and Results.....	184
6.5.3	Nozzle Coefficient of Discharge.....	184
6.5.4	Spray Half-Angle .....	185
6.5.5	Spray Droplet Size Distribution by Number.....	186
6.5.6	Spray Droplet Size Distribution by Mass.....	186
6.5.7	Spray Average Cumulative Droplet Size Distributions .....	187
6.5.8	Validated Local Data Rates .....	188
6.5.9	Local Droplet Velocity.....	188
6.5.10	Inferred Local Gas and Relative Velocity .....	189
6.5.11	Local Droplet AMD and SMD.....	189
6.5.12	Local Droplet Size Spread .....	190
6.5.13	Droplet Secondary Break-up.....	191
6.5.14	Spray Development in the Downstream Direction.....	191
6.5.15	Droplet SMD Correlations from the Literature .....	193
6.5.16	Effect of Aerator Geometry on Global Spray Droplet SMD for Experimental Data .....	193
Chapter 7	: Results – Fluid Properties .....	241
7.1	Test Phase No.8 – Fluid Viscosity, $\eta$ .....	241
7.1.1	Preliminary Investigations.....	241
7.1.2	Spray Characteristics and Results.....	242
7.1.3	Nozzle Coefficient of Discharge.....	242
7.1.4	Mode of Liquid Break-up at Nozzle.....	243
7.1.5	Spray Half-Angle .....	244
7.1.6	Spray Droplet Size Distribution by Number.....	245
7.1.7	Spray Droplet Size Distribution by Mass.....	246
7.1.8	Spray Average Cumulative Droplet Size Distributions .....	246
7.1.9	Validated Local Data Rates .....	247
7.1.10	Local Droplet Velocity.....	248

7.1.11	Inferred Local Gas and Relative Velocity .....	248
7.1.12	Local Droplet AMD and SMD .....	248
7.1.13	Local Droplet Size Consistency .....	249
7.1.14	Spray Development in the Downstream Direction .....	250
7.1.15	Droplet SMD Correlations from the Literature .....	252
7.1.16	Effect of Kinematic Viscosity on Global Spray Droplet SMD for Experimental Data .....	253
7.1.17	Global Spray Droplet SMD Correlations .....	255
Chapter 8 : Conclusions.....		259
Chapter 9 : Further Work .....		247
References .....		248
Appendix A: Pressure Diferential Tests.....		256
Appendix B: Exit Orifice Diameter Tests.....		271
Appendix C: Mixing Chamber Diameter Tests.....		287
Appendix D: Exit Orifice Length-to-Diameter Ratio Tests.....		300
Appendix E: Aerator Geometry Tests.....		315
Appendix F: Kinematic Viscosity Tests.....		327

# List of Figures

---

Figure 1.1.1 World energy consumption by fuel for 1990-2035. ....	1
Figure 2.1.1. Cross-section through a typical effervescent atomiser in operation. ....	9
Figure 2.1.2. Gas-liquid interaction at the exit orifice with typical liquid break-up mechanisms in action. ....	9
Figure 2.2.1 Modes of mechanical jet disintegration .....	11
Figure 2.2.2 Jet break up length varying with jet velocity .....	12
Figure 2.3.1. Gas bubble interaction with circular exit orifice in effervescent atomisers for the case of: (a) large gas bubbles; (b) small gas bubbles; (c) multiple gas bubbles .....	18
Figure 2.3.2. Effervescent atomiser internal flow and external spray response for the case of (a) annular flow with a thin liquid film; (b) annular flow with a thick liquid film..	19
Figure 2.4.1. Typical effervescent atomiser geometry .....	20
Figure 2.4.2. ( $A^*/A_a$ ) ratio versus ALR to produce optimal SMD. ....	21
Figure 2.4.3. Alternative effervescent atomiser geometries: inside-out on the left and outside-in .....	22
Figure 2.4.4. Empirically determined Baker chart used to help with sizing of mixing chamber .....	23
Figure 2.4.5. Flow patterns observed in long, downward pointing pipes for fully developed flows .....	23
Figure 2.5.1. “Single-bubble explosion regime” .....	28
Figure 2.5.2. “Tree-regime fluid break-up” .....	28
Figure 2.5.3. Typical range of operation for different break-up mechanisms with varying ALRs in effervescent atomisation.....	29
Figure 2.6.1. The influence of ALR and injection pressure on spray cone angle .....	42
Figure 2.7.1. Relationship between spray droplet SMD and specific bubble energy....	45
Figure 3.1.1 (a) Photo showing the effervescent atomiser designed, the air supply system (top) and the liquid supply system (middle); (b) Sketch showing important features of the adjustable effervescent atomiser. ....	78
Figure 3.2.1 Schematic of fluid supply systems used.....	80
Figure 3.2.2 The effervescent atomiser with pressure and temperature sensors attached.....	81
Figure 3.2.3 Lowara water pump used to circulate water. ....	81
Figure 3.2.4 CMF 050 coriolis meter.....	82

Figure 3.2.5 The regulator in place on the air line. ....	83
Figure 3.3.1 The first three principle light scattering modes for a water droplet in air. .	85
Figure 3.3.2 Diagram showing the optical parameters governing PDA set-up including beam intersection angle ( $\theta$ ), scattering angle ( $\Phi$ ), and elevation angle ( $\psi$ ).....	85
Figure 3.3.3 A pair of intersecting laser beams creating interference fringes within the control volume .....	86
Figure 3.3.4 (a) Light signal received by photo detector with influence of interference fringe spacing shown; (b) Processed signal showing dependency on Doppler frequency on the right.....	86
Figure 3.3.5 (a) Beam without frequency shift has directional ambiguity; (b) Frequency shifted beam does not suffer from directional ambiguity.....	87
Figure 3.3.6 Light scattered via reflection mode by droplet traversing through PDA control volume .....	88
Figure 3.3.7 (a) Light intensity signal received at photo detectors; (b) The two photo detectors receive the same signal but with a slight phase difference; (c) Phase difference can be used to calculate droplet diameter .....	88
Figure 3.3.8 (a) Light intensity signal received at photo detectors as droplets traverse the control volume; (b) Calculation of phase differences between adjacent photo detectors; (c) $2\pi$ ambiguity as very large and very small droplets are indistinguishable in a two detector PDA system.....	90
Figure 3.3.9 (a) Desired photo detector location to eliminate $2\pi$ ambiguity; (b) Cross-checking the phase differences of the close pair of photo detectors (1-3) and the distant pair (1-2) to calculate diameter .....	91
Figure 3.4.1 The computer-controlled traverse with sending and receiving optics mounted. ....	92
Figure 3.6.1 (a) A photo of the nozzle and issuing spray demonstrating a typical sampling grid; (b) A typical sampling grid in the +X,+Y,0 plane, with the centre of the nozzle at location 0,0,0. ....	94
Figure 4.3.1. Local SMD and AMD for the Effervescent and Y-Jet atomiser sprays. .	106
Figure 4.3.2. Local droplet SMD/AMD ratio for the Effervescent and Y-Jet atomiser sprays.....	107
Figure 4.3.3. Global droplet distributions based on mass, for a Y-Jet and an effervescent atomiser. ....	108
Figure 4.3.4. Cumulative mass-under-size plots for a Y-Jet and an effervescent atomiser.....	109
Figure 5.1.1 Graph of “spray quality” showing liquid flow rates at which optimal effervescent atomisation can be achieved for ranging ALR.....	112



Figure 5.1.2 Graph of “spray quality” showing mixing chamber pressure and total flow rates at which optimal effervescent atomisation can be achieved for ranging ALR....	112
Figure 5.1.3 Graph of “spray quality” showing liquid flow rates and ALRs at which tests were performed for ranging ALR.....	113
Figure 5.1.4 Graph of “spray quality” showing mixing chamber pressures and total flow rates at which tests were performed for ranging ALR.....	113
Figure 5.1.5 Comparison of coefficient of discharge for ALR experiments and of predictions of correlations in the literature for present operating conditions. ....	116
Figure 5.1.6 Calculated liquid disintegration mode for ALR experiments.....	117
Figure 5.1.7 Comparison of spray half-angle from PDA experiments and literature. .	119
Figure 5.1.8 Droplet diameter frequency distribution based on number. ....	120
Figure 5.1.9 Droplet diameter frequency distribution by mass.....	121
Figure 5.1.10 Cumulative droplet size distribution.....	123
Figure 5.1.11 Comparison of global spray droplet SMD from PDA experiments with that predicted by correlations in the literature. ....	142
Figure 5.1.12 The relationship between ALR and global spray droplet SMD as measured using PDA data. ....	143
Figure 5.2.1 Graph of spray quality showing liquid flow rates at which optimal effervescent atomisation can be achieved. ....	147
Figure 5.2.2 Graph of spray quality showing mixing chamber pressures and total flow rates at which tests were performed. ....	147
Figure 5.2.3 Comparison of coefficient of discharge from PDA experiments and literature. ....	149
Figure 5.2.4 Calculated liquid disintegration mode for $\Delta P$ experiments.....	149
Figure 5.2.5 Comparison of spray half-angle from PDA experiments and literature. .	150
Figure 5.2.6 Droplet diameter frequency distribution based on number. ....	151
Figure 5.2.7 Droplet diameter frequency distribution by mass.....	152
Figure 5.2.8 Cumulative droplet size distribution.....	152
Figure 5.2.9 Validated local data rates at 150 mm downstream of the nozzle. ....	154
Figure 5.2.10 Average local droplet velocity at 150 mm downstream of the nozzle...	154
Figure 5.2.11 Inferred average local gas velocity at 150 mm downstream of the nozzle. ....	155
Figure 5.2.12 Inferred average relative velocity at 150 mm downstream of the nozzle. ....	156
Figure 5.2.13 Local droplet AMD at 150 mm downstream of the nozzle.....	157
Figure 5.2.14 Local droplet SMD at 150 mm downstream of the nozzle.....	157
Figure 5.2.15 Local droplet SMD/AMD at 150 mm downstream of the nozzle.....	158

Figure 5.2.16 Average local droplet Weber Number at 150 mm downstream of the nozzle. ....	158
Figure 5.2.17 Comparison of global spray droplet SMD from PDA experiments with that predicted by correlations in the literature. ....	161
Figure 5.2.18 The relationship between $\Delta P$ and global spray SMD as calculated using PDA data. ....	162
Figure 6.1.1 Schematic showing the geometric parameter exit orifice diameter. ....	135
Figure 6.1.2 Combined graphs of “spray quality” showing liquid flow rates at which optimal effervescent atomisation can be achieved with different nozzle diameters. ...	136
Figure 6.1.3 Combined graphs of spray quality showing mixing chamber pressures and total flow rates at which tests were performed with different nozzles. ....	137
Figure 6.1.4 Comparison of coefficient of discharge from PDA experiments and literature. ....	138
Figure 6.1.5 Comparison of spray half-angle from PDA experiments and literature. .	139
Figure 6.1.6 Droplet diameter frequency distribution based on number. ....	140
Figure 6.1.7 Droplet diameter frequency distribution by mass. ....	141
Figure 6.1.8 Cumulative droplet size distribution. ....	142
Figure 6.1.9 Validated local data rates at 150 mm downstream of the nozzle. ....	142
Figure 6.1.10 Average local droplet velocity at 150 mm downstream of the nozzle. ...	143
Figure 6.1.11 Local droplet AMD at 150 mm downstream of the nozzle. ....	144
Figure 6.1.12 Local droplet SMD at 150 mm downstream of the nozzle. ....	144
Figure 6.1.13 Local droplet SMD/AMD at 150 mm downstream of the nozzle. ....	145
Figure 6.1.14 Comparison of global spray SMD from PDA experiments with that predicted by correlations in the literature. ....	148
Figure 6.1.15 The relationship between $D_o$ and global spray droplet SMD as calculated using PDA data. ....	149
Figure 6.2.1 Schematic showing the geometric parameter mixing length. ....	150
Figure 6.2.2 Graph of “spray quality” showing liquid flow rates at which optimal effervescent atomisation can be achieved. ....	151
Figure 6.2.3 Graph of “spray quality” showing mixing chamber pressures and total flow rates at which tests were performed. ....	151
Figure 6.2.4 Droplet diameter frequency distribution by mass. ....	153
Figure 6.2.5 Cumulative droplet size distribution. ....	153
Figure 6.3.1 Schematic showing the geometric parameter mixing chamber diameter. ....	155
Figure 6.3.2 Comparison of coefficient of discharge from PDA experiments and literature. ....	157

Figure 6.3.3 Comparison of spray half-angle from PDA experiments and literature. .	157
Figure 6.3.4 Droplet diameter frequency distribution based on number. ....	158
Figure 6.3.5 Droplet diameter frequency distribution by mass.....	159
Figure 6.3.6 Cumulative droplet size distribution.....	159
Figure 6.3.7 Validated local data rates at 150 mm downstream of the nozzle. ....	161
Figure 6.3.8 Average local droplet velocity at 150 mm downstream of the nozzle.....	161
Figure 6.3.9 Local droplet AMD at 150 mm downstream of the nozzle.....	162
Figure 6.3.10 Local droplet SMD at 150 mm downstream of the nozzle.....	163
Figure 6.3.11 Local droplet SMD/AMD at 150 mm downstream of the nozzle. ....	163
Figure 6.3.12 Comparison of global spray droplet SMD from PDA experiments with that predicted by correlations in the literature. ....	166
Figure 6.3.13 The relationship between $D_{MC}$ and global spray droplet SMD as calculated using PDA data.....	167
Figure 6.4.1 Schematic showing the geometric parameter length-to-diameter ratio. .	168
Figure 6.4.2 Comparison of coefficient of discharge from PDA experiments and literature. ....	170
Figure 6.4.3 Comparison of spray half-angle from PDA experiments and literature. .	171
Figure 6.4.4 Droplet diameter frequency distribution based on number. ....	172
Figure 6.4.5 Droplet diameter frequency distribution by mass.....	172
Figure 6.4.6 Cumulative droplet size distribution.....	173
Figure 6.4.7 Validated local data rates at 150 mm downstream of the nozzle. ....	174
Figure 6.4.8 Average local droplet velocity at 150 mm downstream of the nozzle.....	175
Figure 6.4.9 Local droplet AMD at 150 mm downstream of the nozzle.....	176
Figure 6.4.10 Local droplet SMD at 150 mm downstream of the nozzle.....	176
Figure 6.4.11 Local droplet SMD/AMD at 150 mm downstream of the nozzle.....	177
Figure 6.4.12 Comparison of global spray droplet SMD from PDA experiments with that predicted by correlations in the literature. ....	180
Figure 6.4.13 The relationship between $L_0/D_0$ and global spray SMD as calculated using PDA data.....	181
Figure 6.5.1 Schematic showing the geometric parameter aerator geometry.....	182
Figure 6.5.2 Comparison of coefficient of discharge from PDA experiments and literature. ....	185
Figure 6.5.3 Comparison of spray half-angle from PDA experiments and literature. .	185
Figure 6.5.4 Droplet diameter frequency distribution based on number. ....	186
Figure 6.5.5 Droplet diameter frequency distribution based on volume/mass.....	187
Figure 6.5.6 Cumulative droplet size distribution.....	187
Figure 6.5.7 Validated local data rates at 150 mm downstream of the nozzle. ....	188

Figure 6.5.8 Average local droplet velocity at 150 mm downstream of the nozzle.....	189
Figure 6.5.9 Local droplet AMD at 150 mm downstream of the nozzle.....	190
Figure 6.5.10 Local droplet SMD at 150 mm downstream of the nozzle.....	190
Figure 6.5.11 Local droplet SMD/AMD at 150 mm downstream of the nozzle.....	191
Figure 6.5.12 Comparison of global spray SMD from PDA experiments with that predicted by correlations in the literature. ....	193
Figure 6.5.13 Experimentally determined global spray droplet SMD for all aerator geometries investigated.....	194
Figure 7.1.1 Comparison of coefficient of discharge from PDA experiments with that in the literature.....	243
Figure 7.1.2 Calculated liquid disintegration mode for kinematic viscosity experiments. ....	244
Figure 7.1.3 Comparison of spray half-angle from PDA experiments and literature. .	245
Figure 7.1.4 Droplet diameter frequency distribution based on number. ....	245
Figure 7.1.5 Droplet diameter frequency distribution by mass.....	246
Figure 7.1.6 Cumulative droplet size distribution.....	247
Figure 7.1.7 Validated local data rates at 150 mm downstream of the nozzle. ....	247
Figure 7.1.8 Average local droplet velocity at 150 mm downstream of the nozzle.....	248
Figure 7.1.9 Local droplet AMD at 150 mm downstream of the nozzle.....	249
Figure 7.1.10 Local droplet SMD at 150 mm downstream of the nozzle.....	249
Figure 7.1.11 Local droplet SMD/AMD at 150 mm downstream of the nozzle.....	250
Figure 7.1.12 Comparison of global spray SMD from PDA experiments with that predicted by correlations in the literature. ....	253
Figure 7.1.13 The relationship between kinematic viscosity and global spray SMD as calculated using PDA.....	254
Figure 7.1.14 The relationship between measured and predicted global spray SMD for low and high ALR operation.....	256
Figure 7.1.15 The relationship between measured and predicted global spray SMD.....	257

## List of Tables

---

Table 2.3.1. Bubble diameter ( $D_b$ ) correlations in literature. ....	15
Table 2.4.1. Range of mixing chamber dimensions.....	22
Table 2.6.1. Effervescent Atomiser Produced Spray droplet SMD Correlations in Literature. ....	37
Table 2.6.2. Simplified forms of effervescent atomiser correlations found in literature. ....	39
Table 2.6.3. Relative importance of primary operating parameters on spray droplet SMD as determined by analysis of droplet SMD correlations from the literature. ....	40
Table 2.7.1. Specific bubble Energy ( $E_b$ ) Correlations in Literature. ....	45
Table 2.7.2. Coefficient of Discharge ( $C_d$ ) Correlations in Literature. ....	46
Table 3.1.1 Test matrix designed to facilitate testing.....	79
Table 3.7.1. Output of analyses used to characterise and compare sprays.....	98
Table 3.8.1 The influence of sample size on accuracy representative droplet diameters .....	103
Table 4.1.1. Effervescent and Y-Jet atomiser operating conditions.....	105
Table 4.3.1. Representative droplet diameters of Y-Jet and Effervescent Atomiser sprays.....	110
Table 5.1.1 Operating conditions and controlled parameters for ALR tests.....	111
Table 5.1.2 Summary of average ALR test operating conditions and spray characteristics.....	115
Table 5.1.3 Validates local droplet count varying with ALR increases. ....	125
Table 5.1.4 Average local droplet velocity varying with ALR increases. ....	127
Table 5.1.5 Inferred local gas and relative velocity varying with ALR increases. ....	129
Table 5.1.6 Local droplet AMD and SMD varying with ALR increases. ....	132
Table 5.1.7 Local SMD/AMD ratio varying with ALR increases. ....	135
Table 5.1.8. Local average droplet Weber number varying with ALR increases.....	137
Table 5.1.9 Cumulative mass-under-size plots for entire downstream locations. ....	139
Table 5.2.1 Operating conditions and controlled parameters for pressure differential tests.....	146
Table 5.2.2 Summary of $\Delta P$ test operating conditions and spray characteristics.....	148
Table 5.2.3 Cumulative mass-under-size plots for entire downstream locations. ....	160
Table 6.1.1 Operating conditions and controlled parameters for $D_o$ tests. ....	135
Table 6.1.2 Summary of $D_o$ test operating conditions and spray characteristics. ....	137
Table 6.1.9 Cumulative mass-under-size plots for entire downstream locations. ....	146

Table 6.2.1 Operating conditions and controlled parameters for $L_{MC}$ tests. ....	150
Table 6.2.2 Summary of $L_{MC}$ test operating conditions and spray characteristics. ....	152
Table 6.3.1 Operating conditions and controlled parameters for $D_{MC}$ tests.....	154
Table 6.3.2 Summary of $D_{MC}$ test operating conditions and spray characteristics.....	156
Table 6.3.9 Cumulative mass-under-size plots for entire downstream locations. ....	165
Table 6.4.1 Operating conditions and controlled parameters for $L_O/D_O$ tests.....	168
Table 6.4.2 Summary of $L_O/D_O$ test operating conditions and spray characteristics. .	169
Table 6.4.9 Cumulative mass-under-size plots for entire downstream locations. ....	178
Table 6.5.1 Operating conditions and controlled parameters for aerator geometry tests. .....	182
Table 6.5.2 Side on view of aerators investigated showing location of air injector holes (not to scale).....	183
Table 6.5.3 Summary of aerator geometry test operating conditions and spray characteristics.....	184
Table 6.5.10 Cumulative mass-under-size plots for entire downstream locations.....	192
Table 7.1.1 Operating conditions and controlled parameters for kinematic viscosity tests.....	241
Table 7.1.2 Summary of kinematic viscosity test operating conditions and spray characteristics.....	242
Table 7.1.9 Cumulative mass-under-size plots for entire downstream locations. ....	251
Table 7.1.10 Error between measured and predicted global spray SMD data. ....	257

# Chapter 1 : Introduction

---

## 1.1 Motivation

Fossil (or hydrocarbon) fuels powered the industrial revolution [1] and have continued to be the principal source of energy up until the present day. Nowadays they are widely exploited in a range of important industrial applications, which include fossil fuel power stations and internal combustion engines. The widespread use of hydrocarbon fuels seems unlikely to change in the foreseeable future. For example, projections by the U.S. Energy Information Administration [2], reproduced in Figure 1.1.1, reveal that fossil fuels are expected to provide up to 80% of the world's energy in 2035.

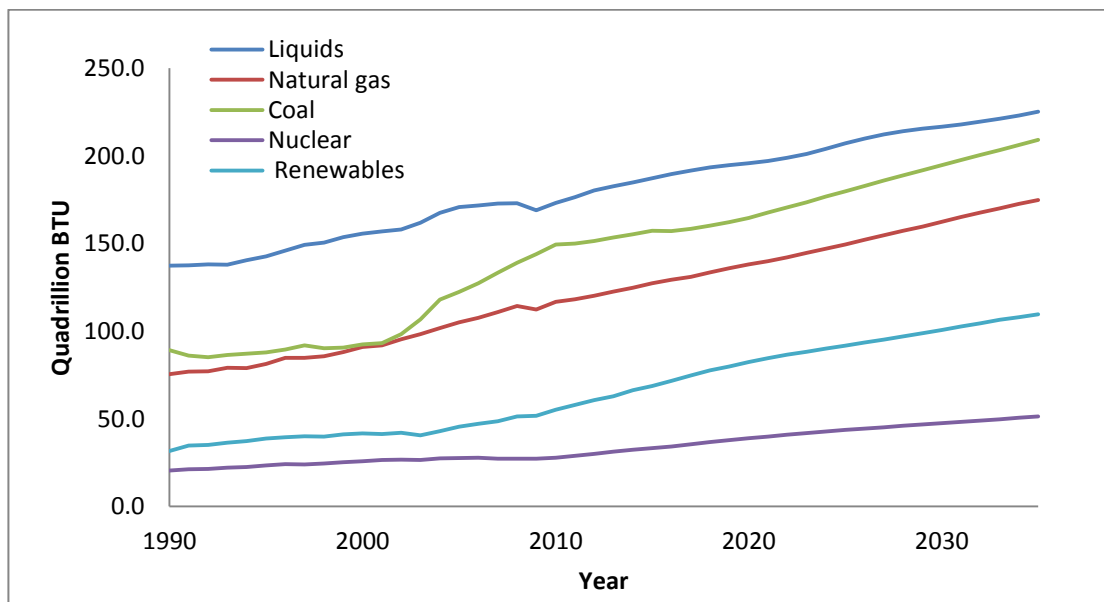


Figure 1.1.1 World energy consumption by fuel for 1990-2035 [2].

This continuing importance of hydrocarbon fuels (especially in newly industrialised countries and developing economies) is unsurprising. Large parts of industry are geared towards the use of such fuels, and are not yet ready to switch to alternative fuel sources. There are many reasons for this which frequently involve considerations of the suitability of fossil fuels towards traditional combustion systems, the difficulties (and costs) involved in drastic changes to power generation practices, as well as the perceived disadvantages of alternative fuel types (e.g. the safety challenges associated with nuclear power [3, 4], the intermittent nature of solar, wind and tidal power [5, 6], the apparent reduction in calorific value [7] or increases in harmful emissions [8] afforded by some alternative fuel types etc).

However fossil fuels have disadvantages, such as the reputation for being “dirty”. Emissions from combustion processes (such as those associated with hydrocarbon fuels) are frequently cited as a major cause of global warming [9-13]. As a result there has been a desire for some decades to begin replacing fossil fuels with “cleaner” and more sustainable alternatives. Global meetings such as the Kyoto Summit 1997 have increased awareness of the unsustainable nature of continued use of hydrocarbon fuels, and put pressure on governments to reduce harmful emissions [14, 15].

In addition, fossil fuels are non-renewable and known to be running out. Depletion dates are difficult to calculate as data on fuel reserves and global consumption are neither readily available nor straightforward to model. One typical study predicts coal being the only remaining fossil fuel by 2042, and being depleted by 2112 [16]. Scarcity, fear of supply issues and pressures arising from international environmental treaties have frequently been responsible, directly or indirectly, for increases in the costs of hydrocarbon fuels [17]. The push to provide “cleaner” energy, as well as the increasing costs and limited supplies of fossil fuels has led to an increased interest in alternative sources of energy.

Simultaneously, these factors forced combustion engineers to look into increasing the efficiency of current fossil fuel combustion systems. Many aspects of traditional combustion systems have been optimised with a view to increasing the power output from the combustion processes or reducing harmful by-products, such as emissions of NO<sub>x</sub>, SO<sub>x</sub> and soot.

However, traditional combustion systems have by no means been fully optimised. For instance, there is further room for improvement in the field of liquid fuel atomisation of viscous fuels (e.g. in the atomisation of Bio-Fuels). The motivation for this study is therefore to further current understanding of liquid fuel injection systems for industrial applications, such as gas turbines, boilers, incinerators and internal combustion engines. This investigation is particularly relevant to combustion systems utilising viscous liquid fuels such as Bio-Fuels.

### 1.2 Liquid Fuel Atomisation

Atomisation – the break-up of large volumes of fluid into small particles – is an important process employed in the chemical industry, agriculture, food processing, fuel injection and power generation. Of particular interest to the power generation sector is the atomisation and injection of liquid fuels into combustors, incinerators and engines.



In order for this to be achieved in an efficient and economical manner the use of a robust, well designed fuel atomiser is critical for the combustion process.

A wide range of atomiser types have been developed for industrial applications – rotary, pressure, air-assist and air-blast. All work on the principle of applying mechanical or kinetic energy to disintegrate a jet or sheet of liquid fuel, in preparation for combustion. This sufficiently increases the surface area to volume ratio of the fuel and presents it in a form suitable for a consistent combustion process. Traditional liquid fuels, such as hydrocarbons, have been employed for some decades and combustion systems (and atomisers) have been optimised for their use. However, combustion engineers have been increasingly forced to look into the use of alternative, biologically-derived hydrocarbon fuels. Such fuels often have very different viscosities, densities and surface tensions or possess complex, non-linear properties when compared to conventional fuels.

The acceptance to utilise such difficult liquid fuels (e.g. Bio-Fuels) was dictated by a combination of government directives, supply issues, fear of depletion of current stocks and increases in fuel prices (e.g. crude oil). For example a boycott by OPEC countries in 1973 lead to a doubling or even tripling of crude oil prices in, amongst other countries, the USA [17].

Traditional combustion systems were not well suited to utilising the new fuels, whether on their own (pure Bio-Diesels) or in combination with established fuel types (blends). Heavier fuels have the potential to clog the fuel injector components, are problematic to atomise to acceptably small sizes and often require pre-heating or treatment prior to use [18]. Bio-Fuels tend to have lower heating values and therefore appear less economical to employ than standard fuels. Solid particulates present in the alternative fuels can increase component wear and possess complicated fluid rheology.

Cost-intensive processing is required to allow fuel firing on current systems while inefficient combustion (resulting from the use of unusual fuels) leads to higher emissions of pollutants such as carbon monoxide, nitrous oxides or partially combusted hydrocarbons.

At various times in the past decades high crude oil prices made research into new technologies for atomising alternative fuel types appear more economically feasible. One promising new atomiser was developed in the 1980's by Lefebvre and co-workers, relying on a novel form of atomisation now called Effervescent Atomisation (EA).

This method, which differs fundamentally from traditional atomisation techniques, relies on the creation of a pressurised “bubbly” two-phase flow upstream of the atomiser exit

orifice. Upon discharge from the exit orifice the compressed gas-phase escapes the mixture, expanding rapidly and shattering the liquid fuel into ligaments and droplets (which can undergo further disintegration to produce smaller droplet sizes). It was found that this type of atomisation was particularly advantageous for comparatively viscous fuels providing several advantages over conventional atomisers [19], such as:

- Large exit orifice diameters could be used on the atomisers helping to avoid nozzle blockage by high viscosity fluids and to reduce component wear.
- Fluid viscosity had a minimal impact on the resulting droplet sizes, allowing a single atomiser to be employed with a range of fluids.
- Equivalent droplet sizes were observed at injection pressures lower than those required by other atomisers (or comparable atomisation at lower pressures thus reducing the need for large pumps and minimising associated energy losses).
- The use of air as the atomising gas was found to improve combustion efficiency as it led to reduced soot formation and exhaust smoke [20].

Since many of the processes are not well understood theoretically, experiments have been performed by researchers to empirically determine the characteristics and limitations of effervescent atomisation.

### 1.3 Aims and Objectives of Thesis

The aim of this thesis is to investigate effervescent atomisation of viscous, difficult-to-atomise fuels such as Bio-Fuels, by performing experiments on a state-of-the-art effervescent atomiser at a simulated 2MW effective power rating based on mass flow. This can be achieved in the following manner:

- Design a testable effervescent atomiser meeting the latest design recommendations and operating at a suitable range of pressures, flow rates and turndown ratios.
- Develop a testing methodology.
- Perform a parametric study to determine the influence of operating conditions, atomiser geometry and fluid properties on effervescent atomisation.
- Perform a comparison between an effervescent atomiser and a typical Y-Jet atomiser at equivalent operating conditions (4.6 barG, 40.59 g/s water, 15.79%

Air-to-Liquid Ratio (ALR), 3.7 mm diameter nozzle) using the same droplet sizing techniques and procedures.

- Develop proportionalities or correlations relating to global droplet spray SMD.

### 1.4 Thesis Layout

Chapter two discusses the current state of the effervescent atomiser literature, and attempts to summarise many of the findings and conclusions relevant to the design of highly-optimised effervescent atomisers, their governing principles and operating parameters.

Chapter three focusses on the design and manufacture of an effervescent atomiser, and on the PDA techniques used to characterise fuel sprays. The atomiser testing facilities available at the Cardiff University School of Engineering are also discussed.

Chapter four compares the effervescent atomiser performance against that of a commonly used industrial-type Y-Jet atomiser running at equivalent operating conditions (4.6 barG, 40.59 g/s water, 15.79% ALR, 3.7 mm diameter nozzle).

Chapters five, six and seven present the results of testing of the important control parameters. The results discuss the influence of the operating conditions, fluid atomiser geometry, and fluid properties on effervescent atomisation, respectively.

Chapter eight summarises the most important conclusions of the study undertaken.

Finally, chapter nine provides recommendations for future work.

## Chapter 2 : Literature Review

---

### 2.1 Effervescent Atomisation – Background

Rising crude oil prices acted as a catalyst for developing new technologies and improving existing ones to help extract more energy from fuels. Some precursors of effervescent atomisation developed in the 1960's and 1970's in response to these incentives included “flashing” and “internal mixing” atomisation which seemed to meet with mixed or limited success (for a thorough review of present-day effervescent atomiser designs, see Konstantinov et al. [21]). In the mid 1980's Chawla reported the use of a two-phase atomising device very similar to an effervescent atomiser [22]. The use of a swirl chamber, however, appeared to limit its performance [18].

Flashing atomisation, which involves atomisation via the action of superheated gas bubbles eluting from the ejected two-phase fluid, can be considered a precursor to the effervescent atomisation technique. Attempts to overcome the difficulties associated with flashing atomisation led to the evolution of the effervescent technique [19]. It should be noted, however, that knowledge of flashing atomisation has subsequently advanced and some of the original difficulties have been circumvented with the development of more efficient models, such as that by Zeng and Lee [23]. Some of the latest designs pioneered by Sher and Bar-Kohany make use of an expansion chamber with optimised dimensions to achieve maximum operating efficiency incorporating internal as well as external flashing [24-28].

Flashing atomisation is a process closely related to effervescent atomisation. This technique relies on the gas bubble nucleation, growth and destructive action on a two-phase superheated jet as it is released into stagnant air at a much lower temperature and pressure than that of the two-phase fluid. When it is released into atmospheric conditions above a certain, critical level of superheat, the fluid begins to rapidly boil or “flash” producing a very fine well-atomised mist. As in the effervescent process, atomisation is achieved via the action of rapidly expanding gas bubbles shattering the liquid phase into ligaments and droplets. Thus the atomisation mechanisms are clearly similar. The main difference between effervescent and flashing atomisation is the heating required to superheat a pre-mixed two-phase fluid prior to flashing atomisation.

Some of the problems early researchers experienced with flashing atomisation included the following:

- Heating to temperatures greater than the fluid boiling point and pressurisation above fluid vapour pressure point were required. This constituted a considerable energy, and hence cost, requirement.
- This superheated mixture often required storage and transportation at elevated temperatures and pressures.
- Bubble nucleation and bubble growth rates (linked to optimal operation) were difficult to control.
- Operating parameters were difficult to optimise since theoretical treatments were involved, requiring complex thermodynamic, two-phase fluid mechanic, atomiser geometry, and surface finish analyses.

By comparison, effervescent atomisation demonstrated the advantages of flashing atomisation, without many of the disadvantages. For these reasons it proved to be a subject of interest to researchers investigating alternative atomisation techniques.

The first systematic study of effervescent atomisation was undertaken by Roesler and Lefebvre in 1987. Since then a great deal of experimentation has been performed to attempt to understand the parameters that control effervescent atomiser performance. Some numerical models of the processes involved have been developed (summarised by Qian et al [29]), most of which attempt to predict spray droplet size. However, none are universally applicable or take into account all primary input parameters that govern the effervescent atomisation process, i.e. a thorough first-principle based understanding of effervescent atomisation has not yet been achieved.

Effervescent atomisation displays some similarities to air-assist and air-blast atomisation, and overlaps with them at certain operating conditions. However, it has lower air-to-liquid ratio (ALR, an important operating parameter in effervescent atomisation) requirements. Effervescent atomisation requires the creation of a steady two-phase flow by bubbling small quantities of gas into the liquid to be atomised upstream of the exit orifice. The gas, which is normally supplied at marginally higher pressures than the liquid, is not expected to atomise the liquid prior to ejection from the exit orifice, but simply to create two-phase flow conditions. Early researchers emphasised the bubbly flow regime as being the optimal flow regime conducive to efficient effervescent atomisation. Although other two-phase flow regimes (such as annular and intermittent flow) are possible, these were thought to be less energy efficient than atomisation with a bubbly flow. Ensuring bubbly flow was therefore a major design consideration for developing an effective and consistent effervescent fuel

injector. By contrast, present-day researchers do not emphasise the importance of the bubbly flow regime for effervescent atomisation.

As discussed, the pressure difference between the injected gas and liquid need only be relatively small. One fluid is injected into the other in the so-called “mixing chamber”, housed in the atomiser body. The two-phase fluid flows through the narrow mixing chamber and escapes via the exit orifice. As it is ejected, the fluid mixture experiences a sudden pressure drop. In doing so, the gas bubbles within the liquid expand and rupture, breaking the fluid up into droplets and ligaments. The destructive action of bubble expansion and explosion is an important characteristic of effervescent atomisation emphasised by early literature, however other liquid break-up mechanisms were also recognised. The break-up mechanisms known to act in effervescent atomisation include:

1. The gas contribution disrupts the liquid phase. The two-phase mixture emerging from the nozzle has no intact liquid core observable above a certain ALR. Compared to a pure liquid jet emerging from a nozzle at the same conditions, the liquid component issuing from an effervescent atomiser nozzle has already gone some way towards disintegrating [30].
2. The gas-liquid mixture ejected from the nozzle undergoes relaxation as fluid conditions rapidly adjust to match ambient conditions. As the gas pressure drops the gas bubbles expand and explode, shattering the liquid into smaller droplets [20, 31].
3. Two-phase mixtures have significantly reduced sonic velocities allowing flow choking at the nozzle to be achieved relatively easily. The resulting shockwaves generate intense shear fields between the gas and liquid phases enhancing liquid atomisation [32].
4. All break-up mechanisms visible in liquid jets emerging from plain orifice atomisers (e.g. primary and secondary atomisation) also act on the liquid phase of an effervescent atomiser produced spray.

The advantages claimed of the effervescent method include the lower pressures needed to achieve good atomisation relative to other techniques. In addition, a number of studies [18, 20, 32-34] indicate that effervescent atomisation is dominated by secondary atomisation, and is therefore less dependent on fluid properties and exit orifice diameter. This makes the technique particularly well-suited to operation with viscous fuels, such as Bio-Fuels.

However the processes involved are not yet fully understood and a great deal of design optimisation still remains. For example, atomiser geometry can be optimised to give more efficient atomisation (smaller representative droplet diameters) and better operation than is possible with current designs.

Figure 2.1.1 shows the aerator, mixing chamber and exit orifice arrangement for a typical “inside-out” (gas inside, liquid outside) type effervescent atomiser such as those investigated by early researchers. Figure 2.1.2 depicts typical gas-liquid behaviour at an effervescent atomiser exit orifice.

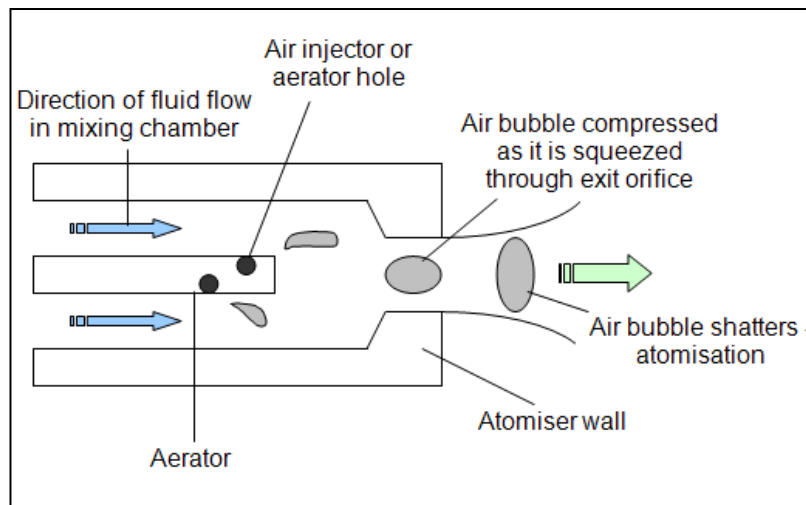


Figure 2.1.1. Cross-section through a typical effervescent atomiser in operation.

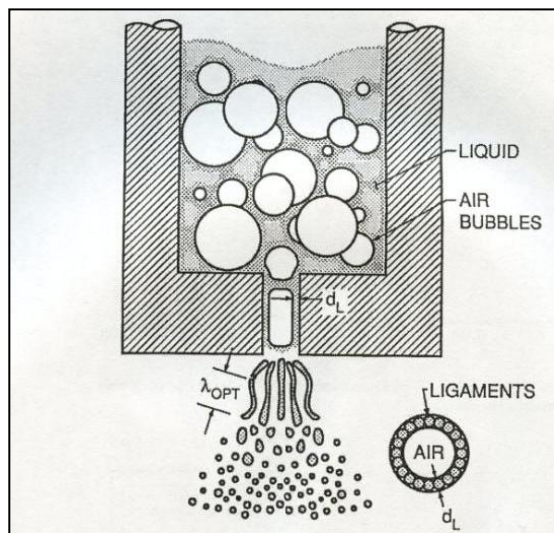


Figure 2.1.2. Gas-liquid interaction at the exit orifice with typical liquid break-up mechanisms in action [35], where  $\lambda_{OPT}$  is Weber's optimum break-up wavelength and  $d_L$  is ligament diameter.

## 2.2 Jet Atomisation Theory

Before the complex behaviour of a disintegrating, two phase, effervescent atomiser jet can be analysed, the more straightforward mechanical jet break-up mechanisms will be considered. These are the mechanisms by which single-phase liquid jets injected into a stagnant gas medium disintegrate as disruptive aerodynamic forces overcome the cohesive action of fluid properties.

### 2.2.1 Mechanical Jet Disintegration

Starting with so-called dripping flow through a plain circular orifice and increasing the flow rate eventually leads to the formation of a liquid jet, which can disintegrate by a number of mechanisms. Jet break-up becomes more efficient and complete as mass flow rate is increased. At low mass flow rates jet break-up begins downstream of the orifice and at the liquid surface, where the gas and liquid phases interact; at very high mass flow rates, disintegration can occur at the nozzle, completely atomising the liquid phase so that no solid liquid core remains intact. The quality of jet atomisation is influenced by operating conditions (mass flow rate or jet velocity or fluid pressure, which have equivalent effects in this context), nozzle geometry (e.g. orifice diameter) and fluid properties (surface tension, viscosity, density). The processes described have been extensively studied and reported in the literature.

For example, droplet formation analysis has been widely investigated [36, 37]; the pioneering work of Lord Rayleigh on jet break-up was published over 130 years ago – more recently it was reviewed and re-analysed [38]; the atomisation mechanisms of liquid jets have been studied in great detail [39] as have the atomisation mechanisms observed in various industrial atomiser types currently in use [40, 41]. In later studies, numerical modelling has been applied to jet break-up analysis [42].

A good overview of mechanical jet break-up theory is provided by Reitz, as reported by Lefebvre [43]. Reitz identified four distinct regimes of jet disintegration which appear to correlate strongly with liquid jet velocity.

1. Rayleigh break-up: occurs at low jet velocities. At the exit orifice axisymmetric oscillations appear at the jet surface induced by fluid surface tension effects. This type of break-up leads to droplets typically larger than the exit orifice diameter.
2. First wind-induced break-up: occurs at increasing jet velocities. A static pressure distribution is induced across the jet by the velocity gradient between



the ambient air and jet surface. This speeds up jet disintegration. Droplets produced are typically similar in size to the exit orifice diameter.

3. Second wind-induced break-up: occurs at even higher jet velocities. The increased relative velocity between the jet surface and the surrounding air causes the creation of short wavelength waves on the jet surface. Wave growth is opposed by surface tension tending to hold the fluid in the shape of a spheroid. The opposing forces cause break-up at the jet surface. Droplets much smaller than the exit orifice diameter result.
4. Atomisation mode break-up: occurs at the highest jet velocities. Break-up begins almost spontaneously at the nozzle exit producing very small droplets. This is the mode of operation of industrial atomisers.

Transition criteria are frequently given as a function of the dimensionless parameters Reynolds number (Re) and Ohnesorge number (Oh). Reitz's four regimes, which are based on empirical data, are graphically represented in Figure 2.2.1, which is taken from Lefebvre [43].

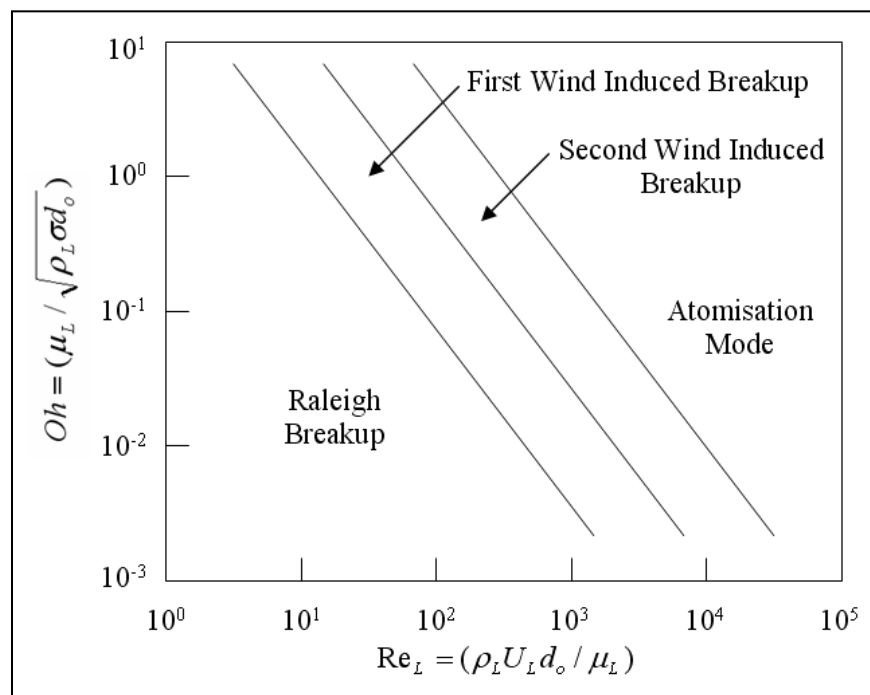


Figure 2.2.1 Modes of mechanical jet disintegration [43].

It can be seen that the so-called “Atomisation Mode” which is required for correct operation of traditional fuel atomisers (pressure atomisers) requires the largest fluid Reynolds and Ohnesorge numbers. Figure 2.2.1 explains why greater relative air-liquid velocities (provided by greater supply pressures or greater fluid mass flow rates),

smaller orifice diameters, and smaller surface tensions, viscosities and densities provide better jet disintegration.

### 2.2.2 Jet Break-up Length

Jet break-up length can be of prime importance in practical atomisation applications (e.g. in physically constrained combustion chambers). Jet break-up length and jet velocity display a characteristic non-linear relationship, given by Lefebvre, and shown in Figure 2.2.2 [43]. The dripping, laminar, turbulent and fully developed spray regimes (corresponding to the atomisation mode of fluid disintegration) are clearly visible. Break-up length can thus be seen to vary with operating conditions.

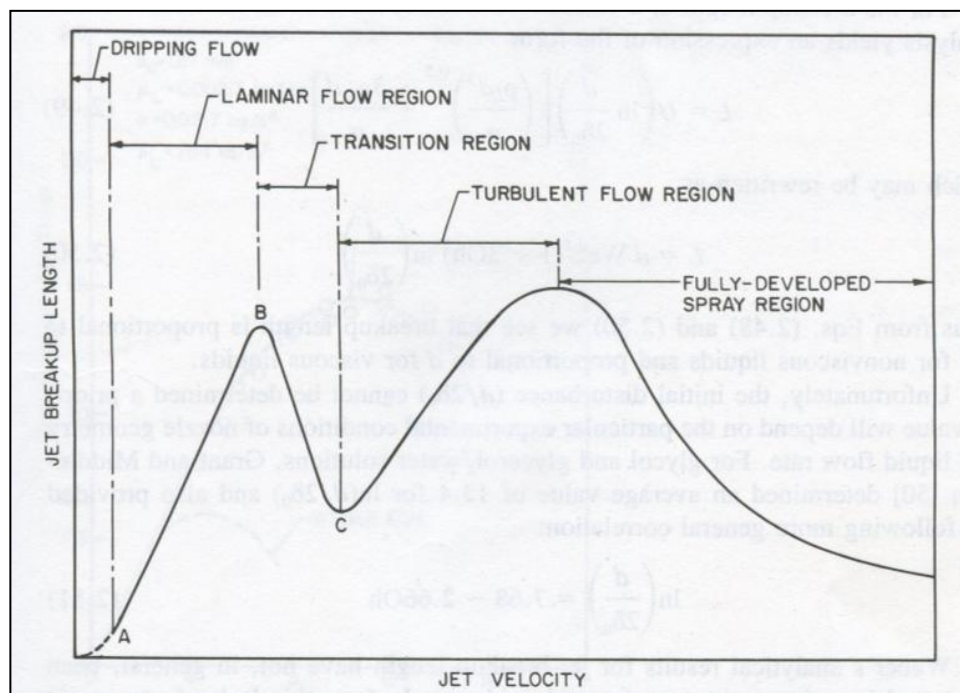


Figure 2.2.2 Jet break up length varying with jet velocity [43].

### 2.2.3 Jet Velocity Profile

The velocity profile of the emerging jet has a strong influence on the method of disintegration observed. According to Schweitzer [44], if the liquid jet emerges from the nozzle exit in streams parallel to the nozzle axis the jet flow is laminar. If however the fluid layers have transverse velocity components, the jet fluid flow is turbulent. Transition occurs at the critical Reynolds number. Turbulent flow is encouraged by high flow velocities, large tube sizes, tube curvature and changes in tube cross sectional area, while laminar flow is encouraged by high liquid viscosity, a rounded entrance to the tube and a lack of tube curvature. Laminar and turbulent jets possess different

kinetic energies per unit mass and consequently behave differently once outside the nozzle. As soon as the constraining effects of the nozzle are removed the kinetic energy carried by the jet is redistributed in a process known as velocity profile relaxation. This affects laminar and turbulent jets differently. For instance, turbulent jets disintegrate without the action of external forces or aerodynamic effects due to the radial components of velocity of the jet itself. However, laminar jets require external forces for break-up to occur. A consideration of fluid turbulence and aerodynamic effects leads to the definition of two distinct types of liquid atomisation – primary and secondary atomisation.

### **2.2.4 Droplet Primary Break-up**

The disintegration of a liquid jet or ligament as it exits the nozzle is termed primary atomisation and is influenced by operating conditions as well as fluid properties. The consensus in the literature is that primary atomisation, although not completely understood, is a phenomenon caused by interactions at the gas-liquid interface. These lead to instabilities (Kelvin-Helmholtz, Rayleigh-Taylor) on the liquid surface which are amplified by energy and momentum transfers from the gas phase. Finally liquid break-up occurs – in the near-nozzle portion of the spray [43, 45, 46].

Lefebvre [43] defines primary atomisation as the atomisation caused by the action of internal (to the liquid) forces – fluid turbulence and inertia, surface tension and velocity profile relaxation. As the liquid jet emerges from an orifice, cohesive and disruptive forces begin to act on its' surface. These give rise to oscillations of the jet surface eventually leading to break-up and disintegration into droplets.

### **2.2.5 Droplet Secondary Break-up**

Lefebvre defines secondary atomisation as the atomisation initiated by forces external to the liquid medium, such as aerodynamic forces [43].

Guildenbecher et al provide a detailed discussion on secondary atomisation and the associated critical Weber number [47]. If the droplets formed as a result of primary atomisation processes are large enough they will disintegrate further by a process termed secondary atomisation. This type of atomisation occurs if the external (aerodynamic) forces on the droplet are large enough to overcome the restoring action of droplet surface tension and viscosity. Since liquid atomisation is a naturally chaotic process, droplet diameter ratios of at least 100:1 are normal, and therefore secondary atomisation frequently occurs. Secondary atomisation correlates strongly with the dimensionless parameter droplet Weber number ( $We$ ) as defined in Equation 2.2.1.

$$We = \frac{\rho_a U_{av,rel}^2 d_{droplet}}{\sigma_{liq}} \quad \text{Equation 2.2.1}$$

Where  $\rho_a$  is the local air density,  $U_{av,rel}$  is the average relative velocity,  $d_{droplet}$  is the average droplet diameter and  $\sigma_{liq}$  is the liquid surface tension.

Droplet Weber number represents the ratio of inertial to viscous forces acting on the droplet. At a certain critical Weber number the disruptive inertial (hydrodynamic) forces overcome the stabilising forces and droplet break-up occurs. Various regimes of secondary break-up have been discovered which relate to different break-up mechanisms, such as vibrational break-up, bag break-up, multimode break-up, sheet-thinning break-up, and catastrophic break-up [48-50]. Empirically determined relationships exist, which aim to determine the break-up mechanism based on droplet Weber number and other dimensionless parameters. For low viscosity fluids ( $Oh < 0.1$ ) such as those used in these tests, almost all correlations in the literature quote a critical Weber number of  $11 \pm 2$  [50]. The value of 12 is also frequently quoted [46]. The critical Weber number indicates the onset of the bag break-up regime (the first secondary break-up regime to occur) and can be used to determine if secondary droplet break-up will follow. Secondary atomisation has been claimed to play an important role in effervescent atomisation [18, 20, 32-34].

### **2.3 Effervescent Atomiser Internal Flow**

The importance of understanding effervescent atomiser internal flow is dictated by the fact that two-phase internal flow approaching the nozzle is believed to strongly correlate to spray structure and therefore representative droplet diameters, such as droplet SMD [51]. However, the precise influence effervescent atomiser internal flow has on spray characteristics is not yet clear. A number of studies have attempted to visualise flow conditions inside the mixing chamber via optical techniques and correlate these with observed external flow conditions. There has been relatively little numerical modelling undertaken on this subject at present; instead recommendations given by researchers on optimal atomiser geometry, desirable flow rates or fluid properties are based mostly on empirical data.

A reasonable starting point in analysing effervescent atomiser internal flow is consideration of the more fundamental process of bubble formation and detachment in quiescent liquids under constant gas flow conditions. Numerous formulae exist to

predict the size and rise velocities of gas bubbles produced at these conditions [52, 53]. These cannot be directly applied to effervescent atomisers as quiescent fluid conditions cannot be assumed. Gas bubble size correlations most relevant to effervescent atomisation have been provided by Lefebvre [54]. These are shown in Table 2.3.1.

Table 2.3.1. Bubble diameter ( $D_b$ ) correlations in literature.

Source	Correlation	Comments
[54]	$D_b = \left( \frac{8\sigma d}{C_d \rho_L U_L^2} \right)^{0.5}$	<p>Where <math>U_L</math> is the velocity of the liquid flowing over the aerator orifice.</p> <p>Corresponds to conditions where bubbles are dislodged from the aerator by the shearing action of the moving liquid stream. <math>C_d</math> (coefficient of discharge) is around 0.5 for a nearly spherical bubble and <math>10^3 &lt; Re &lt; 10^5</math>.</p> <p>Found to be dependent on gas injector orifice diameter.</p>
[54]	$D_b = 2.4 \left( \frac{Q_{aH}}{U_L} \right)^{0.5}$	<p>Where <math>Q_{aH}</math> is the volumetric flow rate of air through each orifice.</p> <p>Results from the Rayleigh analysis where there is no gas-liquid phase slip and density of gas relative to liquid is negligible. Found to over-predict bubble sizes considerably.</p>

In the above study, Lefebvre concludes it is not possible to define an ideal gas bubble size for optimal effervescent atomisation (i.e. smallest representative droplet diameters). Even if optimal bubble sizes and bubble spacings were known, in practice they would be very difficult to achieve.

Further studies have helped clarify the role of gas bubbles in effervescent atomiser internal flow. For example, shadow photography by Buckner et al [32] revealed two distinct bubble sizes, termed microbubbles and macrobubbles. Macrobubbles were of the same order of magnitude as the exit orifice nozzle, while microbubbles were smaller than typical spray droplet sizes. In this study, the authors detected shockwaves and expansion fronts at the nozzle. Upon ejection from the nozzle, the macrobubbles were seen to expand rapidly, shattering the liquid ligaments. This was the principal atomisation mechanism observed. Meanwhile the microbubbles played no role in liquid atomisation.

Sojka et al [18] note that only a small portion of the injected air plays a part in the atomisation process – the rest presumably forming what Buckner et al would call microbubbles. According to a later study the most efficient utilisation of air in

effervescent atomisation occurs when operating in the bubbly flow regime [55]. Finer atomisation is possible in other regimes of operation but these result in significant energy losses to the environment. Bubbly flow, characterised by discrete bubbles of uniform size, is considered stable and desirable while slug flow, producing pulsating sprays is undesirable. The authors do not provide transition criteria but state that the transition between flow regimes is a strong function of air-to-liquid by mass ratio and the ratio of gas to liquid densities. Ferreira et al agree with the above study, claiming that stable bubbly flow inside the nozzle is central to the correct performance of the atomiser [56].

In a similar work Lörcher et al [57] set out to determine flow regimes inside an effervescent atomiser nozzle via an electrical technique (the conductance between a pair of wires is measured to give an indication of which phase is present – gas or liquid) and statistical analysis of the measured axial void fraction. They distinguished between bubbly, annular and plug (or slug) flow regimes of which only the first two produced a continuous, stable spray. The expansion of what other researchers might term macrobubbles, eluting from the gas-liquid mixture upon ejection, provided the dominant fluid break-up mechanism in the bubbly flow regime.

In a different study, ALR increases in the bubbly flow regime were found to produce greater bubble coalescence [58]. This eventually led to large bubble slugs alternating with liquid segments through the exit nozzle. This internal flow behaviour defined slug flow through the exit orifice and resulted in undesirable pulsing sprays.

Beyond the slug flow regime, as ALR is increased further, a gas core forms at the exit orifice with liquid squeezed outwards into the periphery resulting in the annular flow regime. So-called “single bubble expansion” atomisation, characteristic of bubbly flows and low ALRs, is now supplanted by what is called the “tree regime fluid break-up” (these are discussed in a later section). Raising ALR even further converts the effervescent device into a quasi-air-blast atomiser.

In a study similar to that of Lörcher et al, which investigated the relationship between internal and external flow patterns, Kim et al [59] arrive at similar conclusions regarding effervescent atomiser intra-nozzle flow patterns. In this study, bubbly, intermittent (identical to slug flow) and annular flow regimes are identified. Bubbly flow, a feature of which is small individual bubbles passing through the nozzle, produced droplets mostly larger than 100  $\mu\text{m}$ . A characteristic of annular flow was large gas-liquid slip velocity and droplet sizes mainly smaller than 100  $\mu\text{m}$ . Features typical of air-blast atomisation were noted in this atomisation regime. Meanwhile the intermittent mode of atomisation

(sometimes called slug or plug flow) acted as a transition between the two regimes, with both modes seeming to occur alternately. Transition criteria were then developed by the authors based on the Drift Flux Model (DFM).

Huang et al [60] provide a comprehensive study of bubble development and its role in effervescent atomiser flow regimes. A high-speed camera (2000 frames per second at full resolution and up to 100 000 frames per second at reduced resolutions) visualised the flow regime inside the mixing chamber. Phase Doppler Anemometry was used to characterise the sprays produced. Operating conditions included ALRs of 0.5-29% and fluid flow rates of 10-60 kg/hr for a 6 mm diameter mixing chamber. These operating conditions produced numerous so-called macrobubbles. These had a typical diameter of 2 mm as they approached the exit orifice. Each bubble took about 6 ms to develop from inception to maximum size (or 0.59 ms normalized bubble time). Very little bubble coalescence occurred in the bubbly flow regime with an exceptionally steady two-phase flow. The bubbles accelerated as they approached the nozzle increasing their velocity from 0.8-1.9 m/s (or 1.36-3.22 m/s normalized velocity). This acceleration was attributed to the drag effect of fluid flow. Three internal flow regimes were identified: bubbly, intermittent and annular. Starting with initially bubbly flow, as the liquid flow was decreased (equivalent to raising ALR) the two-phase flow in the mixing chamber could no longer maintain a uniform bubbly flow. This led to the intermittent flow regime and pulsing external sprays. Further reductions in the fluid flow resulted in the annular flow regime – the gas bubbles coalesced to occupy most of the mixing chamber. A certain amount of spray unsteadiness was also noticed in this flow regime. The smallest average SMD and highest spray velocities were found to occur in the annular internal flow regime.

One of the important effervescent atomiser internal flow phenomena is the behaviour of gas bubbles as they approach and pass through the exit orifice. A study by Catlin et al provides revealing photographic evidence of this interaction. This is shown in Figure 2.3.1 [61].

At the bubbly flow regime, it was evident that large, small and multiple bubbles approaching the rectangular-shaped exit orifice exhibit similar behaviour: the initially spherical bubbles begin to taper and deform towards the orifice, then expel their contents through the orifice via a puncture at the gas bubble leading edge. A co-annular gas-liquid flow then forms in the nozzle. This expands to occupy most of the nozzle, squeezing the liquid at the periphery into a thin film. According to the authors the gas then appeared to vent from the nozzle at sonic velocity in bursts (for each bubble) to produce a series of explosion-like events along the axis of the annular liquid

jet generating a cyclic fluid break-up mechanism (single bubble expansion atomisation). A similar process was claimed to occur with circular channels.

As expected the different internal flow structures in the annular flow regime produced different break-up mechanisms. In this case a co-annular gas-liquid flow travelled through the mixing chamber and continued throughout the exit orifice with a central gas core squeezing the liquid into a peripherally located film (tree-like atomisation). This can be seen in Figure 2.3.2. However, no evidence of bubble explosion break-up could be found. Instead the authors presumed the external liquid jet to disintegrate as a result of quasi-steady processes.

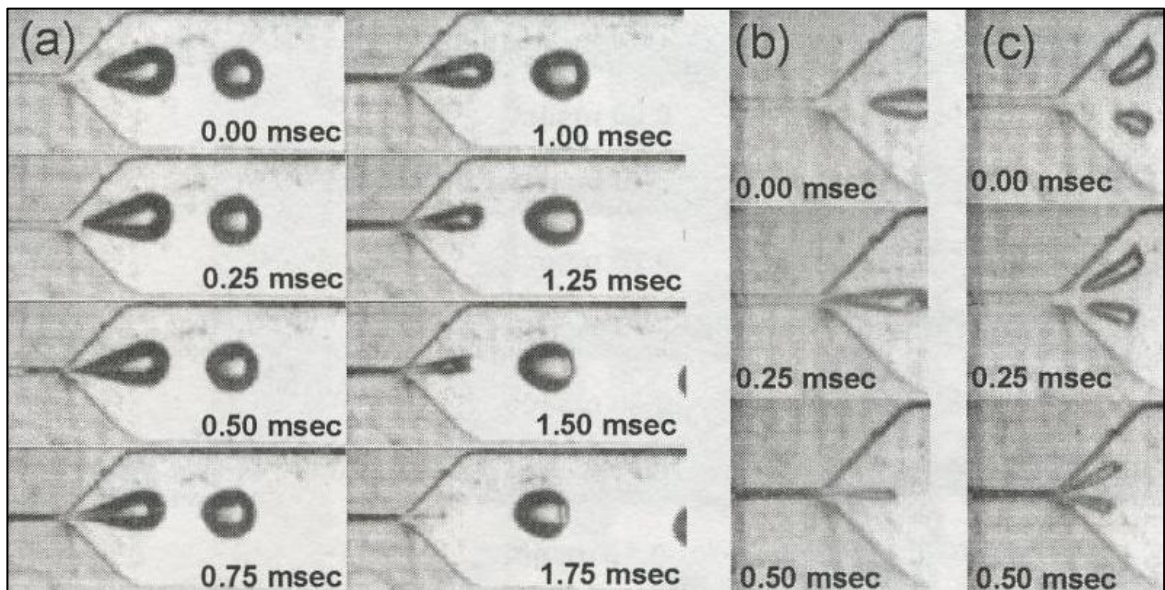


Figure 2.3.1. Gas bubble interaction with circular exit orifice in effervescent atomisers for the case of: (a) large gas bubbles; (b) small gas bubbles; (c) multiple gas bubbles (top to bottom, left to right) [61].

It should be noted that due to the dimensional constraints of the effervescent atomiser the flow regimes described will not be fully developed. For example, mixing chamber is too short to produce fully developed bubbly flow [56]. However this in no way diminishes the importance of the observations discussed concerning flow regimes and their effects on atomisation performance.



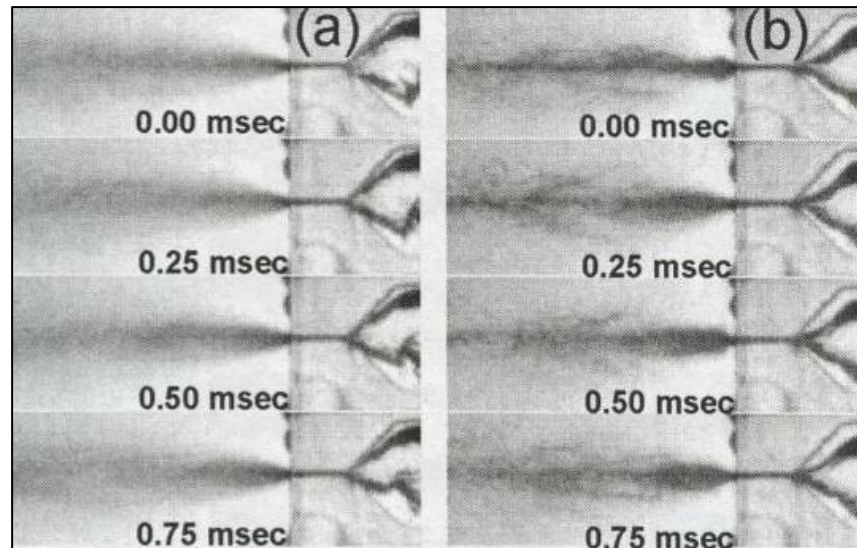


Figure 2.3.2. Effervescent atomiser internal flow and external spray response for the case of (a) annular flow with a thin liquid film; (b) annular flow with a thick liquid film (top to bottom, left to right) [61].

## 2.4 Atomiser Geometry

### 2.4.1 Aerator geometry (size, arrangement of holes)

Figure 2.4.1 shows typical mixing chamber geometry for a single orifice, “inside-out” (gas-inside fluid-outside) type effervescent atomiser.

Early studies showed that gas injector geometry (the method of introducing the atomising gas into the mixing chamber) has little effect on spray SMD [31, 62]. Similar results were revealed in experiments where the gas injection pores were reduced to several micrometres in diameter [32]. Despite this multi-hole gas injection (the use of many gas injection orifices) should lead to more even fluid mixing and therefore a more mono-disperse spray.

For inside-out (or gas *inside*-liquid *outside*) type designs, gas introduction is often achieved by the use of one or more circular injection holes at a right angle to the fluid flow. A newer study claimed that a helically shaped injector surface and centred axial gas injection into swirling fluid flow leads to optimal atomisation [63]. Meanwhile according to Sojka [64] extensive experimental practice seems to indicate that the gas injection orifices should be arranged asymmetrically for best operation.

A further study [65] highlights the ratio of the discharge orifice area ( $A^*$ ) to the area of the air injection holes ( $A_a$ ) as one of the most important parameters affecting spray SMD. The authors employ circular air injection holes whose size is a function of ALR

and the exit orifice area,  $A^*$ . According to this investigation the optimal air injector size (for a finite number of holes) is determined by Equation 2.4.1.

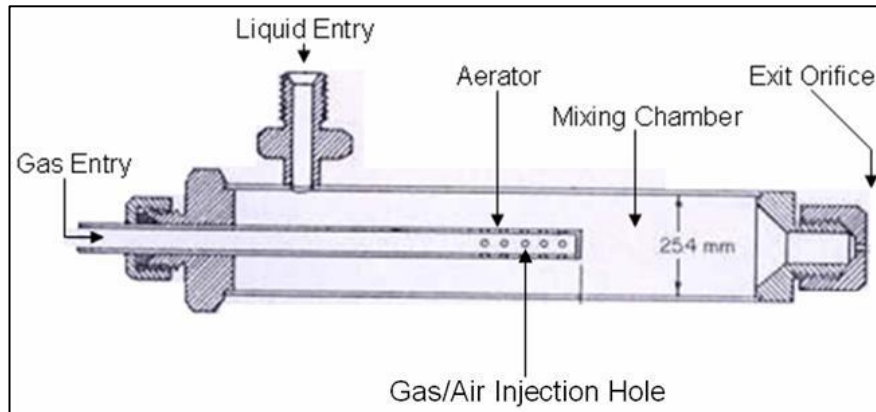


Figure 2.4.1. Typical effervescent atomiser geometry [62].

$$\frac{A^*}{A_a} = 6.3ALR \quad \text{Equation 2.4.1}$$

Equation 2.4.1 (valid for  $0 < A^*/A_a < 3.1$  and  $0 < ALR < 60\%$ ), demonstrating the optimal  $A^*/A_a$  ratio from Chin et al's work, is graphically represented by Figure 2.4.2 [65]. This shows a linear, direct proportionality between the ratio of exit orifice to air injector areas and ALR for optimal operating conditions (where optimal operating conditions translate into smallest achievable spray SMD). For example, if the operating ALR has been selected, then the optimal geometric ratio of  $A^*/A_a$  for minimal spray SMD can be determined from the straight line relationship in Figure 2.4.2. Thus, once the nozzle area is determined (based on required fluid flow rates) the area of the air injectors for the smallest achievable droplets can be calculated.

Implied in their work, and Equation 2.4.1, is the assumption that the number of air injector holes is not important. It can be seen that for an optimal geometric ratio ( $A^*/A_a$ ), the air injector area will always be larger than the exit orifice area. ALR ranges of 1-15% (ranges typically found in effervescent literature) substituted into the right hand side of Equation 2.4.1 yield values of  $A^*/A_a$  between 0.063 and 0.945. Thus  $A_a$  will always be 1.06-15.87 times greater than  $A^*$ , according to Chin et al's equation.

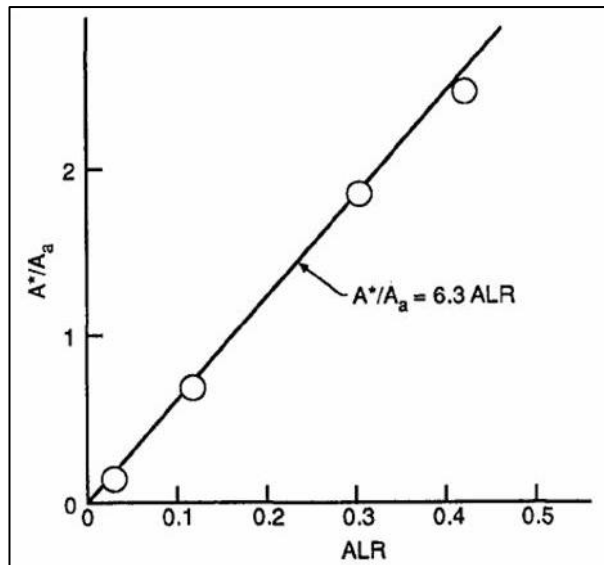


Figure 2.4.2. ( $A^*/A_a$ ) ratio versus ALR to produce optimal SMD [65].

It is instructive to compare the above values to those used by other researchers. Ferreira et al investigated the range 0.0267 – 0.1157 and concluded that for their operating conditions the largest  $A^*/A_a$  ratios they used produced the smallest spray droplet sizes observed [56]. This ties in with the recommendations of Chin et al since the lowest ratios investigated by Ferreira et al correspond to conditions outside the optimal ratios suggested by Equation 2.4.1. Bates et al's study [66] who operated in the range 0.116 – 0.3216  $A^*/A_a$ , also agrees with those of previous researchers. This study also found better atomised sprays at greater  $A^*/A_a$  ratios.

Most designs employ relatively few air injection holes, usually less than thirty. One of the most extreme designs featured eighty circular holes 3.2 mm in diameter providing the largest air injection area ( $A_a$ ) of any effervescent atomiser design encountered in the literature [34]. This design was intended for a high flow rate set-up operating with up to 1 kg/s of liquid.

#### 2.4.2 Mixing Chamber Characteristics

There are many possible configurations for an effervescent atomiser but two contrasting designs commonly recur in the literature: “inside-out” and “outside-in” arrangements (see Figure 2.4.3). Different geometric recommendations exist for each. Discussed here will be the inside-out type, which was widely investigated by early researchers.

Almost all designs reported in the literature possess a cylindrical mixing chamber, at the base of which the liquid phase is introduced. The gas phase is then injected via a centrally located pipe protruding into the chamber containing an arrangement of aerator

holes. During operation, the fluids mix to form a two-phase flow, as shown in Figure 2.4.3. A certain mixing length follows where the two fluid phases mix consistently. Finally the mixing chamber contracts (the arbitrary 45 degrees to the horizontal is recommended by Chin et al [65]) to an exit orifice.

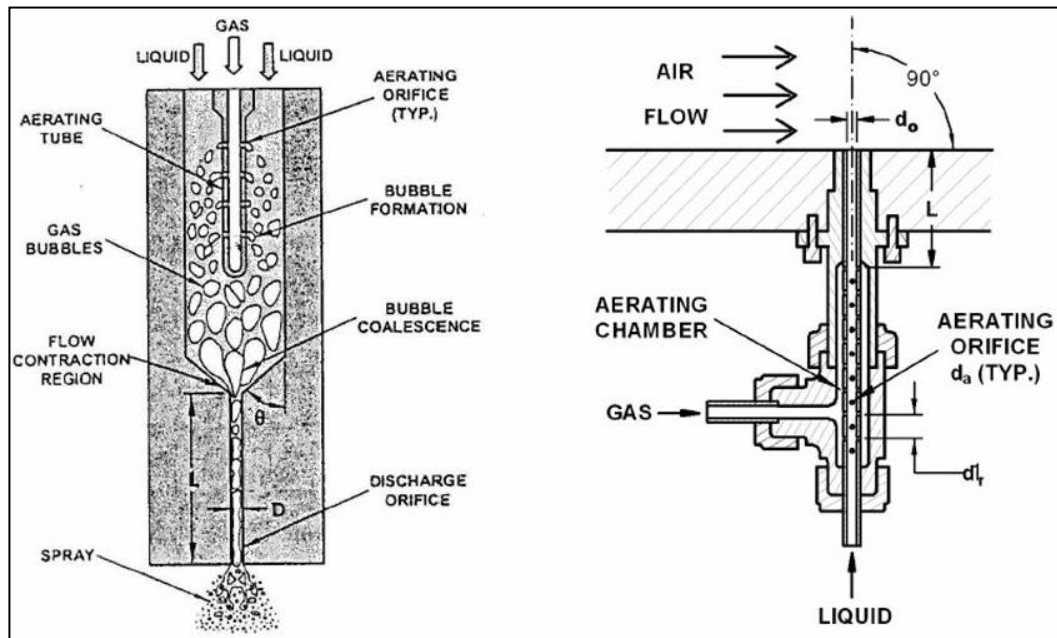


Figure 2.4.3. Alternative effervescent atomiser geometries: inside-out on the left and outside-in (spray ejected upwards into a cross-flow) on the right [67].

Mixing chamber diameter should be small enough to prevent phase separation or gravity effects becoming dominant. For instance gravity effects begin to influence pipe flow at diameters over ten millimetres [59]. Table 2.4.1 lists some typical mixing chamber dimensions from the literature.

Table 2.4.1. Range of mixing chamber dimensions.

Parameter	Minimum	Maximum	Reference
Chamber Diameter (mm)	3	25.4	[20, 63]
Mixing Length (mm)	3.4	250	[20, 68]

The smallest dimensions were used in low flow rate pharmaceutical application designs (35 g/min of water and aqueous solutions of polymers); the largest were used in power generation applications (1 kg/s of viscous fuels). Clearly a wide range of mixing chamber dimensions are possible, which seem to broadly correlate with intended fluid flow rates. However no recommendations were found in the literature on the optimum mixing chamber dimensions. Nevertheless, Chin et al's approach was instructive [65].

They used flow pattern charts (such as the Baker chart in Figure 2.4.4) to help select mixing chamber dimensions for the desired operating conditions.

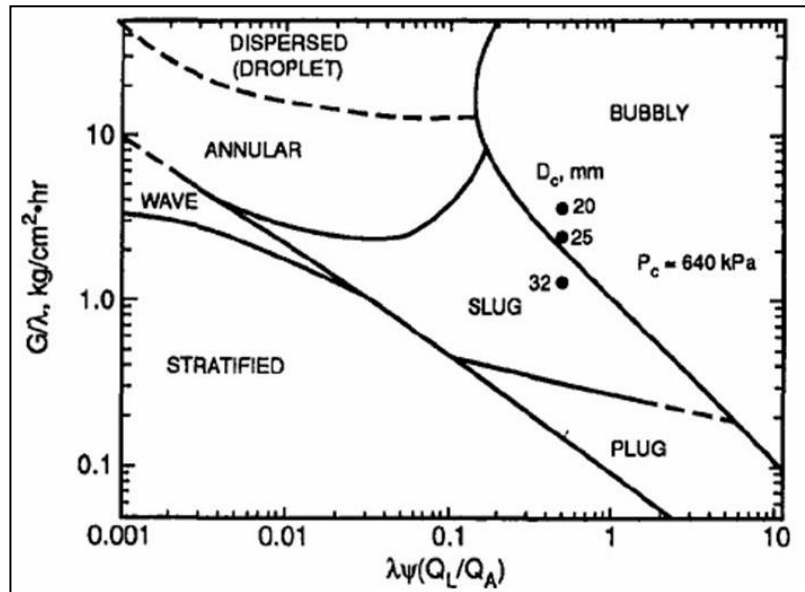


Figure 2.4.4. Empirically determined Baker chart used to help with sizing of mixing chamber [65]. In this approach an optimal flow pattern in the mixing chamber is the desired outcome.

Bubbly flow has already been suggested as producing stable atomiser operation and is therefore claimed to be desirable. Annular flow also results in steady, stable sprays and is suitable for effervescent atomiser operation. However slug or stratified flow needs to be avoided. Figure 2.4.5 shows a depiction of the visual appearance of the fully developed flow patterns possible in long vertical pipes.

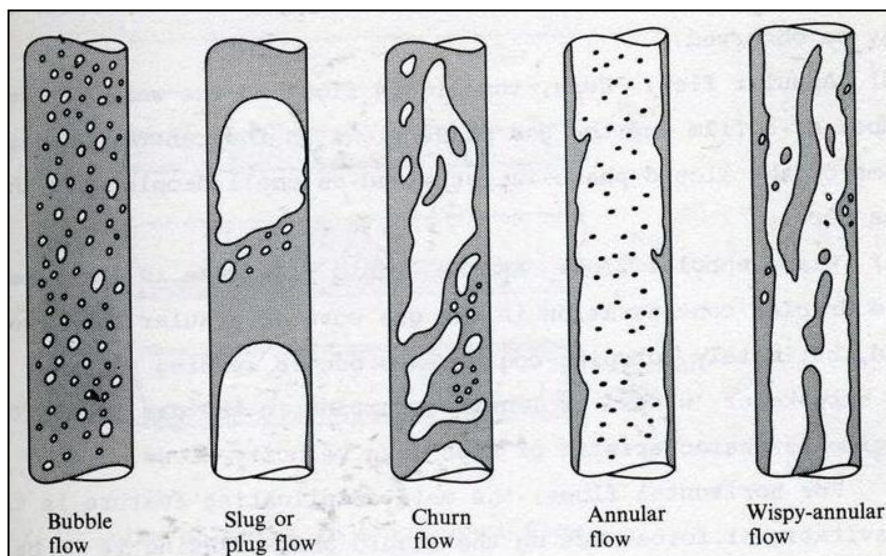


Figure 2.4.5. Flow patterns observed in long, downward pointing pipes for fully developed flows [69].

Experimental studies have shown [70] that axial mixing length can influence spray quality. However the reasons for this have not yet been identified.

Although turbulent mixing and homogenous internal flow is desirable, one study has shown that excessive turbulence in the mixing chamber (through the use of an additional swirl chamber) can be detrimental to the performance of the effervescent atomiser, as it causes fluid phase separation and prevents liquid-gas matrix formation [18].

### **2.4.3 Exit Orifice Geometry**

An important advantage claimed of effervescent atomisation is insensitivity to large exit orifice diameters. This was reported by early researchers [20] and subsequently confirmed by later investigations [19, 31, 62]. Large nozzle diameters help alleviate clogging, which can be a problem when atomising certain fuel types, such as slurry fuels. According to Lefebvre [33] increasing the orifice diameter increases the flow capacity for a given pressure without affecting the size of droplets produced.

In a different study, Wang et al, although agreeing with most of the above findings, reported the lowest spray SMD at the smallest exit orifice diameters and the lowest injection pressures investigated [31]. Meanwhile their largest orifice diameters produced the smallest droplet sizes at the largest injection pressures. From this the authors conclude that effervescent atomisation is fairly insensitive to exit orifice diameter. Wade et al [70] working on effervescent atomisation for a diesel fuel injector found that SMD unexpectedly decreased as exit orifice diameter was increased. No explanation of this is offered but the high pressures (12 to 33 MPa) and small dimensions utilised in this study may have had an impact on the results.

Wade et al make use of the smallest effervescent atomiser nozzle diameters found in the literature with diameters ranging from 0.18-0.34 mm for low flow rate applications. Meanwhile, the largest exit orifice diameter found in published data was 12.7 mm [34] though a more typical upper limit is 2.5 mm [18].

Chen et al [55] and Chin et al [65] recognised the importance of the length-to-diameter ratio of the exit orifice,  $L_o/D_o$ . These authors investigated length-to-diameter ratios of 0.5-1.5 and noted optimal performance at the lowest possible ratios. However, the authors recommend against lower ratios than 0.5 because of manufacturing difficulties and the creation of stress concentrations at the sharp corner of the nozzle.

Larger ratios (2-2.5) were investigated in a later study [56]. In this study a discrepancy between experimental data and coefficient of discharge predicted by Chin et al were

noted. The discrepancies were put down to the use of atomisers with larger  $L_0/D_0$  and smaller  $A^*/A_a$  ratios than those used and recommended by Chin et al. Nevertheless, Chin et al's correlations were claimed to represent underlying trends.

A later study seems to contradict the above findings [63]. Length-to-diameter ratios of 1-5 were studied and their effects on spray SMD were investigated for low flow rate minimal gas flow pharmaceutical applications. No effect on spray quality was observed at an ALR of 10% and only minimal effects seen at greater ALRs. The  $L_0/D_0$  ratio was concluded to have no clear effect on atomiser performance.

So far the exit orifice nozzles discussed herein have been of the circular plain-orifice type. Bates et al investigated the use of a de Laval or convergent-divergent (C-D) circular exit nozzle [66]. They concluded that this type of nozzle is superior to plain orifice types because it facilitates choked flow. Thus as the two-fluid mixture exits the nozzle it exceeds its sonic velocity producing shockwaves and intense shearing between gas and liquid phases. Chin et al [65] similarly report the important influence of  $L_0/D_0$  on spray quality.

#### **2.4.4 Number of Exit Orifices**

Atomisers with multiple exit orifices have also been investigated. These appear to display similar characteristics to single orifice effervescent atomisers [54, 71]. A study by Lefebvre seemed to indicate larger spray droplet SMD produced by multi-hole atomisers compared to single hole designs at similar conditions. A further study by Jedelsky et al [72] claimed multi-hole atomisers are suitable for employment in industrial burners, managing stable sprays and turn-down ratios up to 5:1.

#### **2.5 Parameters Influencing Spray Quality**

Due to the way they are created, sprays produced by atomisers, effervescent included, are not homogenous. They include a wide range of droplet sizes distributed about a given mean. There is no single parameter or formula that can fully describe a given spray distribution and shape. The Rosin-Rammler distribution and its subsequent modifications are empirical distribution functions frequently used by researchers which give a good fit for most atomiser spray data. This distribution attempts to indicate the spread and uniformity of the droplet sizes in the spray by the use of three or four different parameters. A simpler way of characterising a spray is by use of equivalent droplet diameters (also called equivalent spheres). A sphere the only shape that can be

described by one unique number – the particle diameter. This makes equivalent droplet diameters a convenient type of mean. Different kinds of equivalent droplet diameters can be calculated (Sauter Mean Diameter, De Brouckere Diameter, etc.). However in spray and combustion applications the Sauter Mean Diameter (SMD), also called  $D_{32}$ , is the one most frequently used.

SMD is defined as the diameter of a droplet, whose ratio of volume to surface area is equal to that of the spray as a whole [43]. SMD gives an indication of the fineness of the spray in a way particularly important for combustion applications. However, it gives no idea of the spread of the droplet sizes or of the relative droplet diameter frequencies in a spray. It is nevertheless easy to understand and use, and commonly quoted in atomisation literature.

Most studies report the effect a given operating parameter has on spray SMD (or some other representative droplet diameter). A lower spray SMD indicates a spray consisting of larger numbers of smaller sized droplets. Therefore a reduction in spray SMD indicates an improvement in atomiser performance due to the production of a better atomised spray.

Tabulated summaries of previous experimental investigations into effervescent atomisation and ranges covered can be found in the literature [19, 73].

### **2.5.1 Air to Liquid Ratio**

Air to Liquid by mass ratio (ALR) is frequently used by researchers of effervescent atomisation despite the fact that volumetric void fraction is a more appropriate parameter. However, volumetric void fraction at the exit orifice is difficult to measure and so ALR (which is very simple to calculate) is commonly used instead.

Air to Liquid Ratio is sometimes known as Gas to Liquid Ratio (GLR) but in this investigation only ALR will be referred to. The need for a constant air supply is one of the most obvious drawbacks of effervescent atomisation, although the quantity of supplied air is significantly lower compared to some currently used atomisers, such as air-blast atomisers. Early researchers reported good quality effervescent atomiser sprays at relatively low pressures and ALRs. One of the first studies into effervescent atomisation reported droplet SMD less than 50  $\mu\text{m}$  at 138 kPa and at an ALR of 0.04 with nitrogen and water mixtures [62]. Later studies reported further improvements, e.g. Sojka and Lefebvre achieved droplet SMD of 40  $\mu\text{m}$  at pressures less than 100 kPa and ALR less than 0.01 with air and water mixtures [18].



As expected, it was found that use of higher ALRs resulted in decreased droplet sizes and therefore better atomisation. A number of researchers claimed ALR had the greatest effect on SMD for the conditions and fluids they investigated [18, 32, 74, 75].

Believing bubbly flow to be the most favourable internal flow condition leading to optimal atomisation, Lefebvre gave a correlation for the maximum permissible ALR at which bubbly flow could be maintained [33]. This is given in Equation 2.5.1 ( $0 < \text{pressure} < 1 \text{ MPa}$  and  $0 < \text{ALR} < 6\%$ ).

$$ALR_{max} = 4.8(\rho_A/\rho_L) \quad \text{Equation 2.5.1}$$

This correlation assumes a specific type of bubble arrangement, maximum bubble densities and no bubble coalescence. A later study provides a different expression for maximum ALR still providing stable bubbly flow [55]. This is given in Equation 2.5.2 (where  $0 < \rho_A/\rho_L < 0.02$ ,  $0 < \text{ALR} < 40\%$ ,  $0 < \text{pressure} < 1.6 \text{ MPa}$ ,  $1.2 \text{ mm} \leq d_0 \leq 2 \text{ mm}$ ).

$$ALR_{max} = (91 - 127(1 - d_o/d_c)^2)(\rho_A/\rho_L) \quad \text{Equation 2.5.2}$$

These equations were determined for specific atomiser conditions and geometries and so can only be used as guidelines.

Studies have indicated a lower ALR limit of 1% – Lund et al could not obtain droplet SMD less than 100  $\mu\text{m}$  with an ALR less than 1 % using air and water, air and oil or air and water-glycerol mixtures [35]. They reported poor atomisation below this ALR.

Meanwhile operation at the highest ALRs has been shown to marginalise the effects of changes to geometric and fluid physical properties. This was claimed to provide evidence that secondary atomisation (the action of perturbing forces outside the liquid medium) is the dominant mechanism of fluid disintegration in effervescent atomisers [34, 63].

An important study by Santangelo et al [76] revealed two distinct mechanisms of liquid disintegration at different ALRs. The first was termed the “single-bubble explosion regime”, occurring at ALRs below 2%; so-called “tree regime” fluid break-up occurred at ALRs over 5%; a transitional range was observed at  $2\% < \text{ALR} < 5\%$ .

In the first regime, individual gas bubbles expand outside the nozzle, shattering the liquid into ligaments and droplets. At larger ALRs more air is entrained producing a “tree-like” near-nozzle structure which breaks up into droplets via aerodynamically induced shear and disturbances. It was noted that for low ALRs ( $< 5\%$ ) small increases in ALR produced large reductions in droplet size, an effect not observed when break-up

occurred in the “tree regime” mode. The transition from one regime to the other was influenced by the fluid physical properties. These two mechanisms are illustrated in Figure 2.5.1 and Figure 2.5.2.

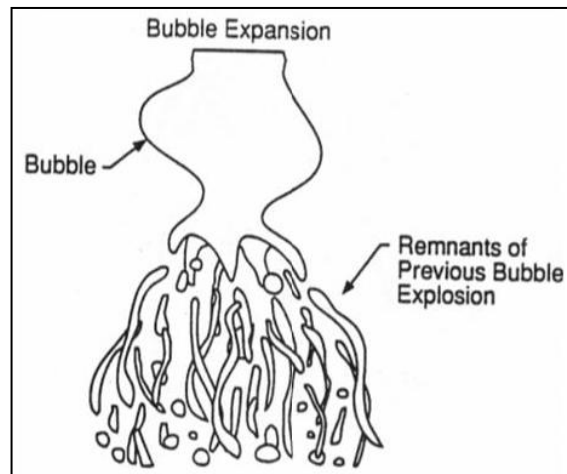


Figure 2.5.1. “Single-bubble explosion regime” [76].

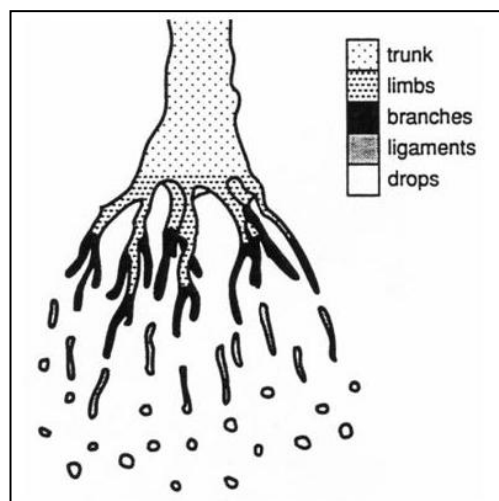


Figure 2.5.2. “Tree-regime fluid break-up” [76].

The positive effect of ALR increases at low ALRs could be due to the growing influence of bubble expansion energy. As ALR is increased much higher and the tree regime ensues, a different break-up mechanism occurs. At these ALRs a large proportion of bubble expansion energy is lost to the environment, decreasing the effect of ALR on spray SMD.

Later investigations found that the use of a ligament (a porous material placed just upstream of the exit orifice) prior to the nozzle or convergent-divergent nozzles, could affect the transition from one regime to the next, allowing operation in the “single-

bubble expansion regime” at higher ALRs than usual. The extension of the single-bubble expansion regime could have been the reason for the better atomisation observed at certain ALRs in these studies [66, 77].

Flow choking, which is linked to optimal effervescent atomiser operation, is reported to occur at ALRs in the tree regime of atomisation. According to Lund et al flow choking occurs at ALRs above 8% [78].

The findings of Morelli et al [79] confirm previous investigations. Looking to develop effervescent atomisers to replace Y-jet atomisers for oil-fired power stations, Morelli found that their effervescent atomiser designs gave the best results with ALRs > 5%. ALRs greater than 5% in the work of Morelli correspond to tree-like atomisation and choked flow for some conditions leading to high quality atomisation.

It is clear that higher ALRs provide increasingly diminishing improvements in spray quality. More break-up mechanisms begin to act at higher ALRs, though losses to the environment are greater, reducing their effects. Higher ALRs are thus generally desirable though increasingly wasteful. Further ALR increases bring operation into the air-blast atomisation regime.

The relative influence of ALR on internal flow regimes and associated break-up mechanisms are illustrated in Figure 2.5.3. The ranges given are typical of those found in the literature and do not denote limits of operation.

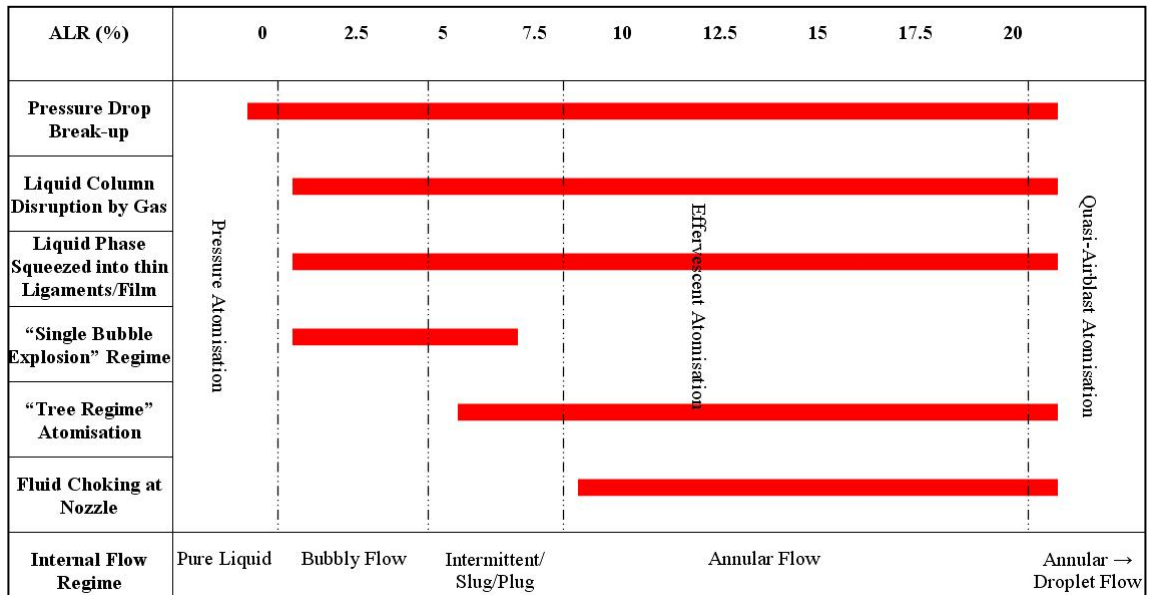


Figure 2.5.3. Typical range of operation for different break-up mechanisms with varying ALRs in effervescent atomisation.

Figure 2.5.3 graphically summarises the fluid break-up mechanism, internal flow regimes and ALRs typical of effervescent atomisation, as well as the interrelation between effervescent and traditional atomiser types.

### **2.5.2 Pressure Drop across Nozzle**

The pressure drop, the difference between the mixing chamber and ambient pressures is a key operating parameter in liquid atomisation. Complex two-phase phenomena make theoretical calculations of mixing chamber parameters, including pressure at the nozzle, challenging. However, gas and liquid supply pressures are always very similar in an effervescent atomiser, by definition [20, 62]. For example, one study recommends maintaining a difference in gas and liquid supply pressures smaller than one order of magnitude less than the absolute pressure of either fluid [71]. For this reason many effervescent atomisation researchers freely quote the fluid supply pressures.

As the two-phase mixture is ejected a nearly instantaneous pressure drop occurs across the nozzle. The gas rapidly expands as it elutes from the mixture and breaks the fluid up into ligaments which break up further to form droplets [18]. As discussed, a number of break-up mechanisms contribute to effervescent atomisation only one of which is pressure drop atomisation (prominent in plain orifice atomisers).

According to Wang et al [31] the superior performance of effervescent atomisation at lower pressures compared to other atomisation types is due to the larger role of expanding gas bubble atomisation more than compensating for the decreased contribution of pressure drop atomisation. As operating pressure decreases, the gas density decreases causing a gas volume increase to maintain equilibrium. This increases the number or size of gas bubbles (the liquid is considered incompressible) and increases the effect of gas-phase liquid disruption aiding lower pressure effervescent atomisation.

Sovani et al [19] agree with the above process. In their view the atomising gas performs two functions. Firstly it forces the liquid to flow through a small fraction of the discharge orifice, squeezing it into ligaments (droplet sizes produced in sprays are known to be proportional to the square root of the thickness of the initial ligaments formed at the nozzle exit orifice [31, 43]). Secondly the gas expands upon exiting the orifice, shattering the fluid ligaments. The latter mechanism could account for comparatively good effervescent atomisation at lower pressures compared to traditional atomiser types. However, both break-up mechanisms increase their contributions at higher pressures and thus decreased spray SMD are expected as pressure is increased.

This very phenomenon – improved atomisation as operating pressures are increased – has been observed and reported in the literature [60, 70]. However, some studies have shown that the beneficial influence of operating pressure increases is relatively minor [57, 58]. Sojka et al also noticed minor benefits but only at an ALR of less than 20 % [18] while Buckner and Sojka [75] noticed this at ALRs less than 15%.

Wade et al [70] reported droplet SMDs less than 10  $\mu\text{m}$  at an injection pressure of 25 MPa in tests using nitrogen and Benz Oil UCF-1 calibration fluid (a Diesel fuel substitute). Higher injection pressures were used by Sovani et al [80], up to 36.5 MPa. Both these studies were looking at developing an effervescent atomiser for use in Diesel engines, and both offered improved atomisation compared to standard fuel injectors. In addition both operated at very large injection pressures, more than ten times larger than most other publications report. In fact, Sojka and Lefebvre [18] report atomisation with 40  $\mu\text{m}$  spray droplet SMD at pressures of just 100 kPa. This result is also considered an improvement compared to other non-effervescent atomisers operating at similar conditions.

### **2.5.3 Viscosity**

Viscosity, together with surface tension, can be thought of as stabilising forces which oppose fluid break-up. Viscosity resists the dynamic forces of the atomising gas and surface tension opposes changes to fluid geometry. Aerodynamic forces compete with the stabilising forces and if large enough, produce liquid disintegration [58].

Viscosity, surface tension and fluid density can vary with fluid temperature. Thus fluid properties can change noticeably during operation. It can be seen therefore that in practice, viscosity, density and surface tension are difficult to isolate and analyse separately.

According to Lefebvre [43] viscosity is the most important fluid property with respect to fluid atomisation for two reasons. It affects the droplet size distributions in the spray and is capable of changing the flow rate through the exit nozzle. The latter can considerably change atomisation characteristics.

There is some disagreement in the literature regarding the effects of fluid viscosity on effervescent atomisation. Initial research reported a relative insensitivity of droplet size to viscosity, which seemed to suggest effervescent atomisation was ideally suited to operation with highly viscous fuels. According to these studies, spray droplet SMD is either independent or nearly independent of viscosity [19, 32, 35, 57, 77]. Lefebvre's correlation [33] for droplet SMD in effervescent atomisation also reveals that, for what

he terms “prompt” atomisation, droplet SMD should be independent of fluid viscosity. In addition it has already been suggested that effervescent atomisation is a process controlled by secondary atomisation [18, 34]. This mechanism is brought on by external pressure forces arising from the high air-liquid relative velocities outside the nozzle. Primary atomisation (influenced by liquid viscosity) is claimed to be less dominant in effervescent atomisation. If this is the case, viscosity should not have a strong effect on atomisation quality.

However some publications contradict these findings. Santangelo and Sojka [76] who studied the flow rate patterns in effervescent atomiser nozzles noticed that increasing fluid viscosity resulted in an increase in the diameter of the fluid elements in the near-nozzle region – and therefore increased droplet SMD. However, this was only noticeable for viscosities over 0.412 kg/ms and ALRs less than 10%. In contrast to previous work, Ferreira et al [56] observed superior atomisation performance for all operating conditions when lower viscosity fluids were utilised. Investigating the effects of polymers for low flow rate applications ( $5 \times 10^{-4}$  kg/s), Petersen et al noticed an increase in spray droplet SMD as fluid viscosity increased [58].

It is clear that fluid viscosity is a parameter whose effect on spray quality requires further investigation.

### **2.5.4 Surface Tension**

Surface tension is a consolidating force, tending to resist expansion of the liquid surface area, maintaining the fluid in a minimum surface energy geometry – that of a sphere. It is well known that traditional twin-fluid atomisers produce smaller droplets (i.e. offer better atomisation) as liquid surface tension is decreased [43, 81]. This seems logical since a decrease in surface tension would translate into a reduction of the cohesive forces holding a droplet or ligament together and thus smaller disruptive forces would produce droplet/ligament disintegration. However, effervescent atomisers appear to exhibit a different kind of behaviour.

Lund et al [35] covering the surface tension range of 0.03-0.067 kg/s<sup>2</sup> reported that increasing surface tension in fact decreased spray droplet SMD for effervescent atomisation. Gosselin et al. [82] advised using fluids with as high a surface tension as possible. Research by Santangelo et al [76] agrees with this statement. These researchers reported that decreasing surface tension reduced the diameter of the fluid elements near the nozzle but also slightly increased spray droplet SMD, concluding that jet break up into ligaments by single bubble expansion (as opposed to ligament

break-up via aerodynamically induced shear and disturbances) dominated the atomisation process for the conditions investigated.

Sutherland et al. [77] investigated the suitability of ligament-controlled effervescent atomisers for consumer product aerosol sprays. Their work contradicts the above findings showing that throughout the surface tension range of 0.03-0.072 kg/s<sup>2</sup> an increase in surface tension resulted in a minor droplet size increase. No explanation is given but it is likely that the porous ligament used (porous mesh just upstream of exit orifice used with the intention of controlling the size of gas bubbles approaching the nozzle) altered the flow dynamics and atomisation mechanisms which ensued.

Despite conflicting data in the published literature regarding whether surface tension increases facilitate (decrease spray droplet SMD) liquid break-up [35, 76] or retard (increase spray droplet SMD) liquid break-up [77], researchers agree that it has a minor effect on the performance of effervescent atomisers. For example, the study by Sutherland et al reports droplet SMD variations of less than 10% when either surface tension or viscosity were varied through their full test ranges.

If, as claimed, effervescent atomisation is dominated by secondary atomisation (which is not a function of fluid properties) then the relatively minor influences of fluid properties, such as surface tension, on atomisation quality are to be expected.

### **2.5.5 Fuel Type (Newtonian and Non-Newtonian Fluids)**

A Newtonian fluid is one where the relationship between shear stress and shear strain is linear and whose gradient is equal to the viscosity. The fluids considered in the preceding sections of this chapter can be characterised by a single non-varying value of viscosity for all conditions. Non-Newtonian fluids have a non-linear relationship between shear stress and shear strain and cannot be defined with a constant viscosity value. Slurries of liquids and solid powder suspensions are examples of such fluids [43].

Traditional atomisers are not well suited to operating with fuel slurries or fuels with solid suspensions. Blockages often occur at the small component passages, excessive wear due to the abrasive action of solid particles is frequent and pre-heating is required to lower fuel viscosity. These increase the economic costs of atomising such fuels.

The applicability of effervescent atomisation to non-Newtonian fluids has been investigated by a number of researchers [18, 34, 75, 83].

Sojka et al altered rheological properties through the addition of polymers to water. Their results showed that fluid rheology (flow behaviour index  $n$ , consistency index  $K$ ) had little to no effect on spray droplet SMD. This led to the conclusion that secondary

atomisation was the dominant mechanism in effervescent atomisation of non-Newtonian and Newtonian fluids.

In a later study, Buckner et al [75] developed an effervescent atomisation model based on mass, momentum and energy conservation. These researchers confirmed previous findings noting, however, that Newtonian and non-Newtonian liquids do atomise differently from each other. An important result was that for the same apparent viscosity, non-Newtonian fluids always produced a larger spray droplet SMD. Nevertheless, effervescent atomisation was claimed to be suitable for spraying highly viscous non-Newtonian fluids.

Of the above studies, Jardine's extended the range of previous investigations by demonstrating the suitability of effervescent atomisation for comparatively high flow rate devices. Up to 940 g/s (typical of industrial processes) of non-Newtonian fluids could be atomised using a high flow rate atomiser.

Meanwhile the study of Geckler et al quoted above, investigated the behaviour of viscoelastic fluids in EA systems. In agreement with previous work on non-Newtonian fluids this study concluded that polymer solutions produced a larger spray droplet SMD than those obtained with pure solvents. The investigation noted that the liquid exited the nozzle in the form of an annular ring. Polymers seemed to retard the formation of disturbances that formed ligaments, tending to create ligaments with larger break-up lengths. Also the ligament diameter was seen to increase as the polymer concentration or weight was raised. Both factors combined to produce an overall droplet SMD increase. Two distinct scaling functions were noticed. At low polymer concentrations, droplet SMD was a strong function of polymer concentration and only a weak function of polymer molecular weight. At high polymer concentrations the opposite was observed.

### **2.5.6 Molecular Weight of Atomising Gas**

In some applications the use of an alternative to air as an atomising gas may be desirable. Lund et al [78] discuss the possibility of using effervescent atomisation as a scale model of an oil well leak (two-phase crude oil and varying methane/ethane/propane ratios as the aerating gas mixture). It is important to know what effect the use of an alternative gas would have on atomisation. Lund et al developed on their earlier model of effervescent atomisation [35] to help analyse operating parameter changes.



Testing and inspection of this model showed that use of a lower molecular weight gas resulted in sprays with smaller droplet SMD for the same conditions at ALRs less than 15 %. At these ALRs, increasing the atomising gas molecular weight was shown to result in the formation of a thicker liquid annulus at the nozzle and hence larger ligaments and droplets.

Despite the above conclusions, it should be remembered that although ALR (gas-to-liquid by mass ratio) is commonly used it is not the parameter that best correlates with the break-up mechanisms in effervescent atomisation. The most appropriate parameter to use is in fact the volumetric void fraction at the exit orifice. Since this parameter is a function of local pressure, which is difficult to measure, ALR is used instead. This has implications in cases where gases with different molecular weights are used.

Gases with different molecular weights will occupy different volumes in the atomiser mixing chamber at seemingly the same conditions. As a result the volumetric void fraction (correlating with the working mechanism of effervescent atomisation) will be different at the same ALRs and operating pressures. Therefore, gases with lighter molecular weights are expected to produce smaller spray droplets at the same operating conditions, since they would occupy a larger volume in the mixing chamber and be accompanied by larger volumetric void fractions. Therefore the findings of Lund et al need to be treated with caution [78].

## **2.6 Effervescent Atomiser Spray Characteristics**

Experimental investigations have been performed for a wide range of conditions and effervescent atomiser arrangements. Researchers have sought to alter the operating parameters in such a way as to produce sprays that are optimal for the intended applications. Most are interested in the operating parameters' effects on SMD. Those looking to develop effervescent atomisers for Diesel injectors for example, will be subjected to considerable spatial constraints and will therefore be interested in the spray penetration and cone angle. Other applications may require careful consideration of the spray velocity profile, gas entrainment rate, spray patternation or spray unsteadiness. These parameters will be considered in this section.

### **2.6.1 Sauter Mean Diameter (SMD)**

Spray droplet SMD is a parameter of prime importance for liquid atomisation. This is because it indicates fineness of spray atomisation, is strongly influenced by large

droplets (which are detrimental to combustion applications), and is easier to use than empirical distribution functions (which do not provide a perfect fit to all data).

Researchers have derived a number of correlations to predict spray droplet SMD for conventional atomisers with fluid properties, operating and geometric conditions as the input parameters. Some such correlations have been adapted to effervescent atomisers and are presented in this chapter. Other researchers have attempted to model important mechanisms of the effervescent atomisation break-up process, in order to provide droplet SMD correlations. Given the range of operating conditions, fluid properties and atomiser geometries (as well as the range of internal and external flow regimes) possible, it is not surprising that no one universal droplet SMD correlation has emerged for effervescent atomisers.

Table 2.6.1 highlights a selection of droplet SMD correlations found in the literature related to effervescent atomisation. These have been developed by various authors.

Inspection of the effervescent atomisation literature led to the identification of a number of frequently recurring operating parameters claimed to have a notable effect on spray droplet SMD. Parameters of interest were found to be:

- Initial operating conditions (ALR, pressure drop across nozzle,  $\Delta P$ ).
- Atomiser geometry (mixing chamber diameter, fluid mixing length, aerator geometry, exit orifice diameter, exit orifice length to diameter ratio).
- Fluid properties (density, surface tension, viscosity).

Some of the main findings are summarised.

Fluid properties (density, surface tension, viscosity) were expected to have a relatively minor effect on spray droplet diameters since it has been claimed effervescent atomisation is dominated by secondary atomisation which is not a function of fluid properties [18, 34]. This property seemed to make effervescent atomisation particularly suitable for use with viscous fuels.

Effervescent atomisation has been reported to be largely insensitive to nozzle diameter [18, 20, 32, 33]. Conversely pressure drop across the nozzle and ALR were expected to have an important influence on spray droplet sizes. For example two fluid break-up mechanisms known to cause fluid disintegration in effervescent atomisation [43] are pressure drop atomisation (as in conventional plain orifice pressure atomisers) and atomisation caused by gas bubble expansion. Thus it can be seen that increases in operating pressure affect pressure drop atomisation and therefore spray droplet diameters. ALR increases raise the atomising contribution of the expanding gas.

Table 2.6.1. Effervescent Atomiser Produced Spray droplet SMD Correlations in Literature.

Correlation	Source and Comments
$SMD = \frac{12\sigma}{\rho_L \left( V_{L1}^2 + \varepsilon ALRV_{A1}^2 - \frac{(V_{L1} + \varepsilon ALRV_{A1})^2}{1 + \varepsilon ALR} \right)}$	<p>[18]; Requires empirical relationship for <math>\varepsilon</math>.</p> $V_{A1} = \left( 2RT_n \ln \frac{P_{AO}}{P_{atm}} \right)^{0.5}$ $V_{L1} = \left( \frac{2(P_{LO} - P_{atm})}{\rho_L} \right)^{0.5}$
$SMD = 3 \left( \frac{1}{t} + \frac{C' \rho_L U_a^2}{4\sigma(1 + 1/ALR)} \right)^{-1}$	<p>[84]; Fits data well for a range of atomiser types. Weaknesses include the need to calculate liquid sheet thickness (<math>t</math>), air velocity (<math>U_a</math>) and process efficiency (<math>C'</math>).</p>
$SMD = \frac{1.5d_o}{1 + \frac{C \rho_L T_A (\Delta P_A / P_A)}{\sigma(1 + 1/ALR)}}$	<p>[33]; Assumes break-up via so-called "prompt" atomisation. SMD assumed independent of viscosity. Process efficiency required (<math>C</math>). Note: dimensionally incorrect.</p>
$SMD = \left[ \frac{3\sqrt{2}\pi d_L^3}{2} \left( 1 + \frac{3\mu_L}{\sqrt{\rho_L \sigma d_L}} \right)^{0.5} \right]^{1/3}$	<p>[35, 54]; Mathematical model based on first principles with no adjustable constants; however, secondary atomisation mechanism is ignored.</p>
$SMD = \sqrt[3]{\frac{3\pi d_L^3}{\zeta_{opt}}}$	<p>[77]; Predicted SMD for ligament controlled EA. Developed from analytical model based on instability of capillary liquid jets. Requires complex solution for <math>\xi_{opt}</math> (critical dimensionless wavenumber).</p>
$SMD = 55D_o^{-0.93} P_{inj}^{-0.9} ALR^{0.005}$	<p>[70]; Development of an EA Diesel injector. Empirically based relationship for ALR: 5-30%, <math>D_o</math>: 0.18-0.34 mm, <math>P_{inj}</math>: 11-33 MPa). Note: dimensionally incorrect.</p>
$SMD = (1 - \varepsilon)SMD_B + \varepsilon SMD_A$ $SMD_B = \left\{ C_1 ALR \frac{\rho_f RT_{env}}{\sigma(k-1)} \left[ 1 - \left( \frac{p_{env}}{p_c} \right)^{\frac{k-1}{k}} \right] + \frac{C_2}{D_o} \right\}^{-1}$ $SMD_A = D_o \left\{ C_3 \left[ \frac{\alpha \sqrt{1-\alpha}}{1 - \sqrt{\frac{\rho_g}{\rho_f} \left( \frac{1+75(1-\alpha)}{\sqrt{\alpha}} \right)^{0.5}}} \right] \left[ \frac{\rho_g j_g^2 D_o}{\sigma} \right]^{-0.5} \right\}$	<p>[59]; Constants <math>C_1</math>, <math>C_2</math> and <math>C_3</math> need to be obtained for operating conditions.</p> <p><math>\varepsilon = 0</math> for (<math>ALR \leq ALR_B</math>),</p> $\varepsilon = \frac{ALR - ALR_B}{ALR_A - ALR_B}$ <p>for (<math>ALR_B &lt; ALR &lt; ALR_A</math>),</p> <p><math>\varepsilon = 1</math> for (<math>ALR \geq ALR_A</math>)</p> <p>Transition criteria developed are based on drift flux model. Correlation represents most measured data <math>\pm 20\%</math>. Note: <math>R</math> has units of <math>Nmkg^{-1}K^{-1}</math>, <math>\alpha</math> = volumetric void fraction.</p>

In addition, ALR affects the flow regime [55] in the mixing chamber – bubbly, annular etc. – as well as the type of break-up process observed: single bubble explosion regime or tree-regime atomisation. It was therefore expected that ALR would have an important influence on droplet sizes. The anticipated influence of each important parameter on spray quality is broadly generalised.

- **ALR**: Droplet diameter was expected to decrease as ALR increased, with ALR and droplet diameter inversely proportional. ALR was expected to have a very strong influence on droplet diameter.
- **$\Delta P$** : Droplet diameter was expected to decrease as the pressure drop,  $\Delta P$  was increased, with  $\Delta P$  and droplet diameter inversely proportional.  $\Delta P$  was anticipated to have a strong influence on droplet diameter, though not as strong as ALR.
- **$D_o$** : Exit orifice diameter was considered to have a minor effect on droplet diameter. However, just like in plain orifice pressure atomisers, increasing exit orifice diameter was expected to result in larger droplets. Therefore exit orifice diameter and droplet diameter were expected to exhibit a weak directly proportional relationship.
- **$L_o/D_o$** : Exit orifice length to diameter ratio was expected to have a minor impact on droplet diameter, with decreases in this ratio causing a decrease in spray droplet diameter. As a result exit orifice diameter and droplet diameter were expected to be directly proportional.
- **$L_{MC}$** : The mixing length was expected to have a minor influence on droplet diameter, with greater mixing length reducing spray droplet diameter. The two were expected to be inversely proportional.
- **$\sigma$** : A minor effect on droplet diameter was anticipated. Surface tension is a consolidating force resisting expansion of fluid surface area. Therefore increasing surface tension is likely to increase droplet diameter. Surface tension and droplet diameter were therefore expected to be directly proportional.
- **$\rho$** : A minor effect on droplet diameter was expected. Liquid density increases were thought likely to increase spray droplet diameter. Consequently liquid density and droplet diameter were expected to be directly proportional.
- **$\mu$** : A minor effect on droplet diameter was anticipated. Viscosity opposes fluid break-up. Increasing viscosity increases the forces holding the liquid ligaments and droplets together and will therefore result in an increased spray droplet diameter. Liquid viscosity and droplet diameter were expected to be directly proportional.

Therefore, based on an extensive literature review, a preliminary droplet SMD relationship for effervescent atomisation was expected to take the approximate form given in Equation 2.6.1, where the indices are expected to differ in magnitude as shown:  $a > b > c, d, e, f, g, h$ .

$$Droplet\ SMD = f \left\{ \frac{D_0^c, \frac{L_0^d}{D_0}, \sigma^f, \rho^g, \mu^h}{ALR^a, \Delta P^b, L_{MC}^e} \right\} \quad \text{Equation 2.6.1}$$

The effervescent atomiser correlations in Table 2.6.1 were re-examined. Only the recurring operating parameters which also corresponded to those in Equation 2.6.1 were analysed. It can be shown that the correlations in Table 2.6.1 are equivalent to those presented in Table 2.6.2.

The correlations from Table 2.6.2 were tabulated and are presented in Table 2.6.3. Table 2.6.3 demonstrates the relative influence of each operating parameter as indicated by the correlation of the respective authors. Thus the relative influence of each parameter was compared against Equation 2.6.1, and across correlations in the literature.

Table 2.6.2. Simplified forms of effervescent atomiser correlations found in literature.

Author and Date	Form of Correlation
Sojka & Lefebvre 1990 [18]	$SMD = f(\Delta P^{-1.204}, \sigma^1, ALR^{-0.0461})$
Lefebvre 1992 [84]	$SMD = f(\rho^{-0.914}, \sigma^{0.0239}, ALR^{-0.0221})$
Lefebvre 1992 [33]	$SMD = f(D^1, \rho^{-0.914}, \sigma^{0.0239}, ALR^{-0.0221})$
Lund 1993 [35]	$SMD = f(\mu^{0.159}, \rho^{-0.014}, \sigma^{-0.014})$
Wade 1999 [70]	$SMD = f(D^{-0.93}, \Delta P^{-0.9}, ALR^{0.005})$
Kim & Lee 2001 [59]	$SMD = f(D^{0.7166}, \Delta P^{0.0062}, \rho^{-0.0062}, \sigma^{0.4846}, ALR^1)$

The lack of agreement between researchers is striking but not unexpected. Correlations in the literature were determined using different models and simplifying assumptions, a range of atomiser geometries (injector types) and operating parameter ranges, as well as a variety of data sampling techniques (e.g. PDA, Malvern Mastersizer etc.). It may also be that effervescent atomisation is too complex a process to be described by one single correlation, covering all atomiser geometries, operating conditions and fluid properties. Previous researchers have arrived at similar conclusions [54].

Table 2.6.3. Relative importance of primary operating parameters on spray droplet SMD as determined by analysis of droplet SMD correlations from the literature.

Source	$\Delta P$	$D_o$	$\rho_L$	$\sigma_L$	$\mu_L$	ALR	Order of Parameter Importance
[18]	-1.204	-	-	1	-	-0.0461	1. $\Delta P$ , 2. $\sigma$ , 3. ALR
[84]	-	-	-0.914	0.0239	-	-0.0221	1. $\rho$ , 2. $\sigma$ , 3. ALR
[33]	-	1	-0.914	0.0239	-	-0.0221	1. D, 2. $\rho$ , 3. $\sigma$ , 4. ALR
[35]	-	-	-0.014	-0.014	0.159	-	1. $\mu$ , 2. $\sigma$ , 3. $\rho$
[70]	-0.9	-0.93	-	-	-	0.005	1. D, 2. $\Delta P$ , 3. ALR
[59]	0.0062	0.7166	-0.0062	0.4846	-	1	1. ALR, 2. D, 3. $\sigma$ , 4. $\Delta P$ , 5. $\rho$

It is important to note that most researchers describe the quality of a given spray using a single value of spray droplet SMD. This value is obtained using a non-intrusive technique such as Phase Doppler Anemometry (in more modern studies), or light scattering techniques based on Fraunhofer diffraction (used in older studies). These sampling techniques collect droplet data from fixed measurement volumes.

In the case of Phase Doppler Anemometry the measurement dimensions are very small – of the order of micrometres. Studies report either a single sampling location within the spray, or several – typically a number of radial points at one single axial location. The droplet data from all sampled locations are then combined and used to calculate one single global value of spray droplet SMD.

The “Malvern Mastersizer” was frequently used in older effervescent atomisation studies. This technique samples a large spray dimension – of the order of centimetres – and relies on the fact that similarly-sized droplets refract light at similar angles. Light diffracted by droplets within the control volume is passed through a lens (Fourier or Reverse Fourier) and collected by detectors before being fed into specialist software. Spray droplet SMD is then calculated from the droplet data collected.

It is these droplet SMD values that are reported in the literature and are used to derive correlations or validate models.

Relatively few studies investigate spray quality variation in the axial and radial spray directions. However, Panchagnula et al [85] reported fairly constant values of droplet SMD across any diameter of the spray they examined – this was ascribed to high

turbulence and good mixing. Gas-phase turbulence levels typical in effervescent atomisation were concluded to be about 10 % higher than the highest measured turbulence in single phase gas jets leading to good mixing and a more homogenous spray.

### 2.6.2 Spray Cone Angle

It should be noted that researchers frequently apply different criteria in determining spray cone angles. Spray edges, and the downstream locations at which these were measured vary between studies. Thus the results presented below can be seen to represent general trends but not necessarily the absolute values of spray cone angles.

The spray cone angle of effervescent atomisers is postulated to be wider than that of plain orifice pressure jet atomisers for all operating conditions, typically by a factor of two [86]. It was found in the above experiments that an increase in atomiser pressure or a decrease in surface tension or viscosity all increased spray cone angle. A non-linear relationship between ALR and spray cone angle was reported. At pressures below 0.5 MPa, spray cone angle attained a maximum value then decreased as ALR was increased. Some characteristic results are presented in Figure 2.6.1.

This peak in spray cone angle was attributed to the effect of high-energy bubble expansion, which enhanced atomisation and widened cone angle at the bubbly regime of internal flow. This was claimed to be replaced at higher ALRs by the annular flow regime and different mechanisms of atomisation. The peak spray cone angle could therefore be attributed to a flow regime transition. At higher pressures, ALR could only slightly increase spray cone angle. This was thought to be a result of diminished bubble energies at higher pressures and poorer momentum transfer between the atomising air and the droplets produced.

Wade et al report spray cone angles of 8-22°, slightly larger than but comparable to the sprays produced by injectors of Diesel internal combustion engines. Conditions in this study included fluid pressures up to 33 MPa, exit orifice diameters of 0.18 mm and typical liquid flow rates of 1.34 g/s [70].

Sovani et al [80] noted similar spray cone angles (11.6-22.3°) with a high pressure effervescent diesel injector prototype. Equation 2.6.2 gives the relationship for spray cone half-angle provided by the authors.

Equation 2.6.2 (for  $0.8 \leq \text{ALR} \leq 13.6\%$ ,  $12.6 \text{ MPa} \leq \text{pressure} \leq 36.5 \text{ MPa}$  and  $0.27 \text{ MPa} \leq \text{ambient pressure} \leq 5.5 \text{ MPa}$  to within 3.7% standard deviation) predicts relatively

minor spray cone angle variations, with ALR having a greater impact than operating and ambient pressures.

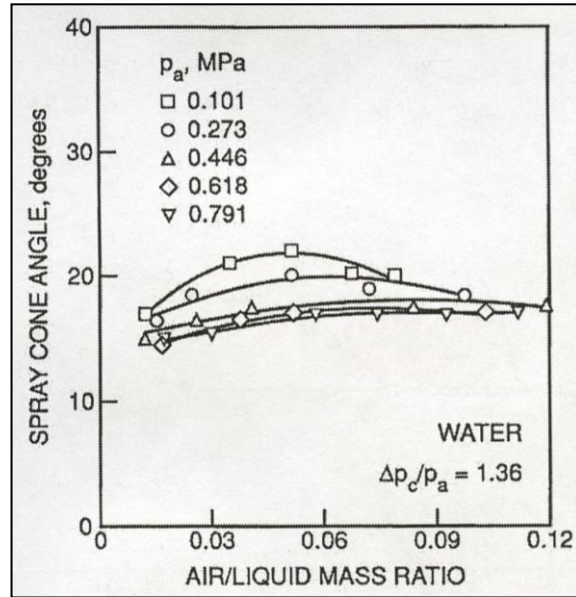


Figure 2.6.1. The influence of ALR and injection pressure on spray cone angle [86].

$$\frac{\alpha}{2} = 0.15ALR + 0.039P_{inj} + 0.0451P_{amb}^4 - 0.6211P_{amb}^3 + 2.7551P_{amb}^2 - 3.62P_{amb} + 7 \quad \text{Equation 2.6.2}$$

Lefebvre, investigating plain orifice effervescent atomisers, agrees with the reports of wide spray cone angles in effervescent atomisation. He reports spray cone angles of 40° which were largely independent of operating conditions. Multi-hole effervescent atomisers (multiple exit orifices) seemed to offer a widening of the spray cone angle although at the cost of increased droplet sizes [54].

### 2.6.3 Velocity Profile

Panchagnula et al [85] investigated the velocity and droplet size profiles of EA produced sprays. Measurements were taken at seven radial locations across the diameter of the spray and at three axial positions. For all operating conditions the axial velocity profile across a given spray radius was found to be bell-shaped with the maximum velocities occurring at the centreline and minimum values at the edges of the spray. This velocity was found to decrease downstream of the nozzle. As anticipated increases in ALR or liquid mass flow rate increased the magnitude of droplet velocities.



The air injected into a typical mixing chamber is known (from calculations) to achieve velocities up to 300 m/s depending on design and operating parameters [54]. However in the study of Panchagnula et al the highest average axial droplet velocities measured were no more than 50 m/s. Therefore, high liquid-gas slip ratios and poor momentum transfer between phases at the nozzle were concluded.

#### **2.6.4 Gas Entrainment**

Gas entrainment can be defined as the quantity of ambient gas drawn in through the spray perimeter as the spray expands after ejecting from the nozzle. Entrainment is important for a number of engineering applications as it can significantly affect liquid evaporation rates and droplet residence times in sprays. Entrainment is also capable of altering local equivalence ratios which affects the formation of oxides of nitrogen.

Gas entrainment in effervescent atomisation and how it is affected by fluid properties is discussed by Sutherland et al [87]. Equation 2.6.3 was proposed for entrainment calculations (valid for  $0 < \text{ALR} < 4\%$ ,  $0 < m_L \leq 1 \text{ g/s}$ ,  $0.001 \text{ Pas} \leq \mu \leq 0.08 \text{ Pas}$ ,  $0.03 \text{ Pam} \leq \sigma \leq 0.072 \text{ Pam}$  and  $998 \text{ kg/m}^3 \leq \rho \leq 1217 \text{ kg/m}^3$ ).

$$E = \frac{m_e}{x\sqrt{\rho_e M_o}} \quad \text{Equation 2.6.3}$$

Where E is dimensionless entrainment number,  $m_e$  is entrained gas mass flow rate,  $\rho_e$  is density of entrained air,  $M_o$  is the spray momentum rate at the exit orifice and x is the distance along the spray axis measured from the exit orifice.

#### **2.6.5 Spray Unsteadiness**

Steady operation, and constant fuel flow is required for all effervescent atomisation applications. Unstable or fluctuating fuel flow patterns can be detrimental.

Studies suggest internal flow regimes can strongly influence effervescent atomiser spray unsteadiness [76]. Perhaps surprisingly, fluid properties (density, surface tension, viscosity) can also noticeably affect spray steadiness [77].

A detailed investigation of spray unsteadiness in effervescent atomisers was performed by Luong et al [88]. After applying the so-called ideal spray theory of Edwards et al [89, 90] they conclude that effervescent atomisation is an inherently unsteady process, with the greatest instability at the spray edges and at downstream locations. Greater unsteadiness was also observed at lower ALRs.

A later study claims the unsteadiness of a spray is a function of both liquid mass flow rates and ALRs. According to this investigation, spray instability can be reduced by mixing schemes involving indirect impingement of the aerating gas onto the mixing chamber, short passage lengths and small converging angles [51].

Further studies suggest an important role played by Kelvin-Helmholtz and sheet instabilities in effervescent atomisation [61]. High velocity gas passing through the exit orifice appears to produce instabilities on the liquid surface. The resulting oscillations ultimately cause spray unsteadiness which is independent of the flow regime in the mixing chamber.

## 2.7 Further Correlations Related to Effervescent Atomisation

Table 2.7.1 describes specific gas bubble energy (energy possessed by expanding gas bubbles outside the exit orifice) correlations found in the literature.

Lefebvre considered the fineness of effervescent atomisation to be a function of the energy possessed by the stream of expanding gas bubbles. In this study [33], the relationship between droplet size and bubble energy was investigated. Experimental droplet SMD was plotted against bubble energy (obtained from the first equation in Table 2.7.1). The relationship deduced is shown in Figure 2.7.1. Clearly flow conditions corresponding to high bubble energies resulted in sprays with a reduced droplet SMD. This is expected since high bubble energy operation translates into high air to liquid injection pressure and mass flow rate ratios.

Table 2.7.2 demonstrates some coefficient of discharge correlations found in the literature. Coefficient of discharge indicates the “effective” flow area at the exit orifice. It is the ratio of the fluid mass flow rate at the nozzle to that of an ideal nozzle which expands an identical working fluid from the same initial conditions to the same exit pressures.

Coefficient of discharge is most frequently calculated using the correlation given in Equation 2.7.1 [31, 62]. This correlation is often used for a variety of traditional atomiser types.

$$C_d = \frac{m_{fuel}}{A(2\rho_{fuel}\Delta P_{fuel})^{0.5}} \quad \text{Equation 2.7.1}$$

Where  $A$  is the nozzle area,  $m_{fuel}$  is the mass flow rate of fuel,  $\rho_{fuel}$  is the fuel density and  $\Delta P_{fuel}$  is the fuel pressure drop across the nozzle (or the fuel supply pressure).

The correlations quoted so far should be used with caution. As Ferreira et al conclude, published effervescent atomisation discharge coefficient correlations, although generally representing underlying trends, are not universally applicable [56].

Table 2.7.1. Specific bubble Energy ( $E_b$ ) Correlations in Literature.

Correlation	Source and Comments
$E_b = RT(m_A/m_L)\ln(P_A/P_L)$	[33]; For a stream of air bubbles to convert a jet of liquid into a fine spray they must possess enough energy to overcome the surface tension forces holding the liquid together. N.B. Units are J/kg.
$E_b = (\gamma - 1)^{-1} p_e \left(\frac{\pi}{6}\right) D_b^3 \left[1 - \left(\frac{p_a}{p_e}\right)^{\frac{\gamma-1}{\gamma}}\right]$	[86]; $\gamma = 1.4$ for isentropic expansions. N.B. Units are J.

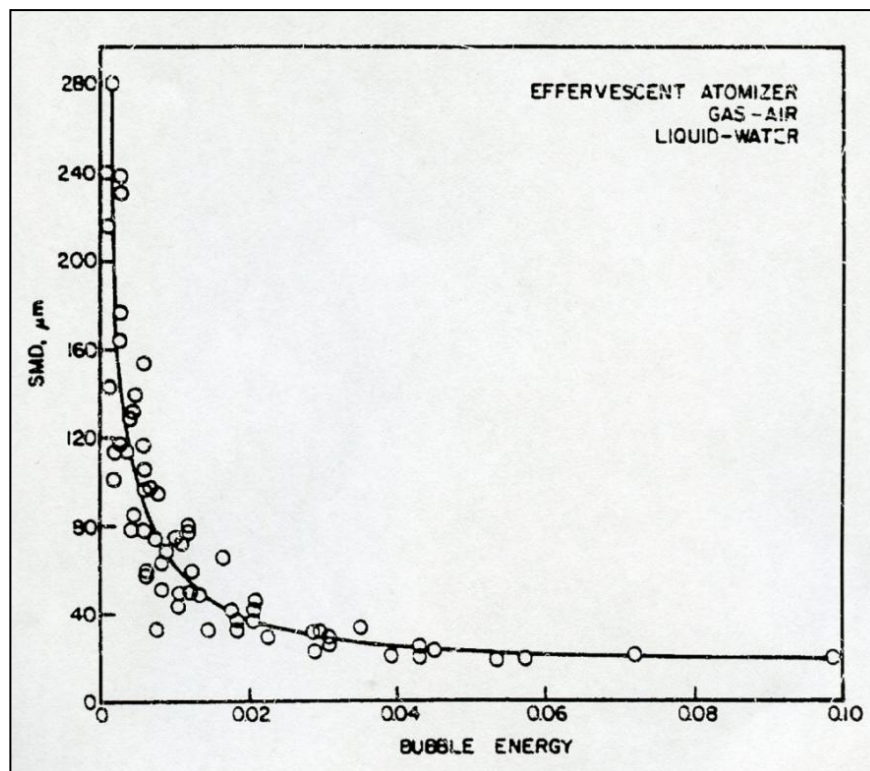


Figure 2.7.1. Relationship between spray droplet SMD and **specific** bubble energy.

Table 2.7.2. Coefficient of Discharge ( $C_d$ ) Correlations in Literature.

Correlation	Source and Comments
$C_d = \frac{m_L}{(\pi/4)d_o^2(2\rho_L\Delta P_L)^{0.5}}$	[31, 62]; Obtained from geometric considerations and flow continuity.
$C_d = [1 + ALR(\rho_L/\rho_A)]^{-1}$	[33]; Assumes no phase slip.
$C_d = c(1 - \beta)^{0.3} \left(1 + \frac{1}{ALR}\right)^{0.15}$	[55] $\beta = \left(1 - \frac{\rho_{AP}}{\rho_L ALR}\right)^{-1}$ The empirical constant $c$ depends on the orifice geometry and varies from 0.25–0.34 for axisymmetric atomisers.
$C_d = C_{dW}(\mu')^{0.04}(\sigma')^{0.02}$ $C_{dW} = aX - b$ $X = \left[\left(\frac{L}{D^*}\right)(\sin 2\alpha)^{0.5}\right]^{-0.1} \left[\left(1 + \frac{1}{ALR}\right)^{0.25} - 1\right] \left[\frac{p_c}{239}\right]$	[65]; Empirically developed. Values for $a$ and $b$ based on geometry and $X$ value. The working fluid coefficient of discharge is then a function of $C_{dW}$ and the ratios of fluid rheological properties (compared to water).
$C_d = C_{D1}C_{D2}C_{D3}$ $C_{D1} = (\mu')^{0.04}(\sigma')^{0.02}$ $C_{D2} = 0.62 \left(\frac{l_o}{d_o} \sin(2\theta)^{0.5}\right)^{-0.11}$ $C_{D3} = \frac{G}{\sqrt{2\Delta p \rho_L}} \left(\frac{1}{1 + ALR}\right)$ $G = 0.5(G_{HFFM} + G_{SFM})$ $G_{HFFM} = \frac{2p_c}{\alpha_1 v_1} \left[ \left(\frac{1 - \alpha_1}{\alpha_1}\right)(1 - \pi) + \left(\frac{k}{k + 1}\right)(1 - \pi^{(k-1)/k}) \right]$ $G_{SFM} = (ALR + 1)\sqrt{p_c} \left[ \frac{1}{\sqrt{2(1 - \pi)\rho_l}} + \frac{ALR}{\pi^{-1/k} \sqrt{2\rho_g \frac{k}{k-1} (1 - \pi^{(k-1)/k})}} \right]^{-1}$	[91] For $\theta$ (mixing chamber convergence half angle) less than $90^\circ$ . Gas mass flux, $G$ , is calculated by combining the Homogenous Frozen Flow Model (HFFM) and the Separated Flow Model (SFM). The multi-phase flow models used (HFFM, SFM) are well known in the literature. $\alpha = \frac{V_g}{V_g + V_l}$ $\pi = \frac{p_{amb}}{p_c}$

## 2.8 Summary

At various times in the past decades, a combination of geo-economic and other factors have led to the need to utilise alternative fuels or bio-fuels for power generation purposes (instead of traditional hydrocarbon fuels). Bio-fuels differ from commonly used fuels in a number of important ways and often require treatment prior to use. Conventional atomisers (pressure, rotary, and air-assist) have been able to run on such viscous fuels but operation was seemingly less effective and economical than when operating with traditional fuels.

A wide range of studies have shown that effervescent atomisation is more efficient than established atomisation techniques when using alternative fuels. Lower operating pressures are needed and fuel properties appear to have only a minor influence on atomisation. Stable effervescent atomisation has been observed with the bubbly and annular regimes of internal flow.

A number of liquid break-up mechanisms acting in effervescent atomisation have been determined. These include pressure drop, liquid column disruption by the gas phase, the gas phase compressing the liquid ligaments at the exit orifice, downstream gas bubble explosions, fluid choking at the nozzle due to the reduced sonic velocity of two-phase mixtures and secondary atomisation outside the nozzle.

A range of parameters' influence on effervescent atomisation has been noted, such as: initial operating conditions (ALR, pressure drop); fluid properties (liquid viscosity, liquid surface tension, liquid density, fuel type, atomising gas molecular weight); and geometric constraints (atomiser geometry, exit orifice geometry). However, current understanding of all of the above parameters can be further developed.

The most important operating parameter, in terms of its effect on spray quality is claimed to be ALR. Also important is pressure drop across the exit orifice. Meanwhile fluid properties are claimed to have a relatively minor effect on spray quality since, it appears that effervescent atomisation is dominated by so-called secondary atomisation. It is clear that considerable changes in effervescent atomiser geometry are possible. Effervescent atomisation has been shown to operate effectively with both Newtonian and Non-Newtonian fluids.

The spray parameter of prime interest is the spray droplet SMD which can be measured using a variety of measurement non-intrusive, light-scattering techniques. Also important is the spray cone angle,  $\theta_s$ . Empirically based formulae from the literature have been investigated. The finest spray droplet SMD have been observed

with the annular flow regime of internal flow. This flow regime is associated with higher ALRs, greater void fractions and phase-slip at the nozzle.

Two distinct spray atomisation regimes have been observed: the single bubble explosion regime and the tree-like atomisation regime. The former is characterised by ALRs of no more than 5%, while the latter occurs at higher air-to-liquid ratios. These broadly correlate with bubbly and annular internal flow regimes, respectively. Meanwhile, well atomised effervescent atomiser sprays could not be obtained at ALRs less than 1%.

Correlations provided in the literature are mostly based on empirical research. Droplet SMD correlations provided so far have proven to be limited to relatively narrow ranges of atomiser geometries, operating conditions and fluid properties. All correlations encountered so far have shortcomings. Some require involved calculations or difficult to measure properties (such as liquid ligament diameter at the nozzle) as their input parameters. Many require calibration constants, are dimensionally incorrect or ignore mechanisms thought to be important to effervescent atomisation (such as secondary atomisation). Finally, the data obtained using earlier versions of the hardware or alternative droplet sizing techniques may not be entirely representative or reliable.

Both practical and theoretical work is required to help further the present knowledge of effervescent atomisation and improve current designs. This is necessary if more efficient effervescent atomisation is to be achieved.

## Chapter 3 : Experimental Methods

---

This chapter describes the objectives of the investigation, outlines the effervescent atomiser design process and describes the test matrix used to facilitate atomiser testing. Also discussed are the testing facilities at the Cardiff University School of Engineering laboratories, including the fluid delivery systems used to supply and operate the atomiser. The underlying principles behind Phase Doppler Anemometry (PDA), which was used to analyse the effervescent atomiser sprays, are explained. Finally, this chapter summarises the data collection procedures and post-processing techniques used to analyse the acquired droplet data.

### 3.1 Effervescent Atomiser Design

The aim of this investigation was to study the effects of a range of operating parameters upon effervescent atomiser spray quality. It was decided to investigate these by designing and testing a 2 MW thermally rated (simulated, based on mass flow) effervescent atomiser fuel injector to be operated at pressures of 3-8 barG and for use with viscous fuels in industrial applications. Atomiser performance was to be characterised by reference to the global spray droplet SMD as calculated using 2-D Phase Doppler Anemometry data. The effervescent atomiser performance could then be compared to the performance of an equivalent Y-jet type industrial atomiser. Also important was the determination of the operating envelopes (in terms of  $\Delta P$ , ALR) within which stable, steady state effervescent atomisation was possible. The objectives of this investigation therefore included:

1. Design and build a 2 MW thermally rated inside-out type effervescent atomiser fuel injector.
2. Investigate achievable operating pressure ranges, ALRs and turndown ratios for stable sprays with water and air as the operating fluids.
3. Investigate the effect of operating conditions, atomiser geometry and fluid properties on both local and global spray quality for the operating ranges possible.
4. Develop a correlation to predict global spray droplet SMD based on the operating parameters investigated.

5. Compare effervescent atomiser performance with that of a typical industrial Y-jet type atomiser operating at equivalent conditions.

Local spray droplet SMD of 150-200  $\mu\text{m}$  was considered a benchmark since these values were known to be achievable using typical industrial Y-jet type [92]. Similarly turndown ratios (the ratio of maximum to minimum fuel mass flow rate) of 3:1 were considered a minimum.

Once the objectives were known some of the effervescent atomiser characteristics could be calculated.

- A 2 MW thermal rating (using the lower heating value of oil – 40000 kJ/kg – and for a 3:1 turndown ratio) gave a total atomiser fuel flow rate range of 10-30 g/s.
- Typical effervescent atomiser ALRs of 1-15 % gave total air flow rate ranges of 0.1-4.5 g/s co-current with the fuel.
- The above flow rates needed to be achievable at fluid pressures of 3-8 barG, as discussed above.
- Atomisation with liquid kinematic viscosities of at least  $1-10 \times 10^{-6} \text{ m}^2/\text{s}$  needed to be possible (water viscosity =  $1 \times 10^{-6} \text{ m}^2/\text{s}$ ; Fuel Oil No.4 viscosity =  $5 \times 10^{-6} \text{ m}^2/\text{s}$ ; fuels with viscosity greater than Fuel Oil No.4 – including typical Bio-Fuels – are considered “viscous”).

The expected fluid flow rates and pressures limited the range of exit orifice diameters and mixing chamber diameters possible, and these in turn impacted on the gas aerator design.

Meanwhile a review of the state-of-the-art effervescent atomisation literature [19, 54, 58, 62, 63, 65, 78, 80, 82, 83, 93] helped determine the key parameters to be investigated. Based on the literature review, parameters of prime importance to effervescent atomisation were found to be:

- Initial operating conditions (ALR, pressure drop across nozzle,  $\Delta P$ ).
- Atomiser geometry (mixing chamber diameter, fluid mixing length, aerator geometry, exit orifice diameter, exit orifice length-to-diameter ratio).
- Fluid properties (density, surface tension, viscosity).

It was decided to investigate the above parameters' influence on local and global spray quality. This could be done by varying each operating parameter individually (it was assumed that each parameter of interest could be investigated independently of all the others) until a stable spray was achieved, and using 2-D Phase Doppler Anemometry



to obtain comprehensive and representative spray droplet data. Once the parameters to be tested were decided, the atomiser design was finalised. A sketch of the effervescent atomiser designed is provided in Figure 3.1.1.

Figure 3.1.1 depicts the effervescent atomiser designed. This adjustable atomiser design allowed many of the important geometric parameters to be modified. For example, nozzle diameter and length to diameter ratio was altered by using different nozzles. Mixing chamber diameter was changed by attaching a new atomiser body. Mixing length was varied by screwing the aerator up or down and aerator geometry could be investigated by the use of an alternate gas aerator. Meanwhile ALR and  $\Delta P$  were controlled by varying the fluid supply pressures, and fluid properties were investigated by using water-glycerol mixtures as the operating fluid.

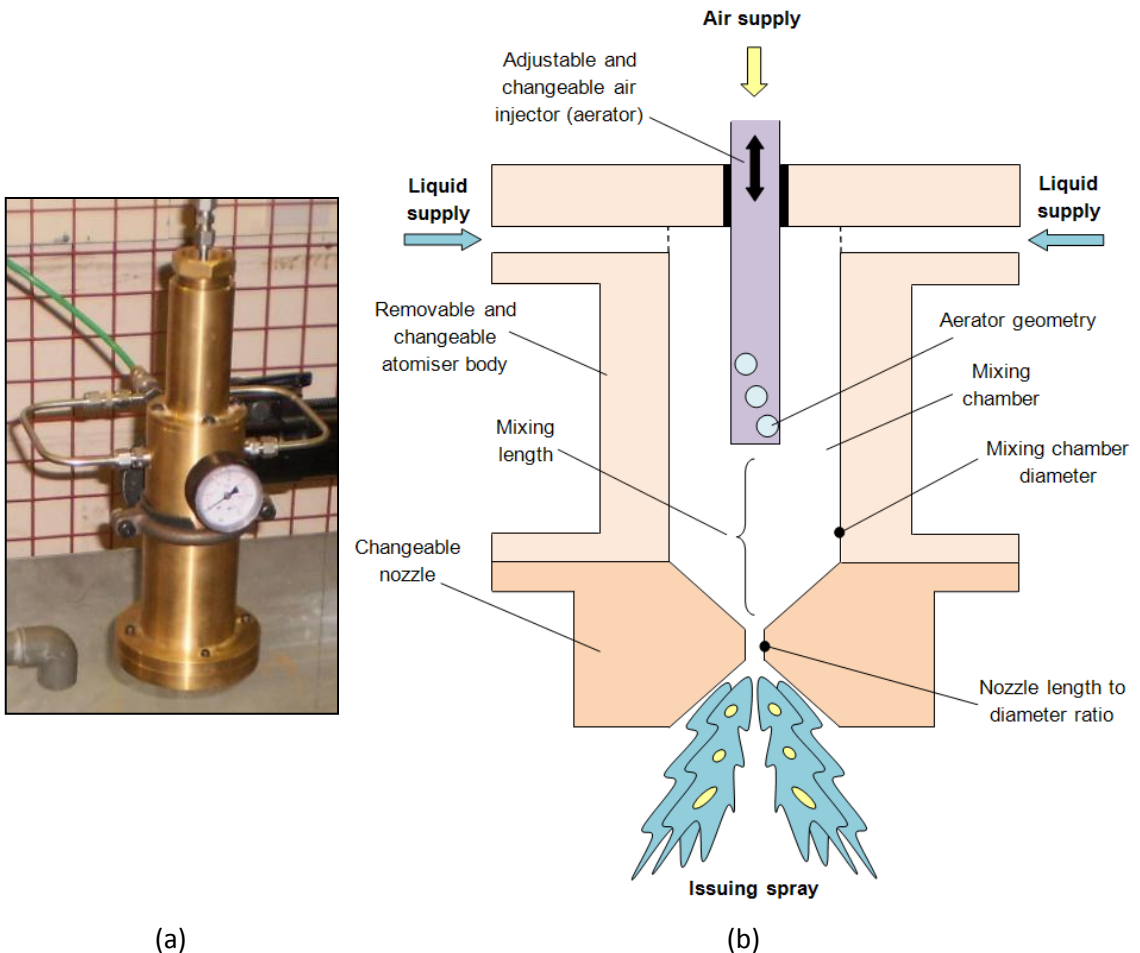


Figure 3.1.1 (a) Photo showing the effervescent atomiser designed, the air supply system (top) and the liquid supply system (middle); (b) Sketch showing important features of the adjustable effervescent atomiser.

Before the tests began, a series of preliminary tests were performed to determine an appropriate test matrix. The test matrix selected is presented in Table 3.1.1. It can be seen from Table 3.1.1 that the testing was divided into three discrete phases. Phase A

investigated initial operating conditions (ALR,  $\Delta P$ ), phase B studied the atomiser geometry (exit orifice diameter, mixing length, mixing chamber diameter, exit orifice length to diameter ratio, aerator geometry) and phase C investigated fluid properties.

Table 3.1.1 Test matrix designed to facilitate testing.

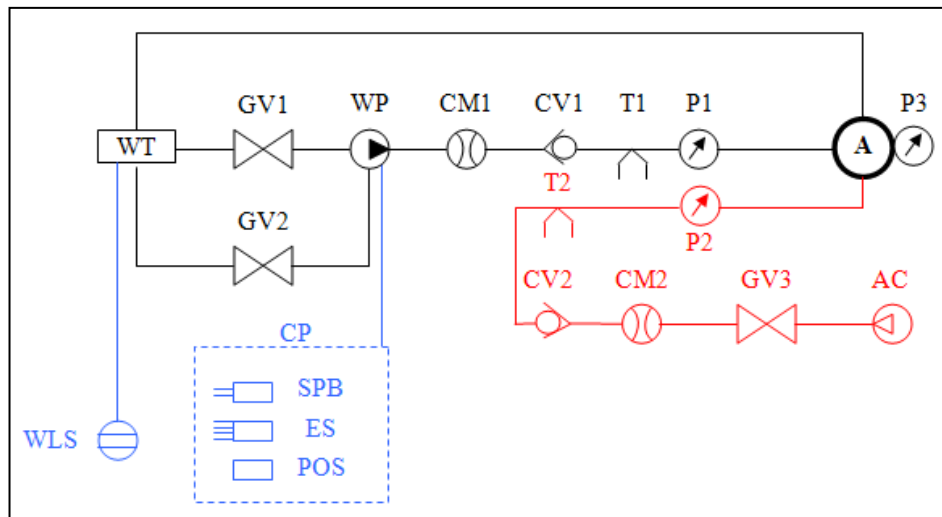
TEST No. PARAMETER VARIED	1 ALR	2 $\Delta P$	3 $D_o$	4 $L_{MC}$	5 $D_{MC}$	6 $L_o/D_o$	7 A. GEOM.	8 $\eta$
TEST PHASE	A. Initial Operating Parameters		B. Atomiser Geometry					C. Fluid properties
ALR (%)	0.8-12.5	2		2				
$\Delta P$ (bar.g)	7	4-7		7				
$D_o$ (mm)	2	2	2-4	2	2	2	2	2
$L_{MC}$ (mm)	140	140	140	64-140	140	140	140	140
$D_{MC}$ (mm)	25.4	25.4	25.4	25.4	20-30	25.4	25.4	25.4
$L_o/D_o$ (-)	1	1	1	1	1	0.5-2	1	1
Aerator Geometry	A1	A1	A1	A1	A1	A1	A2, A3	A1
$\eta \times 10^{-6}$ (m <sup>2</sup> /s)	1	1	1	1	1	1	1	2-10

A review of the fluid property literature [43] led to changes in test phase C. It was found that neither density nor surface tension could be varied independently of other fluid properties. However these properties were known to vary relatively little between fluids used in practical atomisation. In addition, both density and surface tension were claimed to have a relatively small influence on liquid atomisation. By contrast, fluid viscosity can be varied independently of other fluid properties and was known to have an important influence on liquid atomisation. In fact, liquid viscosity can affect both droplet size and flow rate through the nozzle. For these reasons it was decided that, of the fluid properties, only viscosity should be investigated as a parameter of prime importance to effervescent atomisation.

A great number of tests could have been performed to investigate the effect of each individual parameter had on spray quality throughout different parameter ranges. However such a large number of tests were undesirable. A number of factors influenced the choice of test numbers including the minimum tests required to spot non-linearities in results, as well as component manufacturing times. Finally it was decided to perform only up to five or six tests per test parameter with all others kept constant. This would allow non-linear results to be recognised while keeping the number of tests relatively low. However, all test phases were considered individually and, where it seemed justified, some parameters were investigated using fewer test points.

### 3.2 Effervescent Atomiser Testing Facilities

The experiments in this study were performed at Cardiff University, School of Engineering. Since effervescent atomisation requires the use of two pressurised, metered fluids, two fluid supply systems were needed – a water and an air supply system. Most test cases were carried out using air and water as the working fluids. This ensured the tests remained cost effective, safe for the operator, and less damaging to equipment and the laboratory environment. The last phase of testing investigated the effects of fluid viscosity, and here water-glycerol mixtures were used instead of water. The set-up remained the same for these tests. Figure 3.2.1 represents a schematic of the test rig to be used for the experiments. The test rig and its operation are described below.



**Water Supply System:**  
 WT – Water Tank  
 GV1 – Gate Valve 1  
 GV2 – Gate Valve 2  
 WP – Water Pump  
 CM1 – CMF 050  
 CV1 – Check Valve  
 T1 – Air temp. Thermocouple  
 P1 – Air Supply P. Sensor  
 P3 – Mixing Chamber P. Sensor  
**A – Atomiser**

**Air Supply System:**  
 AC – Air Compressor  
 GV3 – Gate Valve 3  
 CM2 – CMF 025  
 CV2 – Check Valve 2  
 T2 – Water Temp. Thermocouple  
 P2 – Water Supply P. Sensor

**Control Components:**  
 CP – Control Panel  
 WLS – Water Level Sensor  
 SPB – Start Pump Button  
 ES – Emergency Stop  
 POS – Power On Switch

Figure 3.2.1 Schematic of fluid supply systems used.

A rectangular water tank (WT) containing up to one cubic metre of water was used both to store water and to capture the spray issuing from the atomiser (A). A Lowara 3SV29F030T 3-phase, vertical, multistage electric pump (WP) capable of pressures up to 25 barG was used to circulate the water. The effervescent atomiser is shown

attached to the test rig in Figure 3.2.2 and the water pump is shown in front of the water tank in Figure 3.2.3.



Figure 3.2.2 The effervescent atomiser with pressure and temperature sensors attached.

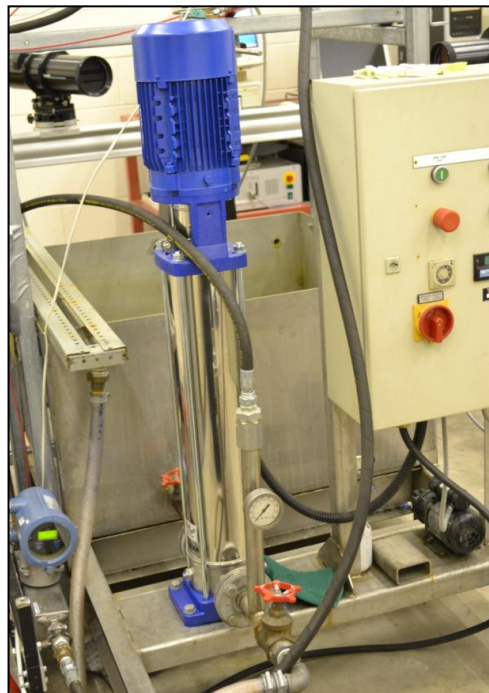


Figure 3.2.3 Lowara water pump used to circulate water.

From the water tank the water was pumped through a calibrated Emerson Micromotion CMF 050 coriolis meter (CM1) – shown in Figure 3.2.4 – before passing through a check valve (CV1) and being supplied to the atomiser mixing chamber.



Figure 3.2.4 CMF 050 coriolis meter.

Water pressure and temperature were measured just prior to injection to the mixing chamber via a calibrated 0-10 barG Druck PTX 1400 pressure transmitter (P1) and a type K thermocouple (T1), respectively. The thermocouple and pressure transmitters are visible in Figure 3.2.2. The atomiser was located centrally over the water tank to ensure the whole spray was captured and recycled, and was far enough from the laser optics to ensure sprays could not wet the optical lenses. Wet optics could either impair the transmitting laser beams or weaken the signal collected by the receiving optics.

Air was provided by the house air compressor (AC) at up to 7 barG. This was fed through a calibrated Emerson Micromotion CMF 025 coriolis meter (CM2), a check valve (CV2), a calibrated 0-10 barG Druck PTX 1400 pressure transmitter (P2) and type K thermocouple (T2) before being injected into the atomiser mixing chamber. The stability of the air compressor and the use of a gate valve (GV3) allowed the air pressure to be set accurately with minimal pressure drift or fluctuations. The gate valve is shown in Figure 3.2.5.

The pressure of the fluids in the mixing chamber was monitored using a calibrated 0-10 barG Druck PTX 1400 pressure transmitter (P3) mounted on the atomiser body.

A 0-2 V input Delta T multi-channel data logger was used to record the pressures, flow rates and temperatures of both fluids at points of interest (pressure within the mixing chamber, pressure, temperature and flow rate just before injection to the atomiser). To achieve this the sensors P1, P2, P3, CM1, CM2, T1 and T2 were wired up to the data logger allowing real-time voltage readings to be viewed and timed recordings to be made. The sampling frequency of the data logger could be varied but was set to 1 Hz for all tests performed. Comparison with a National Instruments Compact RIO 9022 –

NI CRIO 9022 – with NI 9205 analogue input card programmed using the FPGA sampling at 2kHz indicated less than 1 % difference between sampling at 2 kHz and sampling at 1 Hz. The sensors could thus be recorded over the course of a test and post-processed to give average sensor readings for each test performed.



Figure 3.2.5 The regulator in place on the air line.

The pressure transmitters were calibrated individually using a Druck DPI 601 Digital Pressure Indicator for pressures of 0-10 barG. The coriolis meters were calibrated using the logging software.

The following procedure was used to set up a desired spray:

- With the water pump off, the house air was turned on so that only air flowed through the atomiser; the air supply pressure was adjusted until the mixing chamber pressure matched the required  $\Delta P$  value; a live readout from the Delta T data logger was consulted.
- The water pump was turned on and the water flow rate adjusted so that the desired ALR was obtained; this was calculated from the live data logger fluid flow rate readings.
- Minor adjustments to air and water flow rates were then required to achieve the desired  $\Delta P$  (pressure in the mixing chamber) and ALR values; the live data logger readings were continuously consulted.

Readings from the Delta T data logger indicated that steady-state, non-pulsing effervescent atomiser sprays were characterised by relatively stable operating parameters throughout the entire test.

### 3.3 Phase Doppler Anemometry – Theory of Operation

PDA is a non-intrusive optical diagnostic technique capable of simultaneously measuring the diameter, and up to three components of velocity of spherical particles and droplets [94-96]. The measurements are performed on single particles and are applicable to both liquid droplets in a gas medium (e.g. a spray) and gas bubbles in a liquid medium (e.g. gas bubbles in two-phase flows). PDA is also capable of estimating particle concentrations and mass flux via interpolation [97]. Since it is a technique based on absolute physical effects (e.g. light scattering, phase Doppler shift) no in-situ calibration is required. With an appropriate choice of hardware, particle sizes from 0.1  $\mu\text{m}$  to over 1 mm, and velocities up to supersonic can be measured. Maximal data rates of up to 250 kHz can be achieved in special cases [46]. Throughout this study droplet size ranges of 0.1  $\mu\text{m}$  to 600  $\mu\text{m}$ , and velocities up to 100 m/s were measured; validated data rates of up to 10000 droplets per seconds were recorded in 2-D PDA coincident mode.

The technique works by intersecting the waists of a pair of monochromatic, coherent, linearly polarised, collimated laser beams. The waist is that part of the laser beam where beam cross-section attains its lowest value and where the light wave fronts can be assumed to be straight allowing the theory of plane waves to be employed.

Droplet size and velocity measurements are possible only within this ellipsoidal intersection volume or control volume. Because the control volume is very small (dimensions are of the order of tens of micrometres) a high spatial and temporal resolution is possible. As a gas bubble or liquid droplet passes through the control volume, light is scattered in a number of modes such as reflection and refraction. Light from the dominant scattering mode can be collected by optimally positioned photo detectors since the scattering angle ranges for each mode can be calculated from the refractive indices of the media. Figure 3.3.1 demonstrates the typical locations of the first three light scattering modes for a water droplet in air.

Figure 3.3.2 shows the optical set-up for a typical 1-D PDA system where liquid droplets in air are to be measured and light scattered by first order refraction is to be collected.

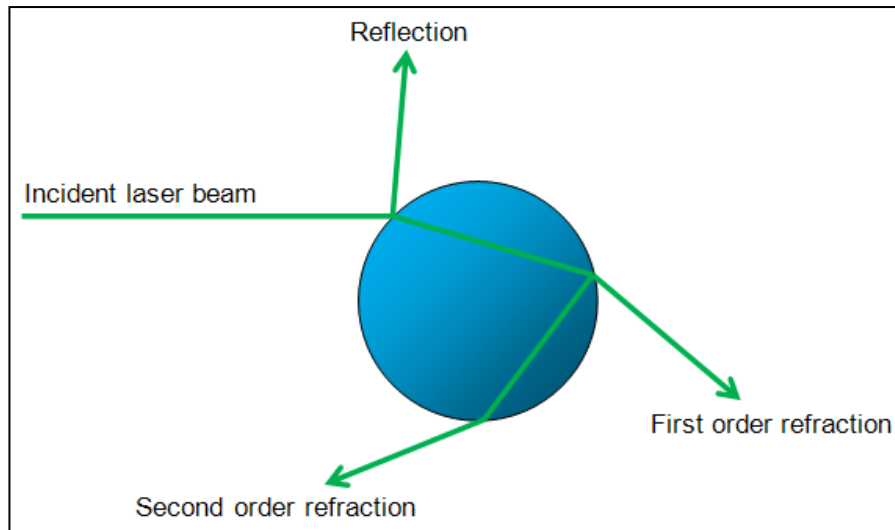


Figure 3.3.1 The first three principle light scattering modes for a water droplet in air [98].

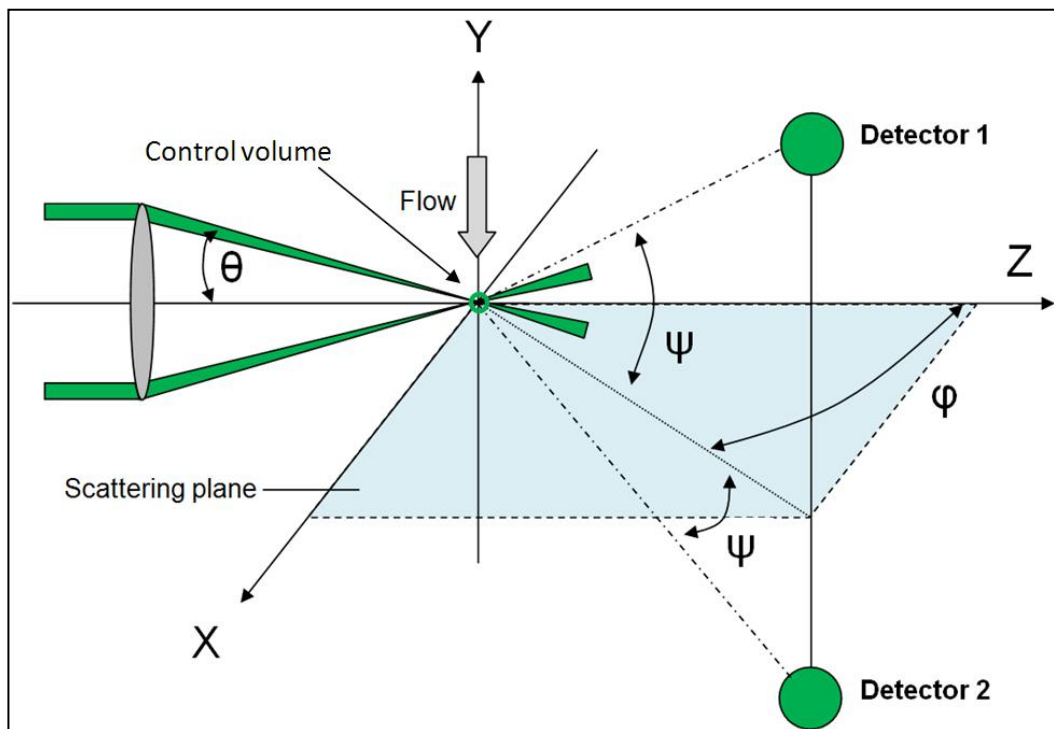


Figure 3.3.2 Diagram showing the optical parameters governing PDA set-up including beam intersection angle ( $\theta$ ), scattering angle ( $\Phi$ ), and elevation angle ( $\psi$ ) [98].

The control volume can be visualised by reference to the fringe model which depicts the control volume as a pattern of parallel interference fringes located perpendicular to the direction of droplet motion. This is illustrated in Figure 3.3.3.



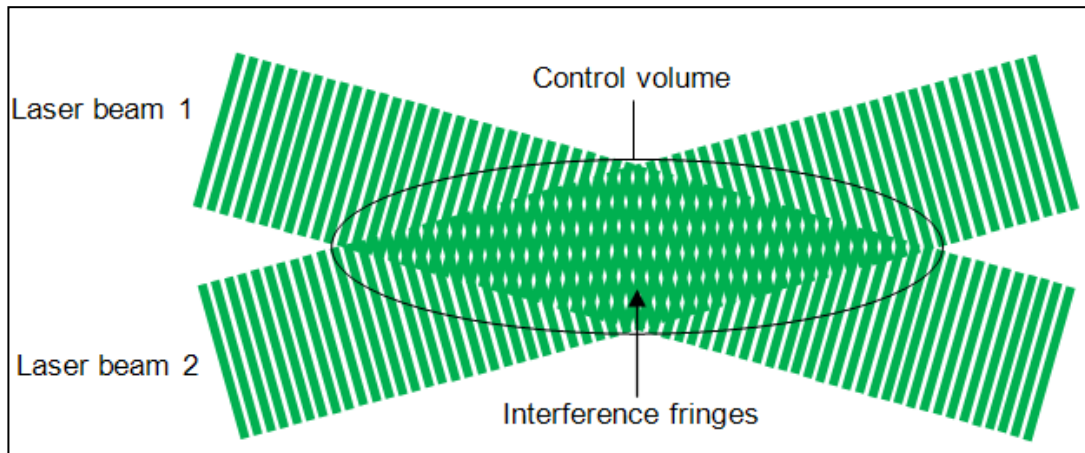


Figure 3.3.3 A pair of intersecting laser beams creating interference fringes within the control volume [98].

As a droplet passes through the control volume light containing components of both beams is scattered. Photo detectors pick up this signal which has alternating regions of high and low light intensity. An example signal received by a photo detector is illustrated in Figure 3.3.4.

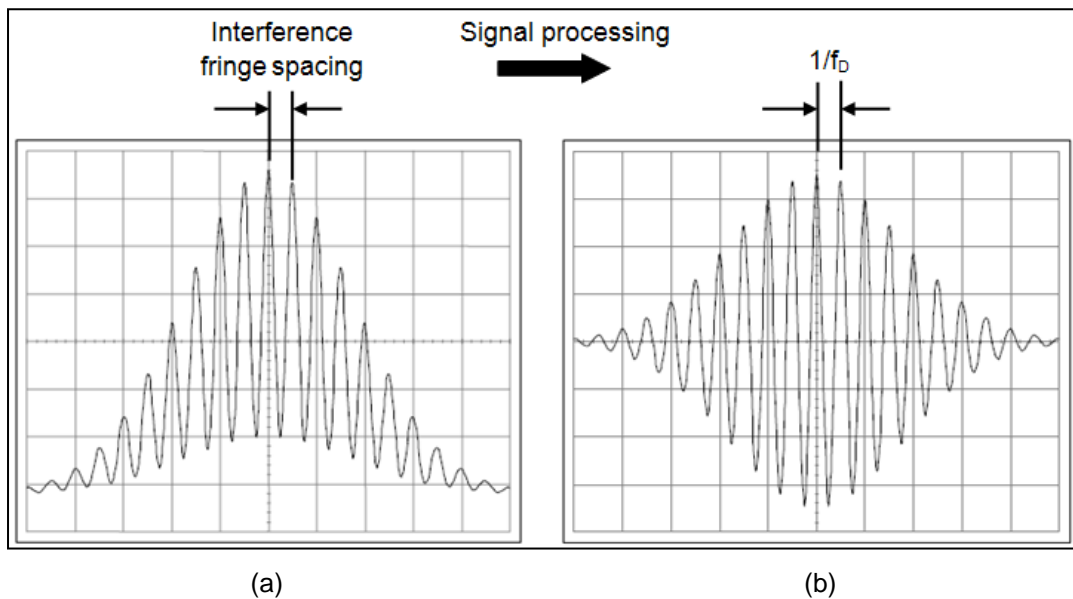


Figure 3.3.4 (a) Light signal received by photo detector with influence of interference fringe spacing shown; (b) Processed signal showing dependency on Doppler frequency on the right [98].

In terms of the Fringe model, the frequency of light intensity pattern received at the photo detectors is directly proportional to the speed with which the droplet traverses the interference fringes of the control volume. The droplet velocity can therefore be calculated from the Doppler frequency. Since Doppler frequency is independent of the position of the receiver, the light collected at any of the photo detectors can be used.

The relationship between droplet velocity and Doppler frequency is given in Equation 3.3.1 where  $\lambda$  is the wavelength of light.

$$U = \frac{\lambda f_d}{2 \sin(\theta/2)} \quad \text{Equation 3.3.1}$$

A drawback of the system described above is that it suffers from directional ambiguity, i.e. a particle moving at the same speed in a positive or negative direction will give the same signal. However, applying a frequency shift to one of the beams using an acousto-optical modulator (such as a Bragg cell) allows positive and negative velocities to be distinguished. This is illustrated in Figure 3.3.5.

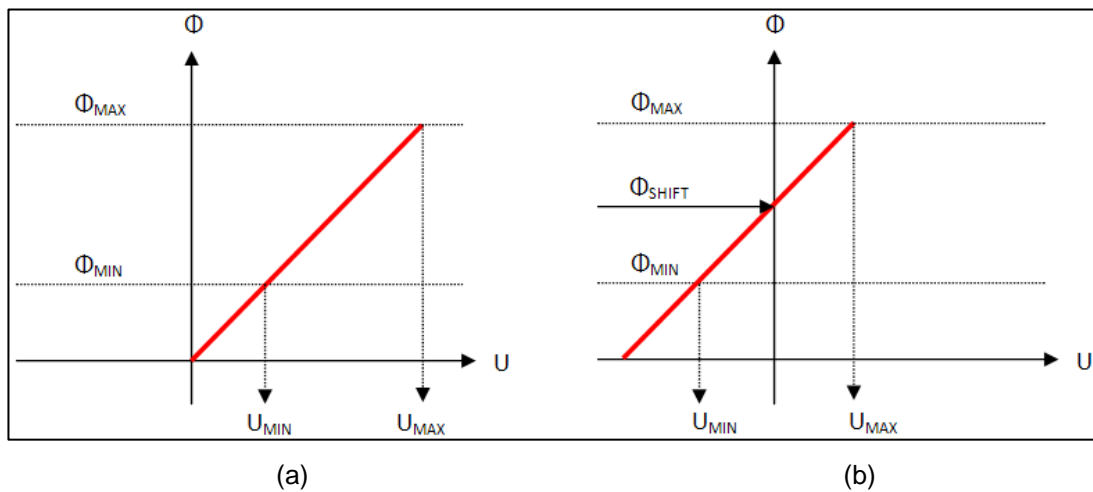


Figure 3.3.5 (a) Beam without frequency shift has directional ambiguity; (b) Frequency shifted beam does not suffer from directional ambiguity [98].

A frequency shift of one of the laser beams would in theory result in a tilting of the interference fringes as depicted by the Fringe model. This would affect calculations and give erroneous results. In this study a frequency shift of 40 MHz was applied to all shifted beams. This value is several orders of magnitude smaller than the frequency of light and therefore resolves the problem of fringe tilting. It can be shown that this kind of frequency shift produces fringe tilting of about  $10^{-5}$  degrees which can be ignored.

A consequence of applying a frequency shift to one of the beams is that the interference fringes within the control volume are no longer stationary but roll at a constant velocity. Therefore a stationary droplet will emit a Doppler burst with frequency equal to the applied frequency shift, a droplet moving with the interference fringes will emit a Doppler burst of lower frequency and a droplet moving in the negative direction will emit a Doppler burst of higher frequency.

A system such as the one described can measure velocity in only one dimension. The addition of an extra pair of beams intersecting at the control volume allows a second component of velocity to be measured. To allow the photo detectors to distinguish between numerous pairs of beams, light of a different wavelength and additional filters will be required for each pair. Once again, a frequency shift needs to be applied to one of the beams from the new pair to overcome the problem of directional ambiguity.

In order to measure particle diameters the use of two photo detectors is needed. As illustrated in Figure 3.3.6 a particle traversing the control volume scatters light which is collected by a pair of photo detectors located in the PDA receiving optics.

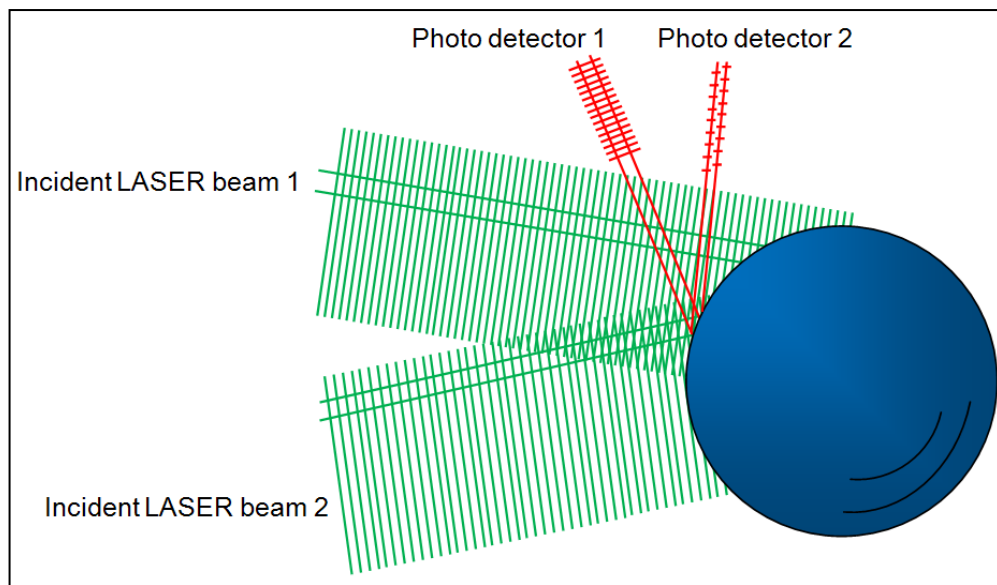


Figure 3.3.6 Light scattered via reflection mode by droplet traversing through PDA control volume (NOT TO SCALE) [98].

Both photo detectors receive the same signal – a burst with the same Doppler frequency but with a slight phase difference due to the different optical lengths travelled by the light. The phase difference ( $\Phi$ ) between the signals received by the two photo detectors is directly proportional to the particle diameter ( $d_p$ ). This is demonstrated in Figure 3.3.7.

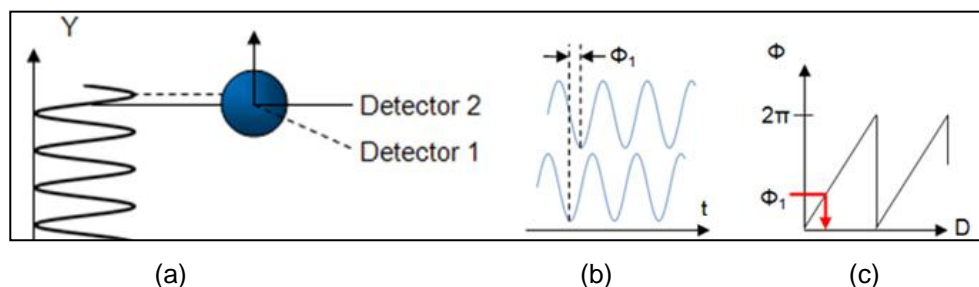


Figure 3.3.7 (a) Light intensity signal received at photo detectors; (b) The two photo detectors receive the same signal but with a slight phase difference; (c) Phase difference can be used to calculate droplet diameter [98].

For reflection as the dominant light scattering mode, the phase difference between adjacent photo detectors is given by Equation 3.3.2. For dominant first order refraction the phase difference is given by Equation 3.3.3. The relative refractive index ( $n_{rel}$ ) can be calculated via Equation 3.3.4 [98].

$$\Phi = \frac{2\pi d_p \sin\theta \sin\psi}{\lambda \sqrt{2(1 - \cos\theta \cos\psi \cos\phi)}} \quad \text{Equation 3.3.2}$$

$$\Phi = \frac{-2\pi d_p n_{rel} \sin\theta \sin\psi}{\lambda \sqrt{2(1 + \cos\theta \cos\psi \cos\phi)(1 + n_{rel}^2 - n_{rel} \sqrt{2(1 + \cos\theta \cos\psi \cos\phi)})}} \quad \text{Equation 3.3.3}$$

$$n_{rel} = \frac{n_{particle}}{n_{medium}} \quad \text{Equation 3.3.4}$$

The relationship between phase difference and particle diameter for higher refraction orders needs to be formulated using a numerical or iterative approach.

Figure 3.3.7 (c) illustrates a linear relationship between phase difference and droplet diameter. This is however only valid when one mode of light scattering dominates. Therefore the scattering angle,  $\Phi$ , needs to be carefully selected to avoid different light scattering modes from interfering. In this research a scattering angle of 70 degrees from forward scatter was used which is where first order refraction light is dominant. This was close to the Brewster's angle for water droplets in air (the angle at which no parallel polarised light is reflected) which is 73.7 degrees.

A PDA system with only two photo detectors can be used to measure particles with a diameter corresponding to a phase shift of up to 360 degrees or  $2\pi$ . A two detector system suffers from what is termed the "2 $\pi$  ambiguity" – a consequence of the fact that because phase is a multiple of  $2\pi$ , a two detector system cannot distinguish between the phase differences produced by very large and very small droplets. This is illustrated in Figure 3.3.8 where particles sized  $D_3$  and  $D_3'$  are indistinguishable.

Figure 3.3.8 (a) shows the light intensity burst as a small, medium and large droplet pass through the control volume. The PDA software compares adjacent and not actual light intensity peaks which are shown in Figure 3.3.8 (b). This means that the large droplet (with phase difference larger than  $2\pi$  corresponding to diameter  $D_3$ ), will be mistakenly identified as a much smaller droplet marked as  $D_3'$  in Figure 3.3.8 (c).

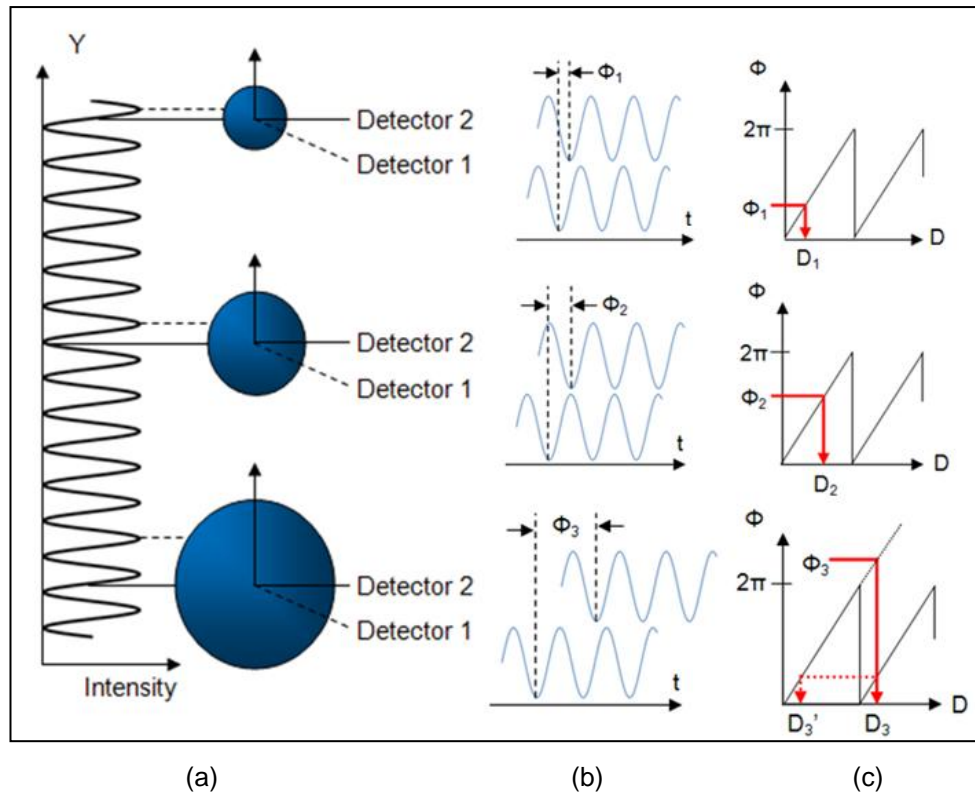


Figure 3.3.8 (a) Light intensity signal received at photo detectors as droplets traverse the control volume; (b) Calculation of phase differences between adjacent photo detectors; (c)  $2\pi$  ambiguity as very large and very small droplets are indistinguishable in a two detector PDA system [98].

The solution employed in PDA systems is to use three photo detectors grouped into two pairs allowing the phase differences between both pairs to be cross-checked. The close pair measure large particle size ranges at a low resolution while the distant pair measure smaller size ranges at a greater resolution. The phase differences of both pairs will then align along the correct droplet diameter as shown in Figure 3.3.9. In this three photo detector set-up cross-checking of the two pairs of phase differences will both extend the measurable particle size ranges and eliminate the  $2\pi$  ambiguity.

Another useful outcome of this approach is the ability to perform validation checks on the phase differences measured. For a perfectly spherical droplet both pairs of phase differences will indicate exactly the same droplet diameter. The particle sphericity validation check, as it is called, is one means of assessing the quality of a PDA set-up. Throughout this study a sphericity error of up to 15% (this value provided a good compromise between high data rates and high validation rates) was deemed acceptable. Droplets with a sphericity error larger than this were rejected by the processor and did not influence results.

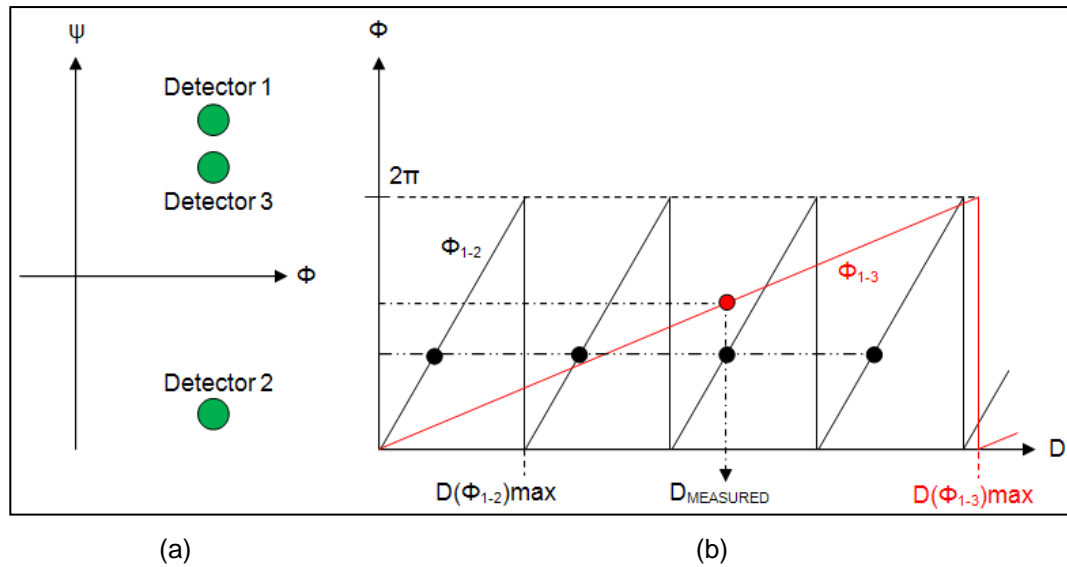


Figure 3.3.9 (a) Desired photo detector location to eliminate  $2\pi$  ambiguity; (b) Cross-checking the phase differences of the close pair of photo detectors (1-3) and the distant pair (1-2) to calculate diameter [98].

### 3.4 PDA System Used

The 112 mm Fiber PDA system used in this study comprised an off-the-shelf system provided by DANTEC DYNAMICS. This included a transmitter, a BSA P60 Flow and Particle mm Processor and a Fiber PDA detector unit. The laser used was a Multiline Coherent Innova 70-5 Series Argon-Ion Laser at an all-line power output set at 2W. The laser light was split into three pairs of beams providing six in total – two green, two blue and two violet beams. One beam from each of the three pairs was shifted in frequency by 40MHz to overcome directional ambiguity inherent in the PDA technique. Four of the six beams (the two greens and two blues) were sent to the transmitting optics via fibre optic cables. The laser wavelengths of 514.5 nm (corresponding to green visible light) and 488 nm (corresponding to blue visible light) were used to perform velocity measurements in the nozzle axial and radial directions respectively. The green pair was used for droplet size measurements and the blue pair was used for validation checks. The violet beams (with a wavelength of 476.5 nm) were not required for 2D PDA systems but were used to help align the green and blue beams within the control volume to ensure an optimal set-up.

The receiving optics were located in the same plane as the transmitting optics but offset at an angle of 70 degrees from forward scatter. This arrangement was suitable for PDA tests with dominant first order refraction for both water, and water-glycerol droplets in air.

A 112 mm Fiber PDA transmitting optic with a beam spacing of 74 mm and a nominal beam diameter of 1.5mm was used. The transmitting and receiving optics were equipped with lenses with a focal length of 600 mm to cope with the large dimensions of the water tank over which the atomiser was located and around which the optics had to be placed. A long focal length was also important in ensuring the optics were far enough from the spray to avoid getting wet during testing.

Both the transmitting and receiving optics were mounted on a computer-controlled traverse allowing remote fine adjustment of the optics location and therefore the control volume. The lightweight traverse employed allowed controlled motion in 3-axes, with over 500 mm of travel and an accuracy of 0.1 mm in each axis. This arrangement allowed any portion of the spray to be reached and investigated. The laser, the transmitting and receiving optics, and the traverse are shown in Figure 3.4.1.



Figure 3.4.1 The computer-controlled traverse with sending and receiving optics mounted.

The measurable droplet size ranges were affected by beam separation, focal length and the collection optics selected. The first two parameters could not be altered in the given set-up (beam separation was determined by the transmitting optics used and focal length could not be less than 600 mm to accommodate the spray housing). However the aperture plates could be used to modify the measurable droplet size ranges and therefore optimise PDA arrangement for the sprays investigated. Throughout this study aperture plate C was used which allowed measurements of droplets up to 577.4  $\mu\text{m}$  (in practice slightly larger droplets than this could be captured – up to 600  $\mu\text{m}$ ) and a droplet resolution up to 0.1  $\mu\text{m}$ . This size range was found to capture droplet size data at all investigated operating conditions. A spherical validation

band of 15% was selected for all tests performed. DANTEC DYNAMICS BSA Flow Software v. 4.50 was used for all PDA tests in this investigation.

### 3.5 PDA Set-up

Once the atomiser was plumbed and wired in, and positioned in the appropriate orientation, the PDA hardware needed to be prepared for testing. This involved the following:

- Aligning the transmitting optics to ensure the green pair and blue pair of beams were in the same vertical and horizontal planes, respectively, as the atomiser.
- Aligning all four fibre optic cables at the laser so as much of the laser beams as possible was captured and sent to the transmitting optics.
- Maximising and regulating beam power (“balancing the beams”) so all beams possessed the same power ratings using a light intensity meter.
- Aligning both pairs of beams within the control volume using a photo-sensitive cell.
- Focussing the receiving optics on the control volume using a controlled spray from a nebuliser.
- Aligning the control volume with the atomiser tip (using the laser beam shadows as the beams approached the nozzle tip from different directions).

The final phases of PDA set-up included focussing the laser beams on a spray and running the PDA software in the “continuous” mode of operation. The data rates and spherical validation checks performed by the processor were then displayed, and could be used to fine tune the optical and software settings for a PDA set-up optimised for the spray to be investigated. From experience it became clear that maximal validated data rates over 8 kHz in 2-D PDA coincident mode at 25 mm from the nozzle (with 600 mm focal length) indicated the achievement of a good set-up. Other parameters used to evaluate and optimise the set-up prior to testing included the Doppler burst signal, the phase plot diagram, the photo detector voltage signals, validations performed by the processor, the droplet diameter and velocity histograms, as well as the changes in data quality as set-up was changed from LDA to PDA, from 1-D to 2-D, and from non-coincident to coincident modes of operation.



### 3.6 PDA Data Collection

The control volume formed when two or more laser beams intersect represents a finite and very small measurement volume (of the order of tens of  $\mu\text{m}$ ). Therefore PDA can be considered a temporal, point sampling technique. A stable fuel spray such as the ones to be investigated does not vary significantly with time. However, the sampling locations are important, and an appropriate sampling grid is required. A sampling grid consists of a series of measurement points chosen in such a way as to obtain results that are representative of the fuel spray as a whole. An example sampling grid is illustrated in Figure 3.6.1.

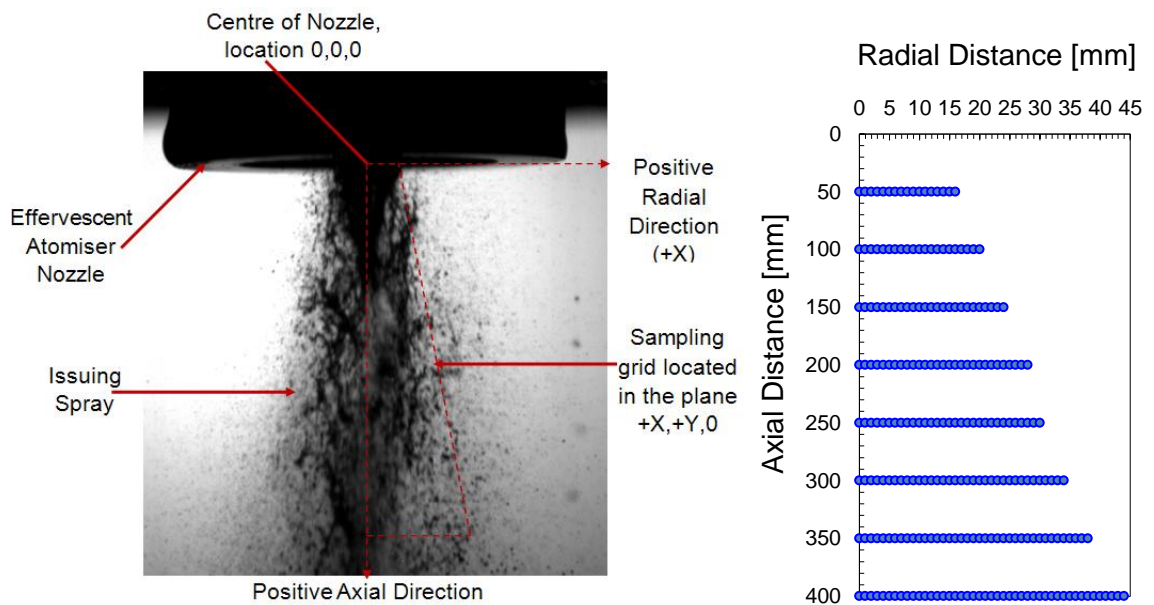


Figure 3.6.1 (a) A photo of the nozzle and issuing spray demonstrating a typical sampling grid; (b) A typical sampling grid in the +X,+Y,0 plane, with the centre of the nozzle at location 0,0,0.

Unlike the densely packed sampling grid demonstrated in Figure 3.6.1, previous effervescent research characterised sprays based on relatively few data points. A number of studies report PDA measurements 150 mm downstream of the nozzle at 5 mm intervals in the radial direction up to  $\pm 50$  mm from the spray centreline [71, 72, 91, 99]. This provides 21 sampling points along a 2-D horizontal plane. In these studies, 50 mm was arbitrarily chosen as the spray edge. Further PDA research investigated the variation of spray quality at 10 mm intervals up to 80 mm in the radial direction, and from 100-254 mm along the centreline in the axial direction [19, 85]. It was noted that spray quality could vary in both the radial and axial directions but no recommendation was given about what axial or radial portion of the spray should be sampled to ensure representative data. Other researchers investigated effervescent atomiser spray quality

using the Malvern Particle Analyzer, a technique based on Fraunhofer diffraction theory. In this type of research, somewhat larger control volumes were utilised, located 150-250 mm downstream of the exit orifice [18, 58, 63, 79, 83, 100]. However, measurements were performed only at this sampling location.

The practices described above are useful for comparison purposes but cannot capture the salient features of a fuel spray or provide truly representative data (since they sample only relatively small portions of the spray). As discussed, the location at which fluid break-up terminates can move axially as operating conditions (such as operating pressure) vary. Therefore sampling at only one axial location while altering operating conditions risks capturing and comparing data from different stages in a spray's downstream development. This could bias results. Meanwhile, only sampling at the centreline will miss many larger droplets whose relatively greater momentum carries them to the spray periphery (preliminary testing has confirmed the possibility of large droplet SMD variations in the radially distant locations). Larger droplets strongly influence global mass-under-size plots as well as representative droplet diameters. From an industrial perspective, large droplets produce fuel cenospheres and unburnt hydrocarbons – all highly undesirable. These highlight the importance of an adequate sampling grid, which should be designed such as to provide comprehensive and representative data, allowing the characterisation of local and global spray quality.

Certain guidelines were used to help simplify the process of determining the optimal sampling grid shape. Some of these are listed below.

- Preliminary PDA tests [101] indicated that stable effervescent atomiser sprays could be considered axisymmetric. This vastly reduced sampling, computational and memory costs. The 2-D sampling plane selected was the one most clearly visible to the PDA receiving optics – perpendicular to the transmitting optics and in the positive x-direction.
- The number and proximity of sampling points needed to be capable of capturing significant features of axial and radial spray development at expected test conditions.
- The radial spray edge at a given axial location was taken to be that radial location at which the validated data rates dropped to below 10% of the maximum at that axial location. This approach has been used before [102] and was applied for all tests performed.
- The spray in the near-nozzle region was very dense leading to multiple scattering and light attenuation effects. This leads to biased data (as light from

smaller droplets is extinguished) and was therefore avoided. Validation and data rates proved to be a good indicator of suitable sampling locations.

A number of effervescent atomisation researchers performed PDA tests at axial locations of 150-200 mm downstream [72, 77, 91]. Lefebvre, who pioneered much of the early effervescent atomisation research, recommends sampling locations well downstream of the nozzle: 200-300 mm, by which point break-up was expected to terminate [43]. However, break-up point is known to move axially and no single axial location is guaranteed to capture exclusively post-break-up data for all conditions investigated. Moreover fewer axial sampling locations would provide a limited and less representative view of the spray and its' development.

Therefore in order to ensure comprehensive and representative data it was decided to sample at a large number of axial locations including very close to the nozzle, with a relatively small radial spacing between points. Preliminary PDA testing helped finalise the sampling grid. It was decided to sample at 25, 50, 100, 150, 200, 250, 300, 350 and 400 mm in the axial direction and in steps of 1 mm in the radial direction from the spray centreline to the spray edge. Spray width would change with each test since spray limits were determined from the data rates at each axial location. The 2-D sampling plane thus formed would be the one most visible to the receiving optics, which is in the positive x-direction.

The PDA sampling grid selected was then imported into the DANTEC software, which controlled the motion of the 3-D traverse. This allowed for automatic data acquisition with no additional input from the human operator.

It was decided that tests should be performed in 2-D PDA mode allowing the measurement of droplet diameters and two components of velocity (axial and radial). Although set-up in this mode was more time consuming, and validation and data rates were lower compared to 1-D PDA, the extra velocity component gained (radial) was felt to be important for determination of possible flow turbulences, vortices, recirculation or other important flow effects.

Preliminary PDA measurements at a range of stable effervescent atomiser test conditions at different locations in the sprays showed that no change in representative droplet diameters (AMD, SMD etc.) occurred after 5 s of sampling, to the nearest  $\mu\text{m}$ . Therefore it was decided to perform PDA tests with a 5 s sampling time at each point in order to reduce testing times, computations and file storage requirements. This seemed justified as data rates were high enough to ensure a representative number of droplets were collected in this sampling period. Typically, data rates were always

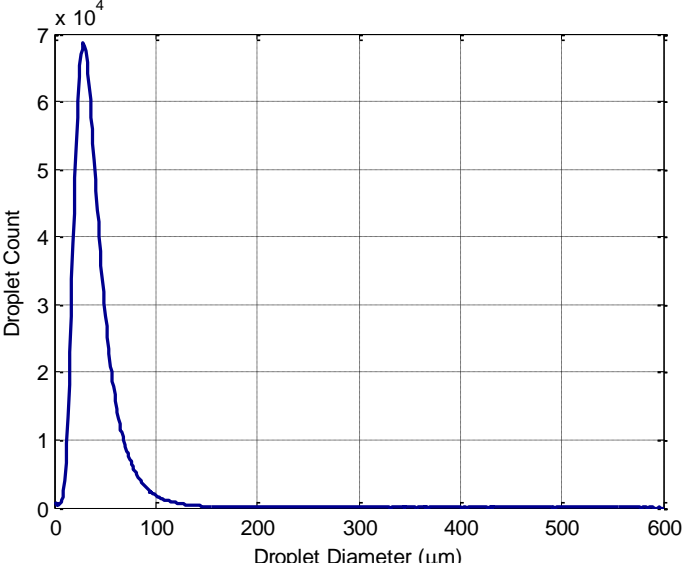
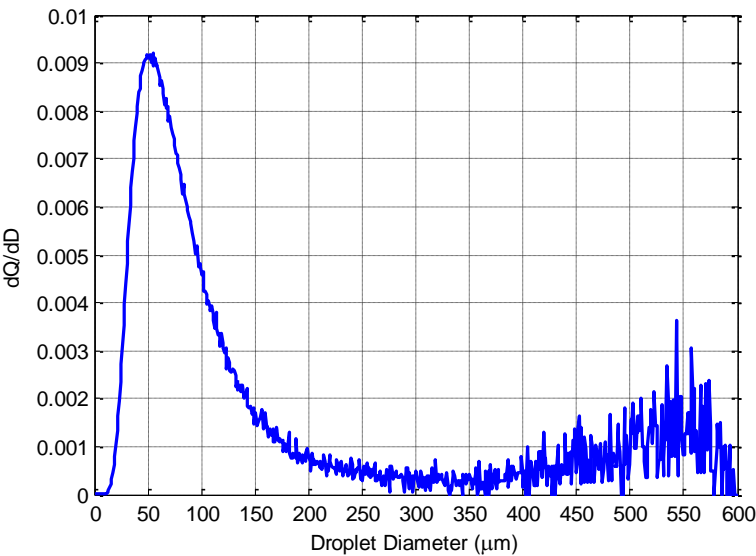
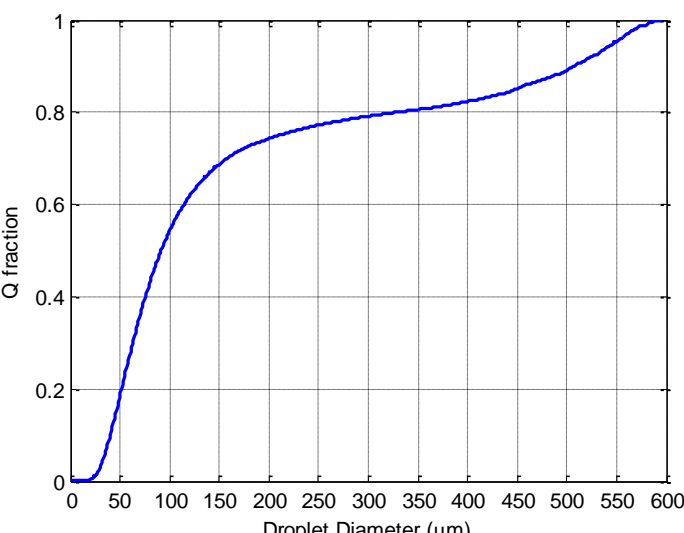
greater than 1 kHz even at the spray edge meaning that the minimum sample size was expected to contain over 5000 droplets. This agreed well with the recommendation of Lefebvre that about 5500 droplets are needed to achieve an estimate of spray quality to within  $\pm 5\%$  of the true value [43]. In practice, sample sizes for all but the very edge of the spray were larger than this recommended figure.

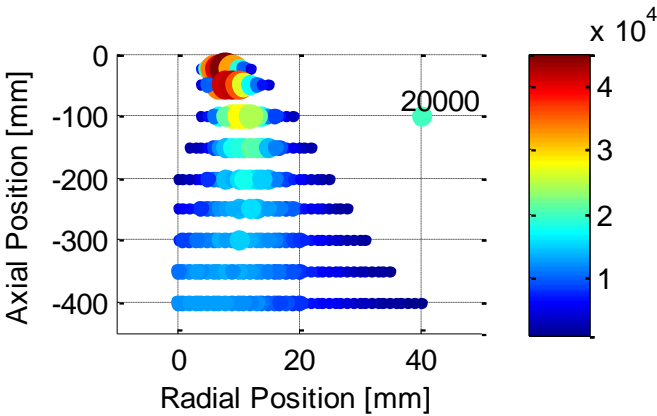
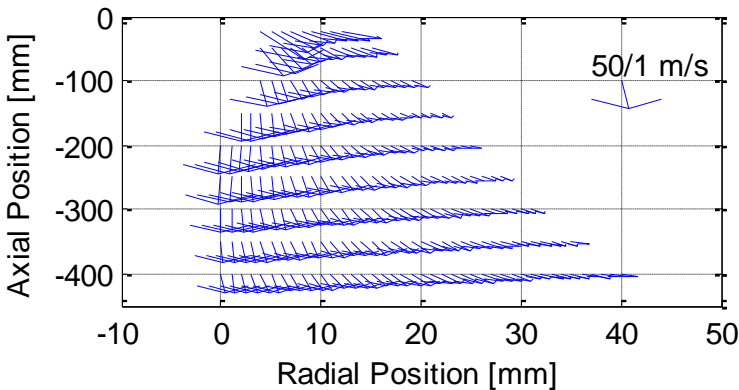
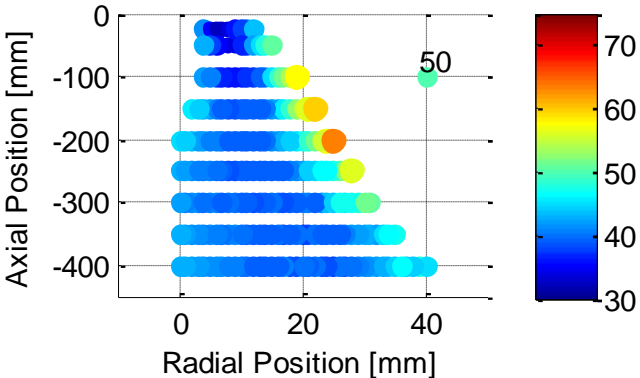
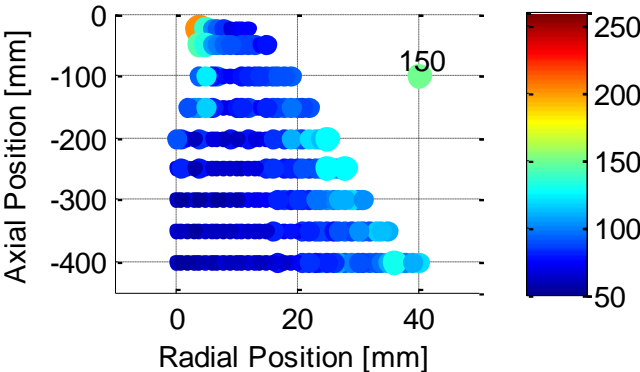
PDA can sample in two different modes: sampling for a fixed time period or until a fixed droplet count is attained. It was decided to sample for a fixed time period at each data point rather than until a fixed sample size (i.e. droplet count) had been reached. This approach was felt to provide better quality data. Due to the nature of effervescent atomisation, the sprays produced (like any other spray) in this study were not homogenous but consisted of more and less dense regions. Therefore sampling for a fixed droplet count would artificially create more data in the less dense regions. These spray locations would contribute equal amounts of data and affect the global spray characteristics, such as global spray droplet SMD. This would provide unrepresentative data. Moreover, sampling for a fixed count still leaves open the question of how to define spray edge at each axial location. Sampling for a fixed time period allows resolution of the spray edge problem by applying the “10% of maximum data rate” criterion. In addition, fixed time PDA sampling avoids biasing the data towards less dense regions of the spray. This approach has been adopted by other researchers [102].

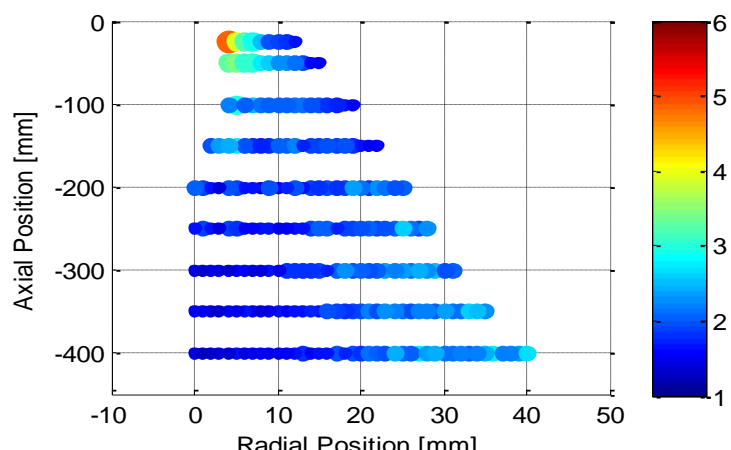
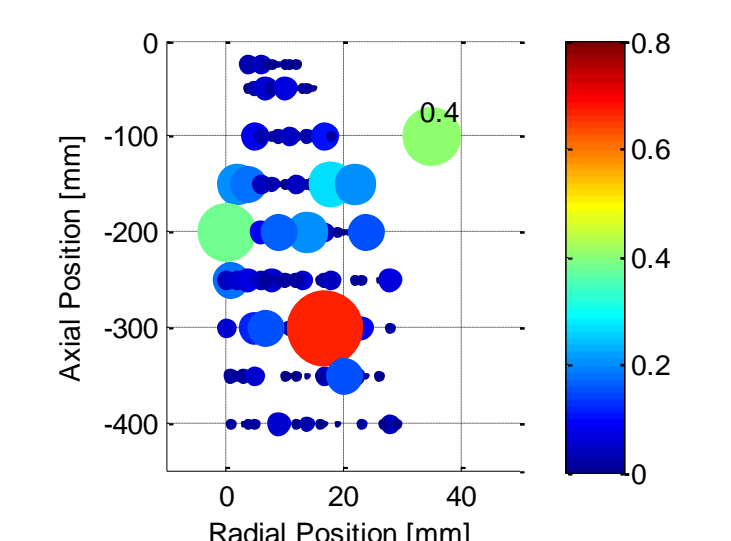
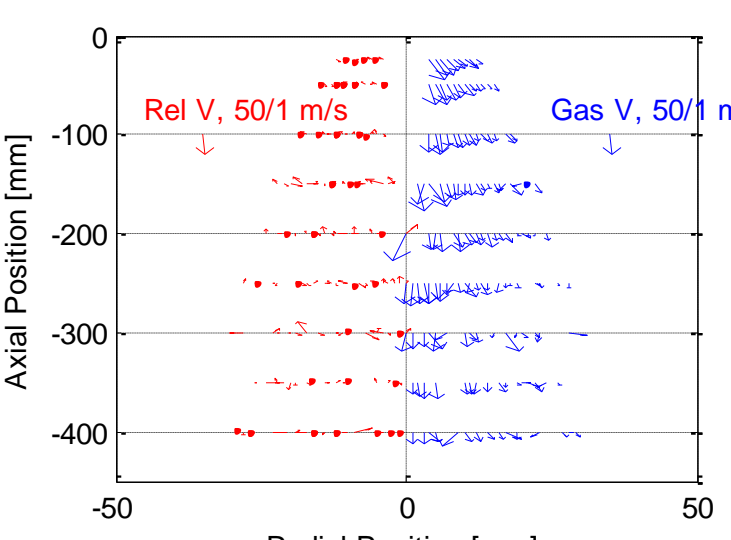
### 3.7 PDA Post-Processing

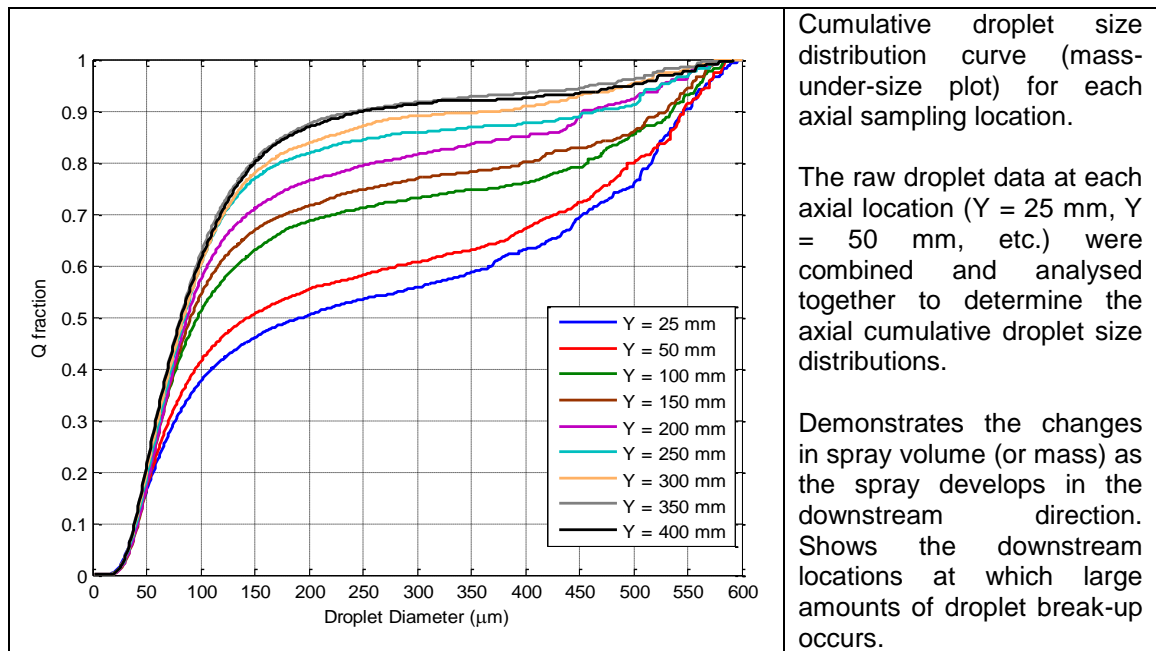
Once the raw droplet data were acquired from PDA tests, they were exported and analysed in MathWorks MATLAB software (R2009b). The results of some typical MATLAB analyses are presented in Table 3.7.1. These graphs could be used to characterise the local and global spray quality of each individual spray. This greatly facilitated comparisons of different sprays. The relevance of each graph (all of which will be used to analyse individual sprays in the results section) is described in Table 3.7.1.

Table 3.7.1. Output of analyses used to characterise and compare sprays.

Analysis Output	Description
	<p>The droplet diameter frequency distribution based on number (size bins 1 µm wide were used in this study).</p> <p>Shows droplet count variation for different droplet diameters. Indicates which droplet diameters within the entire sampled spray, are the most frequent by number.</p> <p>Performed using all sampled points and therefore provides a <b>global</b> characterisation of the spray.</p>
	<p>The droplet diameter frequency distribution based on volume (or mass).</p> <p>Indicates what proportion of the total spray volume (or mass) is contained in droplets of different diameters.</p> <p>Reveals which droplet sizes are providing the largest contribution to the total spray volume (or mass).</p> <p>Performed using all sampled points and therefore provides a <b>global</b> characterisation of the spray.</p>
	<p>Cumulative droplet size distribution curve (also known as the mass-under-size plot).</p> <p>Represents the percentage of the total volume (or mass) of the entire spray contained in droplets smaller than a given diameter.</p> <p>Performed using all sampled points and therefore provides a <b>global</b> characterisation of the spray.</p>

	<p>Plot of validated <b>local</b> droplet count (“cherry” plot) with a reference point of 20000 shown at 40, -100.</p> <p>The x and y axes denote the location within the sampled spray region (Nozzle location: 0,0). Both the size and colour of a given “cherry” corresponds to local droplet count.</p> <p>This plot gives an indication of relatively spray density and/or the spray regions where light attenuation is likely.</p>
	<p>Average <b>local</b> velocity plot (“scatter” plot).</p> <p>The x and y axes denote the location within the sampled spray region. The length of each arrow indicates the average 2D(x-y) droplet velocity at that location.</p> <p>This plot gives an indication of the average droplet motion throughout the spray.</p>
	<p>“Cherry” plot of average <b>local</b> Arithmetic Mean Diameter (AMD).</p> <p>The x and y axes denote the location within the sampled spray region. Both the size and colour of each “cherry” represents the mean droplet diameters at a given location.</p>
	<p>“Cherry” plot of average <b>local</b> Sauter Mean Diameter (AMD).</p> <p>The x and y axes denote the location within the sampled spray region. Both the size and colour of each “cherry” represents the Sauter Mean Diameter at a given location.</p>

	<p>“Cherry” plot of average <b>local</b> SMD/AMD ratio.</p> <p>The x and y axes denote the location within the sampled spray region. Both the size and colour of each “cherry” represents SMD/AMD ratio.</p> <p>This plot indicates the relative spray homogeneity, helping to identify the location of the very large droplets within the spray.</p>
	<p>“Cherry” plot of average <b>local</b> Weber number (<math>We</math>).</p> <p>The x and y axes denote the location within the sampled spray region. Both the size and colour of each “cherry” represents local <math>We</math> (the ratio of inertial to viscous forces acting on the average droplet).</p> <p>This plot indicates whether secondary atomisation occurred throughout the spray.</p>
	<p>Inferred “scatter” plots depicting <b>local</b> gas velocity and <b>local</b> gas-liquid relative velocity (same scale).</p> <p>The x and y axes denote the location within the sampled spray region. The length of each arrow indicates the local average gas and gas-liquid relative velocities respectively.</p> <p>This plot depicts the average entrained gas motion, and shows whether gas-liquid phase slip occurred throughout the spray.</p>



Empirical distribution functions such as the Rosin-Rammler and modified Rosin-Rammler distributions were avoided since they provided a poor fit to the droplet data obtained during preliminary measurements; only the raw droplet diameter distributions are given for all plots shown in this study. Preliminary tests found that empirical distribution functions provided an inadequate fit to most droplet data for the conditions investigated, and as a result these were not utilised.

### 3.8 Experimental Errors

The experimental errors associated with the present investigation result from a number of sources including systematic measurement errors, errors arising from the fluctuations in operating parameters during testing, and errors arising from the estimation of spray characteristics based on a limited number of samples.

#### 3.8.1 Systematic Measurement Errors

- The traverse used to control the receiving and transmitting optics (and therefore the measurement volume) provided a measurement resolution of 0.1 mm, with radial sampling locations spaced 1 mm apart. This allowed spray width to be determined to an accuracy of  $\pm 0.5$  mm which translates into a spray angle error of  $\pm 2^\circ$ .
- The coriolis meters (CMF025) used to measure air and liquid mass flow rate have a combined error (accuracy and repeatability) of up to  $\pm 0.05\%$ .



- The pressure transducer (PTX1400) used to measure air and liquid supply pressure, as well as the pressure drop across the nozzle –  $\Delta P$ , have a combined error (non-linearity, hysteresis and repeatability) up to  $\pm 0.15\%$ .
- The effervescent atomiser tested was manufactured with machining tolerances of  $\pm 0.1$  mm (linear) and  $\pm 0.5^\circ$  (angular). Therefore  $D_O$ ,  $D_{MC}$  were accurate to  $\pm 0.05$  mm;  $L_O/D_O$  was accurate to  $\pm 0.1$ ; the area of the aerator holes may have varied by up to  $\pm 0.1\%$ ; the aerator holes orientation may have varied by up to  $\pm 0.5^\circ$ .
- $L_{MC}$  was measured using a ruler, which provided an error of  $\pm 1$  mm.
- Kinematic viscosity was measured using a Cannon-Fenske Routine Viscometer (range  $3-20 \times 10^{-6} \text{ m}^2/\text{s}$ ) which has a calibration uncertainty (expanded,  $k = 2$ ) of  $\pm 0.156\%$ .
- The PDA system used to obtain the droplet data provided a measurement resolution of  $0.1 \mu\text{m}$ ; it can be shown that for the parameter ranges investigated, this will always result in errors in spray droplet SMD smaller than  $\pm 0.5 \mu\text{m}$  and errors in spray droplet AMD smaller than  $\pm 0.1 \mu\text{m}$ .

### 3.8.2 Operating parameter Fluctuations

All effervescent atomiser tests (excluding the test used to compare effervescent atomiser performance with that of a Y-Jet atomiser) contained 220-270 test points, which were sampled over 5 s. This translated into a total test time of 40-50 minutes for a typical test. During such long testing times the fluid supply pressures and mass flow rates were prone to fluctuate momentarily (e.g. due to pump characteristics), or even to drift. In such cases, in-test corrections (fluid mass flow rates were altered) were necessary to maintain the desired operating conditions. It is clear that although average operating parameters are recorded (ALR,  $\Delta P$ ), the instantaneous values varied throughout the testing process. Analysis of test data has shown that ALR and  $\Delta P$  respectively varied by up to  $\pm 1\%$  and up to  $\pm 0.5$  barG from the average values during a given test. Kinematic viscosity varied by  $\pm 0.5 \times 10^{-6} \text{ m}^2/\text{s}$  at the beginning and at the end of each test.

Despite the presence of operating parameter variations during testing, these are estimated to have had a minor effect on atomiser performance.

### 3.8.3 Limited Sample Sizes

Too small a sample size can lead to inaccuracies in the estimation of spray droplet characteristics. The accuracy of representative droplet diameters (e.g. AMD, SMD) for

95% confidence limits for various sample sizes as estimated by Bowen and Davies [103] and as reported by Lefebvre is given in Table 3.8.1.

Table 3.8.1 The influence of sample size on accuracy representative droplet diameters

<b>Droplets in Sample</b>	<b>Accuracy (%)</b>
500	$\pm 17$
1500	$\pm 10$
5500	$\pm 5$
35000	$\pm 2$

It should be noted that global spray characteristics (e.g. global spray SMD) are based on very large samples (more than 1000000 droplets) and are therefore subject to insignificant experimental error. Local spray characteristics are based on smaller samples, with local droplet count varying from 5000 to 40000 droplets, corresponding to experimental errors of  $\pm 2$ -5%.

Gas and relative velocities are calculated from very small samples (typically less than 50 droplets) and hence will be associated with even greater experimental errors. Errors in relative velocity will also influence the Weber number estimations. It is estimated that gas velocity, relative velocity and Weber number had an experimental error of  $\pm 100\%$ . However, it was not possible to increase the accuracy of the above parameters (by ensuring larger seeding particle samples – particles smaller than 2  $\mu\text{m}$ ) when a sampling time of 5 s was used.

#### **3.8.4 Other Errors**

- The global droplet distributions based on number, mass and the cumulative mass-under-size graphs (which were plotted in MathWorks MATLAB) proved to be very sensitive to the histogram droplet bin width. This was expected. Preliminary investigations were performed using real PDA data sets to study this phenomenon in more detail. It was found that no single droplet bin width could be applied to all data sets to give smooth, continuous distributions (e.g. droplet distributions based on number are a function of droplet diameter whereas droplet distributions based on mass are a function of droplet diameter cubed – the same droplet bin width would provide different effects on both plots). Nevertheless, it was decided to apply one single droplet bin width to all data sets investigated, since attempting to optimise droplet bin width for every droplet distributions based on number and mass, and for every cumulative mass-under-size graph seemed impractical due to the large number of data

sets. Therefore a droplet bin width of 1  $\mu\text{m}$  was applied to all global droplet distributions throughout the present study. This was found to have the effect of providing smooth and continuous global droplet distributions based on number and cumulative mass-under-size graphs; however the global droplet distributions based on mass were usually not smooth at larger droplet diameter ranges, since the droplet counts here were relatively low and the droplet bin width was too small.

- The error associated with a poorly aligned PDA measurement volume results in reductions in data rates and validation rates. This error was minimised by optimising the PDA set-up before each test.
- PDA measurements at  $70^\circ$  from forward scatter rather than at the Brewster angle of  $73.7^\circ$  for a water droplet in air resulted in insignificant experimental errors, since scattering angles of  $25\text{-}75^\circ$  are all suitable when detecting light scattered by first order refraction.
- The PDA software was optimised for collecting light scattered by spherical water droplets in air. However during the kinematic viscosity tests, water-glycerol mixtures were used as the operating fluid. This resulted in a slight variation in the refractive index of the fluid medium (the refractive index of pure water is 1.333 and the refractive index of pure glycerol is 1.470). Nevertheless this can be shown to have an insignificant effect on spray droplet measurements.

### 3.9 Summary

This chapter listed the desired investigation outcomes, and detailed the effervescent atomiser evaluation process. The testing facilities available to perform the current investigation were described. The method by which high-quality 2-D spray data would be obtained (PDA) was explained. Finally, some of the data processing techniques applied to the raw data were presented and potential sources of error were discussed.

## Chapter 4 : Comparison with Industrial Y-Jet Atomiser

### 4.1 Operating Conditions

The effervescent atomiser designed was compared to an industrial-type Y-Jet atomiser. 2-D PDA tests were performed for both atomisers at equivalent operating conditions, using air and water as the operating fluids. The average operating conditions for both tests are summarised in Table 4.1.1.

Table 4.1.1. Effervescent and Y-Jet atomiser operating conditions.

Atomiser	Operating Pressure* (barG)	Liquid Mass Flow Rate (g/s)	ALR (%)	Exit Orifice Diameter (mm)
Effervescent	4.60	40.59	15.79	3.70
Y-Jet	4.50	40.66	13.59	3.66
Difference (%)	2.22	0.17	16.20	1.10

\* Operating Pressure = Effervescent Atomiser Mixing Chamber Pressure,  $\Delta P$ /Y-Jet supply Pressure

Operating pressure in Table 4.1.1 denotes effervescent atomiser mixing chamber pressure,  $\Delta P$ , or Y-Jet supply pressure. Since  $\Delta P$  is measured far from the exit orifice, it was felt that this pressure best corresponds to the supply pressure of the Y-Jet atomiser.

For this experiment, it was considered important to ensure equivalent operating conditions which included: comparable operating pressures and equivalent atomiser capacities (liquid mass flow rates). Similar exit orifice diameters helped ensure equivalent mass flow rates. Meanwhile, there was no control over air-to-liquid by mass ratio (ALR) – an important effervescent atomisation operating parameter. Nevertheless, it can be seen that ALR is broadly similar for both tests. Therefore the above operating conditions can be considered equivalent.

### 4.2 PDA Sampling

As discussed in previous sections, use of the same measurable droplet diameter ranges is vitally important in ensuring an objective comparison between different PDA investigations. Therefore both tests were performed using receiving Mask B, which provided a measurable droplet diameter range of 0.1-300  $\mu\text{m}$ . Sampling was performed at 400 mm downstream of the exit orifice in the traverse positive x-direction, starting at

the spray centreline and up to a radial distance of 50 mm, with radial spacings of 2 mm between each data point. The sampling time was set to 5 s per point.

The selected sampling grid (along a line) could not provide information on downstream spray development; however for the purposes of comparing two stable sprays, the sampling grid was sufficient. The downstream distance chosen was large (over 100 nozzle diameters downstream) and provided a sampling location at which droplet disintegration could be assumed to be largely complete. This assumption seems justified since preliminary investigations have indicated minimal spray development between 350-400 mm downstream of the exit orifice for the effervescent atomiser. Physical constraints did not allow measurements at greater downstream locations.

The investigation was performed without any optimisation of the effervescent atomiser geometry – the baseline mixing chamber and aerator geometries were employed. Only the exit orifice diameter was altered; this was necessary so the required fluid flow rates could be achieved. However, it should be noted that a number of geometric parameters (e.g. aerator geometry, mixing chamber diameter, nozzle length-to-diameter ratio) could be optimised to improve spray quality.

### 4.3 PDA Spray Droplet Data

A comparison of the local droplet SMD and AMD for the effervescent and Y-Jet atomiser sprays is provided in Figure 4.3.1 (where applicable, and where they are large enough to be visible, error bars will be shown on all subsequent graphs).

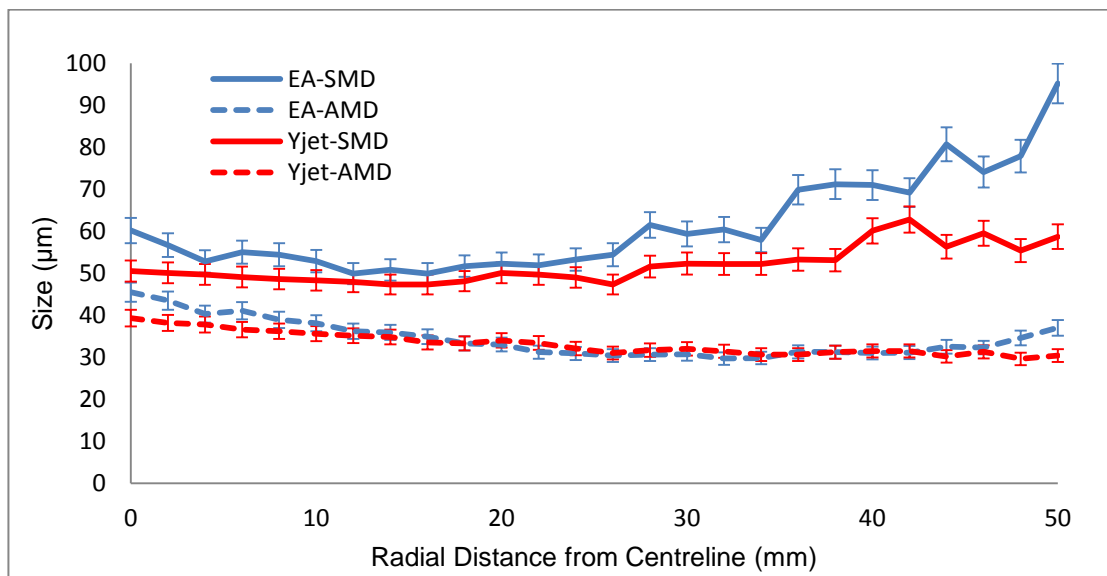


Figure 4.3.1. Local SMD and AMD for the Effervescent and Y-Jet atomiser sprays.

The data seem to indicate that the spray produced by the Y-Jet atomiser was more finely atomised than that of the effervescent atomiser. Local SMD values differ more than AMD, which appear very similar for both sprays. Both sprays display a similar quality of atomisation; however the Y-Jet atomiser does seem to have provided better atomisation, particularly at the spray peripheries. This is likely due to a slightly greater number of larger droplets at the effervescent atomiser spray periphery. Increasing numbers of larger droplets at the effervescent atomiser radial spray periphery have already been observed in the present tests.

The main advantage of the Y-Jet spray can therefore be seen to be the greater droplet homogeneity at the spray periphery. A clearer view of local droplet consistency is provided by Figure 4.3.2.

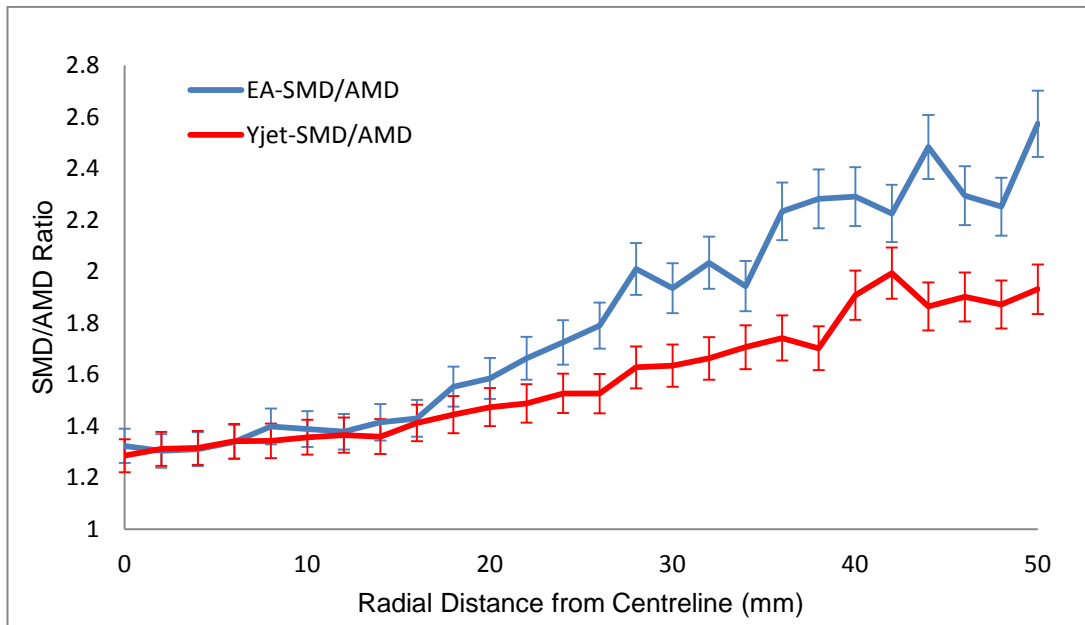


Figure 4.3.2. Local droplet SMD/AMD ratio for the Effervescent and Y-Jet atomiser sprays.

An SMD/AMD ratio of close to unity indicates perfectly uniform droplets and a narrow range of droplet sizes; large SMD/AMD ratios indicate a wide range of droplet sizes present. Figure 4.3.2 shows that both sprays display good droplet consistency nearer the spray centreline, and both become increasingly less consistent in the radial direction. However, the Y-Jet spray is clearly the more consistent (and therefore better atomised) at this distance from the nozzle.

Despite the above results, the limitations of sampling to a fixed radial location should be noted. For example, a radial distance of 50 mm is very close to the spray edge of the effervescent atomiser spray (as defined by the “10%-of-maximum-data-rate” rule, which will be used to define radial spray edges for the tests presented in Chapters 5, 6

and 7), but not of the Y-Jet spray. At 50 mm in the radial direction, the local effervescent atomiser data rate falls to 12% of the maximum, but for the Y-Jet spray the local data rate at this location is still 28% of the maximum. Clearly at the conditions and axial location investigated, the Y-Jet spray is wider. At radially distant spray locations, data rates are low and local spray quality becomes increasingly poorer. Therefore sampling to a fixed radial location somewhat biases the droplet data in favour of the wider spray. In the present example, the Y-Jet spray should ideally be sampled to a radial location where a local data rate equivalent to that of the effervescent atomiser is attained. This approach would result in a greater number of large spray edge droplets, and would appear to worsen Y-Jet spray quality. This would make both sprays somewhat more similar than they currently appear. Nevertheless, sampling to a fixed radial location provides a useful comparison for practical atomiser applications, where the physical (and not idealised) spray is important, and where physical dimensions (and constraints) can be significant.

The local droplet data for each spray were compiled and analysed to determine global spray characteristics. The global droplet distributions based on droplet mass are presented in Figure 4.3.3.

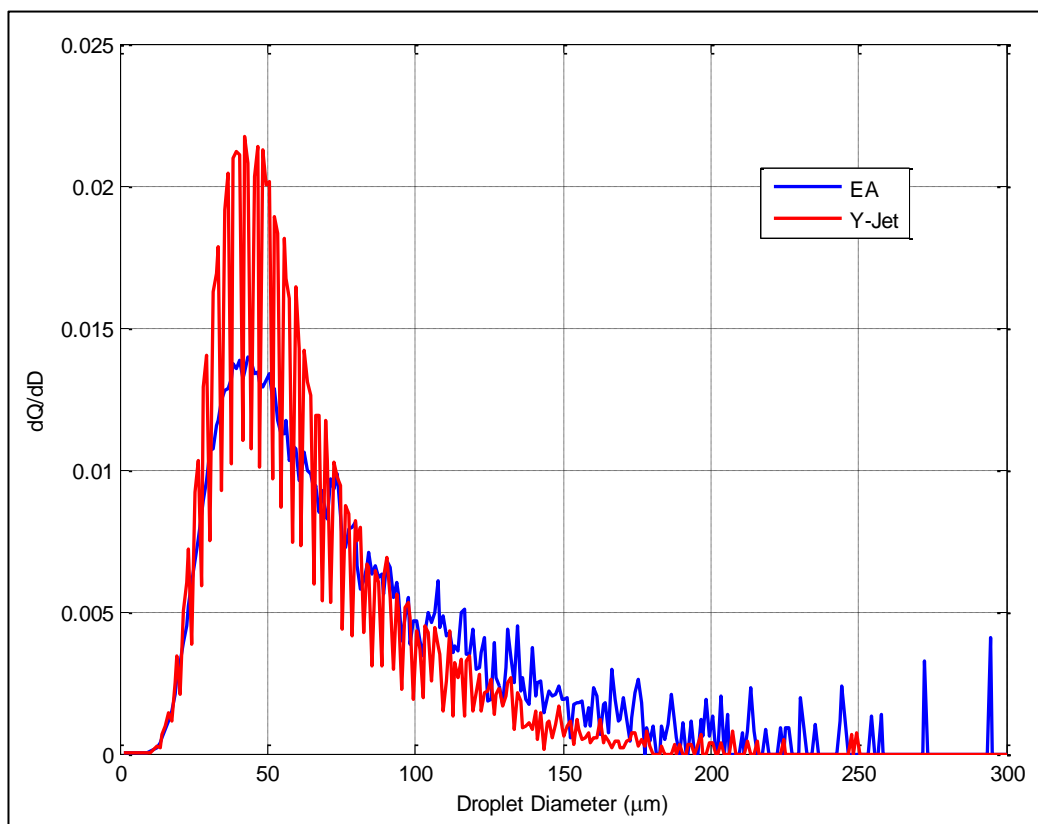


Figure 4.3.3. Global droplet distributions based on mass, for a Y-Jet and an effervescent atomiser.

Figure 4.3.3 indicates that the Y-Jet spray mass was contained in a larger proportion of smaller droplets and in a smaller proportion of larger droplets, compared to the effervescent atomiser spray. This illustrates the previously noted improved atomisation provided by the industrial-type Y-Jet atomiser.

The cumulative mass-under-size plots for both sprays are given in Figure 4.3.4.

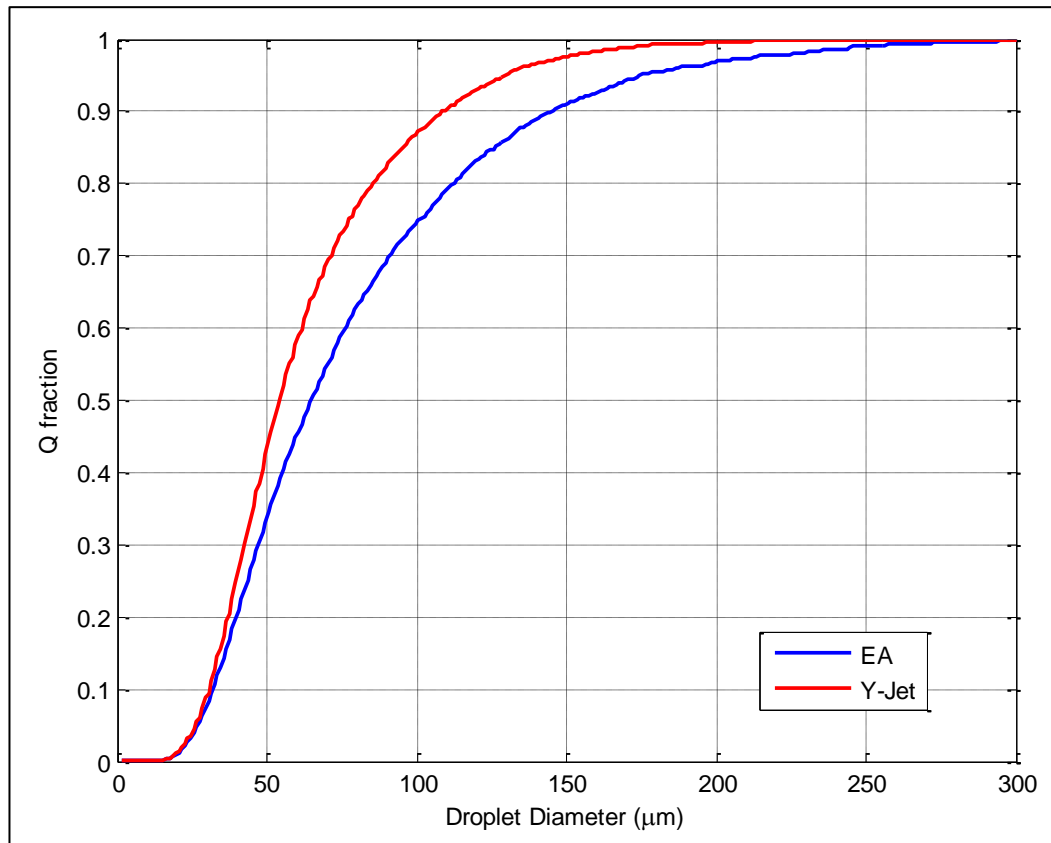


Figure 4.3.4. Cumulative mass-under-size plots for a Y-Jet and an effervescent atomiser.

Figure 4.3.4 indicates a greater proportion of small droplets in the Y-Jet atomiser spray and a smaller proportion of large droplets. Almost no droplets larger than 200 µm are visible. Meanwhile the effervescent atomiser spray clearly contains droplets nearly 300 µm in diameter.

Representative droplet diameters were calculated from the global mass-under-size plots of both sprays. These are summarised in Table 4.3.1 ( $\pm 5\%$  experimental error).  $D_{10\%}$  represents the droplet diameter below which 10% of the spray mass is contained;  $MMD (=D_{50\%})$  is the mass median diameter;  $D_{90\%}$  represents the droplet diameter below which 90% of the spray mass is contained.

Table 4.3.1 indicates a growing difference between the representative droplet diameters of the Y-Jet and effervescent atomiser sprays. This demonstrates that the Y-



Jet spray droplet data groups together into tighter diameter ranges, while the effervescent atomiser data is composed of a larger range of droplet sizes.

The location of the large effervescent atomiser droplets is clear – these occur at the radially distant spray regions. The relatively larger momentum of bigger droplets carries them to the spray edges. This phenomenon (large spray edge droplets), already observed in the effervescent atomiser spray investigations, appears less prominently in the Y-Jet atomiser spray investigated. As discussed, this is partly a result of the different spray dimensions at an axial distance of 400 mm. Since the Y-Jet spray is wider, a more central and consistent portion of this spray is sampled by measuring up to 50 mm from the centreline. The superior performance of the Y-Jet atomiser is therefore slightly exaggerated by the sampling procedure.

Table 4.3.1. Representative droplet diameters of Y-Jet and Effervescent Atomiser sprays.

<b>Atomiser</b>	<b>D<sub>10%</sub> (µm)</b>	<b>SMD (µm)</b>	<b>MMD (µm)</b>	<b>D<sub>90%</sub> (µm)</b>
Effervescent	31.50	57.20	64.50	144.50
Y-Jet	30.50	50.45	54.50	108.50
Difference (%)	3.28	13.38	18.35	33.18

Nevertheless, it is still clear that the Y-Jet atomiser provided marginally better atomisation over the operating conditions investigated. For example Figure 4.3.1 demonstrates the lower local droplet SMD of the Y-Jet spray even at regions close to the spray centreline.

However, optimisations to the effervescent atomiser are clearly possible, which will result in improved atomisation performance. This can help make the adjustable atomiser designed much more competitive compared to traditionally used atomiser types, such as the Y-Jet atomiser analysed.

Optimisations to the effervescent atomiser will be possible after detailed investigations into the effects of operating parameters, atomiser geometry and fluid properties on spray quality. These will be performed in Chapters 5, 6 and 7, respectively.

## Chapter 5 : Results – Operating Parameters

### 5.1 Test Phase No.1 – Air-to-Liquid-by-Mass Ratio (ALR)

#### 5.1.1 Preliminary Investigations

Table 5.1.1 illustrates the position of the ALR tests within the study program, as well as the expected values of the controlled parameters.

Table 5.1.1 Operating conditions and controlled parameters for ALR tests.

TEST No. PARAMETER VARIED	1 ALR	2 $\Delta P$	3 $D_o$	4 $L_{MC}$	5 $D_{MC}$	6 $L_o/D_o$	7 A. GEOM.	8 $\eta$
TEST PHASE	A. Initial Operating Parameters		B. Atomiser Geometry					C. Fluid properties
ALR (%)	0.8-12.5	2		2				
$\Delta P$ (bar.g)	7	4-7		7				
$D_o$ (mm)	2	2	2-4	2	2	2	2	2
$L_{MC}$ (mm)	140	140	140	64-140	140	140	140	140
$D_{MC}$ (mm)	25.4	25.4	25.4	25.4	20-30	25.4	25.4	25.4
$L_o/D_o$ (-)	1	1	1	1	1	0.5-2	1	1
Aerator Geometry	A1	A1	A1	A1	A1	A1	A2, A3	A1
$\eta \times 10^{-8}$ (m <sup>2</sup> /s)	1	1	1	1	1	1	1	2-10

The effervescent atomiser performance was first investigated by undertaking preliminary tests. These helped develop maps of spray quality at the required operating conditions, such as Figure 5.1.1 and Figure 5.1.2. These were used to determine operating conditions which provided a stable spray for PDA analysis. The region within which stable (i.e. steady-state, non-pulsing sprays) effervescent atomisation was achieved is shown bounded by dashed lines and marked “EA”.

It was found that stable operation was only achievable for a certain range of pressures, flow rates and ALRs. As expected, ALR increases improved spray quality. Perhaps surprisingly, ALRs below about 2% could not achieve well-atomised sprays even at high operating pressures. In this region atomisation quality worsened with large droplets and an intact liquid core beginning to appear as ALR was sufficiently lowered. This is similar to the performance of other twin-fluid atomisers. For example, Lefebvre reports that air-blast atomisers, whose ALR ranges overlap with those of effervescent atomisers, experience a considerable deterioration in performance below 2% air-to-liquid by mass ratio [43].

The region marked “transition” is where unsteady, pulsing sprays begin to give way to a steady, stable spray.

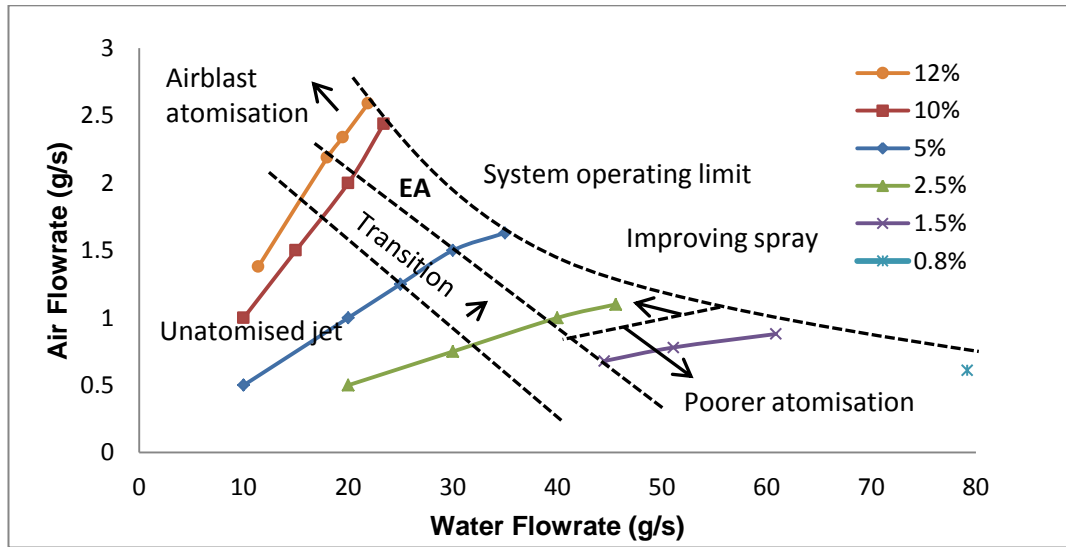


Figure 5.1.1 Graph of “spray quality” showing liquid flow rates at which optimal effervescent atomisation can be achieved for ranging ALR.

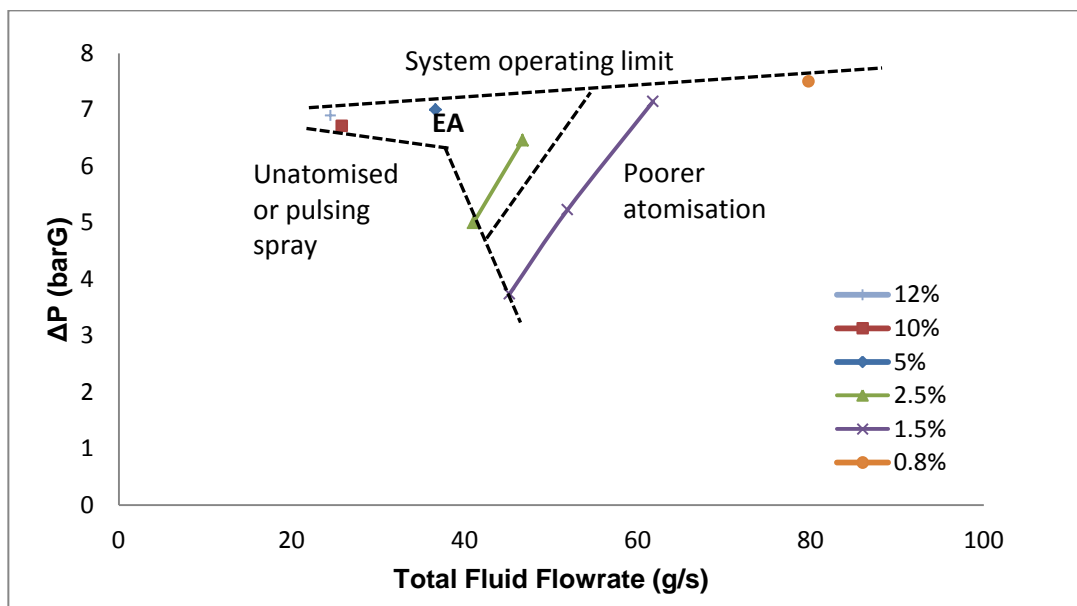


Figure 5.1.2 Graph of “spray quality” showing mixing chamber pressure and total flow rates at which optimal effervescent atomisation can be achieved for ranging ALR.

Since  $\Delta P$  (pressure drop across the nozzle) is a primary operating parameter, it was decided that the sampled sprays of the ALR tests should fall along a line of constant  $\Delta P$  within the band of stable effervescent atomisation. The positions of the five tests within test phase no.1 (see Table 5.1.1) are shown in Figure 5.1.3 and Figure 5.1.4. These Figures show that the above tests were performed at a range of ALRs but at constant mixing chamber pressures.

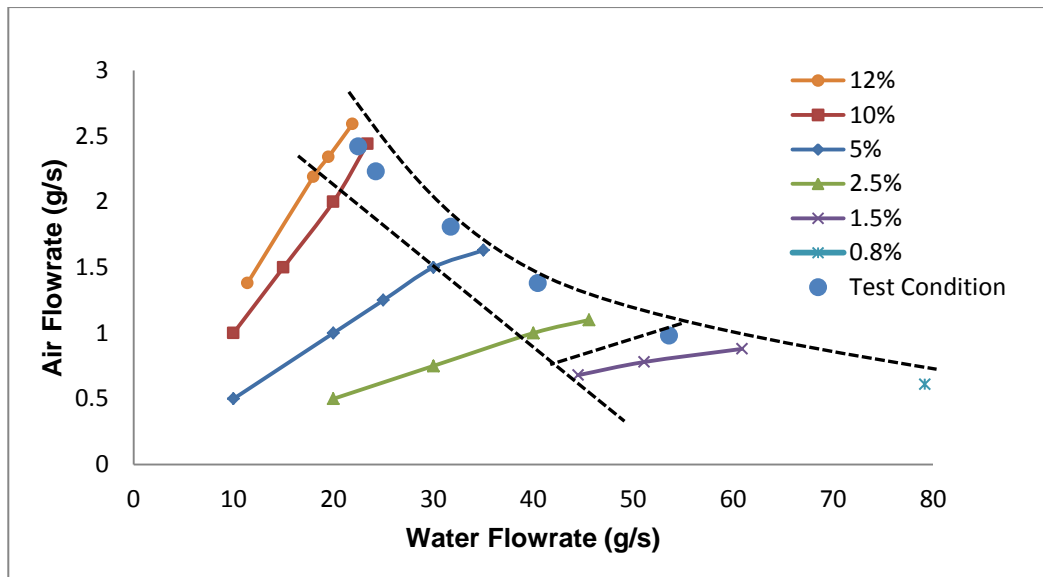


Figure 5.1.3 Graph of “spray quality” showing liquid flow rates and ALRs at which tests were performed for ranging ALR.

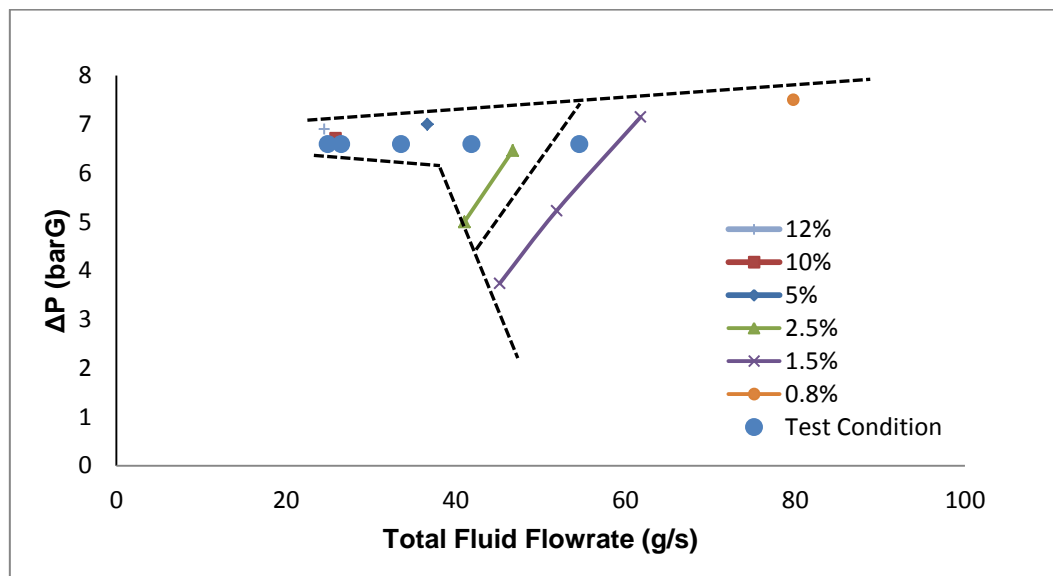


Figure 5.1.4 Graph of “spray quality” showing mixing chamber pressures and total flow rates at which tests were performed for ranging ALR.

### 5.1.2 Assumptions

In order to calculate air density, air and liquid velocities, fluid ligament diameter, void fraction, Reynolds number, Weber number and Ohnesorge number at the nozzle, continuity was applied to the two-phase flow at the nozzle and the following assumptions were made:

- The air and liquid phases travel through the nozzle at velocities that follow Ishii’s slip ratio correlation for annular flow in pipes [104].

- Thermal equilibrium exists at the nozzle with no heat or mass transfer between phases.
- The air bubbles obey the ideal gas laws and behave in an isentropic manner (no energy lost to the environment).

This was similar to the approach used by other researchers to model effervescent atomisation nozzle flow [35, 83].

Meanwhile global SMD values, calculated from the raw PDA droplet data using all data points sampled within a given spray, were determined using the formula given in Equation 5.1.1.

$$SMD = \frac{\sum_{i=1}^{i=N} n_i D_i^3}{\sum_{i=1}^{i=N} n_i D_i^2} \quad \text{Equation 5.1.1}$$

Where  $D_i$  is the diameter of the class size  $i$ ,  $n_i$  is the number of droplets in each size class and  $N$  is the total number of droplets.

A number of effervescent atomiser droplet SMD correlations from the literature were compared to the current experimental data. Two of these correlations required a process efficiency factor (a coefficient describing the efficiency of the assumed atomisation process). Process efficiencies of 1-100% were investigated; the efficiency coefficient giving SMD predictions most consistently matching the PDA data was used for comparison purposes.

Reynolds number, Weber number and Ohnesorge number were calculated using Equation 5.1.2, Equation 5.1.3 and Equation 5.1.4.

$$Re = \frac{\rho_l U_{av,rel} d_{av,lig}}{\mu_l} \quad \text{Equation 5.1.2}$$

$$We = \frac{\rho_l U_{av,rel}^2 d_{av,lig}}{\sigma_l} \quad \text{Equation 5.1.3}$$

$$Oh = \frac{\mu_l}{\sqrt{\rho_l \sigma_l d_{av,lig}}} \quad \text{Equation 5.1.4}$$

The subscripts indicate the following:  $l$  – liquid;  $av$  – average;  $lig$  – liquid ligament;  $rel$  – relative. Relative velocity at the nozzle is then the difference between the calculated liquid and gas velocities.

### 5.1.3 Spray Characteristics and Results

The results are displayed in Table 5.1.2 (all to 2 d.p. excluding volumetric void fraction –  $\alpha$ , Re, We, Oh). Throughout the tests  $\Delta P$  was maintained at a pressure of  $6.59 \pm 0.13$  barG which corresponds to a  $\Delta P$  variation of up to 4% between tests. Meanwhile the investigated parameter, ALR, varied by 510% (where a variation of 100% indicates a doubling of ALR) over the full range of values investigated. Therefore the effects of ALR variation were dominant.

Table 5.1.2 Summary of average ALR test operating conditions and spray characteristics.

Test	1.83 % ALR	3.41 % ALR	5.70 % ALR	9.34 % ALR	11.11 % ALR
Water Supply Pressure (barG)	7.47	7.43	7.38	7.16	7.17
Mixing Chamber Pressure $\Delta P$ (barG)	6.68	6.66	6.65	6.46	6.51
$m_{\text{WATER}}$ (g/s)	53.58	40.47	31.75	24.26	22.50
$P_{\text{AIR}}$ (barG)	7.01	6.97	7.23	7.05	7.11
$m_{\text{AIR}}$ (g/s)	0.98	1.38	1.81	2.23	2.42
Volumetric Void Fraction, $\alpha$ (%)	66.6	78.6	86.1	91.0	92.2
Effective Power Rating (MW)	2.14	1.62	1.27	0.97	0.90
Coefficient of Discharge (-)	0.47	0.35	0.28	0.22	0.20
$\theta/2$ at 25 mm downstream (deg)	27.47	27.47	25.64	25.64	25.64
Liquid Re at Nozzle	22369	26219	29176	29596	29819
Liquid We at Nozzle	8033	14002	21439	27671	30627
Liquid Oh at Nozzle	0.004007	0.004513	0.005018	0.005621	0.005869
$D_{32}$ ( $\mu\text{m}$ )	135.79	98.45	81.06	72.60	69.40

### 5.1.4 Nozzle Coefficient of Discharge

Varying ALR between 1.83% and 11.11% at a constant  $\Delta P$  achieved a turndown ratio of 2.38 (based on water mass flow rates) and corresponded to a power rating range of 0.9-2.14 MW. Accompanying this were relatively low coefficients of discharge ranging from 0.2-0.47 (calculated using measured liquid mass flow rate, measured density, measured mixing chamber pressure and exit orifice diameter; a commonly used coefficient of discharge equation was employed - relating actual to idealised theoretic nozzle throughput [43]). Such low values are to be expected for a twin fluid atomiser. Calculations revealed that operation was accompanied by relatively large volumetric

void fractions at the nozzle, ranging from 66.6-92.2% over the conditions examined. This large air-phase contribution at the nozzle ensured low coefficients of discharge. The experimentally determined values of discharge coefficient, as well as predictions given by effervescent atomiser correlations in the literature are illustrated in Figure 5.1.5. The correlation most accurately matching the experimental data is the one provided by Chen et al [55]. Nevertheless this correlation consistently over-predicted the coefficient of discharge by up to 20%. The correlation of Chin et al predicted coefficients of discharge greater than unity. Closer inspection revealed that this was likely due to flow conditions in the current tests being outside the ranges investigated by Chin et al. A decreasing coefficient of discharge (as ALR was increased) was expected.

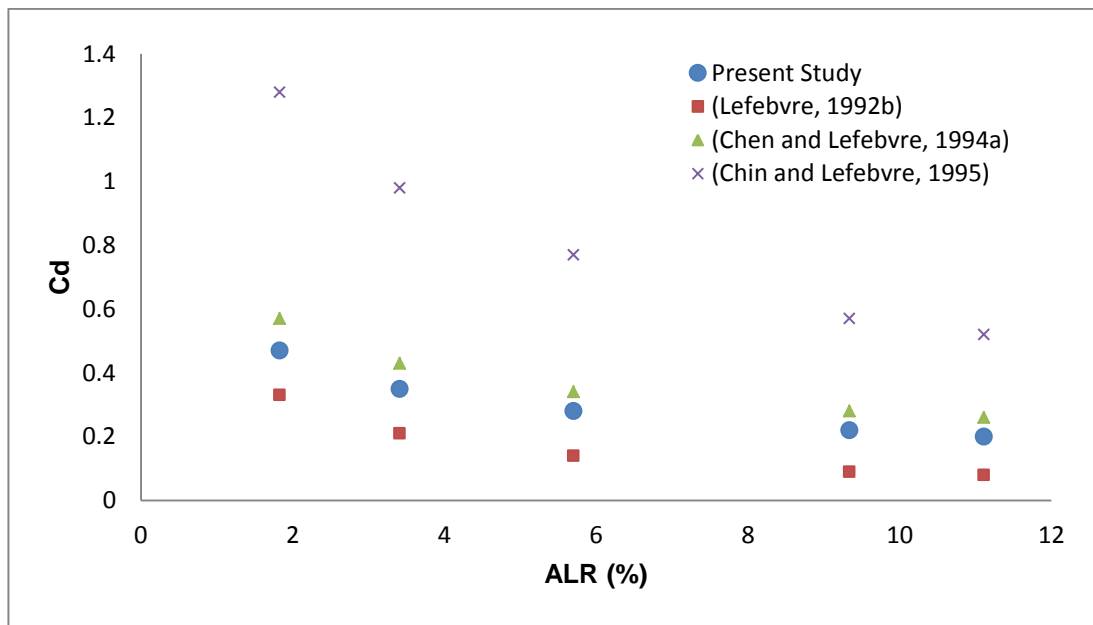


Figure 5.1.5 Comparison of coefficient of discharge for ALR experiments and of predictions of correlations in the literature for present operating conditions.

### 5.1.5 Mode of Liquid Break-up at Nozzle

The fluid disintegration analysis presented is usually performed on single-phase liquid jets as demonstrated in the literature review chapter. However given photographic evidence of co-annular nozzle flow in effervescent atomisation [61], and in keeping with effervescent atomisation researchers who analysed air and liquid phases separately [35, 83], it seemed justified to adopt a similar approach and calculate the dimensions and properties of each phase individually. The assumptions involved in this analysis have already been listed. The theoretical air and liquid characteristics at the nozzle were then calculated allowing the analysis of Reitz as given by Lefebvre [43] to be

applied. The results of this analysis are displayed in Figure 5.1.6, which demonstrates the mode of liquid disintegration at the nozzle according to the classification of Reitz.

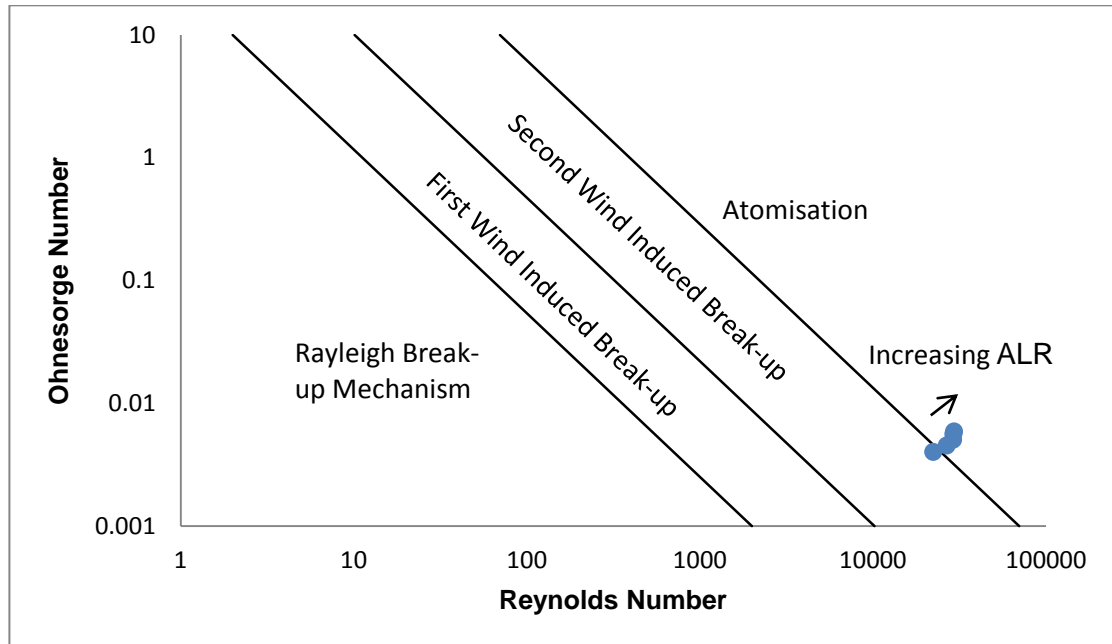


Figure 5.1.6 Calculated liquid disintegration mode for ALR experiments.

According to this classification, the ALR tests were characterised by liquid break-up in both the “second wind induced break-up” and the “atomisation” modes. According to Lefebvre the dominant droplet formation mechanism in second wind induced break-up mode is due to slip between the gas and liquid phases causing an unstable growth of short-wavelength surface waves around the liquid ligaments. Break-up is expected several diameters downstream of the nozzle. The atomisation regime is characterised by liquid disintegration at the nozzle and smaller average droplet diameters [43].

It seems likely that the 1.83% ALR spray (possibly also the 3.41% ALR sprays) with its comparatively poorer atomisation corresponded to operation in the “second wind induced break-up” mode (characterised by the bubble-bursting regime) while the higher ALR sprays corresponded to operation in the “atomisation” mode (characterised by the tree-like atomisation regime). As the ALR was increased second wind induced break-up gave way to the atomisation mode of liquid disintegration. Figure 5.1.6 therefore provides a justification for the unatomised liquid core still visible at ALRs less than about 2% which shortened as ALR was increased, and disappeared altogether at higher ALRs. Conversely, according to this analysis, higher ALR sprays display better atomisation since increasing ALR pushed operation further into the desirable atomisation mode and improved local and global spray quality.



The Reynolds, Weber and Ohnesorge numbers (for this injector) obtained from analysis of each fluid phase individually have been presented in Table 5.1.2. The high values of liquid Reynolds number indicate highly turbulent liquid flows at the nozzle with large radial components of velocity. A highly turbulent liquid jet or ligament does not require the action of aerodynamic effects but will disintegrate under the sole influence of its own turbulence. The large Weber numbers show that the inertial forces acting on the liquid at the nozzle were much larger than the restraining effects of surface tension. At such high Weber numbers the liquid ligaments would be unstable and subject to disintegration under the impact of their own inertial forces. As expected, higher ALR sprays were associated with larger values of Reynolds and Weber number, or in other words, greater turbulence and greater liquid ligament instability.

### **5.1.6 Spray Half-Angle**

Previous experiments indicated axisymmetric sprays could be assumed [100]. Therefore only half of the spray was analysed (a slice through that spray portion most clearly visible to the PDA) and from this the spray half-angle could be calculated. Because the spray angle produced by the effervescent atomiser appeared relatively consistent over time and was axisymmetric, the spray angle was assumed to equal twice the half-angle.

Spray half-angle was defined as the angle subtended by the spray axis and a tangent which touched the spray edge (as defined in previous sections, i.e. based on validated PDA data rates) at an axial distance of 25 mm from the nozzle (corresponding to a downstream distance of  $12.5D_0$  for the nozzle used in the ALR tests). This arbitrary distance was motivated by a desire to use spray dimensions closer to the nozzle and before gravity and aerodynamic effects began to influence droplet motion. An advantage of this approach is that it defines spray dimensions close to the nozzle, an important consideration for practical atomisers.

Use of this definition gave a relatively constant medium sized spray half-angle of 25-28° (to the nearest whole degree). This was about twice as large as the spray half-angle results presented by previous effervescent atomiser researchers [70, 80, 86] and larger than Lefebvre's claim of a relatively constant spray angle of 40° [54]. However this discrepancy is not surprising since previous researchers measured spray angle further downstream and used different criteria to determine the spray edges.

The correlation provided by Sovani et al is shown in Figure 5.1.7 and is compared to the experimental data. This correlation did not match the experimental values well but consistently under-predicted spray half-angles by a factor of four. The large variation

between spray angle in the literature and the results provided by this study are most likely a result of the different spray edge definitions and measurement locations used. For example, the spray half-angles in the present study reduce to 5-7° if the spray edge at 400 mm downstream of the exit orifice (instead of at 25 mm downstream) is used.

Spray half-angle appeared to reduce slightly as ALR was increased. However, it should be remembered that the spray width at an axial distance of 25 mm varied by only 1 mm for all sprays presented. The true location of the data rate minimum (and from this spray edge) can only be determined to an accuracy of  $\pm 1$  mm when using discrete PDA sampling locations spaced 1 mm apart. Therefore the apparent decrease in spray half-angle may be at least in part an artefact of the experimental technique.

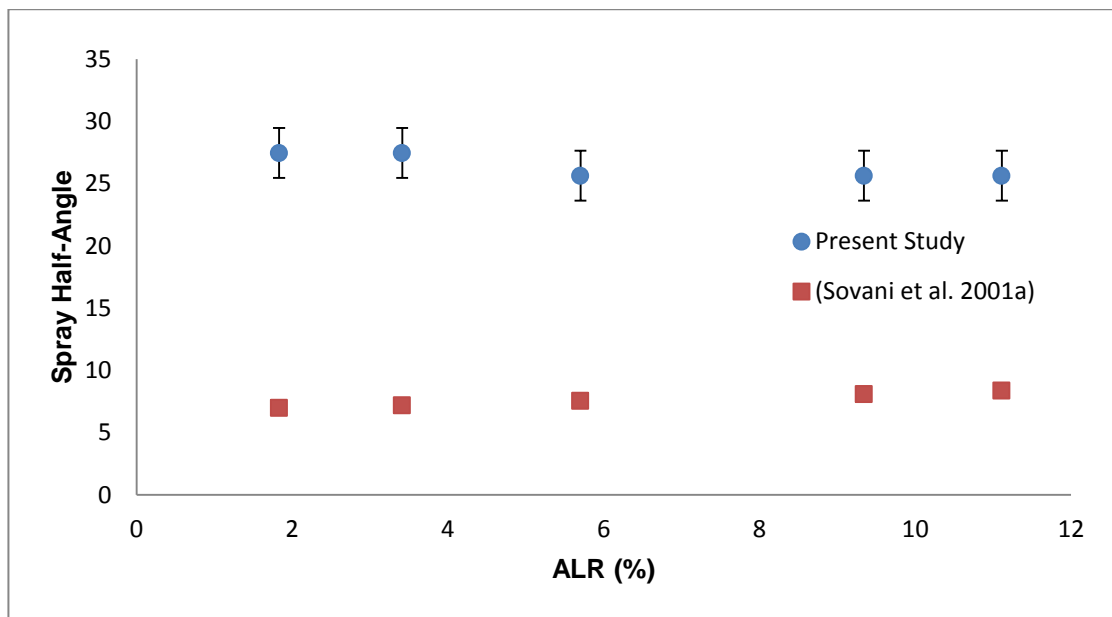


Figure 5.1.7 Comparison of spray half-angle from PDA experiments and literature.

### 5.1.7 Spray Droplet Size Distribution by Number

The droplet diameter frequency-by-number distributions (a global distribution), demonstrated in Figure 5.1.8 appear similar, with distribution shapes and location of maximal peaks comparable for all ALRs. Size bins 1  $\mu\text{m}$  wide were used for all distributions throughout this study.

By number, the majority of the droplet diameters were less than 100  $\mu\text{m}$  for all test cases, with the absolute number of droplets within the larger diameter ranges extremely small. Droplets larger than 180  $\mu\text{m}$  are not visible in this plot.

The varying amplitude of the peaks was a function of the varying sample sizes. Absolute sample sizes were affected by a range of factors including quality of the PDA

setup, different spray densities and validation rates, different spray cone angles (therefore different spray widths and sampling location numbers) as well as instantaneous fluctuations in liquid mass flow rates.

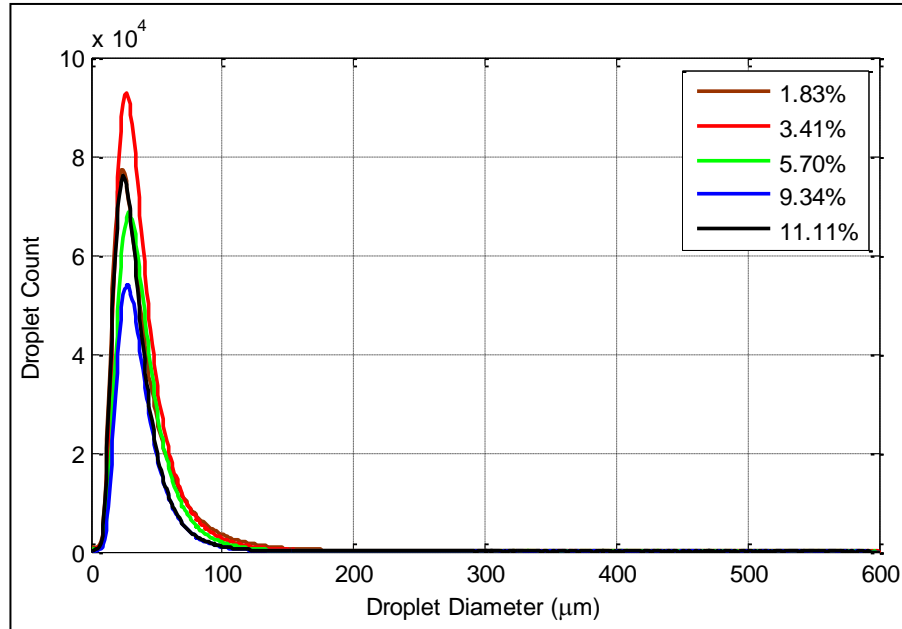


Figure 5.1.8 Droplet diameter frequency distribution based on number.

### 5.1.8 Spray Droplet Size Distribution by Mass

The droplet diameter frequency-by-mass distributions (a global distribution) look considerably different from the frequency distributions by number. The former are shown in Figure 5.1.9.

A significant spray mass was contained in droplets up to 600  $\mu\text{m}$  which was the measurement limit of the optical setup used. This was the case even for the best atomised sprays. The wide range of diameters measured is in keeping with the droplet diameter ranges known to be produced by traditional liquid fuel atomisers, even at optimal operating conditions. For example, conventional atomiser types consistently produce sprays with droplet diameter ratios of at least 100:1 [46].

It should be noted that a very small number of droplets can provide a substantial proportion of the sampled spray mass. For example, only 0.2% of the total droplets in the 1.83% ALR spray (expected to be the most poorly atomised) were contained in droplets larger than 300  $\mu\text{m}$ ; however this accounted for 40% of the sampled spray mass. Meanwhile 0.04% of the droplets in the 11.11% ALR spray had a diameter greater than 300  $\mu\text{m}$ , which represented 16% of the total spray mass.

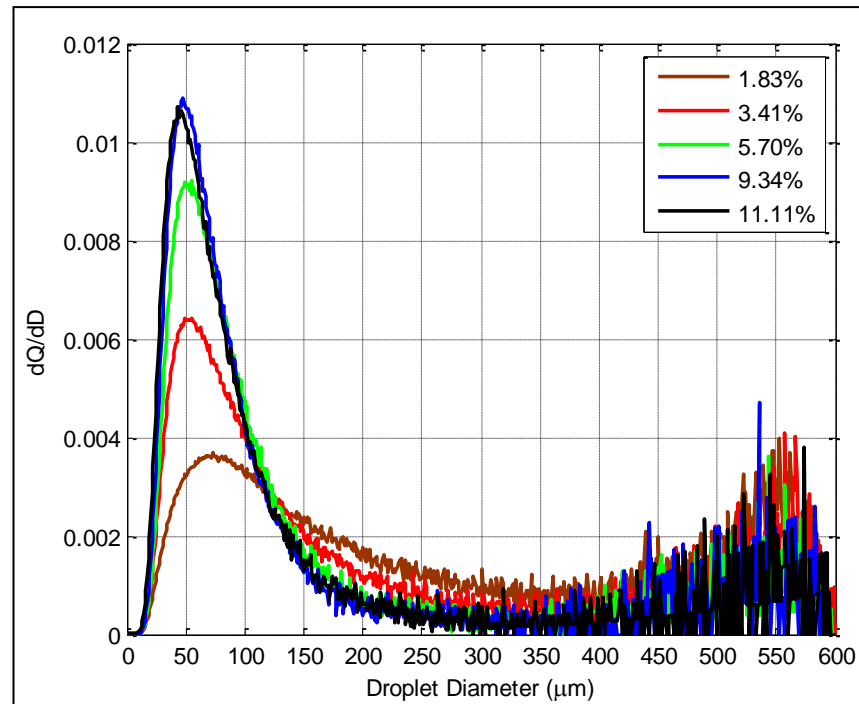


Figure 5.1.9 Droplet diameter frequency distribution by mass.

The sprays in Figure 5.1.9 appear bimodal, a consequence of spray mass being a function of droplet diameter cubed. Since larger droplets can carry a considerably greater mass than smaller ones, only a few larger droplets can create prominent peaks at the upper measurement limits. For instance, one droplet with a diameter of 500  $\mu\text{m}$  contains  $(100)^3$  times more mass than one 5  $\mu\text{m}$  diameter droplet. This trend becomes more extreme at settings with even larger measurable droplet diameter ranges.

All sprays investigated seemed to possess similar absolute numbers of droplets in the range over 350  $\mu\text{m}$ . The effect of increasing the ALR therefore appeared to be that of greatly increasing the absolute spray mass contained in smaller droplets without drastically reducing the absolute spray mass contained in larger droplets. This supports the view that effervescent atomisation (like other types of atomisation) is a process which naturally produces a wide range of droplet sizes, even at optimal operating conditions.

However, it is clear that the higher ALR sprays (5.70%, 9.34% and 11.11%) contained an increasingly larger absolute mass and proportion of droplets in the lower droplet diameter ranges. This is consistent with the improved atomisation expected at higher operating ALRs.

### 5.1.9 Choice of PDA Settings

It could be argued with reference to Figure 5.1.9 that not all the spray data was captured and that even larger droplet ranges need to be investigated. However, as discussed above, at very large droplet diameter ranges, a statistically small number of very large droplets can have a great influence on the spray results. The present sampling range of 0-600  $\mu\text{m}$  already provides a measurable droplet range ratio of close to 1000:1. At these settings one extremely large droplet can provide as much mass as over  $(1000)^3$  droplets at the lower end of the measurable range. One single very large droplet could significantly influence representative droplet diameter values and may adversely affect experimental repeatability, if the largest droplets occur rarely and sampling times are short enough. This effect becomes more extreme at greater measurable diameter ranges.

Performing measurements at larger droplet ranges also reduces the resolution of the diameter-phase relationship causing a reduction in validation and data rates. This was confirmed by preliminary experiments where tests with both Mask B and C were performed. Doubling the diameter ranges (maximum measured data increased from about 270 to 600  $\mu\text{m}$ ) reduced the data rates by a factor of three for identical conditions and for the same set-up quality. Increasing the diameter ranges further would have reduced the validation and data rates even more. To compensate for this larger sampling times might be needed.

Another disadvantage of extending the measurable droplet ranges is that it biases the PDA towards measuring larger droplets since the light they present to the photo detectors is much more prominent than the light from the more numerous but much smaller droplets. This would eventually lead to overestimations of representative droplet diameters.

Finally, there were physical limitations to increasing the measurable droplet diameter range further since the focal length of the optics was already determined by the dimensions of the spray housing.

Therefore to avoid sacrificing validation and data rates, biasing the PDA towards larger droplets, and for practical reasons (spray housing dimensions), it was decided not to increase the measurable droplet diameter range beyond 600  $\mu\text{m}$ . It was felt that this approach would provide high quality PDA data which could be compared to the PDA results of other researchers (providing only the common diameter ranges are compared). An important conclusion from the above discussion is that an objective way of comparing PDA results from investigations performed on different systems is to

ensure the same diameter ranges are used. If this is not the case then only droplet data from diameter ranges common to both systems should be compared.

### 5.1.10 Spray Average Cumulative Droplet Size Distributions

The cumulative droplet distribution graphs (a global distribution) are shown in Figure 5.1.10.

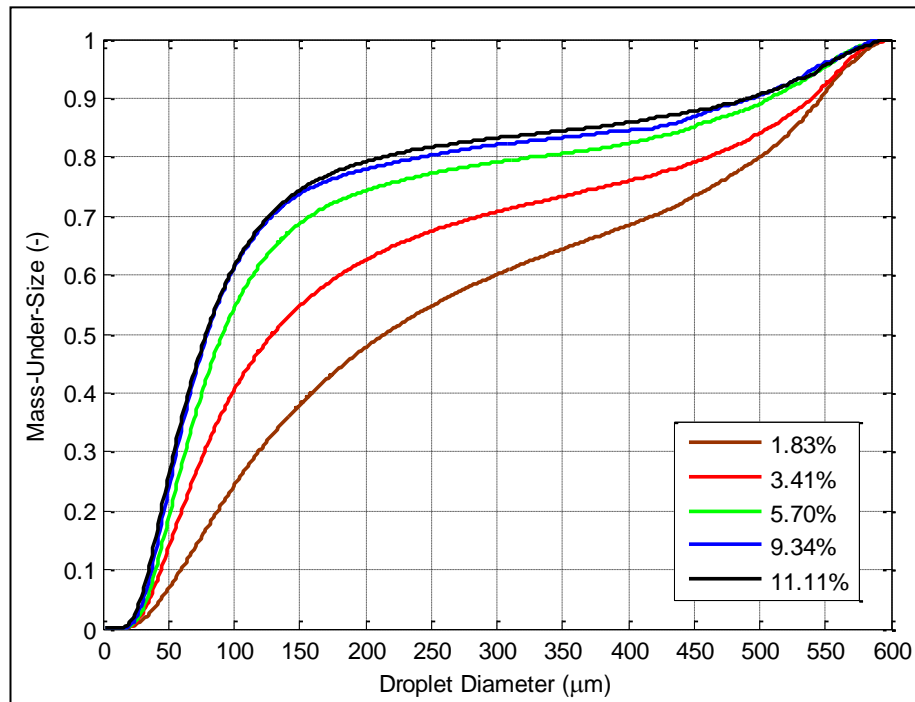


Figure 5.1.10 Cumulative droplet size distribution.

These graphs are arranged in the expected order and with the highest ALR spray curves possessing steeper initial slopes, indicating larger proportions of smaller droplets and therefore better spray quality.

The 11.11% ALR spray was clearly the best atomised one as expected, however, it was only marginally better atomised than the 9.34% spray. In fact the improvement in spray quality afforded by an ALR increase from 5.70-11.11% was considerably smaller than the improvement offered by ALR increases from 3.41-5.70%, or from 1.83-3.41%. This is an important result showing that ALR appears to have a large influence on spray quality at lower ALRs but only a minor influence above 5-6% ALR. It seems likely that the lower ALR sprays correlate with operation in the bubble-bursting atomisation mode, while the higher ALR sprays correspond to the tree-like atomisation mode. In this case it would appear that ALR has a large influence on spray quality in the bubble-bursting mode but only a minor, progressively diminishing influence in the tree-like atomisation mode.

Once again it is clear that even the best atomised sprays contained a considerable spray mass within the larger droplet diameter ranges. The best atomised sprays (5.70% ALR and above) had a steep initial cumulative distribution slope, flattening off noticeably above 200  $\mu\text{m}$ . Only a relatively small spray mass was sampled at higher size ranges. Meanwhile the more poorly atomised sprays had a much more linear cumulative distribution. This indicates a more even distribution of spray mass throughout the entire range of measurable droplet diameter, and therefore poorer atomisation.

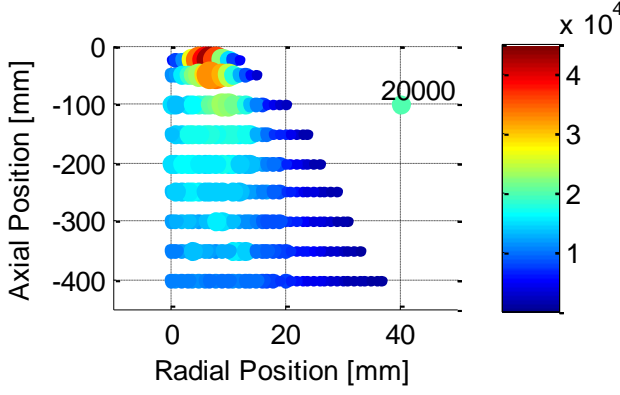
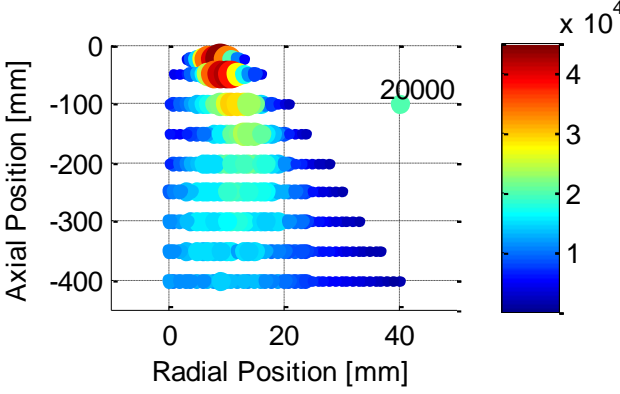
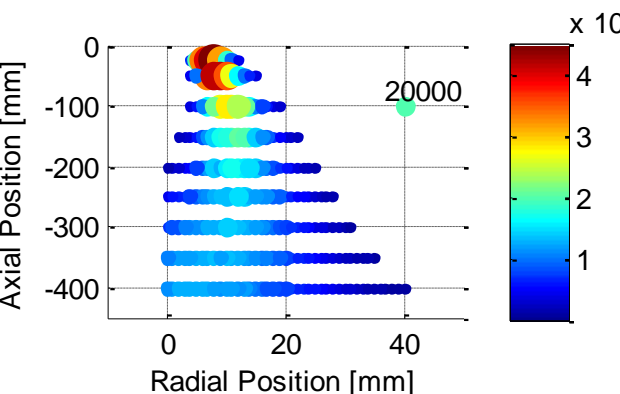
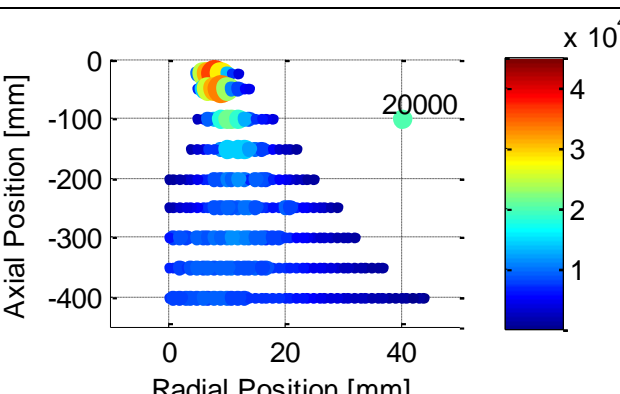
The higher ALR sprays (5.70%, 9.34% and 11.11%) are seen to be considerably more homogenous, with large spray masses contained in tight ranges at the lower droplet diameters. For example the 11.11% ALR spray contained a similar spray mass between 15-40  $\mu\text{m}$  as it did between 200-500  $\mu\text{m}$ . By comparison the 1.83% ALR spray carried a similar spray mass between 50-115  $\mu\text{m}$  and 500-600  $\mu\text{m}$  – a much more even distribution of mass. The latter spray was clearly not well atomised.

#### ***5.1.11 Validated Local Data Rates***

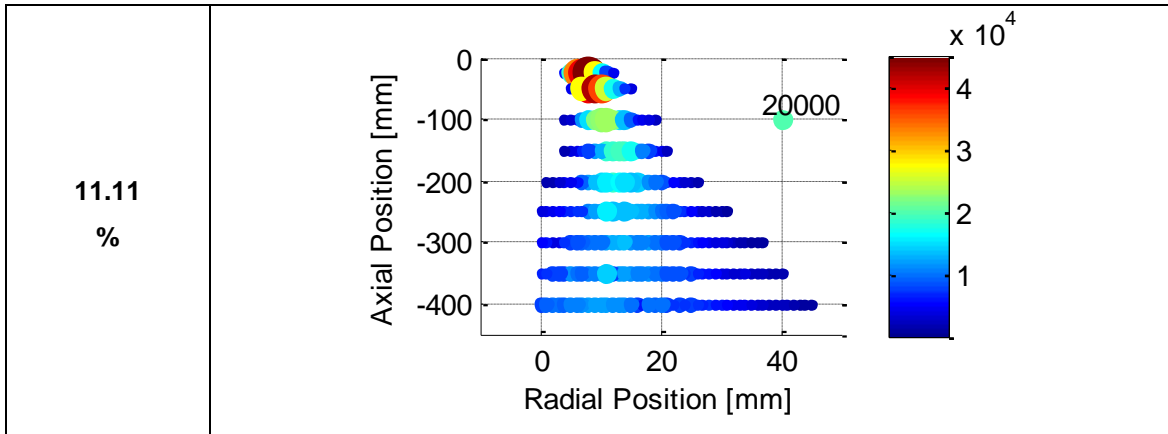
The droplet count graphs shown in Table 5.1.3 are similar for all ALRs in the current configuration and show that the highest data rates occurred halfway between the centreline and the sprays edge. In contrast, the data rates along the centreline at axial distances of 25-200 mm are considerably lower than the data rates throughout the respective axial location, for all sprays investigated.

This might indicate the presence of a hollow cone spray. However based on the visual appearance of the effervescent atomiser sprays and PDA experience with alternative nozzle types (industrial-type Y-Jet and I-Mix atomisers), it appears more likely that a full cone spray did occur, but multiple light scattering and attenuation effects prevented much of the centreline data from being collected (the centreline spray was too dense for the lasers to penetrate making detection of light there difficult).

Table 5.1.3 Validates local droplet count varying with ALR increases.

Spray ALR	Validated Local Droplet Counts
<p style="text-align: center;"><b>1.83</b> %</p>	
<p style="text-align: center;"><b>3.41</b> %</p>	
<p style="text-align: center;"><b>5.70</b> %</p>	
<p style="text-align: center;"><b>9.34</b> %</p>	





Larger data rates nearer the nozzle, which gradually decreased further downstream, were expected. If the spray at a given axial location can be visualised as being contained within the perimeter of a circle whose radius is equal to the spray half-width, then greater downstream distances will be characterised by larger spray circle radii (the spray is wider downstream of the nozzle), and for constant mass flow at all axial locations, the data rates will decrease in regions where the spray has a larger cross-section (i.e. further downstream).

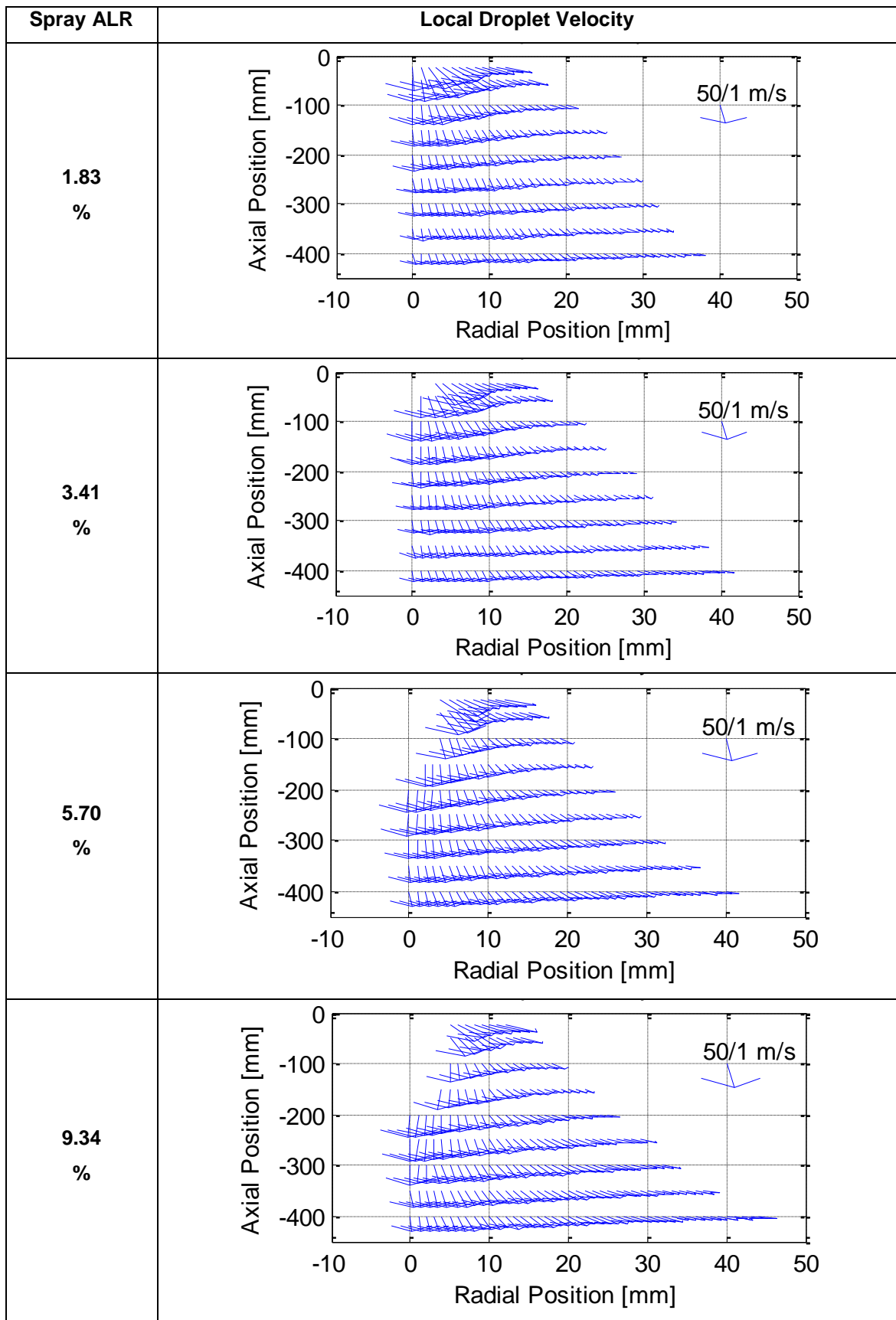
#### 5.1.12 Local Droplet Velocity

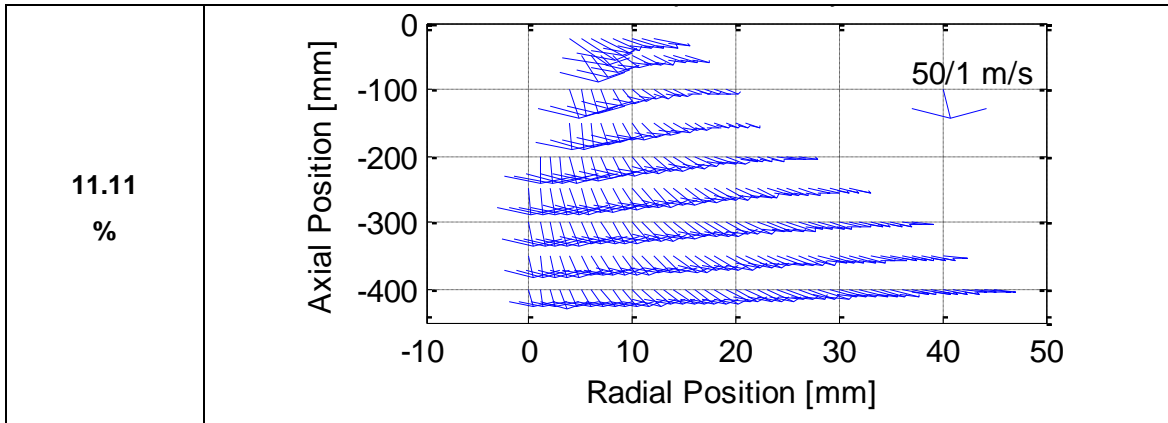
The average droplet velocity plots are presented in Table 5.1.4. The vector plots (“scatter” plots) in Table 5.1.4 show droplet motion throughout the spray for the lower ALR sprays (1.83% and 3.41% ALR) and indicate no downstream changes of droplet direction. For these sprays the droplet motion appears to follow straight lines originating at the nozzle exit orifice. No turbulent droplet behaviour or recirculation zones are visible based on the vectors.

The higher ALR sprays (5.70%, 9.34%, and 11.11%) display a different type of motion. Greater average velocities are visible throughout. With these sprays, the droplets are expelled from the nozzle with larger radial components of velocity (e.g. compare the velocity vector at 25 mm in the axial and 6 mm in the radial direction for all sprays). A reversal in droplet radial velocity is visible further downstream (e.g. at 4 mm in the radial direction and 200-400 mm in the axial direction for the 9.34% and 11.11% sprays). This indicates a somewhat more turbulent droplet motion at higher ALRs.

The large radial components of velocity at 25 mm downstream of the nozzle for the higher ALR sprays (5.70%, 9.34%, and 11.11%) could be explained by the increased contribution of atomising air eluting from the nozzle, which exerts a strong influence on droplet motion.

Table 5.1.4 Average local droplet velocity varying with ALR increases.





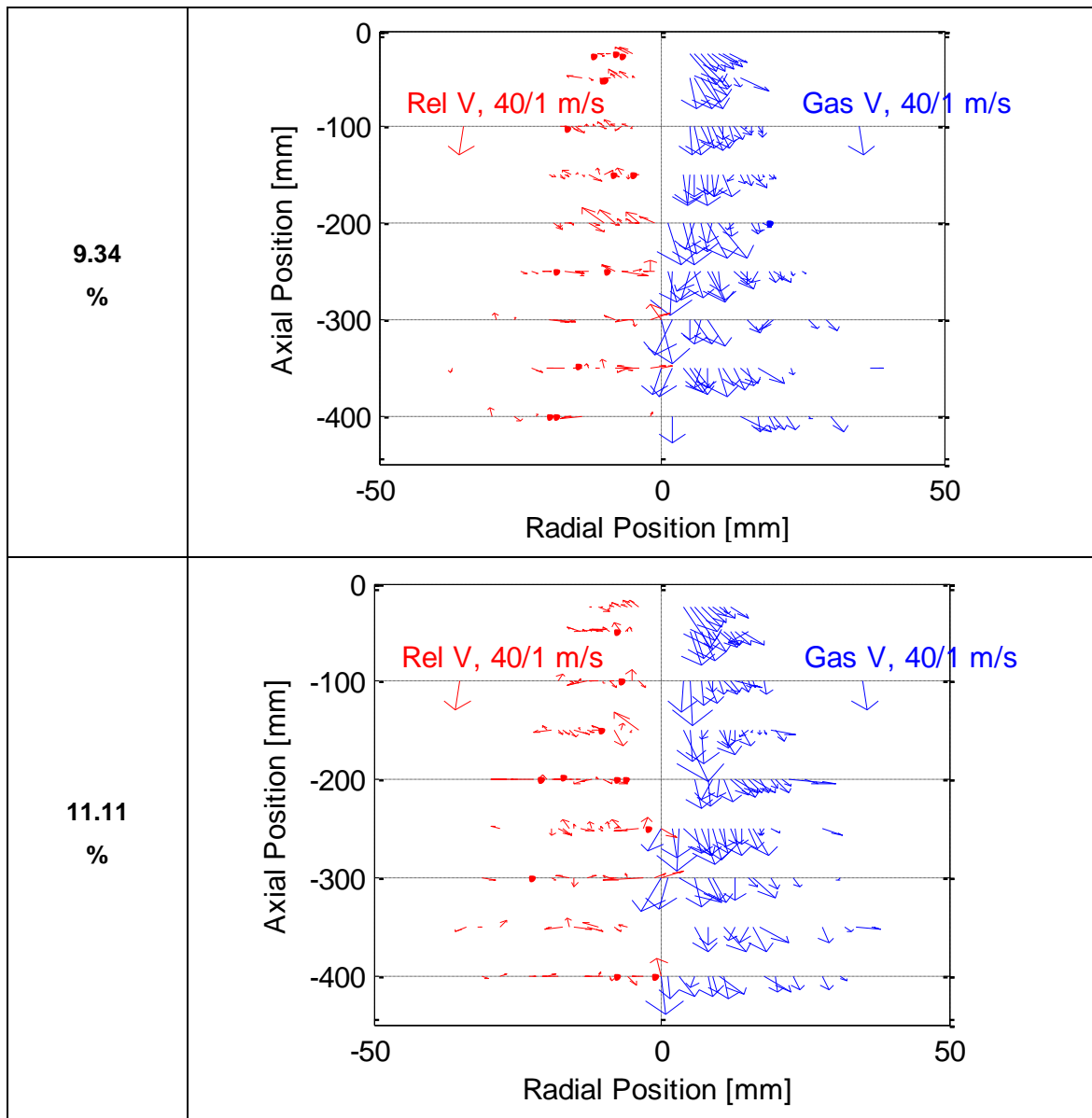
For example, it is known from high-speed photography that effervescent atomisation is characterised by co-annular fluid flow, with the liquid ligaments at the periphery of a centrally located atomising air core [61]. This structure is continuously present in the tree-like atomisation regime of higher ALR effervescent atomiser operation. At lower ALRs (when operating in the bubble-bursting atomisation regime) the co-annular structure is transient – existing only when air bubbles pass through the orifice. An ALR increase usually results in both an increase in air mass flow rate and a reduction in liquid flow rate. Both factors increase the air-phase proportion (which occupied 86-92% of the nozzle volume, according to the volumetric void fraction calculations). Further calculations reveal larger slip ratios and fluid velocities as ALR was increased. Therefore the total effect of increasing ALR was to provide continuous co-annular nozzle flow, with ever greater proportions of centrally located atomising air, travelling at greater velocities, slipping past the liquid phase ever more rapidly and pushing the liquid ligaments radially outwards more strongly. The large droplet radial velocities at 25 mm downstream of the nozzle at higher ALRs in Table 5.1.4 are consistent with operation in the co-annular tree-like atomisation mode, where the atomising air core forces the liquid ligaments and droplets radially outwards.

### 5.1.13 Inferred Local Gas and Relative Velocity

Local and relative gas velocities are shown in Table 5.1.5. “Gas velocity” was calculated by assuming droplets smaller than 2  $\mu\text{m}$  do not move under the influence of their own momentum but act as seeding particles for the gas motion. The velocity of these droplets therefore represents the air velocity at the sampled points. Relative velocity is then the difference between average droplet and average gas velocities at a given sampling location. This approach has been used by other researchers [48]. No gas or relative velocity data is presented in Table 5.1.5 for locations where seeding particles were not discovered. A dot indicates the presence of a data point too small to be seen at the current scale.

Table 5.1.5 Inferred local gas and relative velocity varying with ALR increases.

Spray ALR	Inferred local Gas and Relative Velocity
<p style="text-align: center;"><b>1.83</b> %</p>	<p>Rel V, 40/1 m/s      Gas V, 40/1 m/s</p>
<p style="text-align: center;"><b>3.41</b> %</p>	<p>Rel V, 40/1 m/s      Gas V, 40/1 m/s</p>
<p style="text-align: center;"><b>5.70</b> %</p>	<p>Rel V, 40/1 m/s      Gas V, 40/1 m/s</p>



The motion of the air particles appears relatively uniform (e.g. the arrows – representing axial and radial velocity – are relatively parallel up to 200 mm downstream) at ALRs of 1.83% and 3.41%, becoming less uniform at higher ALRs and further downstream. This is most clearly visible in the gas velocity plots as droplets progress from 25-200 mm downstream. This agrees with the view that higher ALR operation (in what is likely the tree-like atomisation mode) produced more highly turbulent sprays characterised by prominent radial components of velocity near the nozzle. All test cases appear to display non-uniform gas and liquid phase motion further from the nozzle. This may not necessarily be the case since sample sizes and seeding particles decreased downstream. Therefore the data became increasingly less representative, particularly at axial distances greater than 200 mm from the nozzle.

Relative velocity, drawn alongside gas velocity and to the same scale, is an order of magnitude smaller, which indicates only minor gas-liquid phase slip at all sampled positions and for all ALRs investigated. Data 25 mm downstream of the nozzle provides clear evidence of very rapid phase velocity equalisation for all conditions examined. This is an important result when compared to the dynamic conditions at the nozzle. Calculations indicate slip ratios of 3-4 for the three higher ALR sprays with air velocity ranges of 90-115 m/s. Meanwhile PDA measurements show both liquid and gas phase absolute velocities of 40-50 m/s with almost no phase slip at 25 mm downstream. This indicates that complete phase velocity equalisation was achieved after 25 mm of droplet motion. Nevertheless it should be borne in mind that the inferred velocities were based on a relatively small subset of data (droplets smaller than 2  $\mu\text{m}$ ) and may not be entirely representative at certain locations, especially far downstream of the nozzle.

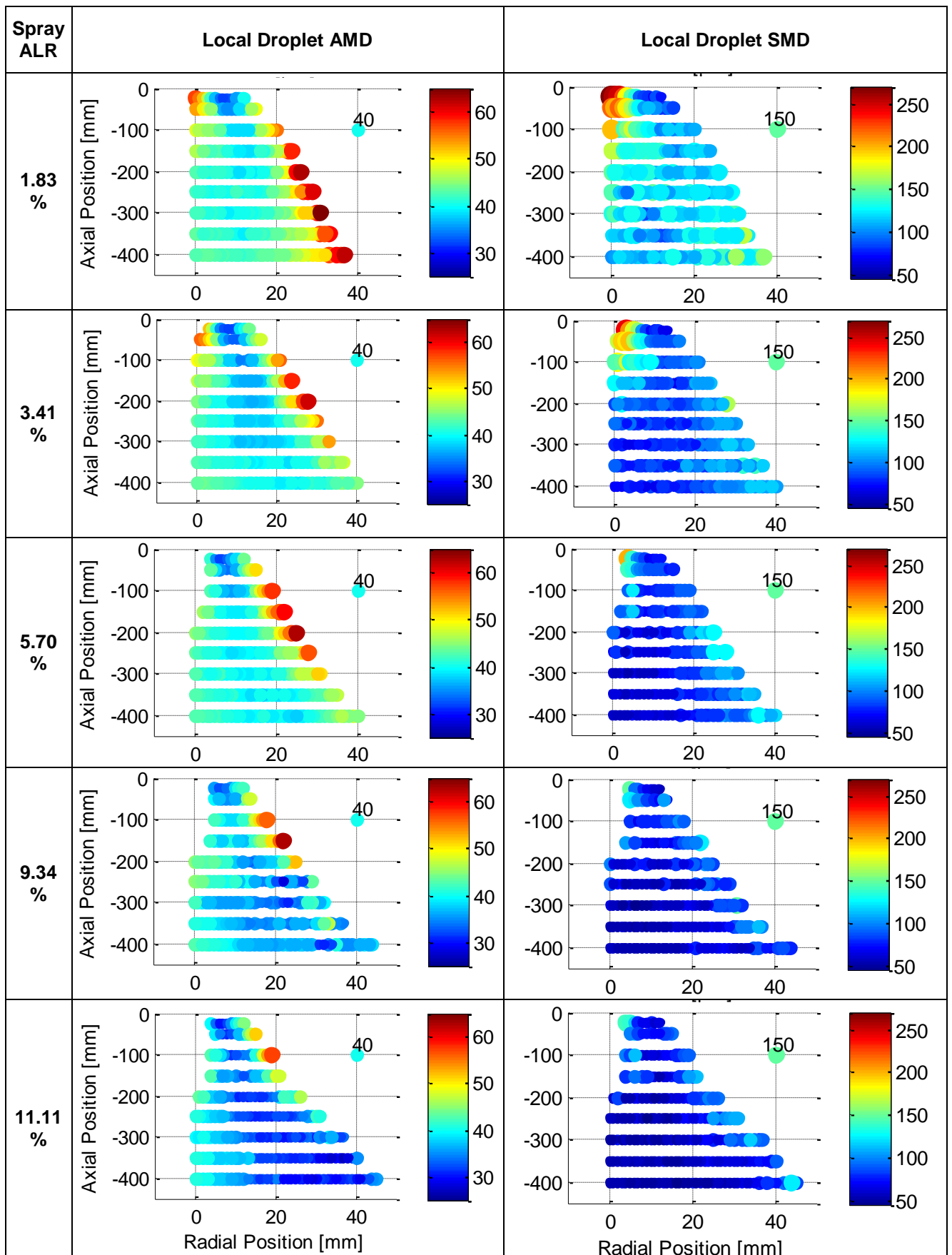
#### **5.1.14 Local Droplet AMD and SMD**

Table 5.1.6 displays the values of local AMD and SMD at all sampled points of every spray. There are two distinct regions of the spray where AMD is relatively large – the spray edge and the central near-nozzle region of the spray, up to 200 mm downstream of the exit orifice. Larger droplets are expected at the spray edge due to their relatively larger momentum (their greater mass means they retain their radial components of velocity better than smaller droplets). Larger AMD at the centreline are most likely the result of an unatomised liquid core (or disintegrating ligaments) still present nearer the nozzle.

In general ALR increases had a small influence on AMD. This is not surprising given that AMD is an arithmetic average giving equal weighting to all the droplet data. Figure 5.1.8, Figure 5.1.9 and Figure 5.1.10 have already indicated that the sprays were comprised of mostly small droplets. The main difference between well-atomised and poorly atomised sprays is then seen to lie in slightly different proportions of larger droplets. Therefore increasing ALR would only affect a comparatively small number of droplets (the larger ones) and this is reflected in only minor changes to AMD throughout all sprays (25-65  $\mu\text{m}$ ).

By contrast, large droplets have a strong influence on SMD (smaller droplets have a minor influence). Therefore the regions of large SMD in Table 5.1.6 clearly indicate the locations of relatively larger droplets. These are along the spray centreline near the nozzle, and at the downstream spray periphery.

Table 5.1.6 Local droplet AMD and SMD varying with ALR increases.



A significant feature of the 1.83% and 3.41% ALR sprays is that they possess larger droplet SMDs throughout, most prominently along the spray centreline, up to 200 mm downstream. Experience with other atomiser types reveals that the most likely reason for the large droplet SMDs at these locations is the presence of a central unatomised liquid core (or region of dense, unatomised ligaments) still intact along the centreline. This receding liquid core (as ALR is increased) seems to correspond to decreasing jet break-up length (within the fully-developed spray regime as either operating pressure or jet velocity are increased).

As ALR was increased jet break-up length and local droplet SMD decreased significantly until the seemingly homogenous higher ALR sprays (5.70%, 9.34% and 11.11%) were achieved. Raising ALR above 5.70% could not noticeably reduce local droplet SMD. The large improvements in local droplet SMD up to an ALR of 5.70% can be explained by a number of mechanisms. For example, it is known from experimental and photographic evidence that increasing ALR squeezes the liquid ligaments at the nozzle into thinner strands. Since the liquid is incompressible and for constant mass flow rate, the liquid exit velocity will increase. This increase in fluid velocity at higher ALRs will lead to enhanced atomisation. Additionally, because liquid ligament diameter is proportional to droplet SMD [43], the larger ALR sprays with their thinner fluid ligaments at the nozzle are likely to produce smaller spray droplet SMDs.

The most significant downstream spray development feature evident from the local droplet SMD plots is the apparent disintegration of the central liquid core (e.g. compare the local droplet SMD along the centreline at axial locations of 25-400 mm for the 1.83% and 3.41% ALR sprays). This demonstrates the locations at which secondary atomisation of a small number of very large droplets occurs.

#### **5.1.15 Local Droplet Size Consistency**

The differences between AMD and SMD are important as they give information about the relative spread of droplet sizes. AMD is insensitive to outlying data and will reflect the fact that by number, most of the droplets sampled were smaller than 100  $\mu\text{m}$ . Local AMD (e.g. Table 5.1.6) only varied between 25-65  $\mu\text{m}$ , which indicates that the bulk of the spray did not change significantly over the full range of ALRs tested. Meanwhile droplet SMD, representing the volume to surface area ratio, is a function of droplet mass and is therefore very sensitive to larger droplets. Only a few larger droplets are enough to significantly influence droplet SMD. In the current investigation, a relatively small number of larger droplets seem to be responsible for the full range of local



droplet SMD variation observed (varying locally between 50-270  $\mu\text{m}$  for all sprays in test phase 1).

The local SMD/AMD ratios shown in Table 5.1.7 provide an indication of the local droplet consistency. A completely uniform spray with identically sized droplets would provide a droplet SMD/AMD ratio of unity. A large ratio would indicate a wide range of droplet sizes.

Since it has already been shown (e.g. Figure 5.1.8, Figure 5.1.9 and Table 5.1.6) that the data demonstrates predominantly smaller droplets in all sprays with only small numbers of larger droplets, it is clear that the regions with large SMD/AMD ratios in Table 5.1.7 must indicate the physical locations where the relatively larger droplets were found.

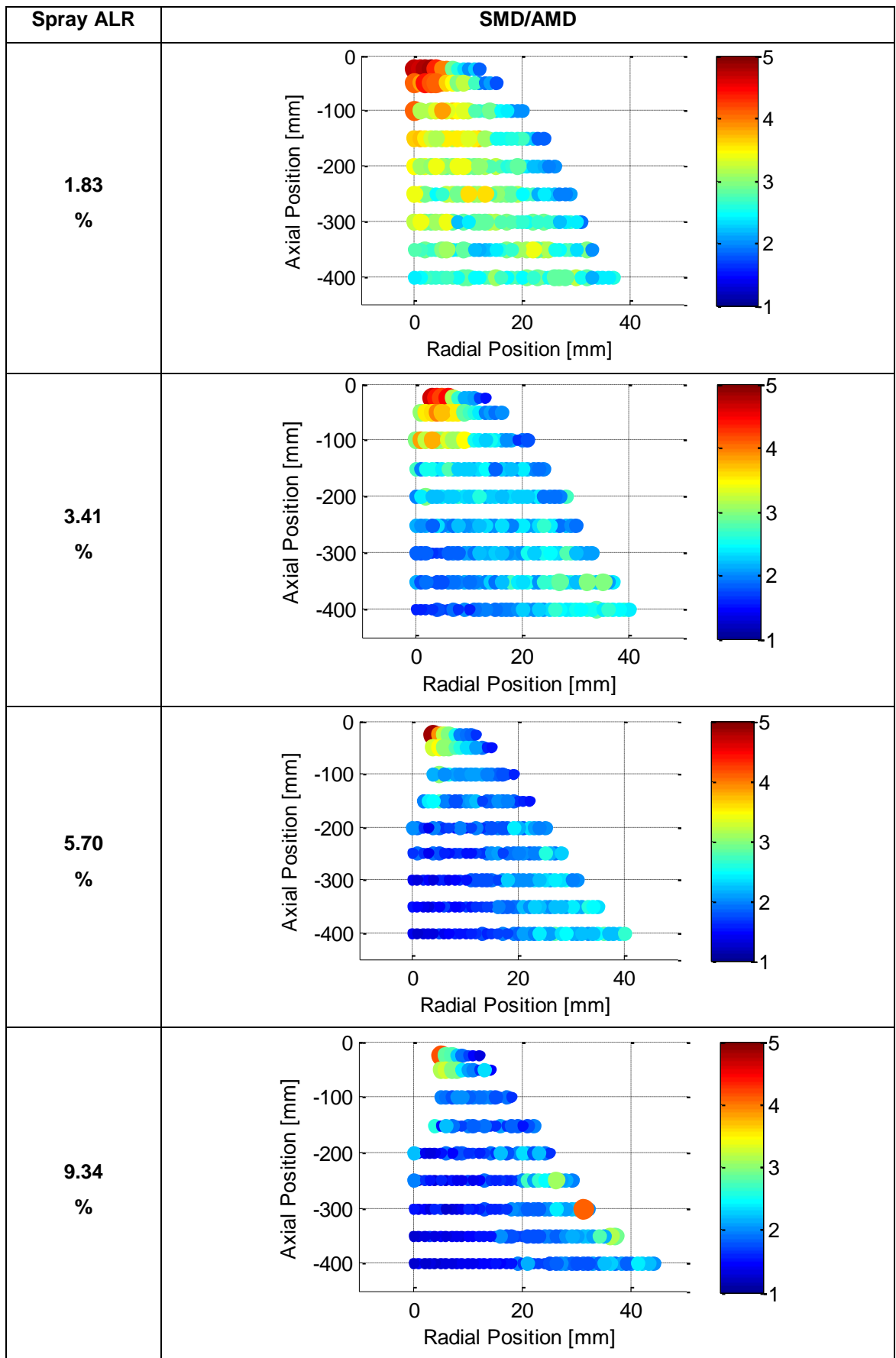
Table 5.1.7 reveals that the 1.83% ALR spray was the least consistent and therefore most poorly atomised. This agrees with previous findings (e.g. Figure 5.1.10). A large range of droplet sizes were present throughout this spray. The largest occur near the nozzle and close to the central axis. A narrowing of droplet size ranges further downstream most likely indicates the gradual disintegration of individual large droplets by secondary atomisation. This spray displays surprising consistency at the radial peripheries, but is poorly atomised elsewhere.

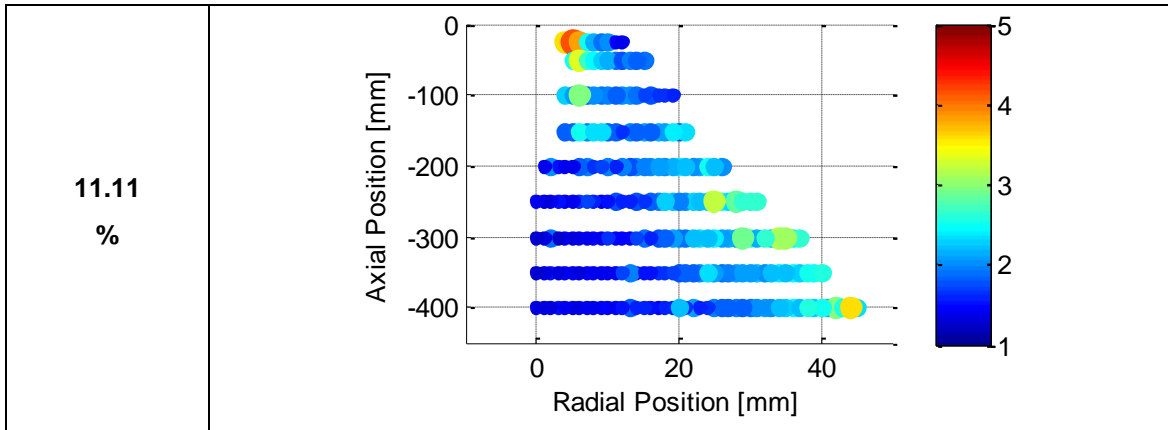
Increasing the ALR to 3.41% had the effect of eliminating many larger droplets as evidenced by greater local droplet size consistency throughout the spray. Nevertheless larger droplets still persist, especially nearer the nozzle.

The remaining sprays (5.70%, 9.34% and 11.11% ALR) were considerably more consistent. Some larger droplets are visible very close to the nozzle (remnants of a disintegrating core or unatomised ligaments) and some occur at the spray radial edges (larger droplets carried outwards by their greater momentum). Elsewhere, these sprays are consistent with local droplet SMD/AMD ratios approaching unity.

The plots in Table 5.1.7 suggests there was a considerable improvement in spray homogeneity as ALR was increased from 1.83% to 3.41% and then to 5.70%, but no significant improvement in homogeneity occurred at higher ALRs. This agrees with the cumulative mass-under-size plots presented in Figure 5.1.10 which show a similar trend, and supports the conclusion that global and local SMD were strongly influenced by ALR up to air-to-liquid ratios of 5-6%, but not much thereafter.

Table 5.1.7 Local SMD/AMD ratio varying with ALR increases.





### 5.1.16 The Importance of Measurement Location

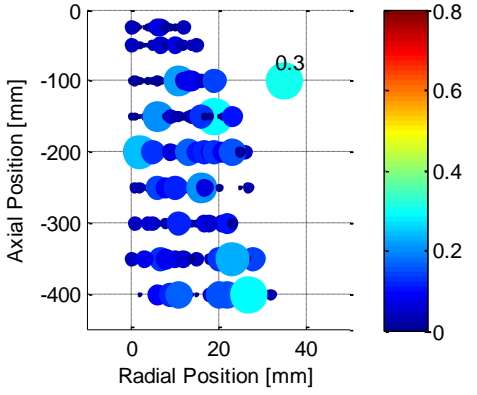
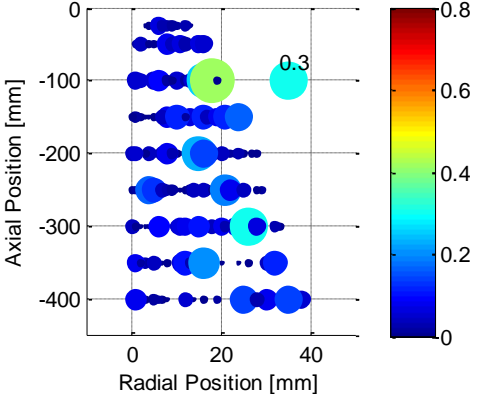
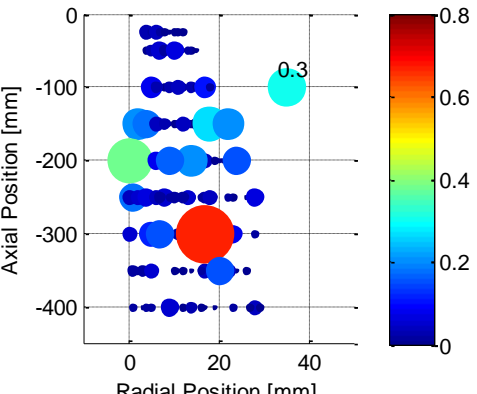
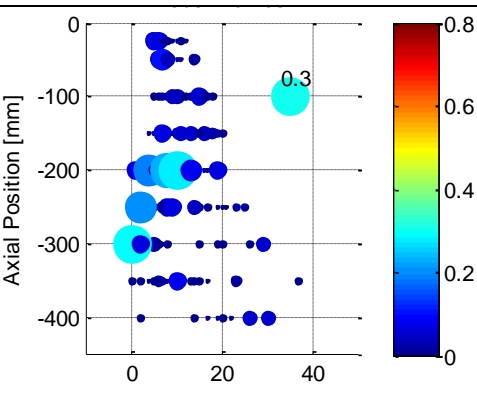
So far it has become clear (for example from Table 5.1.6) that both the measurement location and the definitions of the spray limits are very important and can have a major influence on the results obtained.

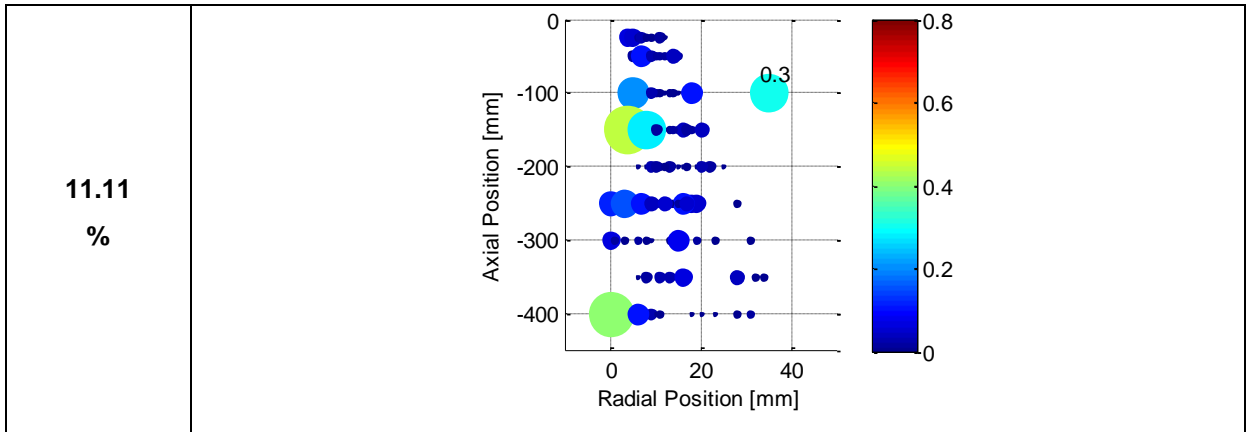
Measuring close to the nozzle will capture large droplets and unatomised ligaments; measuring only at the centreline or at just one axial location will give a limited and not necessarily representative view of a spray; break-up length varies with operating conditions and no single axial sampling location is guaranteed to capture exclusively post-break-up data. For example, as Table 5.1.6 and Table 5.1.7 show, sampling only at 200 mm downstream of the nozzle would not capture representative data for 1.83% and 3.41% ALR sprays. The radial sampling locations are also important. For instance, local SMD varies between 50-150  $\mu\text{m}$  at 150 mm downstream for the 3.41% ALR spray in Table 5.1.6. In the present study, radial spacings of 5 mm or more would have been likely to miss significant features of the spray.

### 5.1.17 Droplet Secondary Break-up

Average relative velocity and average droplet diameter were calculated using PDA. The average Weber number could then be calculated for each data point sampled. The results are presented in Table 5.1.8. Spray data for all tests performed illustrate average local Weber numbers more than an order of magnitude smaller than the commonly quoted critical Weber number values from the literature ( $11 \pm 2$ ).

Table 5.1.8. Local average droplet Weber number varying with ALR increases.

Spray ALR	Local Average Weber Number, $We$
<p style="text-align: center;"><b>1.83</b> %</p>	
<p style="text-align: center;"><b>3.41</b> %</p>	
<p style="text-align: center;"><b>5.70</b> %</p>	
<p style="text-align: center;"><b>9.34</b> %</p>	



Since the disruptive inertial forces were small (as indicated by the local average Weber numbers), secondary break-up was clearly not a significant atomisation mechanism for average sized droplets moving at the average droplet velocities for all sprays investigated. Droplet secondary break-up seems to have only occurred with a small number of very large droplets. This, however, is not visible in Table 5.1.8 where average values little influenced by the larger droplets are presented.

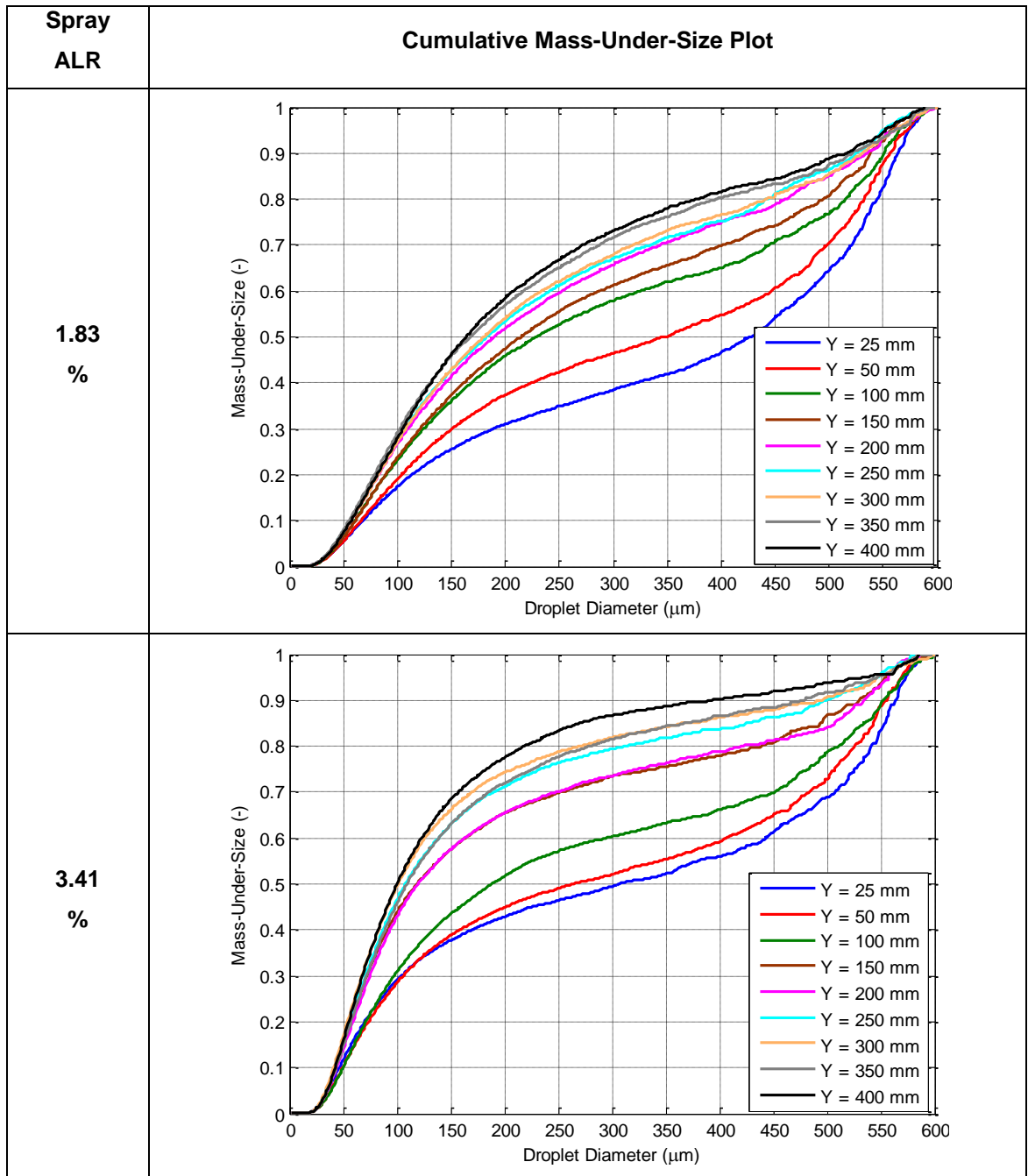
A revealing feature of Table 5.1.8 is the small average Weber numbers near the nozzle (25 mm downstream of the exit orifice), which do not reflect the relatively large droplet SMD values there, shown in Table 5.1.6. This leads to the conclusion that the large near-nozzle droplet SMDs are a result of only a few very large droplets. This is consistent with other results presented so far such as the cumulative droplet distributions by number (Figure 5.1.8).

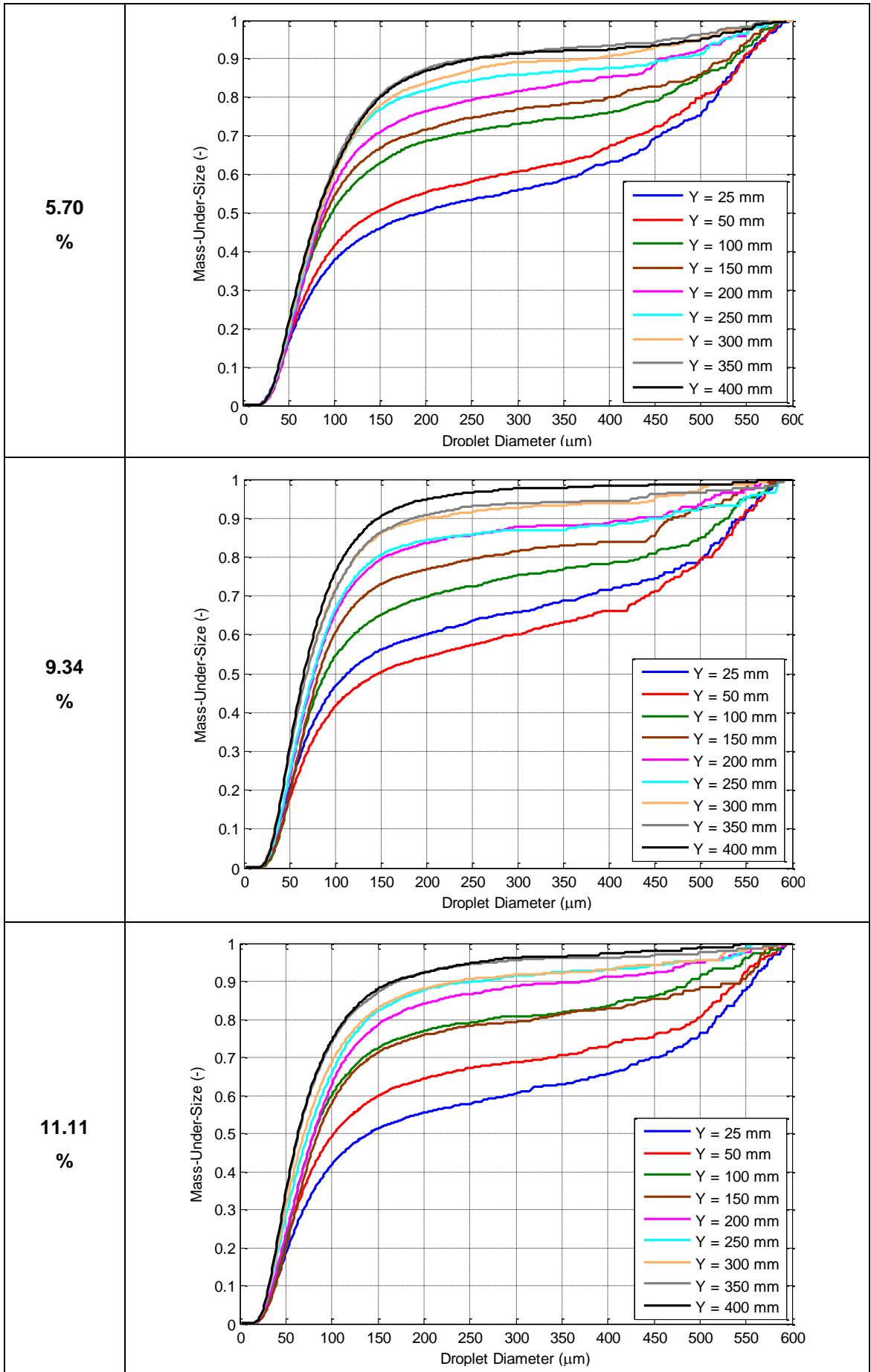
**5.1.18 Spray Development in the Downstream Direction**

The changes in spray mass as the droplets progressed downstream of the nozzle are displayed in the mass-under-size plots of Table 5.1.9. For this analysis, all the data points at a given axial location were compiled and processed together. The resulting mass-under-size plots indicate the cumulative droplet size distributions at each axial locations of every spray.

All tests demonstrate ongoing improvements in downstream spray quality (e.g. compare mass-under-size plots at 25-400 mm for all sprays). In addition, noticeable improvements in spray quality are visible between 350-400 mm downstream (for instance, see the 3.41% spray in Table 5.1.9). This provides evidence of continuing atomisation even up to 400 mm downstream of the exit orifice (i.e. equilibrium had not been achieved at 400 mm downstream of the nozzle).

Table 5.1.9 Cumulative mass-under-size plots for entire downstream locations.





Although Table 5.1.6 and Table 5.1.7 demonstrate a seemingly drastic improvement in downstream spray quality for the 1.83% and 3.41% ALR sprays (as the unatomised core or disintegrating ligaments recede), Table 5.1.9 shows that the spray mass changes between 25-400 mm are comparable for all sprays investigated. Therefore a similar amount of liquid break-up must have occurred for all effervescent atomiser sprays. This is consistent with the large near-nozzle droplet SMDs of the 1.83% and 3.41% ALR sprays being caused by a small total number of droplets (similar to the numbers of large droplets in the near-nozzle region of the higher ALR sprays).

For any given spray, the mass-under-size plots run roughly parallel for droplet size ranges of 200-450  $\mu\text{m}$  at all downstream locations. This indicates that droplets of these sizes appear to have moved downstream relatively intact. While there are considerable downstream increases in the droplets sized 200  $\mu\text{m}$  and less (e.g. the initial gradients of the mass-under-size plots of the 11.11% spray in Table 5.1.9 are noticeably different), there is little change in the mid-range droplets. This leads to the conclusion that the most significant characteristic of a developing spray is a downstream decrease in the absolute number of droplets larger than 450  $\mu\text{m}$  and a simultaneous increase in the absolute number of droplets smaller than 200  $\mu\text{m}$ . This suggests that for the conditions investigated, 450  $\mu\text{m}$  is a critical droplet diameter, with droplets larger than this being unstable and breaking up into numerous droplets smaller than 200  $\mu\text{m}$ . This is similar to the findings of other researchers; for example, one researcher reports that only droplets larger than 100  $\mu\text{m}$  are capable of break-up into smaller droplets, while smaller droplets can only deform [105].

#### ***5.1.19 Droplet SMD Correlations from the Literature***

Figure 5.1.11 shows how experimentally determined global spray droplet SMD varied with ALR. The experimental values are compared to various effervescent atomiser correlations found in the literature. Figure 5.1.11 (also Table 5.1.2) shows that effervescent droplet SMD correlations in the literature could not accurately predict global spray SMD for the conditions investigated. Some of the correlation predictions matched the pattern of droplet SMD decreasing as ALR was increased. However none were satisfactory. This is due to the use of different spray measurement techniques (to obtain experimental data), different atomiser geometries and experimental operating parameters investigated, as well as the utilisation of different sampling locations. In addition the fluid break-up mechanisms outside the nozzle are not well understood and cannot be adequately modelled. All these factors can affect experimentally determined droplet SMD values and influence theoretical models.



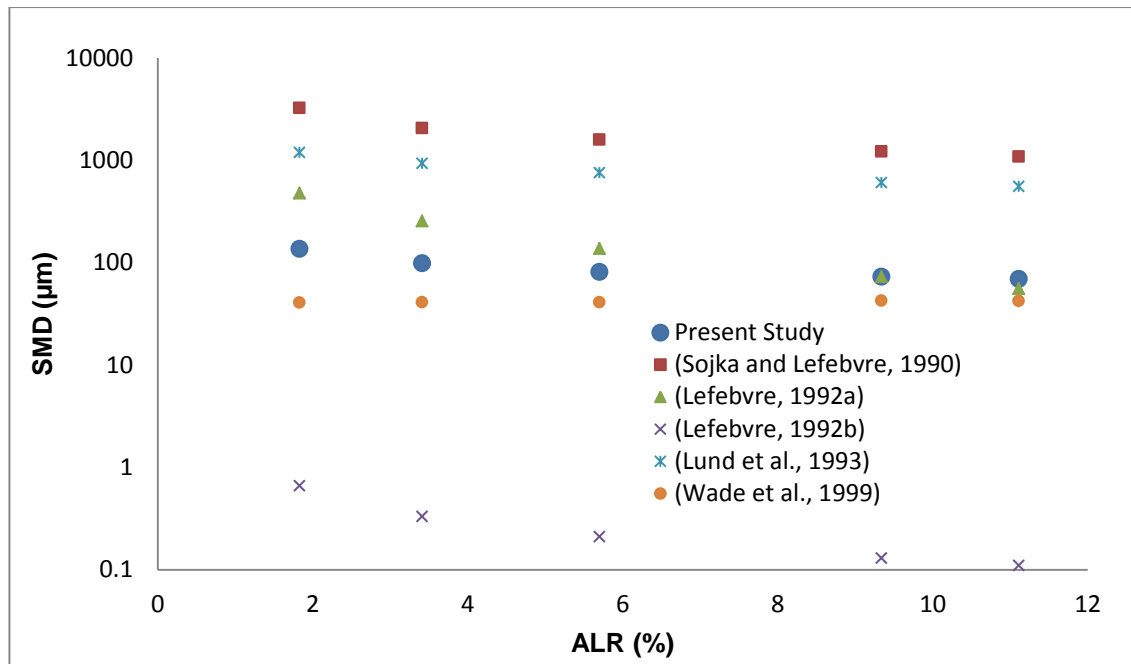


Figure 5.1.11 Comparison of global spray droplet SMD from PDA experiments with that predicted by correlations in the literature.

So far it has become clear that no one measurement technique, droplet diameter sampling range or sampling location can provide an absolute and repeatable value of droplet SMD which completely describes a given spray. In fact, different droplet sizing techniques, droplet measurement ranges and sampling locations will provide varying representative droplet diameters. This can make comparisons across studies difficult. Even the same sampling techniques and sampling locations are not guaranteed to provide identical results. For example preliminary investigations [100] showed that PDA tests at the same locations within a spray could give widely diverging local and global spray droplet SMD if different optical settings were used (optical Masks B or C). Despite these challenges the use of state-of-the-art 2-D PDA, with a high-density probe and a fine sampling grid containing over 230 sampling points at nine axial locations, ensures that the correlations obtained using the present experimental data will be representative of the underlying spray quality trends. The consistent use of the same settings, techniques and methods throughout the current study will ensure that individual tests can justifiably be compared against each other.

### 5.1.20 Effect of ALR on Global Spray SMD for Experimental Data

It has become clear that there are two phenomenologically different modes of effervescent atomiser operation characterised by different ALR ranges. These result in different near-nozzle disintegration modes (Figure 5.1.6), different droplet motion

(Table 5.1.4) and different patterns of droplet SMD and droplet AMD distribution throughout the sprays (Table 5.1.6).

Therefore effervescent atomisation at an ALR below 5% can be characterised by operation in the bubble-bursting mode, with second wind-induced liquid break-up at the nozzle, featuring a prominent unatomised liquid core and somewhat poorer liquid atomisation. Meanwhile ALRs greater than 5% result in the tree-like atomisation mode of operation, with the so-called atomisation mode of liquid disintegration at the nozzle, featuring no detectable solid liquid core and comparatively better liquid atomisation throughout the spray. For these reasons both groups of results were analysed separately.

Figure 5.1.12 graphically depicts the relationship between ALR and global droplet SMD (the values are from Table 5.1.2) for all sprays investigated. The proportionality (assuming linearity) for low ALR operation is given in Equation 5.1.5 and Equation 5.1.6 displays the proportionality for high ALR operation.

$$SMD \propto 185.55ALR^{-0.5166} \quad \text{Equation 5.1.5}$$

$$SMD \propto 121.18ALR^{-0.2306} \quad \text{Equation 5.1.6}$$

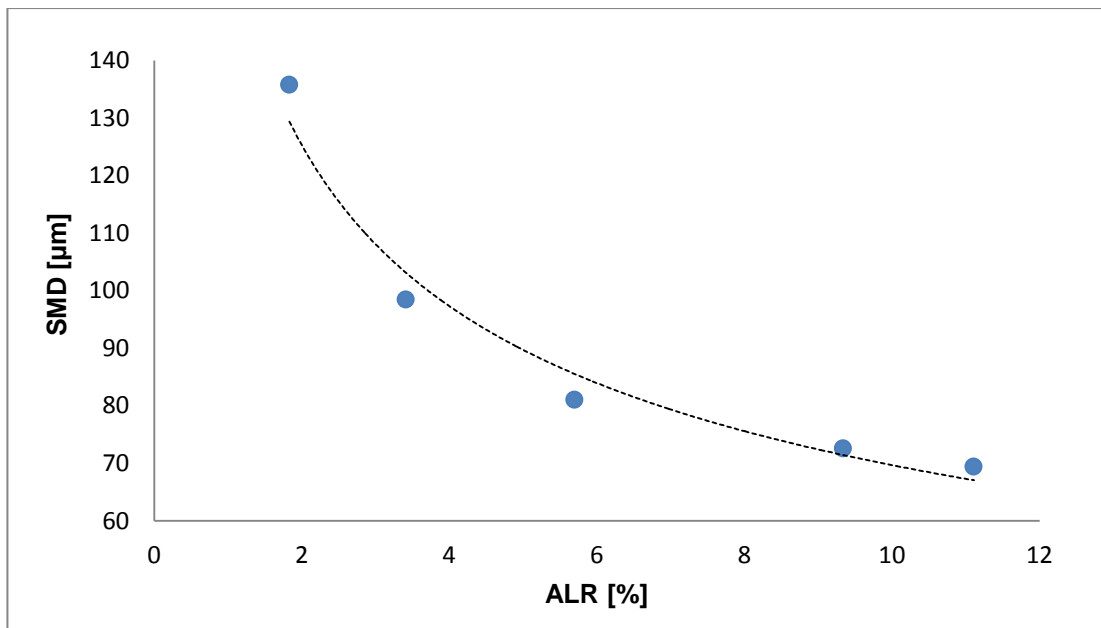


Figure 5.1.12 The relationship between ALR and global spray droplet SMD as measured using PDA data.

Therefore based on the experiments performed, and for the operating conditions, atomiser geometries and fluids used, for  $2\% \geq ALR > 5\%$  global droplet SMD is a function of  $ALR^{-0.5166}$  and for  $5\% \geq ALR \geq 12\%$  global droplet SMD is a function

of  $ALR^{-0.2306}$ . A negative exponent power law is expected since it is well known that increases in ALR will reduce global spray droplet SMD.

The present investigation agrees well with much of the findings of previous researchers. For example, early effervescent atomisation researchers recognised the great importance of ALR and the reduction in spray droplet SMD afforded by ALR increases [18, 32, 74, 75]. However, the current work disagrees with the importance of operation in the low ALR single-bubble explosion regime claimed by some early researchers. This regime, at ALRs below 5%, could not produce well-atomised, homogenous sprays in the current experiments. In fact ALRs below 2% could not produce steady, fully-atomised sprays at all. In contrast, well-atomised, relatively homogenous sprays were only possible at the higher air-to-liquid ratios. This study provides evidence for better atomisation at ALRs above 5%, and therefore confirms the results of Morelli et al, who also reported optimal performance at ALRs greater than 5% [79]. Based on the current work an ALR of 2% can be recommended as a minimum, with operation above 5% ALR preferable.

A considerable discrepancy exists between global spray droplet SMD as calculated in the present study and some of the droplet SMD reported by early researchers. For example, Lefebvre reports droplet SMD less than 50  $\mu\text{m}$  at an ALR of 4% and pressures of 1.38 barG with nitrogen and water mixtures [62]. A related study [18] reports similar findings – droplet SMD of 40  $\mu\text{m}$  at pressures less than 1 barG and ALR less than 1% with air and water mixtures.

There are a number of reasons for this discrepancy, some of which have already been discussed.

- Different sizing techniques (Malvern Particle Size Analyzer, PDA) can give different representative droplet diameters for the same spray. For instance, one study showed a Malvern Particle Size Analyzer consistently reporting lower spray droplet SMD than PDA for the same operating conditions [106].
- The sampled spray areas were different, with the present study utilising a sampling grid encompassing both radial and axial data points contained within a plane cutting through half of the spray. The present sampling grid was somewhat arbitrarily selected and does not necessarily correspond to the sampling areas used in other investigations.
- Global spray droplet SMD as calculated in this investigation made use of spray data up to 25 mm from the nozzle. These included many large droplets or unatomised ligaments which increase the calculated droplet SMD. Other

investigations which only sample further downstream are not necessarily comparable.

- The present study was set to sample droplet ranges up to 600  $\mu\text{m}$  and, as already discussed, the optical setup can influence results. For example, sampling droplet ranges only up to 300  $\mu\text{m}$  would have missed a small total number of large droplets but this would have resulted in considerably lower global spray droplet SMD. Thus different investigations cannot readily be compared without consideration of the measurable sampling ranges.

Therefore the above investigations are difficult to compare to the present work. However, it is likely that 2-D PDA analysis of the sprays analysed by previous researchers (using the settings employed in the current investigation) would have given larger global spray droplet SMD than the droplet SMD reported by the above authors.

#### **5.1.21 Discussion of PDA Findings**

The experimental work performed required an appreciation of the characteristics and limitations of the PDA technique. So far a number of important findings relevant to PDA measurements have been discovered. These include:

- A statistically small number of very large droplets can have a great influence on global spray SMD; for example, with measurable droplet range ratios of up to 1000:1.
- Performing measurements at larger droplet ranges reduces the resolution of the diameter-phase relationship causing a reduction in validation and data rates.
- Operating the PDA with large diameter ranges biases the PDA in favour of larger droplets since the light they present to the photo detectors is much more prominent than the light from the more numerous but smaller droplets.
- Selecting an appropriate measurable diameter range is important in ensuring high-quality droplet data; a large range may introduce the problems discussed above; too low a diameter range may result in the loss of droplet data.
- Sampling location is important enough to be able to influence results, e.g. measuring close to the nozzle will capture large droplets and unatomised ligaments; measuring only at the centreline or at just one axial location will give a limited and not necessarily representative view of a spray; break-up length varies with operating conditions and no single axial sampling location is guaranteed to capture exclusively post-break-up data.

It was discovered that for unbiased spray comparisons of different investigations, it must be ensured that the same sampling techniques and measurable droplet diameter ranges must be used (in addition to ensuring equivalent sampling locations and applying the same spray definitions).

## 5.2 Test Phase No.2 – Pressure Drop across Nozzle, $\Delta P$

The complete data set for the present tests is presented in Appendix A.

### 5.2.1 Preliminary Investigations

Table 5.2.1 illustrates the position of the pressure differential tests within the study program, as well as the calculated values of the controlled parameters.

Table 5.2.1 Operating conditions and controlled parameters for pressure differential tests.

TEST No. PARAMETER VARIED	1 ALR	2 $\Delta P$	3 $D_o$	4 $L_{MC}$	5 $D_{MC}$	6 $L_o/D_o$	7 A. GEOM.	8 $\eta$
TEST PHASE	A. Initial Operating Parameters		B. Atomiser Geometry					C. Fluid properties
ALR (%)	0.8-12.5	2		2				
$\Delta P$ (bar.g)	7	4-7		7				
$D_o$ (mm)	2	2	2-4	2	2	2	2	2
$L_{MC}$ (mm)	140	140	140	64-140	140	140	140	140
$D_{MC}$ (mm)	25.4	25.4	25.4	25.4	20-30	25.4	25.4	25.4
$L_o/D_o$ (-)	1	1	1	1	1	0.5-2	1	1
Aerator Geometry	A1	A1	A1	A1	A1	A1	A2, A3	A1
$\eta \times 10^{-8}$ (m <sup>2</sup> /s)	1	1	1	1	1	1	1	2-10

For test phase 2, the control variable ALR needed to be kept constant. The spray quality maps shown in Figure 5.2.1 and Figure 5.2.2 were consulted in order to choose an appropriate operating region where  $\Delta P$  could be varied over a wide range of values while still ensuring a well atomised spray. Previous investigations had already shown that 2% was the lower ALR limit for well atomised sprays. An arbitrary upper ALR limit of 12% was selected; this was done to avoid the operation in the air-blast atomisation regime.

After consulting Figure 5.2.2 it was decided to perform test phase 2 tests at the lowest ALRs which still gave stable sprays, as this would allow for the widest range of  $\Delta P$  values to be achieved with a constant ALR. Therefore it was decided to aim for stable

ALR conditions between 2-2.5% air-to-liquid ratio. Figure 5.2.1 and Figure 5.2.2 shows the precise positions of the  $\Delta P$  tests in terms of flow rates and pressure drop across the nozzle ( $\Delta P$ ).

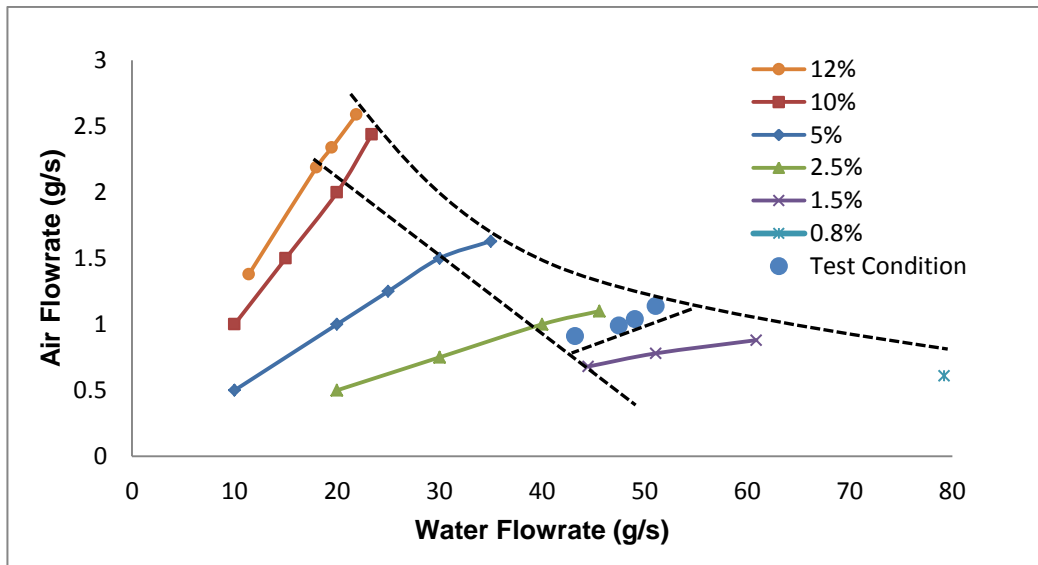


Figure 5.2.1 Graph of spray quality showing liquid flow rates at which optimal effervescent atomisation can be achieved.

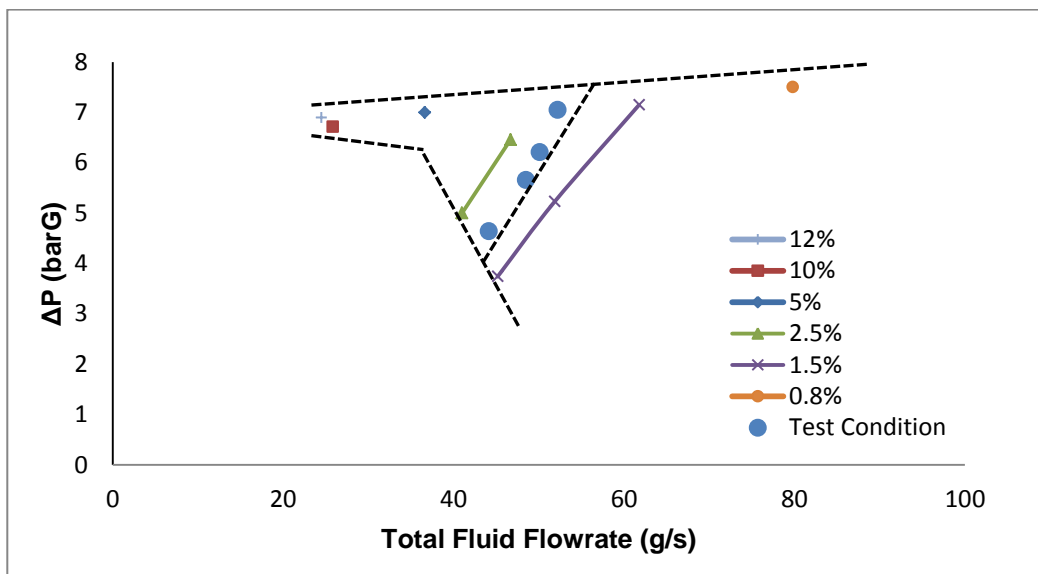


Figure 5.2.2 Graph of spray quality showing mixing chamber pressures and total flow rates at which tests were performed.

### 5.2.2 Spray Characteristics and Results

The  $\Delta P$  tests were performed at an average ALR of 2.08-2.25%, varying by up to 8%. Meanwhile  $\Delta P$  was varied over a total range of 2.41 barG or 52%. Therefore  $\Delta P$  was the dominant operating parameter. The test results are summarised in Table 5.2.2.

Table 5.2.2 Summary of  $\Delta P$  test operating conditions and spray characteristics.

Test	4.64 barG $\Delta P$	5.66 barG $\Delta P$	6.21 barG $\Delta P$	7.05 barG $\Delta P$
Water Supply Pressure (barG)	5.42	6.46	7.02	7.87
ALR (%)	2.10	2.08	2.12	2.25
$m_{\text{WATER}}$ (g/s)	43.22	47.51	49.07	51.07
$P_{\text{AIR}}$ (barG)	5.06	6.09	6.60	7.52
$m_{\text{AIR}}$ (g/s)	0.91	0.99	1.04	1.14
Volumetric Void Fraction, $\alpha$ (%)	75.7	72.4	70.8	69.9
Effective Power Rating (MW)	1.73	1.90	1.96	2.04
Coefficient of Discharge (-)	0.45	0.45	0.44	0.43
$\theta/2$ at 25 mm downstream (deg)	23.75	25.64	27.47	27.47
Calculated Nozzle Re	33389	28183	25151	22899
Calculated Nozzle We	19137	13459	10741	9073
Calculated Nozzle Oh	0.004143	0.004116	0.004121	0.004160
$D_{32}$ ( $\mu\text{m}$ )	156.93	137.93	136.89	122.27

### 5.2.3 Nozzle Coefficient of Discharge

Figure 5.2.3 compares the experimentally determined coefficients of discharge with those predicted by correlations in the literature. The correlation of Chen and Lefebvre once again is closest to the experimental data values. The correlation of Chin et al predicts values greater than unity – a result of the different geometric and operating parameter ranges investigated.

The experimentally determined coefficient of discharge remained relatively constant varying from 0.43-0.45 for all tests. This closely matches the coefficient of discharge of the 1.83% ALR test from test phase 1 (0.47). It seems logical that tests at similar ALRs will possess similar coefficients of discharge since ALR directly affects the air-phase proportion at the atomiser nozzle.

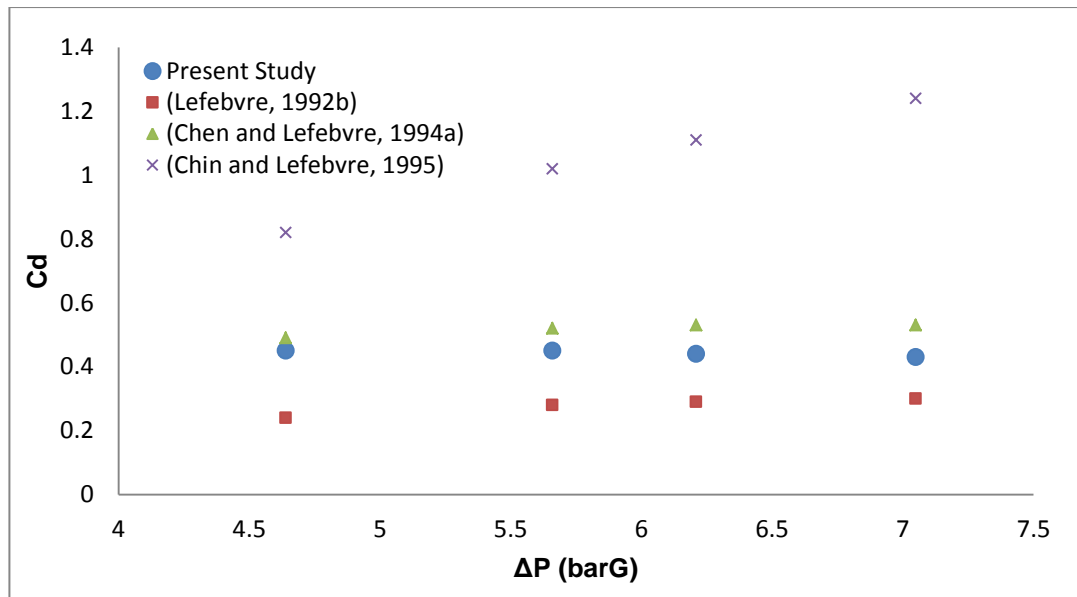


Figure 5.2.3 Comparison of coefficient of discharge from PDA experiments and literature.

### 5.2.4 Mode of Liquid Break-up at Nozzle

The map of liquid disintegration at the nozzle is shown in Figure 5.2.4.

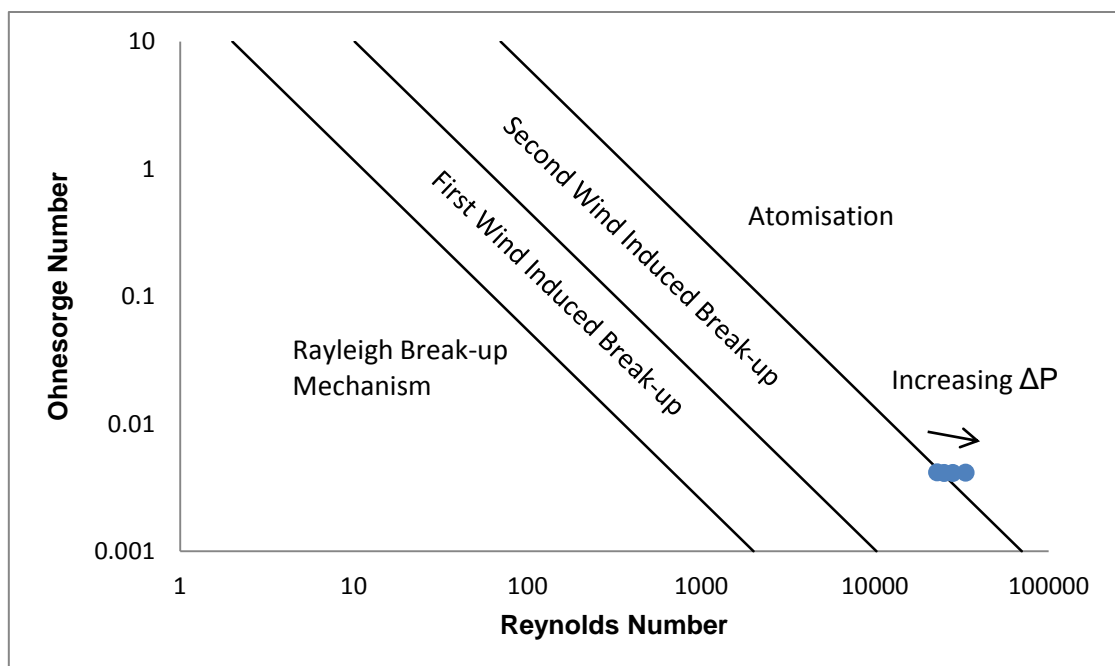


Figure 5.2.4 Calculated liquid disintegration mode for ΔP experiments.

This analysis indicates improving atomisation as ΔP is increased. This was expected and is confirmed by the reduction in global spray droplet SMD as ΔP was increased in Table 5.2.2. The lowest ΔP test appears to be on the border between the desirable atomisation regime and the second wind induced break-up regime. This agrees with



the spray quality maps in Figure 5.2.1 and Figure 5.2.2. Increases in  $\Delta P$  pushed operation into the “atomisation” regime and improved spray quality.

### 5.2.5 Spray Half-Angle

Experimentally determined spray half angle is shown in Figure 5.2.5, where it is compared against the correlation provided by Sovani et al. The experimental data is a factor of three to four larger than the predictions of the correlation. This discrepancy was expected given the different measurement techniques and sampling locations employed.

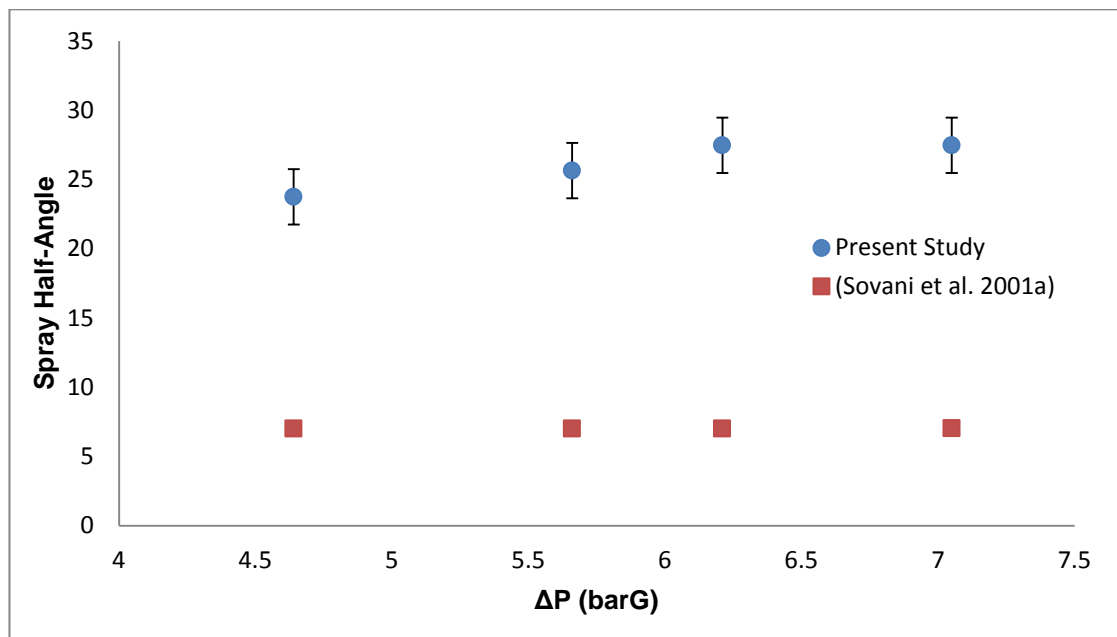


Figure 5.2.5 Comparison of spray half-angle from PDA experiments and literature.

Spray width at 25 mm downstream was used for determining spray half-angles in the current investigation. Further downstream spray widths will give spray half-angles smaller than the ones currently quoted by a factor of up to four. Therefore axial measurement location is important and can account for the differences between the experimental data and the predictions of Sovani et al.

Spray half-angle is seen to vary between 23-28° to the nearest whole degree, and an accuracy of  $\pm 3^\circ$ . Therefore these data very closely matched the spray half-angles of test phase 1.

### 5.2.6 Spray Droplet Size Distribution by Number

Figure 5.2.6 displays the diameter frequency distributions by number for all sprays investigated. Just as in the ALR tests (Figure 5.1.8), the sprays of test phase 2 have a prominent peak at lower droplet size ranges and possess few droplets larger than 180  $\mu\text{m}$ .

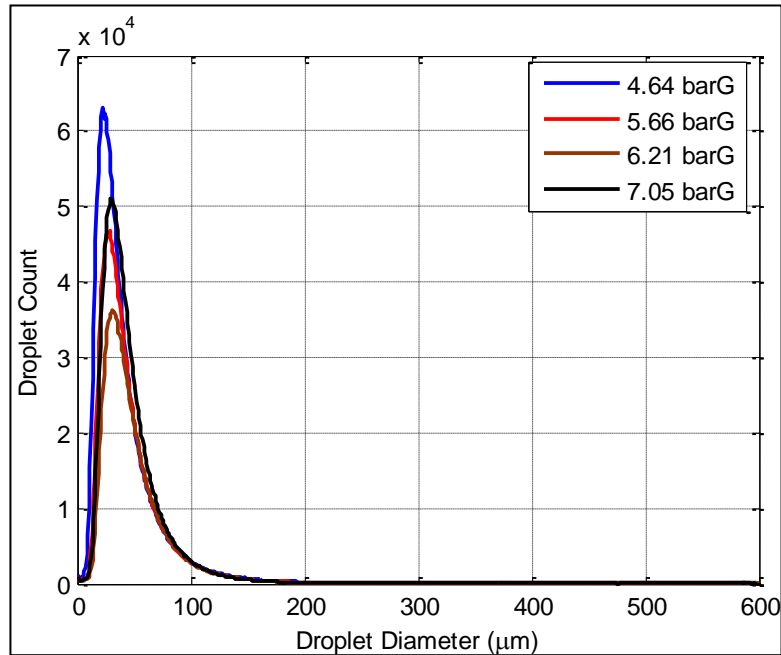


Figure 5.2.6 Droplet diameter frequency distribution based on number.

### 5.2.7 Spray Droplet Size Distribution by Mass

The diameter frequency distributions by mass, shown in Figure 5.2.7, are of a similar shape to the equivalent plots from test phase 1. A number of important features can be seen in Figure 5.2.7.

The sprays appear bimodal with the second peak a result of a small number of very large droplets. In terms of absolute mass, all sprays are very similar above droplet diameters of 200  $\mu\text{m}$ . This seems to indicate that increasing  $\Delta P$  had no noticeable effect on the larger droplets. The only difference provided by increasing  $\Delta P$  was to increase the total spray mass proportion carried in the lower droplet ranges without changing the absolute mass carried in droplets sized 200  $\mu\text{m}$  and over. Once again it is clear that effervescent atomisation produces a wide range of droplet sizes many of which cannot necessarily be eliminated by improving the operating conditions.

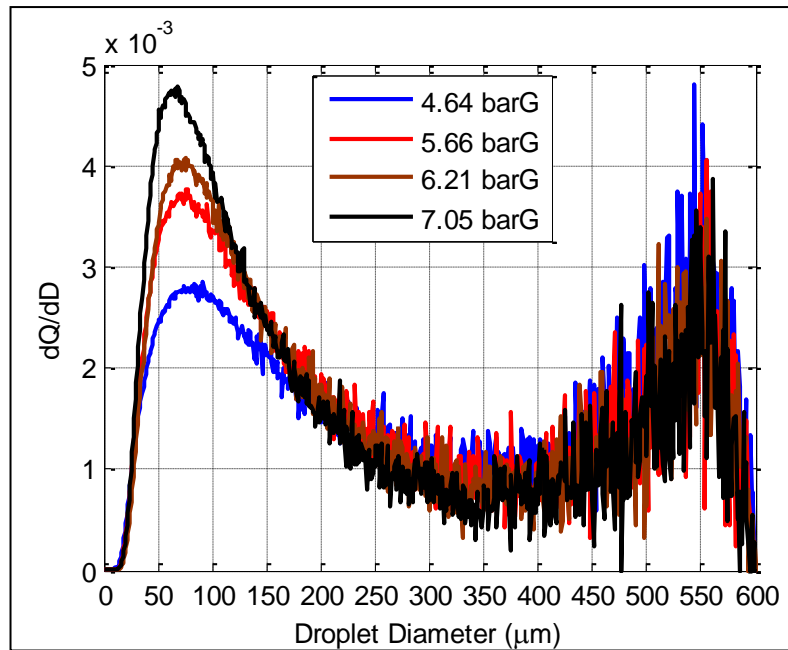


Figure 5.2.7 Droplet diameter frequency distribution by mass.

### 5.2.8 Spray Average Cumulative Droplet Size Distributions

The mass-under-size curves in Figure 5.2.8 identify the same trend with the largest  $\Delta P$  sprays possessing steeper gradients at lower droplet ranges and more parallel gradients thereafter. The mass-under-size curves are arranged in the expected order with the 7.05 barG spray at the top and the 4.64 barG spray at the bottom. The former spray was clearly the best atomised. The plots in Figure 5.2.8 agree with the trend indicated by the global spray SMDs shown in Table 5.2.2.

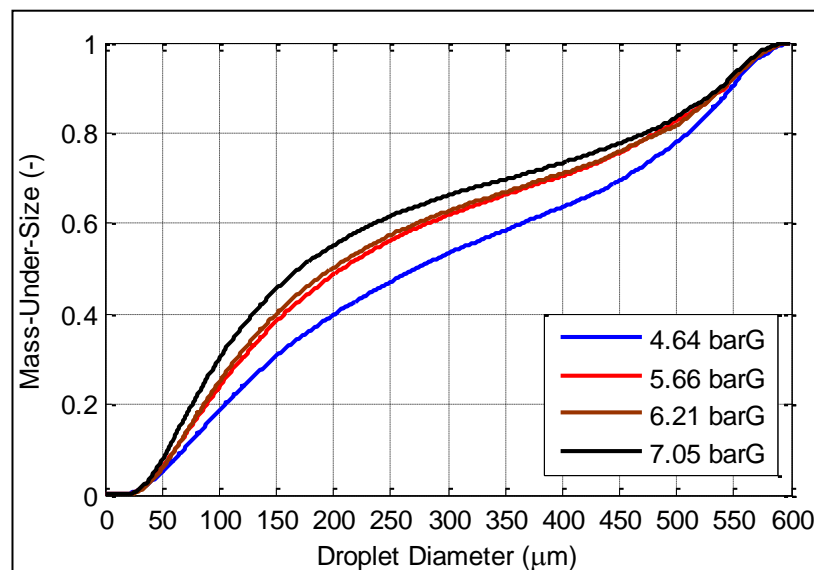


Figure 5.2.8 Cumulative droplet size distribution.

### 5.2.9 Validated Local Data Rates

Appendix A presents the complete data set for the present test phase including the plots of validated local droplet count varying with  $\Delta P$ . For brevity, in this section, the data from only one axial location will be presented and this will be compared against a reference case. The reference case selected was the 1.83% ALR spray from test phase 1 (6.68 barG pressure differential, 2 mm exit orifice diameter, 25.4 mm mixing chamber diameter, exit orifice length-to-diameter ratio of 1, aerator geometry 1, with air and water as the operating fluids). This test point was selected as the reference case since, as Figure 5.1.3 and Figure 5.1.4 show, this is the operating point at which poor quality atomisation gives way to effervescent atomisation (good quality sprays could not be achieved at lower ALRs). All remaining tests had a larger ALR than the reference case, which can be considered to be one of the lower limits at which effervescent atomisation is possible.

The axial location selected was 150 mm downstream of the exit orifice since this is the location at which combustion typically begins for steam/air-assist boiler combustion systems, and is therefore the location at which spray quality is particularly important. Although one axial sampling location will provide a limited view of the spray, this is the only way to provide a brief and clear comparison of the droplet data.

Figure 5.2.9 compares the validated local data rates at 150 mm downstream of the exit orifice for the reference test case and for the pressure differential tests. The data at this axial location can be considered typical. The local data rates show a similar pattern for all sprays investigated. The highest data rates were obtained at a radial location slightly offset from the centreline. The centreline regions frequently proved very dense and therefore light attenuation and multiple scattering effects resulted in the loss of data (mainly from smaller droplets). It is clear that light attenuation effects became significant at radial locations of less than 10 mm away from the spray centreline. It should be noted that the absolute values of validated data rates cannot readily be compared across different tests since data rates are a function of the PDA software and hardware set-up, which can change between tests.

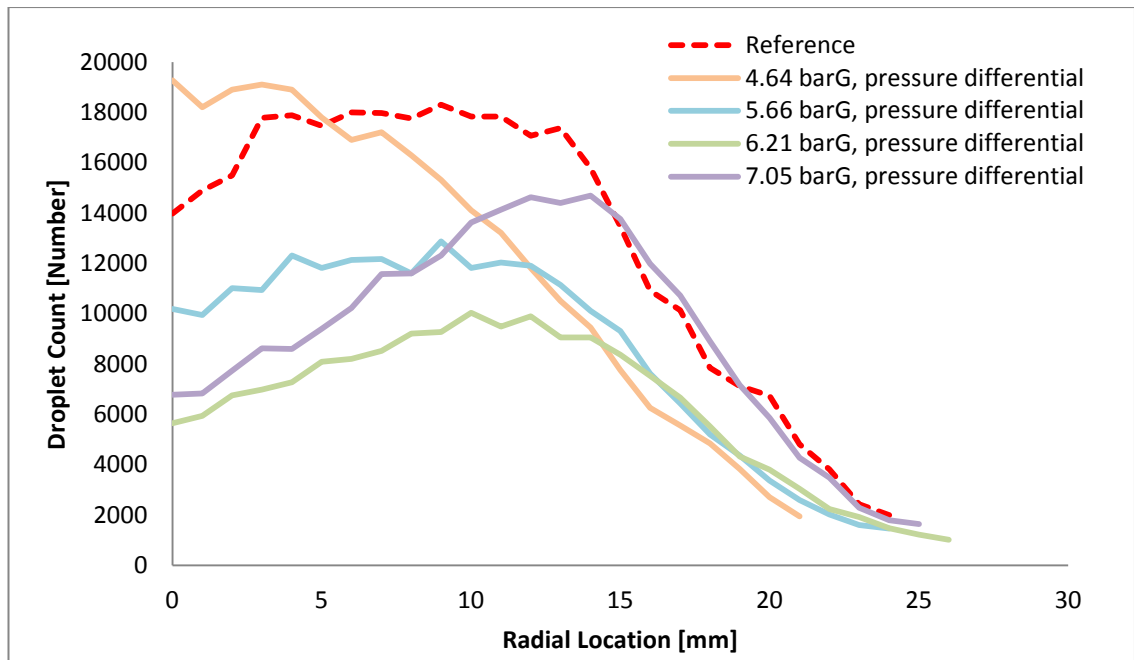


Figure 5.2.9 Validated local data rates at 150 mm downstream of the nozzle.

### 5.2.10 Local Droplet Velocity

The average local droplet velocity at 150 mm downstream of the exit orifice is shown for the reference test case and for the pressure differential tests in Figure 5.2.10.

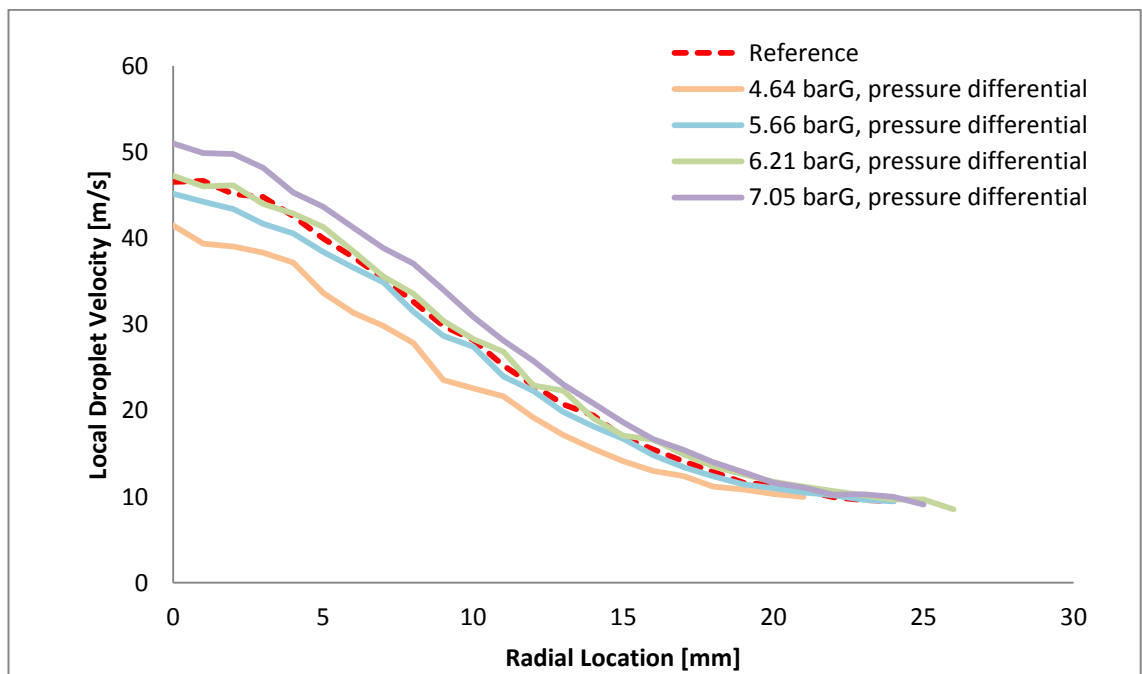


Figure 5.2.10 Average local droplet velocity at 150 mm downstream of the nozzle.

The results presented can be considered representative. It can clearly be seen that increases in pressure differential resulted in an increase in average local droplet velocity at all radial locations. This result is expected since greater pressures are associated with larger forces acting on the droplets and greater momentum for all droplets in the spray.

### 5.2.11 Inferred Local Gas and Relative Velocity

The inferred average local gas velocity and the inferred average relative velocity (which gives an indication of estimated gas-liquid phase slip) at 150 mm downstream of the exit orifice is shown in Figure 5.2.11 and Figure 5.2.12, respectively.

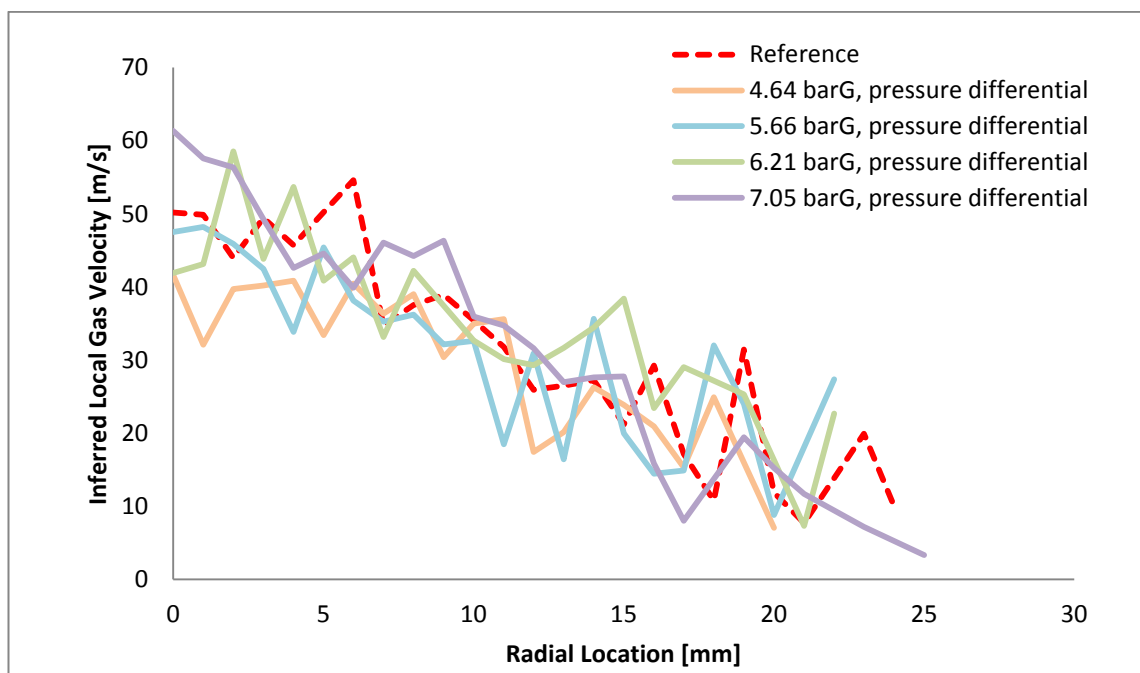


Figure 5.2.11 Inferred average local gas velocity at 150 mm downstream of the nozzle.

It should be noted that seeding particles were relatively few in number, which led to uncertainties in the estimates of gas and relative velocity (this can be seen in both Figure 5.2.11 and Figure 5.2.12). However, to aid clarity, error bars have not been drawn. Nevertheless it is clear that increasing pressure differential had an insignificant influence on both inferred gas and inferred relative velocities. The inferred relative velocities shown in Figure 5.2.12 demonstrate that phase slip with an average value of about -5 m/s, occurred for all tests. Small, negative values of phase slip were expected since the entrained ambient air will begin to increase its velocity to match that of the faster moving droplets.

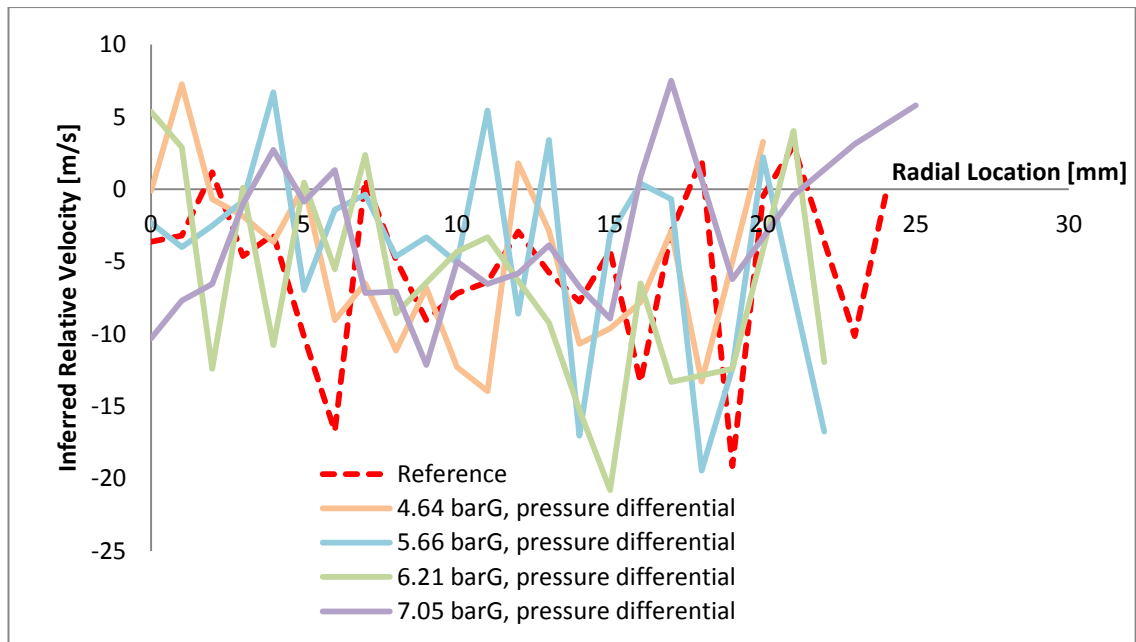


Figure 5.2.12 Inferred average relative velocity at 150 mm downstream of the nozzle.

### 5.2.12 Local Droplet AMD and SMD

Local droplet AMD and local droplet SMD at 150 mm downstream of the exit orifice diameter is shown in Figure 5.2.13 and Figure 5.2.14, respectively.

The large droplet SMD (Figure 5.2.14) at the centreline indicates that this is the location at which the largest droplets are to be found. These very large droplets or disintegrating liquid ligaments could correspond to an intact unatomised central liquid core (or to the predominance of non-spherical particles).

A notable effect of  $\Delta P$  increases is to slightly reduce droplet SMD at most sampled locations within each spray. This reduction in droplet SMD (but not droplet AMD, which in fact increases slightly) can mostly be attributed to the elimination of a small numbers of larger droplets (with few other changes throughout the sampled spray regions) as mixing chamber pressure was raised. It is clear that increasing  $\Delta P$  improved the atomising contribution of so-called primary atomisation, which left fewer large droplets and unatomised ligaments throughout the spray.

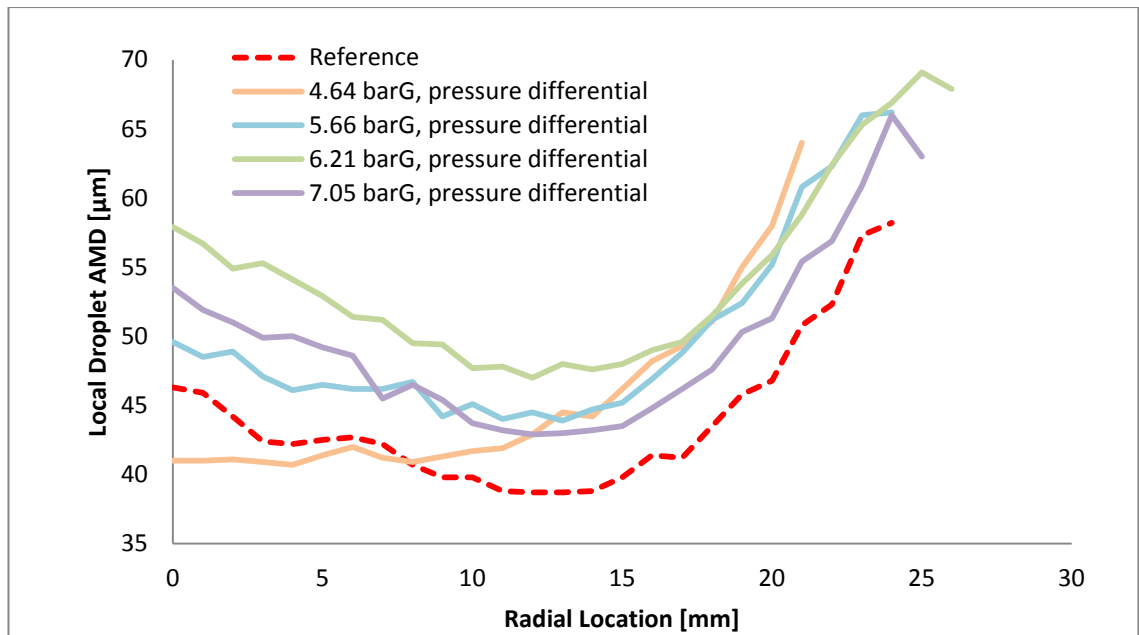


Figure 5.2.13 Local droplet AMD at 150 mm downstream of the nozzle.

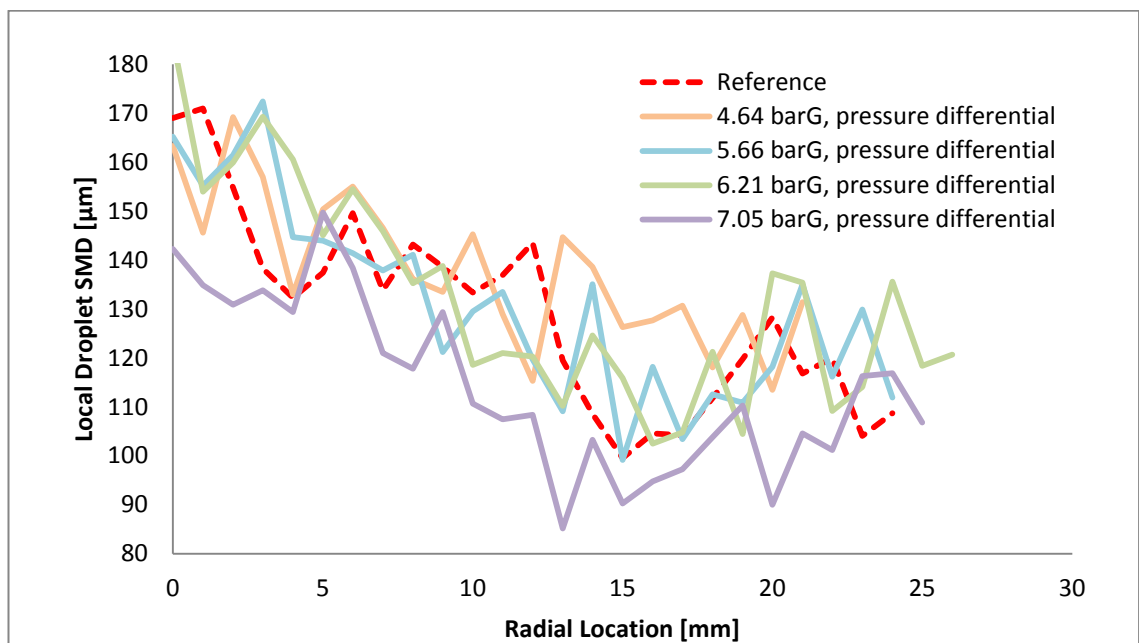


Figure 5.2.14 Local droplet SMD at 150 mm downstream of the nozzle.

### 5.2.13 Local Droplet Size Consistency

Local droplet SMD/AMD ratio for all  $\Delta P$  sprays and for the reference test case at 150 mm downstream of the exit orifice is presented in Figure 5.2.17.

As previously discussed, droplet SMD/AMD ratios close to unity indicate very narrow droplet size distributions while large ratios indicate a large range of droplet sizes. It is clear from Figure 5.2.17 that increasing  $\Delta P$  reduced local droplet size spread and



produced a more consistent and therefore better atomised spray throughout. As suggested, this could be explained by larger primary atomisation contributions at higher pressures, leaving fewer large droplets throughout the spray.

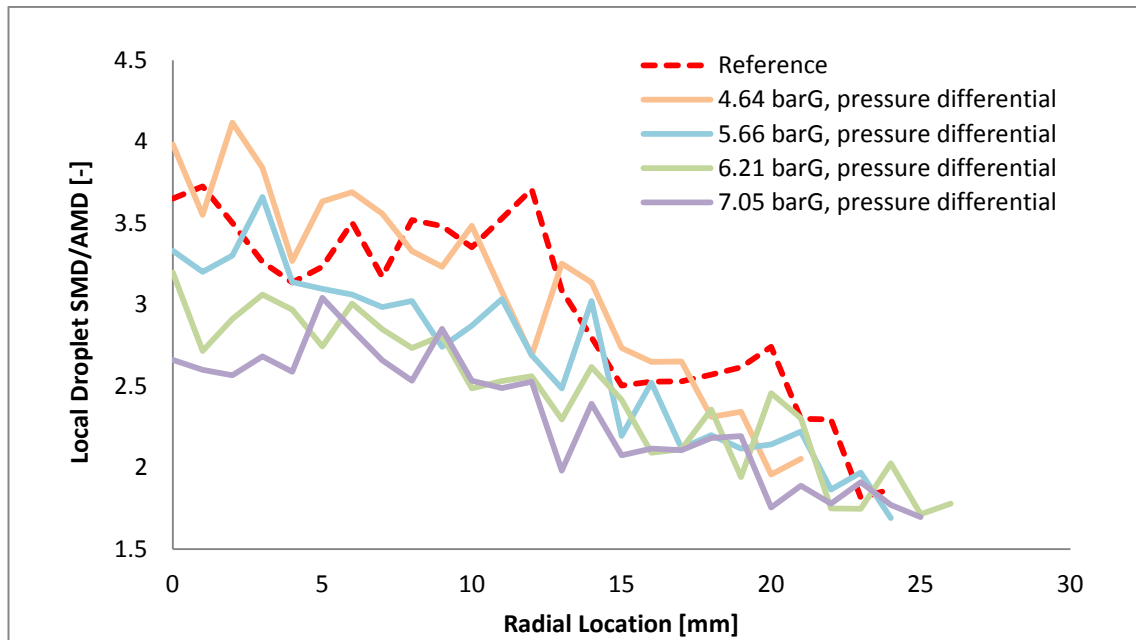


Figure 5.2.15 Local droplet SMD/AMD at 150 mm downstream of the nozzle.

#### 5.2.14 Droplet Secondary Break-up

Figure 5.2.16 shows the average local Weber number at 150 mm downstream of the exit orifice.

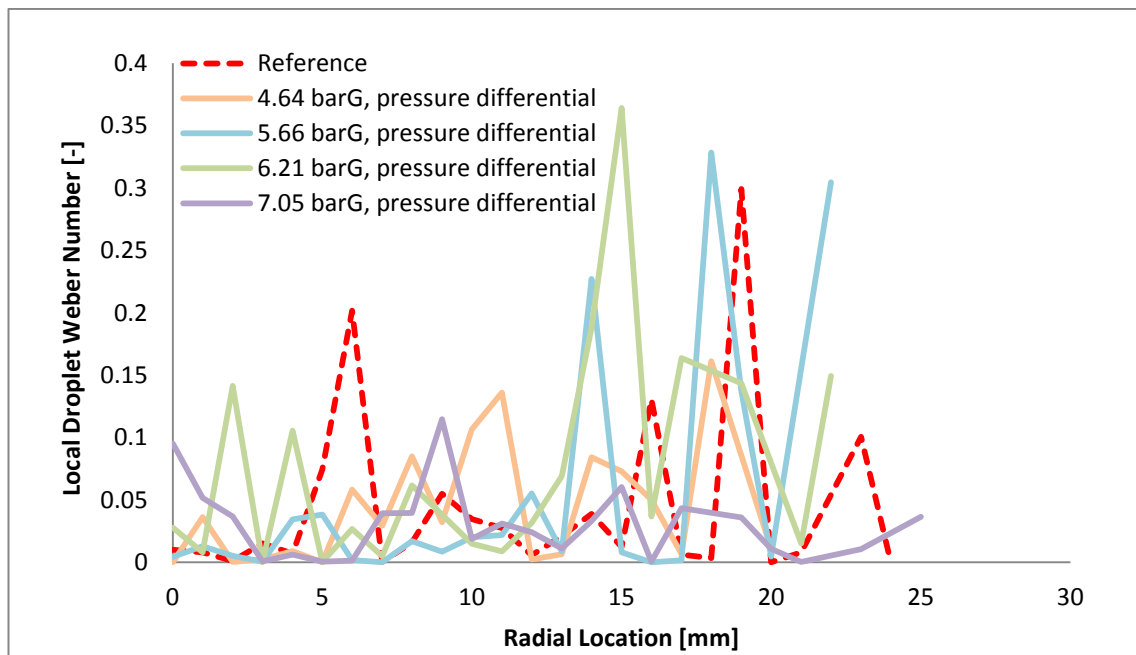


Figure 5.2.16 Average local droplet Weber Number at 150 mm downstream of the nozzle.

Just as in test phase 1, average local Weber number is more than an order of magnitude smaller than commonly quoted values of critical Weber number ( $11 \pm 2$ ). Clearly the average local droplet Weber number plots do not provide evidence for secondary atomisation since this affected a small total number of droplets (only the very large ones), and these were not numerous enough to influence the average Weber number values.

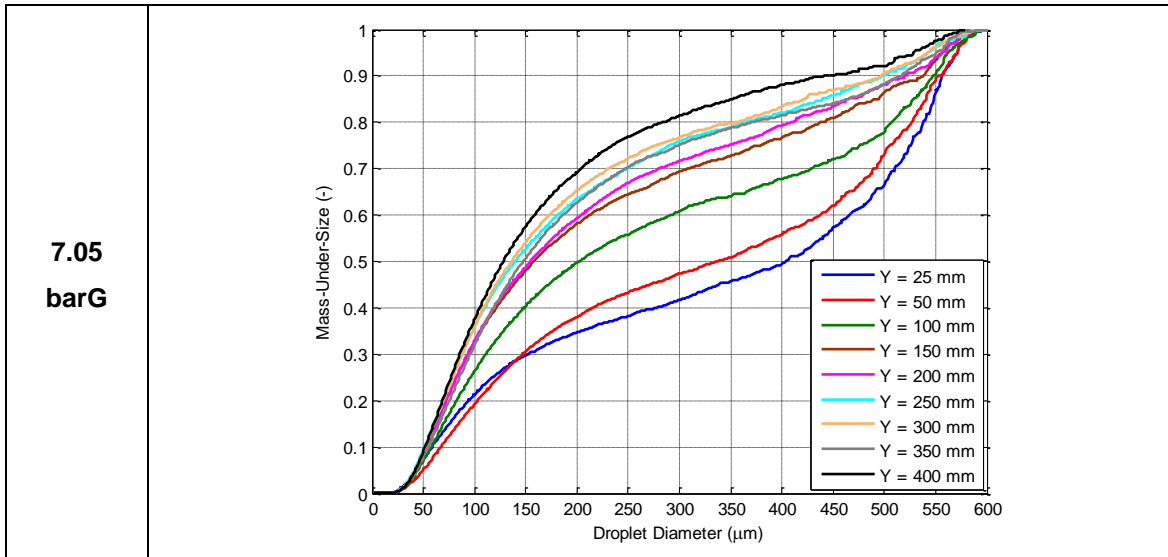
#### ***5.2.15 Spray Development in the Downstream Direction***

The changes in spray mass as the droplets progressed in the downstream direction are displayed in Table 5.2.3. Downstream spray quality improvements are visible in the mass-under-size plots (25-400  $\mu\text{m}$  downstream) of all sprays investigated. This downstream improvement in spray quality is likely to be the result of the disintegration of a relatively small numbers of larger droplets.

Just as in test phase 1, the relatively similar mass-under-size gradients for droplet diameters between 250  $\mu\text{m}$  and 400  $\mu\text{m}$  at all spray axial locations indicates that the droplets of these size ranges appear to progress through the spray relatively unchanged. By contrast, droplets larger than 400  $\mu\text{m}$  reduce further downstream while droplets smaller than 250  $\mu\text{m}$  simultaneously increase. This would indicate a critical droplet size of about 400  $\mu\text{m}$  for the conditions investigated. Droplets larger than this seem to have exceeded the critical Weber number and disintegrated via secondary break-up mechanisms into multiple smaller droplets. Calculations indicate that a 400  $\mu\text{m}$  droplet typically requires a relative gas-liquid velocity of 40 m/s to attain a Weber number of 11 (critical Weber number). Figure 5.2.10 shows that this velocity is realistic, especially for droplets located along the spray centreline.

Table 5.2.3 Cumulative mass-under-size plots for entire downstream locations.

Spray $\Delta P$	Mass-Under-Size Plot
4.64 barG	
5.66 barG	
6.21 barG	



**5.2.16 Droplet SMD Correlations from the Literature for EA**

Figure 5.2.17 displays experimentally determined global spray droplet SMD for each  $\Delta P$  spray of test phase 2. These are compared against droplet SMD predicted by correlations from the literature (shown in Table 5.2.2). It is clear that none of the correlations could accurately predict global spray droplet SMD variation as  $\Delta P$  was varied. Amongst other factors, this discrepancy is due to different spray sampling techniques, differing sampling locations and different atomiser geometries and parameter ranges investigated.

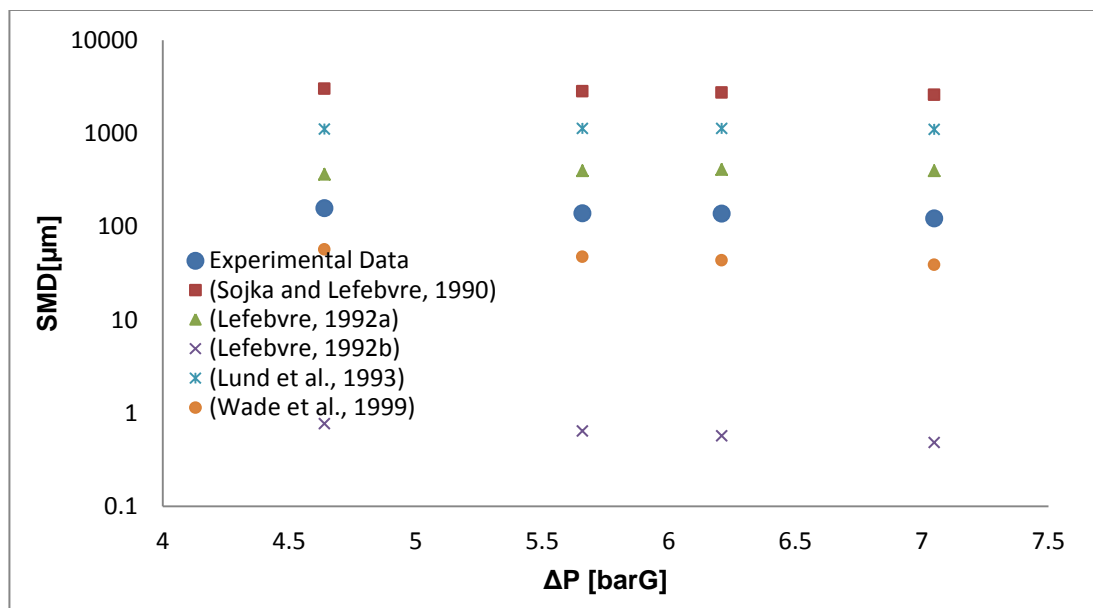


Figure 5.2.17 Comparison of global spray droplet SMD from PDA experiments with that predicted by correlations in the literature.

### 5.2.17 Effect of $\Delta P$ on Global Spray droplet SMD for Experimental Data

Figure 5.2.18 graphically illustrates the relationship between global spray droplet SMD and  $\Delta P$ , and Equation 5.2.1 displays the proportionality obtained for a power law relationship (this provided the best fit to the experimental data). Equation 5.2.1 shows that  $\Delta P$  is as influential an operating parameter as ALR in the bubble-bursting regime ( $ALR < 5\%$ ), and is more important than ALR in the tree-like regime of operation ( $ALR > 5\%$ ).

It may seem surprising (given the global droplet SMD values listed in Table 5.1.2 and Table 5.2.2) that all but the worst ALR sprays were better atomised (lower global droplet SMD) than any of the  $\Delta P$  sprays. This, however, is a consequence of the regions where the ALR and  $\Delta P$  tests were conducted. Test phase 1 was characterised by a large ALR range and large  $\Delta P$ , generally providing good quality atomisation. In contrast, test phase 2 was characterised by a relatively small range of  $\Delta P$  and a low ALR, providing somewhat poorer atomisation. Overall it is clear that  $\Delta P$  had a marginally greater influence on global spray SMD than air-to-liquid by mass ratio for the atomiser geometry and conditions investigated.

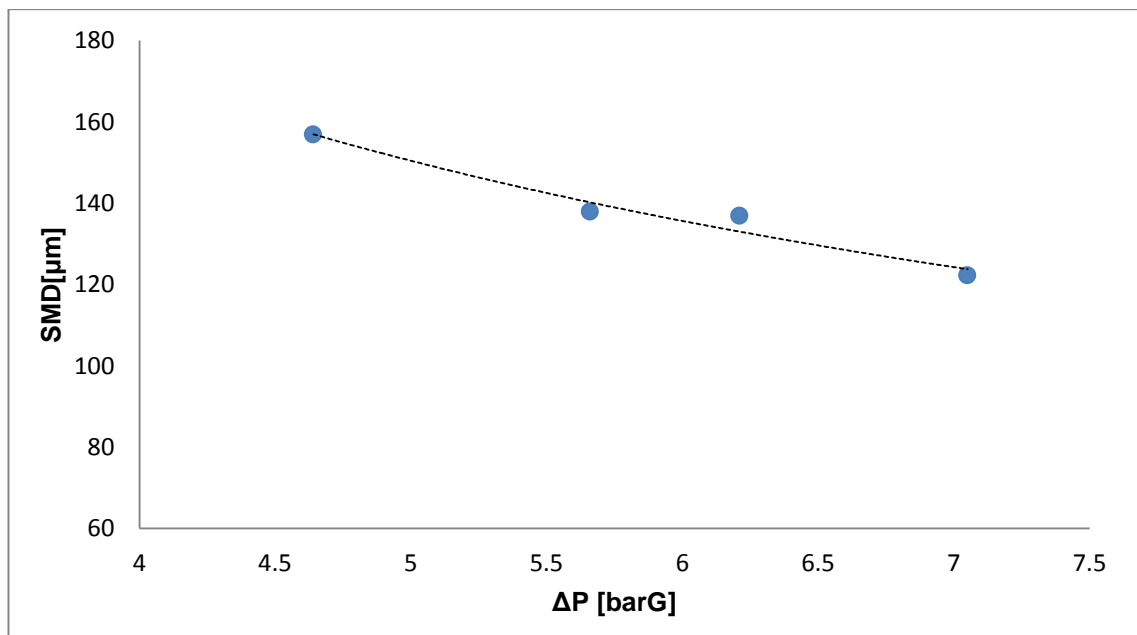


Figure 5.2.18 The relationship between  $\Delta P$  and global spray SMD as calculated using PDA data.

$$SMD \propto 375.07\Delta P^{-0.5677}$$

Equation 5.2.1

The strong influence of  $\Delta P$  on global spray SMD demonstrated by the present study supports the findings of some previous researchers who report pressure having a

strong influence on spray quality [60, 70]. Other researchers claimed pressure drop had only a minor influence compared to ALR [18, 57, 58, 75]. However, some of these studies (e.g. Lörcher et al, Petersen et al) investigated very low flow rates. The different parameter ranges and atomiser geometries investigated are likely to be responsible for the discrepancy in findings.

Despite the conflicting reports from previous research, the present study provides clear evidence that mixing chamber pressure had an important influence on spray quality, over the parameter ranges (and atomiser geometries) investigated. A linear, inversely proportional relationship between  $\Delta P$  and global spray droplet SMD is seen to emerge. This is not altogether unexpected since greater operating pressures are known to improve atomisation quality.

However it should be noted that only a relatively small pressure range was investigated (4.64-7.05 barG). The house air supply (limited to 8 barG) and the baseline atomiser geometry (which permitted a steady-state, stable spray only for certain operating conditions – see Figure 5.2.1 and Figure 5.2.2) somewhat limited the testable pressure ranges. In order to extend the present investigation, a superior air supply system or an alternative atomiser geometry is required (e.g.  $D_o$ , see testable pressure ranges for test phase 3).

## Chapter 6 : Results – Atomiser Geometry

### 6.1 Test Phase No.3 – Exit Orifice Diameter, $D_o$

#### 6.1.1 Preliminary Investigations

The geometric parameter exit orifice diameter is shown in Figure 6.1.1 and Table 6.1.1 illustrates the position of the  $D_o$  investigations within the test program.

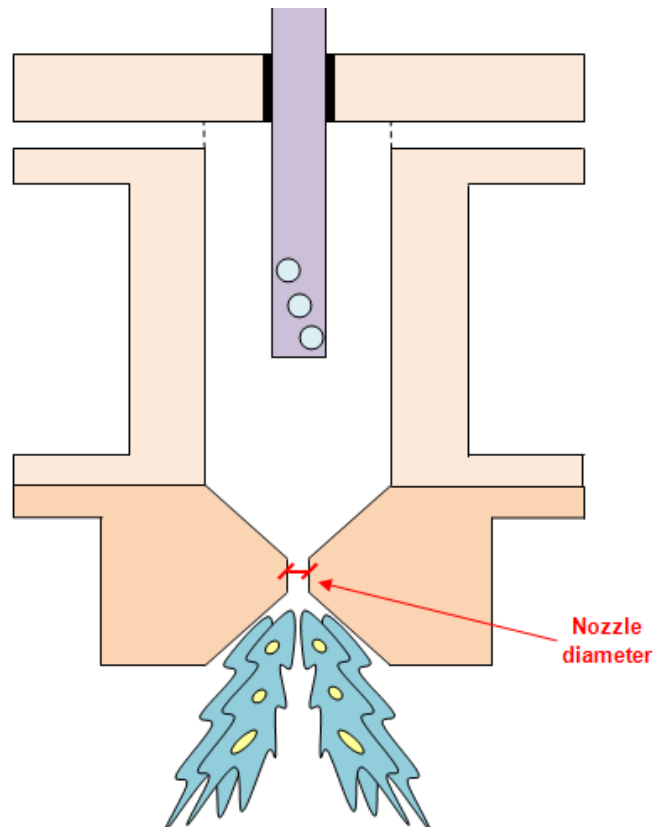


Figure 6.1.1 Schematic showing the geometric parameter exit orifice diameter.

Table 6.1.1 Operating conditions and controlled parameters for  $D_o$  tests.

TEST No. PARAMETER VARIED	1 ALR	2 $\Delta P$	3 $D_o$	4 $L_{MC}$	5 $D_{MC}$	6 $L_o/D_o$	7 A. GEOM.	8 $\eta$
TEST PHASE	A. Initial Operating Parameters			B. Atomiser Geometry				C. Fluid properties
ALR (%)	0.8-12.5	2		2				
$\Delta P$ (bar.g)	7	4-7		7				
$D_o$ (mm)	2	2	2-4	2	2	2	2	2
$L_{MC}$ (mm)	140	140	140	64-140	140	140	140	140
$D_{MC}$ (mm)	25.4	25.4	25.4	25.4	20-30	25.4	25.4	25.4
$L_o/D_o$ (-)	1	1	1	1	1	0.5-2	1	1
Aerator Geometry	A1	A1	A1	A1	A1	A1	A2, A3	A1
$\eta \times 10^{-8}$ ( $m^2/s$ )	1	1	1	1	1	1	1	2-10

Figure 6.1.2 and Figure 6.1.3 indicate the regions where well-atomised, steady-state sprays could be achieved for an ALR of 2-12% for the system used.

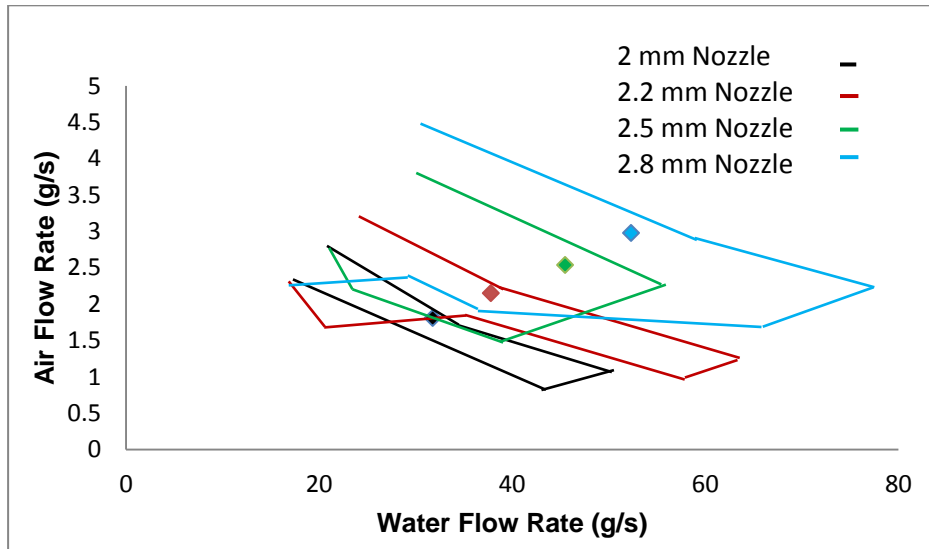


Figure 6.1.2 Combined graphs of “spray quality” showing liquid flow rates at which optimal effervescent atomisation can be achieved with different nozzle diameters.

The coloured, diamond-shaped points show the test conditions investigated for each nozzle, with the point colours matching the line colours.

It can be seen from Figure 6.1.2 and Figure 6.1.3 that larger nozzles widened and shifted the operating envelopes (indicating the regions of good-quality effervescent atomisation). This was expected as greater flow rate ranges are achievable with larger nozzles.

In order to isolate the variable  $D_o$ , the values of ALR and  $\Delta P$  were kept constant throughout the entirety of test phase 3.



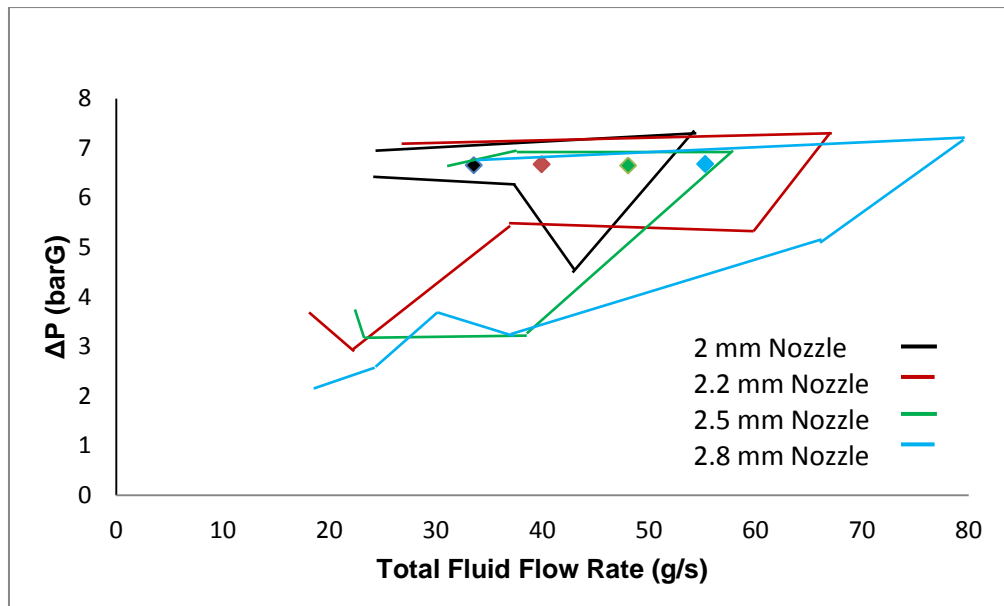


Figure 6.1.3 Combined graphs of spray quality showing mixing chamber pressures and total flow rates at which tests were performed with different nozzles.

### 6.1.2 Spray Characteristics and Results

The results are given in Table 6.1.2. These indicate the average values of ALR varied between 5.59-5.7% while  $\Delta P$  varied between 6.65-6.67 barG, giving a variation of 2% and 1% respectively. Meanwhile  $D_o$  varied from 2-2.8 mm giving a total variation of 40%. Since  $D_o$  varied by an order of magnitude more than any other variable it is clear that exit orifice diameter was the dominant operating parameter.

Table 6.1.2 Summary of  $D_o$  test operating conditions and spray characteristics.

Test	2 mm $\emptyset$	2.2 mm $\emptyset$	2.5 mm $\emptyset$	2.8 mm $\emptyset$
<b>Water Supply Pressure (barG)</b>	7.38	7.44	7.44	7.52
<b>ALR (%)</b>	5.70	5.70	5.59	5.70
<b>Mixing Chamber Pressure, <math>\Delta P</math> (barG)</b>	6.65	6.67	6.65	6.68
<b><math>m_{\text{WATER}}</math> (g/s)</b>	31.75	37.79	45.50	52.32
<b><math>P_{\text{AIR}}</math> (barG)</b>	7.23	7.23	7.27	7.32
<b><math>m_{\text{AIR}}</math> (g/s)</b>	1.81	2.15	2.54	2.98
<b>Volumetric Void Fraction, <math>\alpha</math> (%)</b>	86.1	86.1	85.9	86.1
<b>Effective Power Rating (MW)</b>	1.27	1.51	1.82	2.09
<b>Coefficient of Discharge (-)</b>	0.28	0.33	0.40	0.46
<b><math>\theta/2</math> at 25 mm downstream (deg)</b>	25.64	27.47	30.96	29.25
<b><math>D_{32}</math> (<math>\mu\text{m}</math>)</b>	81.06	97.27	109.25	103.66

It should be noted that the  $D_o = 2$  mm test was performed during test phase 1. For greater economy, the test campaign was arranged such as to allow some test points to be re-used for later test phases. However, since data and validation rates were high (up to 10 kHz and over 90% for most test points, respectively) for each test performed, the results can justifiably be compared across test phases.

### 6.1.3 Nozzle Coefficient of Discharge

Figure 6.1.4 compares the experimental coefficient of discharge to those predicted by correlations in the literature. The correlation provided by Chen and Lefebvre most closely matched the experimental data. Very low experimental coefficients of discharge (0.28-0.46) were observed with discharge coefficient increasing as exit orifice diameter was increased.

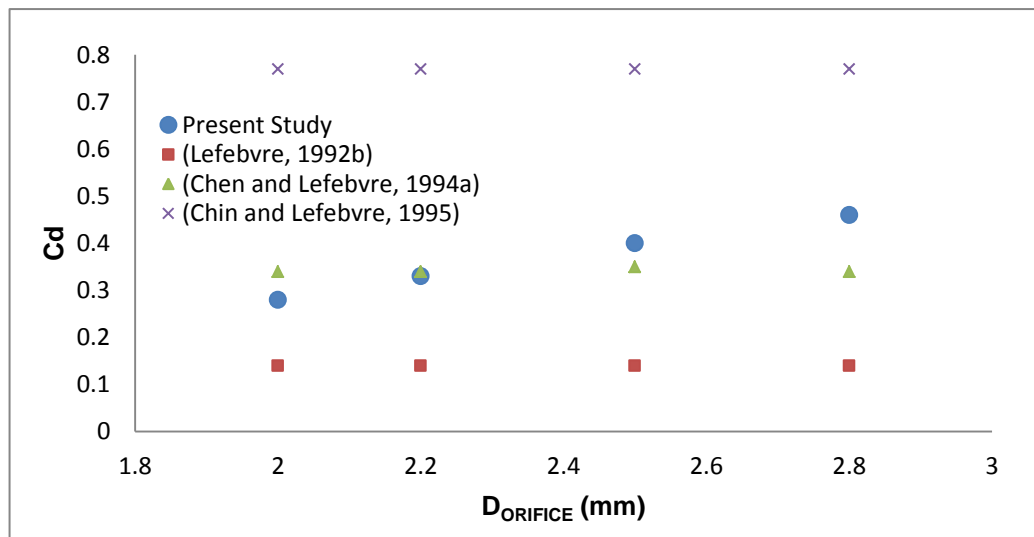


Figure 6.1.4 Comparison of coefficient of discharge from PDA experiments and literature.

### 6.1.4 Mode of Liquid Break-up at Nozzle

The liquid break-up mode analysis proved to be a beneficial tool in comparing spray quality at different operating conditions. However, this analysis does not appear to provide useful insights when applied to analysis of effervescent atomiser geometry. For example, larger exit orifice diameters are predicted to improve spray quality. This prediction is a result of the larger Reynolds numbers expected as  $D_o$  is increased. According to continuity, larger nozzles should allow greater fluid velocities since mass flow rate increases more quickly than nozzle cross-sectional area. These result in larger gas-liquid relative velocities at the nozzle and therefore (for the same fluid properties and similar liquid ligament diameters) Reynolds number at the nozzle is predicted to increase. This should translate into operation further inside the desirable

atomisation regime which is expected to result in improved atomisation. However improved atomisation with larger exit orifice diameters is instinctively (and from experiments) known to not occur in most atomiser types, including the present one (e.g. see Table 6.1.2).

It is possible that the weakness of the liquid break-up mode analysis when applied to exit orifice diameter is due to deviation from the assumed fluid behaviour at greater nozzle diameters (e.g. increasing nozzle dimensions make the assumptions of a discrete number of circular liquid jets at the nozzle less plausible). As a result, this analysis will not be performed when investigating the influence of atomiser geometric parameters on spray quality.

### 6.1.5 Spray Half-Angle

Experimentally determined spray half-angle is displayed in Figure 6.1.5 where it is compared to the correlation of Sovani et al. There is a significant discrepancy between experimental data and predictions, most likely due to different definitions of spray dimensions as well as differing measurement techniques and sampling locations.

Exit orifice diameter appears to have slightly increased spray width (25-31°) though this may partly be due to experimental error since spray half-angle could have varied by  $\pm 3^\circ$ .

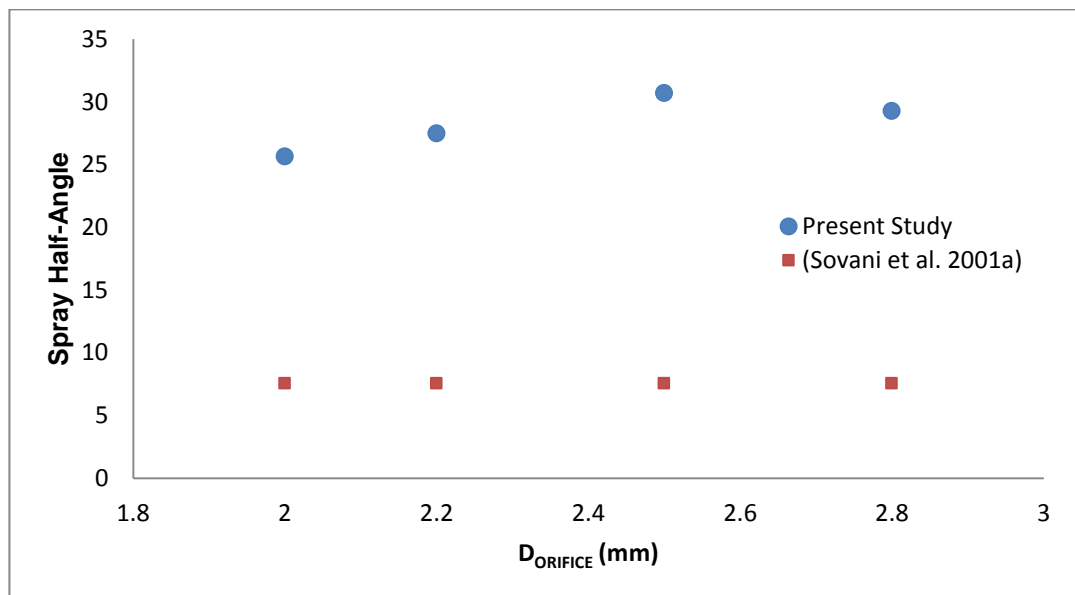


Figure 6.1.5 Comparison of spray half-angle from PDA experiments and literature.

### 6.1.6 Spray Droplet Size Distribution by Number

The droplet diameter frequency distributions by number for all experiments of test phase 3 are given in Figure 6.1.6. These graphs appear very similar, demonstrating that the majority of the droplets were small for all sprays investigated.

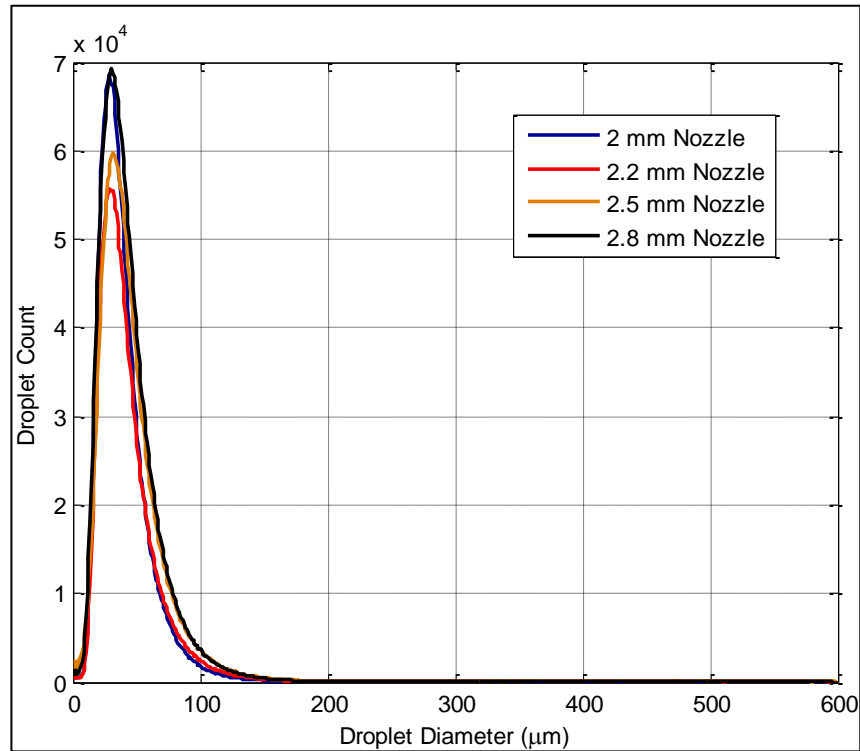


Figure 6.1.6 Droplet diameter frequency distribution based on number.

### 6.1.7 Spray Droplet Size Distribution by Mass

The droplet diameter frequency distributions by mass for all experiments of test phase 3 are given in Figure 6.1.7.

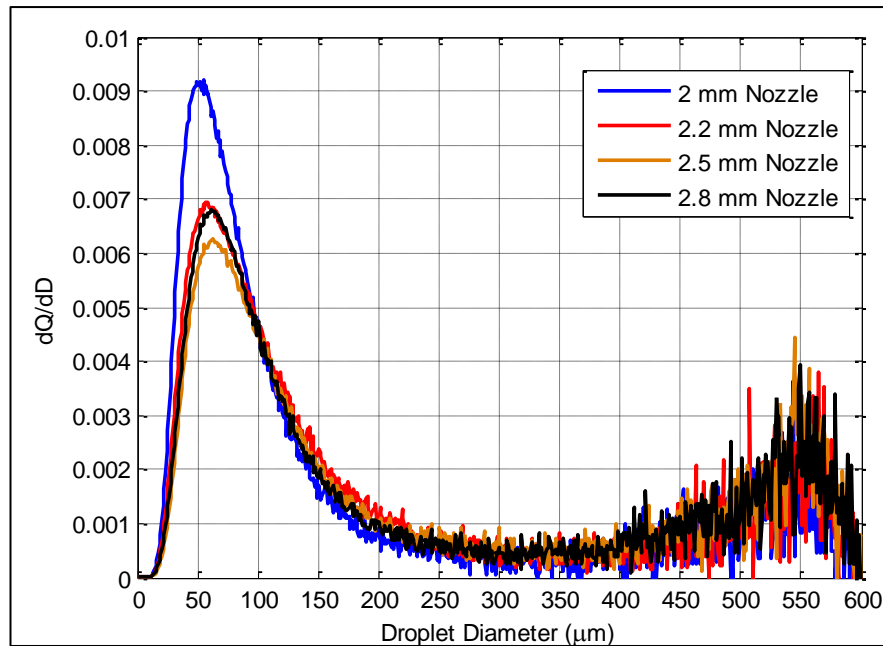


Figure 6.1.7 Droplet diameter frequency distribution by mass.

This graph shows a difference in spray distributions only at droplet sizes smaller than 100  $\mu\text{m}$ . It is clear that the spray produced by the smallest diameter orifice (2 mm) had the largest proportion of smaller droplets and was therefore the best atomised. The most poorly atomised spray appears to be the one produced by the 2.5 mm nozzle.

### 6.1.8 Spray Average Cumulative Droplet Size Distributions

Figure 6.1.8 displays the cumulative mass-under-size plots for all sprays tested.

This graph provides a clear view of the relative spray qualities and supports the results of Figure 6.1.7, demonstrating that the 2 mm nozzle produced the most finely atomised spray. As nozzle diameter was increased to 2.5 mm, spray behaviour comparable to that of plain orifice atomisers was observed, as spray quality worsened with increasing  $D_o$ . Increasing nozzle diameter further to 2.8 mm resulted in a slight improvement in spray quality. This finding was unexpected. In order to verify the accuracy of the test data, the PDA runs for the 2.5 mm and 2.8 mm nozzles were repeated. The results of these tests agreed well with the existing data, confirming the apparent improvement in spray quality as diameter was increased from 2.5 mm to 2.8 mm for the atomiser and conditions investigated.

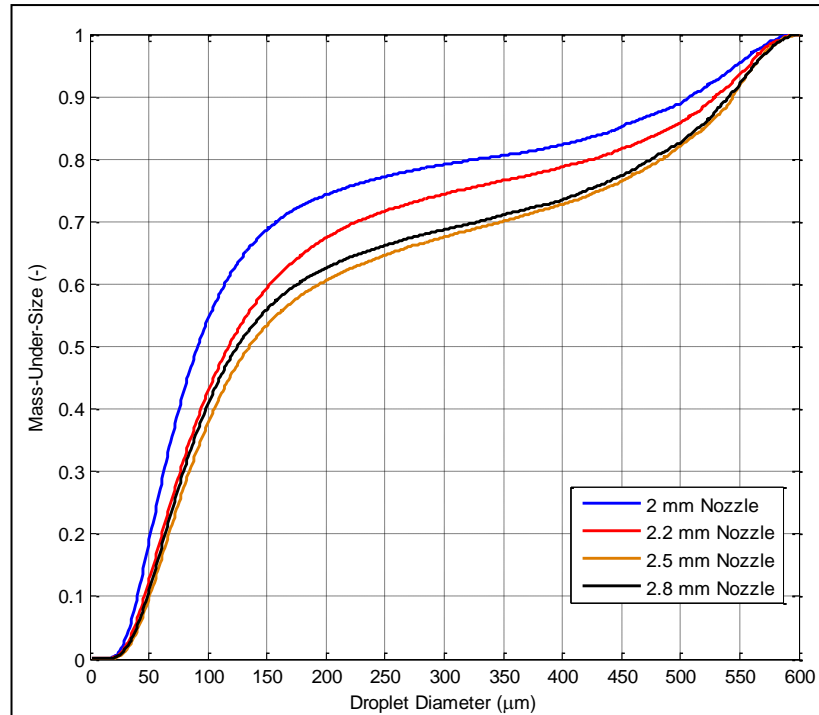


Figure 6.1.8 Cumulative droplet size distribution.

### 6.1.9 Validated Local Data Rates

The complete data set for this test phase is presented in Appendix B. Figure 6.1.9 shows the local data rates 150 mm axially downstream of the exit orifice. Just as in previous test phases, the highest data rates were found about half-way between the spray centreline and edge.

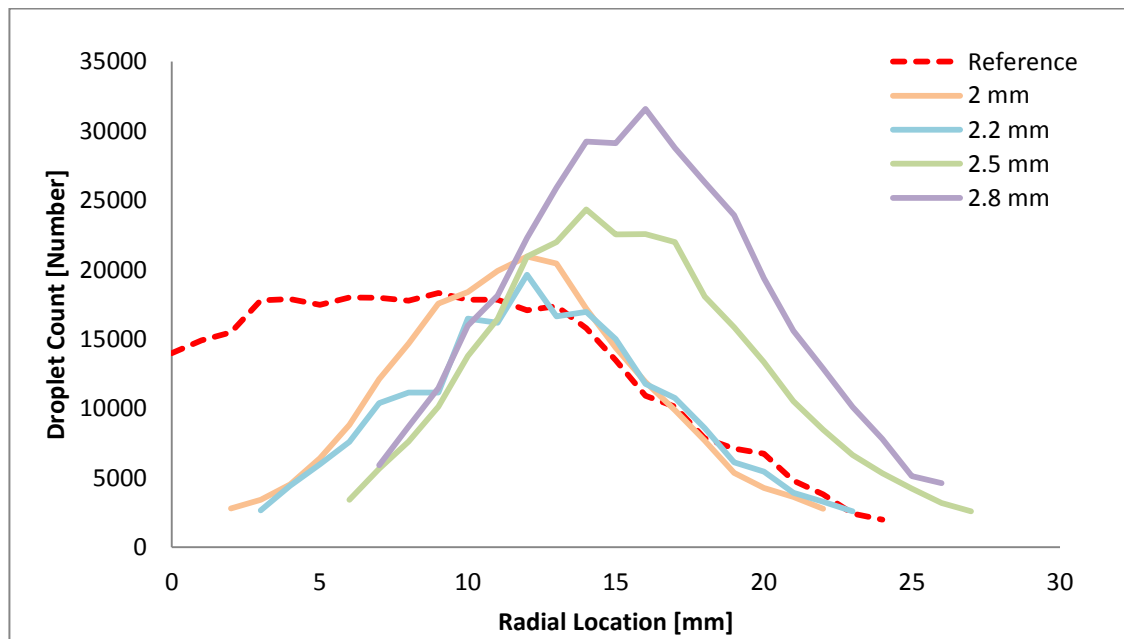


Figure 6.1.9 Validated local data rates at 150 mm downstream of the nozzle.

### 6.1.10 Local Average Droplet Velocity

The local droplet velocities 150 mm downstream of the exit orifice are presented in Figure 6.1.10. It appears that increases in nozzle diameter have resulted in minor increases in local droplet velocity. These are likely to be linked to the higher fluid mass flow rates required with larger exit orifice diameters.

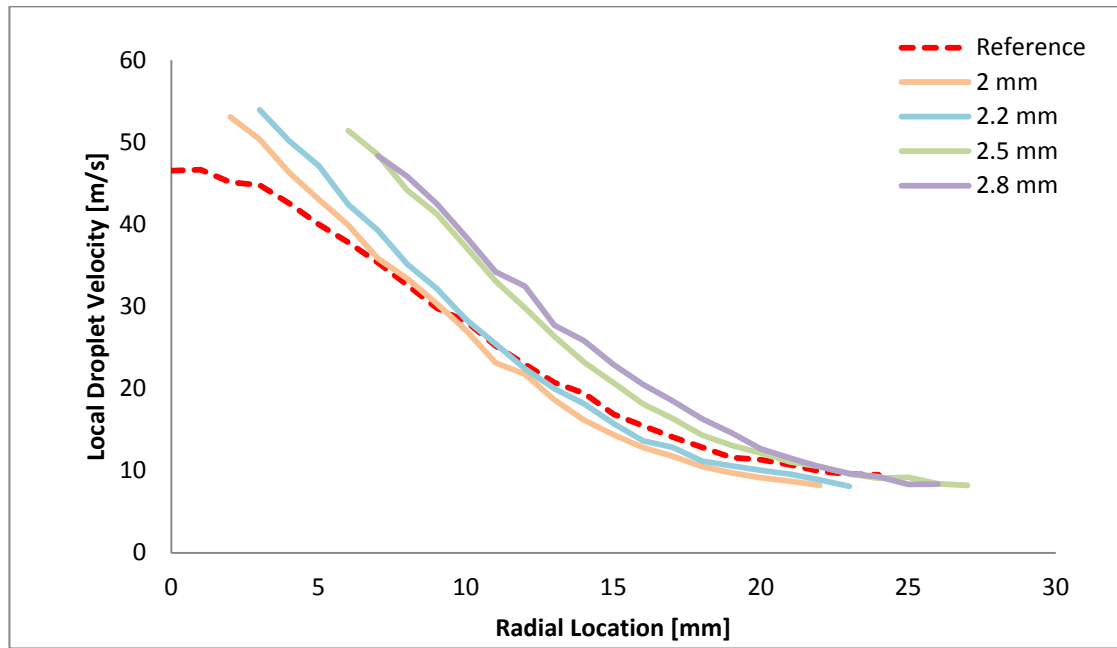


Figure 6.1.10 Average local droplet velocity at 150 mm downstream of the nozzle.

### 6.1.11 Inferred Local Gas and Relative Velocity

The PDA droplet data shows that exit orifice diameter had an insignificant effect on inferred gas and inferred relative velocity. As before, inferred relative velocity seems to centre on an average value of -5 m/s which indicates a small amount of phase slip. The full data sets are presented in Appendix B.

### 6.1.12 Local Droplet AMD and SMD

Local droplet AMD and SMD at 150 mm downstream of the exit orifice are presented in Figure 6.1.11 and Figure 6.1.12, respectively.

There is no clear relationship between exit orifice diameter and AMD (Figure 6.1.11), however SMD (Figure 6.1.12) appears to slightly increase as exit orifice diameter is increased. This provides evidence for deteriorating spray quality at larger nozzle diameters. This behaviour indicates that effervescent atomisation shows some similarities to traditional atomiser which perform better with smaller exit orifice diameters.

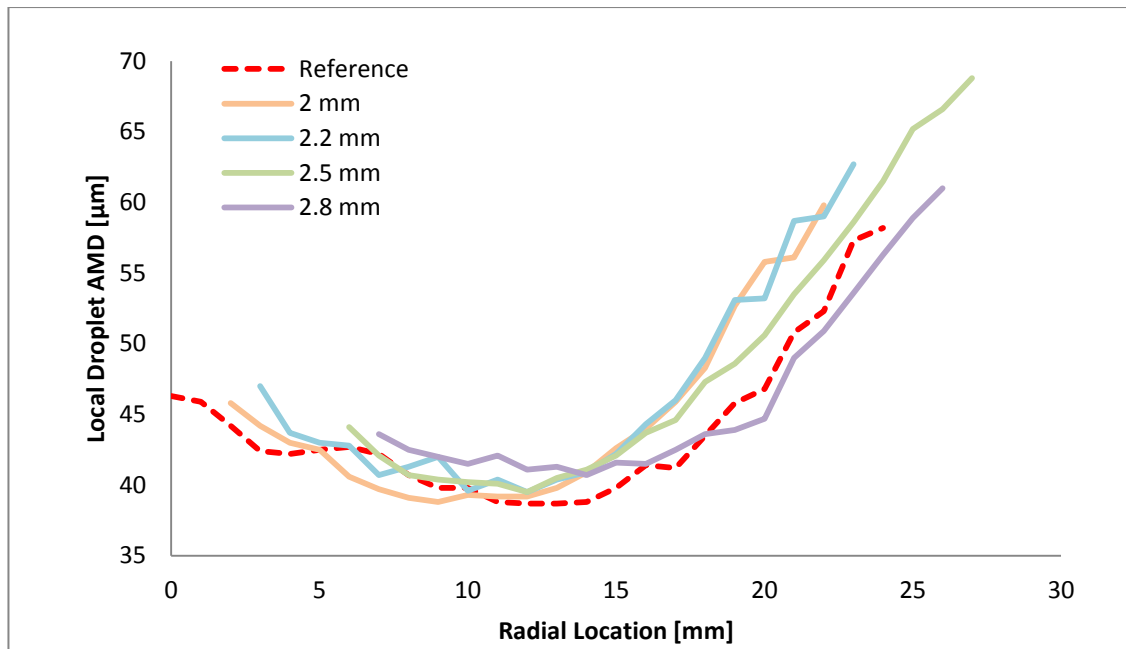


Figure 6.1.11 Local droplet AMD at 150 mm downstream of the nozzle.

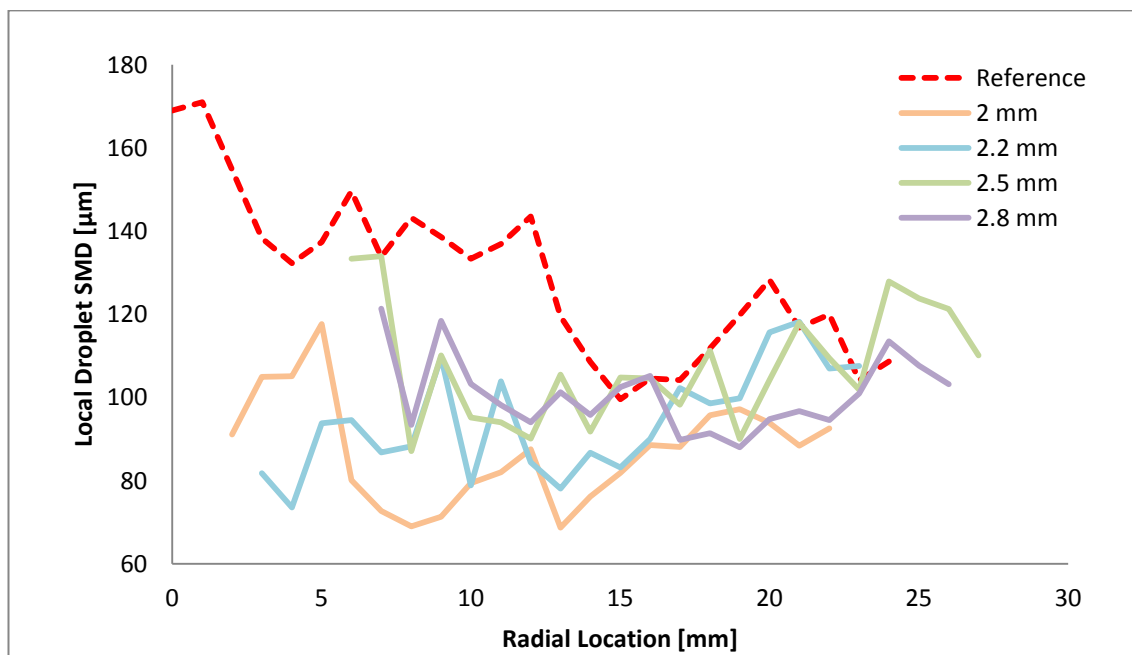


Figure 6.1.12 Local droplet SMD at 150 mm downstream of the nozzle.

### 6.1.13 Local Droplet Size Consistency

The droplet SMD/AMD ratio, presented in Figure 6.1.13, gives an indication of the droplet size consistency at every radial sampling location 150 mm downstream of the exit orifice. These graphs seem to indicate decreasing droplet consistency and therefore worsening atomisation performance as exit orifice diameter is increased.



However the 2.5 mm and 2.8 mm sprays appear similar in consistency at this axial location.

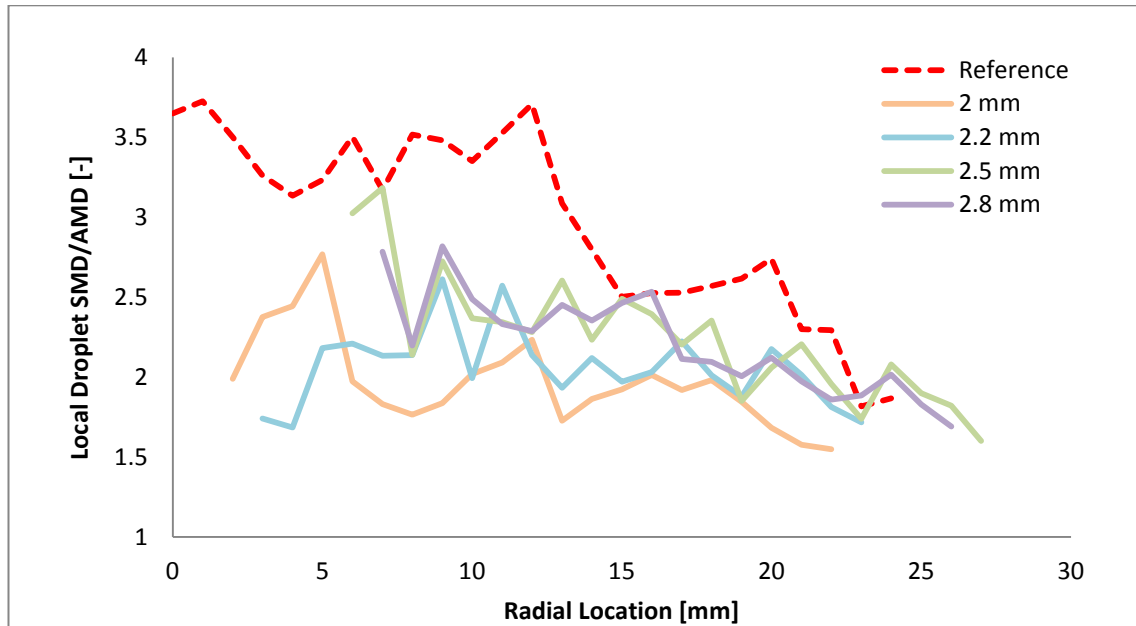


Figure 6.1.13 Local droplet SMD/AMD at 150 mm downstream of the nozzle.

#### 6.1.14 Droplet Secondary Break-up

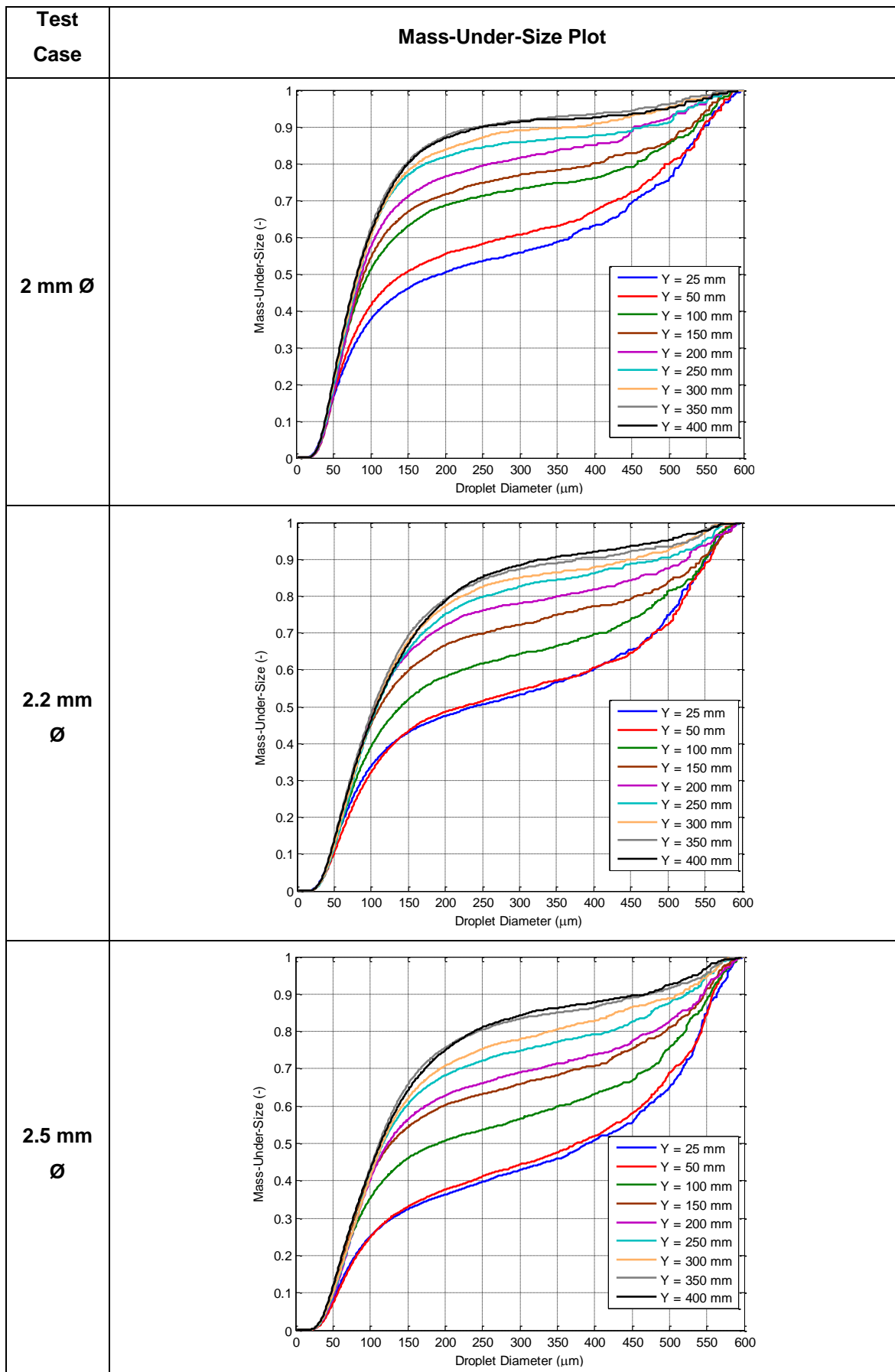
The average local Weber number throughout the spray is much smaller than critical Weber number (commonly take to be about  $11 \pm 2$ ), and therefore secondary atomisation cannot be detected. Complete sets of Weber number plots are provided in Appendix B.

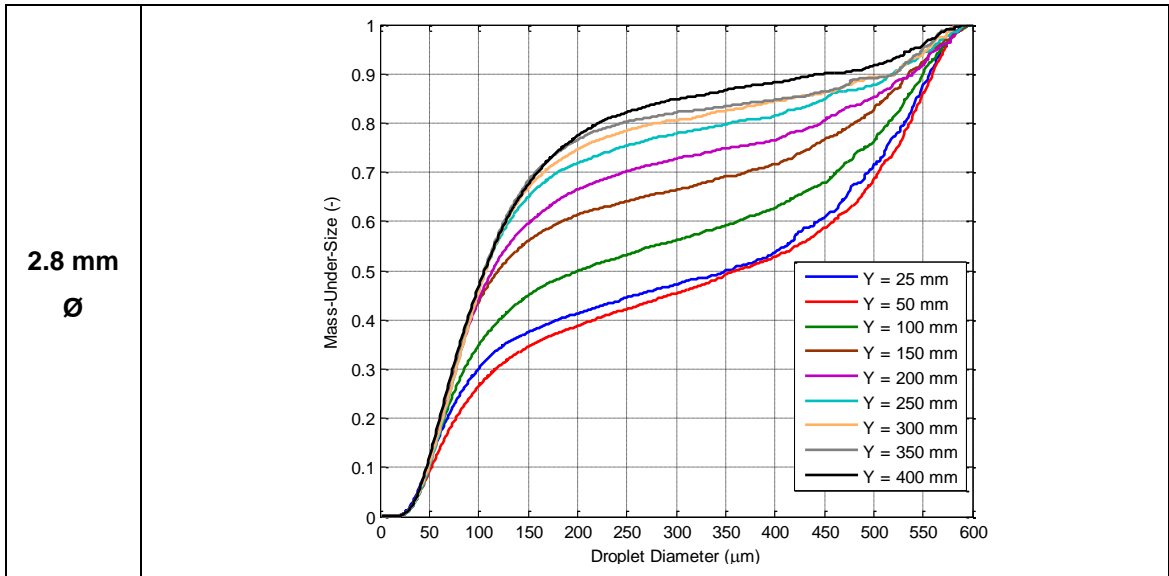
#### 6.1.15 Spray Development in the Downstream Direction

The downstream cumulative mass-under-size plots are given in Table 6.1.3. These plots show a comparable amount of downstream droplet disintegration for all sprays (compare the difference between mass-under-size plots at 25 mm and 400 mm downstream for all sprays). This is likely to be the result of the downstream disintegration of only small numbers of very large droplets (by secondary atomisation processes).

It is evident that downstream droplet break-up continued through the full range of axial locations sampled. For example, Table 6.1.3 shows changes in mass-under-size plots for the 2.8 mm spray from 350-400 mm downstream. In fact equilibrium may not have been achieved even at 400 mm downstream of the exit orifice, with more break-up due further downstream.

Table 6.1.3 Cumulative mass-under-size plots for entire downstream locations.





The total downstream spray quality improvements seen (from 25-400 mm in the axial direction) are considerable and emphasise the important influence only a small number of larger droplets can have on local and global spray quality. This in turn emphasises the important influence axial sampling location can have on spray quality.

#### 6.1.16 Droplet SMD Correlations from the Literature

Figure 6.1.14 displays the global spray droplet SMD (as defined in this investigation) as it varied with exit orifice diameter. Also plotted are the droplet SMD predicted by effervescent atomiser correlations from the literature. It is clear that no correlations from the literature could accurately predict droplet SMD for the conditions investigated in the present research. This discrepancy was expected and is due to, amongst other factors, alternative sampling techniques, different sampling locations and differing parameter ranges investigated.

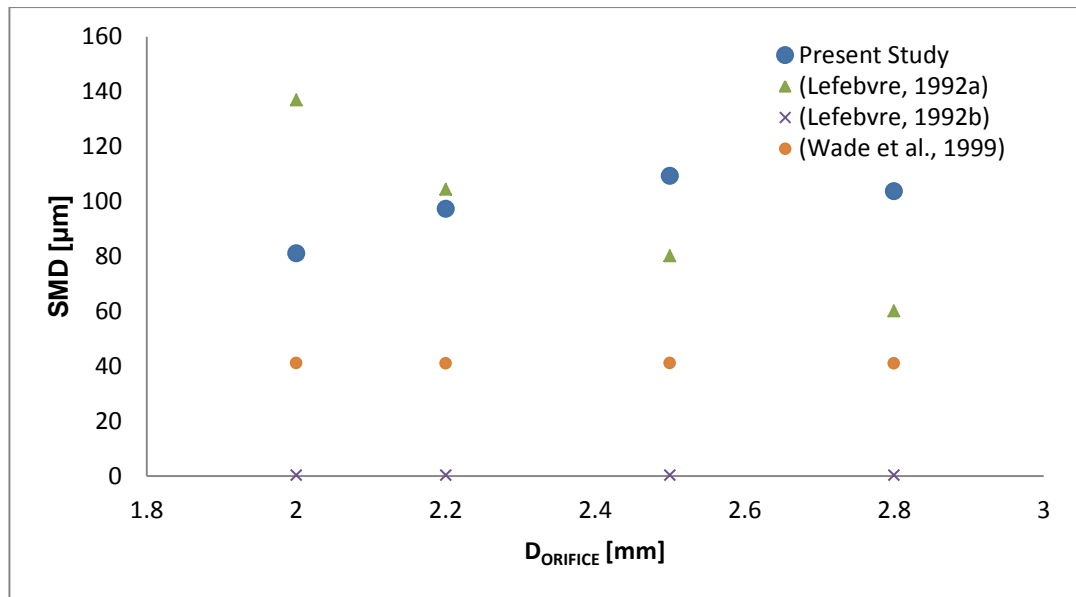


Figure 6.1.14 Comparison of global spray SMD from PDA experiments with that predicted by correlations in the literature.

### 6.1.17 Effect of $D_o$ on Global Spray Droplet SMD for Experimental Data

Many researchers consider  $D_o$  to have a minor or non-existent effect on droplet SMD [31, 33, 54, 62]. One study investigating low flow rate effervescent atomisation found an increase in droplet SMD as  $D_o$  was increased [63]. Meanwhile one study into very high-pressure effervescent atomisation surprisingly reported the reverse effect [70].

The relationship between  $D_o$  and global spray droplet SMD for the current investigation is illustrated in Figure 6.1.15, where a second order polynomial line of best fit has been added. In the present study increasing  $D_o$  led to worsening atomisation performance for  $2 \text{ mm} < D_o < 2.5 \text{ mm}$  (comparable to the behaviour of plain orifice atomisers). Nevertheless, the 2.8 mm spray was better atomised than the 2.5 mm spray (confirmed by repeated PDA tests). This matches previous analyses of the test phase 3 experimental data (e.g. Figure 6.1.8). Clearly exit orifice diameter and droplet SMD exhibit a complex relationship, where the differences in atomiser performance are likely to be related to the creation of different flow conditions through the nozzle as  $D_o$  was increased.

Although a non-linear relationship is evident, the range  $2 \text{ mm} < D_o < 2.5 \text{ mm}$  appears to correlate linearly with global spray droplet SMD. Therefore assuming linearity and for  $2 \text{ mm} < D_o < 2.5 \text{ mm}$  (and for the atomiser geometries and conditions investigated), it can be shown that the relationship between diameter and global spray droplet SMD is given by Equation 6.1.1. A deterioration in atomisation quality is observed as  $D_o$  is increased further to 2.8 mm. Further work is required to investigate the nature of the

relationship between nozzle diameter and spray quality at orifice diameters larger than 2.8 mm.

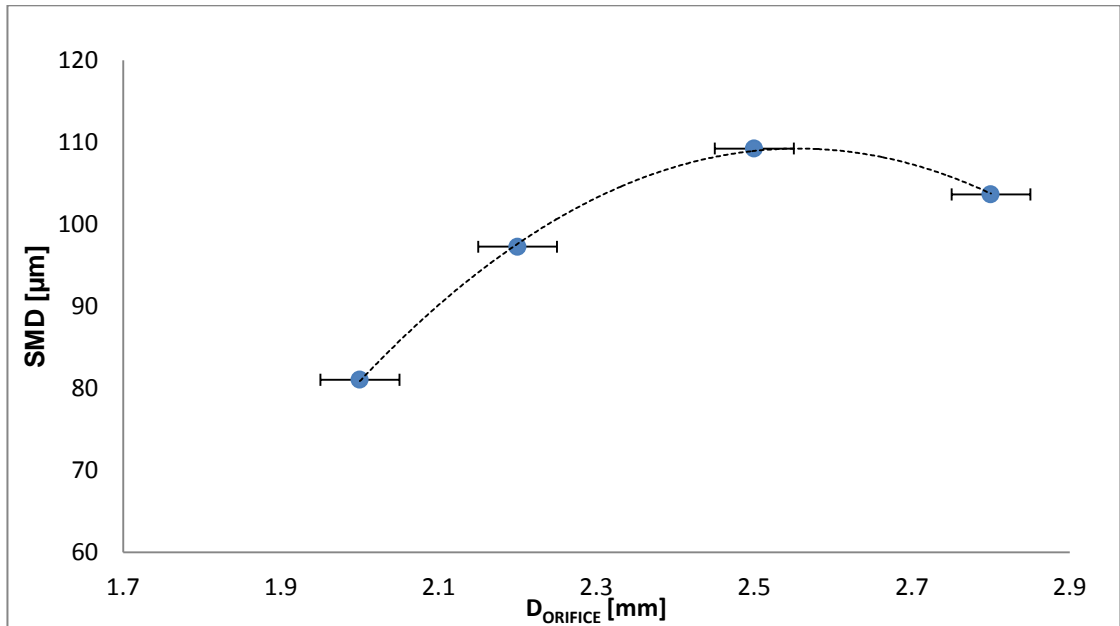


Figure 6.1.15 The relationship between  $D_o$  and global spray droplet SMD as calculated using PDA data.

$$SMD \propto 33.29D_o^{1.3138} \quad \text{Equation 6.1.1}$$

The results indicate that  $D_o$  has an important influence on spray quality, being even more important than the operating parameters ALR and  $\Delta P$  over certain operating ranges. The present work contradicts those studies which claim no relation between exit orifice diameter and droplet SMD. However the discrepancy in findings may be the result of different sampling locations employed, as well as different atomiser geometries and operating conditions investigated.

## 6.2 Test Phase No.4 – Mixing Chamber Length, $L_{MC}$

### 6.2.1 Preliminary Investigations

The geometric parameter mixing length is shown in Figure 6.2.1, and the position of the  $L_{MC}$  tests (test phase 4) within the test program is illustrated in Table 6.2.1.

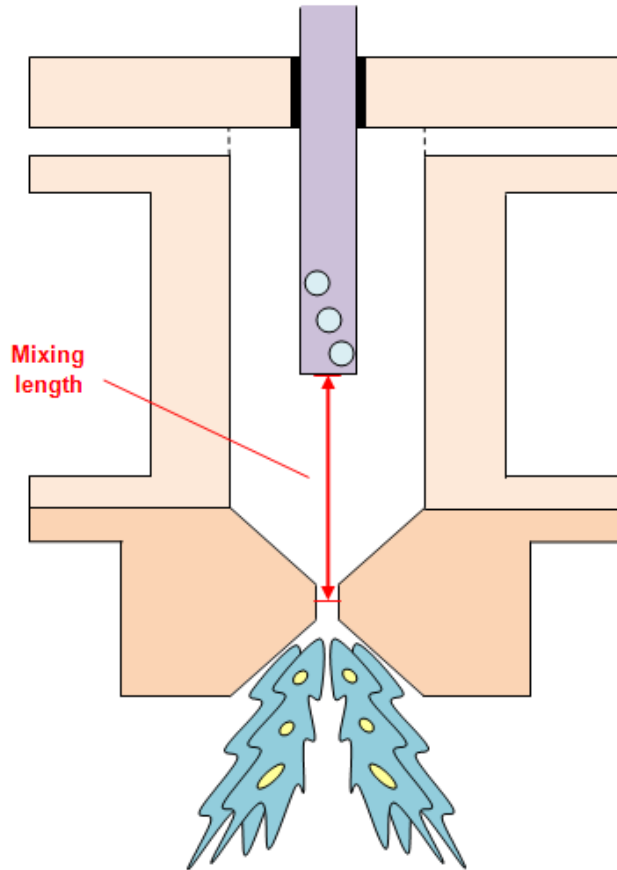


Figure 6.2.1 Schematic showing the geometric parameter mixing length.

Table 6.2.1 Operating conditions and controlled parameters for  $L_{MC}$  tests.

TEST No. PARAMETER VARIED	1 ALR	2 $\Delta P$	3 $D_O$	4 $L_{MC}$	5 $D_{MC}$	6 $L_O/D_O$	7 A. GEOM.	8 $\eta$
TEST PHASE	A. Initial Operating Parameters		B. Atomiser Geometry					C. Fluid properties
ALR (%)	0.8-12.5	2		2				
$\Delta P$ (bar.g)	7	4-7		7				
$D_O$ (mm)	2	2	2-4	2	2	2	2	2
$L_{MC}$ (mm)	140	140	140	64-140	140	140	140	140
$D_{MC}$ (mm)	25.4	25.4	25.4	25.4	20-30	25.4	25.4	25.4
$L_O/D_O$ (-)	1	1	1	1	1	0.5-2	1	1
Aerator Geometry	A1	A1	A1	A1	A1	A1	A2, A3	A1
$\eta \times 10^{-8}$ (m <sup>2</sup> /s)	1	1	1	1	1	1	1	2-10

The sprays investigated in test phase 4 are shown on the spray quality maps in Figure 6.2.2 and Figure 6.2.3. As can be seen, these tests (performed at the same operating conditions) lie within the region of good quality effervescent atomisation, with relatively high values of average  $\Delta P$  and ALR. Mixing length was altered by winding the adjustable air injector to the required length. The  $L_{MC}$  range of 60-136 mm could be investigated.

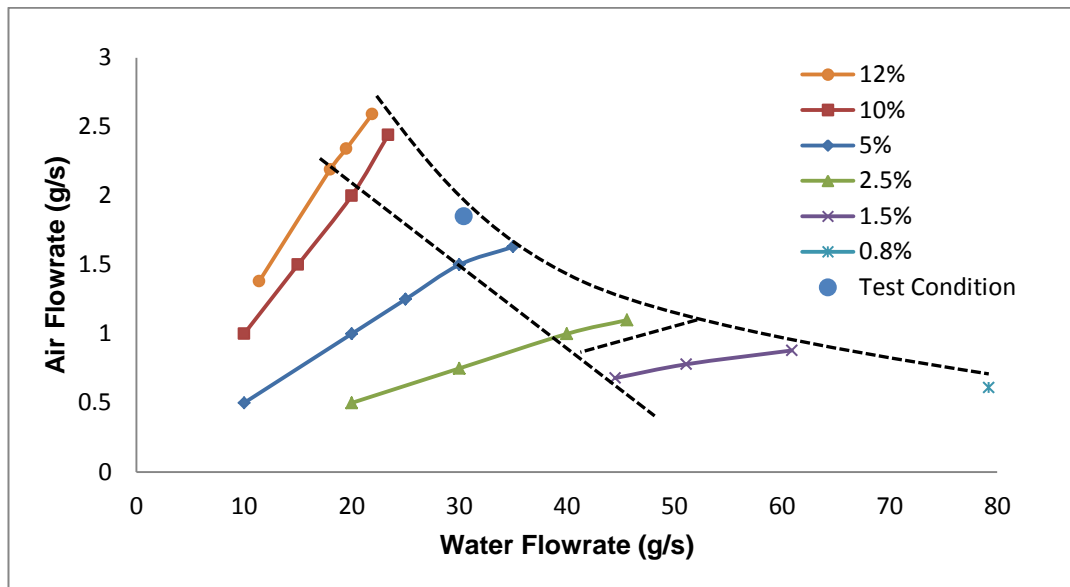


Figure 6.2.2 Graph of “spray quality” showing liquid flow rates at which optimal effervescent atomisation can be achieved.

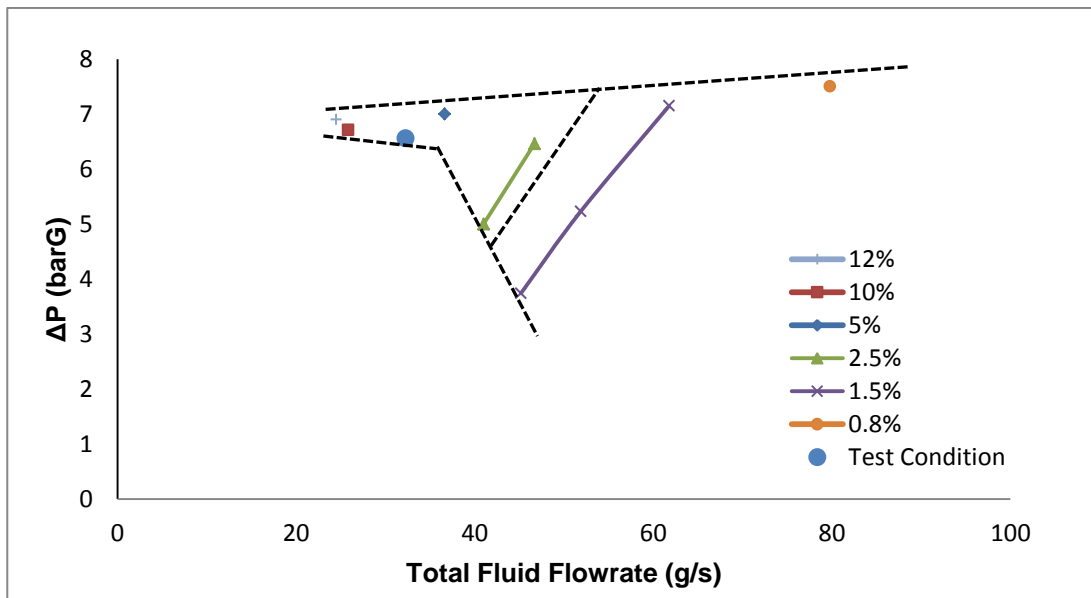


Figure 6.2.3 Graph of “spray quality” showing mixing chamber pressures and total flow rates at which tests were performed.

### 6.2.2 Spray Characteristics and Results

The results of the  $L_{MC}$  tests are presented in Table 6.2.2. The  $L_{MC} = 136$  mm test was obtained during test phase 1.

Table 6.2.2 Summary of  $L_{MC}$  test operating conditions and spray characteristics.

Test	$L_{MC} = 136$ mm	$L_{MC} = 99$ mm	$L_{MC} = 60$ mm
Water Supply Pressure (barG)	7.30	7.33	7.27
ALR (%)	6.24	6.06	5.97
Mixing Chamber Pressure, $\Delta P$ (barG)	6.57	6.58	6.53
$m_{WATER}$ (g/s)	30.38	30.73	30.13
$P_{AIR}$ (barG)	7.09	7.10	7.10
$m_{AIR}$ (g/s)	1.89	1.86	1.79
Volumetric Void Fraction, $\alpha$ (%)	87.1	86.8	86.7
Effective Power Rating (MW)	1.22	1.23	1.21
Coefficient of Discharge (-)	0.27	0.27	0.27
$\theta/2$ at 25 mm downstream (deg)	29.25	25.64	27.47
$D_{32}$ ( $\mu m$ )	82.10	82.91	81.55

### 6.2.3 Spray Droplet Size Distribution by Mass

Figure 6.2.4 shows droplet diameter frequency distributions based on mass, for all sprays.



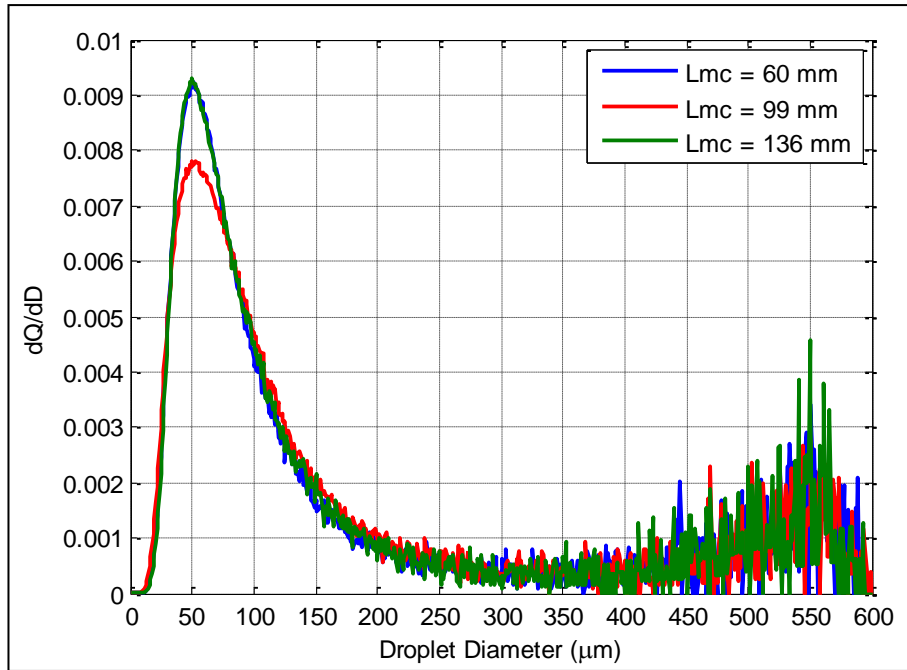


Figure 6.2.4 Droplet diameter frequency distribution by mass.

#### 6.2.4 Spray Average Cumulative Droplet Size Distributions

The cumulative mass-under-size distributions for each spray are given in Figure 6.2.5.

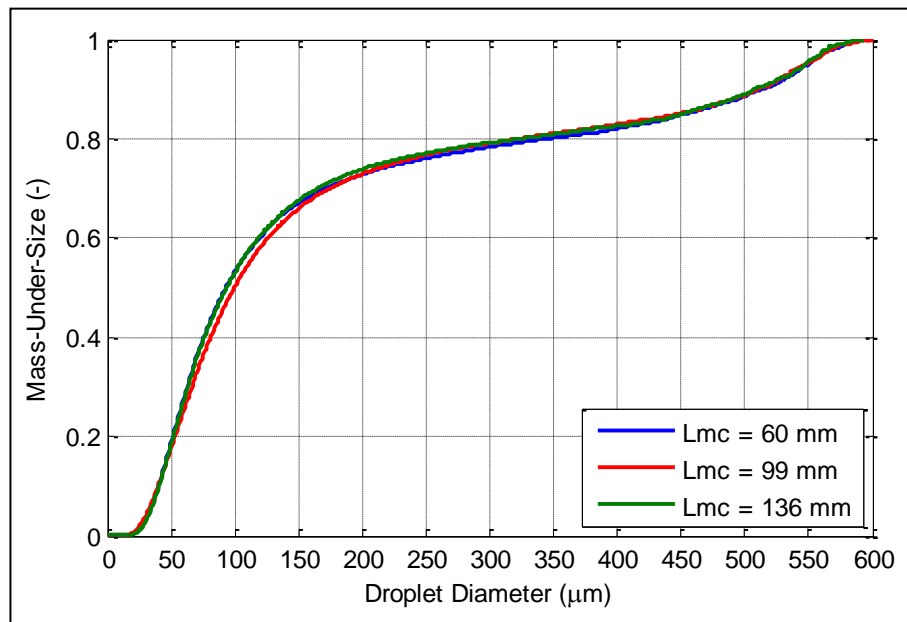


Figure 6.2.5 Cumulative droplet size distribution.

It is clear from Figure 6.2.4, Figure 6.2.5 and the global SMD droplet values in Table 6.2.2 that the three sprays investigated are extremely similar. No overall trend can be

identified. Mixing length appears to have no influence on global spray droplet SMD for the atomiser and operating conditions tested.

However, the results display two important findings.

1. Figure 6.2.4, Figure 6.2.5 and the global droplet SMD values in Table 6.2.2 indicate that PDA test results for the same operating conditions were highly repeatable. There is almost no variation in results which gives confidence in the measurement technique, setup and the results obtained.
2. The  $L_{MC} = 136$  mm test from test phase 1 agrees very well with the results from test phase 4. This provides strong evidence that comparison across test phases (which are characterised by slightly different software and optical setups, e.g. voltage sensitivities) is justified provided the setup is good (e.g. high validation rates) and only the same diameter ranges are compared.

### 6.3 Test Phase No.5 – Mixing Chamber Diameter, $D_{MC}$

#### 6.3.1 Preliminary Investigations

The geometric parameter mixing chamber diameter is shown in Figure 6.3.1, and the position of the  $D_{MC}$  tests (test phase 5) within the test campaign is demonstrated in Table 6.3.1.

Table 6.3.1 Operating conditions and controlled parameters for  $D_{MC}$  tests.

TEST No.	1	2	3	4	5	6	7	8
PARAMETER VARIED	ALR	$\Delta P$	$D_o$	$L_{MC}$	$D_{MC}$	$L_o/D_o$	A. GEOM.	$\eta$
TEST PHASE	A. Initial Operating Parameters		B. Atomiser Geometry				C. Fluid properties	
ALR (%)	0.8-12.5	2		2				
$\Delta P$ (bar.g)	7	4-7		7				
$D_o$ (mm)	2	2	2-4	2	2	2	2	2
$L_{MC}$ (mm)	140	140	140	64-140	140	140	140	140
$D_{MC}$ (mm)	25.4	25.4	25.4	25.4	20-30	25.4	25.4	25.4
$L_o/D_o$ (-)	1	1	1	1	1	0.5-2	1	1
Aerator Geometry	A1	A1	A1	A1	A1	A1	A2, A3	A1
$\eta \times 10^{-8}$ (m <sup>2</sup> /s)	1	1	1	1	1	1	1	2-10

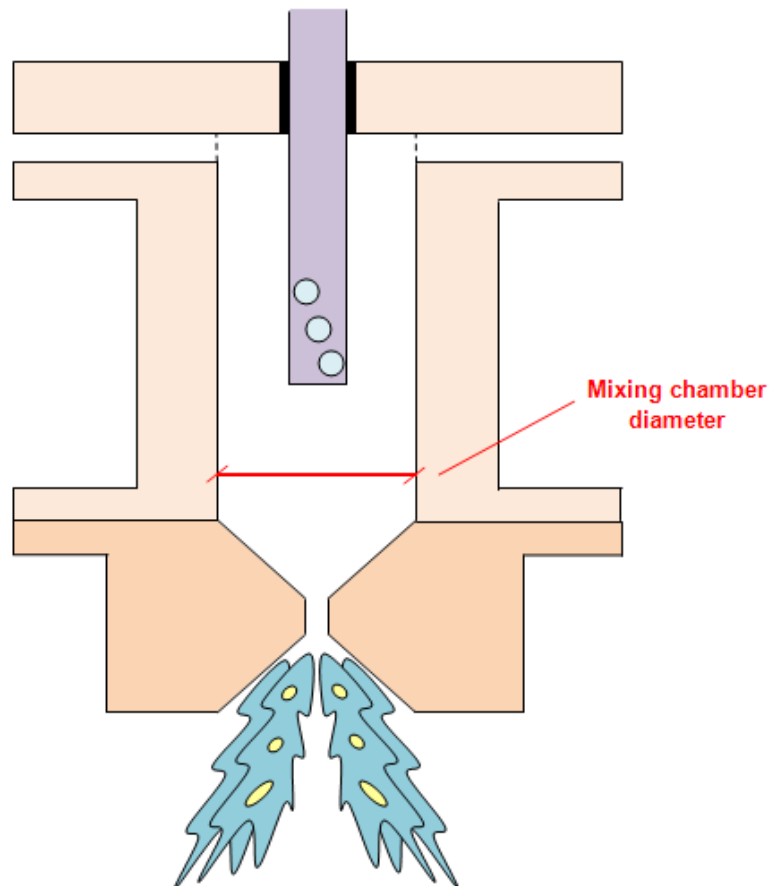


Figure 6.3.1 Schematic showing the geometric parameter mixing chamber diameter.

### 6.3.2 Spray Characteristics and Results

The results of test phase 5 are summarised in Table 6.3.2. The  $D_{MC} = 25.4$  mm test was taken from test phase 1. The other two tests ( $D_{MC} = 20$  mm,  $D_{MC} = 30$  mm) were performed by changing the atomiser body of the adjustable effervescent atomiser. Two atomiser bodies of different internal diameters were specially manufactured for this purpose.

The tests in this test phase were performed at the same operating conditions. ALR and  $\Delta P$  were kept constant throughout all tests: average ALR varied by 3% and average  $\Delta P$  varied by 1% between individual tests. Meanwhile the control parameter  $D_{MC}$  varied by 50% throughout the tests (an order of magnitude more than any other control parameter) and was therefore the dominant operating parameter.

Table 6.3.2 Summary of  $D_{MC}$  test operating conditions and spray characteristics.

Test	$D_{MC} = 20$	$D_{MC} = 25.4$	$D_{MC} = 30$
Water Supply Pressure (barG)	7.35	7.38	7.25
ALR (%)	5.61	5.70	5.78
Mixing Chamber Pressure, $\Delta P$ (barG)	6.63	6.65	6.58
$m_{WATER}$ (g/s)	31.70	31.75	31.25
$P_{AIR}$ (barG)	7.10	7.23	6.57
$m_{AIR}$ (g/s)	1.77	1.81	1.81
Volumetric Void Fraction, $\alpha$ (%)	85.9	86.1	86.3
Effective Power Rating (MW)	1.27	1.27	1.25
Coefficient of Discharge (-)	0.28	0.28	0.27
$\theta/2$ at 25 mm downstream (deg)	27.47	25.64	27.47
$D_{32}$ ( $\mu m$ )	83.28	81.06	87.11

### 6.3.3 Nozzle Coefficient of Discharge

The experimentally determined discharge coefficient is shown in Figure 6.3.2 as it varies with  $D_{MC}$ . Shown alongside experimentally determined coefficient of discharge are the discharge coefficients predicted by correlations from the literature (for operation at the same conditions). It can be seen that the correlation of Chen et al (1994a) is closest to the experimental values. The remaining correlations are seen to provide a poor match to the experimental data. A constant value of discharge coefficient was expected since mixing chamber diameter was not expected to significantly alter the fluid flow rates through the nozzle.

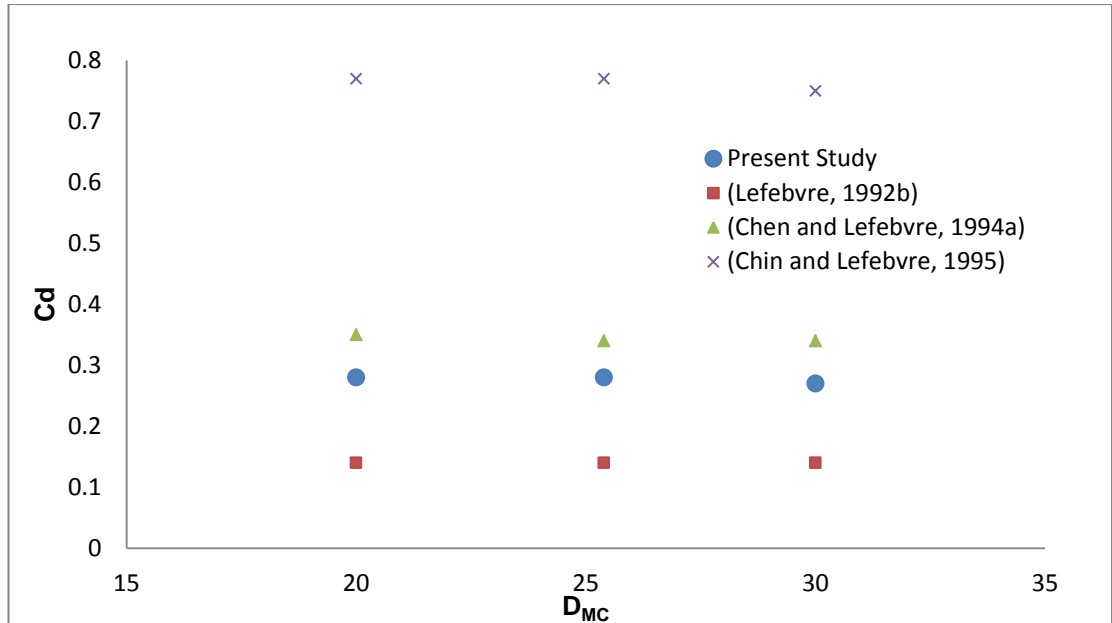


Figure 6.3.2 Comparison of coefficient of discharge from PDA experiments and literature.

### 6.3.4 Spray Half-Angle

Experimentally determined spray half-angle is presented in Figure 6.3.3.

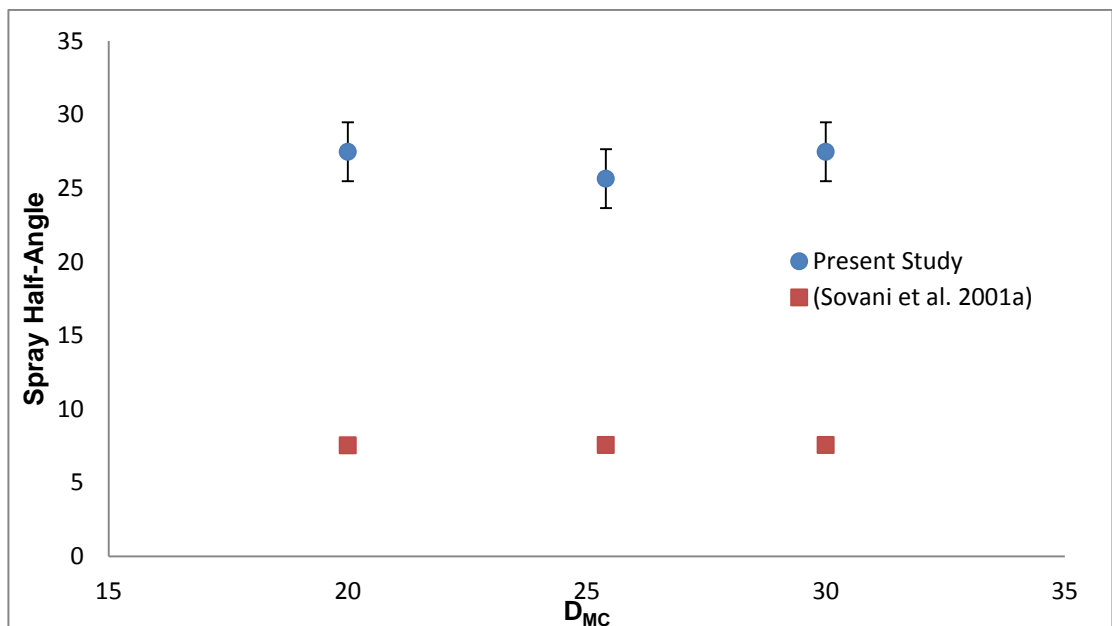


Figure 6.3.3 Comparison of spray half-angle from PDA experiments and literature.

This is shown together with spray half-angle predicted by the correlation of Sovani et al for the same operating conditions. As in previous test phases, the correlation of Sovani does not match the experimental data well, but considerably under-predicts the experimental values. This is unsurprising given the different sampling locations employed.

It can be seen that spray half-angle remained relatively constant at values of 25-28°. An experimental error of  $\pm 3^\circ$  is predicted.

### 6.3.5 Spray Droplet Size Distribution by Number

The droplet diameter frequency distributions by number are shown in Figure 6.3.4. As in previous test phases, the sprays of test phase 5 can be seen to be largely comprised of smaller droplets. Droplets larger than 140  $\mu\text{m}$  are not visible in Figure 6.3.4.

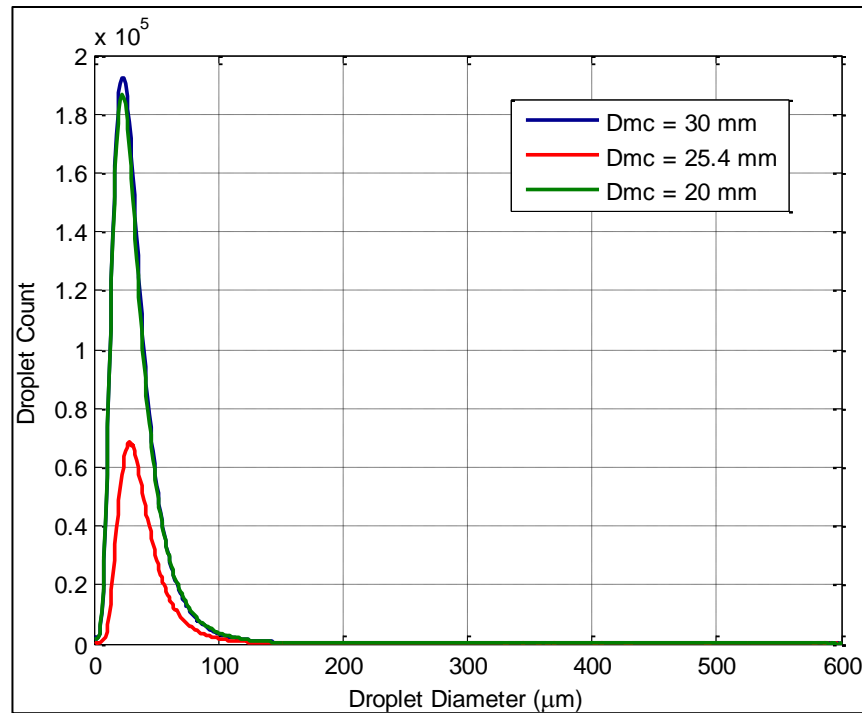


Figure 6.3.4 Droplet diameter frequency distribution based on number.

### 6.3.6 Spray Droplet Size Distribution by Mass

The droplet diameter frequency distributions by mass are shown in Figure 6.3.5.

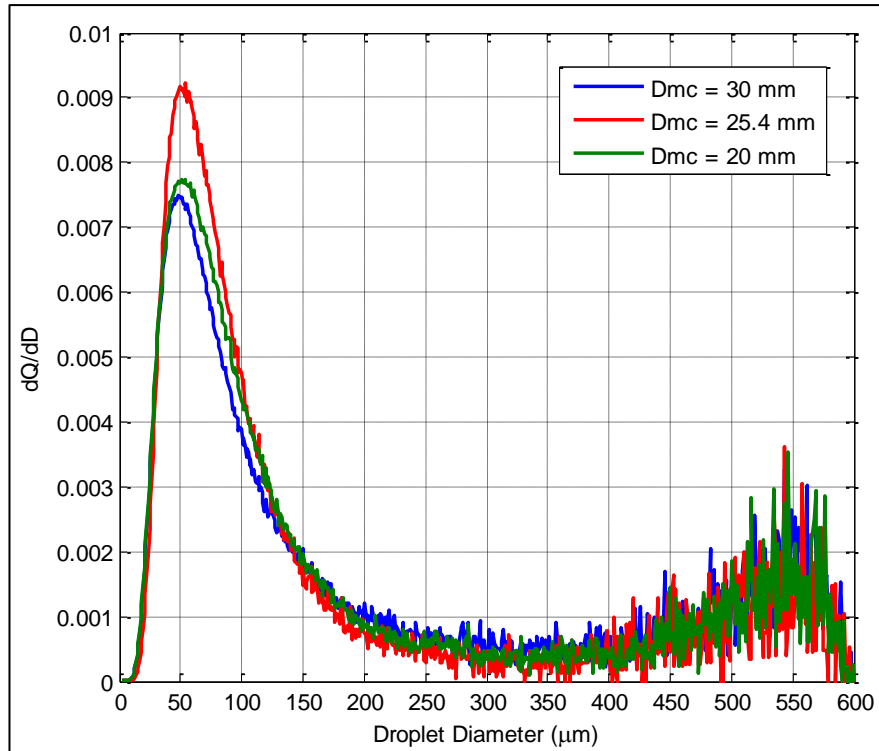


Figure 6.3.5 Droplet diameter frequency distribution by mass.

### 6.3.7 Spray Average Cumulative Droplet Size Distributions

The cumulative mass-under-size plots are presented in Figure 6.3.6.

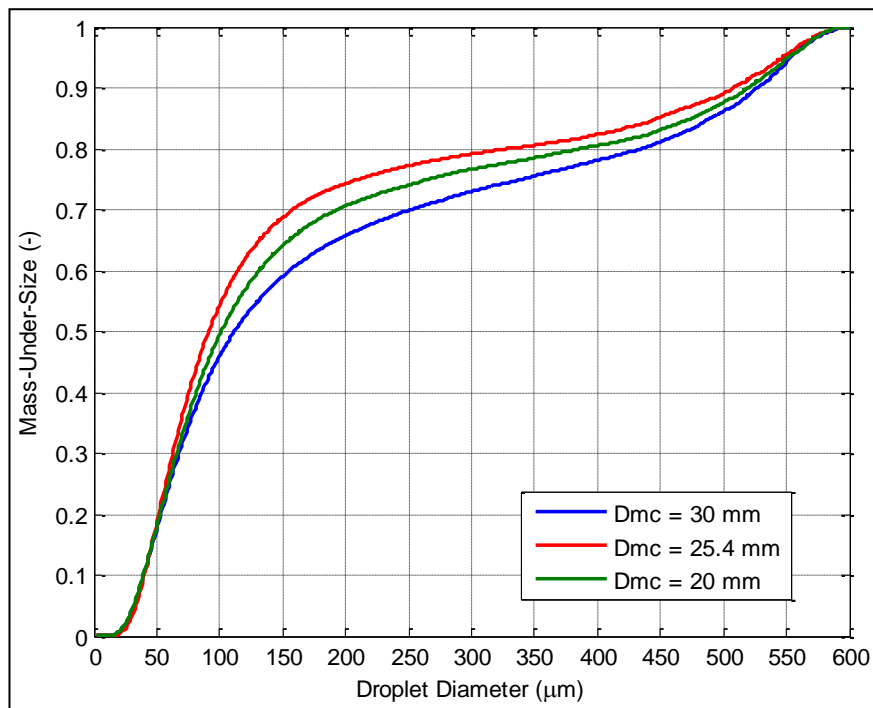


Figure 6.3.6 Cumulative droplet size distribution.

The relatively low value of the  $D_{MC} = 25.4$  mm curve maximal peak in Figure 6.3.4 is due to the different optical settings in test phase 1 (where the  $D_{MC} = 25.4$  mm data was obtained) resulting in comparatively lower data rates and therefore lower total droplet counts.

The droplet diameter frequency distributions by mass given in Figure 6.3.5 indicate very similar proportions of droplets larger than 130  $\mu\text{m}$  in diameter for all sprays in test phase 5. However, the relative proportions of smaller droplets clearly demonstrate that the  $D_{MC} = 25.4$  mm spray was the best atomised.

The cumulative mass-under-size plots in Figure 6.3.6 confirm the superior atomisation of the  $D_{MC} = 25.4$  mm spray, and also clearly show that the  $D_{MC} = 30$  mm spray was the most poorly atomised. This suggests a relatively minor influence on spray quality, with a non-linear relationship between spray quality and  $D_{MC}$ .

Although the differences between them are small, the variation in the mass-under-size plots of Figure 6.3.6 cannot be a result of experimental error. This is demonstrated by the mass-under-size plots of test phase 4, which show good agreement despite individual tests being performed during different test phases and at slightly different PDA settings (as well as at slightly different average operating conditions).

### **6.3.8 Validated Local Data Rates**

The average local droplet counts at 150 mm downstream of the exit orifice are presented in Figure 6.3.7. The difference in PDA settings between test phase 1 and test phase 5 is responsible for the different local droplet counts of the  $D_{MC} = 25.4$  mm spray (e.g. at axial distances of 200-400 mm). However as has been discussed, this does not influence global spray droplet SMD or the mass-under-size plot.

As expected, the maximal data rates were obtained roughly halfway between the spray centreline and edge.



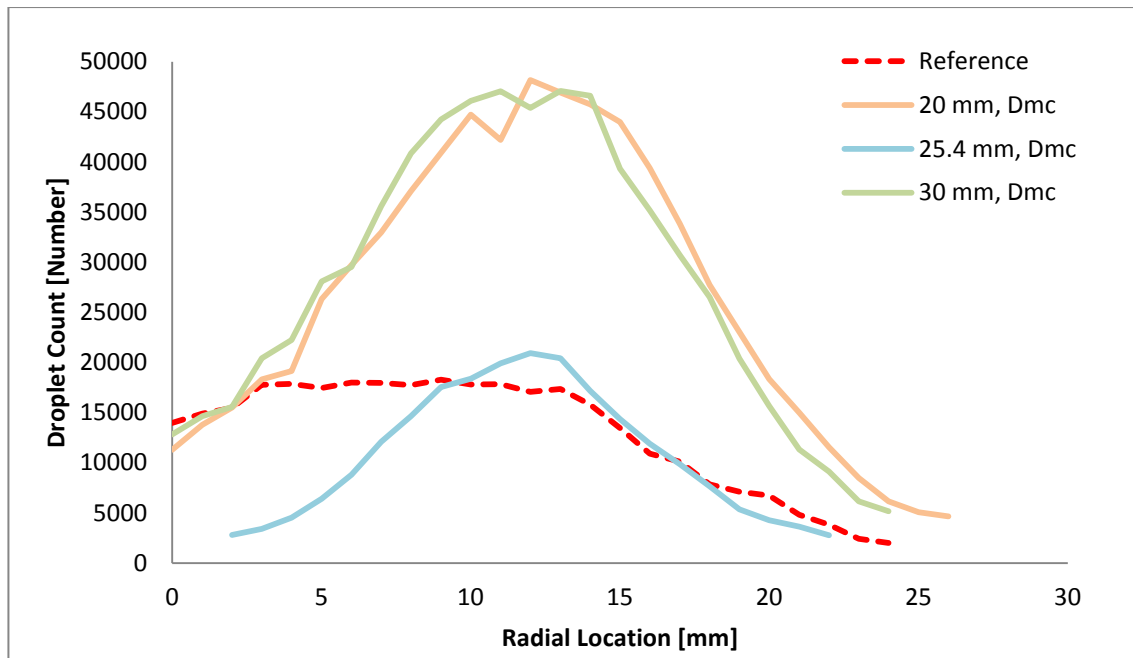


Figure 6.3.7 Validated local data rates at 150 mm downstream of the nozzle.

### 6.3.9 Local Droplet Velocity

The average local droplet velocity at 150 mm downstream of the exit orifice is shown in Figure 6.3.8. The  $D_{MC} = 20$  mm and  $D_{MC} = 30$  mm sprays appear very similar and no clear relationship is seen to emerge. However, as in other test phases, the average local droplet velocity is seen to reduce in magnitude further away from the centreline. This is an important, but expected finding.

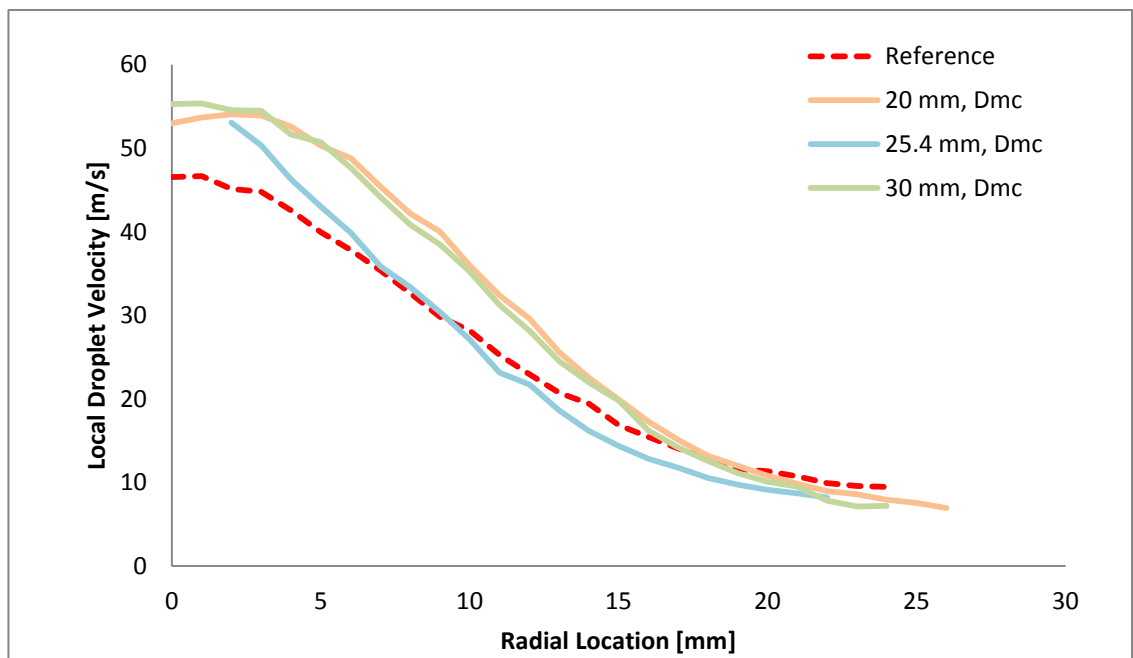


Figure 6.3.8 Average local droplet velocity at 150 mm downstream of the nozzle.

### 6.3.10 Inferred Local Gas and Relative Velocity

The inferred local gas and relative velocities were seen to remain unaffected by mixing chamber diameter. The complete data set of inferred gas and relative velocities are presented in Appendix C.

### 6.3.11 Local Droplet AMD and SMD

Local droplet AMD and SMD are shown in Figure 6.3.9 and Figure 6.3.10, respectively. The plots in Figure 6.3.9 indicate no clear relationship between mixing chamber diameter and AMD. However slightly larger local droplet AMD visible in the  $D_{MC} = 25.4$  mm spray are most likely the result of the lower data rates associated with this test. By number the majority of all sprays throughout this investigation are comprised of relatively small droplets. These droplets (which are fewer in the  $D_{MC} = 25.4$  mm spray, due to lower data rates) are known to have a noticeable effect on AMD but only a minor effect on SMD. Therefore comparatively larger local droplet AMD are expected for the  $D_{MC} = 25.4$  mm spray.

Local spray droplet SMD (Figure 6.3.10) appear similar for all sprays in the present test phase indicating relatively similar atomisation quality at this axial location.

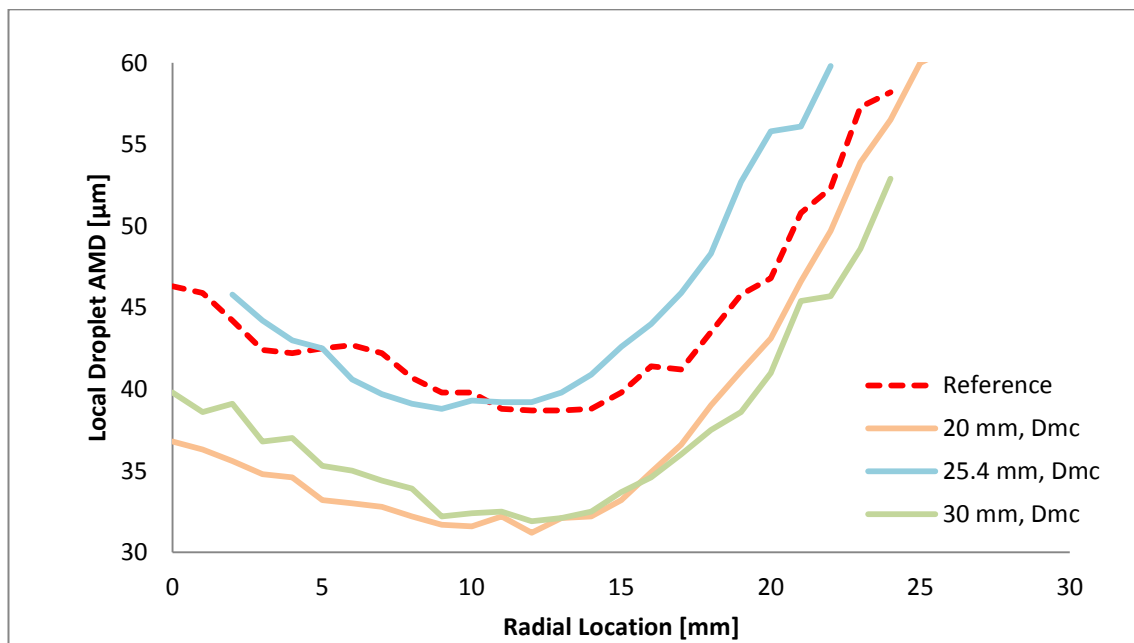


Figure 6.3.9 Local droplet AMD at 150 mm downstream of the nozzle.

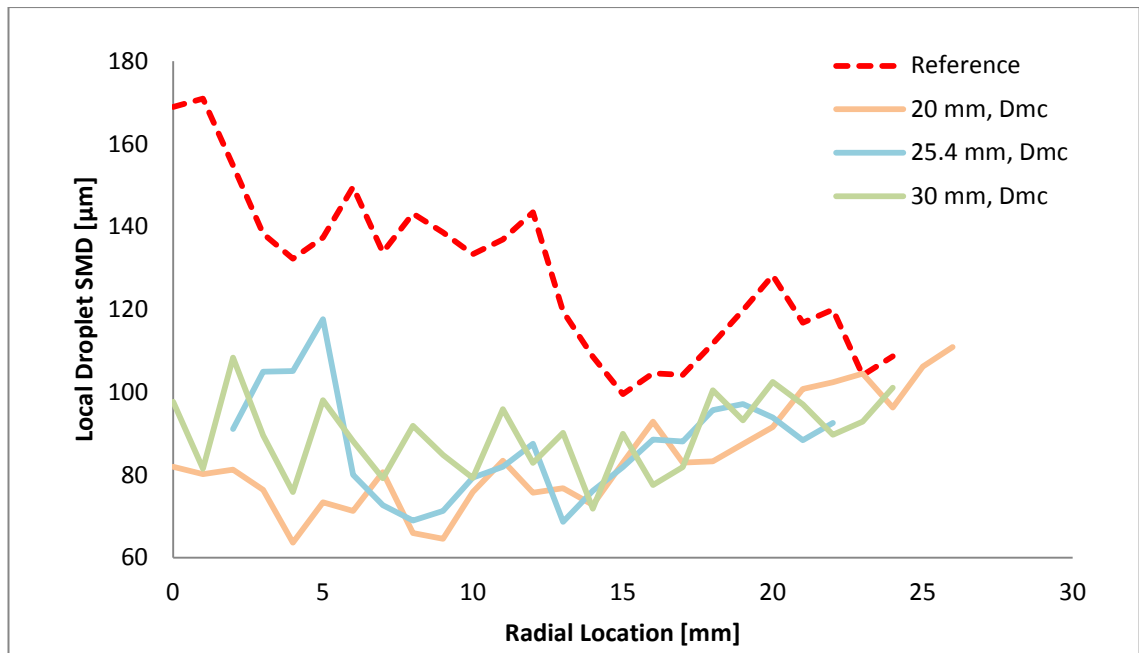


Figure 6.3.10 Local droplet SMD at 150 mm downstream of the nozzle.

### 6.3.12 Local Droplet Size Consistency

The local droplet consistency is displayed in Figure 6.3.11, which shows the average local droplet SMD/AMD ratio. This graph demonstrates that the  $D_{MC} = 25.4$  mm spray is the most consistent and therefore the best atomised, while the  $D_{MC} = 30$  mm spray is the least consistent and therefore most poorly atomised, at this axial location.

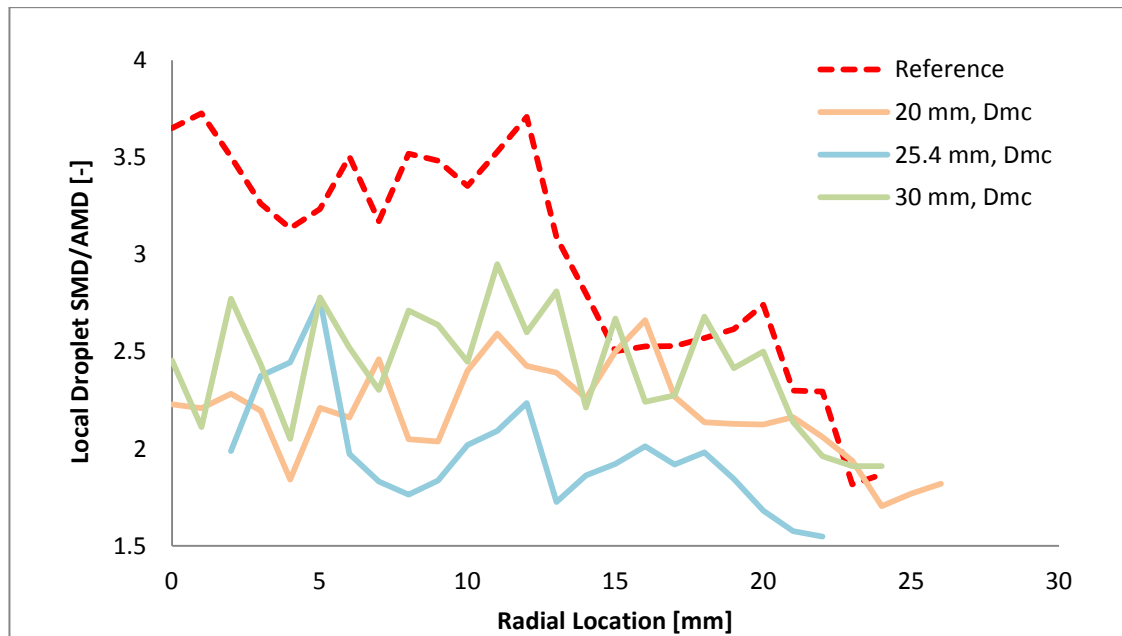


Figure 6.3.11 Local droplet SMD/AMD at 150 mm downstream of the nozzle.

### **6.3.13 Droplet Secondary Break-up**

Local average Weber number was found to be more than an order of magnitude smaller than the critical Weber number (usually quoted as  $11 \pm 2$ ). The low local values of Weber number indicate that the majority of droplets sampled could not have been subjected to secondary break-up mechanisms. This was expected since it is clear that most of the spray is contained in smaller droplets, and only the relatively few larger droplets could have disintegrated via secondary break-up mechanisms. The complete Weber number data set is presented in Appendix C.

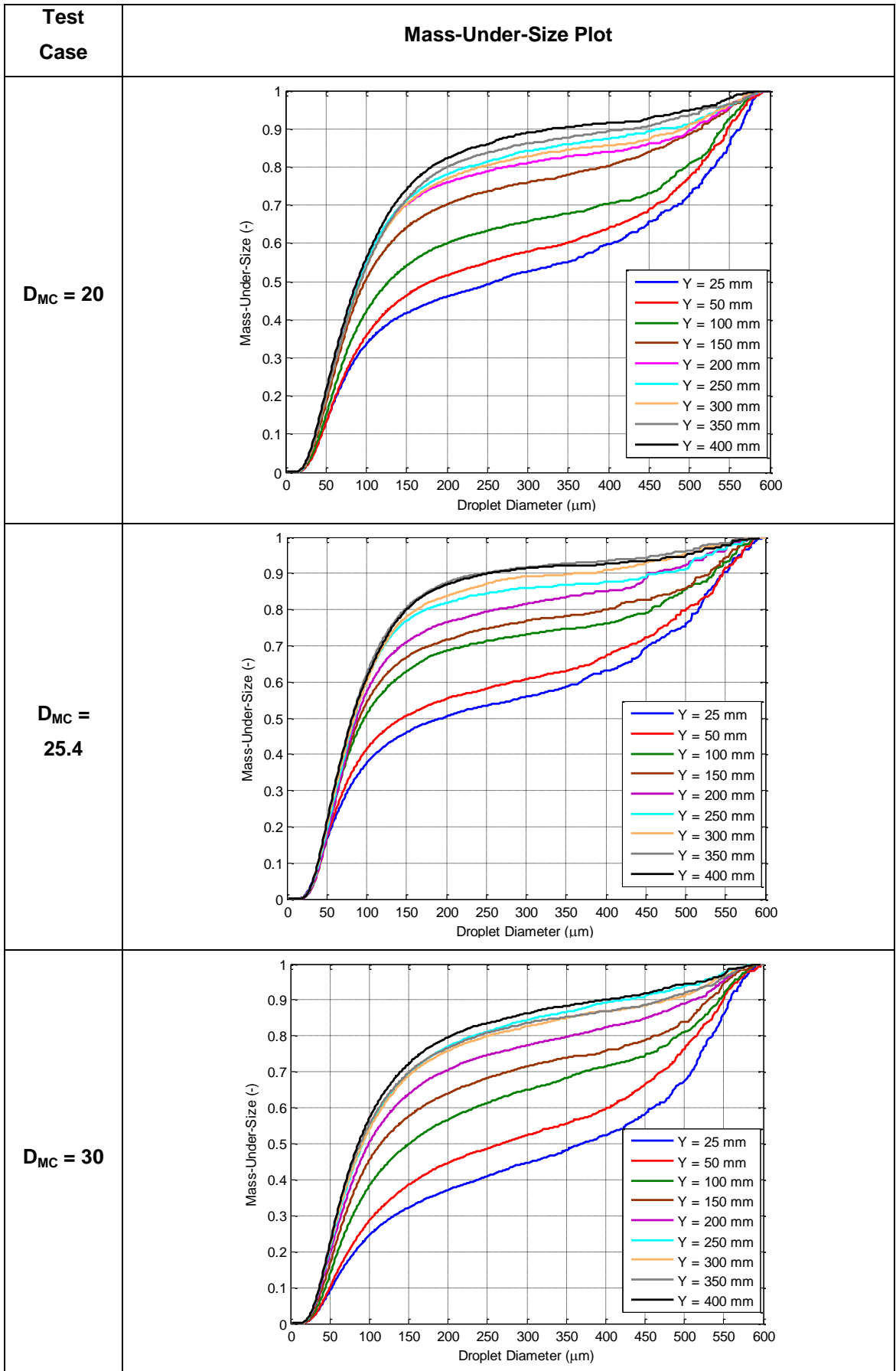
### **6.3.14 Spray Development in the Downstream Direction**

The cumulative mass-under-size plots are shown in Table 6.3.3. Inspection of the mass-under-size plots at axial distances of 25 mm and 400 mm for all sprays indicates that a comparable amount of break-up occurred for all sprays in test phase 5.

It is noticeable that droplets in the range 150-450  $\mu\text{m}$  appear to progress downstream with almost no changes (e.g. the downstream mass-under-size plots of the  $D_{MC} = 20$  mm spray run approximately parallel to one another at diameter ranges of 150-450  $\mu\text{m}$ ). This shows that as the sprays progressed downstream, a small number of droplets larger than 450  $\mu\text{m}$  disintegrate via secondary break-up mechanisms to produce multiple droplets smaller than 150  $\mu\text{m}$  in diameter, with the mid-sized droplets remaining relatively intact.

As in previous test phases, ongoing secondary atomisation was detected in all test phase 5 sprays even at axial locations of 400 mm downstream of the exit orifice.

Table 6.3.3 Cumulative mass-under-size plots for entire downstream locations.



### 6.3.15 Droplet SMD Correlations from the Literature

The droplet SMD predicted by correlations from the literature are compared to the experimentally determined values of global spray droplet SMD from the present investigation in Figure 6.3.12. It can be seen that none of the existing correlations could accurately predict global spray droplet SMD. However this is expected given the different spray sampling techniques and sampling locations employed.

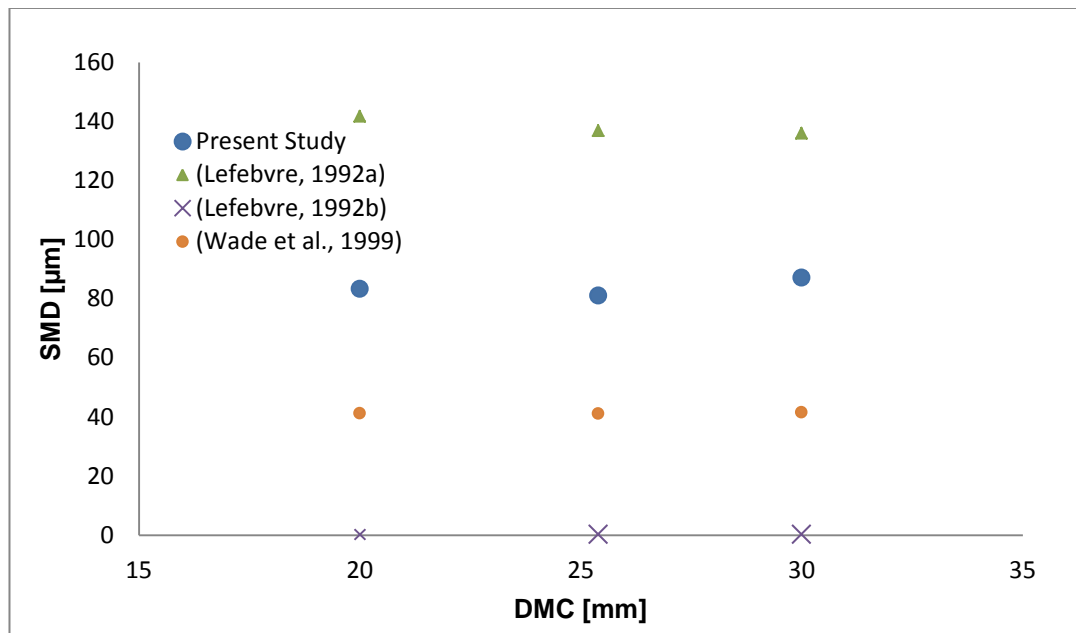


Figure 6.3.12 Comparison of global spray droplet SMD from PDA experiments with that predicted by correlations in the literature.

### 6.3.16 Effect of $D_{MC}$ on Global Spray Droplet SMD for Experimental Data

It is likely that the effects  $D_{MC}$  has on spray quality are similar to the effects  $D_O$  has on droplet SMD since both nozzle diameter and mixing chamber diameter can influence internal flow.

The relationship between global spray droplet SMD and mixing chamber diameter ( $D_{MC}$ ) is illustrated in Figure 6.3.13. Only three test points could be obtained as the lead and manufacturing times required to fabricate an atomiser body were long.

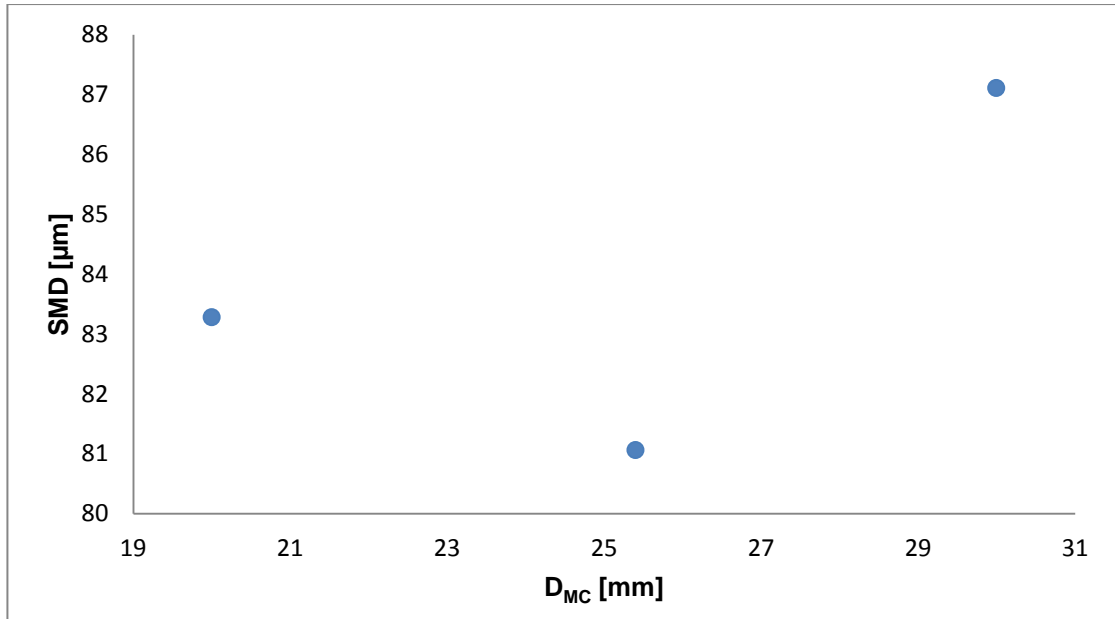


Figure 6.3.13 The relationship between  $D_{MC}$  and global spray droplet SMD as calculated using PDA data.

The results show that global spray droplet SMD and  $D_{MC}$  exhibit no clear relationship, with the 25.4 mm diameter mixing chamber providing the best atomisation for the conditions and atomiser geometries investigated. The results clearly demonstrate that mixing chamber diameter had a noticeable though relatively small effect on spray quality (global spray droplet SMD only varied between 81.06-87.11  $\mu\text{m}$ ).

This result is significant given the fact that, to the authors' knowledge, no investigations which consider the effects of mixing chamber diameter on spray quality exist in the literature. Early researchers typically sized their mixing chambers such as to ensure bubbly flow in the atomiser [65]. However, as far as the author is aware, this design recommendation has never been experimentally validated.

A precise knowledge of the nature of the relationship between droplet SMD and mixing chamber diameter requires further PDA investigations using a larger range of  $D_{MC}$ .

### 6.4 Test Phase No.6 – Exit Orifice Length-to-Diameter Ratio, $L_o/D_o$

#### 6.4.1 Preliminary Investigations

The geometric parameter exit orifice length-to-diameter ratio is shown in Figure 6.4.1, and the position of the  $L_o/D_o$  tests within the test campaign are demonstrated in Table 6.4.1.

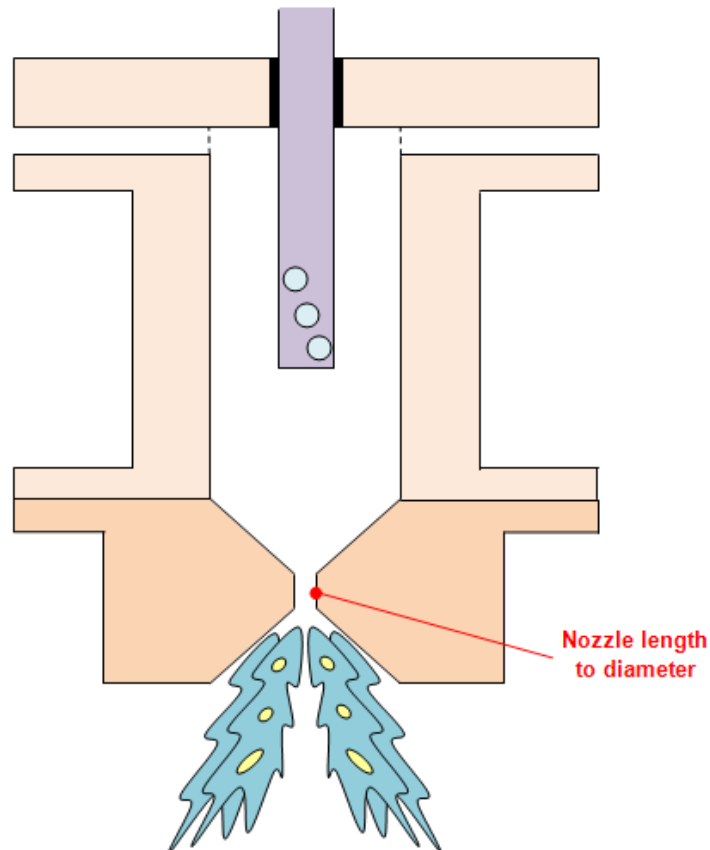


Figure 6.4.1 Schematic showing the geometric parameter length-to-diameter ratio.

Table 6.4.1 Operating conditions and controlled parameters for  $L_o/D_o$  tests.

TEST No. PARAMETER VARIED	1 ALR	2 $\Delta P$	3 $D_o$	4 $L_{MC}$	5 $D_{MC}$	6 $L_o/D_o$	7 A. GEOM.	8 $\eta$
TEST PHASE	A. Initial Operating Parameters		B. Atomiser Geometry				C. Fluid properties	
ALR (%)	0.8-12.5	2		2				
$\Delta P$ (bar.g)	7	4-7		7				
$D_o$ (mm)	2	2	2-4	2	2	2	2	2
$L_{MC}$ (mm)	140	140	140	64-140	140	140	140	140
$D_{MC}$ (mm)	25.4	25.4	25.4	25.4	20-30	25.4	25.4	25.4
$L_o/D_o$ (-)	1	1	1	1	1	0.5-2	1	1
Aerator Geometry	A1	A1	A1	A1	A1	A1	A2, A3	A1
$\eta \times 10^{-6}$ (m <sup>2</sup> /s)	1	1	1	1	1	1	1	2-10



### 6.4.2 Spray Characteristics and Results

The results of the  $L_0/D_0$  tests (test phase 6) are displayed in Table 6.4.2. It became clear during preliminary investigations that  $L_0/D_0$  influenced the flow behaviour of the nozzle, altering the flow rates achievable for the same operating pressures and ALRs. This is reflected in the variation of discharge coefficient in Table 6.4.2. A variation in flow rate was expected since length-to-diameter ratio can affect the fluid dynamics of the flow through the nozzle.

It should be noted that the data point for  $L_0/D_0 = 1$  was obtained during test phase 1. Each test phase was performed at constant optical and software settings to ensure consistent, congruent results. However some software settings were re-optimised before each new test phase began (e.g. photo-detector sensitivity). This seems to have led to different distributions of maximum axial data rate values in test phase 6 compared to test phase 1. For this reason the spray half-angle of the  $L_0/D_0 = 1$  spray appeared somewhat smaller than it may have been had it been performed at test phase 6 settings. However, as demonstrated by test phase 4, parameters such as global spray droplet SMD are not affected by such differences in settings, since the data and validation rates were high during both test phases.

Table 6.4.2 Summary of  $L_0/D_0$  test operating conditions and spray characteristics.

Test	$L_0/D_0 = 0.5$	$L_0/D_0 = 1$	$L_0/D_0 = 1.5$	$L_0/D_0 = 2$
<b>Water Supply Pressure (barG)</b>	7.49	7.38	7.32	7.51
<b>ALR (%)</b>	5.79	5.70	5.76	5.85
<b>Mixing Chamber Pressure, <math>\Delta P</math> (barG)</b>	6.71	6.65	6.57	6.75
<b><math>m_{\text{WATER}}</math> (g/s)</b>	40.02	31.75	34.12	33.97
<b><math>P_{\text{AIR}}</math> (barG)</b>	7.31	7.23	7.13	7.29
<b><math>m_{\text{AIR}}</math> (g/s)</b>	2.31	1.81	1.96	1.98
<b>Volumetric Void Fraction, <math>\alpha</math> (%)</b>	86.3	86.1	86.3	86.4
<b>Effective Power Rating (MW)</b>	1.60	1.27	1.36	1.36
<b>Coefficient of Discharge (-)</b>	0.35	0.28	0.30	0.29
<b><math>\theta/2</math> at 25 mm downstream (deg)</b>	29.25	25.64	29.25	29.25
<b><math>D_{32}</math> (<math>\mu\text{m}</math>)</b>	89.12	81.06	94.77	113.04

### 6.4.3 Nozzle Coefficient of Discharge

The experimentally determined coefficient of discharge remained low throughout test phase 6 due to the large atomising air contribution associated with steady-state, good quality effervescent atomisation (as in previous test phases). Figure 6.4.2 compares experimentally determined discharge coefficients of the current investigation with those predicted by correlations in the literature. The correlation of Chen and Lefebvre most closely matches the experimental data; the remaining correlations provide a poor match. The relatively small variations in experimentally determined discharge coefficient (0.28-0.34) are closely linked to the changes in fluid flow through the nozzle as  $L_0/D_0$  was changed.

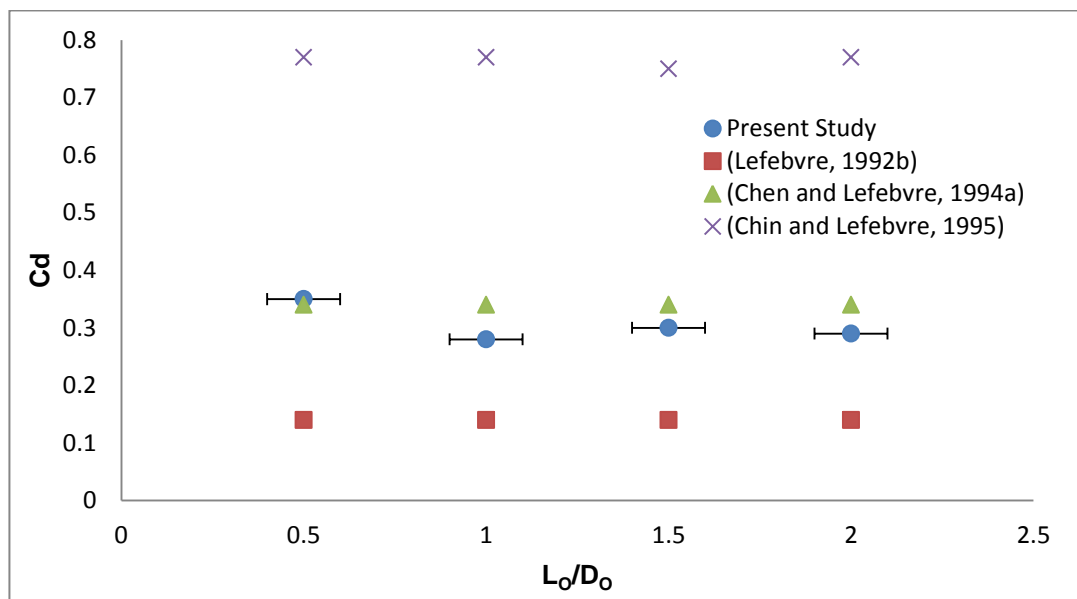


Figure 6.4.2 Comparison of coefficient of discharge from PDA experiments and literature.

### 6.4.4 Spray Half-Angle

Experimentally determined spray half-angles are presented in Figure 6.4.3.

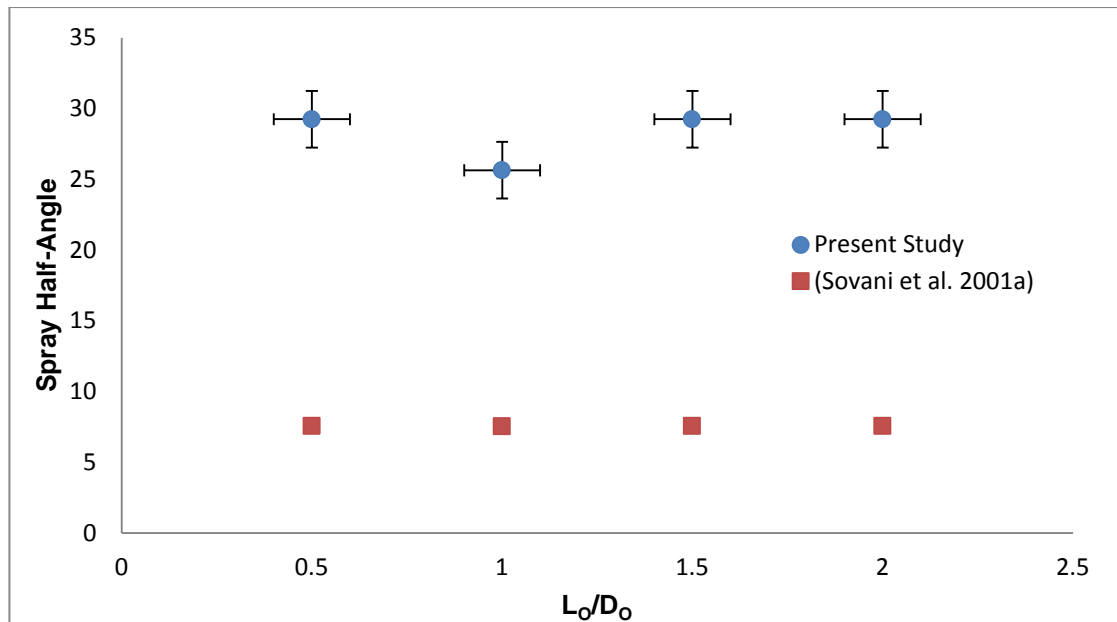


Figure 6.4.3 Comparison of spray half-angle from PDA experiments and literature.

These are shown alongside the spray half-angles predicted by the correlation of Sovani et al for the same operating conditions. The large discrepancy between experimental and predicted values is expected and can be attributed to different measurement techniques, different sampling locations and spray width definitions.

As discussed, spray half-angle at  $L_0/D_0 = 1$  is slightly lower than a test phase 6 investigation of the same spray may have indicated (due different maximal data rate distributions in test phase 1 compared to test phase 6). Notwithstanding this, spray half-angle appears relatively constant throughout the ranges tested (25-30°, with an experimental error of  $\pm 3^\circ$ ) indicating that  $L_0/D_0$  had a minor influence on spray angle.

#### 6.4.5 Spray Droplet Size Distribution by Number

Figure 6.4.4 shows the droplet diameter frequency-by-number distributions which indicate that all sprays were mostly comprised of smaller droplets, e.g. droplets larger than 160  $\mu\text{m}$  are so few in number that they are not visible in Figure 6.4.4.

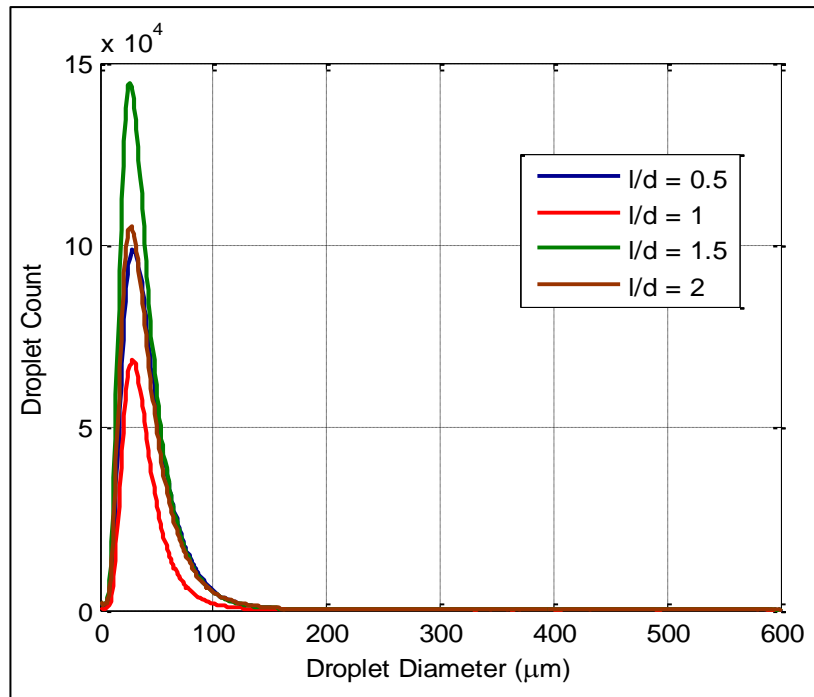


Figure 6.4.4 Droplet diameter frequency distribution based on number.

### 6.4.6 Spray Droplet Size Distribution by Mass

Figure 6.4.5 demonstrates the droplet diameter frequency-by-mass distributions.

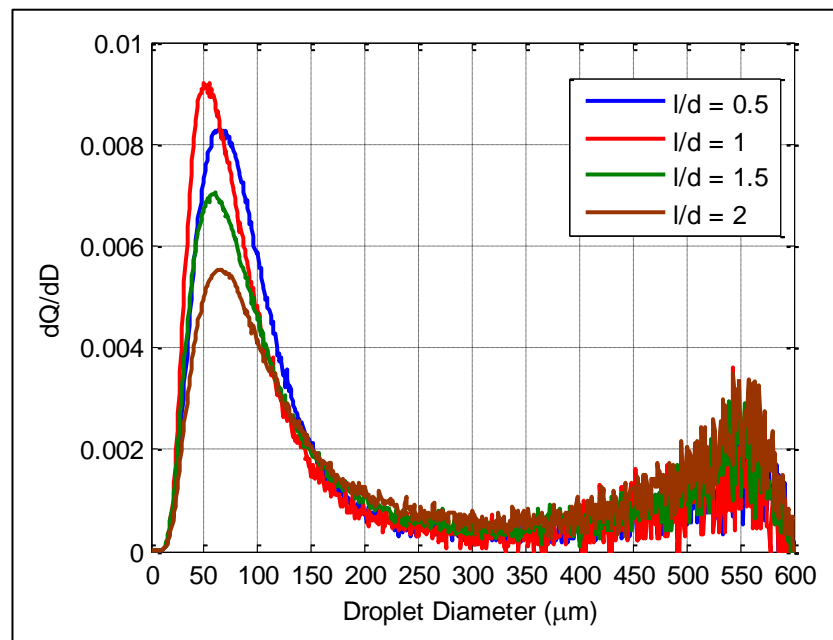


Figure 6.4.5 Droplet diameter frequency distribution by mass.

It is clear that the test phase 6 sprays exhibit differences only in the lower droplet size ranges. For example, noticeable differences in droplet distributions by mass are visible

at droplet diameters smaller than 150  $\mu\text{m}$ , but not at larger size ranges. The mass-under-size graphs in Figure 6.4.5 show that the best atomised spray appears to have been produced by the  $L_0/D_0 = 1$  nozzle. This spray clearly contained the largest proportion of small droplets.

#### 6.4.7 Spray Average Cumulative Droplet Size Distributions

The cumulative droplet size distributions are given in Figure 6.4.6. It is clear that although the  $L_0/D_0 = 0.5$  and  $L_0/D_0 = 1$  sprays appear very similar, the latter spray is marginally better atomised than the former. This agrees with the respective global droplet SMD values given for each spray in Table 6.4.2 (where a difference of over 8  $\mu\text{m}$  is noted). Nozzle length-to-diameter ratios larger than these (within the range  $1 < L_0/D_0 < 2$ ) are seen to increasingly reduce spray quality.

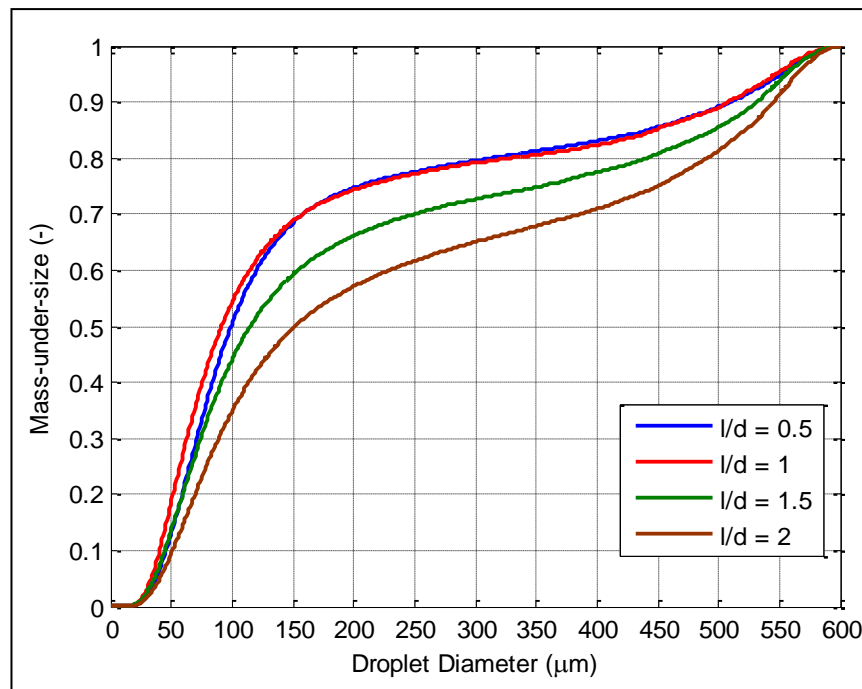


Figure 6.4.6 Cumulative droplet size distribution.

#### 6.4.8 Validated Local Data Rates

Local data rates at 150 mm downstream of the exit orifice are presented in Figure 6.4.7. These appear to display a similar pattern. However, as discussed, the  $L_0/D_0 = 1$  spray (also the Reference case) was analysed during test phase 1 (which was characterised by slightly different settings, e.g. different photo detector sensitivities) and displays slightly lower data rate values.

However as test phase 4 has shown, comparisons across test phases are justified so long as data rates and validation rates remain high, and only the common diameter ranges are compared. Although local data rates and spray half-angles can be affected by changes in PDA settings, global spray droplet SMD and mass-under-size plots have been shown to remain unaffected.

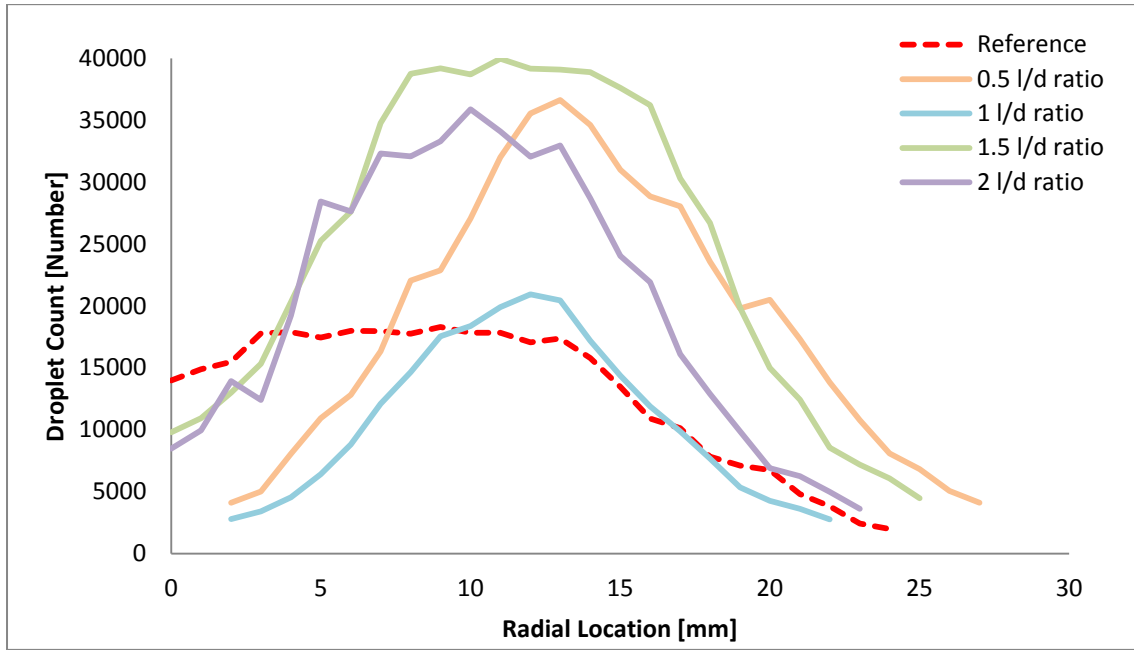


Figure 6.4.7 Validated local data rates at 150 mm downstream of the nozzle.

#### 6.4.9 Local Droplet Velocity

Local droplet velocity at 150 mm downstream of the exit orifice is presented in Figure 6.4.8. Nozzle length-to-diameter ratio does not appear to have had any clear effect on average droplet velocity at this location. The droplet velocities appear similar to each other and to the reference case.

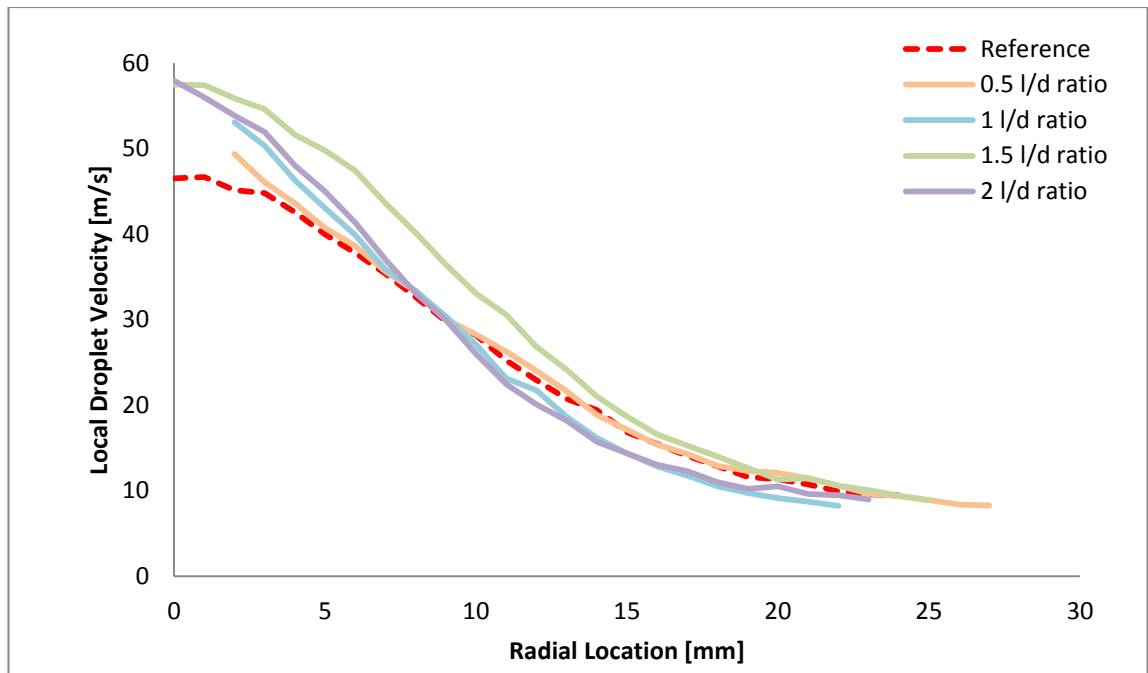


Figure 6.4.8 Average local droplet velocity at 150 mm downstream of the nozzle.

#### 6.4.10 Inferred Local Gas and Relative Velocity

The inferred local gas and relative velocities were seen to remain unaffected by length-to-diameter ratio. The complete data set of inferred gas and relative velocities are presented in Appendix D.

#### 6.4.11 Local Droplet AMD and SMD

Local droplet AMD and SMD at 150 mm downstream of the exit orifice are shown in Figure 6.4.9 and Figure 6.4.10, respectively. It is clear that the largest local droplet AMD (Figure 6.4.9) were provided by the  $l/d = 2$  spray, indicating relatively poorer atomisation. The local droplet SMD graphs (Figure 6.4.10) provide similar results, with increasing nozzle length-to-diameter ratios tending to increase local droplet SMD and therefore reducing atomisation quality.

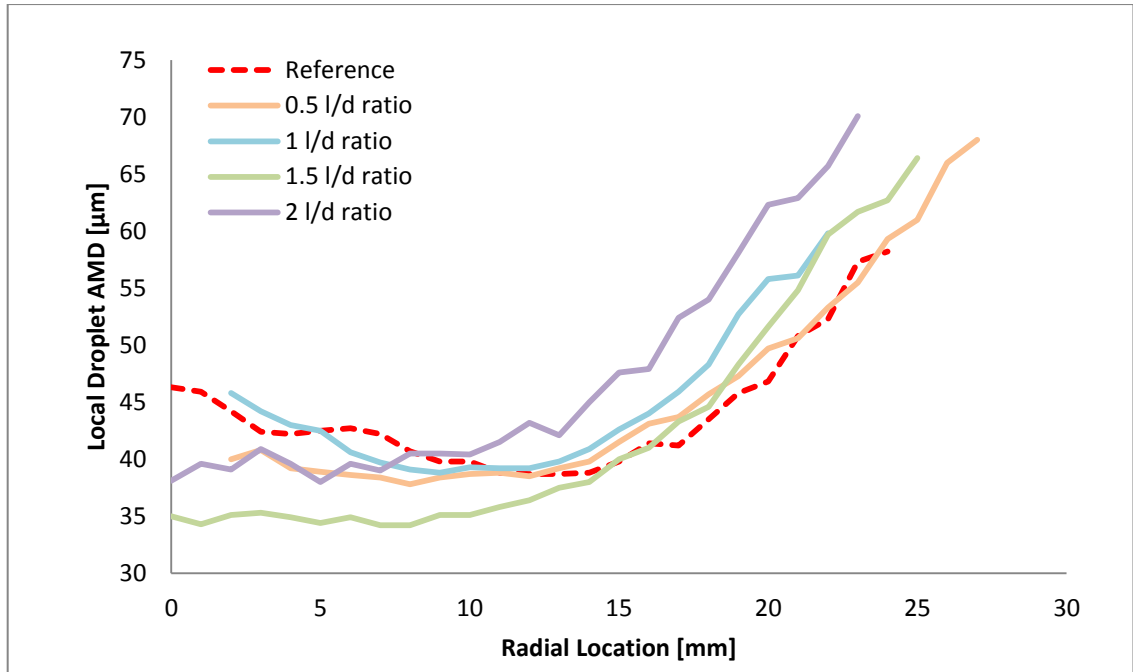


Figure 6.4.9 Local droplet AMD at 150 mm downstream of the nozzle.

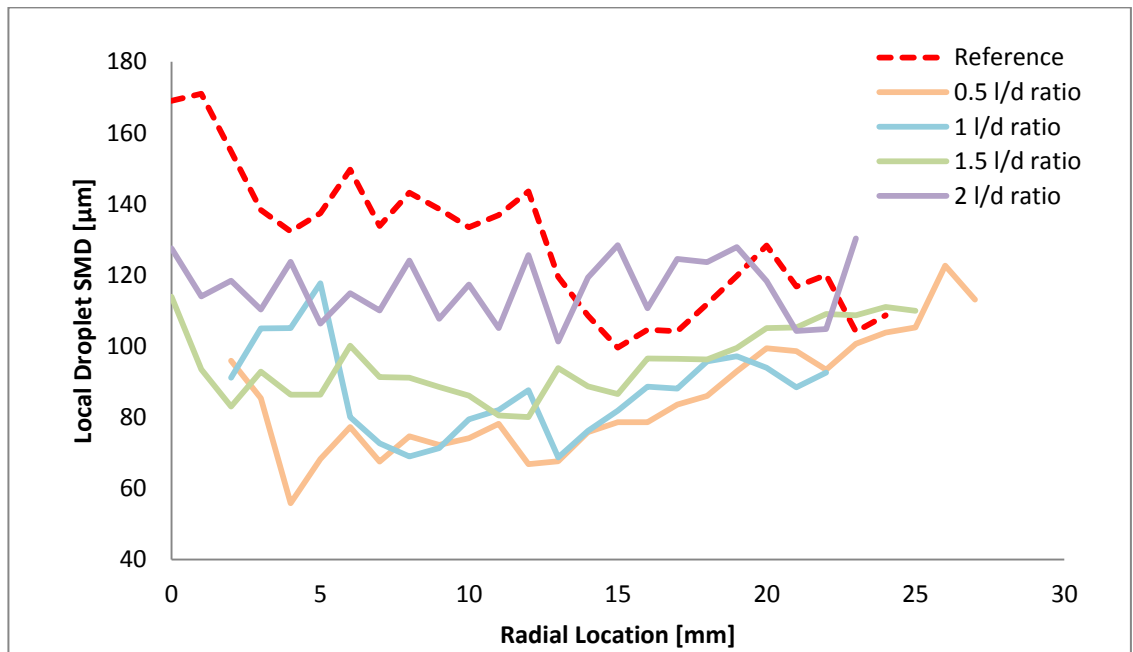


Figure 6.4.10 Local droplet SMD at 150 mm downstream of the nozzle.

#### 6.4.12 Local Droplet Size Consistency

Local droplet SMD/AMD ratio, representing local spray consistency, is presented in Figure 6.4.11. These data agree well with the local droplet AMD and SMD data. It can be seen that increasing nozzle length-to-diameter ratio reduced spray droplet



consistency resulting in a wider range of droplet sizes. This provides evidence of poorer atomization at higher nozzle length-to-diameter ratios.

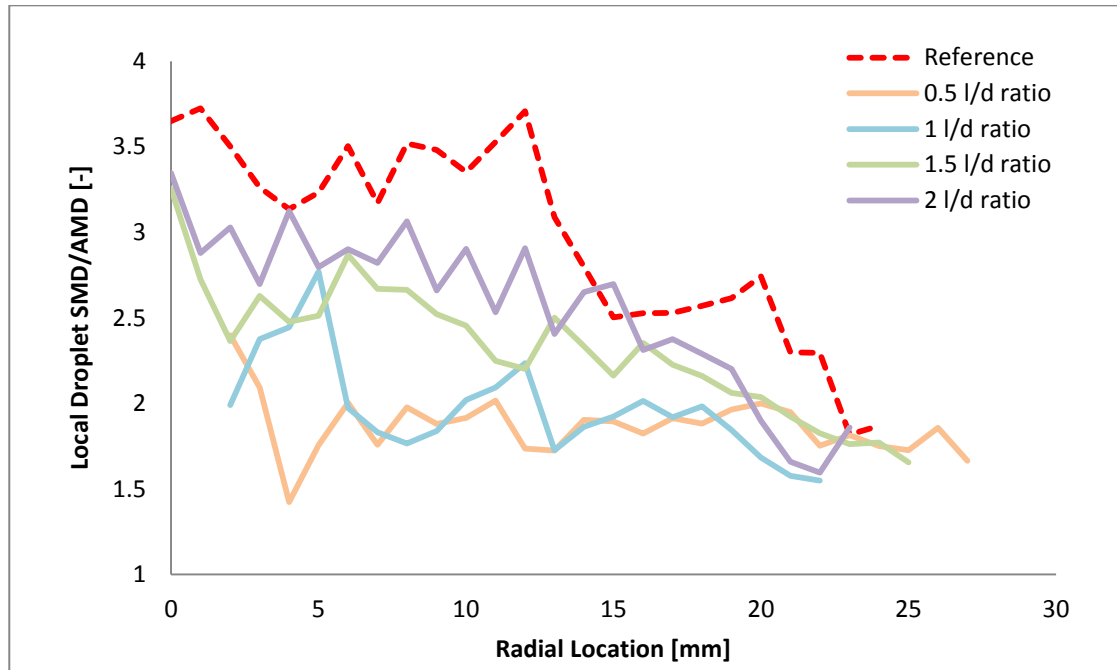


Figure 6.4.11 Local droplet SMD/AMD at 150 mm downstream of the nozzle.

#### 6.4.13 Droplet Secondary Break-up

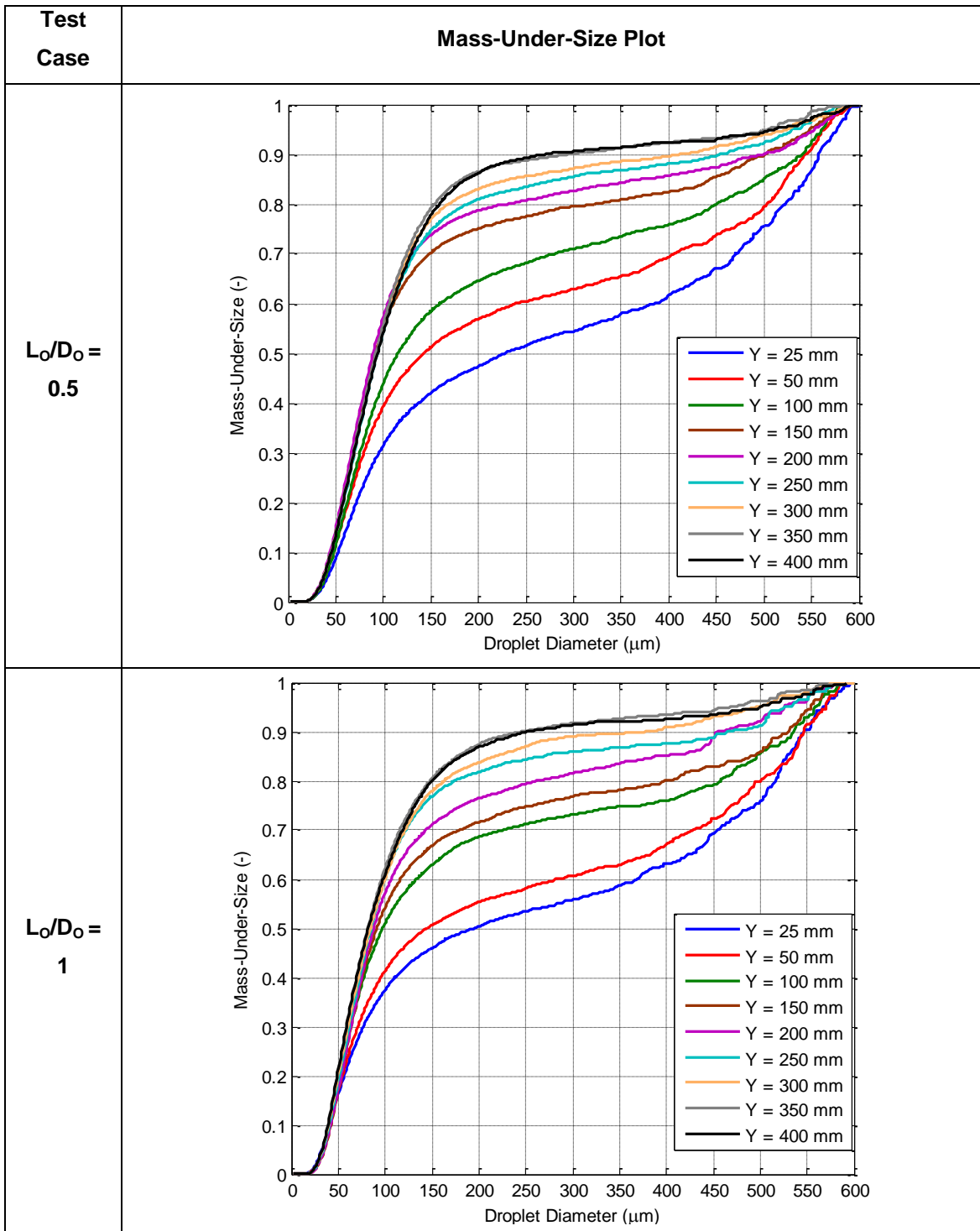
Local average Weber number was found to be more than an order of magnitude smaller than the critical Weber number ( $11 \pm 2$ ). The low local values of Weber number indicate that the majority of droplets sampled could not have been subjected to secondary break-up mechanisms. The complete Weber number data set is presented in Appendix D.

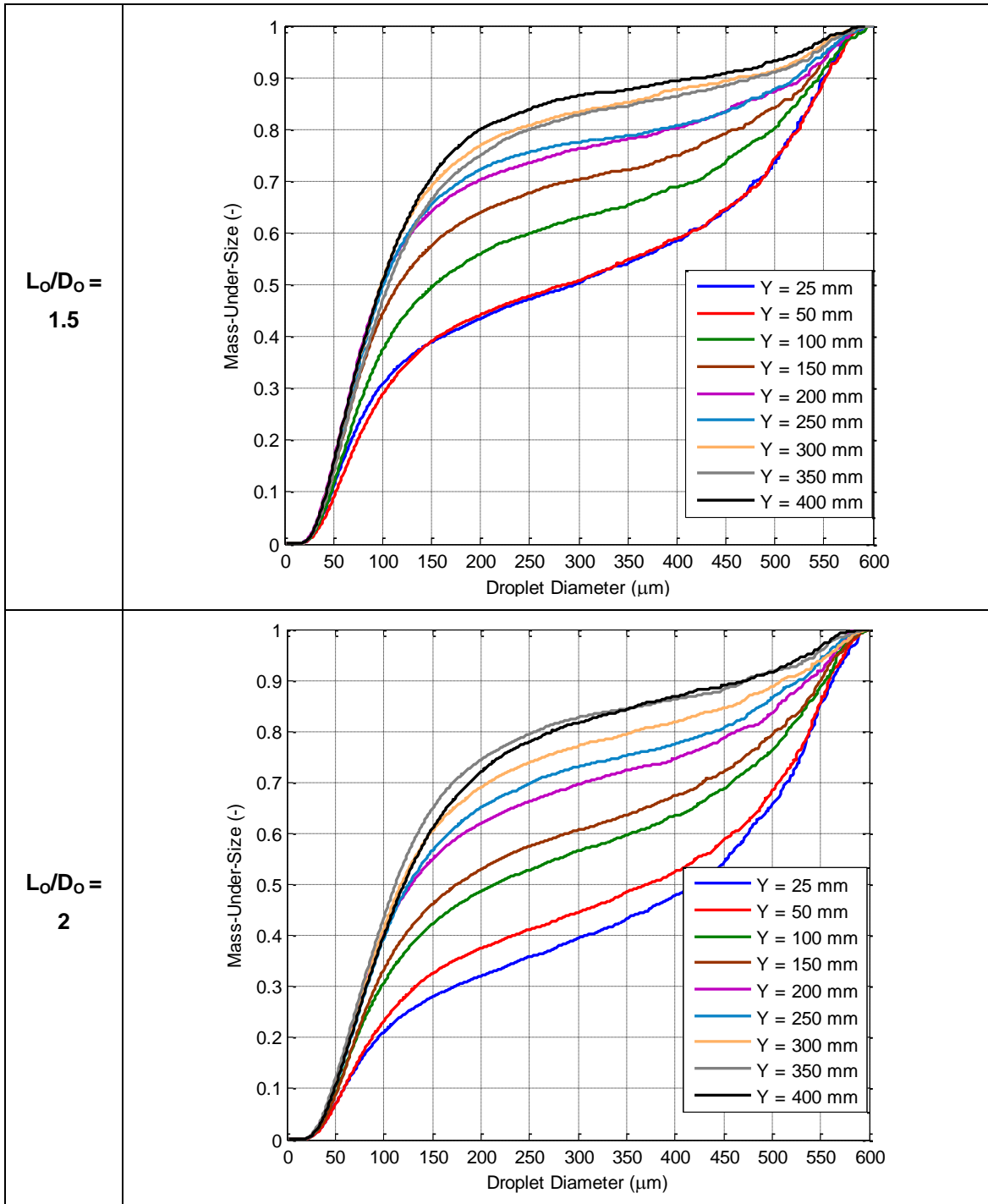
#### 6.4.14 Spray Development in the Downstream Direction

Downstream spray development is shown in Table 6.4.3. All sprays demonstrate similar amounts of downstream droplet disintegration for the axial ranges investigated. For instance the difference between the mass-under-size plots at axial distances of 25 mm and 400 mm are comparable for all test phase 6 sprays. It is evident that equilibrium may not have been achieved even at 400 mm downstream of the nozzle (e.g. the  $L_0/D_0 = 1.5$  spray shows differences in the mass-under-size plots at 350 mm and 400 mm downstream of the nozzle).

It appears that for a given spray the differences in downstream spray mass are due to different relative proportions of the very large and very small droplets (with the mid-range droplets seemingly unaffected). For example, the  $L_0/D_0 = 1$  spray in Table 6.4.3, shows different downstream proportions only in the droplets smaller than 150  $\mu\text{m}$  and those larger than 450  $\mu\text{m}$ . This is consistent with the disintegration of relatively few larger droplets by secondary atomisation in the downstream direction.

Table 6.4.3 Cumulative mass-under-size plots for entire downstream locations.





**6.4.15 Droplet SMD Correlations from the Literature**

Experimentally determined global spray droplet SMD is displayed in Figure 6.4.12, alongside droplet SMD predicted by correlations from the literature. It is clear that no correlation could accurately predict global spray droplet SMD. However this is expected as different droplet sizing techniques and sampling locations were used.

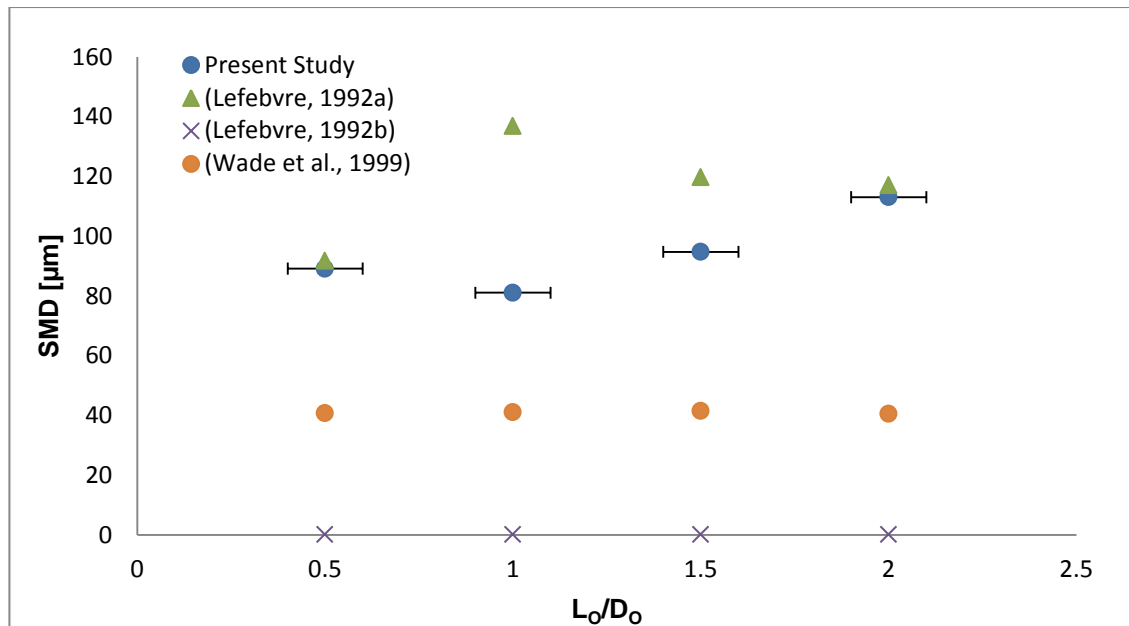


Figure 6.4.12 Comparison of global spray droplet SMD from PDA experiments with that predicted by correlations in the literature.

#### 6.4.16 Effect of $L_0/D_0$ on Global Spray Droplet SMD for Experimental Data

Since nozzle length-to-diameter ratio can alter the dynamics of the fluid flow through the nozzle, the mechanisms by which  $L_0/D_0$  affects global spray droplet SMD may be similar to the mechanisms by which nozzle and mixing chamber diameter affect spray quality. The relationship between experimentally determined global spray droplet SMD and  $L_0/D_0$  is displayed in Figure 6.4.13, where a second order polynomial line of best fit has been added.

Previous researchers [55, 65], investigating the  $L_0/D_0$  range of 0.5-1.5 claimed improved atomisation at lower length-to-diameter ratios. A later study [63] found no clear effect on droplet SMD, for the  $L_0/D_0$  range of 1-5 and for low mass flow rate pharmaceutical applications.

The present investigation demonstrates a clear relationship between  $L_0/D_0$  and global spray droplet SMD at  $L_0/D_0$  ratios of 0.5-2, in contrast to the study by Petersen et al (although that study was conducted at very low flow rates, which may result in different flow behaviour). The results of the current investigation exhibit some agreement with the findings of Chen et al and Chin et al, as lower length-to-diameter ratios generally appears to improve atomisation. However, it was not the case that the lowest  $L_0/D_0$  ratios always provided the best atomisation. In fact the best atomised spray was produced by the  $L_0/D_0 = 1$  nozzle (for instance see Figure 6.4.13).

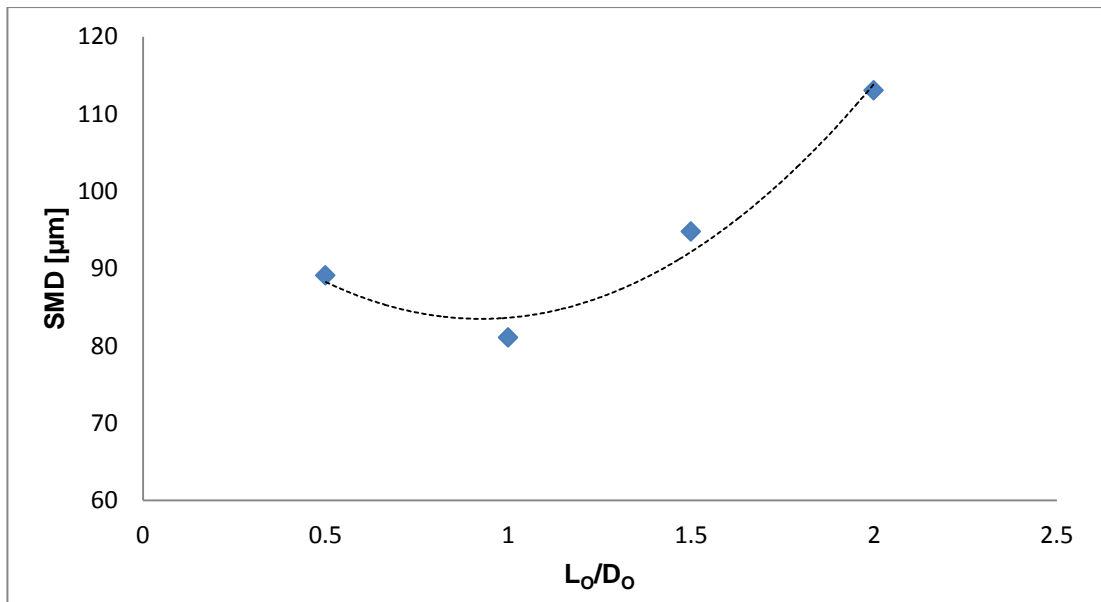


Figure 6.4.13 The relationship between  $L_0/D_0$  and global spray SMD as calculated using PDA data.

Although the relationship between SMD and  $L_0/D_0$  seems to be non-linear, the length-to-diameter ratio range  $1 < L_0/D_0 < 2$  appears highly linear. It can therefore be shown that for the geometries and conditions investigated (for  $1 < L_0/D_0 < 2$ ) the relationship between global spray SMD and nozzle length-to-diameter ratio is given by Equation 6.4.1 (a power law correlation provided the best fit to the experimental data). A reduction in  $L_0/D_0$  below unity is seen to slightly reduce spray quality. The reasons for this are not entirely clear. However further investigations of the  $L_0/D_0$  range of 0.5-1 would help improve understanding of this phenomenon.

$$\text{SMD} \propto 80.214 \left( \frac{L_0}{D_0} \right)^{0.4736} \quad \text{Equation 6.4.1}$$

## 6.5 Test Phase No.7 – Aerator Geometry

### 6.5.1 Preliminary Investigations

The geometric parameter aerator geometry is shown in Figure 6.5.1, and the position of the Aerator geometry tests within the test campaign are demonstrated in Table 6.5.1.

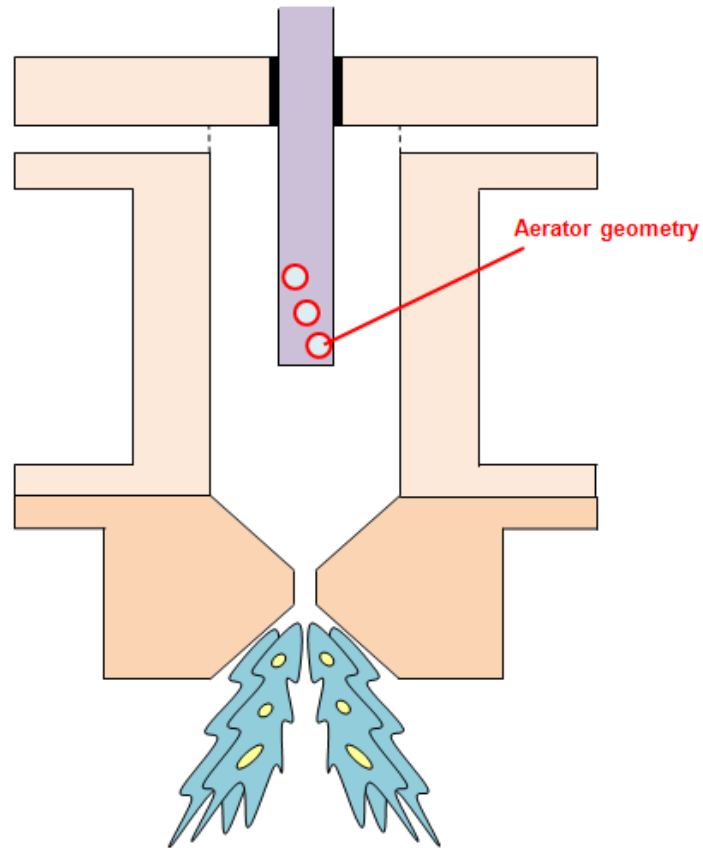


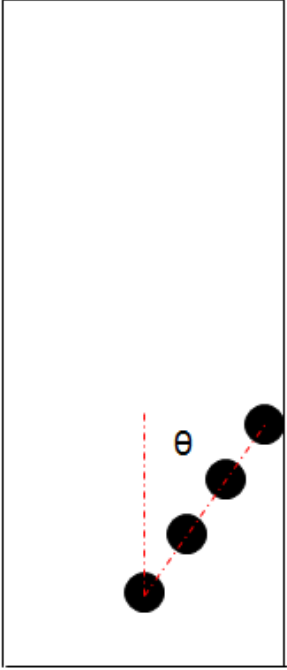
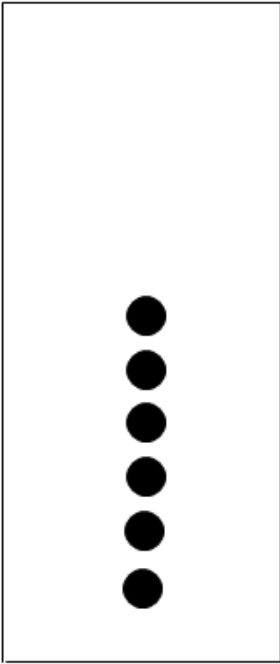
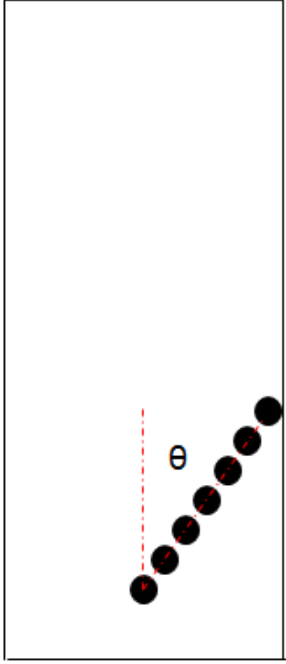
Figure 6.5.1 Schematic showing the geometric parameter aerator geometry.

Table 6.5.1 Operating conditions and controlled parameters for aerator geometry tests.

TEST No. PARAMETER VARIED	1 ALR	2 $\Delta P$	3 $D_O$	4 $L_{MC}$	5 $D_{MC}$	6 $L_O/D_O$	7 A. GEOM.	8 $\eta$
TEST PHASE	A. Initial Operating Parameters		B. Atomiser Geometry					C. Fluid properties
ALR (%)	0.8-12.5	2		2				
$\Delta P$ (bar.g)	7	4-7		7				
$D_O$ (mm)	2	2	2-4	2	2	2	2	2
$L_{MC}$ (mm)	140	140	140	64-140	140	140	140	140
$D_{MC}$ (mm)	25.4	25.4	25.4	25.4	20-30	25.4	25.4	25.4
$L_O/D_O$ (-)	1	1	1	1	1	0.5-2	1	1
Aerator Geometry	A1	A1	A1	A1	A1	A1	A2, A3	A1
$\eta \times 10^{-6}$ (m <sup>2</sup> /s)	1	1	1	1	1	1	1	2-10

It was decided to use data from test phase 1 for the A1 geometry investigation of test phase 7. Two further geometries were investigated – geometry A2 and geometry A3. Table 6.5.2 illustrates the three atomiser geometries investigated during test phase 7.

Table 6.5.2 Side on view of aerators investigated showing location of air injector holes (not to scale)

Aerator Geometry 1	Aerator Geometry 2	Aerator Geometry 3
		
6 x 2.5 mm diameter aerator holes; $\theta = 26.57^\circ$	6 x 2.6 mm diameter aerator holes; $\theta = 0^\circ$	10 x 2 mm diameter aerator holes; $\theta = 26.57^\circ$
Baseline aerator	Investigates influence of <b>air injector hole radial symmetry</b>	Investigates influence of <b>aerating hole diameter</b>

Geometry A1 represents the baseline air injector (aerator) used in all tests of the present study. This aerator geometry makes use of six evenly-spaced circular air injection holes 2.6 mm in diameter located at a measured angle of  $26.57^\circ$  to the vertical axis. This geometry was selected based on recommendations from the effervescent atomisation literature [65].

Atomiser geometry A2 employs six evenly-spaced 2.6 mm diameter holes located along the vertical axis (providing the same vertical distance between holes and the same total injection area as geometry A1). Geometry A2 aimed to investigate the effects air injector hole radial symmetry can have on spray quality. This parameter required investigation since evidence existed to suggest a possible influence on spray quality [64].

Atomiser geometry A3 makes use of ten evenly-spaced 2 mm diameter holes located at an angle of  $26.57^\circ$  to the vertical axis. The hole locations were designed to overlap with the area of hole coverage of geometry A1 in order to ensure equivalent average mixing lengths. The total injection area was the same as that of geometry A1 (and

geometry A2). This geometry aims to investigate the effects aerating hole diameter can have on spray quality.

### 6.5.2 Spray Characteristics and Results

The average operating conditions and spray results of test phase 7 are summarised in Table 6.5.3.

Table 6.5.3 Summary of aerator geometry test operating conditions and spray characteristics.

Test	A1	A2	A3
Water Supply Pressure (barG)	7.38	7.37	7.28
ALR (%)	5.70	5.71	5.62
Mixing Chamber Pressure, $\Delta P$ (barG)	6.65	6.69	6.60
$m_{\text{WATER}}$ (g/s)	31.75	33.26	31.55
$P_{\text{AIR}}$ (barG)	7.23	7.18	6.95
$m_{\text{AIR}}$ (g/s)	1.81	1.90	1.77
Volumetric Void Fraction, $\alpha$ (%)	86.1	86.2	86.0
Effective Power Rating (MW)	1.27	1.33	1.26
Coefficient of Discharge (-)	0.28	0.29	0.28
$\theta/2$ at 25 mm downstream (deg)	25.64	27.47	27.47
$D_{32}$ ( $\mu\text{m}$ )	81.06	69.14	84.28

### 6.5.3 Nozzle Coefficient of Discharge

Figure 6.5.2 shows the experimentally determined coefficients of discharge for the test phase 7 sprays. These are compared to the coefficients of discharge predicted by correlations in the literature. It can be seen that atomiser geometry had no influence on coefficient of discharge (calculated to be 0.28-0.29) and that the predictions of most equations in the literature provided a poor match to the experimental data. An exception is the correlation of Chen et al which provided a moderate match to the experimental data.



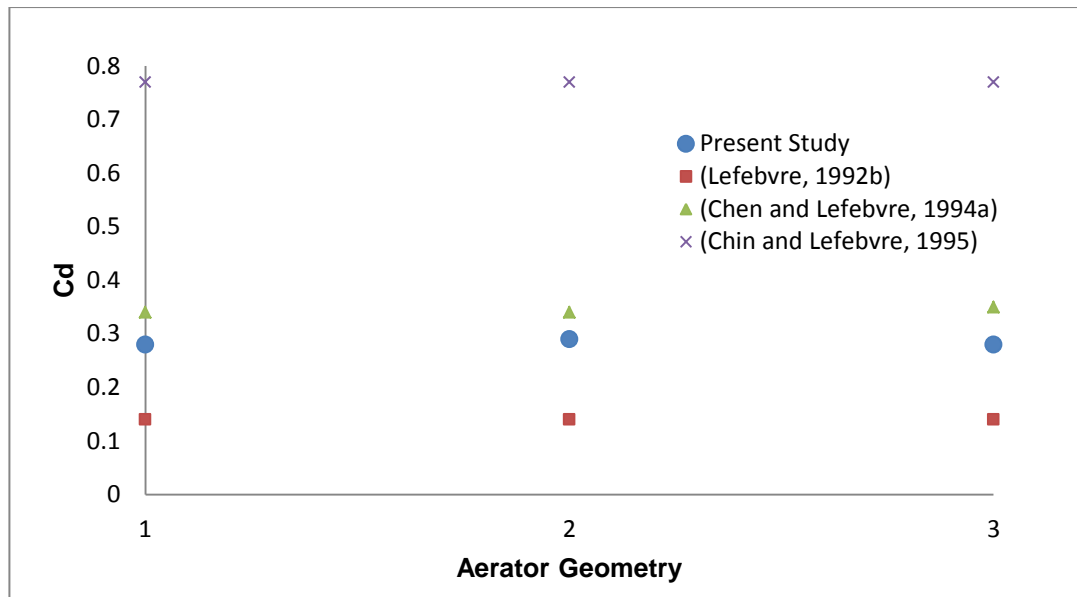


Figure 6.5.2 Comparison of coefficient of discharge from PDA experiments and literature.

#### 6.5.4 Spray Half-Angle

Figure 6.5.3 displays experimentally determined spray half-angle.

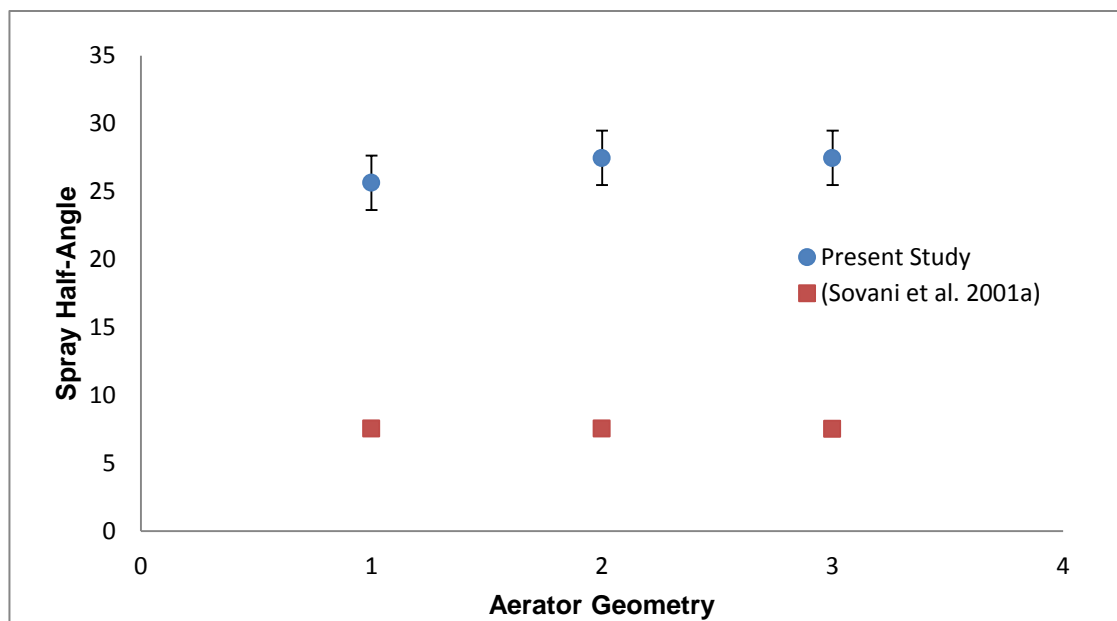


Figure 6.5.3 Comparison of spray half-angle from PDA experiments and literature.

This is compared to spray half-angle predicted by the correlation of Sovani et al. The discrepancy between the two sets of values is a result of the different data collection techniques, measurement locations and definitions of spray half-angle. The results seem to show that aerator geometry had no effect on spray half angle which varied between 25-28°.

### 6.5.5 Spray Droplet Size Distribution by Number

Figure 6.5.4 shows the droplet diameter frequency-by-number distributions for the three geometric configurations investigated during test phase 7. Geometric configuration A1, the results of which were obtained during test phase 1, displays lower total droplet counts. This is due to slightly different PDA settings which led to different data rates and therefore different spray widths (this directly influences the total droplet count).

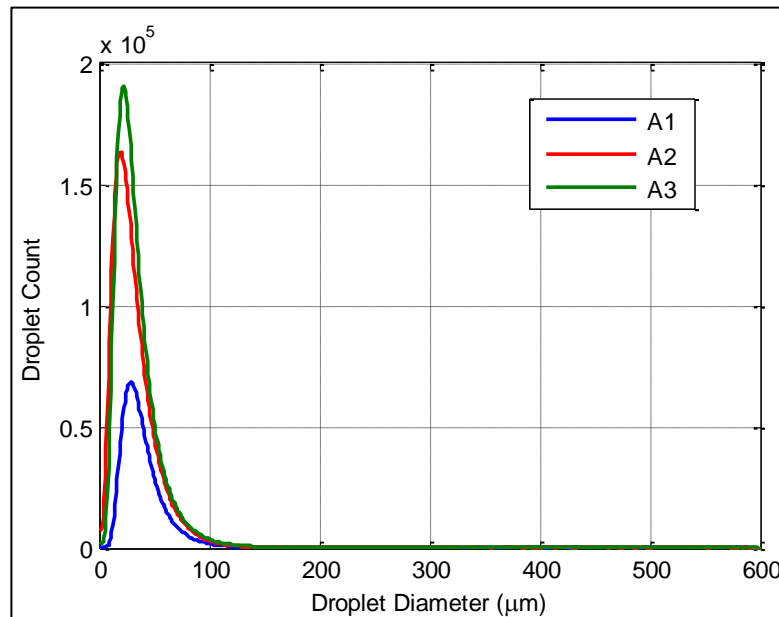


Figure 6.5.4 Droplet diameter frequency distribution based on number.

### 6.5.6 Spray Droplet Size Distribution by Mass

Figure 6.5.5 displays the droplet diameter frequency-by-mass distributions. This graph clearly shows that the spray produced by the A2 configuration was the best atomised, while the one produced by the A3 geometry was the worst atomised, respectively. For example, the former spray has the largest, while the latter spray has the smallest proportion of droplets smaller than  $150 \mu\text{m}$  (all sprays have similar droplet distributions at larger diameter ranges).

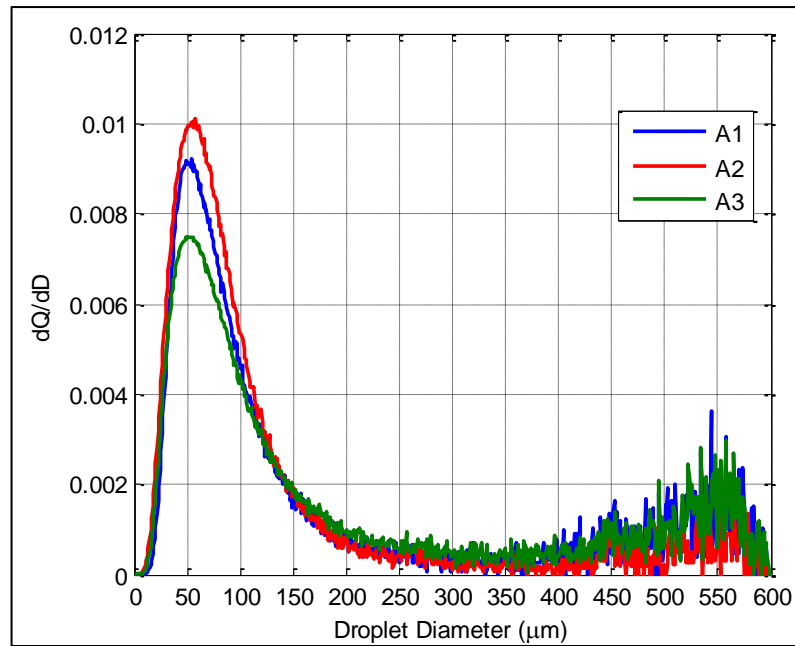


Figure 6.5.5 Droplet diameter frequency distribution based on volume/mass.

### 6.5.7 Spray Average Cumulative Droplet Size Distributions

Figure 6.5.6 displays the cumulative mass-under-size plots of all sprays investigated.

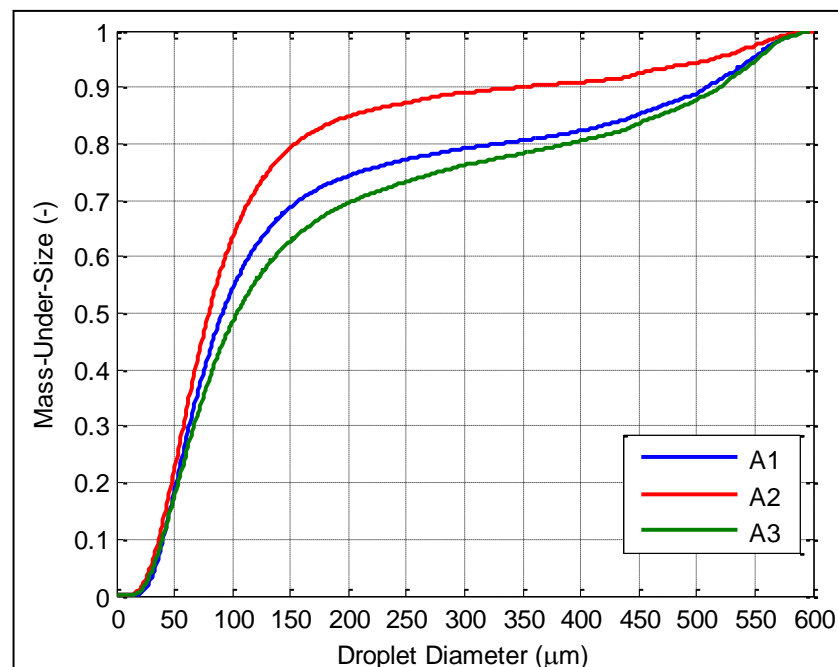


Figure 6.5.6 Cumulative droplet size distribution.

Figure 6.5.6 confirms the superior atomisation provided by the A2 atomiser geometry. This spray is comprised of a much greater mass of droplets smaller than 150 µm. In

agreement with the frequency-by-mass distributions shown in Figure 6.5.5, atomising geometry A1 provided somewhat better atomisation than geometry A3.

### 6.5.8 Validated Local Data Rates

Figure 6.5.7 illustrates the validated local data rates attained at 150 mm downstream of the exit orifice. As before, a similar pattern of droplet count variation is seen for all sprays investigated, with maximal values at a radial location of 10-15 mm and with light attenuation effects reducing data rates closer to the spray centreline.

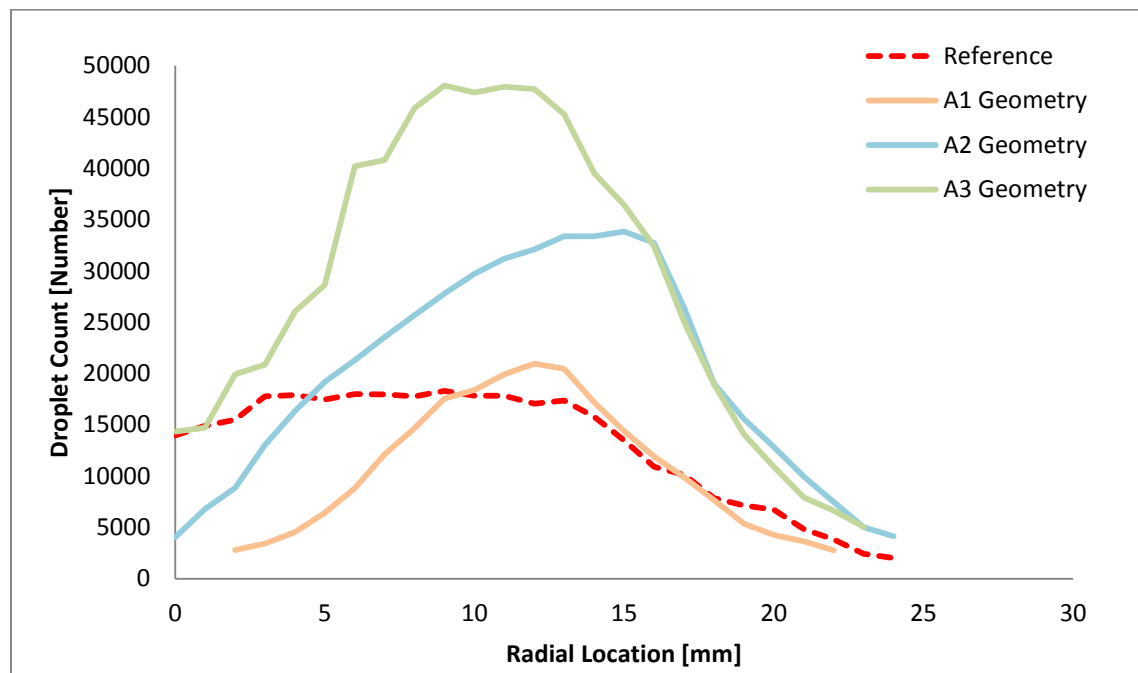


Figure 6.5.7 Validated local data rates at 150 mm downstream of the nozzle.

### 6.5.9 Local Droplet Velocity

Figure 6.5.8 shows average local droplet velocities. The minimal variation in local droplet velocity shows that air injector geometry had a small effect on average droplet velocity.

It is interesting to note that the A2 Geometry spray most closely matches the reference case (performed using the A1 Geometry). This indicates that air injector geometry had a smaller effect on local droplet velocity than atomiser operating conditions.

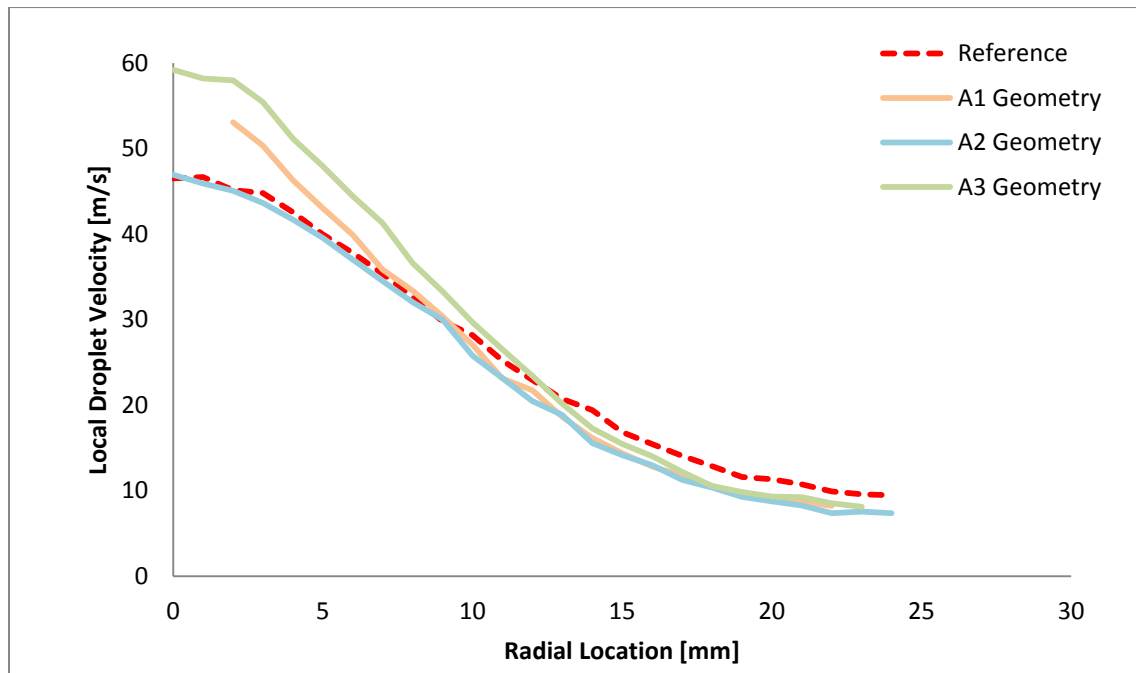


Figure 6.5.8 Average local droplet velocity at 150 mm downstream of the nozzle.

#### 6.5.10 Inferred Local Gas and Relative Velocity

The inferred local gas and relative velocities were seen to remain unaffected by air injection geometry. The complete data set of inferred gas and relative velocities are presented in Appendix E.

#### 6.5.11 Local Droplet AMD and SMD

Figure 6.5.9 and Figure 6.5.10 show local droplet AMD and local droplet SMD, respectively, at an axial location of 150 mm. Both figures demonstrate that the best atomisation was provided by the A2 Geometry (lowest droplet AMD and SMD) and the worst atomisation was provided by the A 1 Geometry (largest droplet AMD and SMD). However all sprays were more finely atomised than the reference case, which is expected since the reference case was characterised by lower ALR and pressure drop across the nozzle.

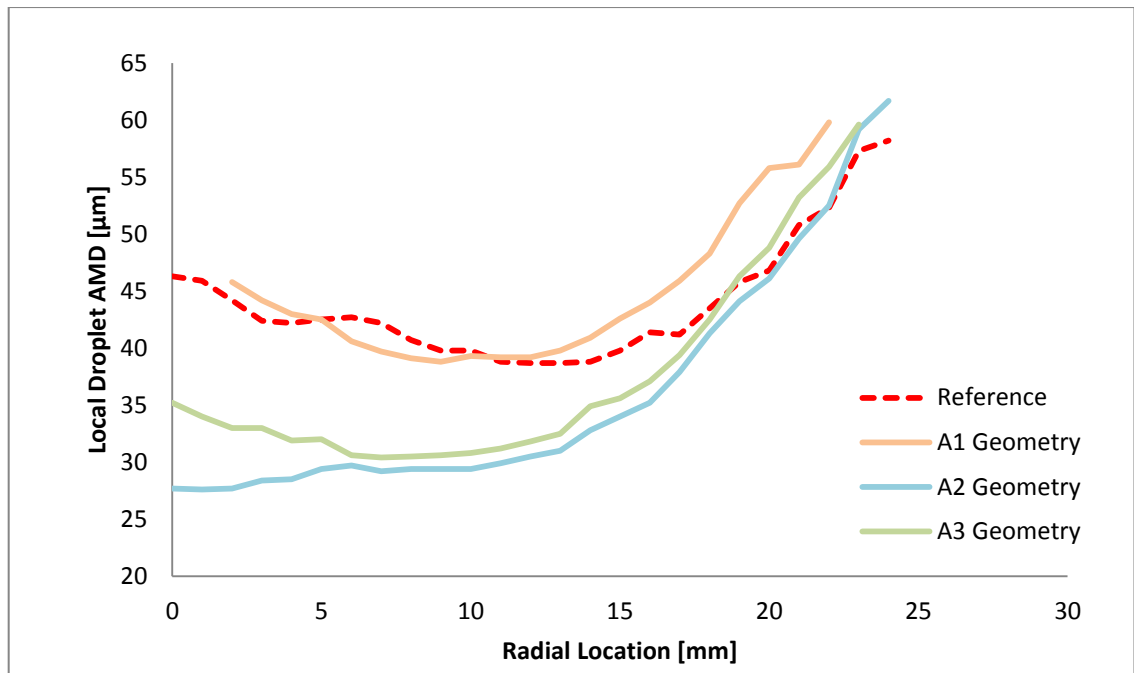


Figure 6.5.9 Local droplet AMD at 150 mm downstream of the nozzle.

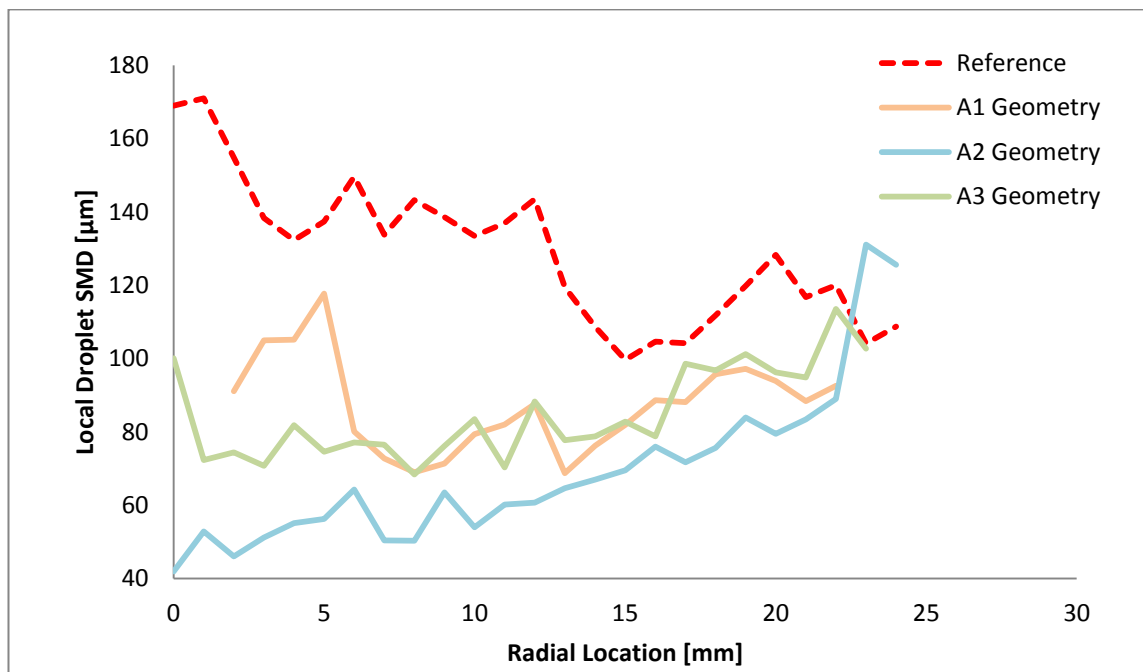


Figure 6.5.10 Local droplet SMD at 150 mm downstream of the nozzle.

### 6.5.12 Local Droplet Size Spread

The local droplet consistency of the sprays analysed is shown in Figure 6.5.11. This graph indicates that the greatest droplet consistency was provided by the A2 Geometry and that the poorest droplet consistency was provided by the A3 Geometry. Meanwhile, all sprays are more consistent than the reference case. This agrees well with the conclusions drawn from Figure 6.5.9 and Figure 6.5.10.

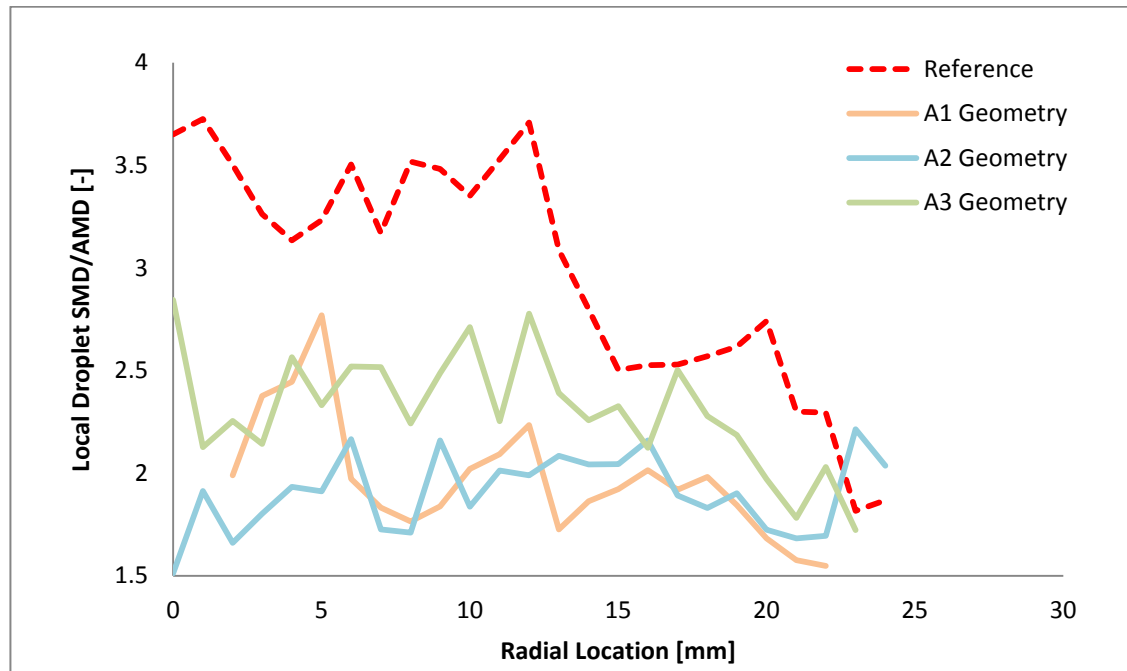


Figure 6.5.11 Local droplet SMD/AMD at 150 mm downstream of the nozzle.

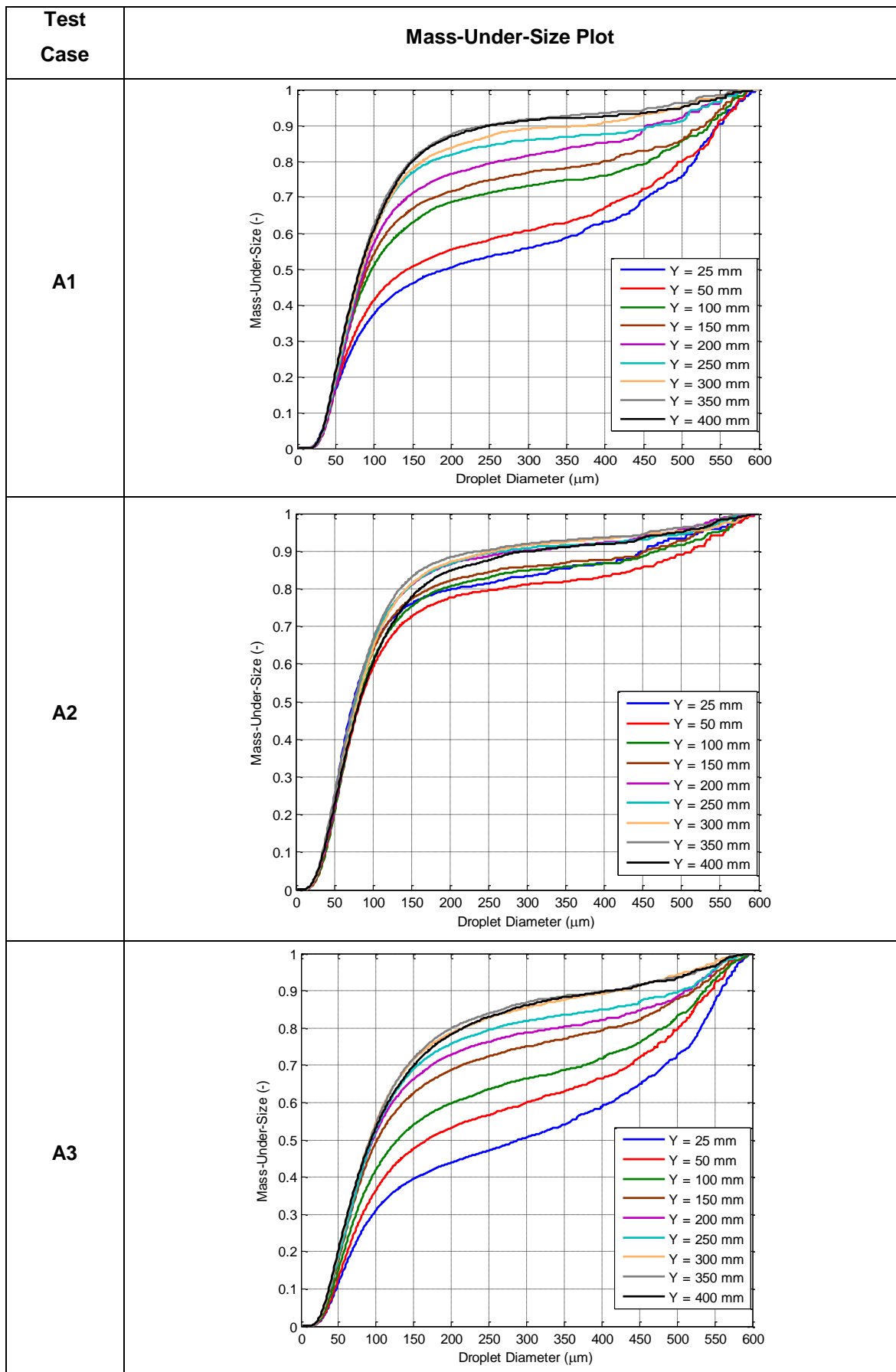
### 6.5.13 Droplet Secondary Break-up

Local average Weber number was found to be more than an order of magnitude smaller than the critical Weber number ( $11 \pm 2$ ). The low local values of Weber number indicate that the majority of droplets sampled could not have been subjected to secondary break-up mechanisms. The complete Weber number data set is presented in Appendix E.

### 6.5.14 Spray Development in the Downstream Direction

Table 6.5.4 displays the cumulative mass-under-size plots for every axial sampling location of every spray investigated in test phase 7. The closely-lying mass-under-size plots of the A2 geometry graph shows comparatively little spray development in the downstream direction. This indicates that this spray was subject to significantly less secondary atomisation than the other two sprays; instead this spray was already well atomised at 25 mm downstream of the exit orifice with very few large droplets present. This supports the conclusions of other analyses performed which demonstrate that the A2 geometry provided the best atomisation of any aerator geometry investigated.

Table 6.5.4 Cumulative mass-under-size plots for entire downstream locations.





### 6.5.15 Droplet SMD Correlations from the Literature

Figure 6.5.12 compares experimentally determined global spray SMD to SMD predicted by correlations from the effervescent atomisation literature. Clearly none of the correlations found could accurately predict global spray SMD for the atomiser geometries and conditions investigated. However this is expected as different authors employed a range of droplet sizing techniques and sampling locations in order to obtain their experimental data. As discussed in previous chapters, sampling technique and location can have a considerable influence on SMD.

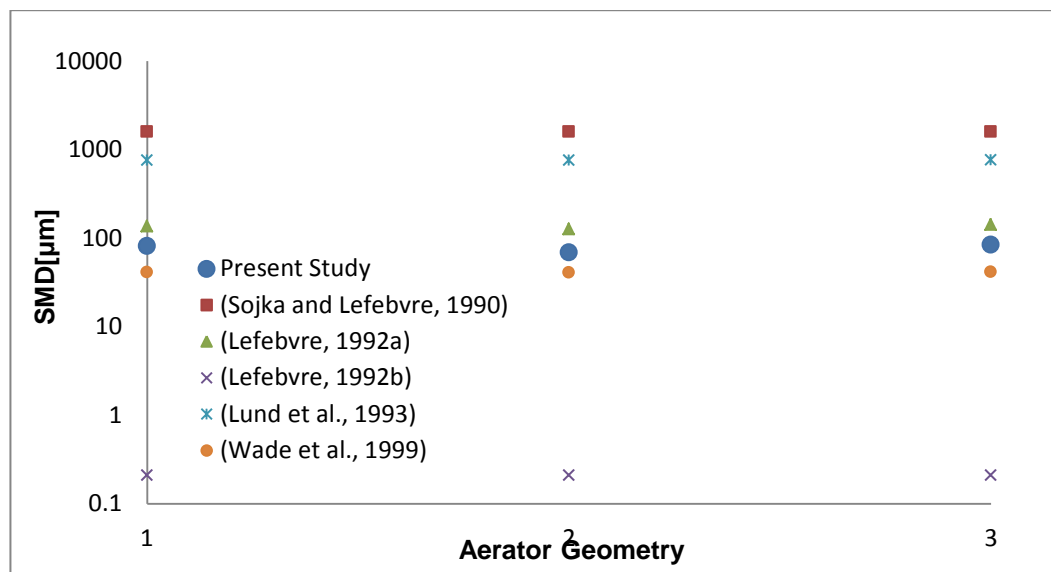


Figure 6.5.12 Comparison of global spray SMD from PDA experiments with that predicted by correlations in the literature.

### 6.5.16 Effect of Aerator Geometry on Global Spray Droplet SMD for Experimental Data

Figure 6.5.13 shows global spray SMD for all three atomiser geometries investigated in test phase 7. The results indicate that both air injector hole radial symmetry and air injector diameter influenced spray quality. It is clear that the A2 atomiser geometry provided significantly better atomisation performance than any other aerator geometry.

In agreement with the findings of Sojka [64] an asymmetric arrangement of air injector holes was found to provide considerable improvements in spray quality. In the context of the present study, complete air injector hole asymmetry translates into all air injector holes being placed on the same radial location as shown in the A2 geometry sketch of Table 6.5.2. This finding is significant when contrasted with the test phase 4 results which demonstrated no relation between axial mixing length (i.e. the axial location of the air injector holes) and spray quality.

In keeping with previous investigations which report that air injector hole diameter had only a minor effect on spray quality [31, 32, 62], air injector hole diameter was seen to have a small influence on spray quality over the diameter ranges investigated (2-2.6 mm diameter air injector holes). Aerator geometry A1 provided marginally better spray atomisation than geometry A3 which shows that over the ranges investigated (for the same total air injector area) larger air injector diameter holes offered marginally better atomisation performance.

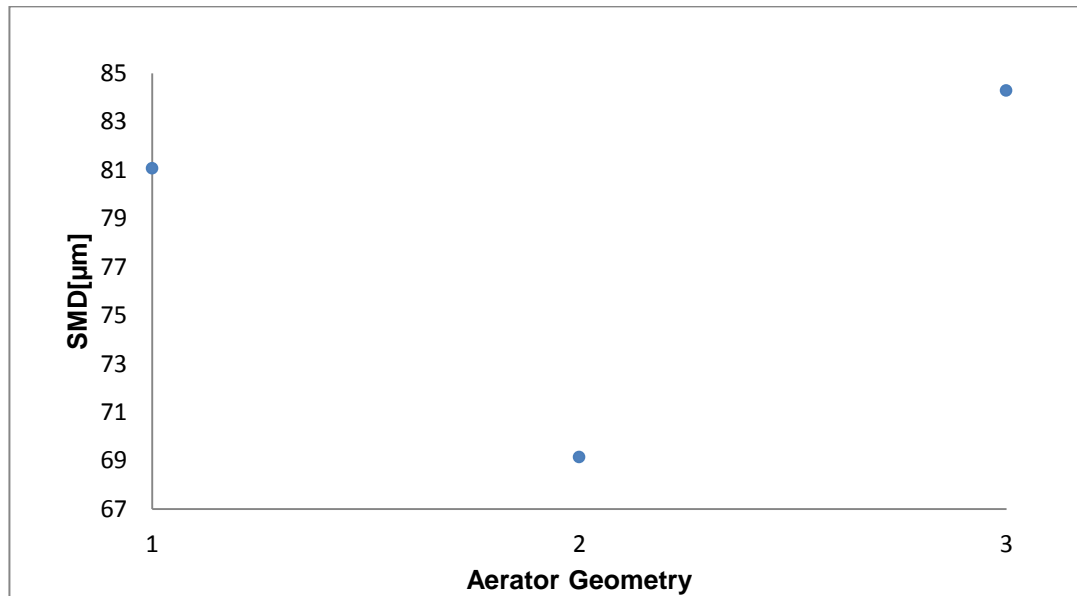


Figure 6.5.13 Experimentally determined global spray droplet SMD for all aerator geometries investigated.

## Chapter 7 : Results – Fluid Properties

### 7.1 Test Phase No.8 – Fluid Viscosity, $\eta$

#### 7.1.1 Preliminary Investigations

Table 7.1.1 illustrates the position of the tests to investigate kinematic viscosity (test phase 8) within the test program.

Table 7.1.1 Operating conditions and controlled parameters for kinematic viscosity tests.

TEST No. PARAMETER VARIED	1 ALR	2 $\Delta P$	3 $D_O$	4 $L_{MC}$	5 $D_{MC}$	6 $L_O/D_O$	7 A. GEOM.	8 $\eta$
TEST PHASE	A. Initial Operating Parameters		B. Atomiser Geometry					C. Fluid properties
ALR (%)	0.8-12.5	2		2				
$\Delta P$ (bar.g)	7	4-7		7				
$D_O$ (mm)	2	2	2-4	2	2	2	2	2
$L_{MC}$ (mm)	140	140	140	64-140	140	140	140	140
$D_{MC}$ (mm)	25.4	25.4	25.4	25.4	20-30	25.4	25.4	25.4
$L_O/D_O$ (-)	1	1	1	1	1	0.5-2	1	1
Aerator Geometry	A1	A1	A1	A1	A1	A1	A2, A3	A1
$\eta \times 10^{-6}$ (m <sup>2</sup> /s)	1	1	1	1	1	1	1	2-10

Fluid viscosity was investigated by running the effervescent atomiser with water-glycerol mixtures (instead of plain water, as in previous test phases) as the operating fluid, and with air as the assist medium. By mixing water and glycerol, fluids with the desired properties could be created and investigated. A calibrated Cannon-Fenske Routine Viscometer was used to measure the kinematic viscosity of a given fluid. Each mixture was homogenised by stirring for half an hour (the pump was used to recycle the fluid back to the storage tank) prior to viscosity measurements being taken. It was found that prolonged operation imparted heat energy to the fluid causing noticeable increases in fluid temperature and therefore viscosity. To account for this, fluid viscosity was measured immediately before and immediately after each test to allow an average value of kinematic viscosity to be calculated. This average value of viscosity is reported (as a whole number or to 1 d.p.) in the present work. Throughout all tests, initial and final kinematic viscosities varied by up to  $\pm 0.5 \times 10^{-6}$  m<sup>2</sup>/s from the average values given.

Pure water was assumed to have a kinematic viscosity of  $1 \times 10^{-6}$  m<sup>2</sup>/s.

### 7.1.2 Spray Characteristics and Results

The Table 7.1.2 summarises the results. An average viscosity range of  $1\text{--}18 \times 10^{-6} \text{ m}^2/\text{s}$  was achieved, corresponding to a variation of 1700%. Meanwhile the average values of the control parameters ALR and  $\Delta P$  varied by 5% and 8% respectively. This shows that viscosity was the dominant parameter, as it varied by two orders of magnitude more than any other control parameter.

Table 7.1.2 Summary of kinematic viscosity test operating conditions and spray characteristics.

Test	Kinematic Viscosity = $1 \times 10^{-6} \text{ m}^2/\text{s}$	Kinematic Viscosity = $5.1 \times 10^{-6} \text{ m}^2/\text{s}$	Kinematic Viscosity = $10.1 \times 10^{-6} \text{ m}^2/\text{s}$	Kinematic Viscosity = $18 \times 10^{-6} \text{ m}^2/\text{s}$
Water Supply Pressure (barG)	7.38	7.10	7.21	7.56
ALR (%)	5.70	5.57	5.84	5.70
Mixing Chamber Pressure, $\Delta P$ (barG)	6.65	6.52	6.69	7.00
$m_{\text{WATER}}$ (g/s)	31.75	32.91	31.70	34.35
$P_{\text{AIR}}$ (barG)	7.23	6.81	7.03	7.19
$m_{\text{AIR}}$ (g/s)	1.81	1.83	1.85	1.95
Volumetric Void Fraction, $\alpha$ (%)	86.1	85.9	86.4	86.1
Effective Power Rating (MW)	1.27	1.32	1.27	1.37
Coefficient of Discharge (-)	0.28	0.29	0.28	0.29
$\theta/2$ at 25 mm downstream (deg)	25.64	32.62	30.96	30.96
$D_{32}$ ( $\mu\text{m}$ )	81.06	88.16	95.28	146.58

### 7.1.3 Nozzle Coefficient of Discharge

Figure 7.1.1 shows how discharge coefficient varied with increasing viscosity, and how this compares to the predictions of other correlations from the literature. It is clear that discharge coefficient was almost entirely unaffected by changes in fluid viscosity and that most correlations in the literature provided a poor match with the experimental data. Closest to the experimental data was the correlation of Chen et al.

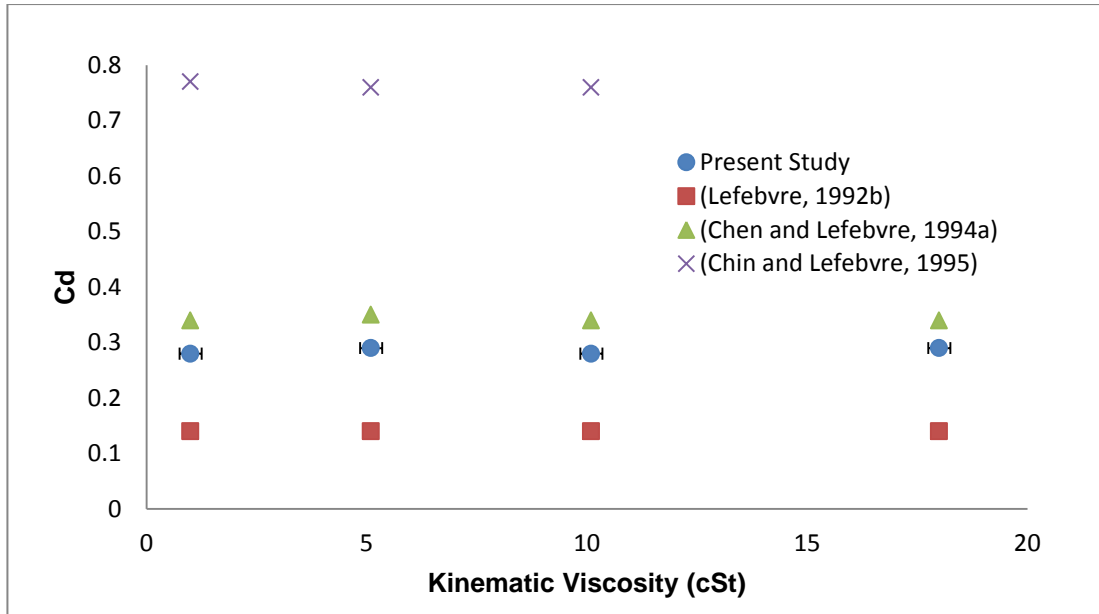


Figure 7.1.1 Comparison of coefficient of discharge from PDA experiments with that in the literature.

#### 7.1.4 Mode of Liquid Break-up at Nozzle

Figure 7.1.2 displays the calculated mode of liquid break-up at the nozzle. This shows that all sprays investigated in this test phase were characterised by the atomisation regime of near-nozzle break-up. Unexpectedly this analysis shows that increases in kinematic viscosity pushed operation further into the atomisation regime which would be expected to result in superior atomisation performance at higher viscosities. However this is contrary to the expected results, since increases in fluid viscosity are known to generally reduce atomisation quality.

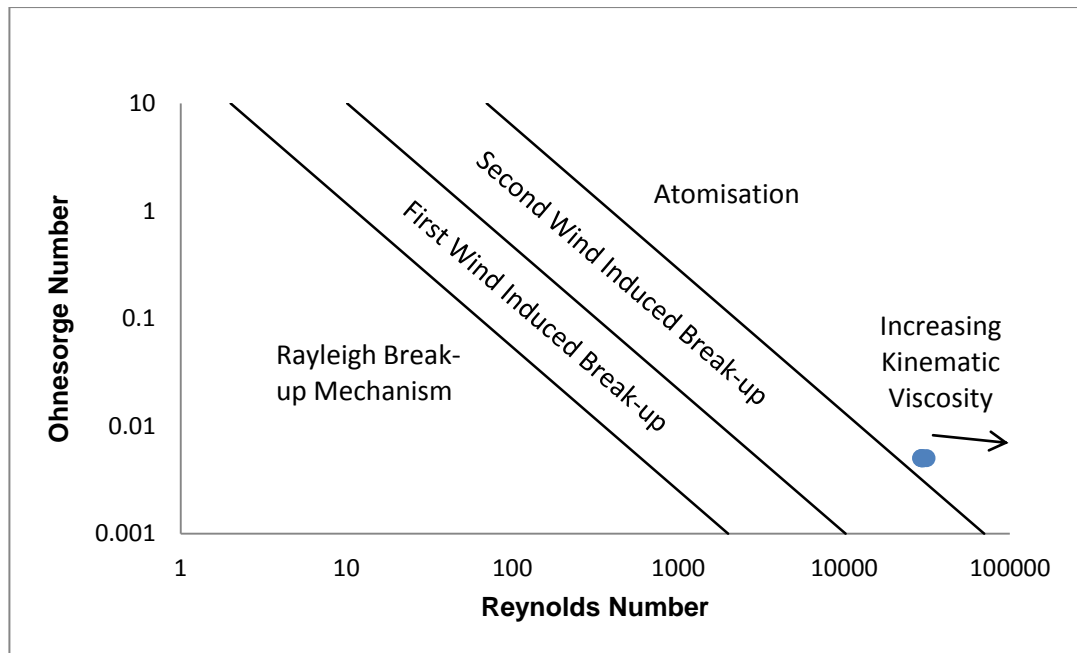


Figure 7.1.2 Calculated liquid disintegration mode for kinematic viscosity experiments.

### 7.1.5 Spray Half-Angle

Figure 7.1.3 shows experimentally determined spray half-angle, and compares this to the half-angle predicted by the correlation of Sovani et al. It can be seen that spray half-angle, initially low at a kinematic viscosity of  $1 \times 10^{-6} \text{ m}^2/\text{s}$ , increases by about  $5^\circ$  to a roughly constant value for the viscosity ranges of  $5\text{-}18 \times 10^{-6} \text{ m}^2/\text{s}$ . This finding is in contrast to the work of Chen et al who reported decreasing spray angles at larger viscosities [86].

Meanwhile the correlation of Sovani et al is seen to considerably under-predict spray half-angle. This is a result of the different spray angle definitions and measurement techniques used by Sovani et al.

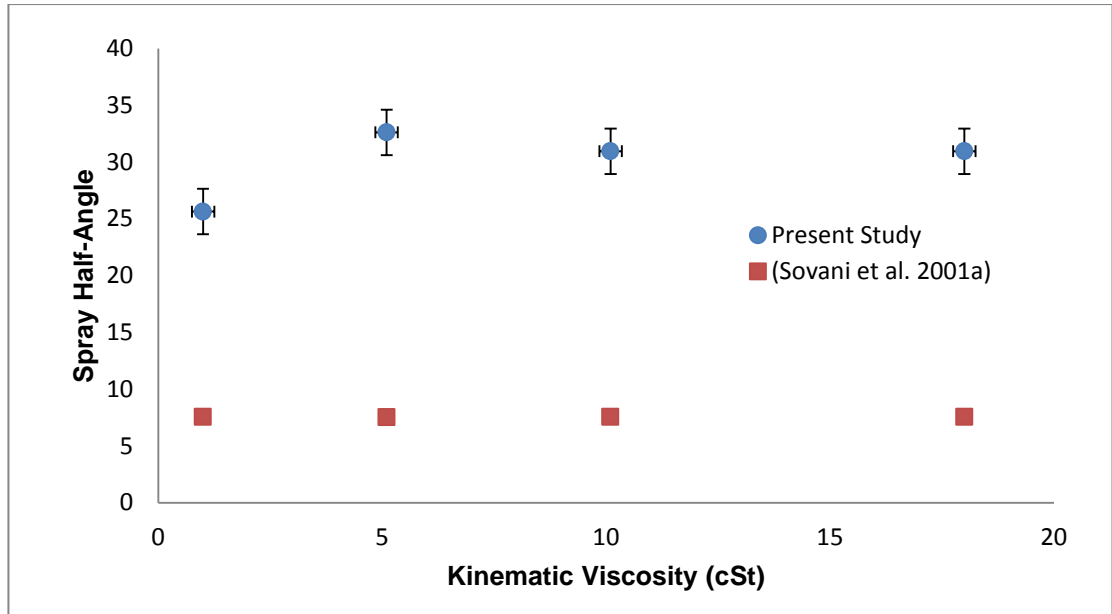


Figure 7.1.3 Comparison of spray half-angle from PDA experiments and literature.

### 7.1.6 Spray Droplet Size Distribution by Number

Figure 7.1.4 displays the droplet diameter frequency distributions based on number. These graphs show that by number most of the droplets found in all sprays measured were smaller than 150  $\mu\text{m}$ .

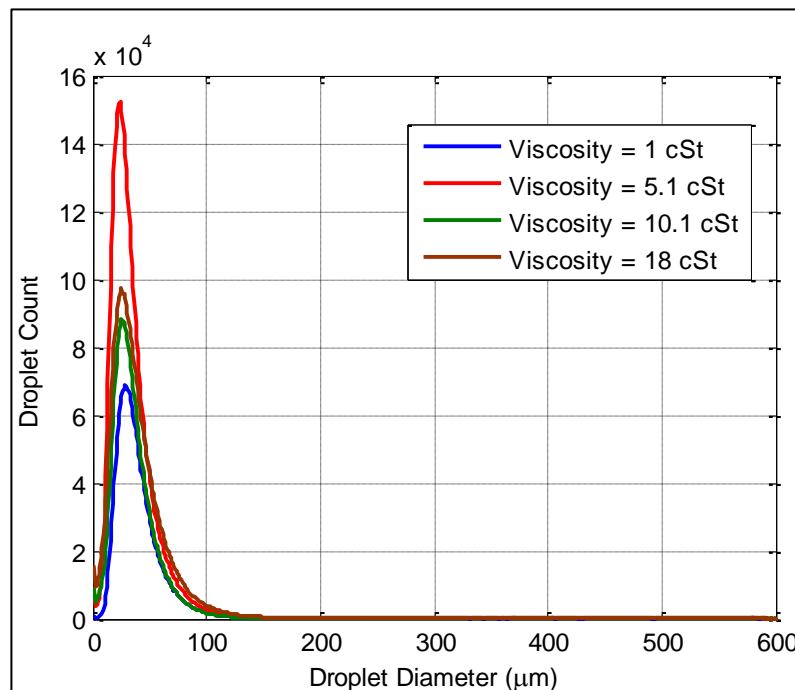


Figure 7.1.4 Droplet diameter frequency distribution based on number.

### 7.1.7 Spray Droplet Size Distribution by Mass

Droplet diameter frequency distributions based on mass are shown in Figure 7.1.5. This graph clearly shows that the frequency distributions by mass increasingly become bimodal at greater viscosities, with one peak in the low droplet diameter and one peak in the large droplet diameter ranges. This is a result of the increasing contribution of very large droplets as viscosity is increased, and is a clear indication that the larger viscosity sprays are more poorly atomised as they possess a greater number of larger droplets.

Figure 7.1.5 shows that  $1 \times 10^{-6} \text{ m}^2/\text{s}$  spray is the best atomised, the  $18 \times 10^{-6} \text{ m}^2/\text{s}$  spray is the most poorly atomised, with the remaining two sprays ( $5.1 \times 10^{-6} \text{ m}^2/\text{s}$  and  $10.1 \times 10^{-6} \text{ m}^2/\text{s}$ ) appearing very similar.

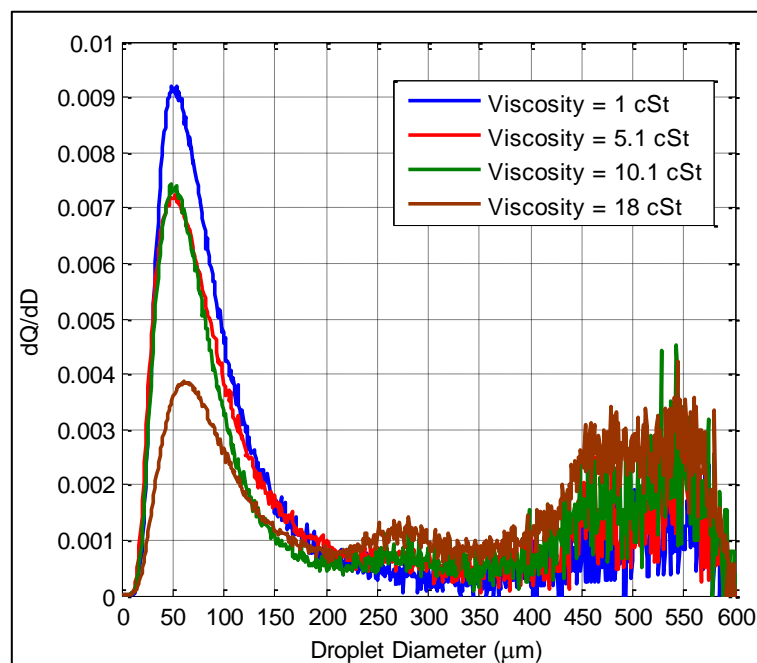


Figure 7.1.5 Droplet diameter frequency distribution by mass.

### 7.1.8 Spray Average Cumulative Droplet Size Distributions

Figure 7.1.6 shows the cumulative mass-under-size plots for all sprays investigated.

This graph provides support for Figure 7.1.5 and clearly shows that viscosity increases resulted in progressively less well-atomised sprays. Despite not being clear from Figure 7.1.5, Figure 7.1.6 demonstrates that the  $5.1 \times 10^{-6} \text{ m}^2/\text{s}$  spray was in fact better atomised than the  $10.1 \times 10^{-6} \text{ m}^2/\text{s}$  spray.



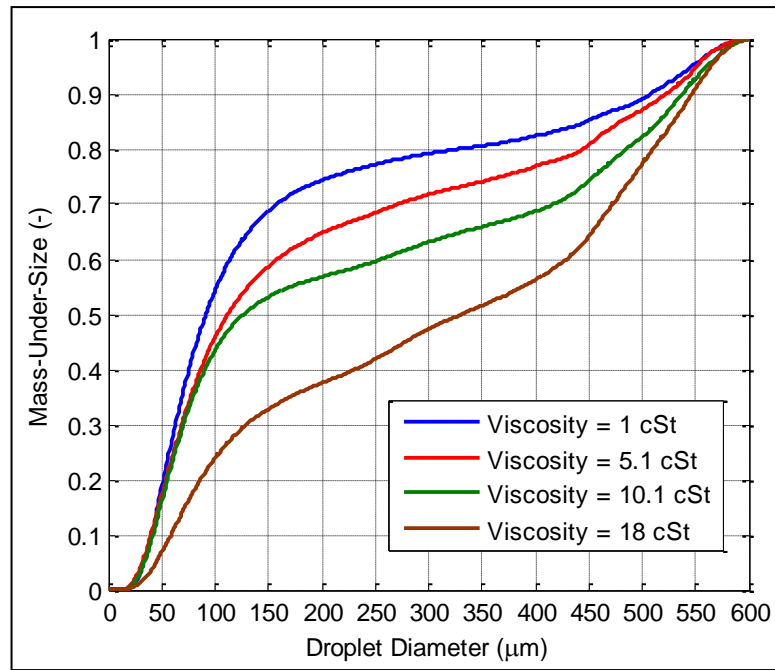


Figure 7.1.6 Cumulative droplet size distribution.

### 7.1.9 Validated Local Data Rates

Figure 7.1.7 displays validated local droplet count at an axial location of 150 mm. As expected, the highest data rates were observed about halfway between the centreline and the spray edge. Meanwhile the relatively low data rates along the centreline are a result of multiple scattering and light attenuation effects in the dense spray.

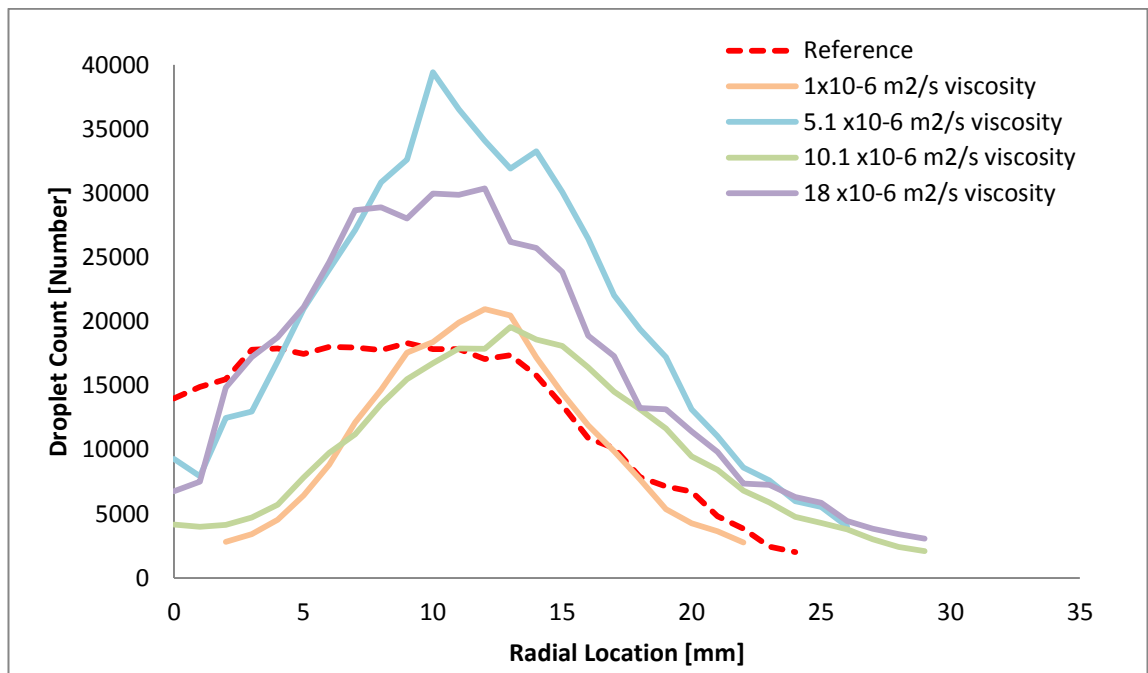


Figure 7.1.7 Validated local data rates at 150 mm downstream of the nozzle.

### 7.1.10 Local Droplet Velocity

Figure 7.1.8 displays the average local droplet velocities 150 mm downstream of the exit orifice. Although a similar droplet velocity pattern emerges for all sprays analysed (for the kinematic viscosity ranges investigated), no clear relationship can be seen between fluid viscosity and average local droplet velocity.

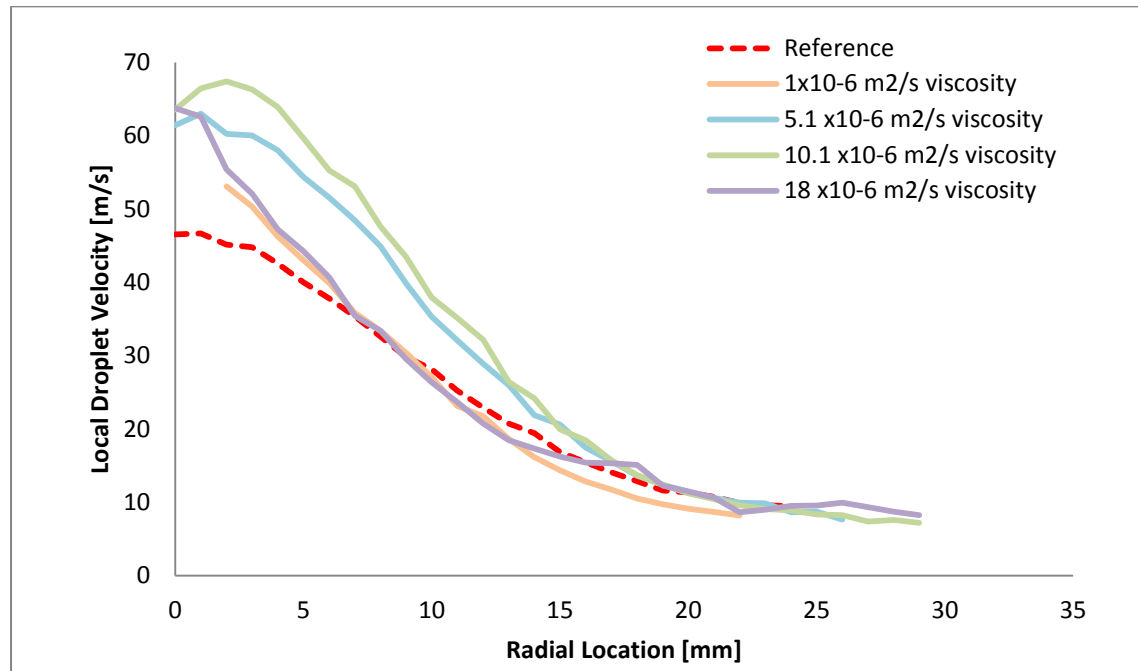


Figure 7.1.8 Average local droplet velocity at 150 mm downstream of the nozzle.

### 7.1.11 Inferred Local Gas and Relative Velocity

The inferred local gas and relative velocities were seen to remain unaffected by air injection geometry. The complete data set of inferred gas and relative velocities are presented in Appendix F.

### 7.1.12 Local Droplet AMD and SMD

Figure 7.1.9 and Figure 7.1.10 display the average local droplet AMD and SMD, respectively, at an axial location of 150 mm. The graph of local droplet AMD (Figure 7.1.9) does not provide any clear trends. However the graph of local droplet SMD clearly demonstrates that the  $18 \times 10^{-6} \text{ m}^2/\text{s}$  spray was the most poorly atomised (largest droplet SMD), with the remaining three sprays somewhat similar in terms of

their local droplet SMD values. This shows that the highest viscosity spray was the most poorly atomised.

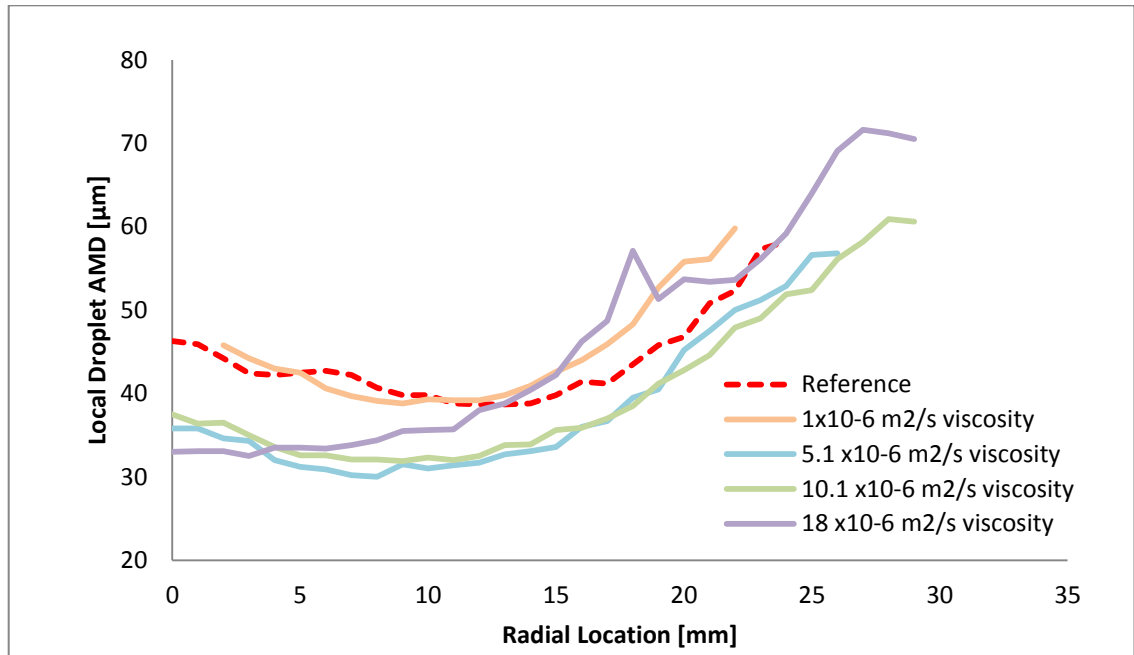


Figure 7.1.9 Local droplet AMD at 150 mm downstream of the nozzle.

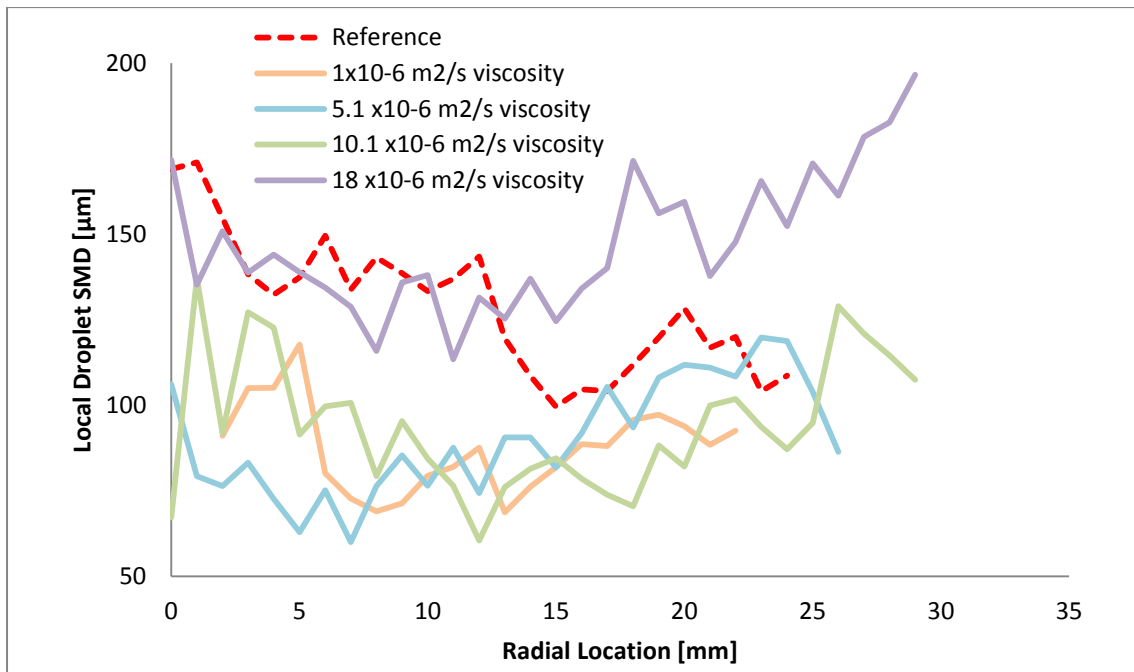


Figure 7.1.10 Local droplet SMD at 150 mm downstream of the nozzle.

### 7.1.13 Local Droplet Size Consistency

Figure 7.1.11 displays the local droplet SMD/AMD ratio of each spray. This figure provides clear evidence for a reduction in atomiser performance at higher fluid

viscosities: the  $18 \times 10^{-6} \text{ m}^2/\text{s}$  spray was the least consistent, while the  $1 \times 10^{-6} \text{ m}^2/\text{s}$  spray displayed the greatest local droplet consistency. This supports the conclusions drawn from Figure 7.1.9 and Figure 7.1.10.

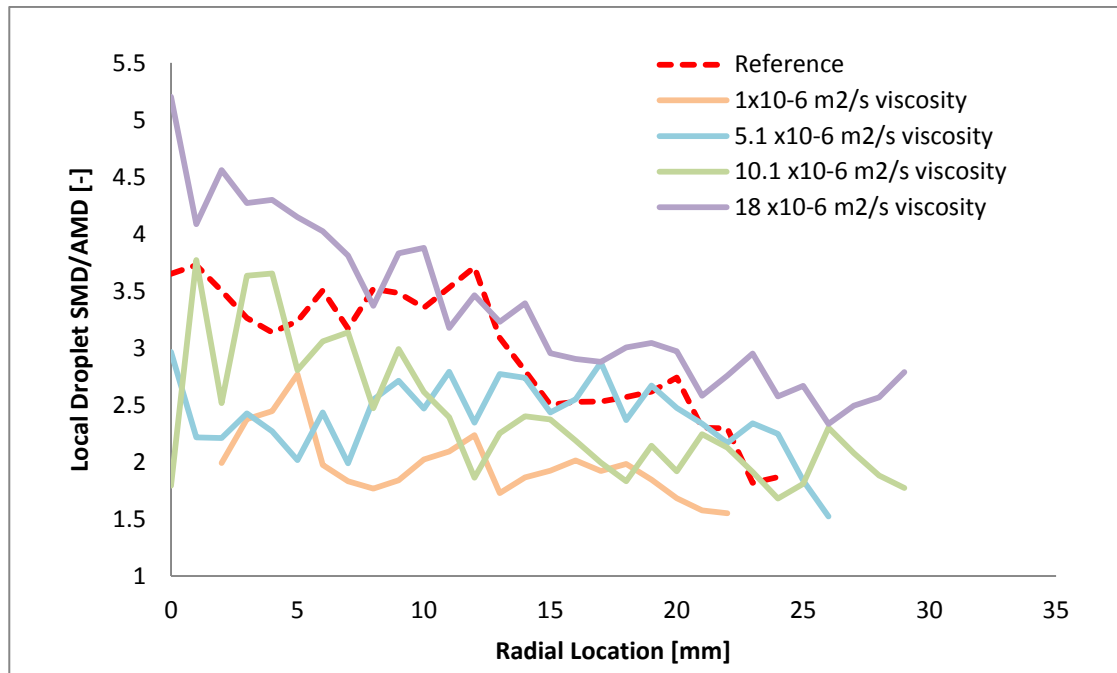


Figure 7.1.11 Local droplet SMD/AMD at 150 mm downstream of the nozzle.

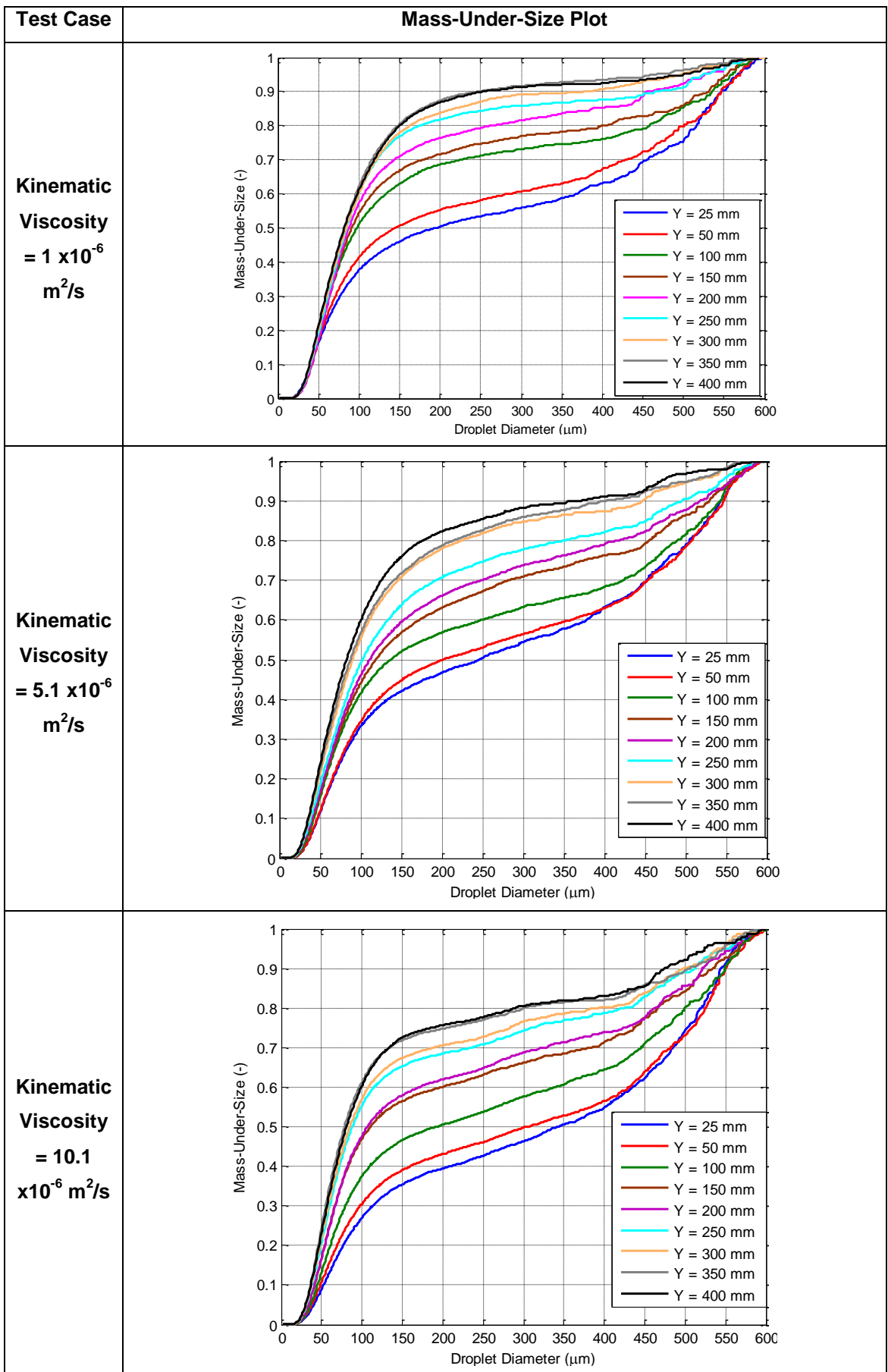
### ***Droplet Secondary Break-up***

Local average Weber number was found to be more than an order of magnitude smaller than the critical Weber number ( $11 \pm 2$ ). The low local values of Weber number indicate that the majority of droplets sampled could not have been subjected to secondary break-up mechanisms. The complete Weber number data set is presented in Appendix F.

### ***7.1.14 Spray Development in the Downstream Direction***

Table 7.1.3 shows the mass-under-size plots at each sampled axial location of every spray. These graphs give an indication of the downstream spray development at nine different axial locations, from 25 mm to 400 mm downstream of the nozzle.

Table 7.1.3 Cumulative mass-under-size plots for entire downstream locations.



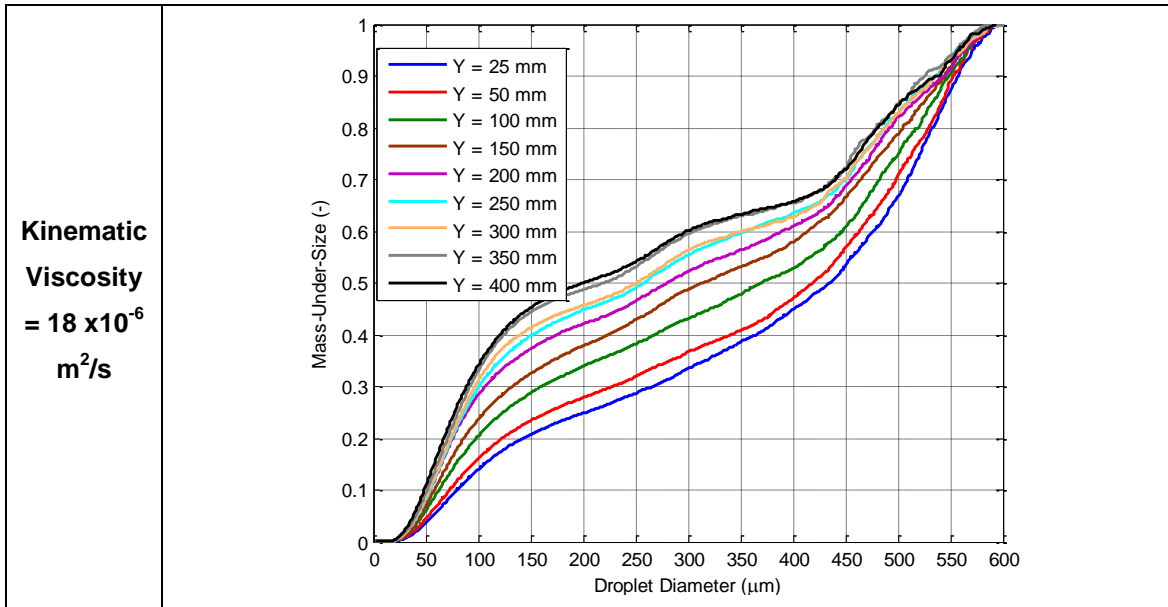


Table 7.1.3 clearly demonstrates a similar amount of liquid break-up from 25-400 mm downstream of the nozzle for all sprays investigated. For example, the difference between the mass-under-size plots at axial distances of 25 mm and 400 mm is similar for all four sprays. This shows that a comparable amount of break-up occurred over the axial ranges investigated at all fluid viscosities.

The fluid break-up which did occur (most likely the disintegration of small numbers of larger droplets) does not necessarily appear to have been completed by 400 mm downstream of the exit orifice. Liquid break-up after 350 mm downstream is visible (for instance the mass-under-size plots at the 350 mm and 400 mm axial locations of the  $5.1 \times 10^{-6} \text{ m}^2/\text{s}$  sprays are different) and it is possible that further break-up may have occurred even after 400 mm downstream. This indicates that equilibrium may not have been achieved even at 400 mm downstream of the nozzle. In turn this highlights the effects axial measurement location can have on spray quality. Therefore in order to compare results from different PDA tests it is clear that the measurement locations need to be comparable.

### 7.1.15 Droplet SMD Correlations from the Literature

Figure 7.1.12 shows the experimentally determined global spray SMD for all sprays analysed, and compares these to SMD predicted by correlations in the literature. It is clear that none of the correlations from the literature could accurately predict experimental SMD. This was expected since a range of sampling techniques, measurement locations and atomiser geometries were employed in deriving the

equations presented. Evidently, none of the effervescent atomiser equations from the literature are universal to all operating conditions and atomiser geometries.

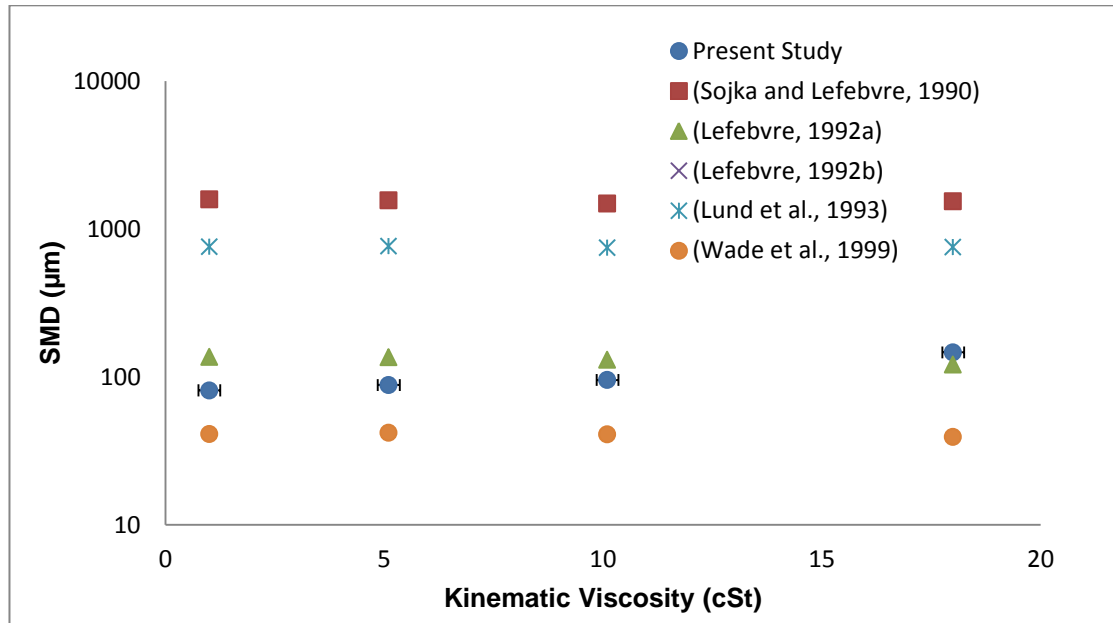


Figure 7.1.12 Comparison of global spray SMD from PDA experiments with that predicted by correlations in the literature.

### 7.1.16 Effect of Kinematic Viscosity on Global Spray Droplet SMD for Experimental Data

Figure 7.1.13 displays the experimentally determined global spray droplet SMD plotted against kinematic viscosity.

It can be shown that Equation 7.1.1 represents the relationship between kinematic viscosity and droplet SMD for the range  $1 \times 10^{-6} \text{ m}^2/\text{s} < \eta < 10.1 \times 10^{-6} \text{ m}^2/\text{s}$  (a power law provided the best fit to the experimental data).

$$\text{SMD} \propto 80.61\eta^{0.0666} \quad \text{Equation 7.1.1}$$

It is clear that above  $10.1 \times 10^{-6} \text{ m}^2/\text{s}$ , viscosity starts to influence global spray droplet SMD much more strongly. For example calculations reveal that for the  $10.1\text{-}18 \times 10^{-6} \text{ m}^2/\text{s}$  range (assuming linearity) the relationship between kinematic viscosity and droplet SMD could take the form  $\text{SMD} \propto \eta^{0.7455}$ . This would indicate that viscosity has only a minor influence on spray quality at lower viscosities ( $1 \times 10^{-6} \text{ m}^2/\text{s} < \eta < 10.1 \times 10^{-6} \text{ m}^2/\text{s}$ ) but a strong influence on spray quality at larger viscosity ranges. This contrasts with a number of effervescent atomisation studies which found that spray droplet SMD is independent or nearly independent of fluid viscosity [19, 32, 35, 57, 77]. The present work is more in line with a study by Santangelo et al [76] which reported that increasing

fluid viscosity above 0.412 kg/ms at ALRs less than 10% resulted in increased droplet SMD, with little correlation between viscosity and droplet SMD at lower viscosities or higher ALRs. The dynamic viscosity at which Santangelo et al noticed the effects of viscosity increases on droplet SMD is much larger than the range of kinematic viscosities covered in the present study. However, the relationship between viscosity and global spray droplet SMD appears to follow a similar pattern.

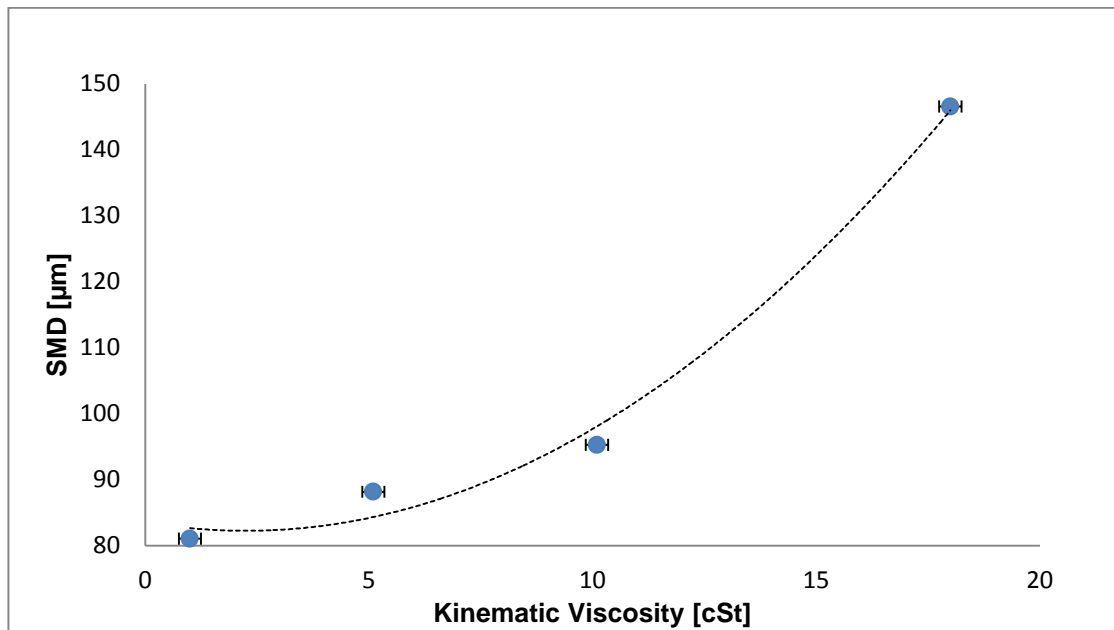


Figure 7.1.13 The relationship between kinematic viscosity and global spray SMD as calculated using PDA.

Despite discovering that viscosity has a relatively small influence on global spray SMD at kinematic viscosities of 1-10.1  $\times 10^{-6}$  m<sup>2</sup>/s, it is still the case that for all conditions investigated, superior atomisation was always achieved with the lower viscosity fluid. This matches the findings of a number of researchers who reported a reduction in spray quality as fluid viscosity was increased [56, 58].

It is clear from the tests performed so far (and the literature reviewed) that viscosity and spray quality display a complex, non-linear relationship which is affected by a number of operating and geometric parameters. It appears that SMD may be relatively insensitive to the effects of fluid viscosity, but only at certain viscosity ranges and at certain operating conditions and atomiser geometries. The conditions at which this might occur are not entirely clear. Further work is required to investigate kinematic viscosities in the range 10.1-18  $\times 10^{-6}$  m<sup>2</sup>/s.



### 7.1.17 Global Spray Droplet SMD Correlations

The present study investigated the effects a number of operating parameters (air-to-liquid by mass ratio, pressure differential), atomiser geometries (exit orifice diameter, mixing length, mixing chamber diameter, exit orifice length-to-diameter ratio, air injector geometry) and the fluid property kinematic viscosity had on effervescent atomiser spray quality. The above eight parameters were analysed using 2-D PDA data obtained on the same PDA system. One parameter was altered at any one time and it was assumed that each parameter could be investigated independently of all the others. As a result of the present study, five global spray SMD correlations were developed (for the parameters ALR,  $\Delta P$ ,  $D_o$ ,  $L_o/D_o$ ,  $\eta$ ). Meanwhile three of the parameters investigated could not be used to develop global spray correlations (mixing length,  $L_{MC}$ , was found to have no effect on spray quality; there were not enough test points to determine a clear relationship between mixing chamber diameter,  $D_{MC}$ , and global spray SMD; the aerator geometry tests could not be quantified and manipulated into equation form).

The five correlations obtained can now be combined to give a universal global spray SMD correlation (for the operating conditions and atomiser geometry investigated). For operation in the bubble-bursting mode ( $ALR < 5\%$ ,  $4.64 \text{ barG} < \Delta P < 7.05 \text{ barG}$ ,  $2 \text{ mm} < D_o < 2.5 \text{ mm}$ ,  $1 < \frac{L_o}{D_o} < 2$ ,  $1 \times 10^{-6} \text{ m}^2/\text{s} < \eta < 10.1 \times 10^{-6} \text{ m}^2/\text{s}$ ), it can be shown that a universal global droplet SMD correlation would take the form shown in Equation 7.1.2.

$$SMD = A \left( D_o^{1.3138} \Delta P^{-0.5677} ALR^{-0.5166} \left( \frac{L_o}{D_o} \right)^{0.4736} \eta^{0.0666} \right) \quad \text{Equation 7.1.2}$$

Where A is an appropriate constant.

In the region of “tree-like” atomisation mode ( $ALR > 5\%$ ,  $4.64 \text{ barG} < \Delta P < 7.05 \text{ barG}$ ,  $2 \text{ mm} < D_o < 2.5 \text{ mm}$ ,  $1 < \frac{L_o}{D_o} < 2$ ,  $1 \times 10^{-6} \text{ m}^2/\text{s} < \eta < 10.1 \times 10^{-6} \text{ m}^2/\text{s}$ ), it can be shown that a universal global droplet SMD correlation can take the form shown in Equation 7.1.3.

$$SMD = B \left( D_o^{1.3138} \Delta P^{-0.5677} \left( \frac{L_o}{D_o} \right)^{0.4736} ALR^{-0.2306} \eta^{0.0666} \right) \quad \text{Equation 7.1.3}$$

Where B is an appropriate constant.

Analysis of the data from the present investigation has shown that for the current atomiser design and for the operating conditions investigated,  $A = 13.24503$  and  $B =$

8.097166. These values were substituted into Equation 7.1.2 and Equation 7.1.3 and the predicted values of global spray SMD were compared to those calculated using PDA data. This comparison is presented in Figure 7.1.14 where the low ALR (ALR < 5%) and high ALR data (ALR > 5%) are plotted in red and blue, respectively (data at ALR's between 5-6% was included in both data sets since this is a transitional zone between low and high ALR operation). Both data sets seem to show good agreement between measured and predicted global spray SMD, with the greater disparity shown by the more poorly atomised, low ALR sprays (ALR < 5%).

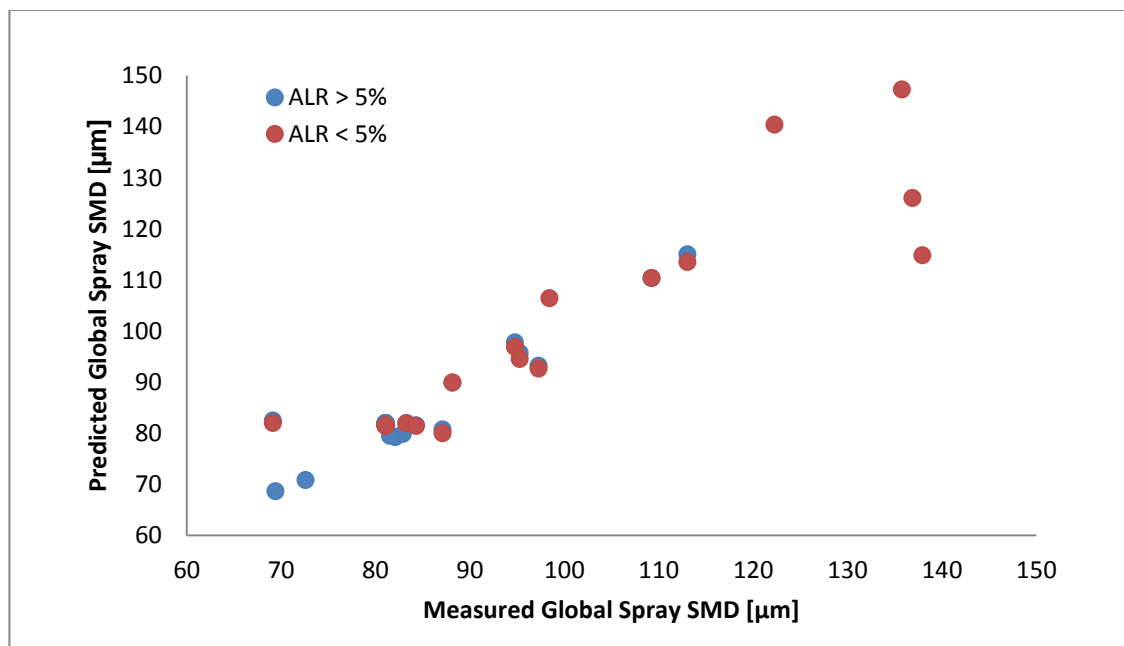


Figure 7.1.14 The relationship between measured and predicted global spray SMD for low and high ALR operation.

In order to evaluate the accuracy of prediction of Equation 7.1.2 and Equation 7.1.3, the two data sets were combined, and measured global spray SMD was plotted against predicted global spray SMD. This is shown in Figure 7.1.15.

Figure 7.1.15 shows good agreement between predicted and measured data. The largest disparity between predicted and measured global spray SMD is provided by the pressure differential tests ( $\Delta P$ , test phase 2) which are the three points on the top right corner of Figure 7.1.15.

To quantify the agreement between predicted and measured global spray SMD, two statistical parameters were employed: the mean relative error (MRE) and the standard deviation (SD). Mean relative error is defined in Equation 7.1.4, and standard deviation is defined in Equation 7.1.5. MRE and SD provide an indication of the agreement

between measured and predicted global spray SMD data; the better the agreement, the smaller the values of both MRE and SD will be.

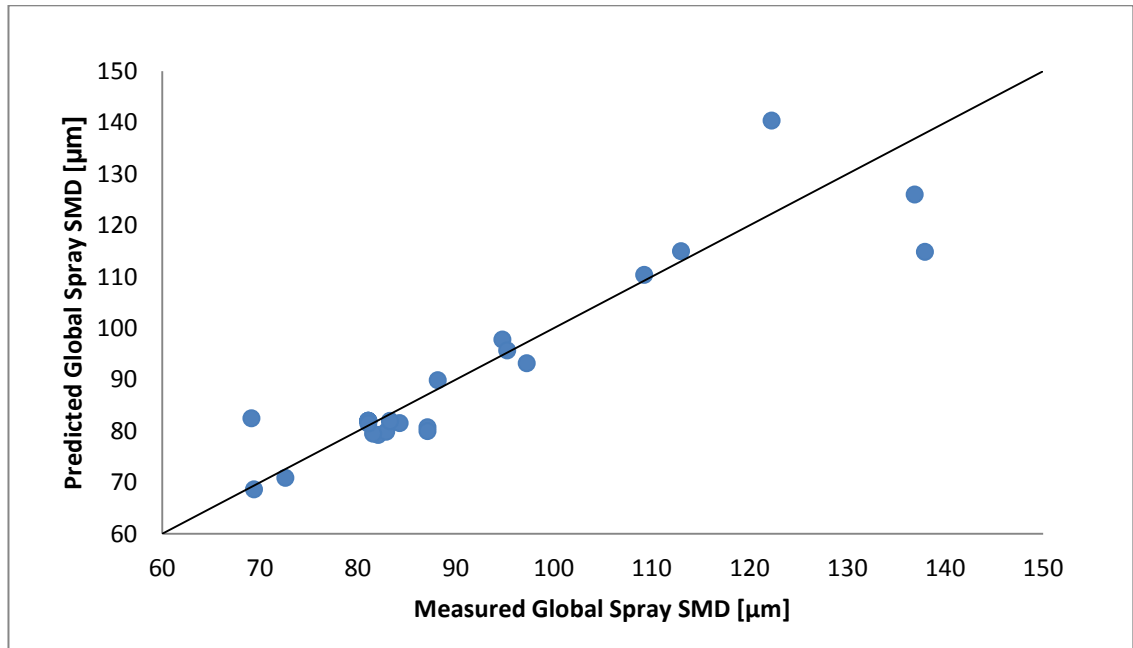


Figure 7.1.15 The relationship between measured and predicted global spray SMD.

$$MRE = \frac{1}{N} \sum_{i=1}^N \left| \frac{(SMD)_i^{measured} - (SMD)_i^{predicted}}{(SMD)_i^{predicted}} \right| \quad \text{Equation 7.1.4}$$

$$SD = \sqrt{\frac{1}{N} \sum_{i=1}^N (x_i - \bar{x})^2} \quad \text{Equation 7.1.5}$$

Where  $x_i = \left| \frac{(SMD)_i^{measured}}{(SMD)_i^{predicted}} \right|$  and  $\bar{x} = \frac{1}{N} \sum_{i=1}^N x_i$

MRE and SD were calculated for the data set containing all test points. The results are shown in Table 7.1.4 to 3 d.p.

Table 7.1.4 Error between measured and predicted global spray SMD data.

Statistical Parameter	Mean Relative Error (MRE)	Standard Deviation (SD)
Numerical Value	0.042	0.065

The MRE value is close to zero indicating very good agreement between predicted and measured values (exact agreement would give an MRE value of zero). Meanwhile SD

is also very small indicating minimal deviation between the mean values of the measured and predicted data sets.

Therefore Equation 7.1.2 and Equation 7.1.3 can be rewritten taking into account the calculated calibration constants. It can be shown that for the current atomiser geometry and for the operating conditions investigated, effervescent atomiser global spray SMD can be predicted to a high degree of accuracy using Equation 7.1.6 when operating at  $ALR < 5\%$ , and using Equation 7.1.7 when operating at  $ALR > 5\%$ .

$$SMD = 13.24503 \left( D_o^{1.3138} \Delta P^{-0.5677} ALR^{-0.5166} \left( \frac{L_o}{D_o} \right)^{0.4736} \eta^{0.0666} \right) \quad \text{Equation 7.1.6}$$

$$SMD = 8.097166 \left( D_o^{1.3138} \Delta P^{-0.5677} \left( \frac{L_o}{D_o} \right)^{0.4736} ALR^{-0.2306} \eta^{0.0666} \right) \quad \text{Equation 7.1.7}$$

## Chapter 8 : Conclusions

---

In this chapter the work performed and main findings of the present study will be summarised and important correlations derived from the experimental data will be listed.

A wide range of atomiser types have been developed for industrial applications – such as rotary, pressure, air-assist and air-blast. Each type works on the principle of applying mechanical or kinetic energy to disintegrate a jet or sheet of liquid fuel in preparation for combustion. The aim is to sufficiently increase the surface area to volume ratio of the fuel and present it in a form suitable for a consistent combustion process. Traditional liquid fuels such as fossil fuels, have been employed for some decades and combustion systems (and atomisers) have been optimised for their use. However combustion engineers are being increasingly forced to consider the use of alternative, biologically-derived hydrocarbon fuels. Such fuels often have very different or non-linear properties when compared to conventional fuels. This can make Bio-Fuels difficult to use on traditional liquid fuel atomisation systems.

Effervescent atomisation is a promising two-phase atomisation technique offering potential improvements in fluid atomisation quality and reductions in fluid operating pressures. It appears particularly well suited to the atomisation of viscous fuels such as Bio-Fuels; for example it seems to be relatively insensitive to large orifice diameters which can relieve the problem of component clogging and wear, a common occurrence when running Bio-Fuels through conventional liquid atomisers. This applicability to alternative fuels has led to a renewed interest in the method, particularly with a view to designing efficient, practical atomisers.

An extensive literature review of the current state of this technology was performed and the important parameters controlling effervescent atomisation were investigated. As a result of the literature review an adjustable geometry, “inside-out” type effervescent atomiser rated at 2MW effective power was designed, built and studied at the Cardiff School of Engineering. Both water and water-glycerol mixtures were used as the operating fluids; air was used as the assist medium.

Comparisons between the baseline (unoptimised) effervescent atomiser and an industrial-type Y-Jet atomiser were performed at equivalent operating conditions, using air and water as the operating fluids. Identical PDA settings and sampling locations were used. The results indicated that the spray produced by the Y-Jet atomiser was

narrower and more finely atomised than that of the effervescent atomiser. One important difference was that the Y-Jet atomiser displayed greater droplet consistency at the spray periphery. An optimised geometry needed to be developed to improve effervescent atomiser performance. This was performed and was reported in subsequent chapters.

The atomiser designed was then tested at a range of operating conditions to investigate its operating boundaries. A test plan, which allowed for a detailed analysis of multiple control parameters over a wide range of values, was designed. The operating parameters investigated in this manner included operating conditions (air-to-liquid by mass ratio – ALR, and pressure drop across the exit orifice –  $\Delta P$ ), geometric parameters (exit orifice diameter, effective mixing length, mixing chamber diameter, exit orifice length-to-diameter ratio and air injector geometry) and fluid properties (kinematic viscosity).

The parameter ranges investigated included 1.83-11.11% ALR, 4.64-7.05 barG  $\Delta P$ , 2-2.8mm  $D_O$ , 60-136 mm  $L_{MC}$ , 20-30 mm  $D_{MC}$ , 0.5-2  $L_O/D_O$  and  $1-18 \times 10^{-6}$  m/s<sup>2</sup> kinematic viscosity. In addition 3 different air injector geometries were studied which investigated the influence of air injector hole radial symmetry and aerating hole diameter.

In each of the cases, the sprays produced by the atomiser were characterised using a Phase Doppler Anemometry (PDA) system which allowed for simultaneous real-time droplet size and velocity measurements to be obtained. High quality data was achieved with data rates up to 10 kHz and validation rates over 90 % for measurements in the 2-D PDA coincident mode of operation. A PDA probe designed for dense spray applications was utilised. A suitable sampling grid comprising between 220-270 data points at 9 different axial locations was designed to ensure representative data was obtained for each spray investigated.

The important operating parameters identified during the literature review phase were altered by performing adjustments to the operating conditions or atomiser geometry and their effects on fuel spray quality were investigated by performing PDA tests on the stable, steady-state liquid sprays produced by the atomiser.

The operating parameters for each test (fluid pressures, temperatures and mass flow rates) were measured using calibrated pressure transducers, type K thermocouples and coriolis meters, respectively. The use of a Delta-T datalogger recording at a frequency of 1 Hz allowed average operating conditions to be measured. A calibrated Cannon-Fenske Routine Viscometer was used to measure fluid kinematic viscosity for each water-glycerol mixture investigated.

The droplet data obtained from the 2-D PDA tests for each spray investigated were post-processed and imported into a MathWorks MATLAB environment; a software program was written to facilitate the calculation of a range of local and global parameters which could be used to determine spray quality.

Most PDA tests were performed only once but some were repeated. This was usually done when the results seemed unexpected. The repeatability of the results (as well as the high validation rates achieved) gave good confidence in the PDA set-up, the testing procedures and the results.

Spray quality (or atomisation quality, the amount by which the surface area of a given volume of fluid was increased as it passed through the exit orifice) was most frequently determined by reference to the global spray SMD – Sauter Mean Diameter ( $D_{32}$ ) calculated for all droplet data obtained from a given spray. Other parameters used to evaluate spray quality included arithmetic mean diameter (AMD), SMD/AMD ratio, mass-under-size plots, a number of droplet frequency distribution plots, droplet velocity vector plots, inferred gas velocity vector and, relative velocity vector plots and local average Weber number.

Findings relevant to atomiser operation and to spray characteristics included the following:

- Stable, well-atomised sprays could not be achieved at ALRs below 2% for all operating conditions investigated.
- It was found that effervescent atomisation at ALRs below 5% are characterised by operation in the bubble-bursting mode, featuring a prominent unatomised liquid core and somewhat poorer liquid atomisation.
- ALRs greater than 5% resulted in the tree-like atomisation mode of operation, featuring no detectable solid liquid core, and comparatively better liquid atomisation throughout the spray.
- By number, the vast majority of most sprays investigated were comprised of droplets smaller than 100  $\mu\text{m}$ ; only a small fraction of the droplets fell in the larger diameter ranges.
- By mass all sprays investigated had significant proportions of their total mass contained in droplets in the diameter ranges up to the PDA measurement limits.
- Even the best performing sprays contained very large droplets; most sprays seemed to possess similar absolute spray masses in droplet diameter ranges of 350-600  $\mu\text{m}$ ; this supports the view that effervescent atomisation is a process

which produces a wide range of droplet sizes, even at optimal operating conditions. However this is not surprising as it is known that conventional atomiser types consistently produce sprays characterised by droplet diameter ratios of at least 100:1 [46].

- The spray near the nozzle, along the central spray axis (axial distances of 25-50 mm) was too dense for high-quality data to be obtained; data here was lost due to attenuation and multiple light scattering effects.
- Sprays possessed two regions where larger droplets were typically found: the central, near-nozzle region (unatomised ligaments and larger droplets) and further downstream along the spray radial edges (larger droplets further downstream would be carried radially outwards due to their relatively larger momentum).
- Poorly atomised sprays typically possessed larger regions containing bigger droplets – both near the nozzle and further downstream at the spray periphery; well-atomised sprays possessed only a small number of larger droplets and unatomised ligaments near the nozzle, which rapidly disintegrated in the downstream direction and gave way to small, homogenous and uniform droplets.
- The most significant feature of downstream spray development for all investigated sprays was the disintegration of the relatively small number of larger droplets and ligaments seen nearer the nozzle, with little further changes to the droplets.
- Plots of average local Weber number revealed that secondary break-up did not play an active role in liquid disintegration at any of the sampling locations of any spray; only a very small number of very large droplets could have disintegrated via secondary break-up mechanisms.
- Continuous downstream droplet break-up is evidenced by the axial mass-under-size plots which show that even at 400 mm downstream of the exit orifice, a state of equilibrium (i.e. stable droplets with no further break-up) may not yet have been achieved.
- Inferred gas velocity matched droplet velocity very well for all sprays and at all sampling locations.
- Inferred relative velocities near the nozzle were small indicating that gas and liquid phase velocity equalisation was complete by 25 mm downstream of the nozzle for all sprays investigated.



- The mode of liquid break-up at the nozzle analysis offered helpful insights when investigating operating conditions (ALR,  $\Delta P$ ) but not when considering atomiser geometry or fluid viscosity.

The effects of the control parameters upon the global spray droplet SMD were approximated by the following terms:

- For ALRs less than 5%,  $SMD \propto ALR^{-0.5166}$  down to the minimum ALR.
- For ALRs greater than 5%,  $SMD \propto ALR^{-0.2306}$  up to the maximum ALR.
- $SMD \propto \Delta P^{-0.5677}$  (for 4.64 barG < pressure differential,  $\Delta P < 7.05$  barG).
- For 2 mm < exit orifice diameter,  $D_o < 2.5$  mm,  $SMD \propto D_o^{1.3138}$
- Mixing length,  $L_{MC}$  had no impact on global spray droplet SMD over the ranges investigated.
- Global spray droplet SMD and mixing chamber diameter,  $D_{MC}$  exhibit a non-linear relationship, and the 25.4 mm diameter mixing chamber provided the best atomisation over the diameter ranges investigated.
- For 1 < length-to-diameter ratio,  $L_o/D_o < 2$ ,  $SMD \propto \left(\frac{L_o}{D_o}\right)^{0.4736}$
- An asymmetric arrangement of air injector holes (such as was used in the A2 aerator geometry) was found to provide considerable improvements in spray quality.
- Air injector hole diameter was seen to have a minor influence on spray quality over the diameter ranges investigated (2-2.6 mm diameter air injector holes), with the larger air injector diameter holes providing better atomisation.
- For  $1 \times 10^{-6} \text{ m}^2/\text{s} < \text{kinematic viscosity}, \eta < 10.1 \times 10^{-6} \text{ m}^2/\text{s}$ ,  $SMD \propto \eta^{0.0666}$

Therefore it can be shown that based on the present study and for the operating parameters and ranges investigated, for operation in the bubble-bursting mode (ALR < 5%, 4.64 barG <  $\Delta P < 7.05$  barG, 2 mm <  $D_o < 2.5$  mm,  $1 < \frac{L_o}{D_o} < 2$ ,  $1 \times 10^{-6} \text{ m}^2/\text{s} < \eta < 10.1 \times 10^{-6} \text{ m}^2/\text{s}$ ), a universal global droplet SMD correlation would take the form presented at the end of Chapter 7 (Equation 7.1.6) and shown below.

$$SMD = 13.24503 \left( D_o^{1.3138} \Delta P^{-0.5677} ALR^{-0.5166} \left( \frac{L_o}{D_o} \right)^{0.4736} \eta^{0.0666} \right)$$

In the region of “tree-like” atomisation (ALR > 5%, 4.64 barG <  $\Delta P < 7.05$  barG, 2 mm <  $D_o < 2.5$  mm,  $1 < \frac{L_o}{D_o} < 2$ ,  $1 \times 10^{-6} \text{ m}^2/\text{s} < \eta < 10.1 \times 10^{-6} \text{ m}^2/\text{s}$ ), a universal global

droplet SMD correlation would take the form presented at the end of Chapter 7 (Equation 7.1.7) and shown below .

$$\text{SMD} = 8.097166 \left( D_o^{1.3138} \Delta P^{-0.5677} \left( \frac{L_o}{D_o} \right)^{0.4736} ALR^{-0.2306} \eta^{0.0666} \right)$$

It should be noted that the calibration constants in Equation 7.1.2 and Equation 7.1.3 (constants A and B in, respectively), will be influenced by factors such as mixing chamber diameter, air injector hole arrangement and air injector hole diameter. These need to be determined for the effervescent atomiser being investigated. For the present study A = 13.24503 and B = 8.097166.

Relevant correlations in the literature were compared to the experimental data from the present study. The results showed that:

- Of the discharge coefficient equations found in the literature, the one most closely matching the experimental data for all conditions investigated was the one provided by Chen et al [55].
- Spray half-angle could not be accurately predicted by the correlation of Sovani et al [80] for all conditions investigated. This was due to differences in measurement techniques and sampling locations.
- No droplet SMD correlation from the literature could accurately match the experimentally determined values of global spray SMD; this was due to a range of factors such as different spray measurement techniques, atomiser geometries, parameter ranges and sampling locations used by various researchers.

## Chapter 9 : Further Work

---

Recommendations for further work include:

- Extend the investigation of ALR further – perform ALR tests both at constant pressures and constant mass flow rates and compare results; this will enable the influence of ALR on spray droplet SMD to be calculated while discounting dilution effects.
- Investigate the performance of exit orifice diameters greater than 2.8 mm.
- Perform a more thorough investigation into the influence of mixing chamber diameter on spray quality involving a greater number of mixing chamber diameters.
- Investigate the influence of  $L_0/D_0$  ratios in the critical 0.5-1 range.
- Extend the range of air hole injector diameters investigated beyond 2-2.6 mm, investigating both smaller and larger diameters.
- Further investigate the effects of fluid viscosity, particularly the range  $10.1-18 \times 10^{-6} \text{ m}^2/\text{s}$ , but also larger kinematic viscosity ranges.
- Compare the performance of a fully optimised geometry effervescent atomiser to the Y-Jet atomiser at equivalent conditions using both water and higher viscosity liquids as the operating fluid.
- Perform an investigation into exit orifice design, for example comparing the performance of plain orifice and convergent-divergent (de Laval) nozzles.
- Investigate gas motion in the spray by using seeding particles.
- Perform CFD investigations of effervescent atomisation.
- Investigate the performance of an effervescent atomiser using Bio-Fuel as the operating fluid.
- Perform combustion tests using effervescent fuel injectors.
- Investigate spray quality using a greater range of representative droplet diameters, such as  $D_{20}$ ,  $D_{30}$ ,  $D_{50\%}$  etc.
- Perform a detailed Weber number analysis to help clarify the influence of secondary atomisation upon effervescent atomisation.
- Investigate effervescent atomisation with cross-flow injection.

## References

---

1. Barca, S., *Energy, property, and the industrial revolution narrative*. Ecological Economics, 2011. 70(7): p. 1309-1315.
2. Administration, U.S.E.I., *International Energy Outlook 2011*, 2011.
3. Abu-Khader, M. M., *Recent advances in nuclear power: A review*. Progress in Nuclear Energy, 2009. 51(2): p. 225-235.
4. Adamantiades, A. and I. Kessides, *Nuclear power for sustainable development: Current status and future prospects*. Energy Policy, 2009. 37(12): p. 5149-5166.
5. Sovacool, B.K., *The intermittency of wind, solar, and renewable electricity generators: Technical barrier or rhetorical excuse?* Utilities Policy, 2009. 17(3-4): p. 288-296.
6. Moriarty, P. and D. Honnery, *Intermittent renewable energy: The only future source of hydrogen?* International Journal of Hydrogen Energy, 2007. 32(12): p. 1616-1624.
7. Kumar, J.V. and B.C. Pratt, *Determination of calorific values of some renewable biofuels*. Thermochemica Acta, 1996. 279(0): p. 111-120.
8. Lopes, H., Gulyurtlu, I., Abelha, P., Crujeira, T., Salema, D., Freire, M., Pereira, R., Cabrita, I., *Particulate and PCDD/F emissions from coal co-firing with solid biofuels in a bubbling fluidised bed reactor*. Fuel, 2009. 88(12): p. 2373-2384.
9. Akorede, M.F., Hizam, H., Ab Kadir, M. Z. A., Aris, I., Buba, S. D., *Mitigating the anthropogenic global warming in the electric power industry*. Renewable and Sustainable Energy Reviews, 2012. 16(5): p. 2747-2761.
10. Zecca, A. and L. Chiari, *Fossil-fuel constraints on global warming*. Energy Policy, 2010. 38(1): p. 1-3.
11. Chiari, L. and A. Zecca, *Constraints of fossil fuels depletion on global warming projections*. Energy Policy, 2011. 39(9): p. 5026-5034.
12. Nel, W.P. and C.J. Cooper, *Implications of fossil fuel constraints on economic growth and global warming*. Energy Policy, 2009. 37(1): p. 166-180.
13. Abbasi, T. and S.A. Abbasi, *Decarbonization of fossil fuels as a strategy to control global warming*. Renewable and Sustainable Energy Reviews, 2011. 15(4): p. 1828-1834.
14. Dagoumas, A.S., G.K. Papagiannis, and P.S. Dokopoulos, *An economic assessment of the Kyoto Protocol application*. Energy Policy, 2006. 34(1): p. 26-39.

15. Quirion, P., *Complying with the Kyoto Protocol under uncertainty: Taxes or tradable permits?* Energy Policy, 2010. 38(9): p. 5166-5173.
16. Shafiee, S. and E. Topal, *When will fossil fuel reserves be diminished?* Energy Policy, 2009. 37(1): p. 181-189.
17. Greene, D.L., D.W. Jones, and P.N. Leiby, *The outlook for US oil dependence.* Energy Policy, 1998. 26(1): p. 55-69.
18. Sojka, P.E. and A.H. Lefebvre, *A novel method of atomizing coal-water slurry fuels*, 1990. p. Size: Pages: (116 p).
19. Sovani, S.D., P.E. Sojka, and A.H. Lefebvre, *Effervescent atomization.* Progress in Energy and Combustion Science, 2001. 27(4): p. 483-521.
20. Lefebvre, A.H., X.F. Wang, and C.A. Martin, *Spray Characteristics of Aerated-Liquid Pressure Atomizers.* Journal of Propulsion Power, 1988. 4(4): p. 293-298.
21. Konstantinov, D.D., Marsh, R., Bowen, P.J., Crayford, A., *Effervescent atomization for industrial energy - technology review.* 2010. 20(6): p. 525-552.
22. Chawla, J.B. *Atomisation of Liquids Employing the Low Sonic Velocity of Liquid/Gas Mixtures.* in *ICLASS 1985: 3rd International Conference of Liquid Atomization and Spray Systems.* 1985. London, UK.
23. Zeng, Y. and C.-F.F. Lee, *An atomization model for flash boiling sprays.* Combustion Science and Technology, 2001. 169(1): p. 45-67.
24. Bar-Kohany, T. and E. Sher. *Spray formation by bi-component liquid flashing: a theoretical approach.* in *The 18th ILASS Conference.* 2002. Zaragoza, Spain.
25. Bar-Kohany, T. and E. Sher, *Subsonic Effervescent Atomization: A Theoretical Approach.* Atomization and Sprays, 2004. 14: p. 495-509.
26. Rashkovan, A., V. Kholmer, and E. Sher, *Effervescent Atomization of Gasoline Containing Dissolved CO<sub>2</sub>.* Atomization and Sprays, 2004. 14: p. 341-354.
27. Bar-Kohany, T. and E. Sher, *Effervescent atomization under sub-sonic and choked conditions--a theoretical approach.* Chemical Engineering Science, 2004. 59(24): p. 5987-5995.
28. Sher, E., T. Bar-Kohany, and A. Rashkovan, *Flash-boiling atomization.* Progress in Energy and Combustion Science, 2008. 34(4): p. 417-439.
29. Qian, L. and J. Lin, *Modeling on effervescent atomization: A review.* Science China: Physics, Mechanics and Astronomy, 2011. 54(12): p. 2109-2129.
30. Lin, K.C., Carter, C., Fezzaa, K., Wang, J., Liu, Z., *X-Ray Study of Pure- and Aerated-Liquid Jets in a Quiescent Environment.* American Institute of Aeronautics and Astronautics, 2009. 2009-0994.

31. Wang, X., J.S. Chin, and A.H. Lefebvre, *Influence of Gas Injector Geometry on Atomization Performance of Aerated Liquid Nozzles*. International Journal of Turbo and Jet Engines, 1989. 6: p. 271-279.
32. Buckner, H.N. and P.E. Sojka, *Effervescent atomization of high-viscosity fluids: part I. Newtonian liquids*. Atomization and Sprays, 1991. 1(3): p. 239-252.
33. Lefebvre, A.H., *Twin-fluid atomization: factors influencing mean drop size*. Atomization and Sprays, 1992. 2(2): p. 101-119.
34. Jardine, K.J., *Effervescent Atomization of Non-Newtonian Fluids at High Flow Rates*, 1991, Purdue University: Purdue. p. 97.
35. Lund, M.T., Sojka, P.E., Lefebvre, A.H., Gosselin, P.G., *Effervescent Atomization at Low Mass Flow rates. Part I: the Influence of Surface Tension*. Atomization and Sprays, 1993. 3: p. pp. 77-89.
36. Eggers, J., *A brief history of drop formation*, in Nonsmooth Mechanics and Analysis, Springer, 2006.
37. Lin, S.P. and R.D. Reitz, *Drop and spray formation from a liquid jet*. Annual Review of Fluid Mechanics, 1998. 30(1): p. 85.
38. Pimbley, W.T., *Drop Formation from a Liquid Jet: A Linear One-Dimensional Analysis Considered as a Boundary Value Problem*. IBM J. Res. Dev., 1976: p. 148-156.
39. Li, X., *Mechanism of Atomization of a Liquid Jet*. Atomization and Sprays, 1995. 5(1): p. pp. 89-105.
40. Song, S.H. and S.Y. Lee, *Study of Atomization Mechanism of Gas/Liquid Mixtures flowing through Y-jet Atomizers*. Atomization and Sprays, 1996. 6(2): p. pp. 193-209.
41. Hiroyasu, H., *Spray Breakup Mechanism from the Hole-Type Nozzle*. Atomization and Sprays, 2000. 10(3): p. 511-527.
42. Xu, Z., Samulyak, R., Li, X., Tzanos, C., *Atomization of a High Speed Jet*. American Physical Society, 2005.
43. Lefebvre, A.H., *Atomization and Sprays*. Combustion: An International Series, ed. N. Chigier 1989: Hemisphere Publishing Corporation. 421.
44. Schweitzer, P.H., *Mechanism of Disintegration of Liquid Jets*. Journal of Applied Physics, 1937. 8(8): p. 513-521.
45. Shinjo, J. and A. Umemura, *Surface instability and primary atomization characteristics of straight liquid jet sprays*. International Journal of Multiphase Flow, 2011. 37(10): p. 1294-1304.
46. Nasr, G.G., A.J. Yule, and L. Bendig, *Industrial Sprays and Atomization* 2002.

47. Gueldenbecher, D., C. López-Rivera, and P. Sojka, *Secondary atomization*. *Experiments in Fluids*, 2009. 46(3): p. 371-402.
48. Kay, P.J., *Characterising Thermofluid Spray Dynamics For Energy-Efficient Automotive Engines*, 2006, Cardiff University.
49. Zhao, H., Liu, H.F., Xu, J.F., Li, W.F., *Experimental Study of Drop Size Distribution in the Bag Breakup Regime*. *Industrial & Engineering Chemistry Research*, 2011. 50(16): p. 9767-9773.
50. Zhao, H., Liu, H.F., Xu, J.F., Li, W.F., Cao, X.K., *Breakup characteristics of liquid drops in bag regime by a continuous and uniform air jet flow*. *International Journal of Multiphase Flow*, 2011. 37(5): p. 530-534.
51. Lin, K.C., P.J. Kennedy, and T.A. Jackson, *Structures of Internal Flow and the Corresponding Spray for Aerated-Liquid Injectors*. *American Institute of Aeronautics and Astronautics*, 2001. AIAA 2001-3569.
52. Gaddis, E.S. and A. Vogelpohl, *Bubble formation in quiescent liquids under constant flow conditions*. *Chemical Engineering Science*, 1986. 41(1): p. 97-105.
53. Kulkarni, A.A. and J.B. Joshi, *Bubble Formation and Bubble Rise Velocity in Gas-Liquid Systems: A Review*. *Industrial & Engineering Chemistry Research*, 2005. 44(16): p. 5873-5931.
54. Lefebvre, A.H., *Some Recent Developments in Twin-Fluid Atomization*. *Particle and Particle Systems Characterization*, 1996. 13(3): p. 205-216.
55. Chen, S.K. and A.H. Lefebvre, *Discharge Coefficients for Plain-Orifice Effervescent Atomizers*. *Atomization and Sprays*, 1994. 4: p. 275-290.
56. Ferreira, M.E., Texeira, J.C.F., Bates, C.J., Bowen, P.J., *Detailed Investigation of the Influence of Fluid Viscosity on the Performance Characteristics of Plain-Orifice Effervescent Atomizers*. *Atomization and Sprays*, 2001. 11: p. pp. 107-124.
57. Lörcher, M. and D. Mewes, *Atomization of Liquids by Two-phase Gas-liquid Flow through a Plain-orifice Nozzle: Flow Regimes inside the Nozzle*. *Chemical Engineering & Technology*, 2001. 24(2): p. 167-172.
58. Petersen, F.J., Worts, O., Schaeffer, T., Sojka, P.E., *Effervescent atomization of aqueous polymer solutions and dispersions*. *Pharmaceutical Development and Technology*, 2001. 6(2): p. 201-210.
59. Kim, J.Y. and S.Y. Lee, *Dependence of Spraying Performance on the Internal Flow Pattern in Effervescent Atomizers*. *Atomization and Sprays*, 2001. 11: p. 735-756.
60. Huang, X., X. Wang, and G. Liao, *Visualization of Two Phase Flow inside an Effervescent Atomizer*. *Journal of Visualization*, 2008. 11(4): p. 299-308.

61. Catlin, C.A. and J. Swithenbank, *Physical Processes Influencing Effervescent Atomizer Performance in the Slug and Annular Flow Regimes*. *Atomization and Sprays*, 2001. 11: p. 575-595.
62. Lefebvre, A.H., *A novel method of atomization with potential gas turbine applications*. *Defence Science Journal*, 1988. 38(4): p. 353-362.
63. Petersen, F.J., Worts, O., Schaeffer, T., Sojka, P.E., *Design and Atomization Properties for an Inside-Out Type Effervescent Atomizer*. *Drug Development and Industrial Pharmacy*, 2004. 30(3): p. 319-326.
64. Sojka, P.E., to D.D. Konstantinov, Personal Communication, 2009: Cardiff.
65. Chin, J.S. and A.H. Lefebvre, *A Design Procedure for Effervescent Atomizers*. *Journal of Engineering for Gas Turbines and Power*, 1995. 117(2): p. 266-271.
66. Bates, C.J., P.J. Bowen, and J.C.F. Teixeira. *Influence of Exit Orifice Characteristics on Transition between Effervescent Atomization Flow Regimes*. in *Proceedings of the Eighth International Conference on Liquid Atomization and Spray Systems (ICLASS-2000)*. 2000. Pasadena, California.
67. Tian, M., *Numerical Simulation of the Internal Two-Phase Flow within an Aerated-Liquid Injector and its Injection into the Corresponding High-speed Crossflows*, 2005, NCSU.
68. Flachs Nielsen, A., Bertelsen, P., Gjelstrup Kristensen, H., Kristensen, J., Hovgaard, L., *Investigation and Comparison of Performance of Effervescent and Standard Pneumatic Atomizer Intended for Soluble Aqueous Coating*. *Pharmaceutical Development and Technology*, 2006. 11: p. 243-253.
69. Butterworth, D. and G.F. Hewitt, *Two-phase flow and heat transfer* 1977: Oxford University Press.
70. Wade, R.A., Weerts, J.M., Sojka, P.E., Gore, J.P., *Effervescent atomization at injection pressures in the MPa range*. *Atomization and Sprays*, 1999. 9(6): p. 651-667.
71. Jedelsky, J., M. Jicha, and J. Slama, *Discharge coefficient and operational flow characteristics of multihole effervescent atomizer*, in *ICLASS 20032003*: Sorrento, Italy.
72. Jedelsky, J., M. Jicha, and J. Slama, *Characterization of spray generated by multihole efferevescent atomizer and comparison with standard y-jet atomizer*, in *ICLASS 20032003*: Sorrento, Italy.
73. Lörcher, M., F. Schmidt, and D. Mewes, *Effervescent Atomization of Liquids*. *Atomization and Sprays*, 2005. 15: p. 145-168.
74. Buckner, H.N., P.E. Sojka, and A.H. Lefebvre, *Effervescent atomization of coal-water slurries*. *ASME, Petroleum Division*, 1990. 30: p. 105-108.



75. Sojka, P.E. and H.N. Buckner, *Effervescent atomization of high-viscosity fluids: part II. Non-newtonian liquids*. *Atomization and Sprays*, 1993. 3(2): p. 157-170.
76. Santangelo, P.J. and P.E. Sojka, *A Holographic Investigation of the Near-Nozzle Structure of an Effervescent Atomizer-Produced Spray*. *Atomization and Sprays*, 1995. 5: p. 137-155.
77. Sutherland, J.J., P.E. Sojka, and M.W. Plesniak, *Ligament-controlled effervescent atomization*. *Atomization and Sprays*, 1997. 7: p. 383-406.
78. Lund, M.T., Jian, C.Q., Sojka, P.E., Gore, J.P., Panchagnula, M.V., *The Influence of Atomizing Gas Molecular Weight on Low Mass Flowrate Effervescent Atomizer Performance*. *Journal of Fluids Engineering*, 1998. 120(4): p. 750-754.
79. Morelli, F., S. Ligasacchi, and M. Bizzarri, *Development of Effervescent Atomisers for Oil-Fired Power Stations*, in *ICLASS 2003*: Sorrento, Italy.
80. Sovani, S.D., Chou, E., Sojka, P.E., Gore, J.P., Eckerle, W.A., Crofts, J.D., *High pressure effervescent atomization: effect of ambient pressure on spray cone angle*. *Fuel*, 2001. 80(3): p. 427-435.
81. Dorfner, V., Domnick, J., Durst, F., Kohler, R., *Viscosity and Surface Tension Effects in Pressure Swirl Atomization*. *Atomization and Sprays*, 1995. 5: p. 261-285.
82. Gosselin, P.G., Lund, M.T., Sojka, P.E., Lefebvre, A.H., *Consumer Product package incorporating a spray device utilizing large diameter bubbles*, U.S.P. Office, Editor 1994, The Procter & Gamble Company: U.S.A.
83. Geckler, S.C. and P.E. Sojka, *Effervescent Atomization of Viscoelastic Liquids: Experiment and Modeling*. *Journal of Fluids Engineering*, 2008. 130(6): p. 061303-11.
84. Lefebvre, A.H., *Energy Considerations in Twin-Fluid Atomization*. *Journal of Engineering for Gas Turbines and Power*, 1992. 114(1): p. 89-96.
85. Panchagnula, M.V. and P.E. Sojka, *Spatial droplet velocity and size profiles in effervescent atomizer-produced sprays*. *Fuel*, 1999. 78(6): p. 729-741.
86. Chen, S.K. and A.H. Lefebvre, *Spray Cone Angles of Effervescent Atomizers*. *Atomization and Sprays*, 1994. 4: p. 291-301.
87. Sutherland, J.J., P.E. Sojka, and M.W. Plesniak, *Entrainment by ligament-controlled effervescent atomizer-produced sprays*. *International Journal of Multiphase Flow*, 1997. 23(5): p. 865-884.
88. Luong, J.T.K. and P.E. Sojka, *Unsteadiness in Effervescent Sprays*. *Atomization and Sprays*, 1999. 9: p. 87-109.

89. Edwards, C.F. and K.D. Marx, *Multipoint statistical structure of the ideal spray. Part I: Fundamental concepts and the realization density*. *Atomization and Sprays*, 1995. 5: p. 435-455.
90. Edwards, C.F. and K.D. Marx, *Multipoint statistical structure of the ideal spray. Part II: Evaluating steadiness using the interparticle time distribution*. *Atomization and Sprays*, 1995. 5: p. 457-505.
91. Jedelsky, J., Jicha, M., Slama, J., Otahal, J., *Development of an Effervescent Atomizer for Industrial Burners*. *Energy and Fuels*, 2009. 23: p. 6121-6130.
92. Derksen, M., to D.D. Konstantinov, Personal Communication, 2009: Cardiff.
93. Perry, R.H. and D.W. Green, *Perry's Chemical Engineers' Handbook*. 6th ed 1984: McGraw-Hill Co.
94. Soo, S.L., *Instrumentation for Fluid Particle Flow*, William Andrew Publishing/Noyes, 1999.
95. Xu, R., *Particle Characterization: Light Scattering Methods*, Kluwer Academic Publishers, 2002.
96. Zhang, Z., *LDA Application Methods*, 2010: Springer.
97. Aísa, L., Garcia, J.A., Cerecedo, L.M., Garcia Palacin, I., Calvo, E., *Particle concentration and local mass flux measurements in two-phase flows with PDA. Application to a study on the dispersion of spherical particles in a turbulent air jet*. *International Journal of Multiphase Flow*, 2002. 28(2): p. 301-324.
98. Dantec Dynamics A/S, BSA Flow Software, Version 4.10, Installation and User Guide, 2006.
99. Broukal, J. and J. Hájek, *Validation of an effervescent spray model with secondary atomization and its application to modeling of a large-scale furnace*, *Applied Thermal Engineering*, 2011.
100. Sovani, S.D., et al., *Structure and steady-state spray performance of an effervescent diesel injector*. *Fuel*, 2005. 84(12-13): p. 1503-1514.
101. Konstantinov, D.D., *Effervescent Atomisation for Industrial Energy*, in *ECM2011: Cardiff*.
102. Crayford, A.P., Bowen, P.J., Kay, P.J., Laget, H., *Comparison of Gas-Oil and Bio-Oil Spray Performance for Use in a Gas Turbine*. *ASME Conference Proceedings*, 2010. 2010(43963): p. 659-667.
103. Bowen, I.G., Davies, G.P., *Report ICT 28*, 1951, Shell Research Ltd.: London.
104. Ishii, M. and T. Hibiki, *Thermo-Fluid Dynamics of Two-Phase Flows* 2006.
105. Yeom, G.-S. and K.-S. Chang, *Dissipation of shock wave in a gas-droplet mixture by droplet fragmentation*. *International Journal of Heat and Mass Transfer*, (0).

106. Zaidi, S.H., A. Altunbas, and B.J. Azzopardi, *A comparative study of phase Doppler and laser diffraction techniques to investigate drop sizes in annular two-phase flow*. Chemical Engineering Journal, 1998. 71(2): p. 135-143.

## Appendix A: Pressure Differential Tests

Table A.1 Operating conditions and controlled parameters for pressure differential tests.

TEST No.	1	2	3	4	5	6	7	8
PARAMETER VARIED	ALR	$\Delta P$	$D_O$	$L_{MC}$	$D_{MC}$	$L_O/D_O$	A. GEOM.	$\eta$
TEST PHASE	A. Initial Operating Parameters		B. Atomiser Geometry					C. Fluid properties
ALR (%)	0.8-12.5	2		2				
$\Delta P$ (bar.g)	7	4-7		7				
$D_O$ (mm)	2	2	2-4	2	2	2	2	2
$L_{MC}$ (mm)	140	140	140	64-140	140	140	140	140
$D_{MC}$ (mm)	25.4	25.4	25.4	25.4	20-30	25.4	25.4	25.4
$L_O/D_O$ (-)	1	1	1	1	1	0.5-2	1	1
Aerator Geometry	A1	A1	A1	A1	A1	A1	A2, A3	A1
$\eta \times 10^{-6}$ (m <sup>2</sup> /s)	1	1	1	1	1	1	1	2-10

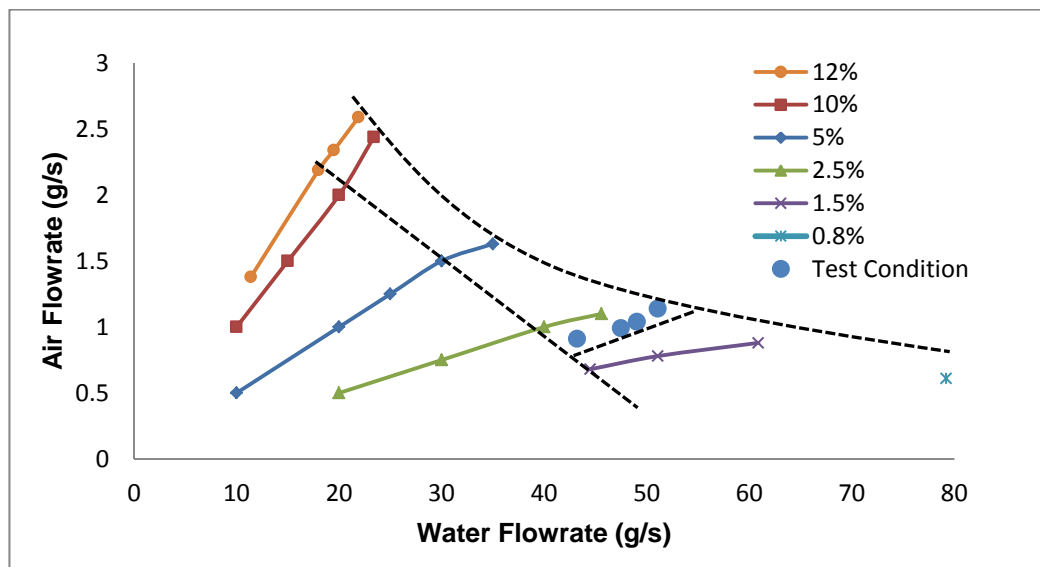


Figure A.1 Graph of spray quality showing liquid flow rates at which optimal effervescent atomisation can be achieved.

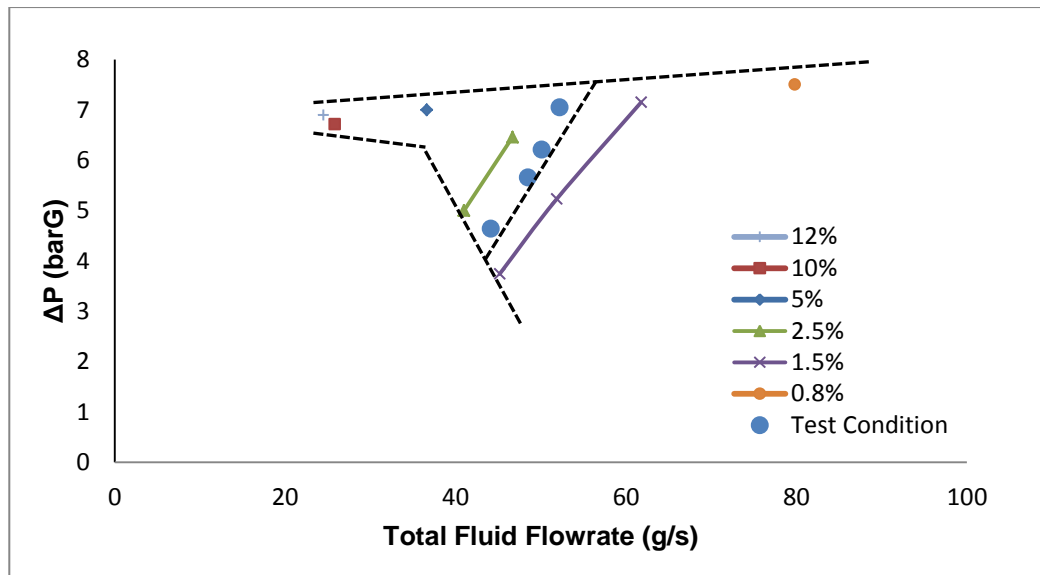


Figure A.2 Graph of spray quality showing mixing chamber pressures and total flow rates at which tests were performed.

Table A.2 Summary of  $\Delta P$  test operating conditions and spray characteristics.

Test	4.64 barG $\Delta P$	5.66 barG $\Delta P$	6.21 barG $\Delta P$	7.05 barG $\Delta P$
<b>Water Supply Pressure (barG)</b>	5.42	6.46	7.02	7.87
<b>ALR (%)</b>	2.10	2.08	2.12	2.25
<b><math>m_{\text{WATER}}</math> (g/s)</b>	43.22	47.51	49.07	51.07
<b><math>P_{\text{AIR}}</math> (barG)</b>	5.06	6.09	6.60	7.52
<b><math>m_{\text{AIR}}</math> (g/s)</b>	0.91	0.99	1.04	1.14
<b>Volumetric Void Fraction, <math>\alpha</math> (%)</b>	75.7	72.4	70.8	69.9
<b>Effective Power Rating (MW)</b>	1.73	1.90	1.96	2.04
<b>Coefficient of Discharge (-)</b>	0.45	0.45	0.44	0.43
<b><math>\theta/2</math> at 25 mm downstream (deg)</b>	23.75	25.64	27.47	27.47
<b>Calculated Nozzle <math>Re</math></b>	33389	28183	25151	22899
<b>Calculated Nozzle <math>We</math></b>	19137	13459	10741	9073
<b>Calculated Nozzle <math>Oh</math></b>	0.004143	0.004116	0.004121	0.004160
<b><math>D_{32}</math> (<math>\mu\text{m}</math>)</b>	156.93	137.93	136.89	122.27

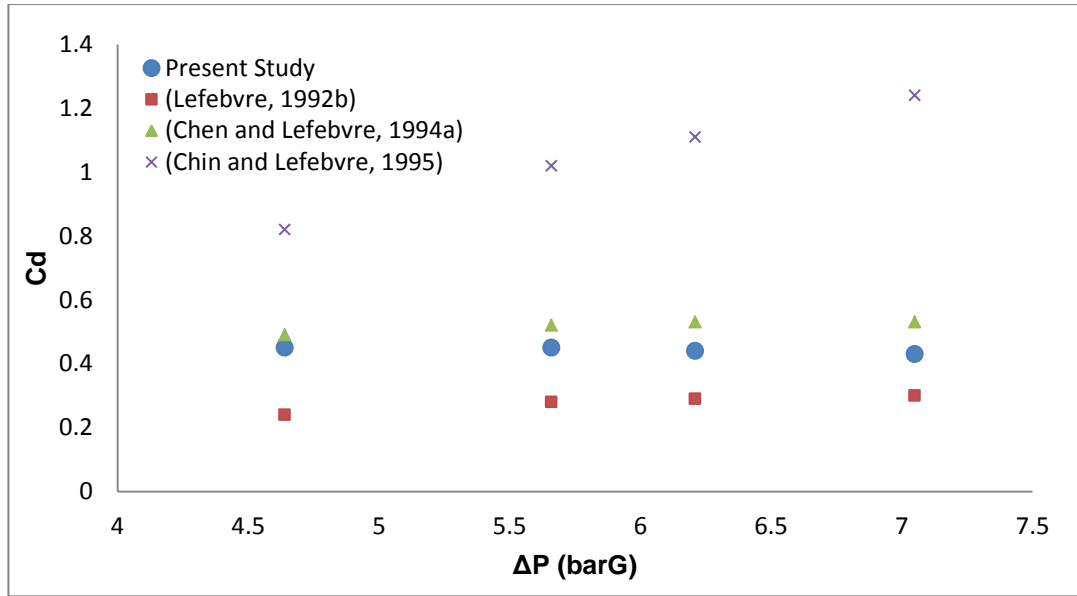


Figure A.3 Comparison of coefficient of discharge from PDA experiments and literature.

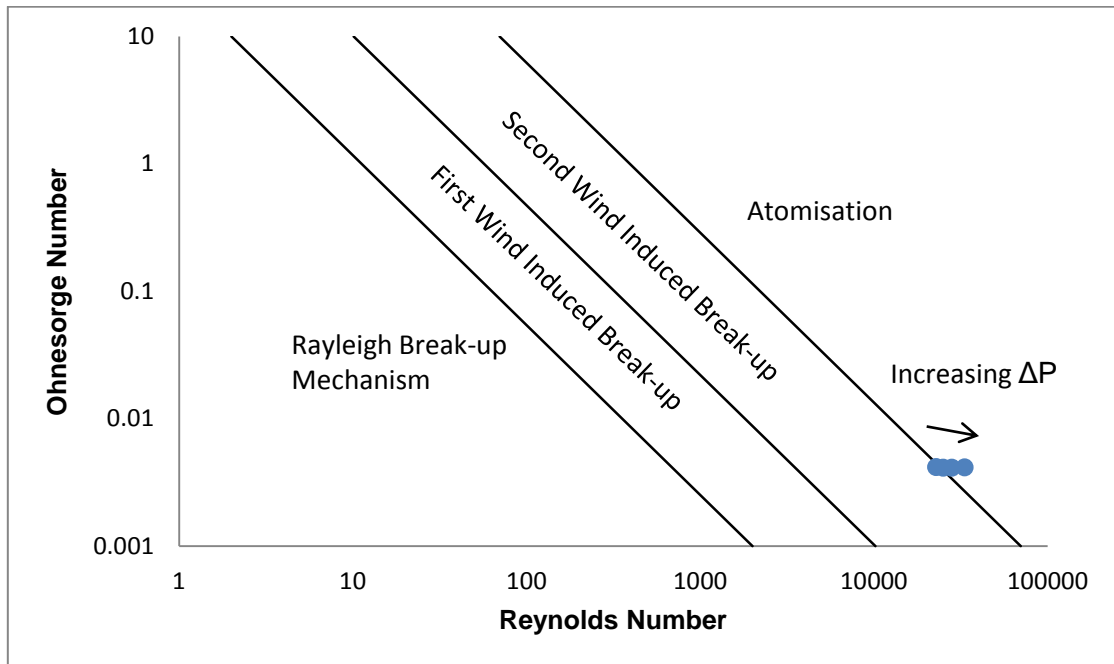


Figure A.4 Calculated liquid disintegration mode for  $\Delta P$  experiments.

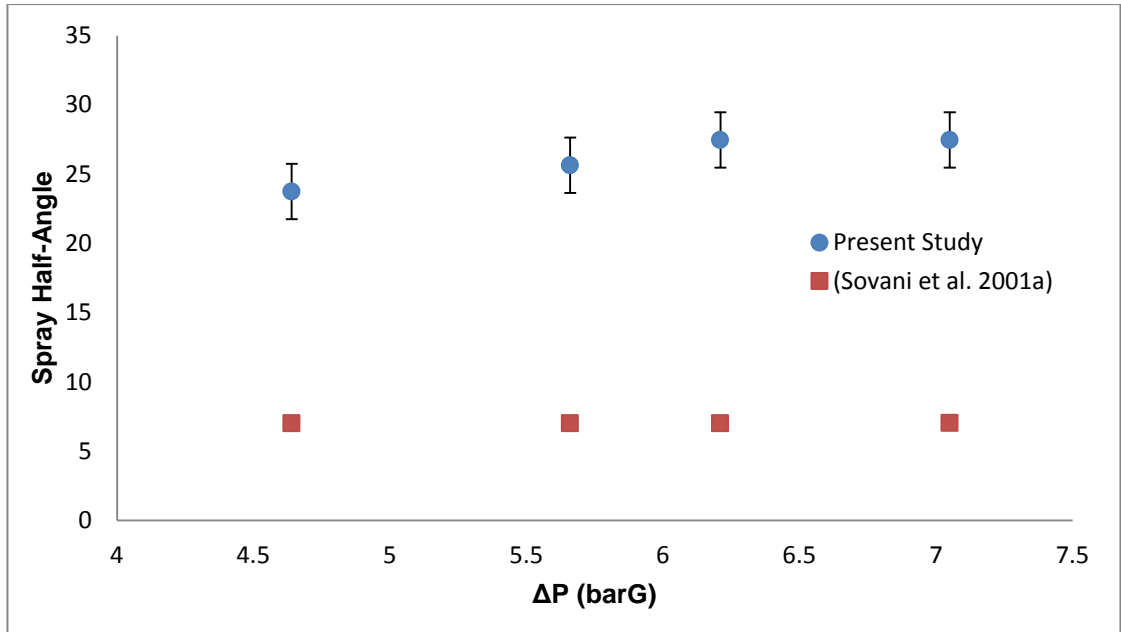


Figure A.5 Comparison of spray half-angle from PDA experiments and literature.

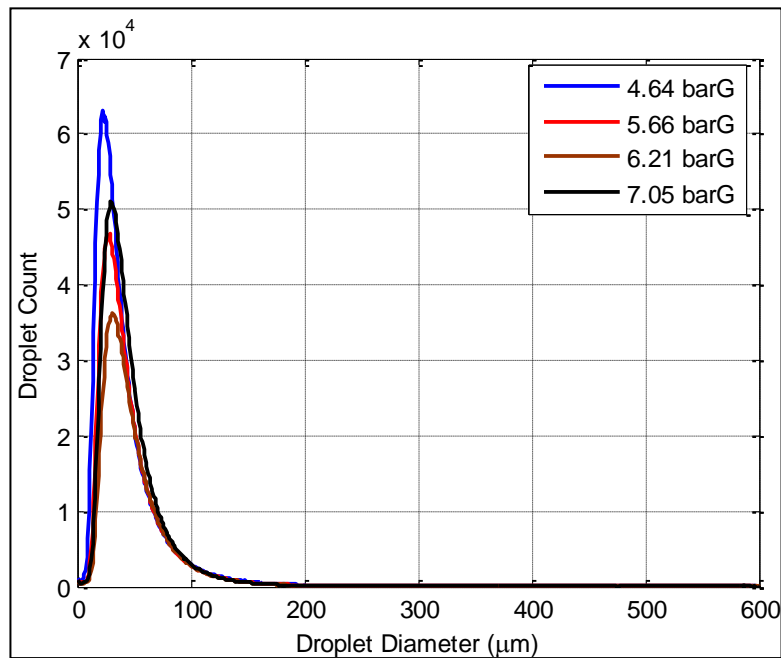


Figure A.6 Droplet diameter frequency distribution based on number.

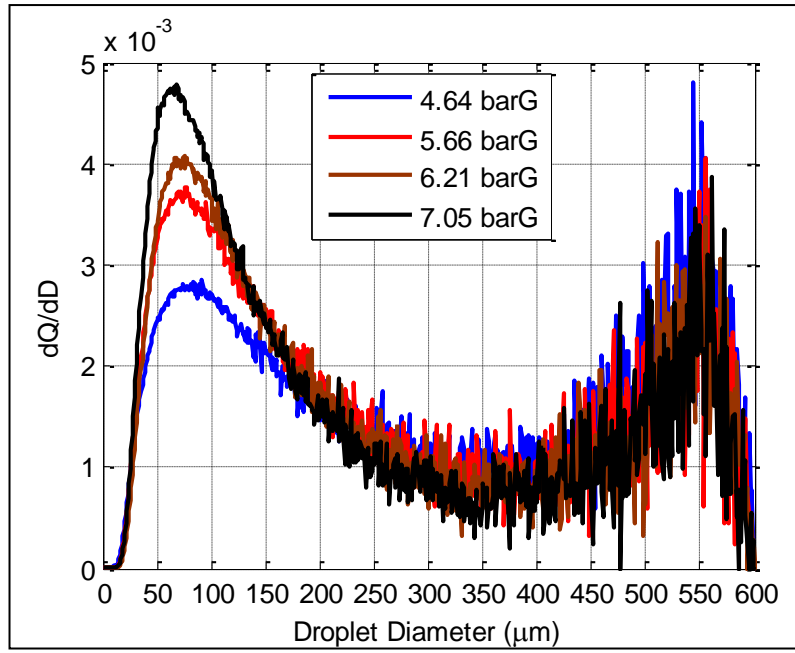


Figure A.7 Droplet diameter frequency distribution by mass.

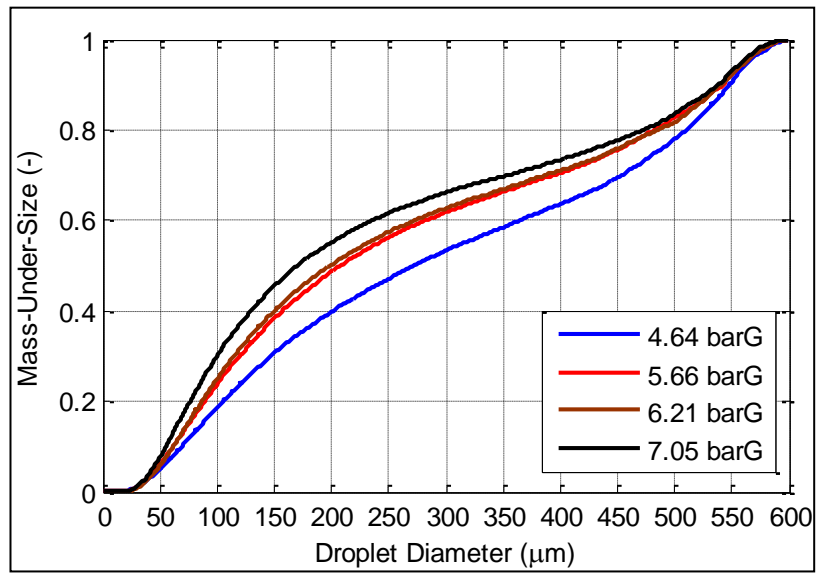


Figure A.8 Cumulative droplet size distribution.



Table A.3 Validated local droplet count varying with  $\Delta P$  increases.

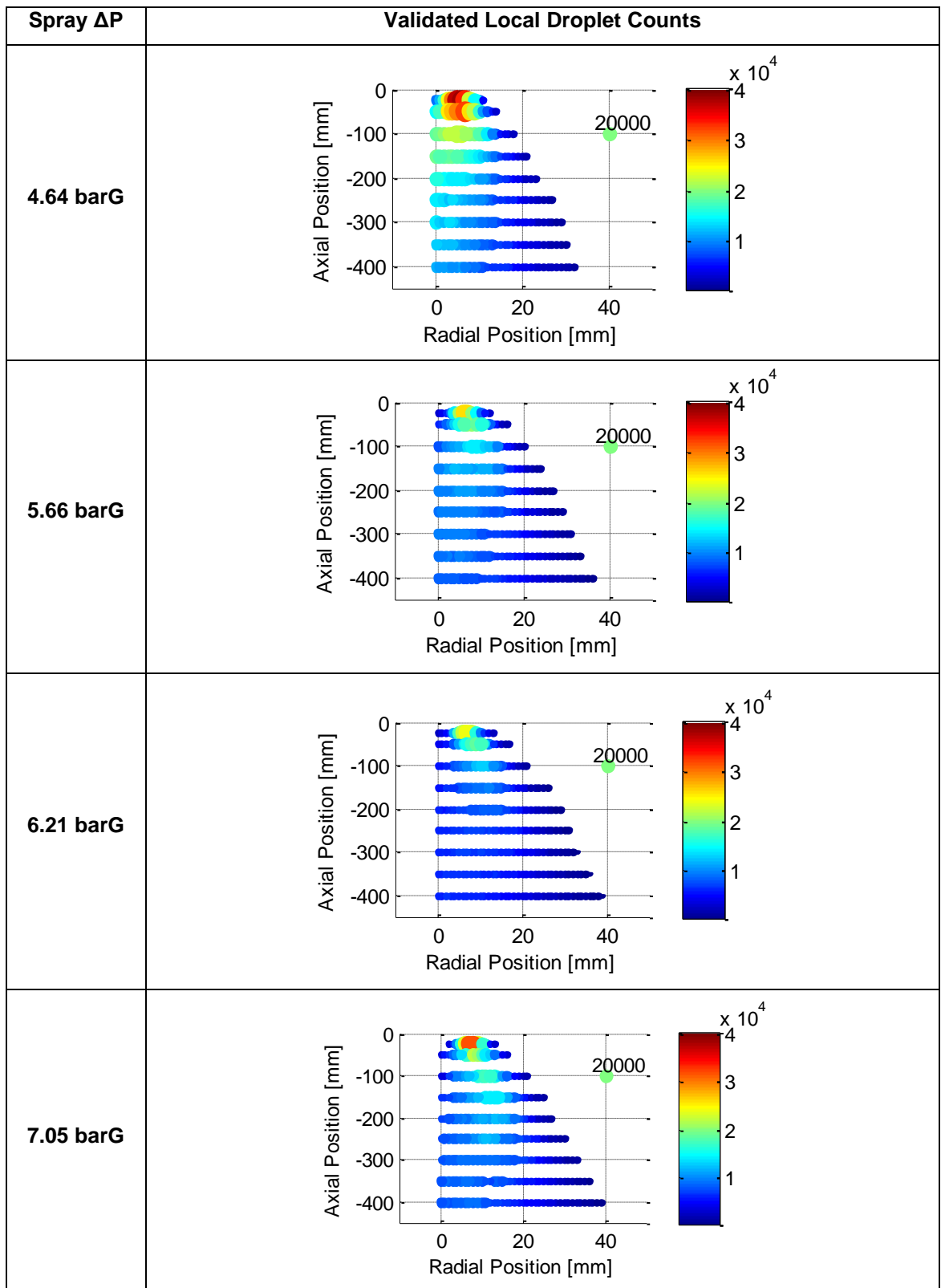


Table A.4 Average local droplet velocity varying with  $\Delta P$  increases.

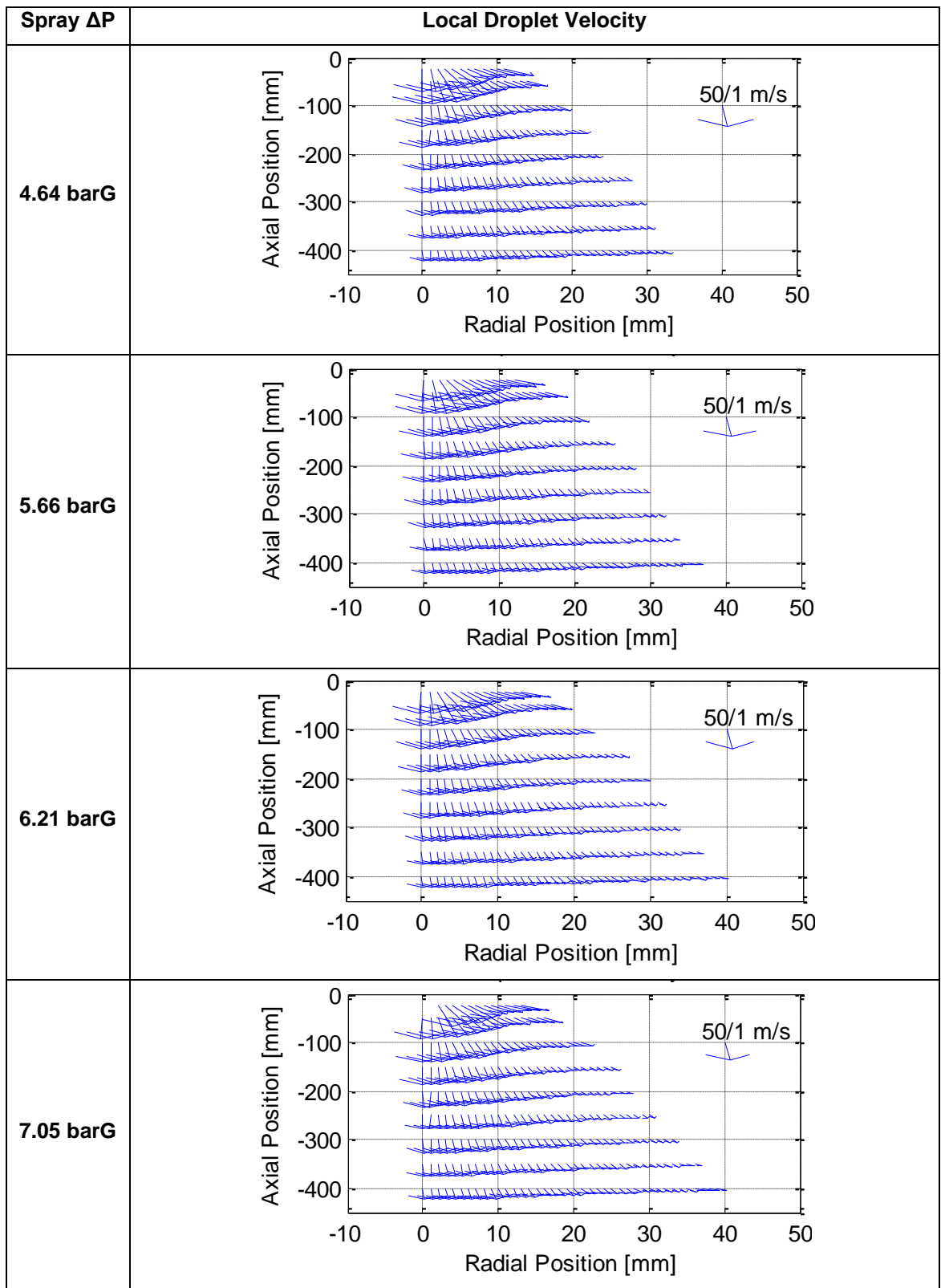
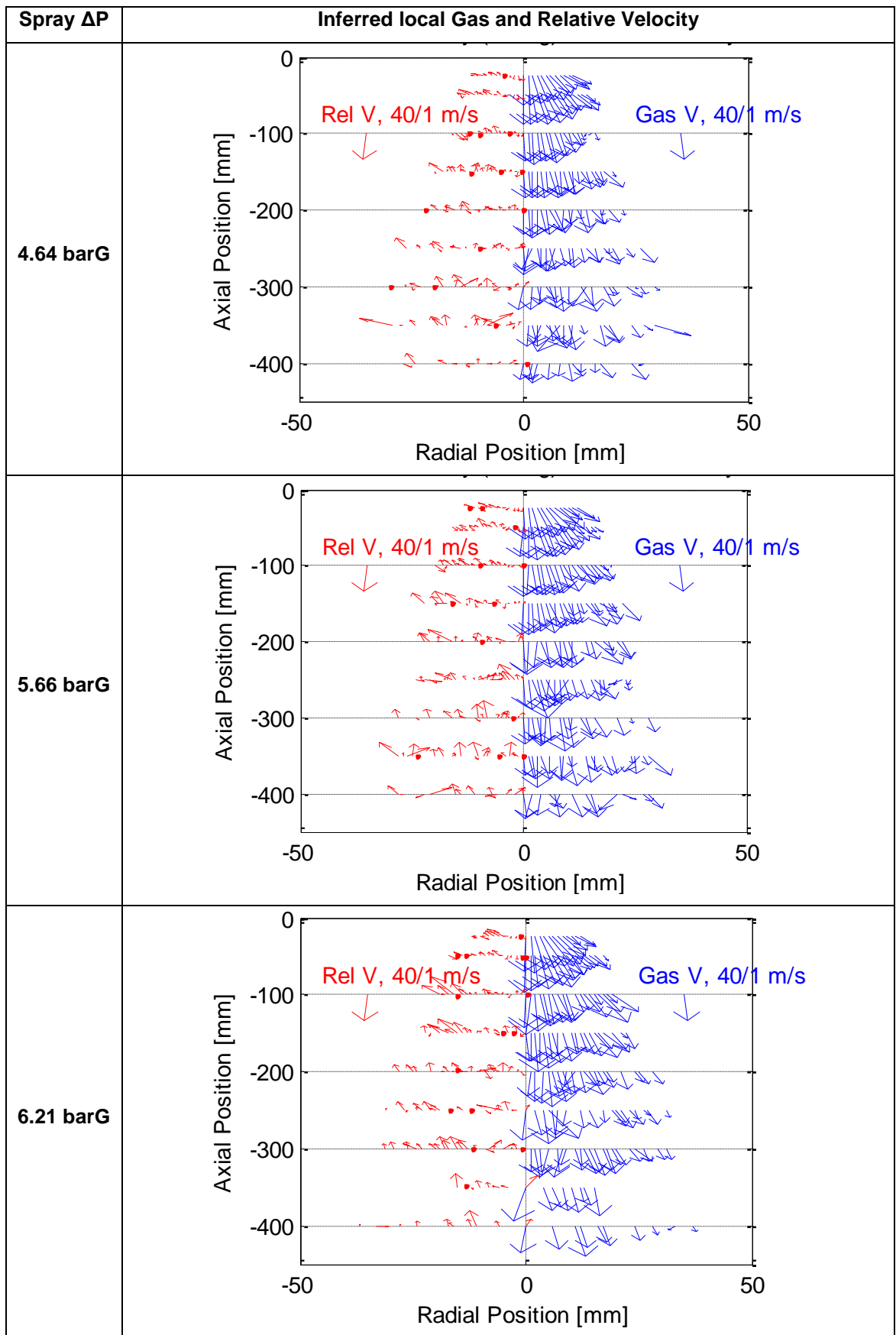


Table A.5 Inferred local gas and relative velocity varying with  $\Delta P$  increases.



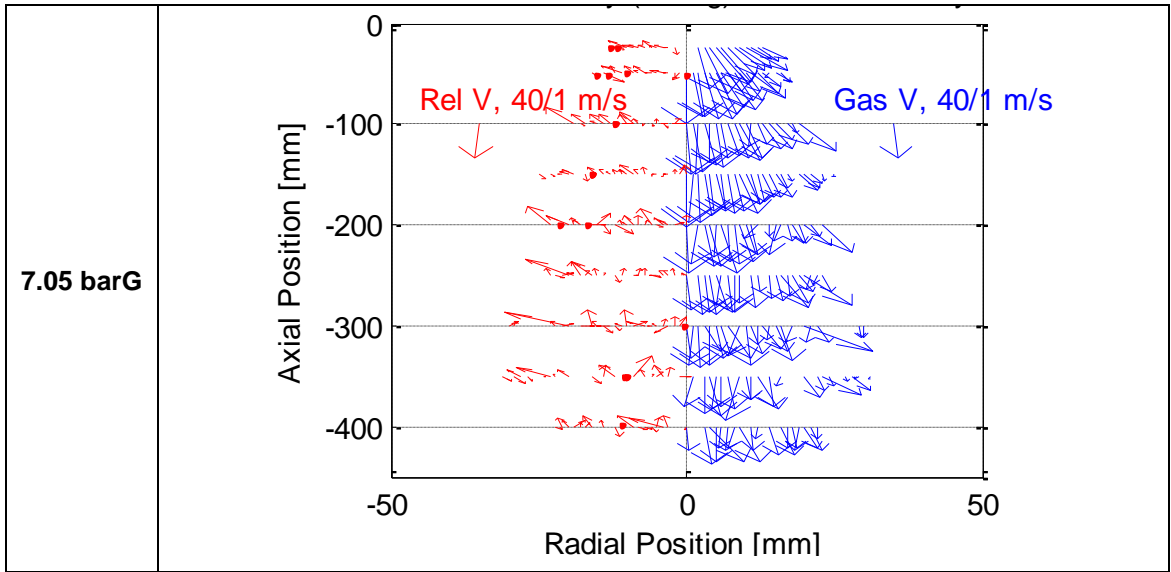


Table A.6 Average local droplet velocity varying with  $\Delta P$  increases.

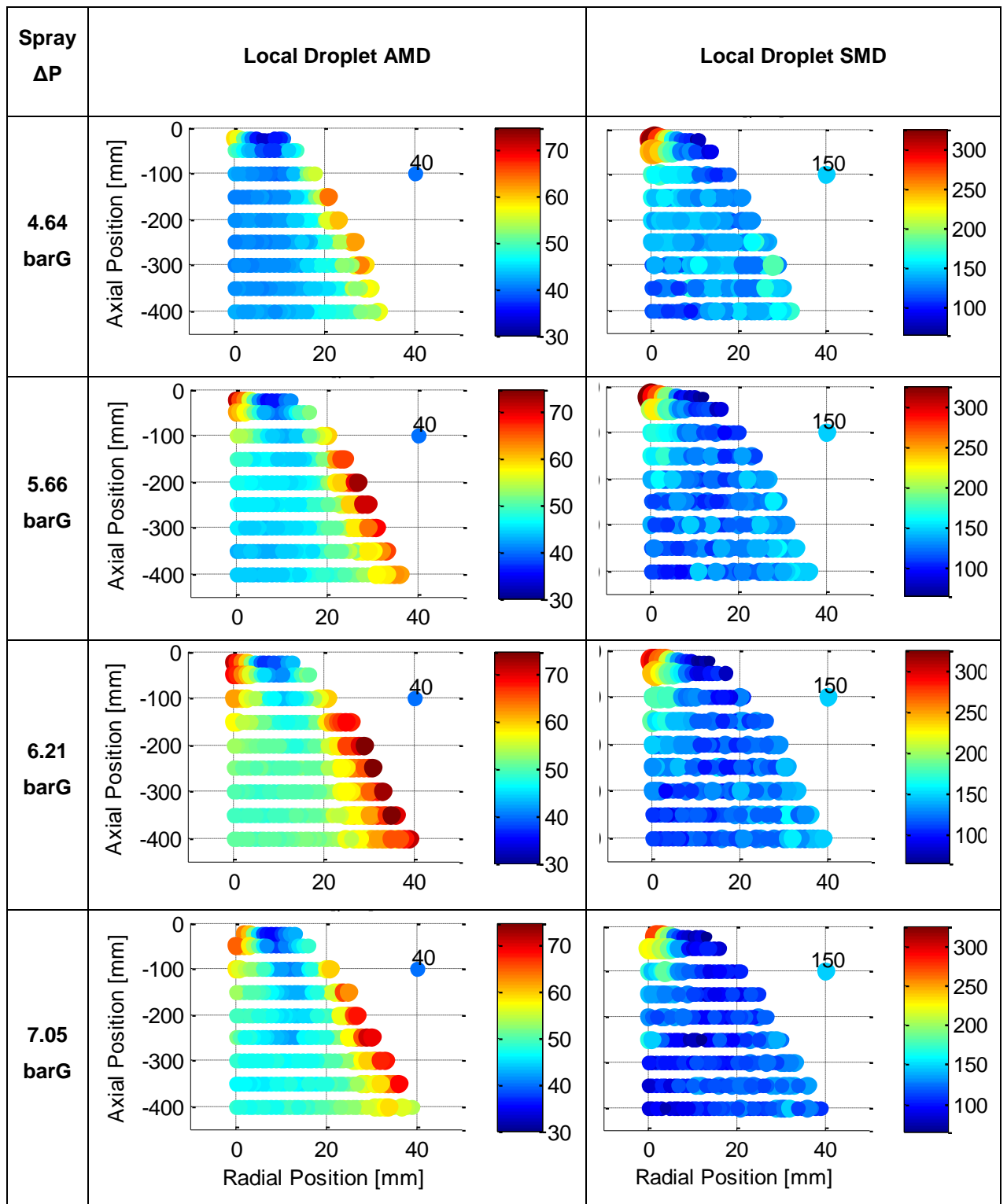


Table A.7 Local droplet SMD/AMD ratio varying with  $\Delta P$  increases.

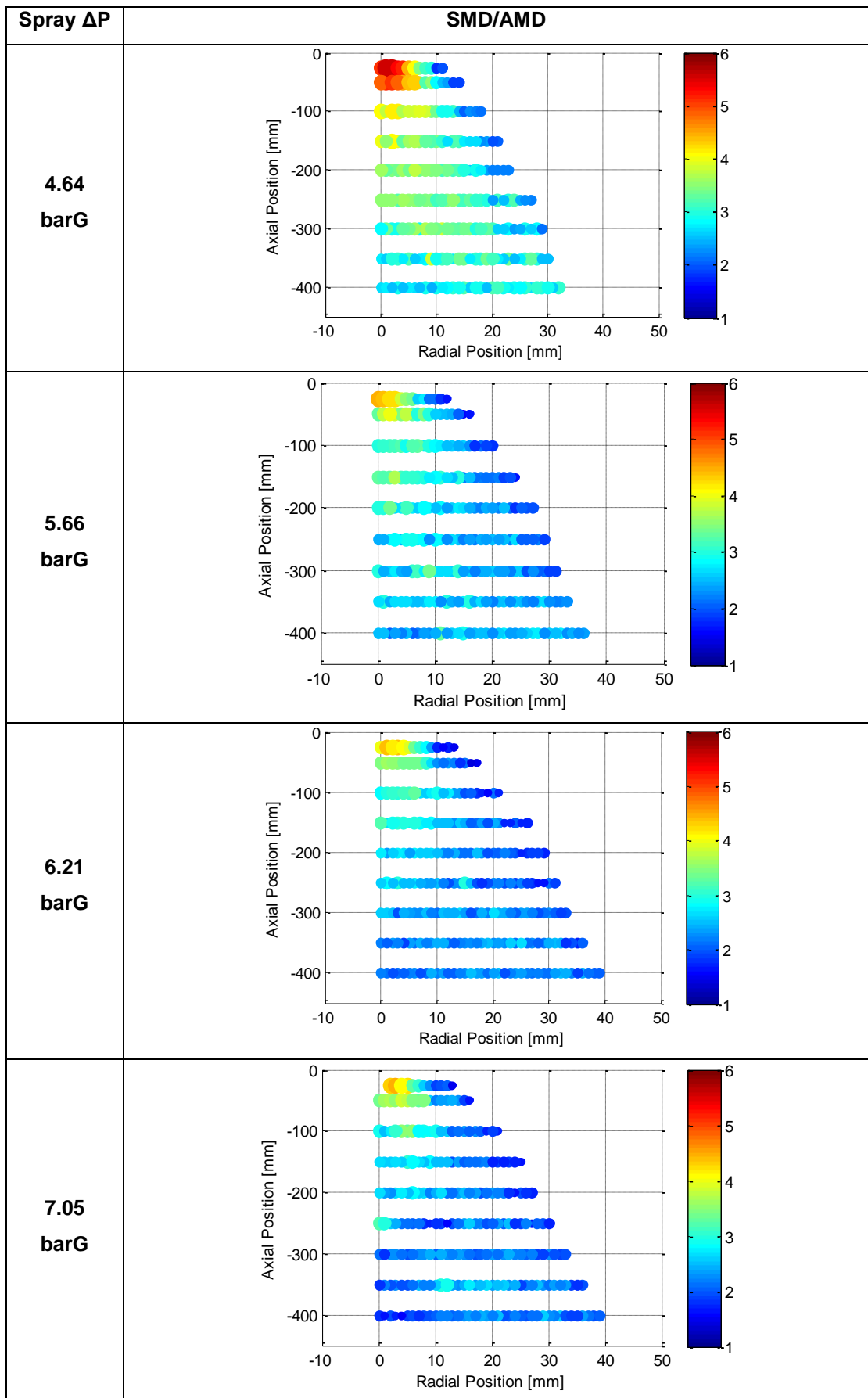


Table A.8 Local average droplet Weber number varying with  $\Delta P$  increases.

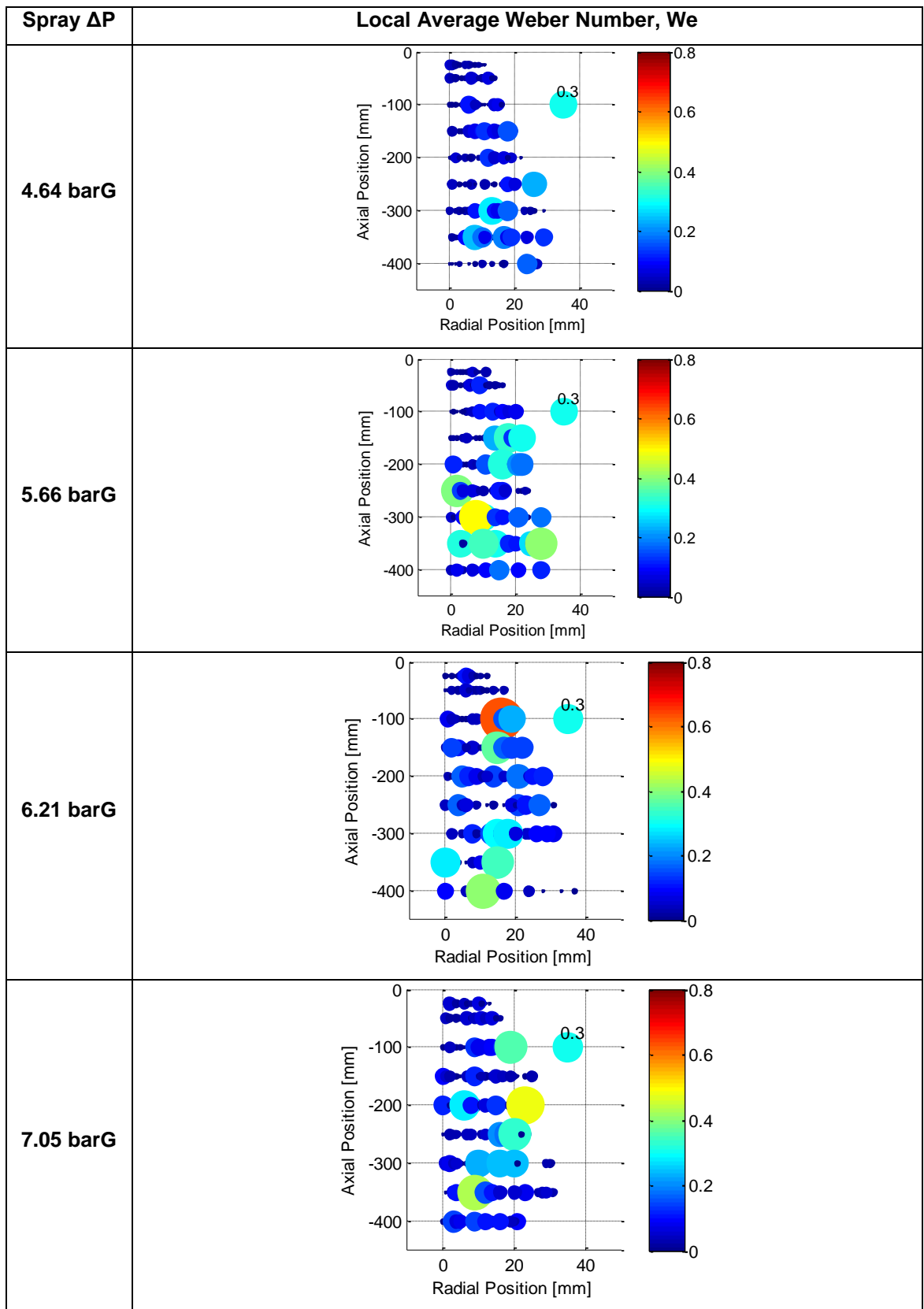
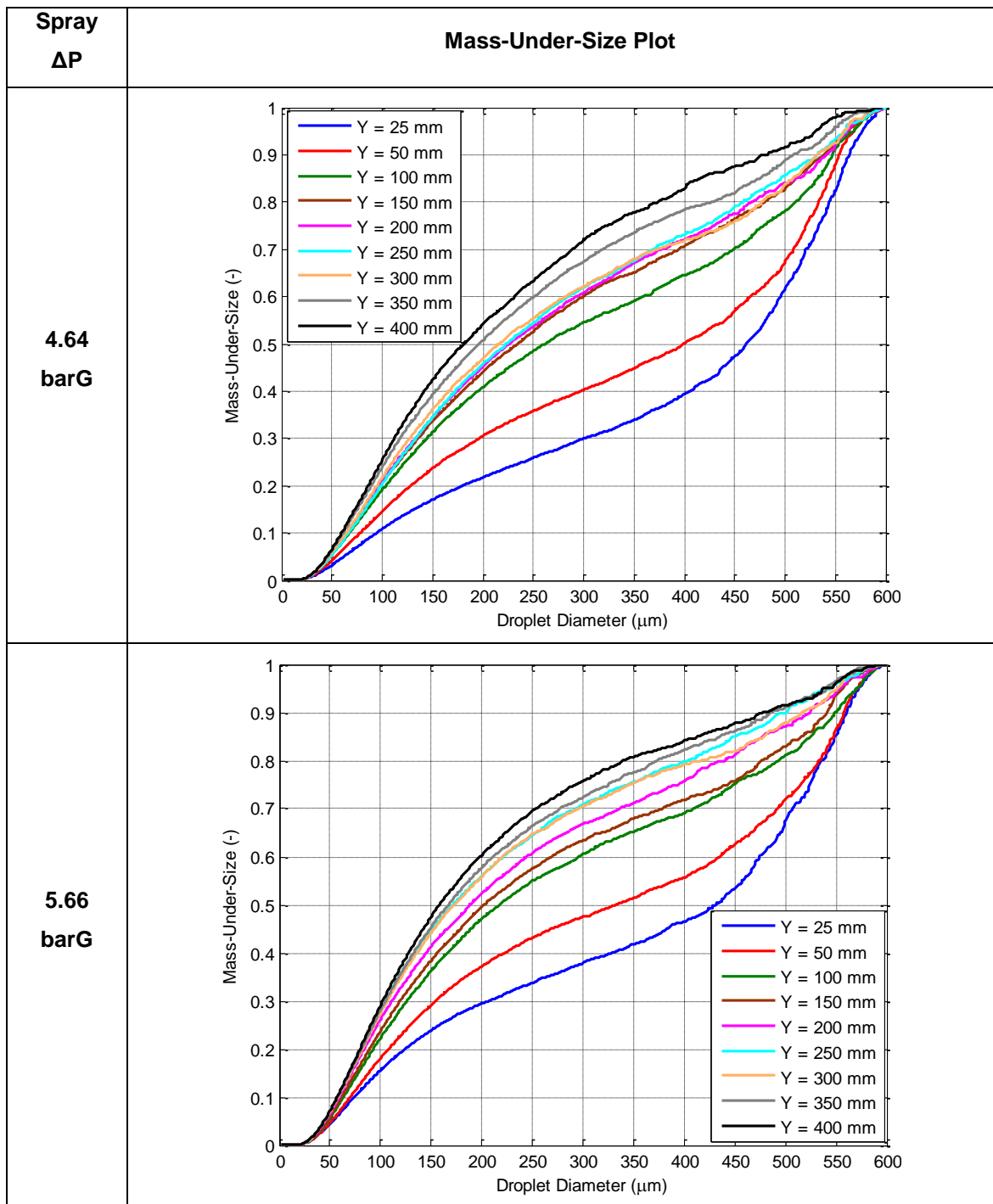
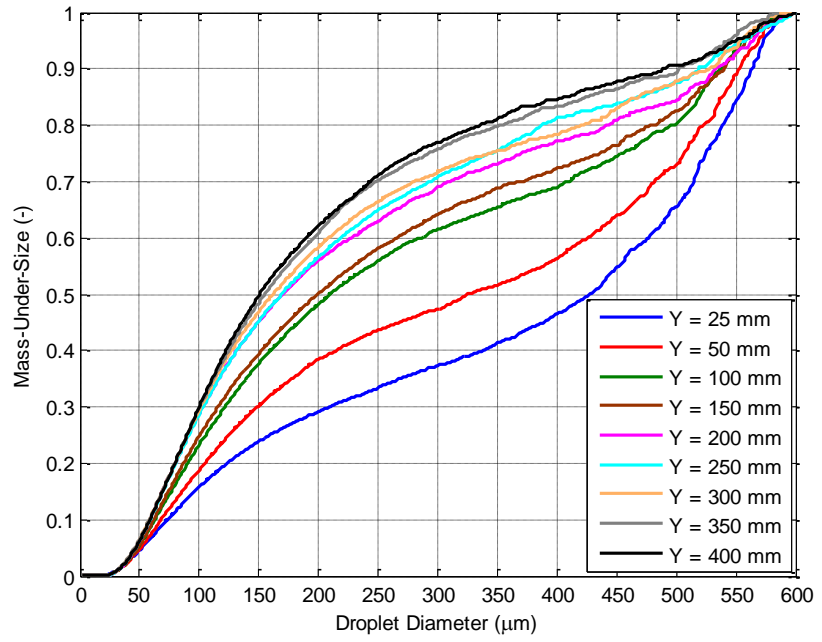


Table A.9 Cumulative mass-under-size plots for entire downstream locations.

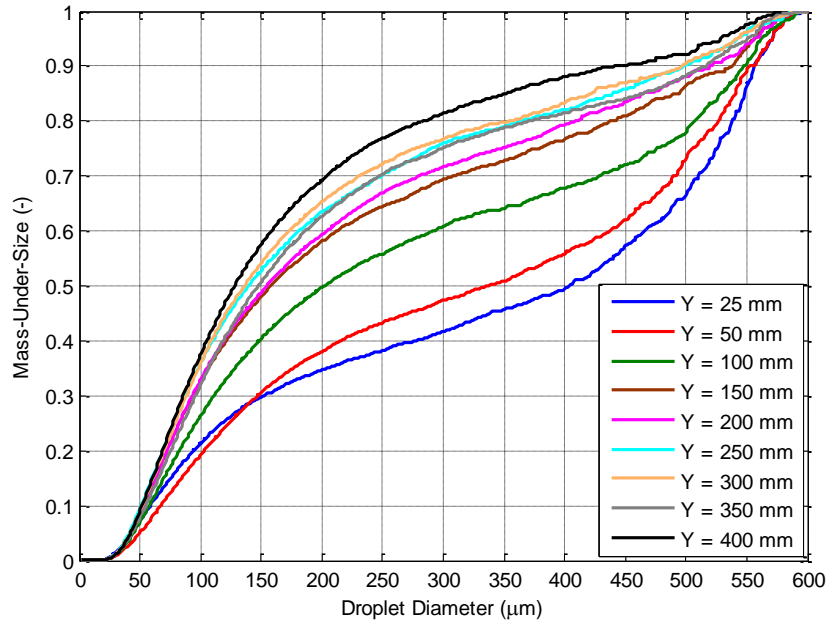




**6.21  
barG**



**7.05  
barG**



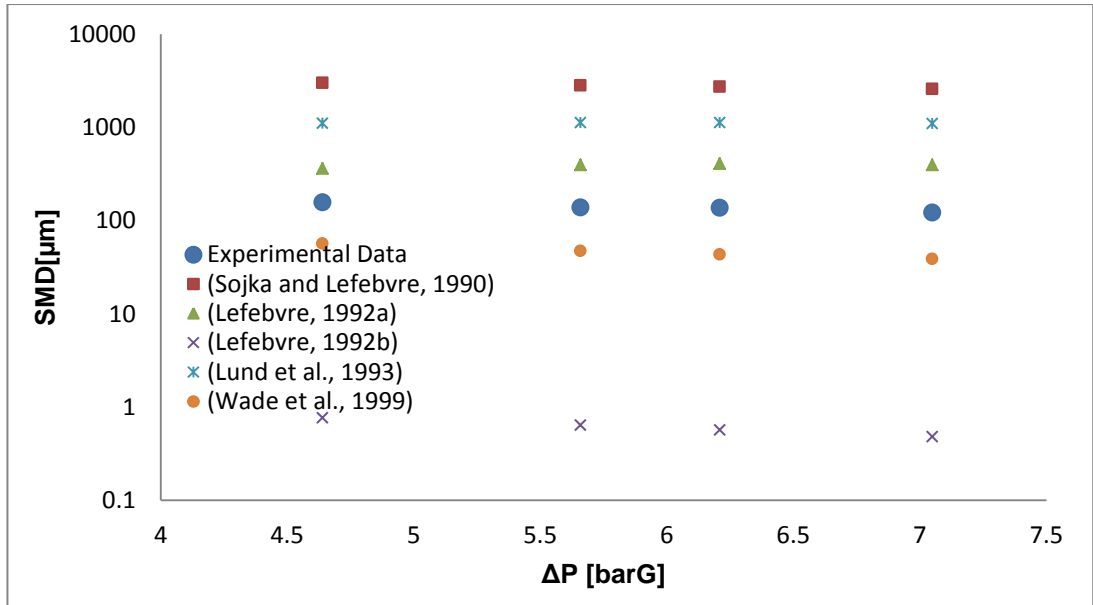


Figure A.9 Comparison of global spray droplet SMD from PDA experiments with that predicted by correlations in the literature.

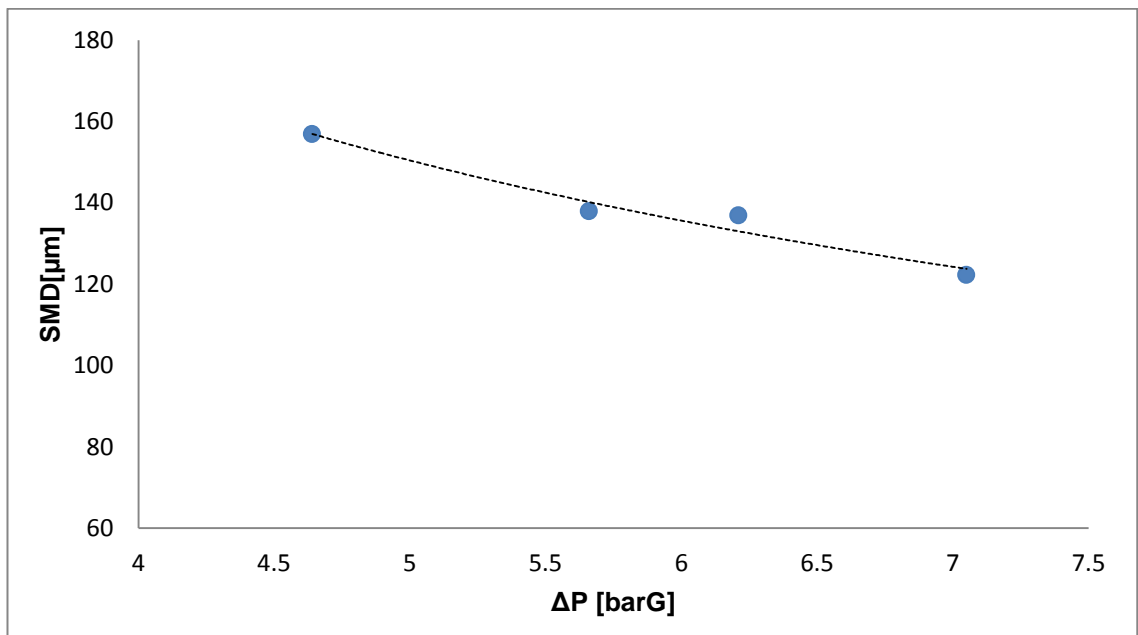


Figure A.10 The relationship between ΔP and global spray SMD as calculated using PDA data.

## Appendix B: Exit Orifice Diameter Tests

Table B.1 Operating conditions and controlled parameters for  $D_o$  tests.

TEST No. PARAMETER VARIED	1 ALR	2 $\Delta P$	3 $D_o$	4 $L_{MC}$	5 $D_{MC}$	6 $L_o/D_o$	7 A. GEOM.	8 $\eta$
TEST PHASE	A. Initial Operating Parameters			B. Atomiser Geometry				C. Fluid properties
ALR (%)	0.8-12.5	2		2				
$\Delta P$ (bar.g)	7	4-7		7				
$D_o$ (mm)	2	2	2-4	2	2	2	2	2
$L_{MC}$ (mm)	140	140	140	64-140	140	140	140	140
$D_{MC}$ (mm)	25.4	25.4	25.4	25.4	20-30	25.4	25.4	25.4
$L_o/D_o$ (-)	1	1	1	1	1	0.5-2	1	1
Aerator Geometry	A1	A1	A1	A1	A1	A1	A2, A3	A1
$\eta \times 10^{-8}$ (m <sup>2</sup> /s)	1	1	1	1	1	1	1	2-10

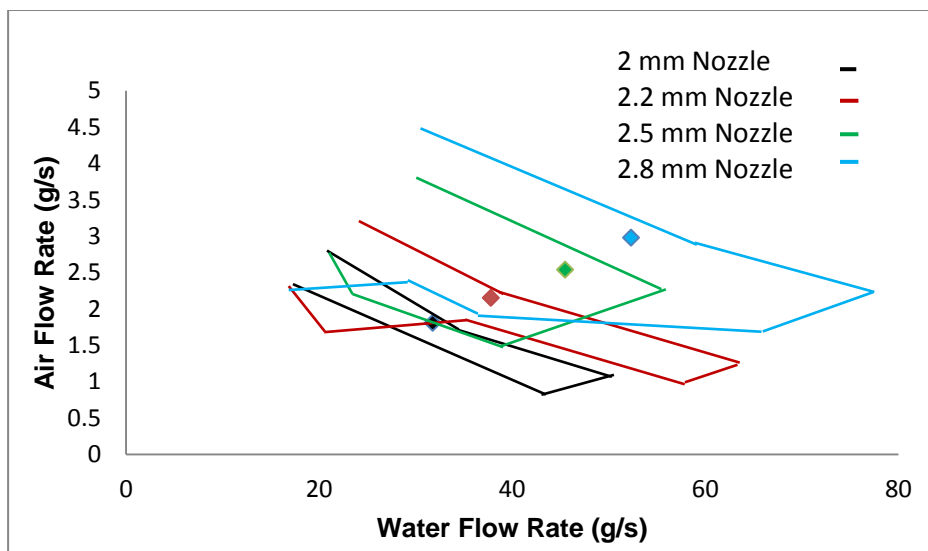


Figure B.1 Combined graphs of “spray quality” showing liquid flow rates at which optimal effervescent atomisation can be achieved with different nozzle diameters.

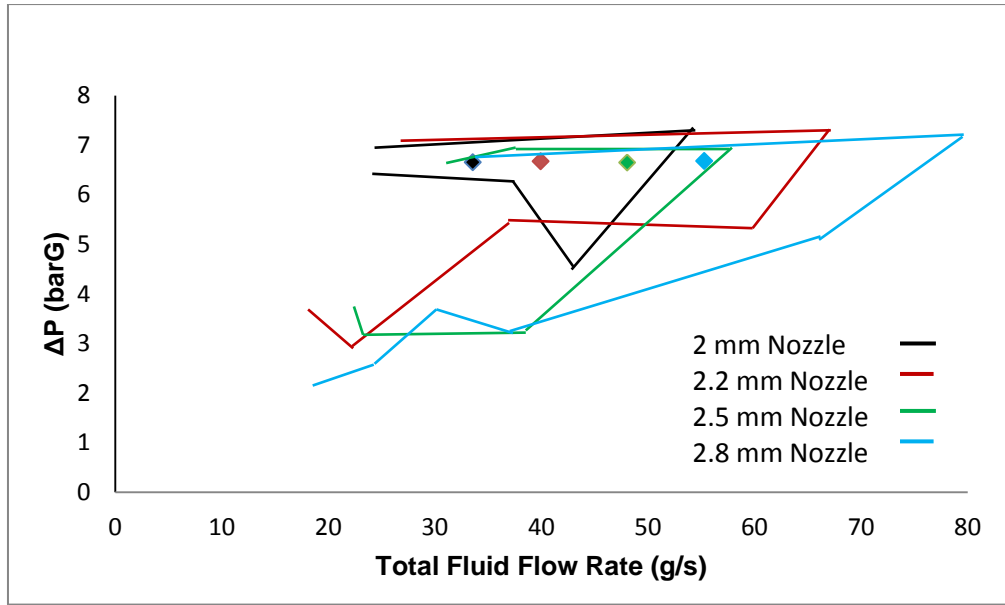


Figure B.2 Combined graphs of spray quality showing mixing chamber pressures and total flow rates at which tests were performed with different nozzles.

Table B. 2 Summary of  $D_0$  test operating conditions and spray characteristics.

Test	2 mm Ø	2.2 mm Ø	2.5 mm Ø	2.8 mm Ø
<b>Water Supply Pressure (barG)</b>	7.38	7.44	7.44	7.52
<b>ALR (%)</b>	5.70	5.70	5.59	5.70
<b>Mixing Chamber Pressure, <math>\Delta P</math> (barG)</b>	6.65	6.67	6.65	6.68
<b><math>m_{\text{WATER}}</math> (g/s)</b>	31.75	37.79	45.50	52.32
<b><math>P_{\text{AIR}}</math> (barG)</b>	7.23	7.23	7.27	7.32
<b><math>m_{\text{AIR}}</math> (g/s)</b>	1.81	2.15	2.54	2.98
<b>Volumetric Void Fraction, <math>\alpha</math> (%)</b>	86.1	86.1	85.9	86.1
<b>Effective Power Rating (MW)</b>	1.27	1.51	1.82	2.09
<b>Coefficient of Discharge (-)</b>	0.28	0.33	0.40	0.46
<b><math>\theta/2</math> at 25 mm downstream (deg)</b>	25.64	27.47	30.96	29.25
<b><math>D_{32}</math> (<math>\mu\text{m}</math>)</b>	81.06	97.27	109.25	103.66

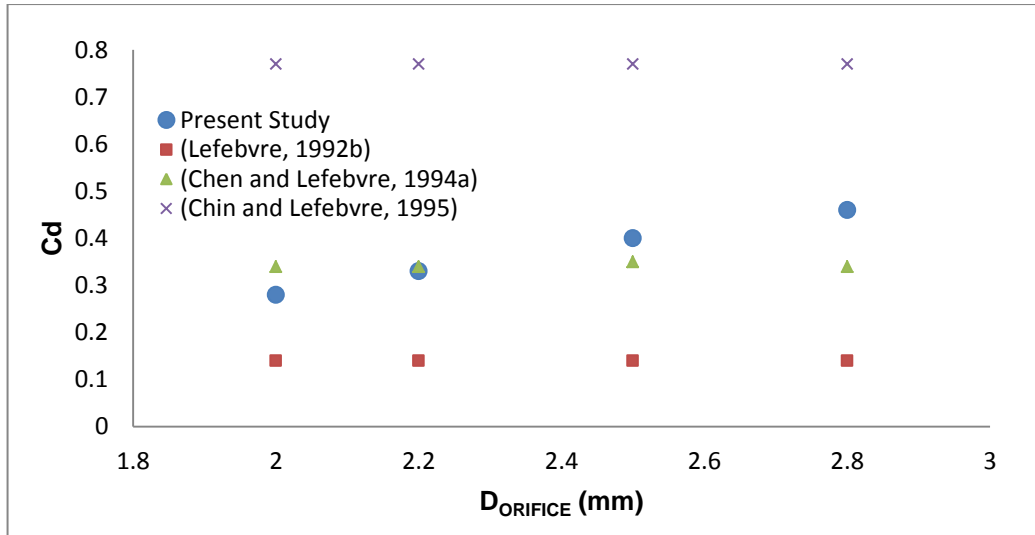


Figure B.3 Comparison of coefficient of discharge from PDA experiments and literature.

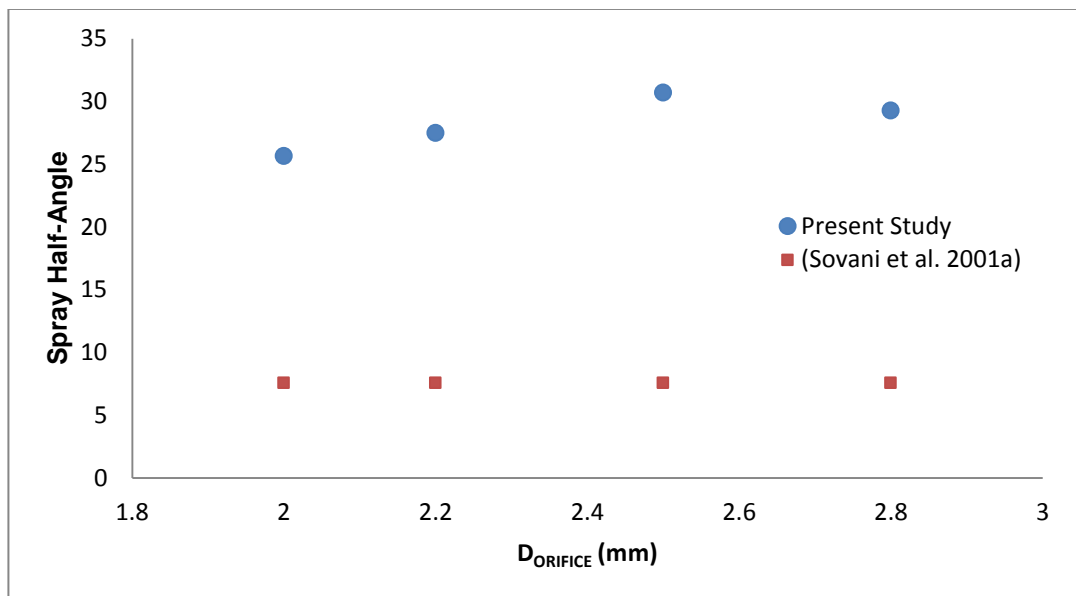


Figure B.4 Comparison of spray half-angle from PDA experiments and literature.

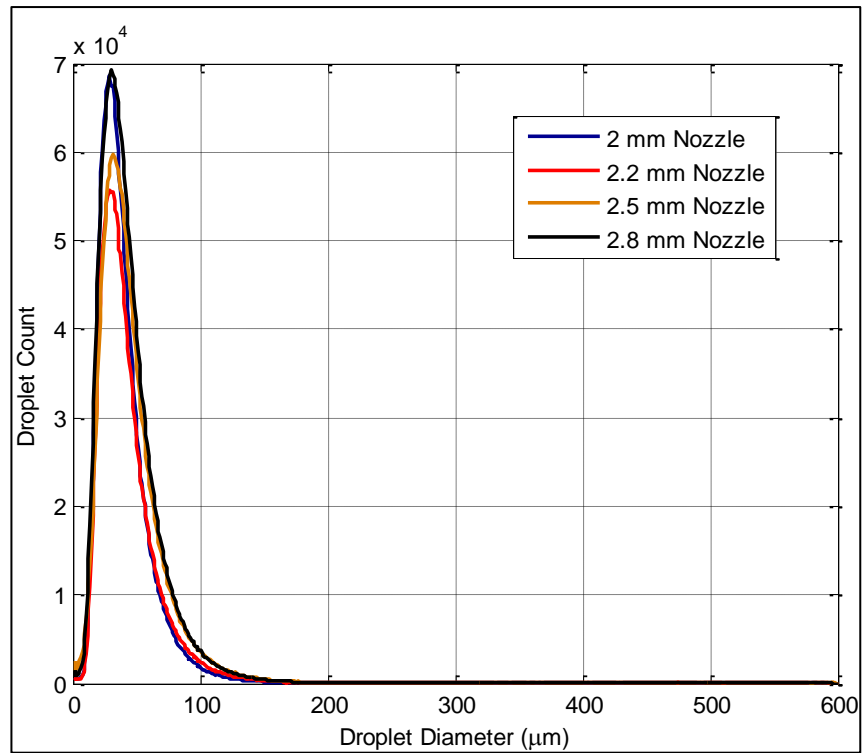


Figure B.5 Droplet diameter frequency distribution based on number.

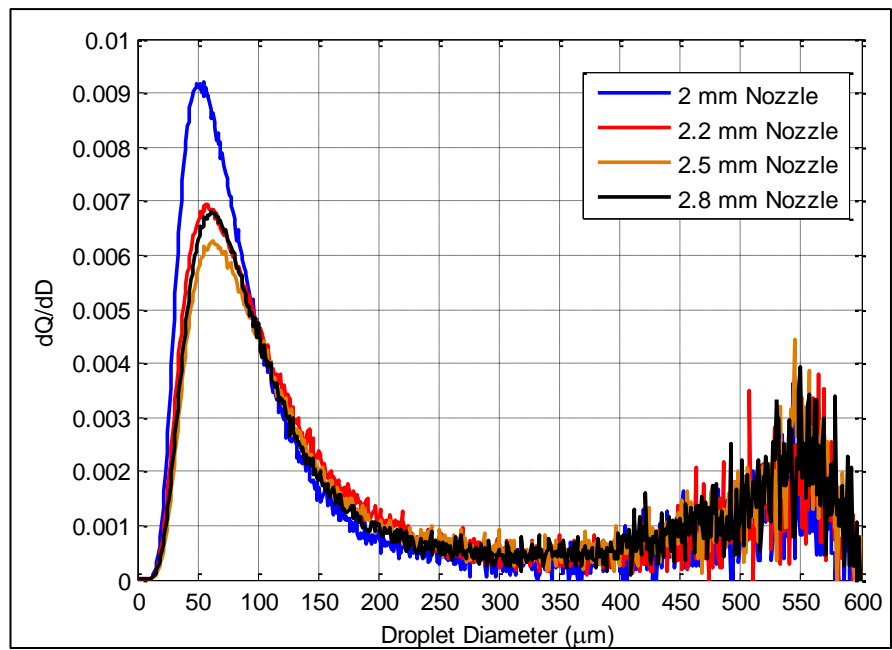


Figure B.6 Droplet diameter frequency distribution by mass.

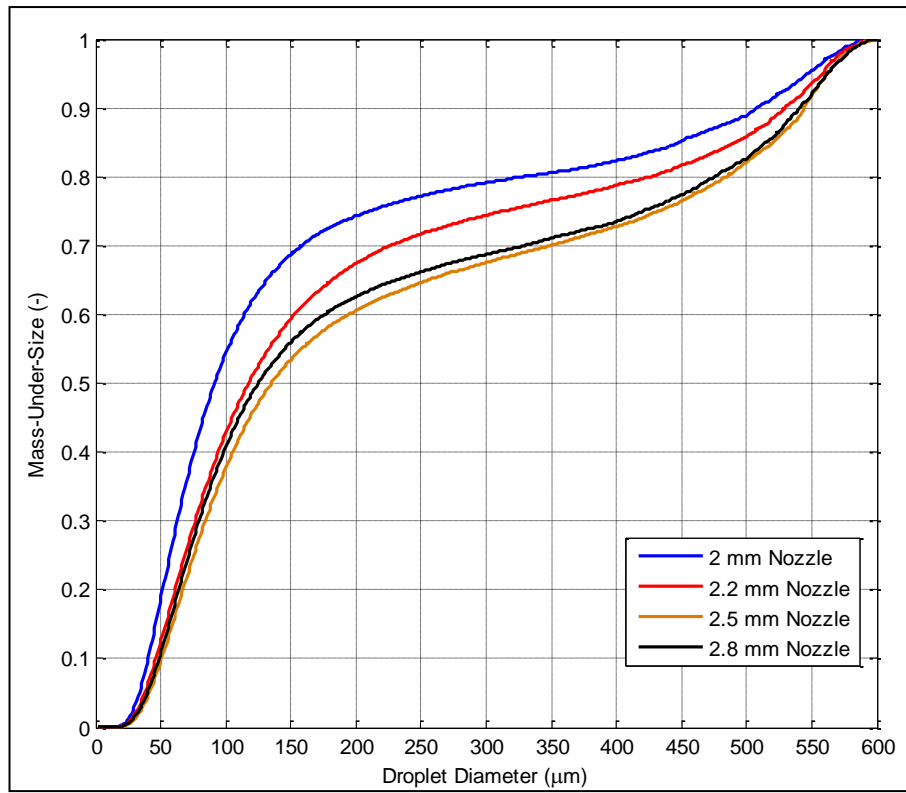


Figure B.7 Cumulative droplet size distribution.

Table B. 3 Validated local droplet count varying with  $D_o$  increases.

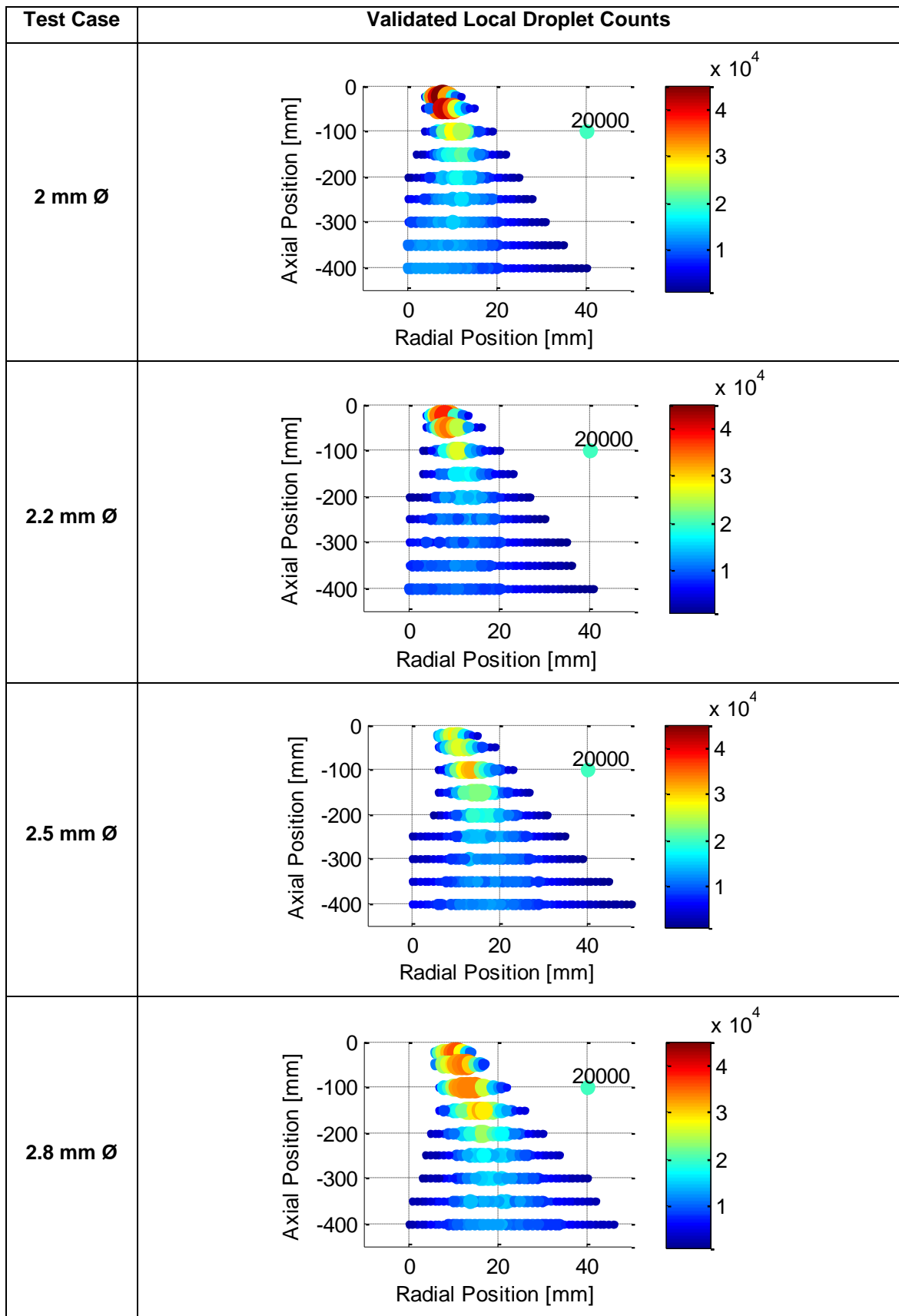
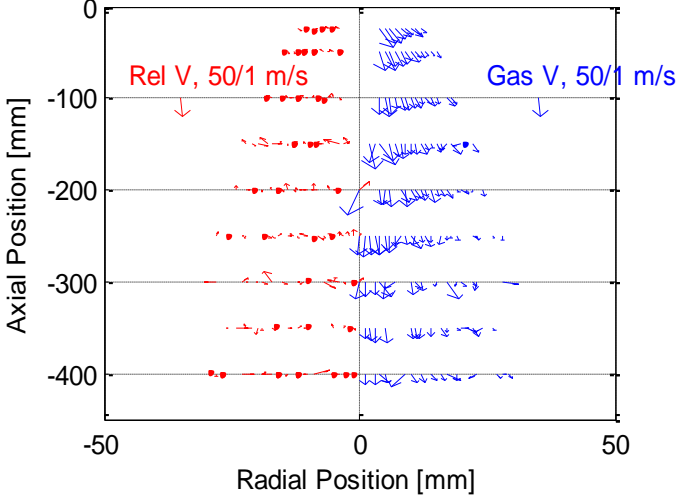
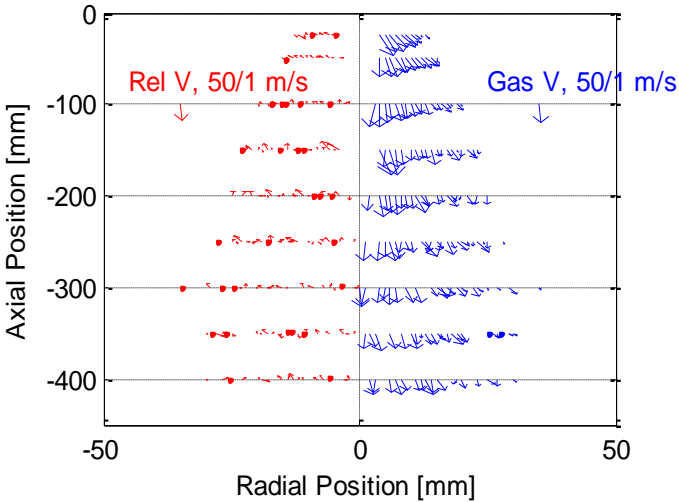
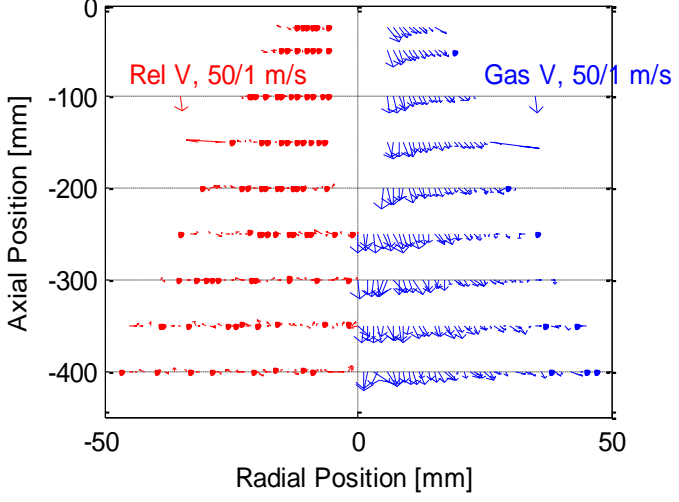




Table B. 4 Average local droplet velocity varying with  $D_0$  increases.

Test Case	Local Droplet Velocity
2 mm $\varnothing$	
2.2 mm $\varnothing$	
2.5 mm $\varnothing$	
2.8 mm $\varnothing$	

Table B. 5 Inferred Local gas and relative velocity varying with  $D_0$  increases.

Test Case	Inferred Local Gas and Relative Velocity
2 mm $\emptyset$	 <p>The plot for a 2 mm diameter shows relative velocity (red) and gas velocity (blue) as a function of radial position (mm) at various axial positions (mm). The radial position ranges from -50 to 50 mm, and the axial position ranges from 0 to -400 mm. The relative velocity is labeled 'Rel V, 50/1 m/s' and the gas velocity is labeled 'Gas V, 50/1 m/s'. Both velocities show a peak near the center (radial position = 0) and decrease towards the edges. The gas velocity is generally higher than the relative velocity.</p>
2.2 mm $\emptyset$	 <p>The plot for a 2.2 mm diameter shows relative velocity (red) and gas velocity (blue) as a function of radial position (mm) at various axial positions (mm). The radial position ranges from -50 to 50 mm, and the axial position ranges from 0 to -400 mm. The relative velocity is labeled 'Rel V, 50/1 m/s' and the gas velocity is labeled 'Gas V, 50/1 m/s'. Both velocities show a peak near the center (radial position = 0) and decrease towards the edges. The gas velocity is generally higher than the relative velocity.</p>
2.5 mm $\emptyset$	 <p>The plot for a 2.5 mm diameter shows relative velocity (red) and gas velocity (blue) as a function of radial position (mm) at various axial positions (mm). The radial position ranges from -50 to 50 mm, and the axial position ranges from 0 to -400 mm. The relative velocity is labeled 'Rel V, 50/1 m/s' and the gas velocity is labeled 'Gas V, 50/1 m/s'. Both velocities show a peak near the center (radial position = 0) and decrease towards the edges. The gas velocity is generally higher than the relative velocity.</p>

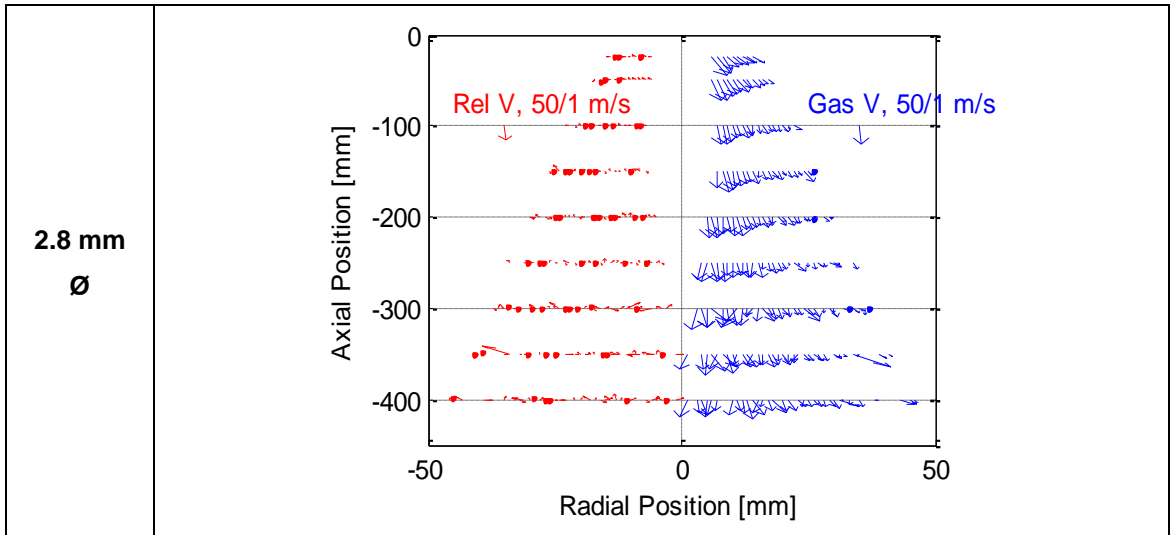


Table B. 6 Average local droplet AMD and SMD varying with  $D_o$  increases.

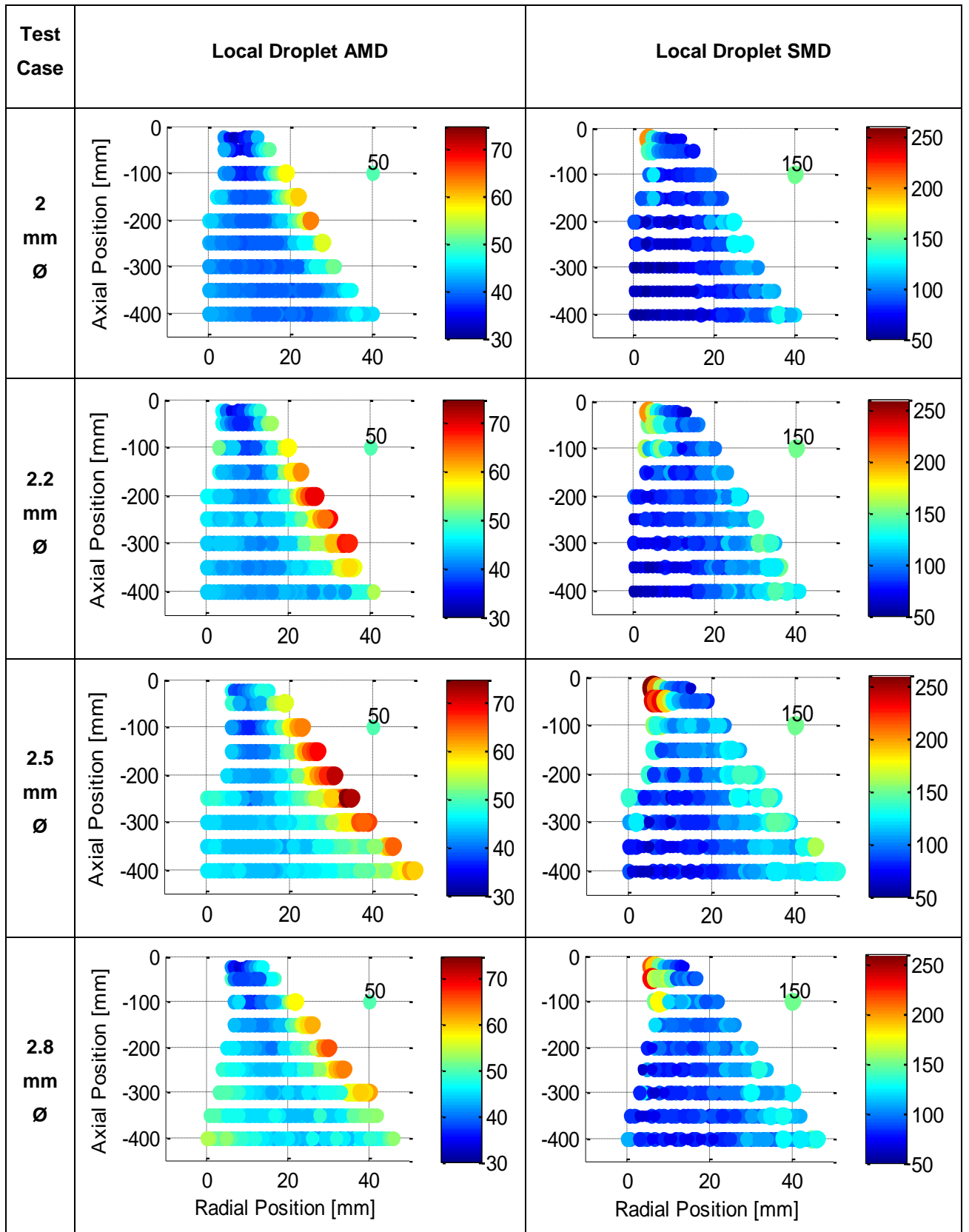
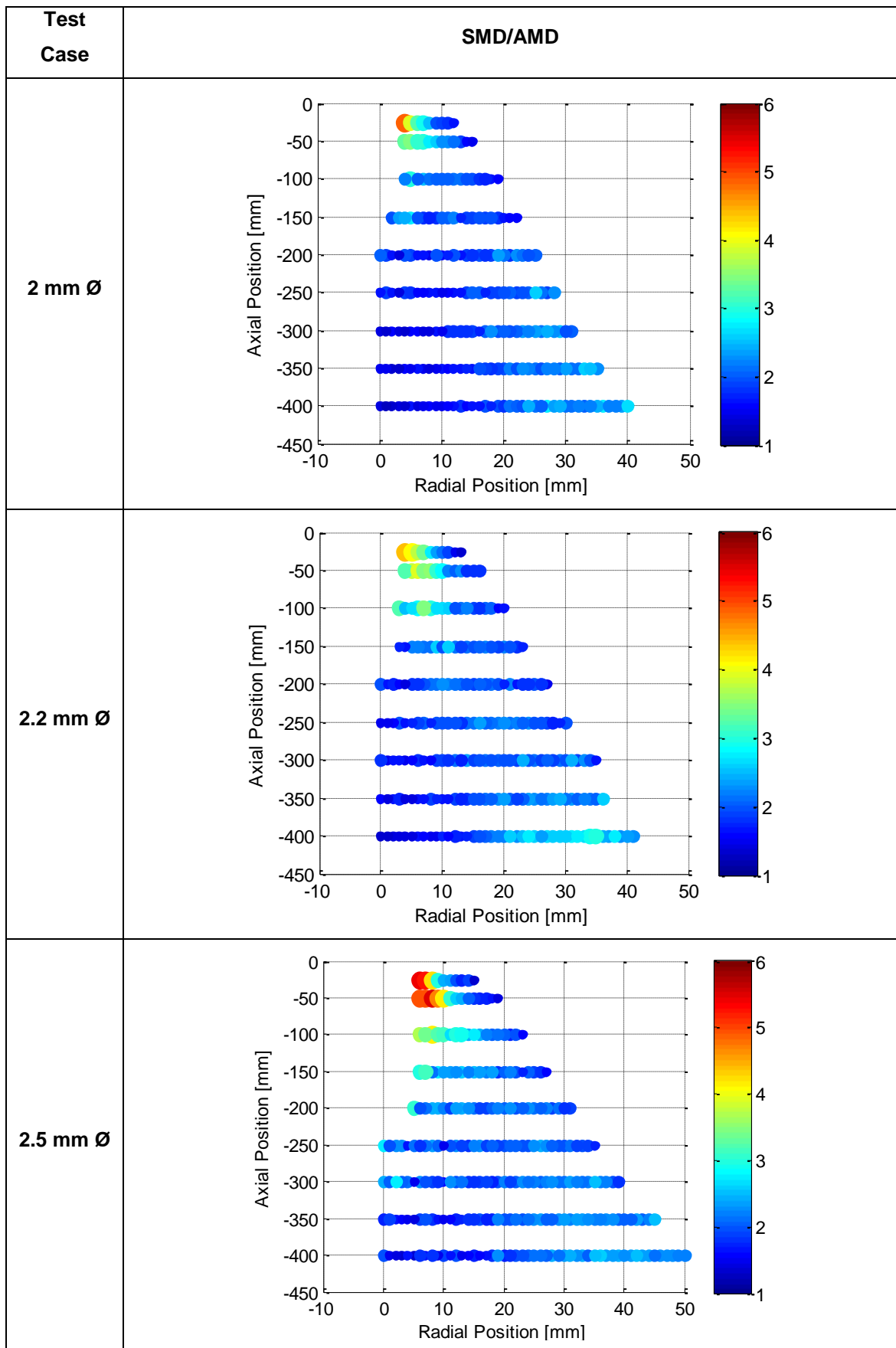


Table B. 7 Local droplet SMD/AMD ratio varying with  $D_o$  increases.



2.8 mm  $\varnothing$

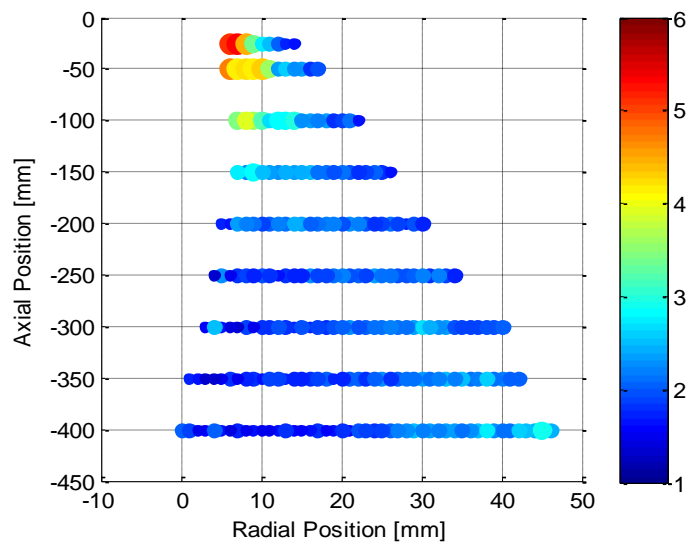


Table B. 8 Local average droplet Weber number varying with  $D_0$  increases.

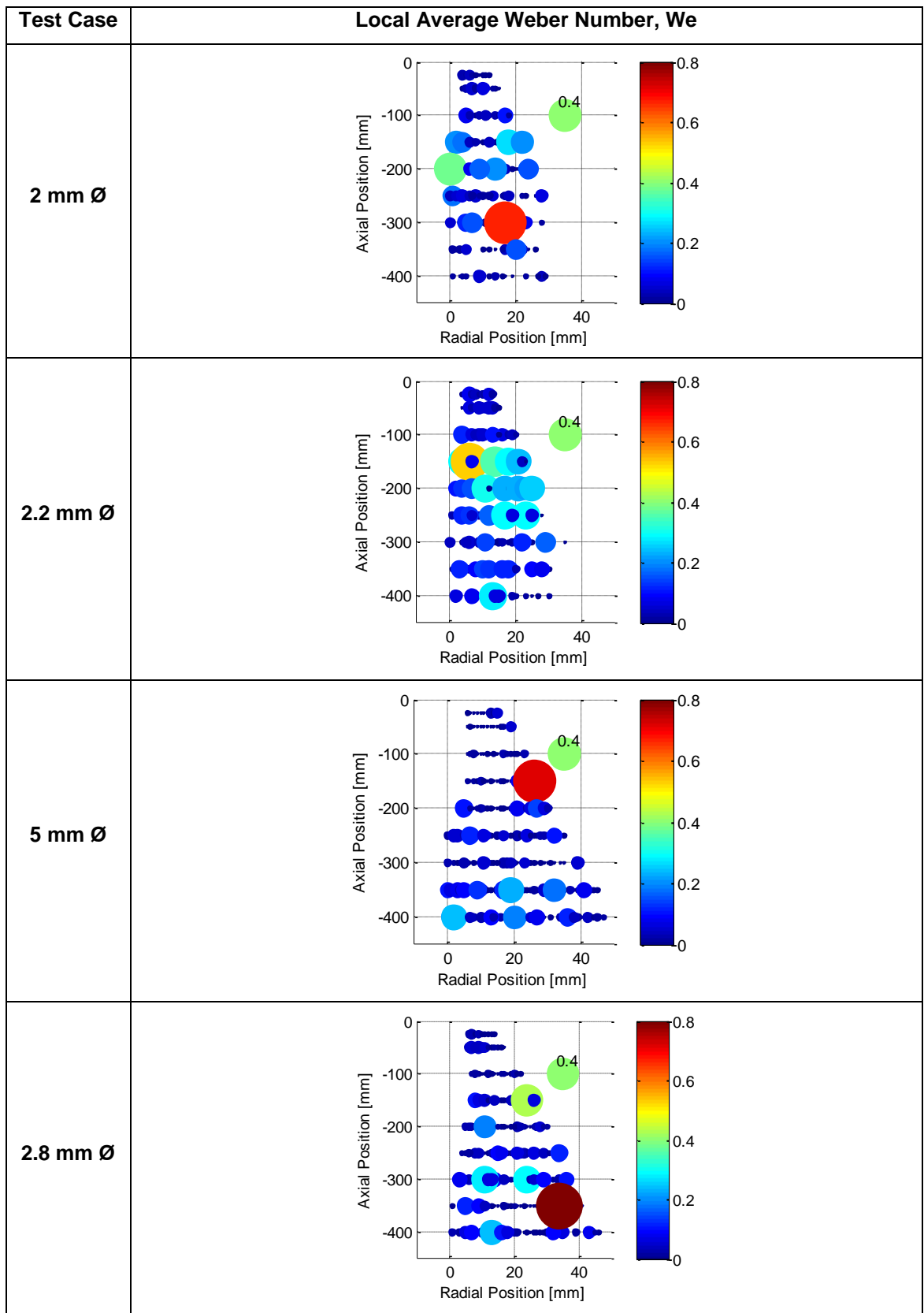
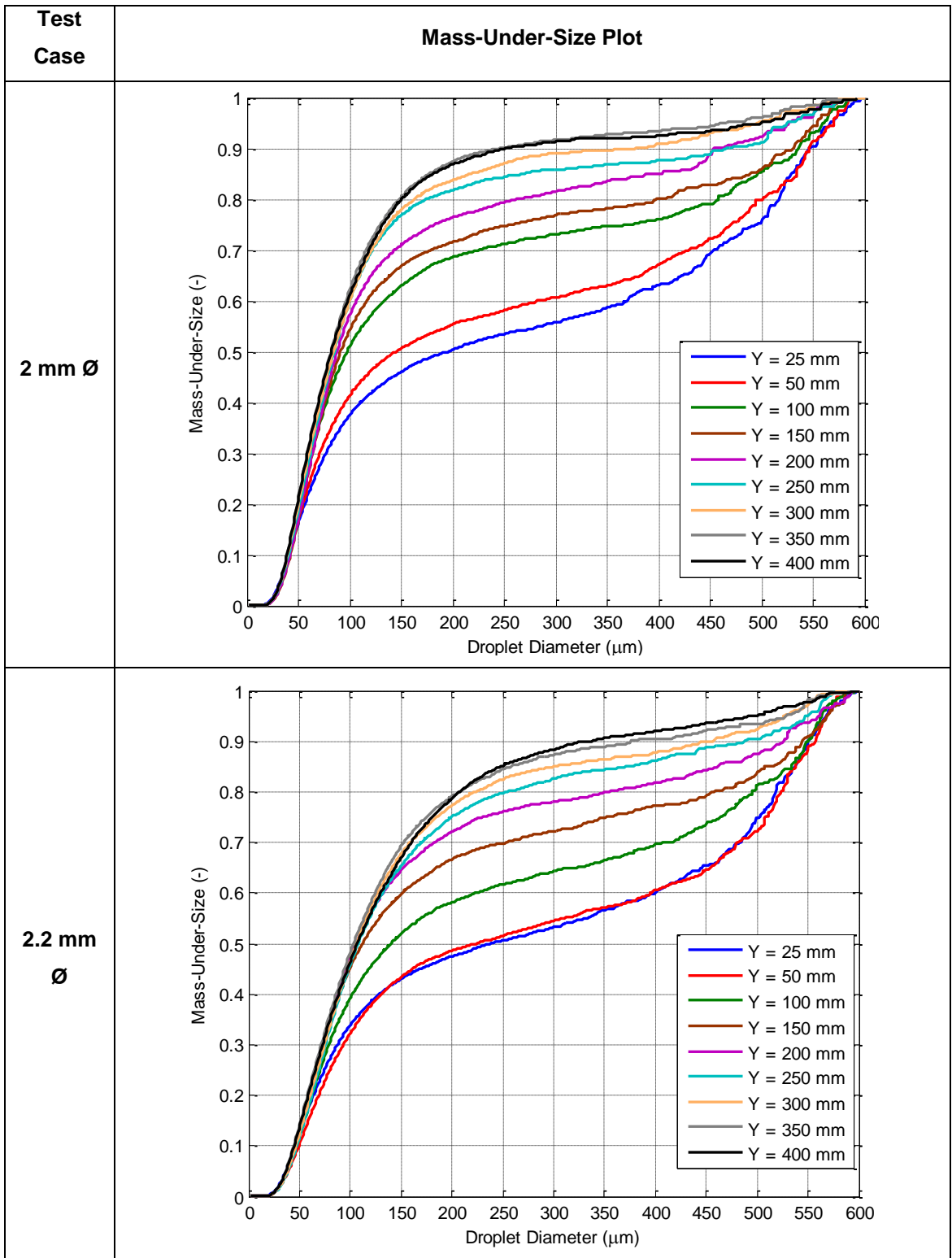
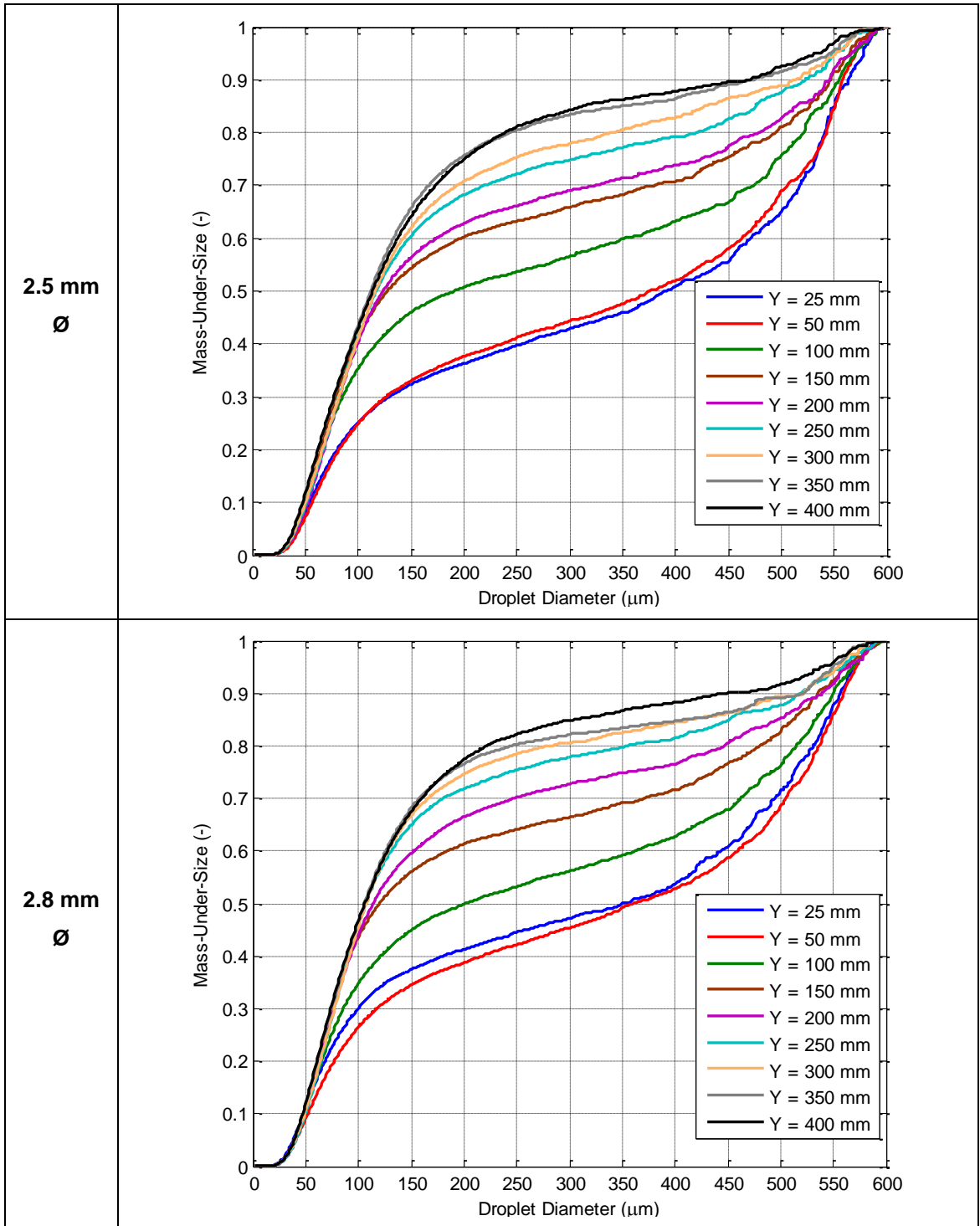


Table B. 9 Cumulative mass-under-size plots for entire downstream locations.







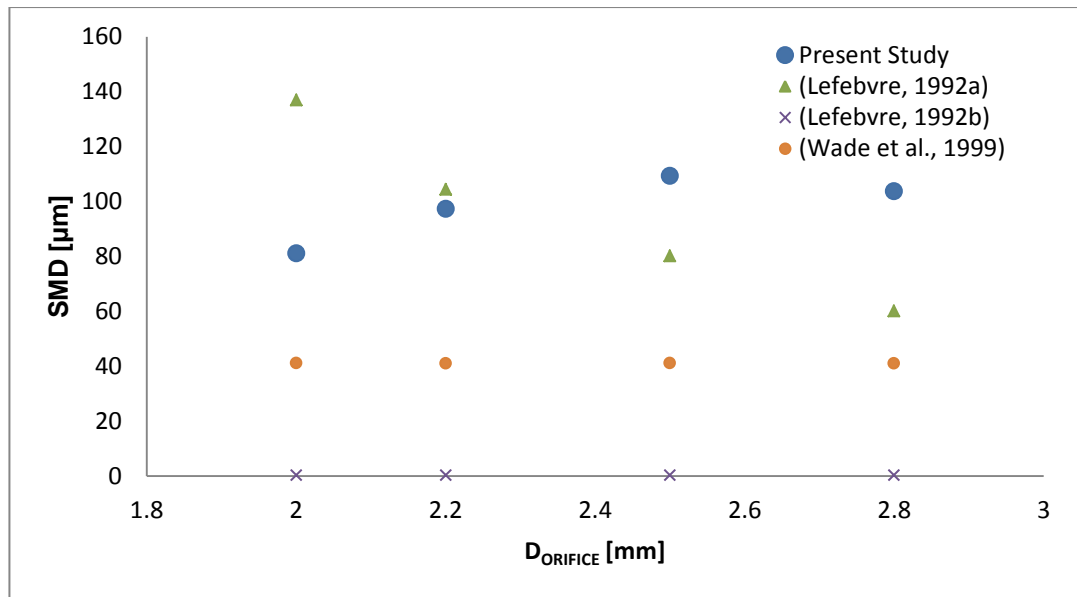


Figure B.8 Comparison of global spray SMD from PDA experiments with that predicted by correlations in the literature.

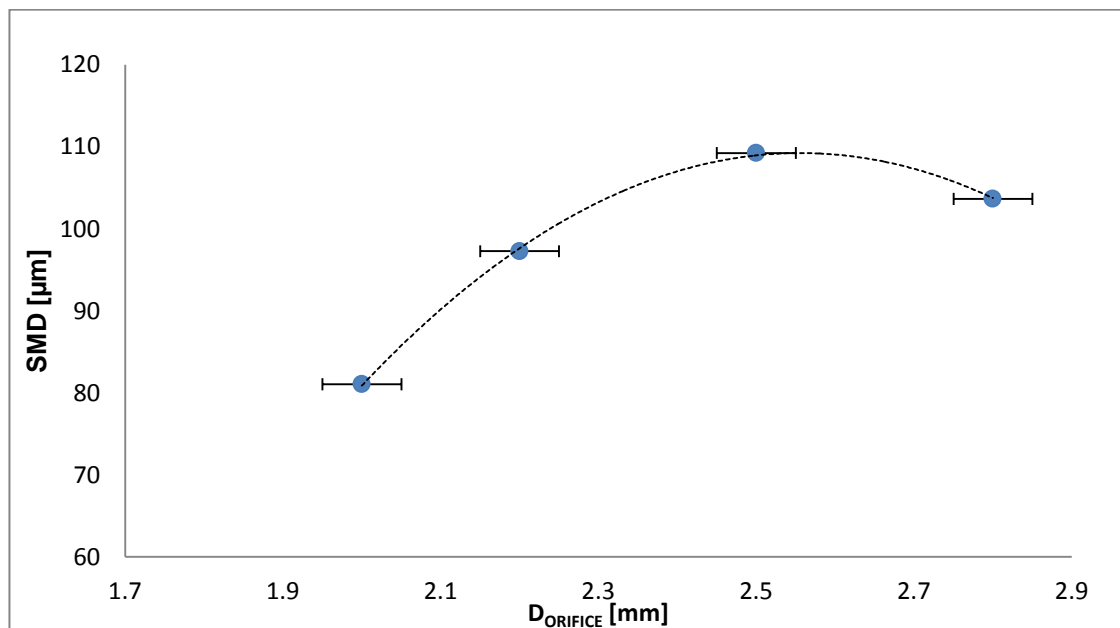


Figure B.9 The relationship between  $D_o$  and global spray droplet SMD as calculated using PDA data.

## Appendix C: Mixing Chamber Diameter Tests

Table C.1 Operating conditions and controlled parameters for  $D_{MC}$  tests.

TEST No. PARAMETER VARIED	1 ALR	2 $\Delta P$	3 $D_O$	4 $L_{MC}$	5 $D_{MC}$	6 $L_O/D_O$	7 A. GEOM.	8 $\eta$
TEST PHASE	A. Initial Operating Parameters		B. Atomiser Geometry				C. Fluid properties	
ALR (%)	0.8-12.5	2		2				
$\Delta P$ (bar.g)	7	4-7		7				
$D_O$ (mm)	2	2	2-4	2	2	2	2	2
$L_{MC}$ (mm)	140	140	140	64-140	140	140	140	140
$D_{MC}$ (mm)	25.4	25.4	25.4	25.4	20-30	25.4	25.4	25.4
$L_O/D_O$ (-)	1	1	1	1	1	0.5-2	1	1
Aerator Geometry	A1	A1	A1	A1	A1	A1	A2, A3	A1
$\eta \times 10^{-8}$ (m <sup>2</sup> /s)	1	1	1	1	1	1	1	2-10

Table C.2 Summary of  $D_{MC}$  test operating conditions and spray characteristics.

Test	$D_{MC} = 20$	$D_{MC} = 25.4$	$D_{MC} = 30$
<b>Water Supply Pressure (barG)</b>	7.35	7.38	7.25
<b>ALR (%)</b>	5.61	5.70	5.78
<b>Mixing Chamber Pressure, <math>\Delta P</math> (barG)</b>	6.63	6.65	6.58
<b><math>m_{WATER}</math> (g/s)</b>	31.70	31.75	31.25
<b><math>P_{AIR}</math> (barG)</b>	7.10	7.23	6.57
<b><math>m_{AIR}</math> (g/s)</b>	1.77	1.81	1.81
<b>Volumetric Void Fraction, <math>\alpha</math> (%)</b>	85.9	86.1	86.3
<b>Effective Power Rating (MW)</b>	1.27	1.27	1.25
<b>Coefficient of Discharge (-)</b>	0.28	0.28	0.27
<b><math>\theta/2</math> at 25 mm downstream (deg)</b>	27.47	25.64	27.47
<b><math>D_{32}</math> (<math>\mu m</math>)</b>	83.28	81.06	87.11

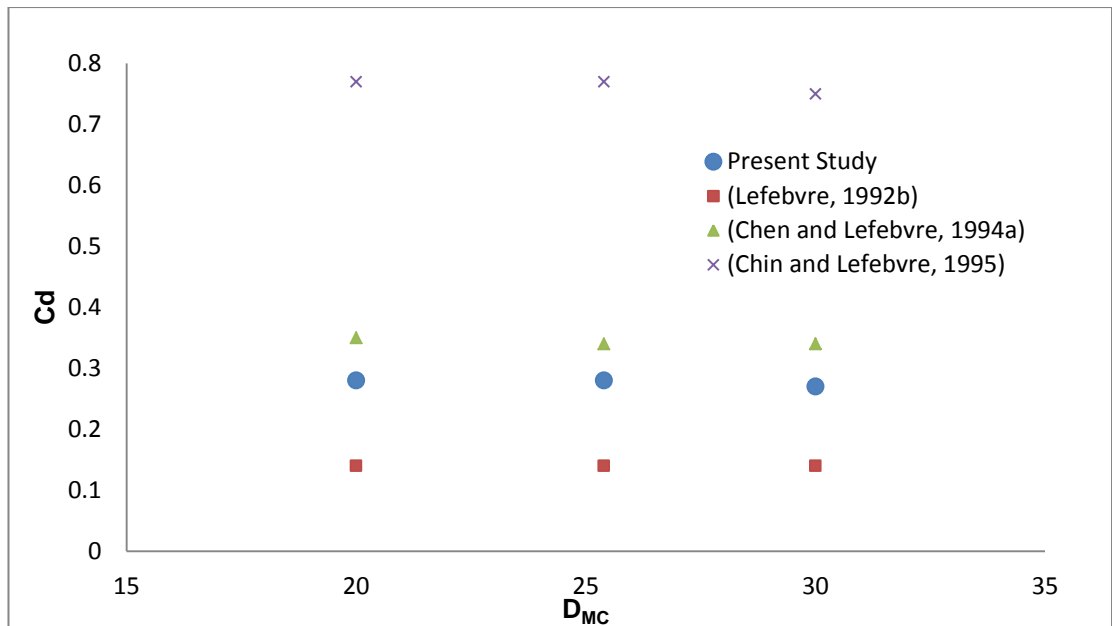


Figure C.1 Comparison of coefficient of discharge from PDA experiments and literature.

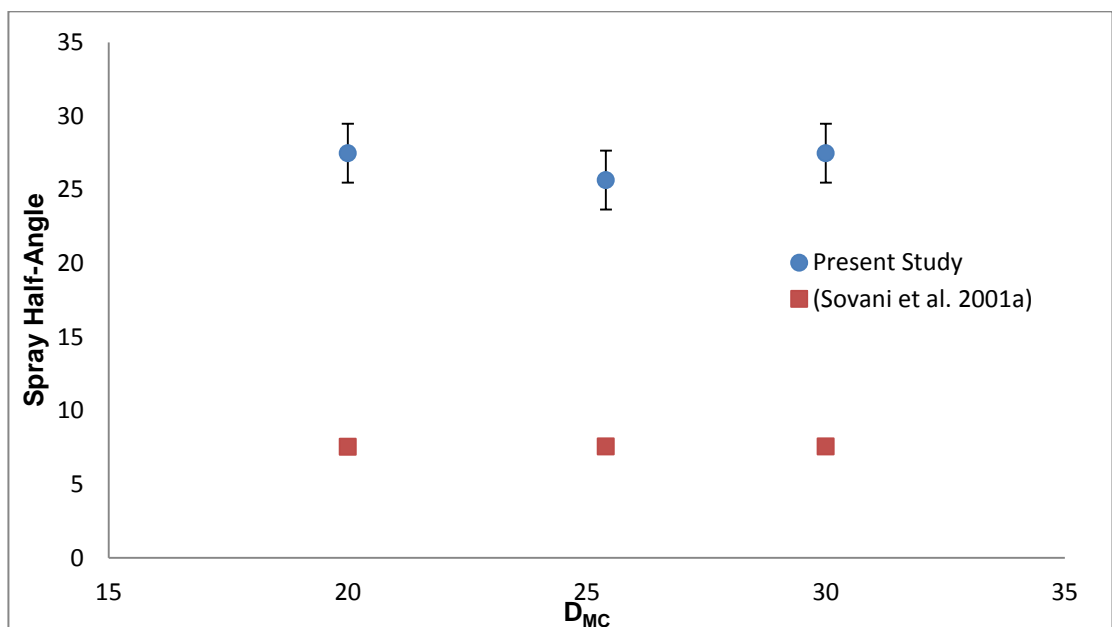


Figure C.2 Comparison of spray half-angle from PDA experiments and literature.

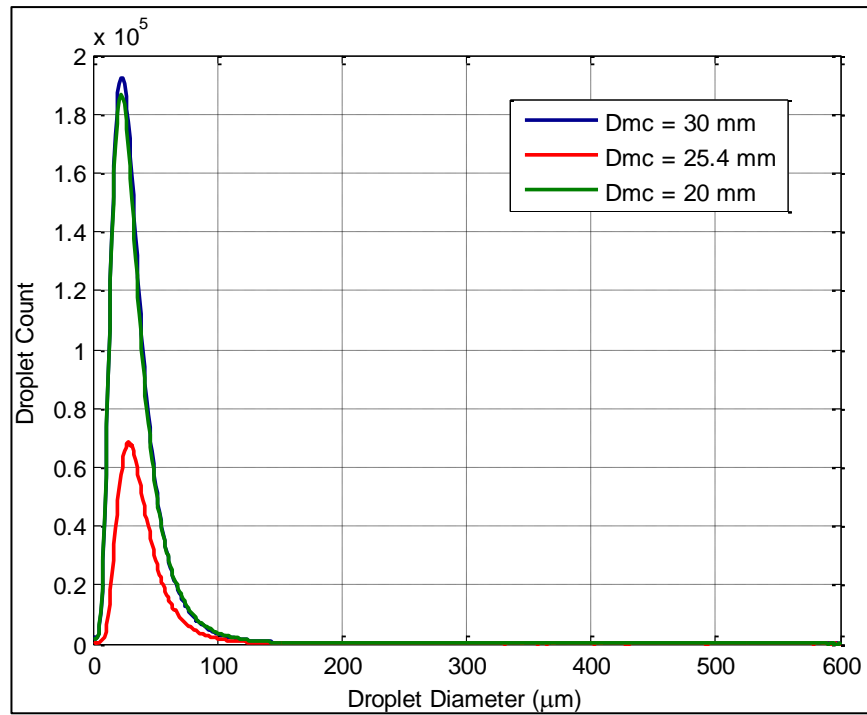


Figure C.3 Droplet diameter frequency distribution based on number.

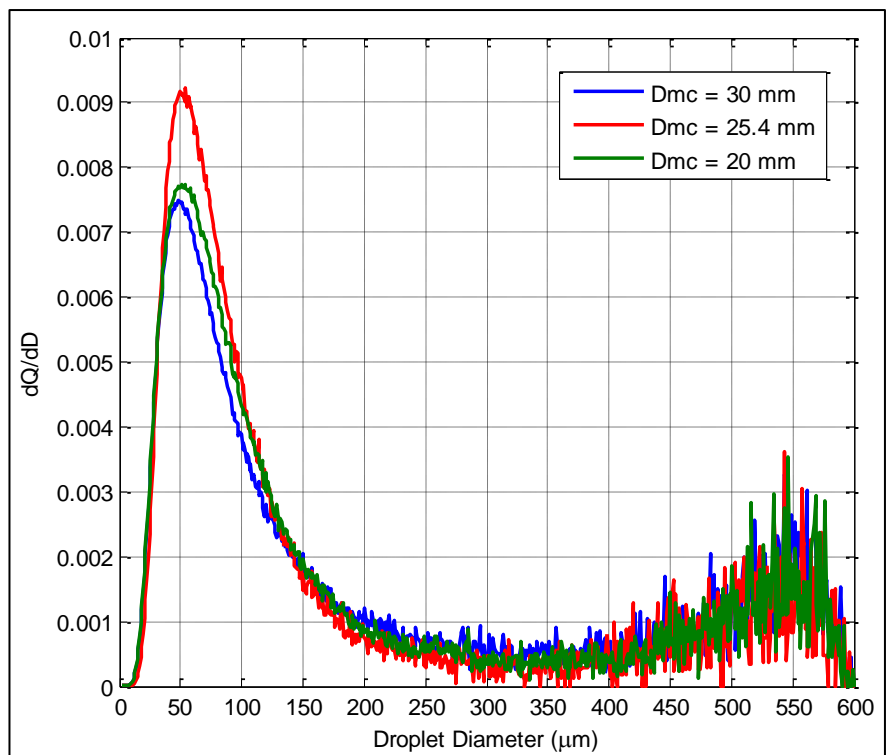


Figure C.4 Droplet diameter frequency distribution by mass.

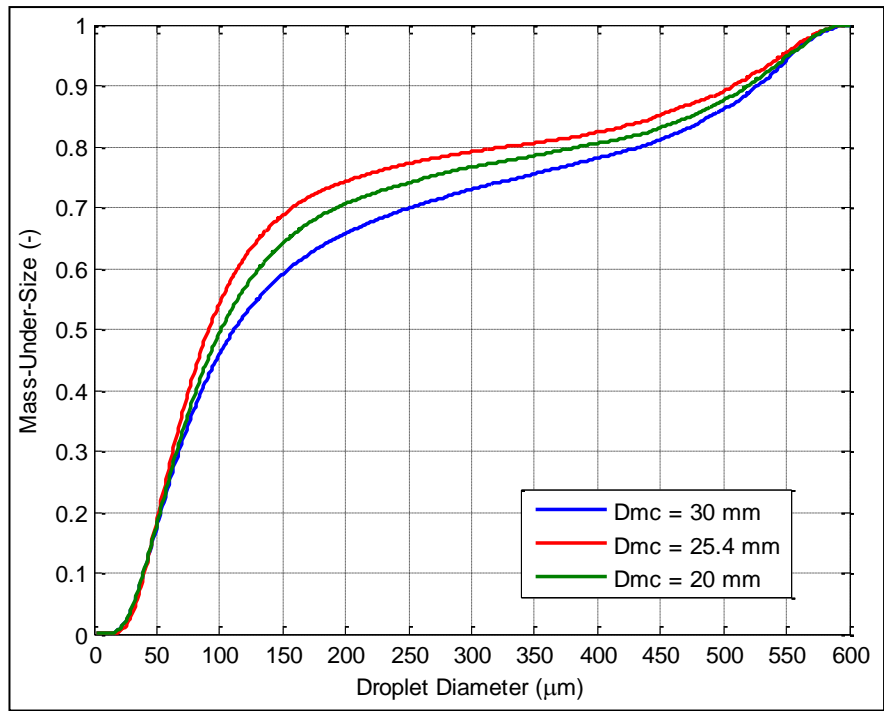


Figure C.5 Cumulative droplet size distribution.

Table C.3 Validated local droplet count varying with  $D_{MC}$  increases.

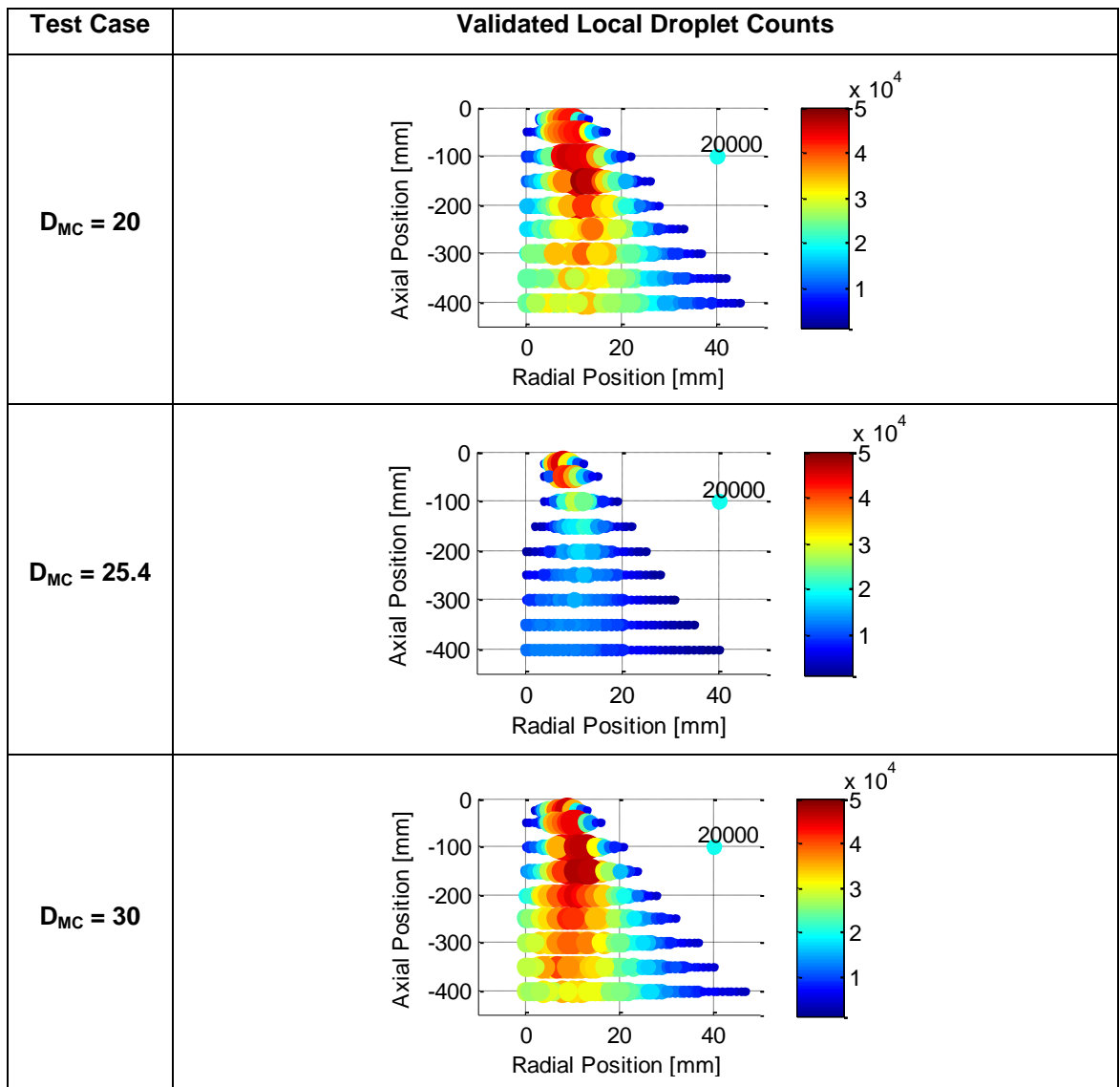


Table C.4 Average local droplet velocity varying with  $D_{MC}$  increases.

Test Case	Local Droplet Velocity
$D_{MC} = 20$	<p>Local Droplet Velocity for <math>D_{MC} = 20</math>. The plot shows velocity vectors in blue on a grid of Axial Position [mm] (0 to -400) and Radial Position [mm] (-10 to 50). A scale bar indicates 50/1 m/s.</p>
$D_{MC} = 25.4$	<p>Local Droplet Velocity for <math>D_{MC} = 25.4</math>. The plot shows velocity vectors in blue on a grid of Axial Position [mm] (0 to -400) and Radial Position [mm] (-10 to 50). A scale bar indicates 50/1 m/s.</p>
$D_{MC} = 30$	<p>Local Droplet Velocity for <math>D_{MC} = 30</math>. The plot shows velocity vectors in blue on a grid of Axial Position [mm] (0 to -400) and Radial Position [mm] (-10 to 50). A scale bar indicates 50/1 m/s.</p>



Table C.5 Inferred local gas and relative velocity varying with  $D_{MC}$  increases.

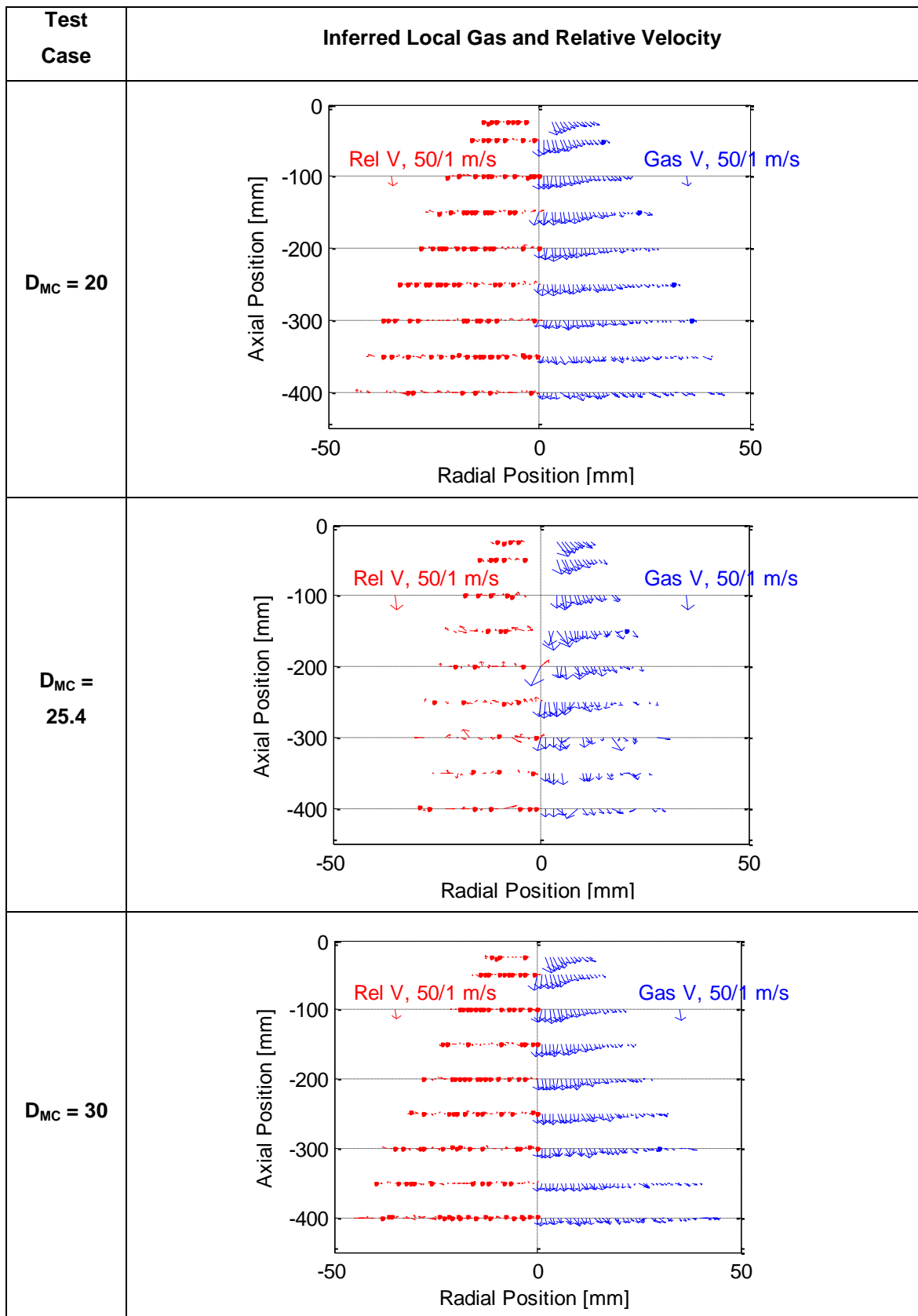


Table C.6 Average local droplet AMD and SMD varying with  $D_{MC}$  increases.

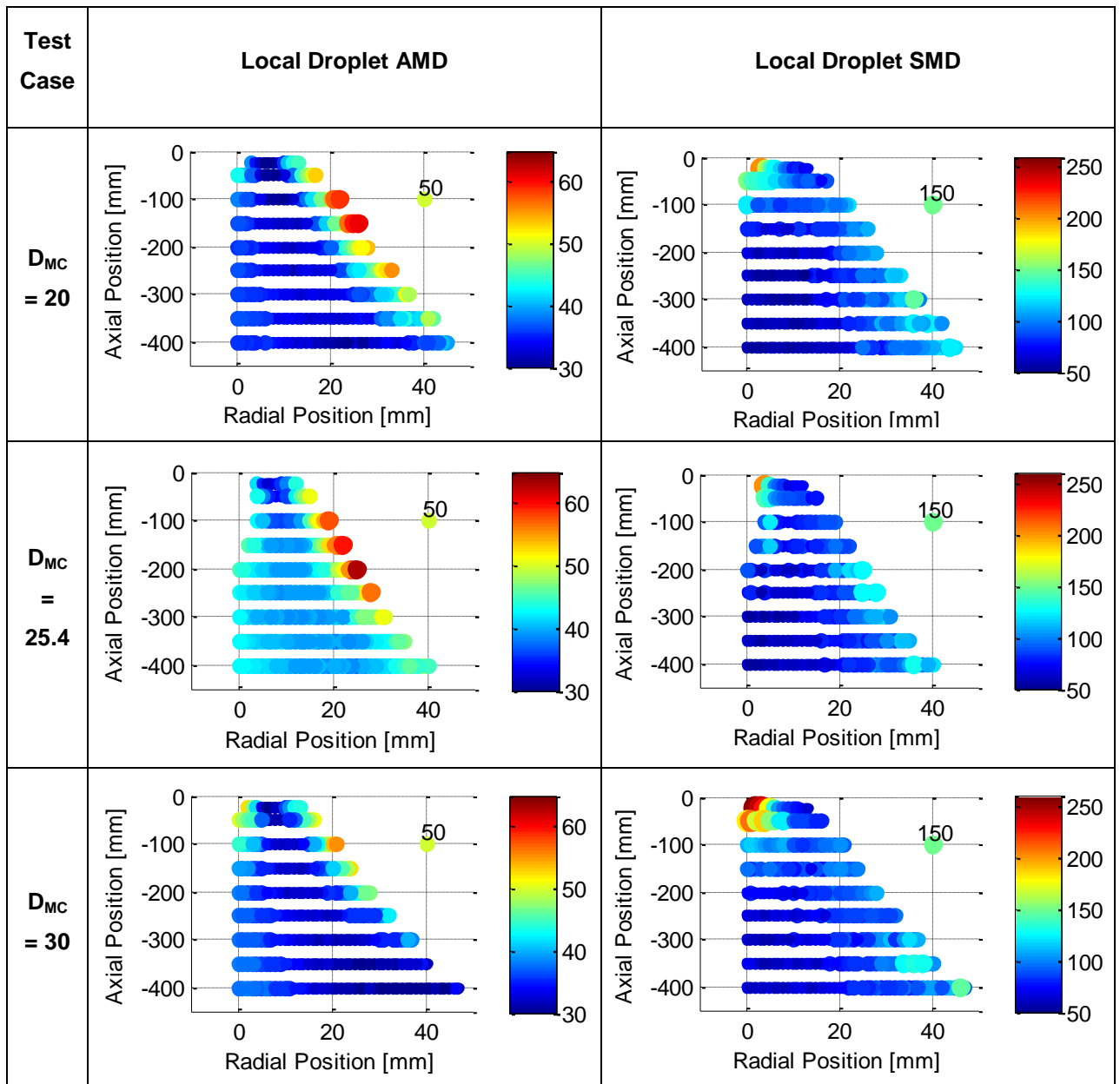


Table C.7 Local SMD/AMD ratio varying with  $D_{MC}$  increases.

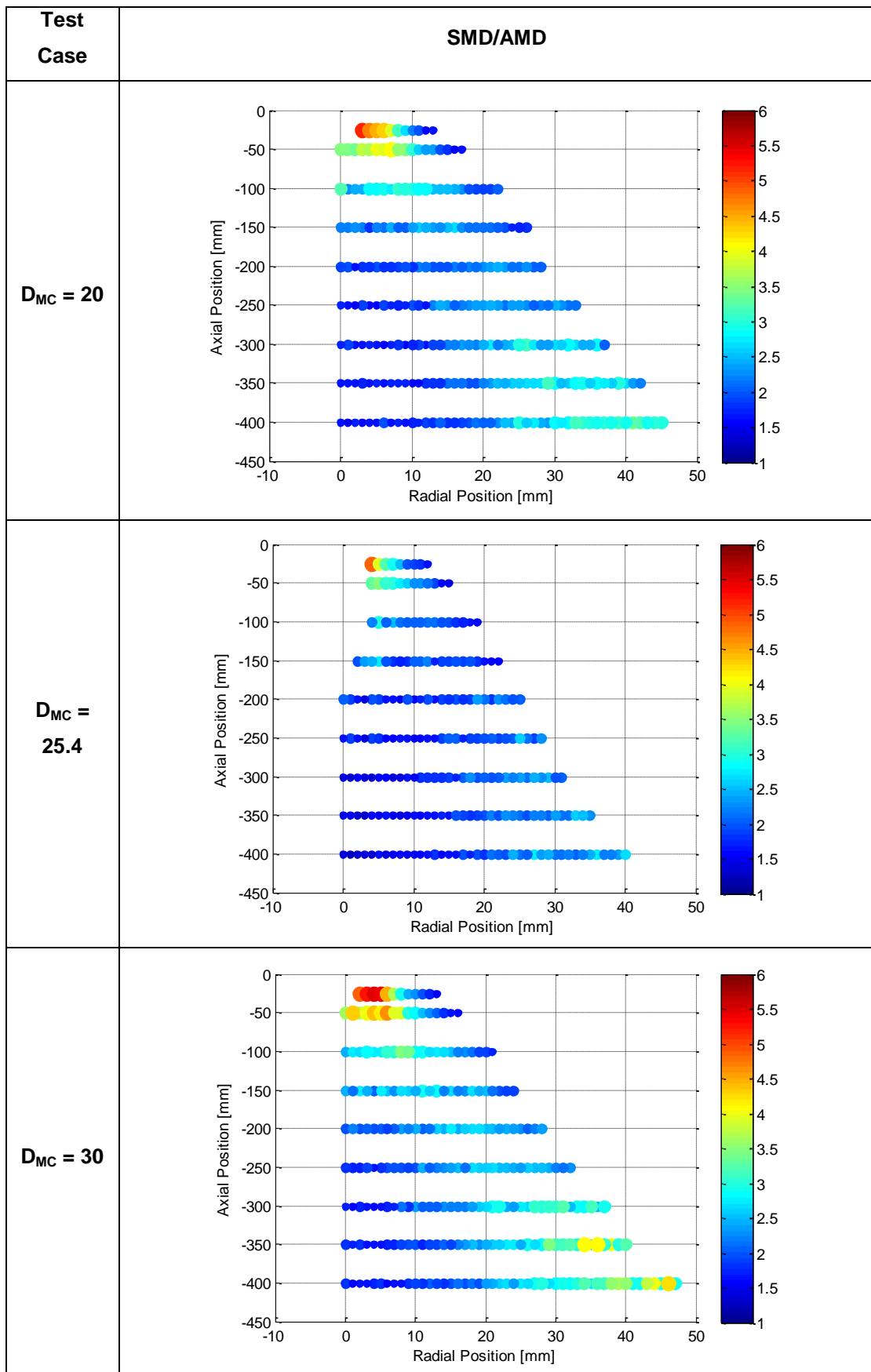


Table C.8 Local average droplet Weber number varying with  $D_{MC}$  increases.

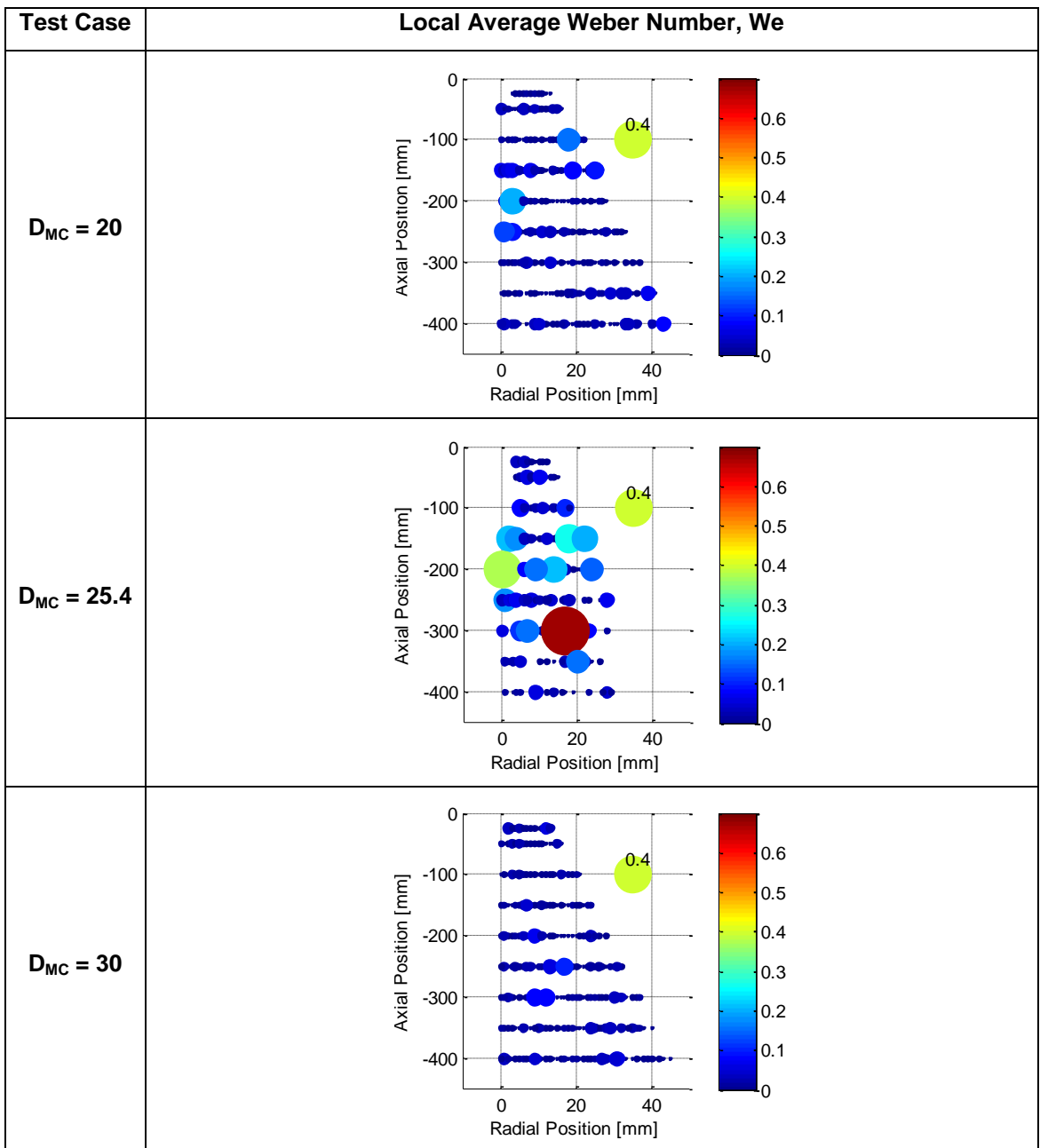
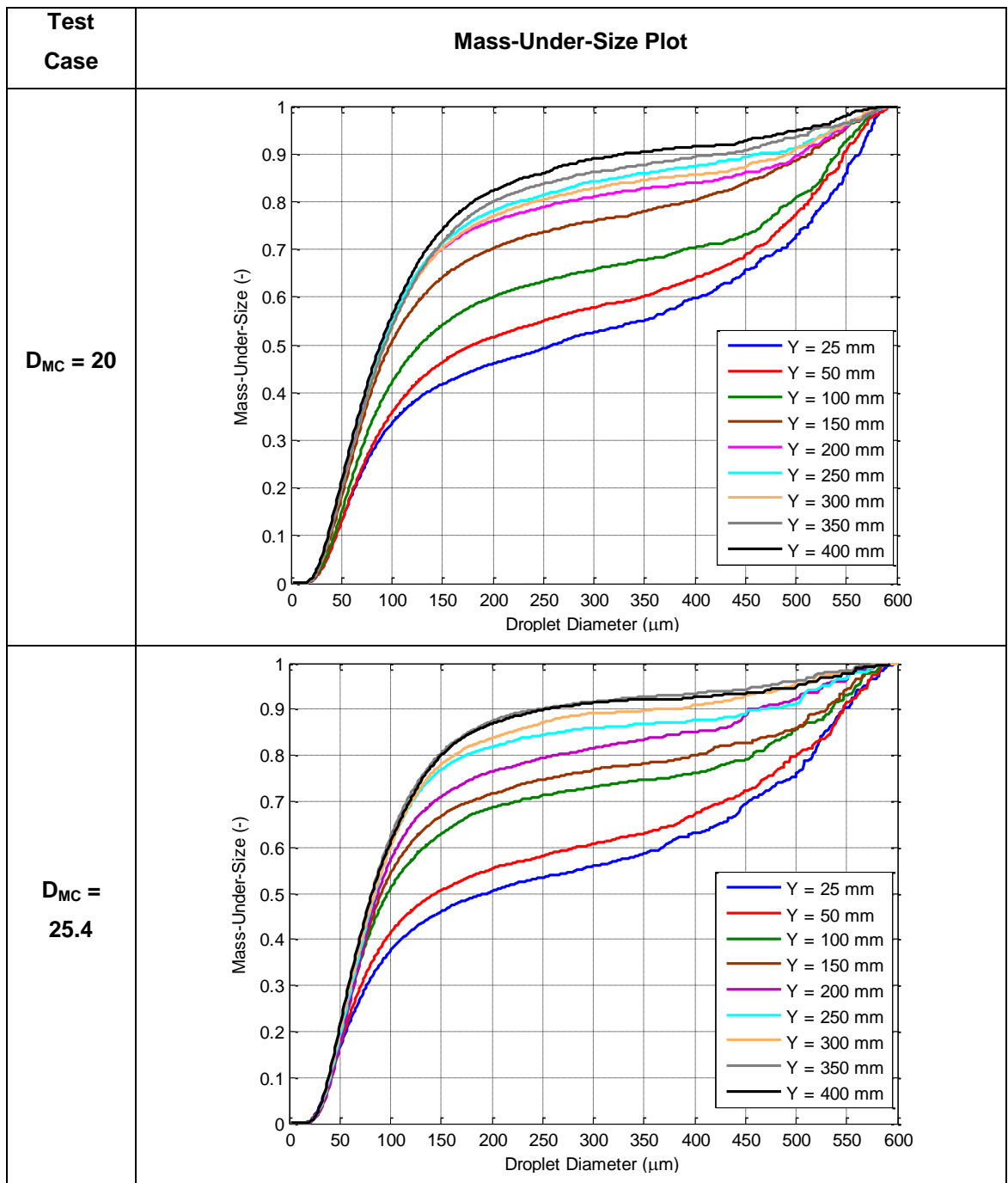
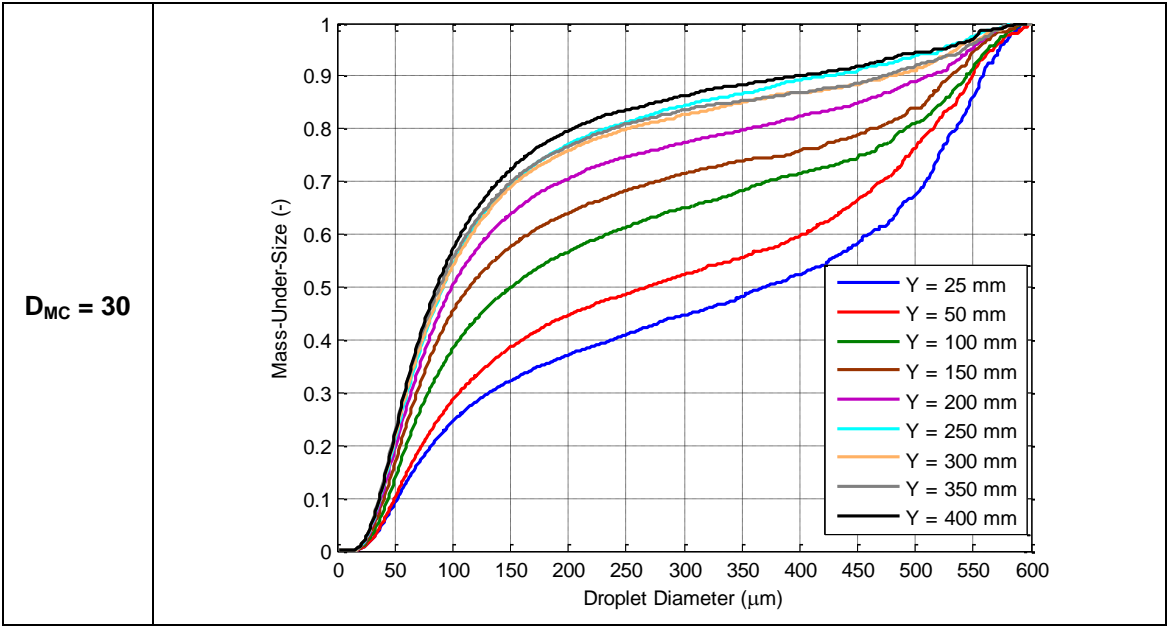


Table C.9 Cumulative mass-under-size plots for entire downstream locations.





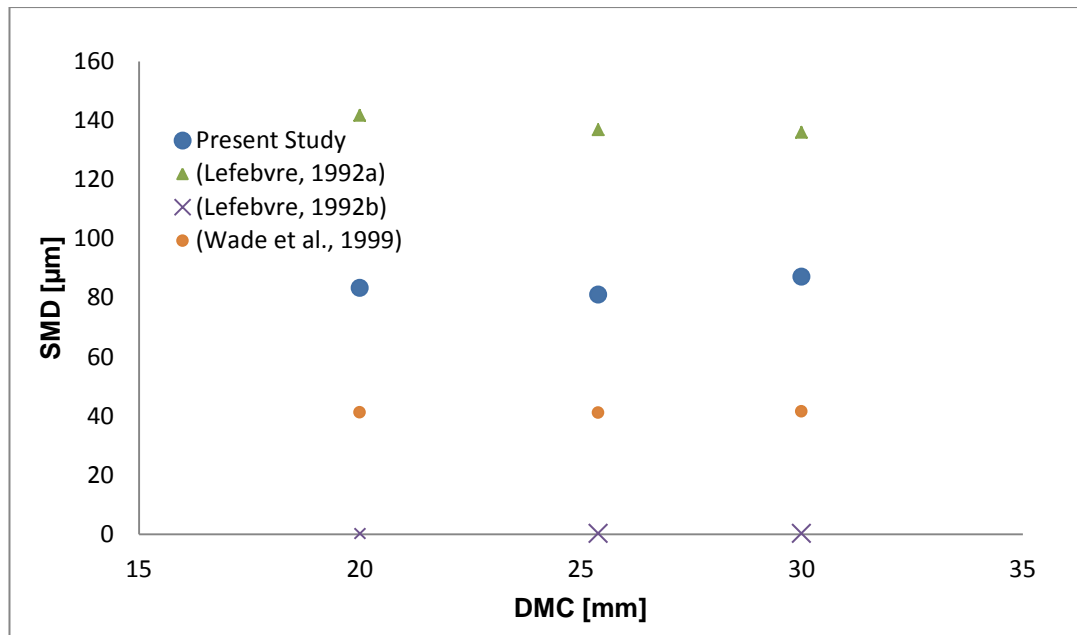


Figure C.6 Comparison of global spray droplet SMD from PDA experiments with that predicted by correlations in the literature.

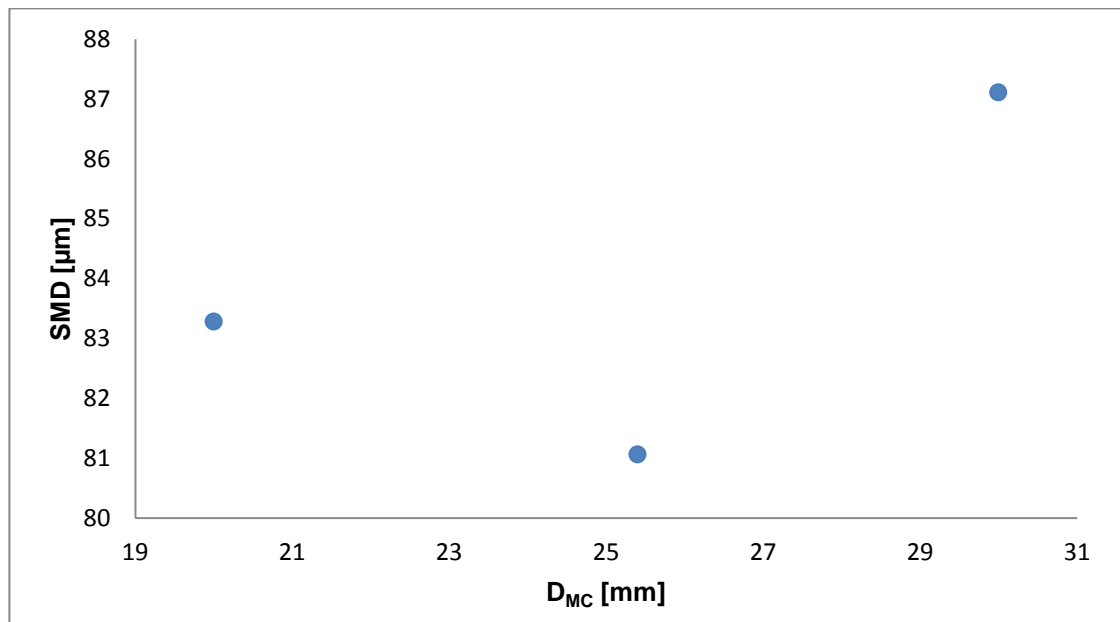


Figure C.7 The relationship between  $D_{MC}$  and global spray droplet SMD as calculated using PDA data.

## Appendix D: Exit Orifice Length-to-Diameter Ratio Tests

Table D.1 Operating conditions and controlled parameters for  $L_o/D_o$  tests.

TEST No. PARAMETER VARIED	1 ALR	2 $\Delta P$	3 $D_o$	4 $L_{MC}$	5 $D_{MC}$	6 $L_o/D_o$	7 A. GEOM.	8 $\eta$
TEST PHASE	A. Initial Operating Parameters		B. Atomiser Geometry				C. Fluid properties	
ALR (%)	0.8-12.5	2		2				
$\Delta P$ (bar.g)	7	4-7		7				
$D_o$ (mm)	2	2	2-4	2	2	2	2	2
$L_{MC}$ (mm)	140	140	140	64-140	140	140	140	140
$D_{MC}$ (mm)	25.4	25.4	25.4	25.4	20-30	25.4	25.4	25.4
$L_o/D_o$ (-)	1	1	1	1	1	0.5-2	1	1
Aerator Geometry	A1	A1	A1	A1	A1	A1	A2, A3	A1
$\eta \times 10^{-6}$ (m <sup>2</sup> /s)	1	1	1	1	1	1	1	2-10

Table D.2 Summary of  $L_o/D_o$  test operating conditions and spray characteristics.

Test	$L_o/D_o = 0.5$	$L_o/D_o = 1$	$L_o/D_o = 1.5$	$L_o/D_o = 2$
<b>Water Supply Pressure (barG)</b>	7.49	7.38	7.32	7.51
<b>ALR (%)</b>	5.79	5.70	5.76	5.85
<b>Mixing Chamber Pressure, <math>\Delta P</math> (barG)</b>	6.71	6.65	6.57	6.75
<b><math>m_{WATER}</math> (g/s)</b>	40.02	31.75	34.12	33.97
<b><math>P_{AIR}</math> (barG)</b>	7.31	7.23	7.13	7.29
<b><math>m_{AIR}</math> (g/s)</b>	2.31	1.81	1.96	1.98
<b>Volumetric Void Fraction, <math>\alpha</math> (%)</b>	86.3	86.1	86.3	86.4
<b>Effective Power Rating (MW)</b>	1.60	1.27	1.36	1.36
<b>Coefficient of Discharge (-)</b>	0.35	0.28	0.30	0.29
<b><math>\theta/2</math> at 25 mm downstream (deg)</b>	29.25	25.64	29.25	29.25
<b><math>D_{32}</math> (<math>\mu m</math>)</b>	89.12	81.06	94.77	113.04



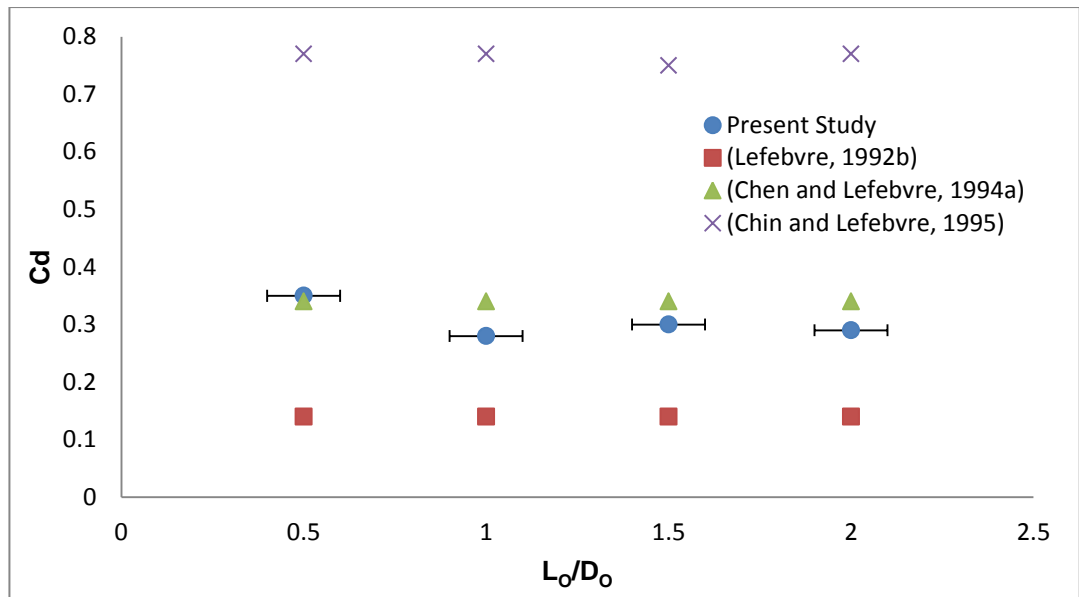


Figure D.1 Comparison of coefficient of discharge from PDA experiments and literature.

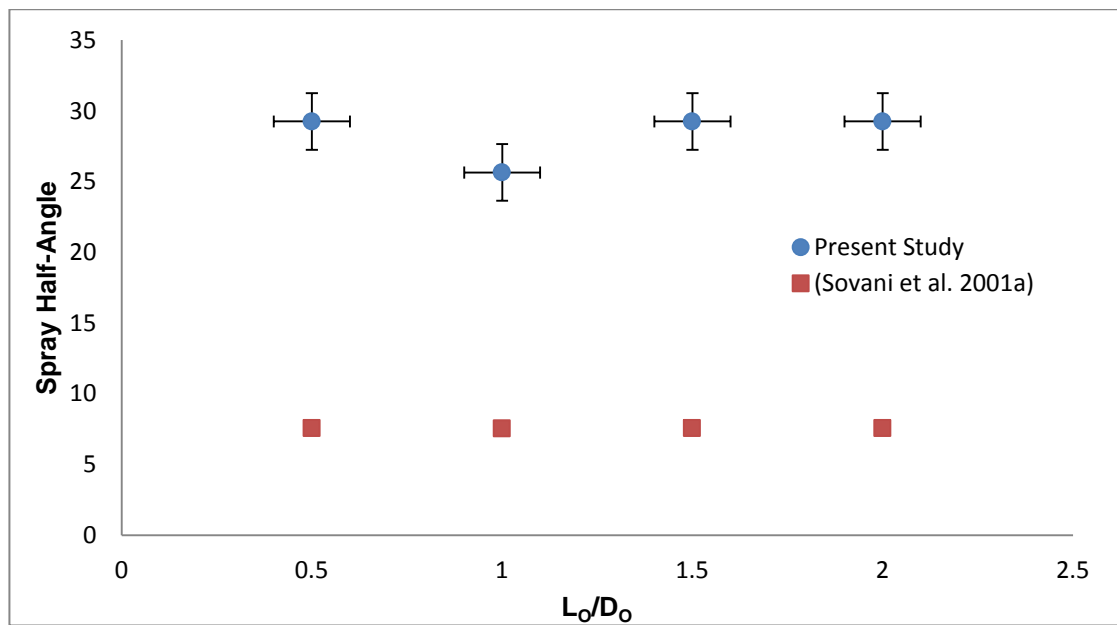


Figure D.2 Comparison of spray half-angle from PDA experiments and literature.

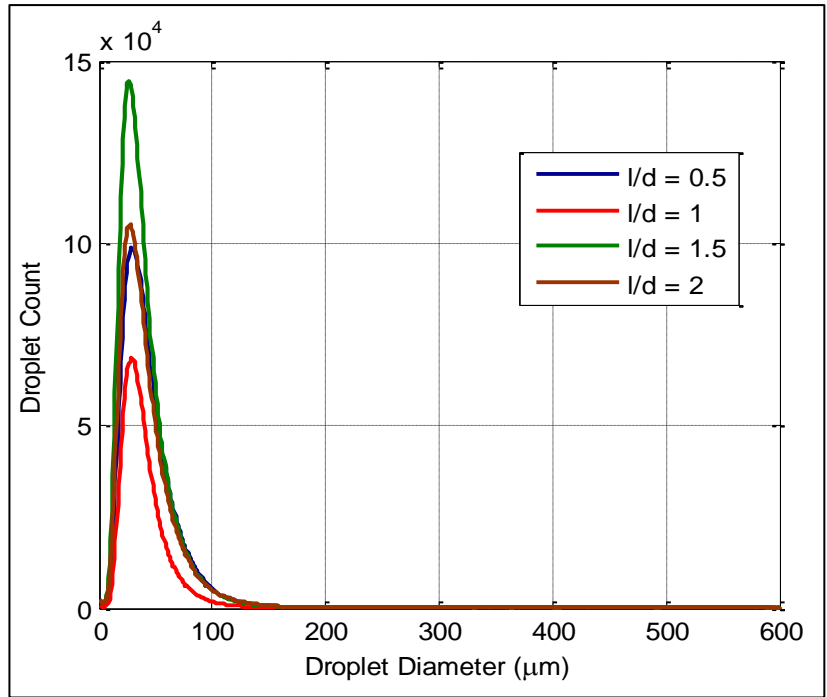


Figure D.3 Droplet diameter frequency distribution based on number.

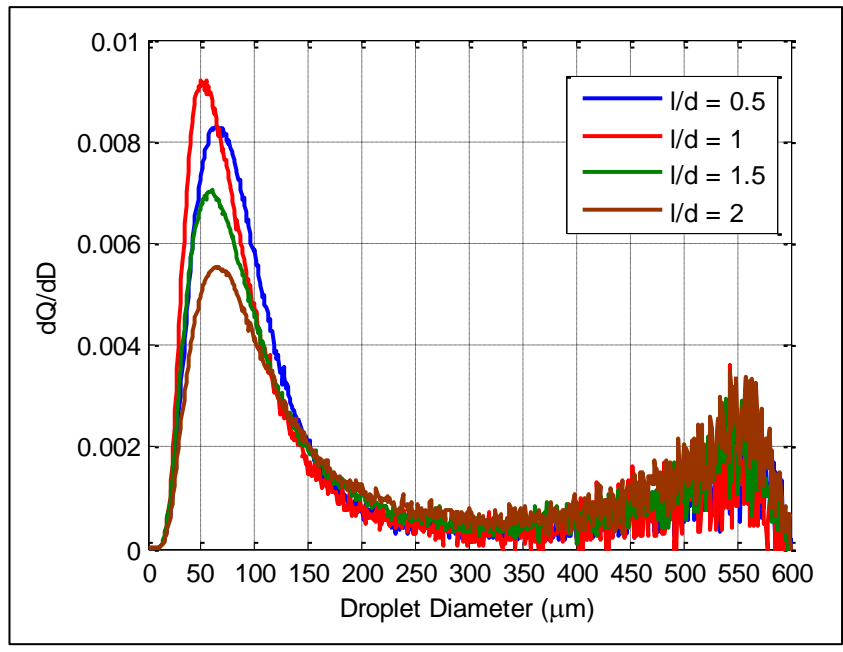


Figure D.4 Droplet diameter frequency distribution by mass.

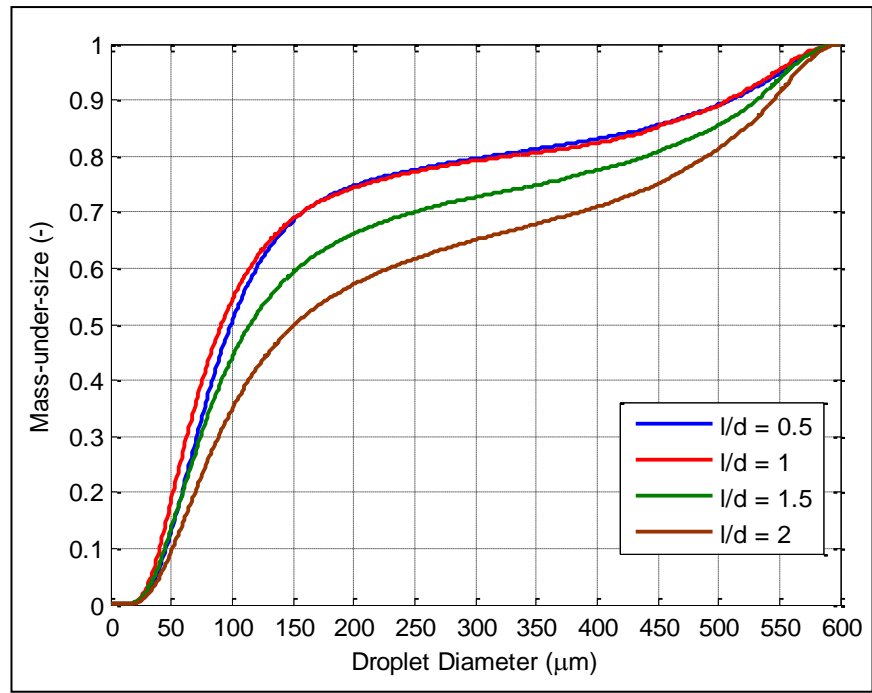


Figure D.5 Cumulative droplet size distribution.

Table D.3 Validated local droplet count varying with  $L_0/D_0$  increases.

Test Case	Validated Local Droplet Counts
$L_0/D_0 = 0.5$	
$L_0/D_0 = 1$	
$L_0/D_0 = 1.5$	
$L_0/D_0 = 2$	

Table D.4 Average local droplet velocity varying with  $L_o/D_o$  increases.

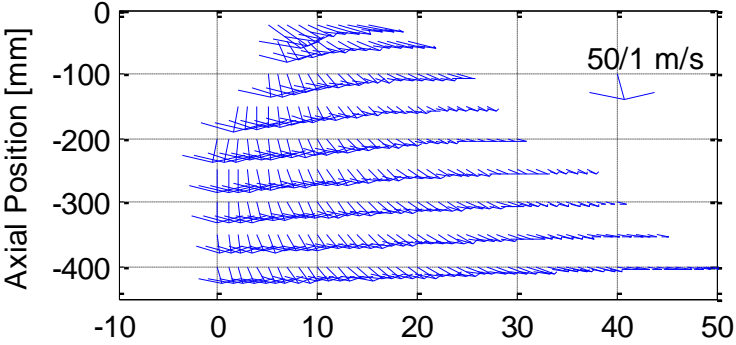
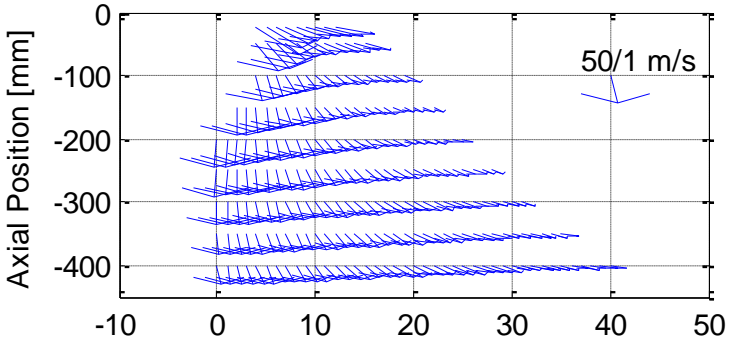
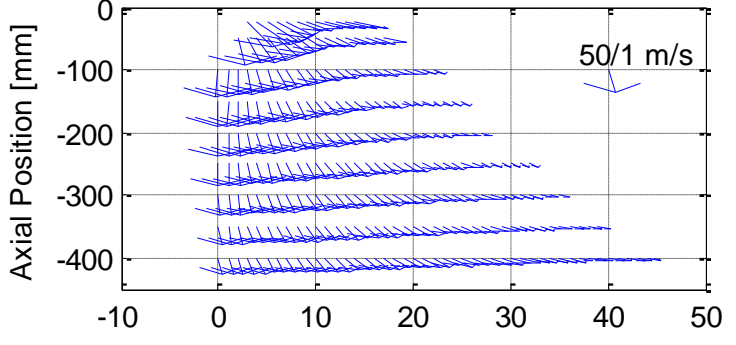
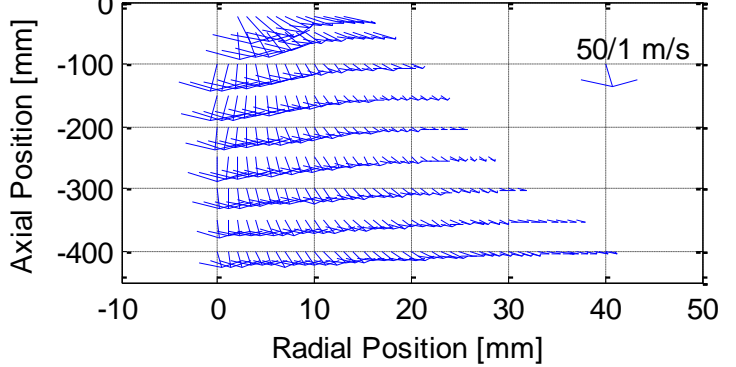
Test Case	Local Droplet Velocity
$L_o/D_o = 0.5$	
$L_o/D_o = 1$	
$L_o/D_o = 1.5$	
$L_o/D_o = 2$	

Table D.5 Inferred local gas and relative velocity varying with  $L_0/D_0$  increases.

Test Case	Inferred Local Gas and Relative Velocity
$L_0/D_0 = 0.5$	
$L_0/D_0 = 1$	
$L_0/D_0 = 1.5$	

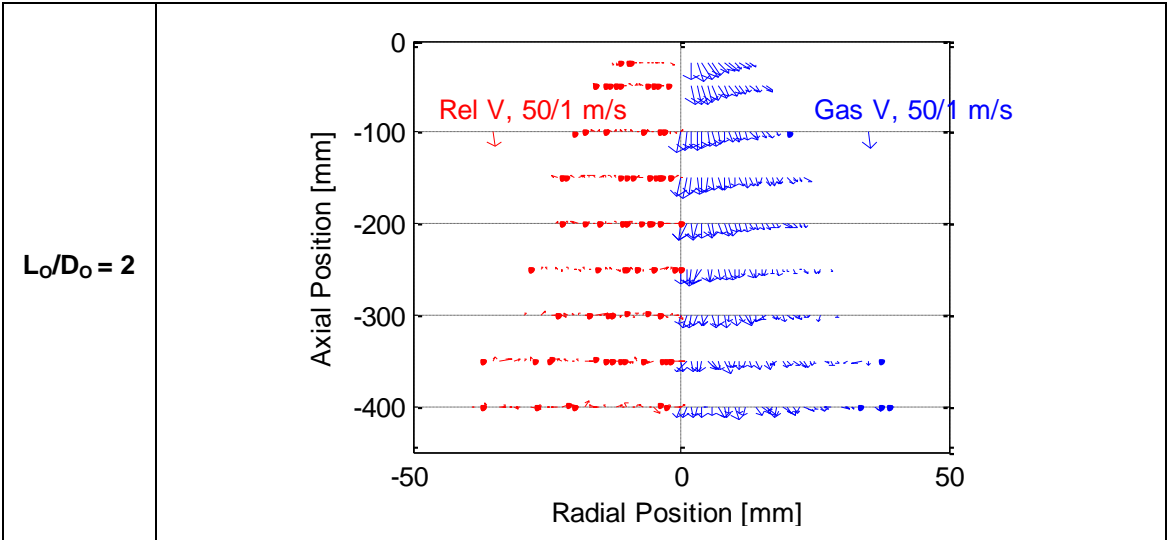


Table D.6 Average local droplet AMD and SMD varying with  $L_o/D_o$  increases.

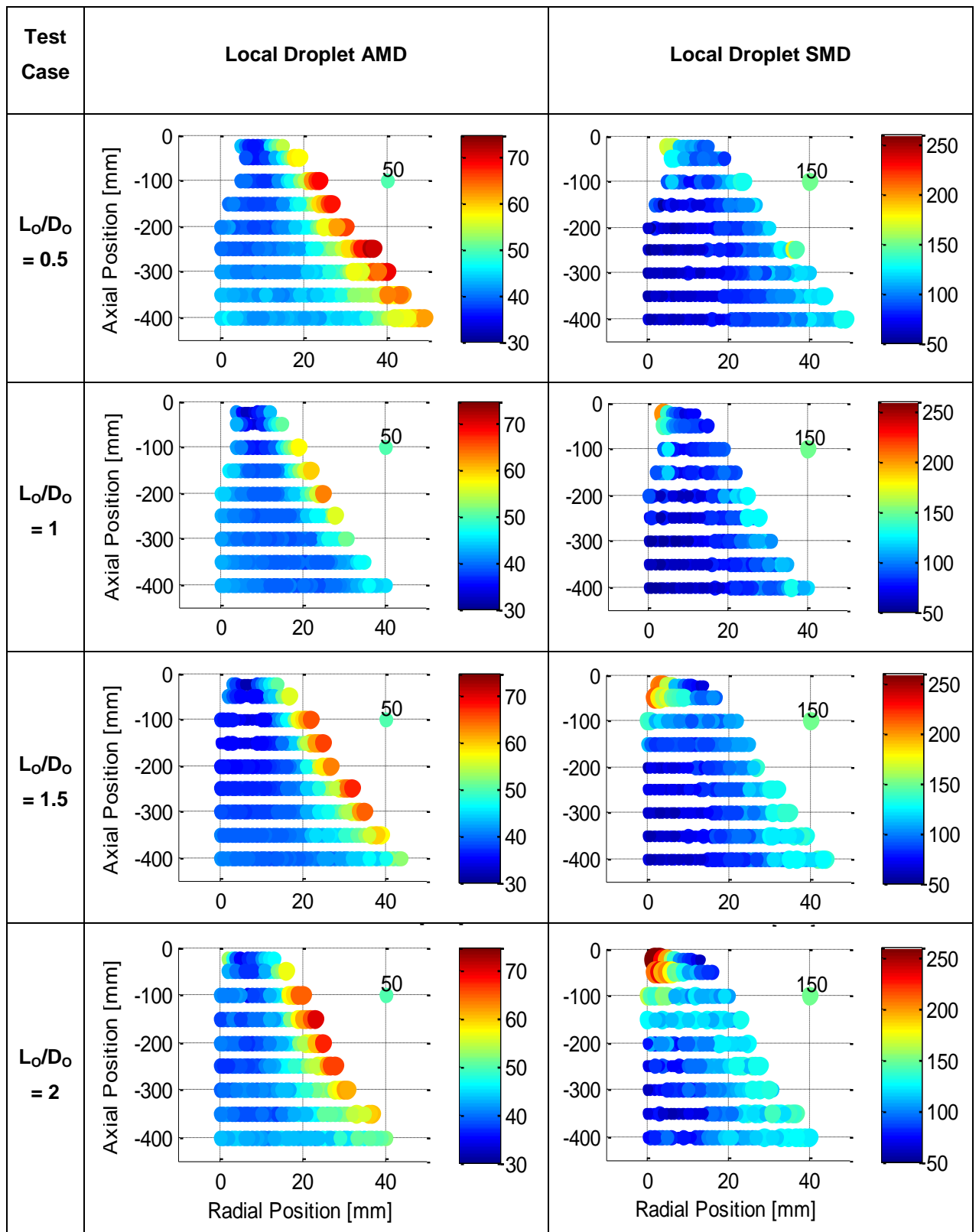
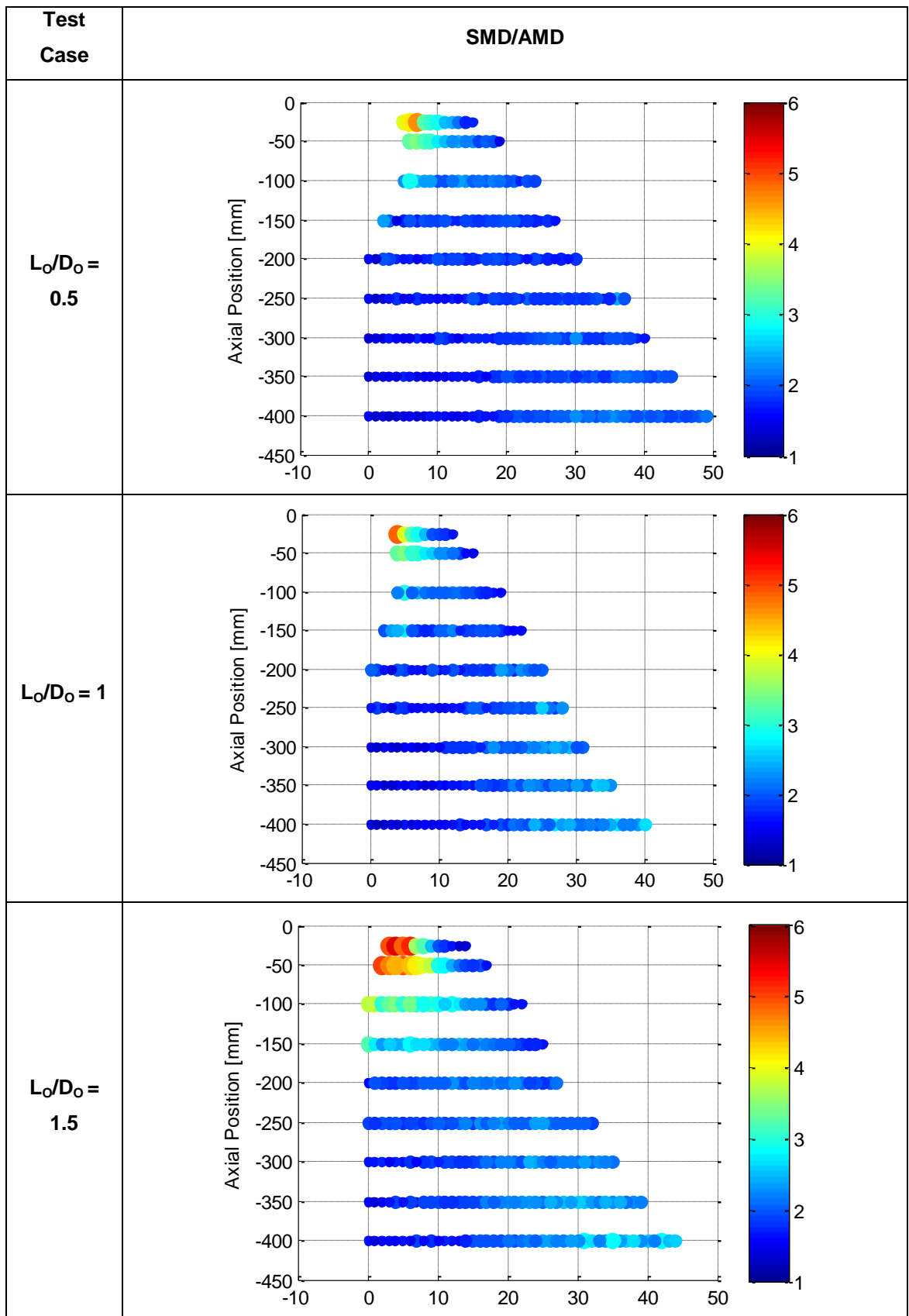




Table D.7 Local SMD/AMD ratio varying with  $L_0/D_0$  increases.



$L_0/D_0 = 2$

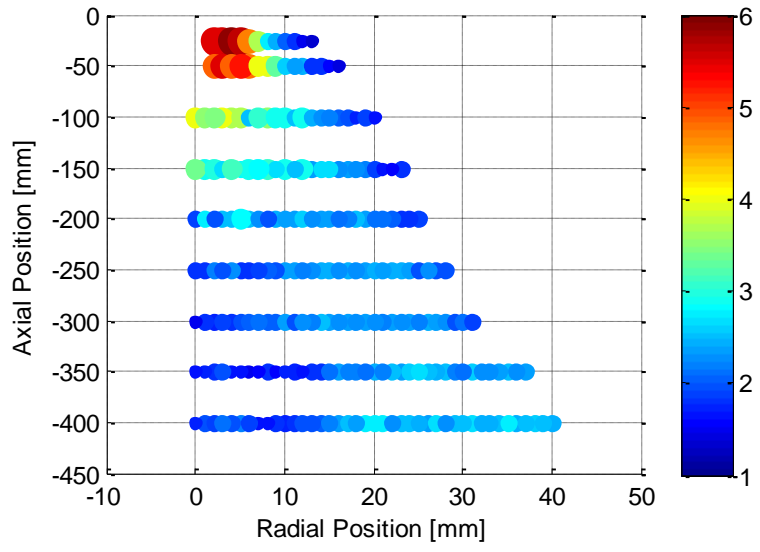


Table D.8 Local average droplet Weber number varying with  $L_0/D_0$  increases.

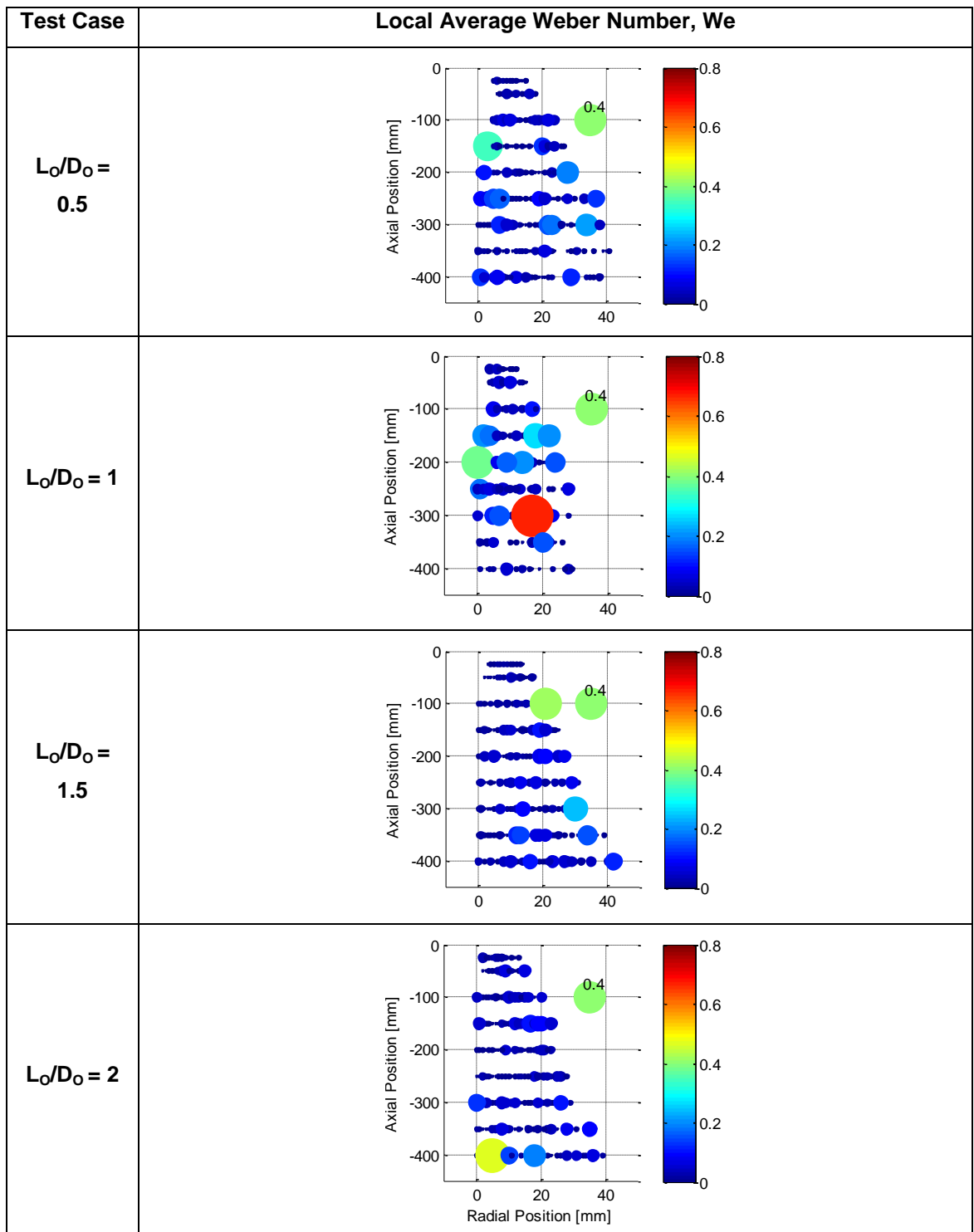
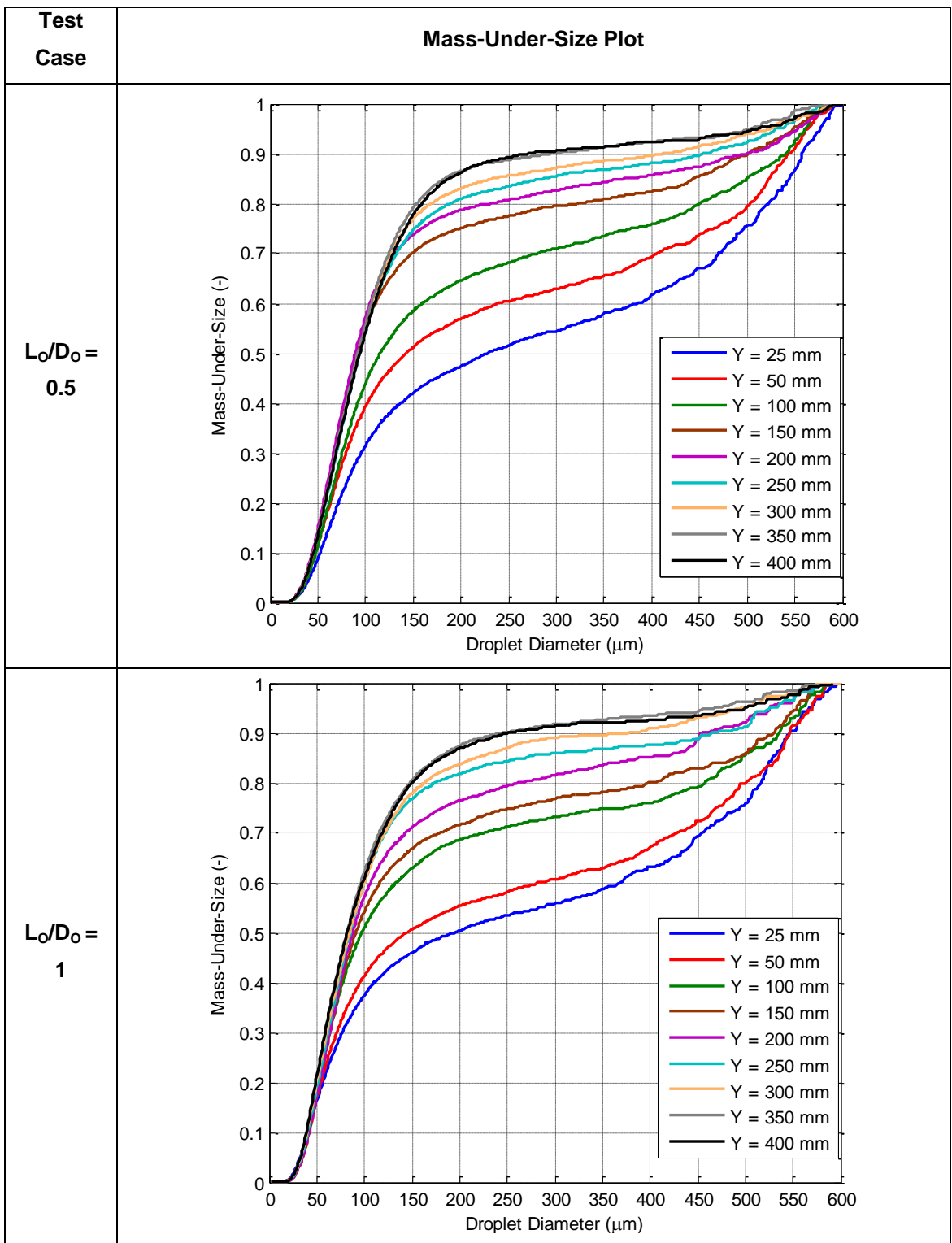
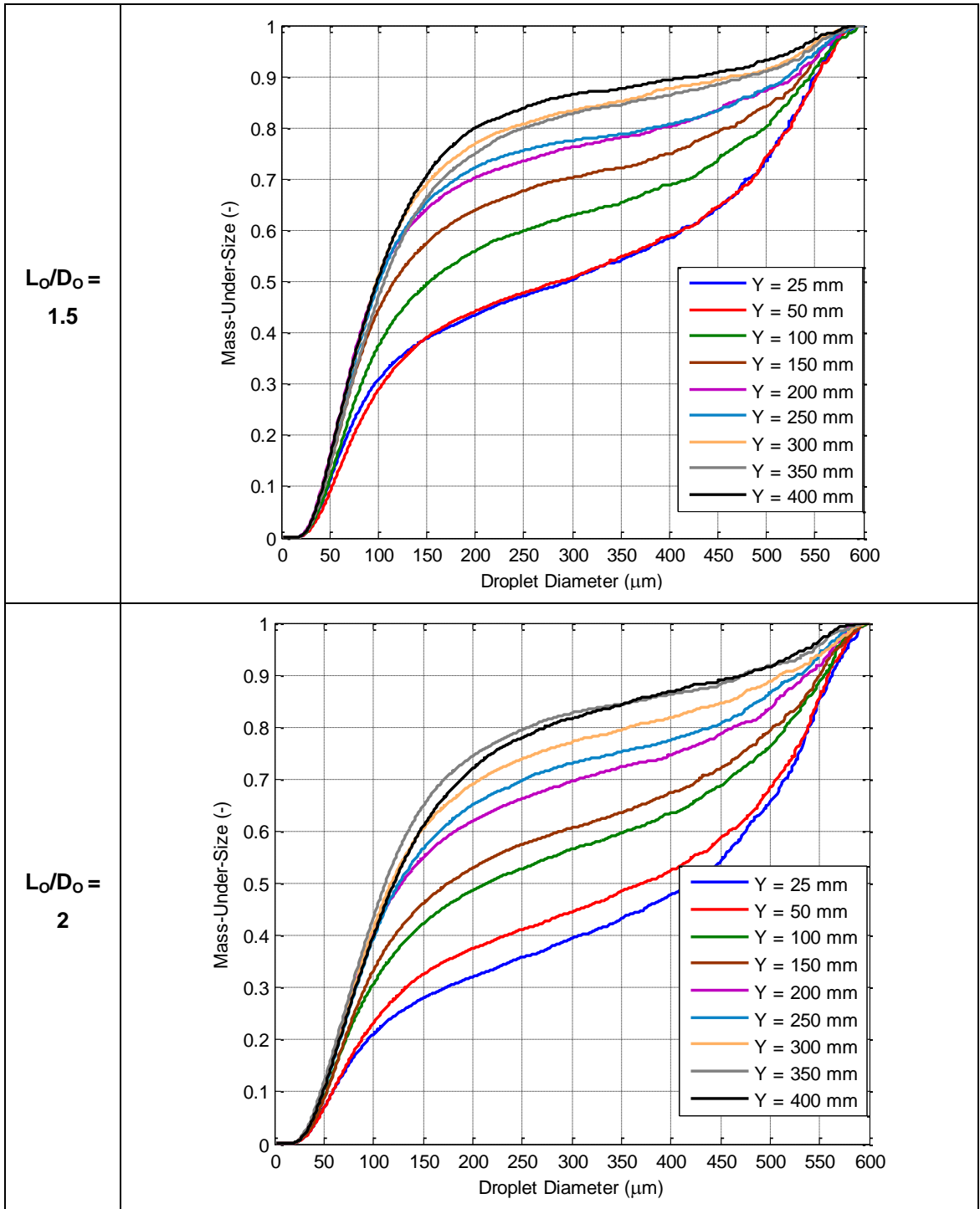


Table D.9 Cumulative mass-under-size plots for entire downstream locations.





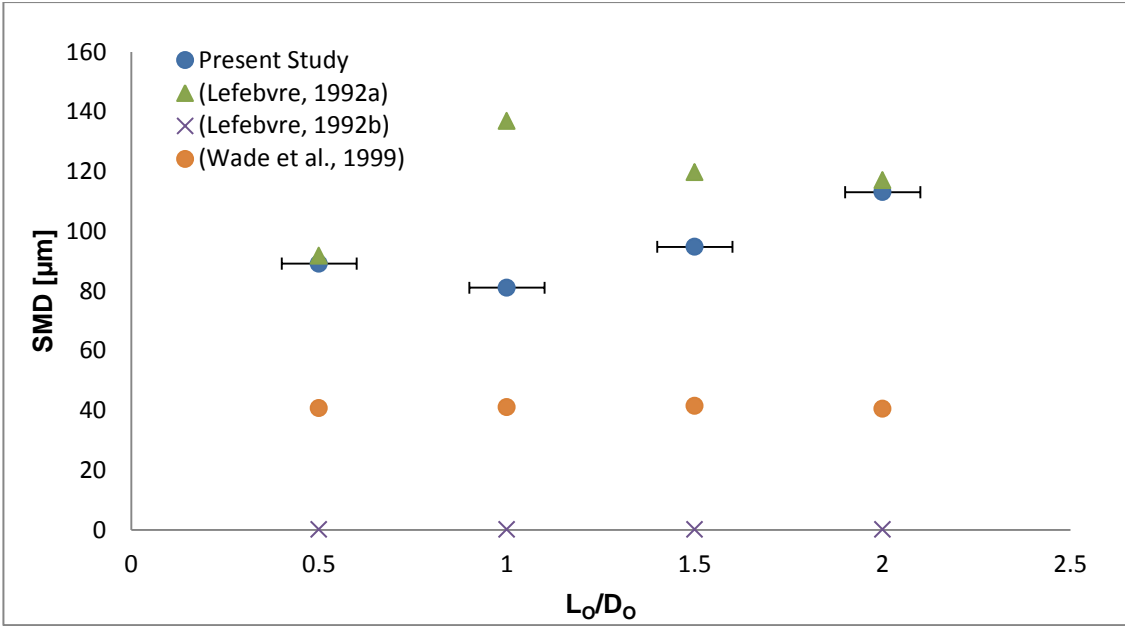


Figure D.6 Comparison of global spray droplet SMD from PDA experiments with that predicted by correlations in the literature.

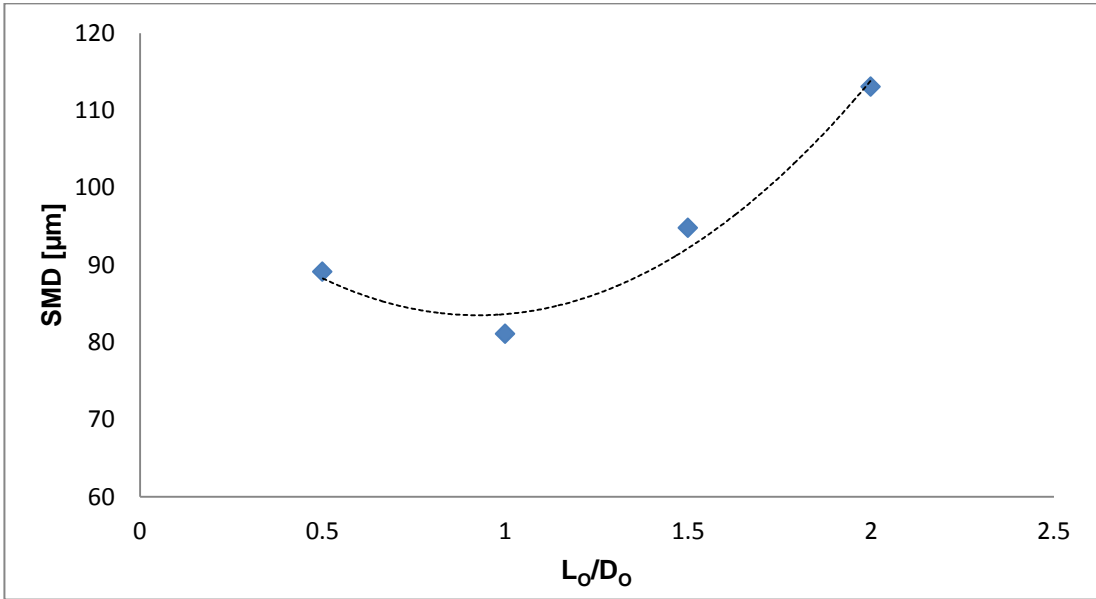


Figure D.7 The relationship between  $L_0/D_0$  and global spray SMD as calculated using PDA data.

## Appendix E: Aerator Geometry Tests

Table E.1 Operating conditions and controlled parameters for aerator geometry tests.

TEST No. PARAMETER VARIED	1 ALR	2 $\Delta P$	3 $D_O$	4 $L_{MC}$	5 $D_{MC}$	6 $L_O/D_O$	7 A. GEOM.	8 $\eta$
TEST PHASE	A. Initial Operating Parameters		B. Atomiser Geometry				C. Fluid properties	
ALR (%)	0.8-12.5	2		2				
$\Delta P$ (bar.g)	7	4-7		7				
$D_O$ (mm)	2	2	2-4	2	2	2	2	2
$L_{MC}$ (mm)	140	140	140	64-140	140	140	140	140
$D_{MC}$ (mm)	25.4	25.4	25.4	25.4	20-30	25.4	25.4	25.4
$L_O/D_O$ (-)	1	1	1	1	1	0.5-2	1	1
Aerator Geometry	A1	A1	A1	A1	A1	A1	A2, A3	A1
$\eta \times 10^{-6}$ (m <sup>2</sup> /s)	1	1	1	1	1	1	1	2-10

Table E.2 Side on view of aerators investigated showing location of air injector holes (not to scale)

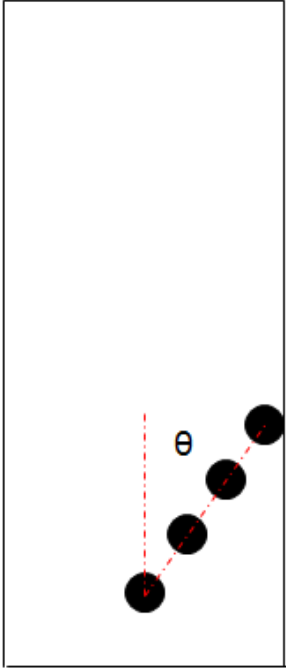
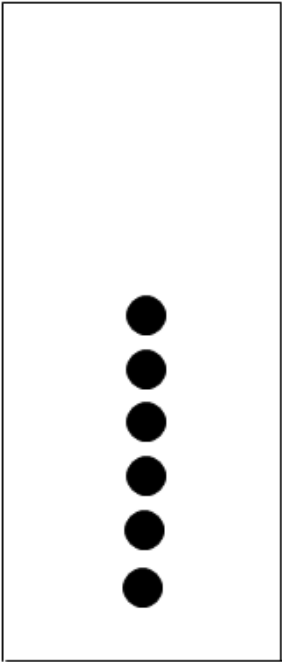
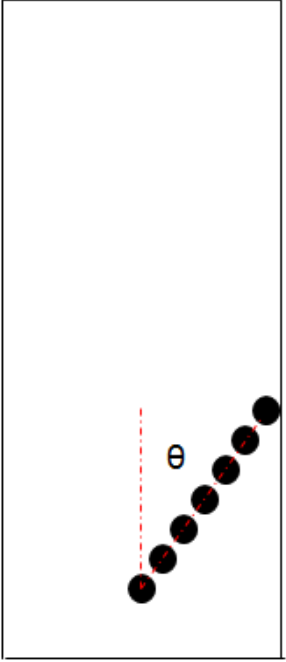
Aerator Geometry 1	Aerator Geometry 2	Aerator Geometry 3
		
6 x 2.5 mm diameter aerator holes; $\theta = 26.57^\circ$	6 x 2.6 mm diameter aerator holes; $\theta = 0^\circ$	10 x 2 mm diameter aerator holes; $\theta = 26.57^\circ$
Baseline aerator	Investigates influence of <b>air injector hole radial symmetry</b>	Investigates influence of <b>aerating hole diameter</b>

Table E.3 Summary of aerator geometry test operating conditions and spray characteristics.

Test	A1	A2	A3
Water Supply Pressure (barG)	7.38	7.37	7.28
ALR (%)	5.70	5.71	5.62
Mixing Chamber Pressure, $\Delta P$ (barG)	6.65	6.69	6.60
$m_{\text{WATER}}$ (g/s)	31.75	33.26	31.55
$P_{\text{AIR}}$ (barG)	7.23	7.18	6.95
$m_{\text{AIR}}$ (g/s)	1.81	1.90	1.77
Volumetric Void Fraction, $\alpha$ (%)	86.1	86.2	86.0
Effective Power Rating (MW)	1.27	1.33	1.26
Coefficient of Discharge (-)	0.28	0.29	0.28
$\theta/2$ at 25 mm downstream (deg)	25.64	27.47	27.47
$D_{32}$ ( $\mu\text{m}$ )	81.06	69.14	84.28

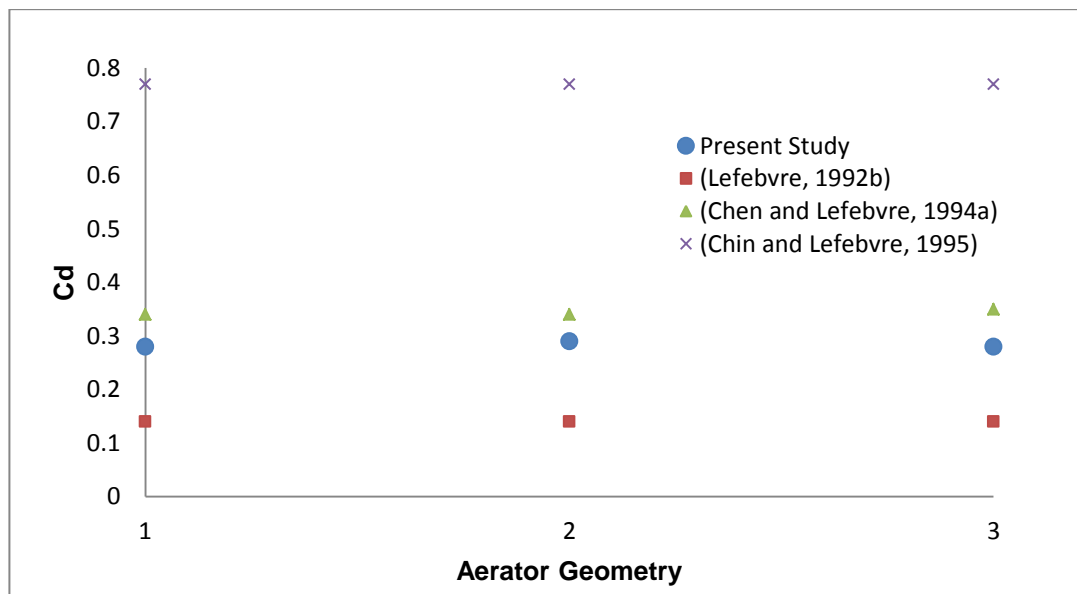


Figure E.1 Comparison of coefficient of discharge from PDA experiments and literature.



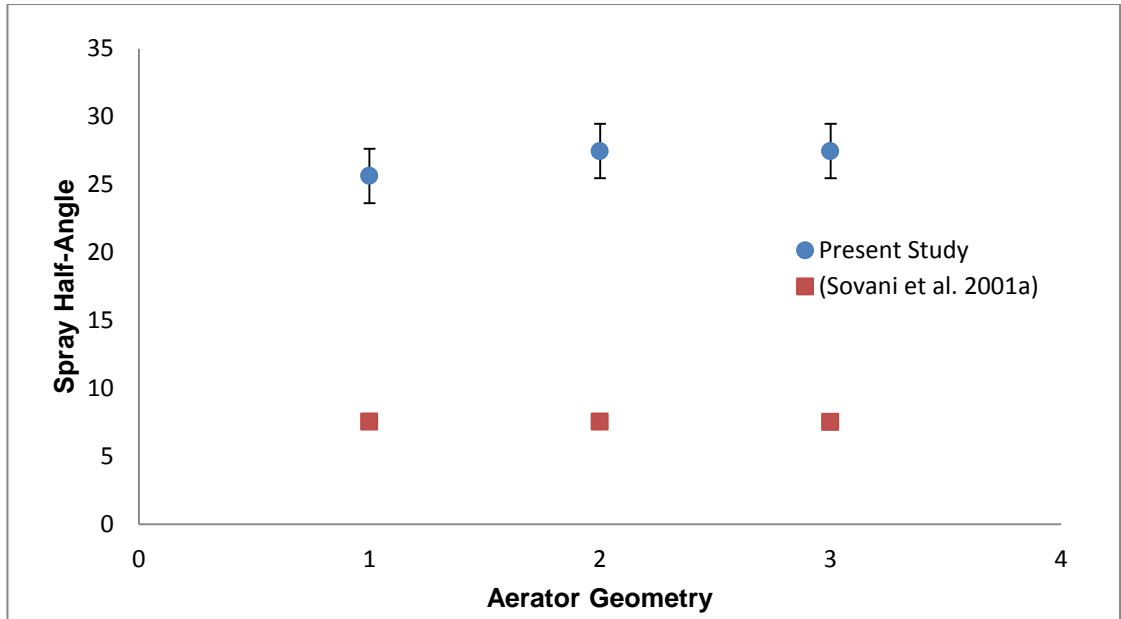


Figure E.2 Comparison of spray half-angle from PDA experiments and literature.

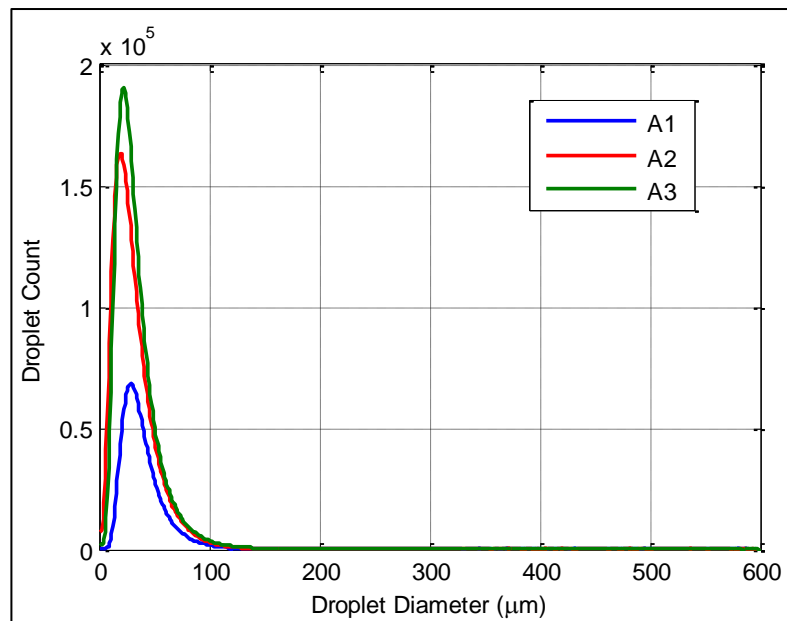


Figure E.3 Droplet diameter frequency distribution based on number.

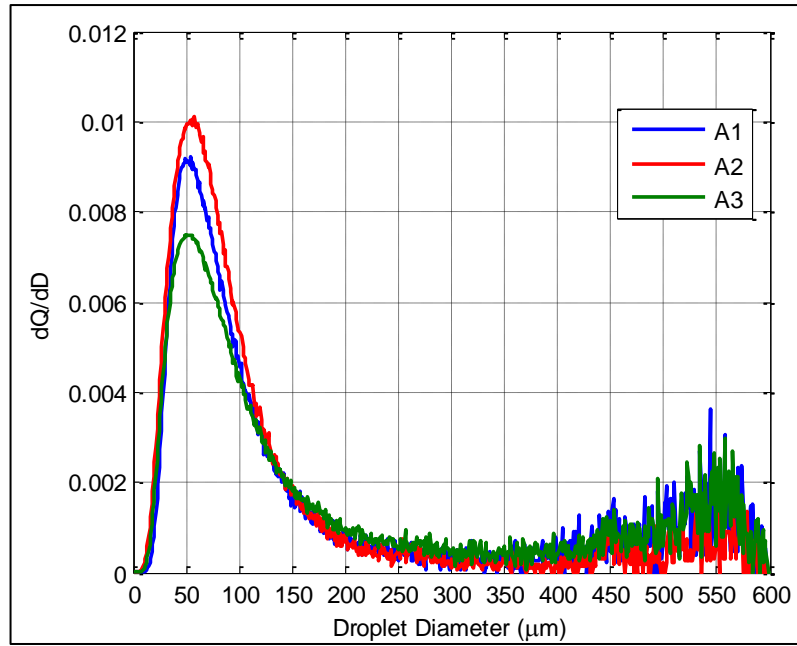


Figure E.4 Droplet diameter frequency distribution based on volume/mass.

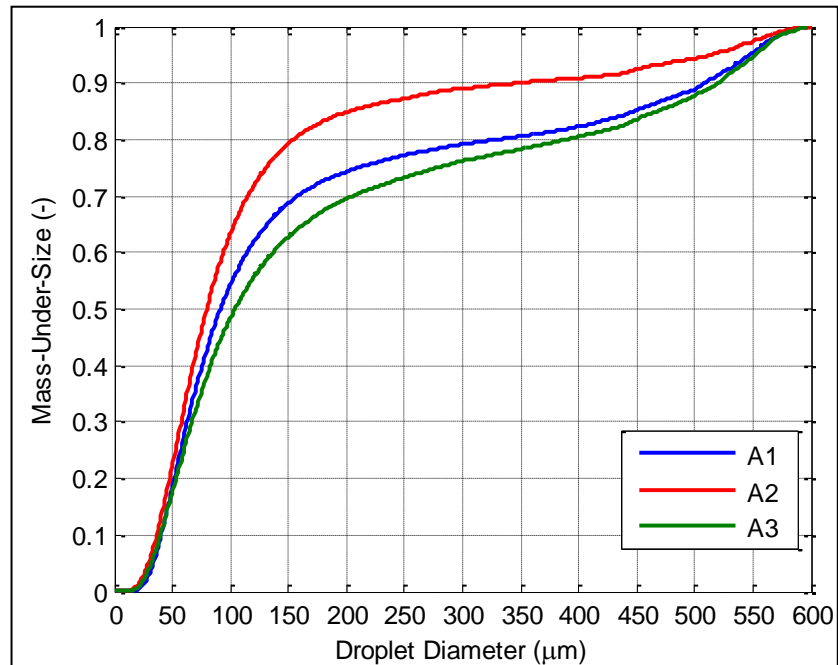


Figure E.5 Cumulative droplet size distribution.

Table E.4 Validated local droplet count varying with atomiser geometry.

Test Case	Validated Local Droplet Counts
A1	<p>Heatmap showing validated local droplet counts for Test Case A1. The y-axis is Axial Position [mm] (0 to -400) and the x-axis is Radial Position [mm] (0 to 40). A color scale on the right indicates droplet counts from 1 to 5 <math>\times 10^4</math>. A specific point at (40, 0) is labeled 20000.</p>
A2	<p>Heatmap showing validated local droplet counts for Test Case A2. The y-axis is Axial Position [mm] (0 to -400) and the x-axis is Radial Position [mm] (0 to 40). A color scale on the right indicates droplet counts from 1 to 5 <math>\times 10^4</math>. A specific point at (40, 0) is labeled 20000.</p>
A3	<p>Heatmap showing validated local droplet counts for Test Case A3. The y-axis is Axial Position [mm] (0 to -400) and the x-axis is Radial Position [mm] (0 to 40). A color scale on the right indicates droplet counts from 1 to 5 <math>\times 10^4</math>. A specific point at (40, 0) is labeled 20000.</p>

Table E.5 Average local droplet velocity varying with atomiser geometry.

Test Case	Local Droplet Velocity
A1	<p>Vector plot for Test Case A1. The y-axis is Axial Position [mm] (0 to -400) and the x-axis is Radial Position [mm] (-10 to 50). Blue arrows represent velocity vectors. A scale bar indicates 50/1 m/s.</p>
A2	<p>Vector plot for Test Case A2. The y-axis is Axial Position [mm] (0 to -400) and the x-axis is Radial Position [mm] (-10 to 50). Blue arrows represent velocity vectors. A scale bar indicates 50/1 m/s.</p>
A3	<p>Vector plot for Test Case A3. The y-axis is Axial Position [mm] (0 to -400) and the x-axis is Radial Position [mm] (-10 to 50). Blue arrows represent velocity vectors. A scale bar indicates 50/1 m/s.</p>

Table E.6 Inferred local gas and relative velocity varying with atomiser geometry.

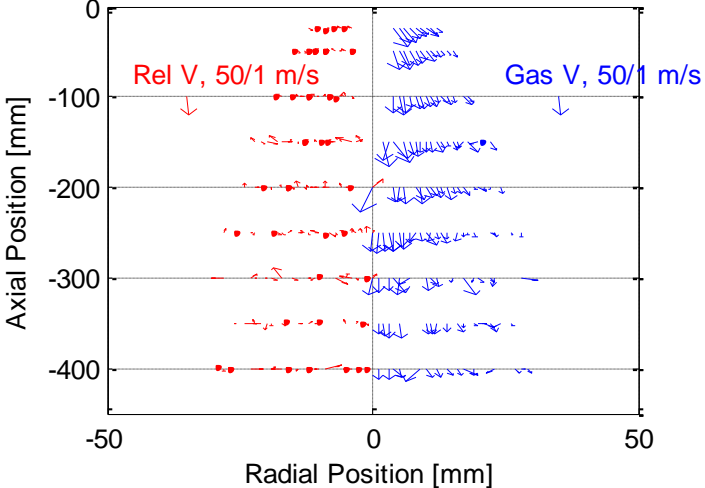
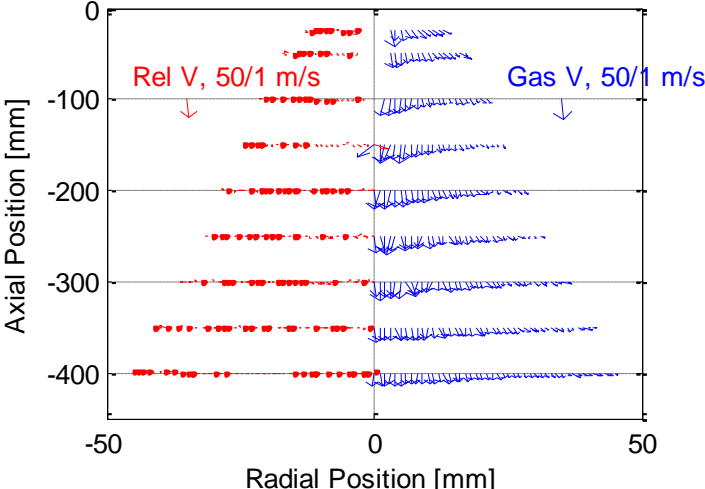
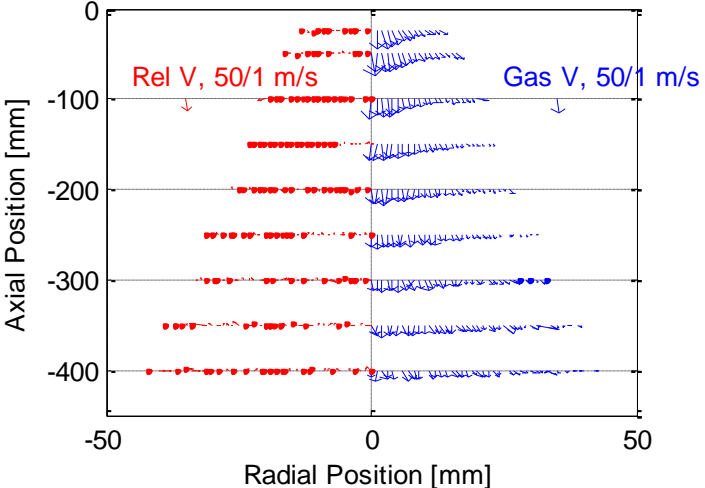
Test Case	Inferred Local Gas and Relative Velocity
A1	 <p>Plot for Test Case A1 showing relative velocity (Rel V, 50/1 m/s) and gas velocity (Gas V, 50/1 m/s) versus radial position (mm) at various axial positions (mm). The y-axis ranges from 0 to -400 mm, and the x-axis ranges from -50 to 50 mm. Red arrows indicate relative velocity, and blue arrows indicate gas velocity.</p>
A2	 <p>Plot for Test Case A2 showing relative velocity (Rel V, 50/1 m/s) and gas velocity (Gas V, 50/1 m/s) versus radial position (mm) at various axial positions (mm). The y-axis ranges from 0 to -400 mm, and the x-axis ranges from -50 to 50 mm. Red arrows indicate relative velocity, and blue arrows indicate gas velocity.</p>
A3	 <p>Plot for Test Case A3 showing relative velocity (Rel V, 50/1 m/s) and gas velocity (Gas V, 50/1 m/s) versus radial position (mm) at various axial positions (mm). The y-axis ranges from 0 to -400 mm, and the x-axis ranges from -50 to 50 mm. Red arrows indicate relative velocity, and blue arrows indicate gas velocity.</p>

Table E.7 Average local droplet AMD and SMD varying with atomiser geometry.

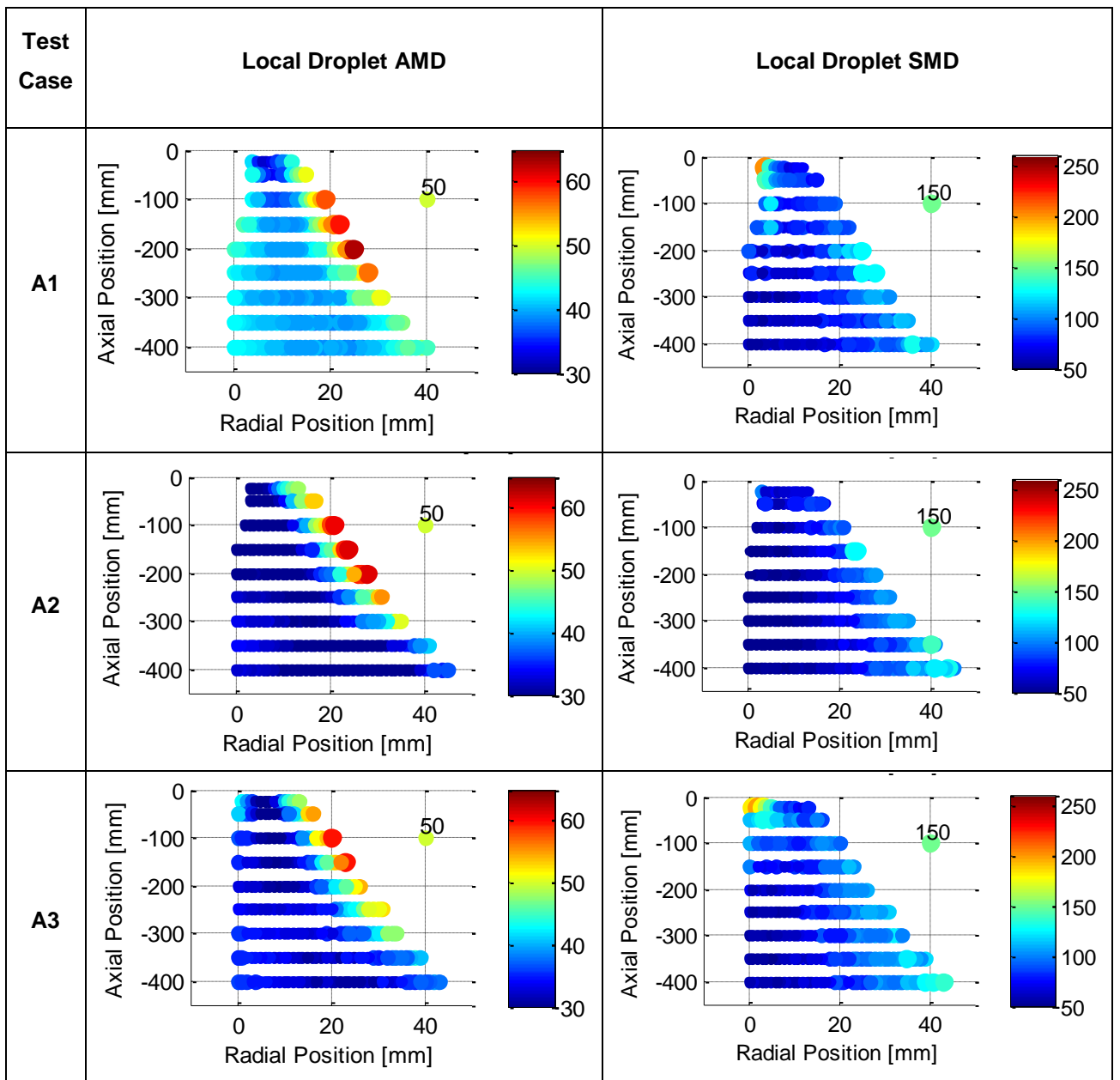


Table E.8 Local SMD/AMD ratio varying with atomiser geometry.

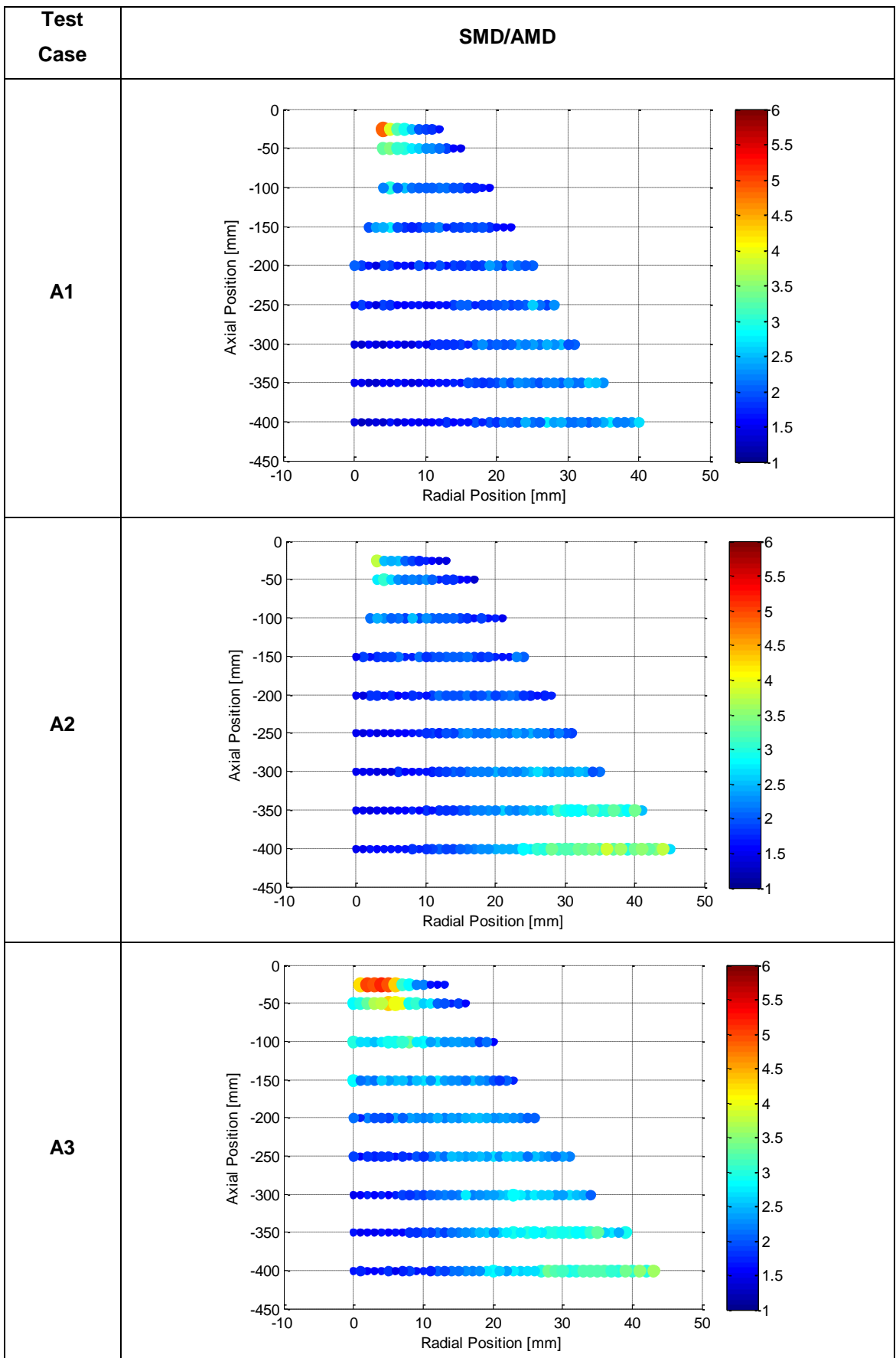


Table E.9 Local average droplet Weber number varying with atomiser geometry.

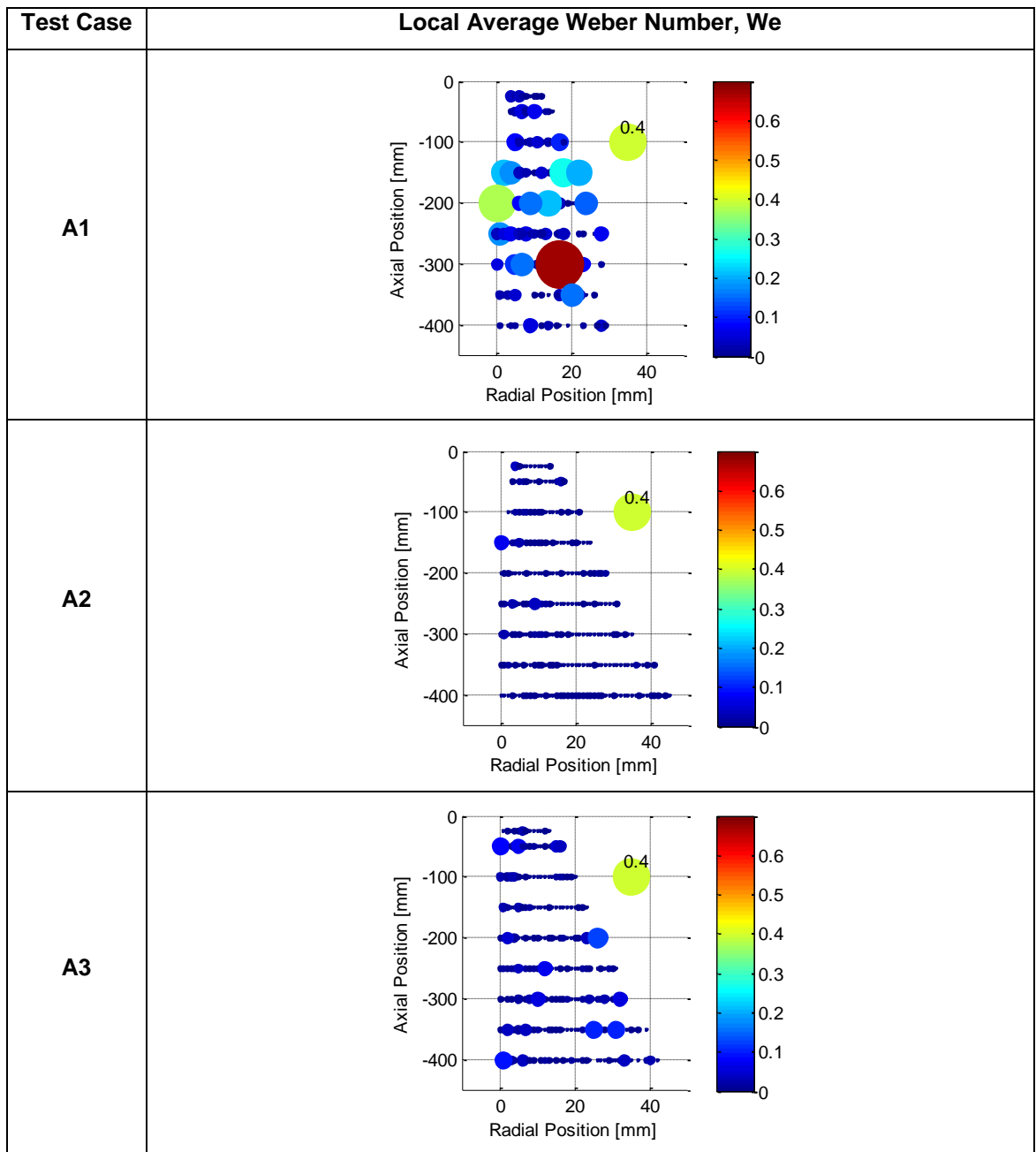
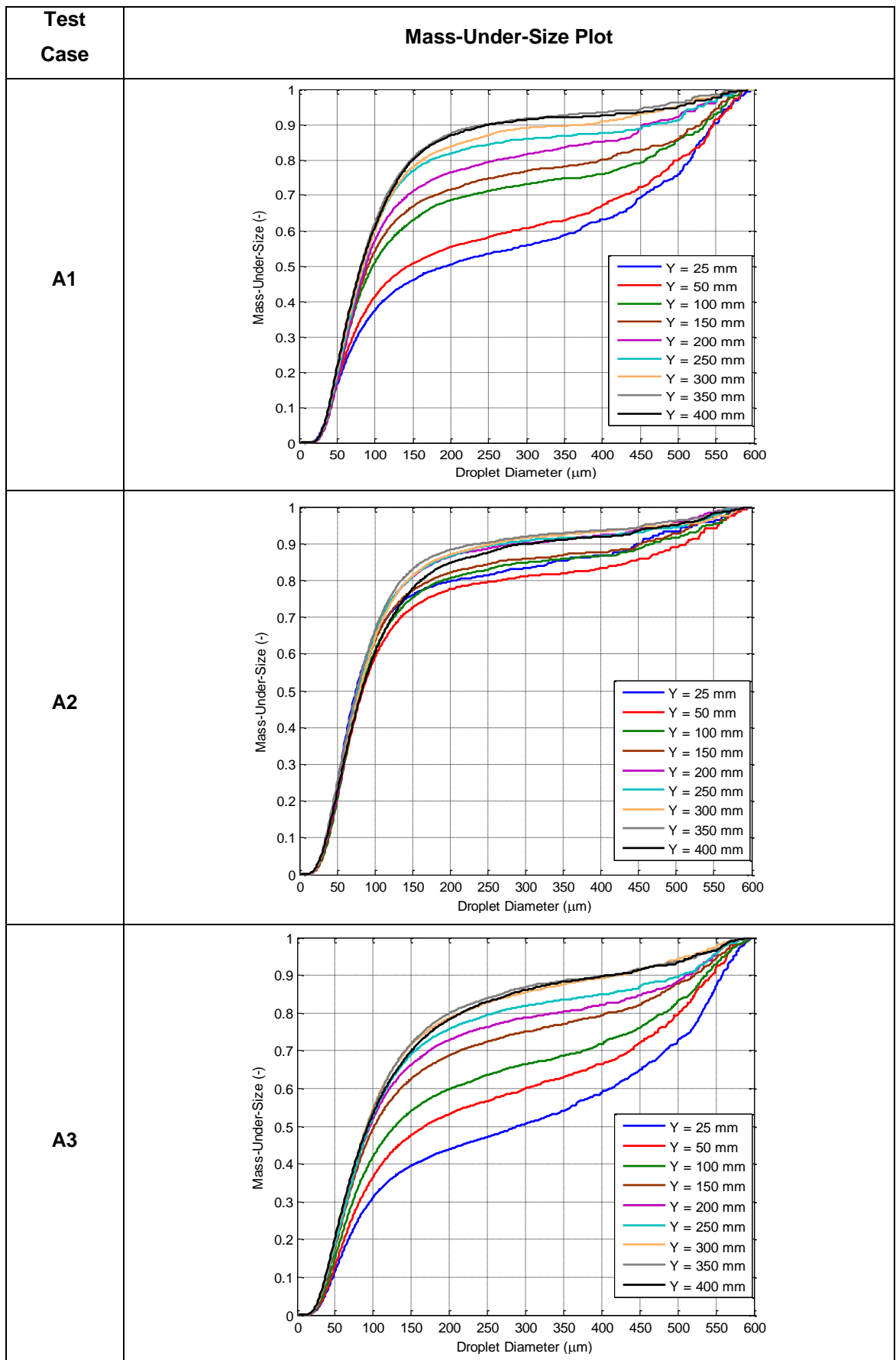




Table E.10 Cumulative mass-under-size plots for entire downstream locations.



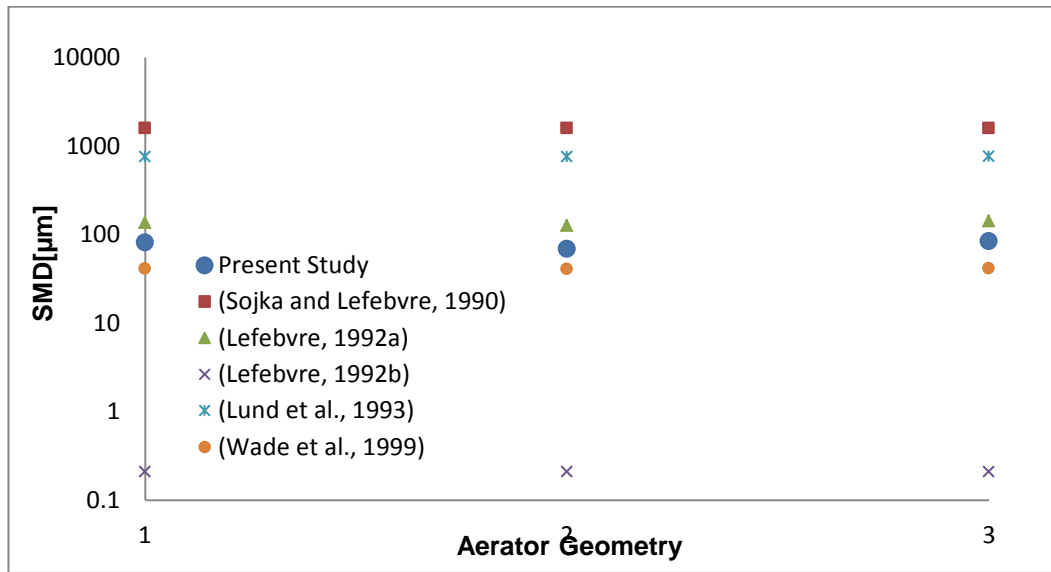


Figure E.6 Comparison of global spray SMD from PDA experiments with that predicted by correlations in the literature.

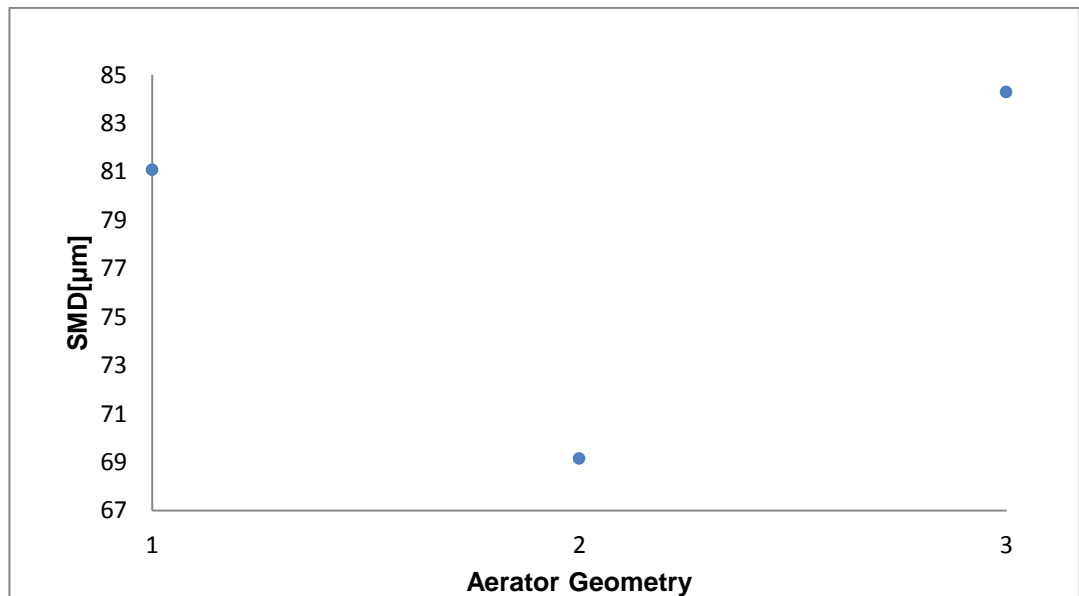


Figure E.7 Experimentally determined global spray droplet SMD for all aerator geometries investigated.

## Appendix F: Kinematic Viscosity Tests

Table F.1 Operating conditions and controlled parameters for kinematic viscosity tests.

TEST No. PARAMETER VARIED	1 ALR	2 $\Delta P$	3 $D_o$	4 $L_{MC}$	5 $D_{MC}$	6 $L_o/D_o$	7 A. GEOM.	8 $\eta$
TEST PHASE	A. Initial Operating Parameters		B. Atomiser Geometry					C. Fluid properties
ALR (%)	0.8-12.5	2		2				
$\Delta P$ (bar.g)	7	4-7		7				
$D_o$ (mm)	2	2	2-4	2	2	2	2	2
$L_{MC}$ (mm)	140	140	140	64-140	140	140	140	140
$D_{MC}$ (mm)	25.4	25.4	25.4	25.4	20-30	25.4	25.4	25.4
$L_o/D_o$ (-)	1	1	1	1	1	0.5-2	1	1
Aerator Geometry	A1	A1	A1	A1	A1	A1	A2, A3	A1
$\eta \times 10^{-6}$ (m <sup>2</sup> /s)	1	1	1	1	1	1	1	2-10

Table F.2 Summary of kinematic viscosity test operating conditions and spray characteristics.

Test	Kinematic Viscosity = $1 \times 10^{-6}$ m <sup>2</sup> /s	Kinematic Viscosity = $5.1 \times 10^{-6}$ m <sup>2</sup> /s	Kinematic Viscosity = $10.1 \times 10^{-6}$ m <sup>2</sup> /s	Kinematic Viscosity = $18 \times 10^{-6}$ m <sup>2</sup> /s
Water Supply Pressure (barG)	7.38	7.10	7.21	7.56
ALR (%)	5.70	5.57	5.84	5.70
Mixing Chamber Pressure, $\Delta P$ (barG)	6.65	6.52	6.69	7.00
$m_{WATER}$ (g/s)	31.75	32.91	31.70	34.35
$P_{AIR}$ (barG)	7.23	6.81	7.03	7.19
$m_{AIR}$ (g/s)	1.81	1.83	1.85	1.95
Volumetric Void Fraction, $\alpha$ (%)	86.1	85.9	86.4	86.1
Effective Power Rating (MW)	1.27	1.32	1.27	1.37
Coefficient of Discharge (-)	0.28	0.29	0.28	0.29
$\theta/2$ at 25 mm downstream (deg)	25.64	32.62	30.96	30.96
$D_{32}$ ( $\mu m$ )	81.06	88.16	95.28	146.58

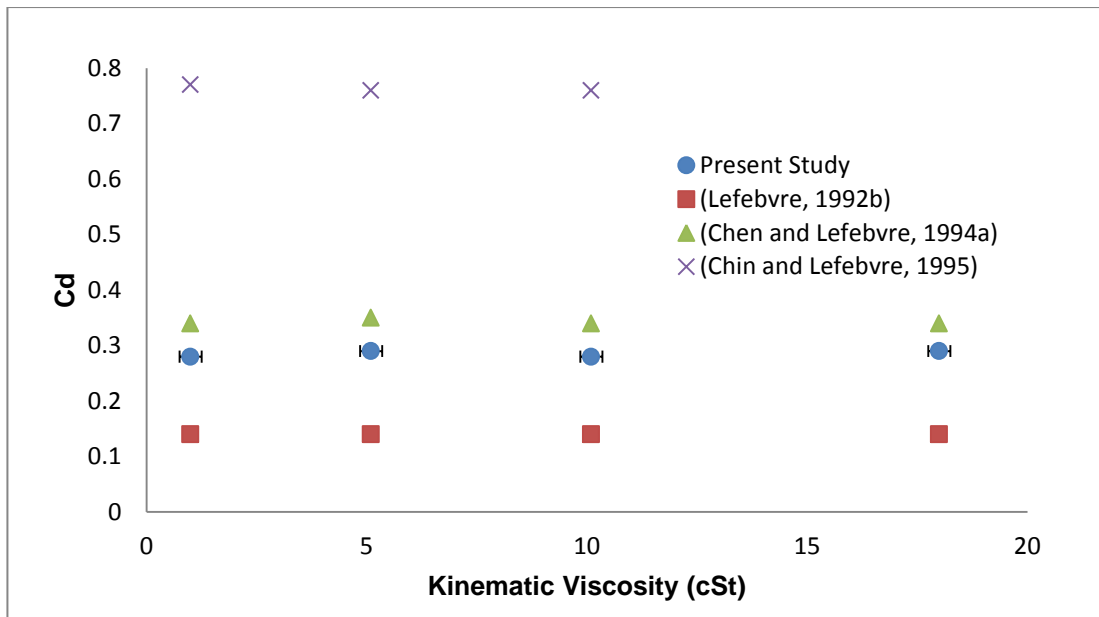


Figure F.1 Comparison of coefficient of discharge from PDA experiments with that in the literature.

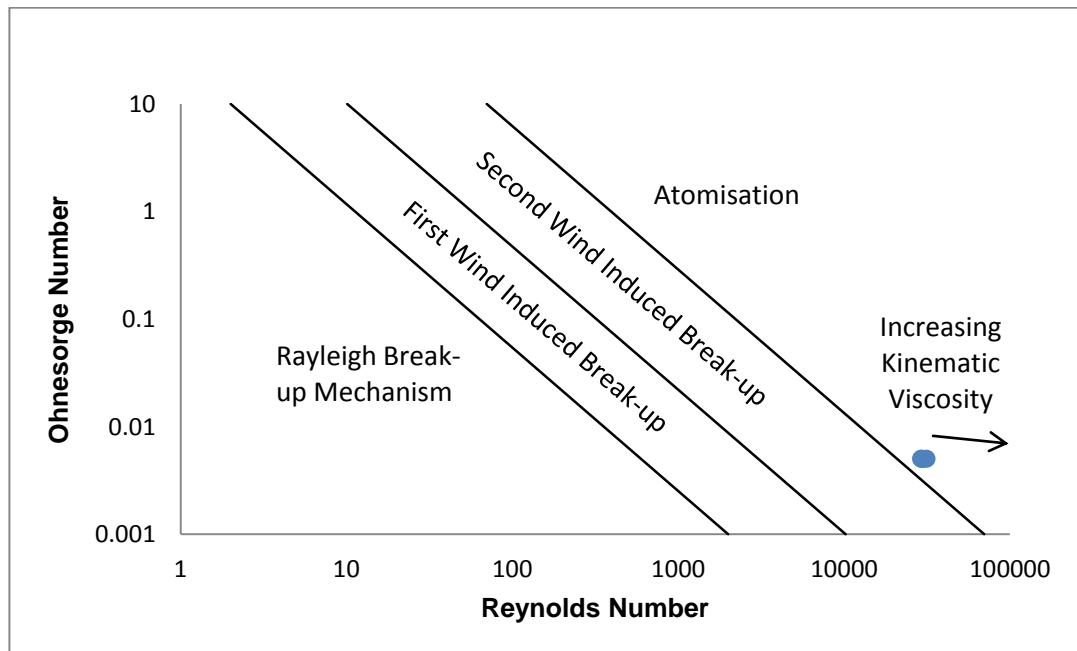


Figure F.2 Calculated liquid disintegration mode for kinematic viscosity experiments.

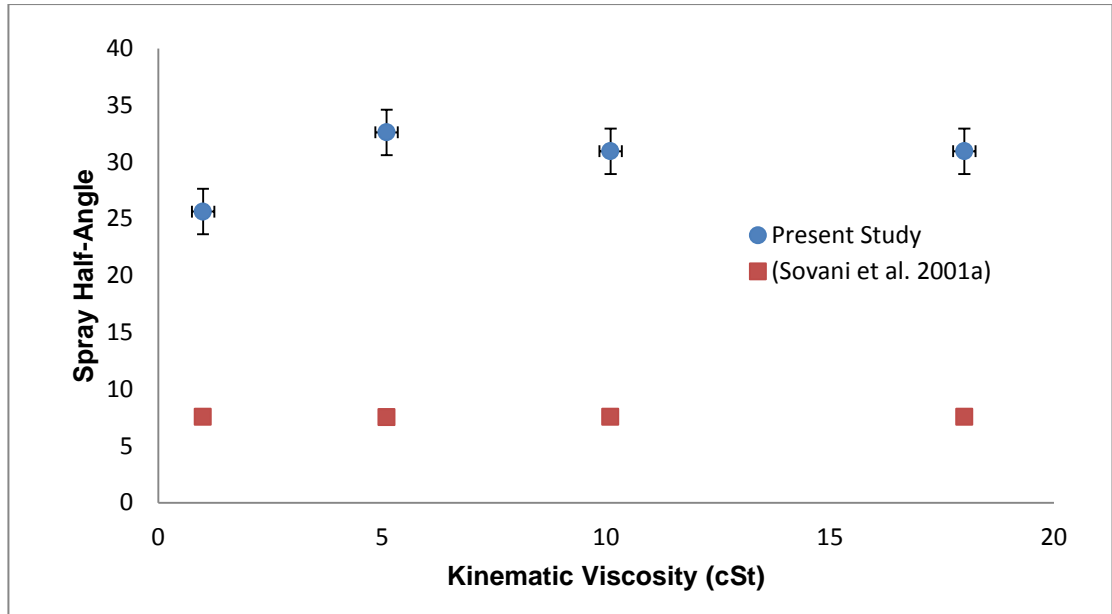


Figure F.3 Comparison of spray half-angle from PDA experiments and literature.

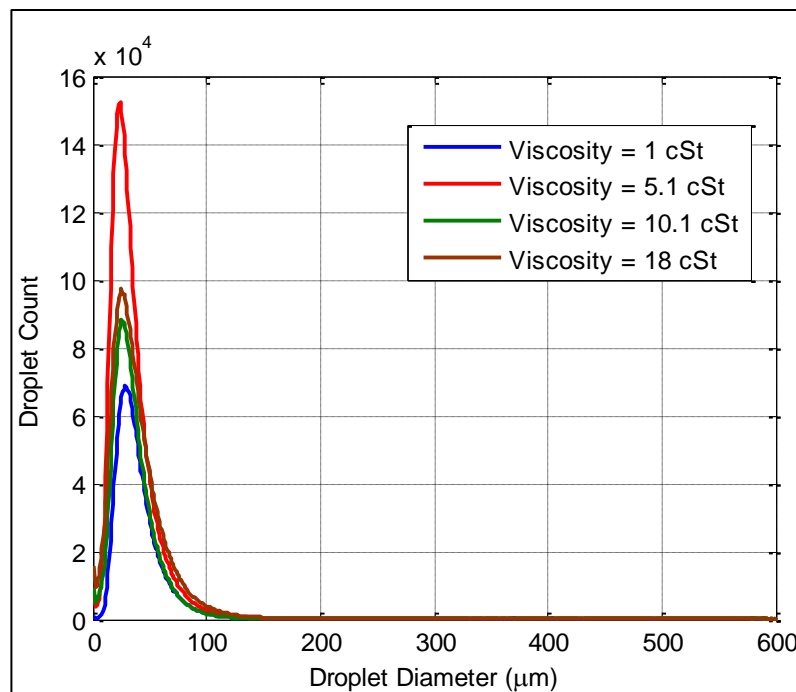


Figure F.4 Droplet diameter frequency distribution based on number.

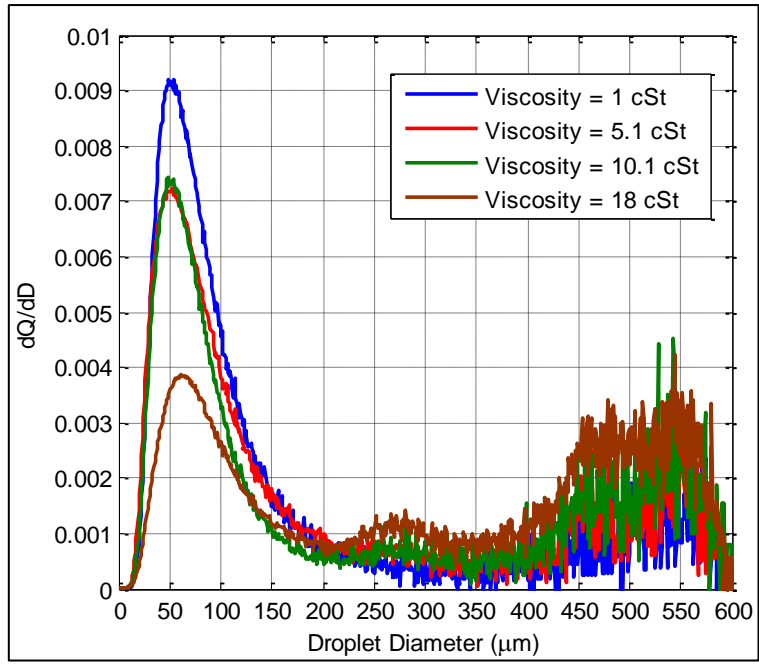


Figure F.5 Droplet diameter frequency distribution by mass.

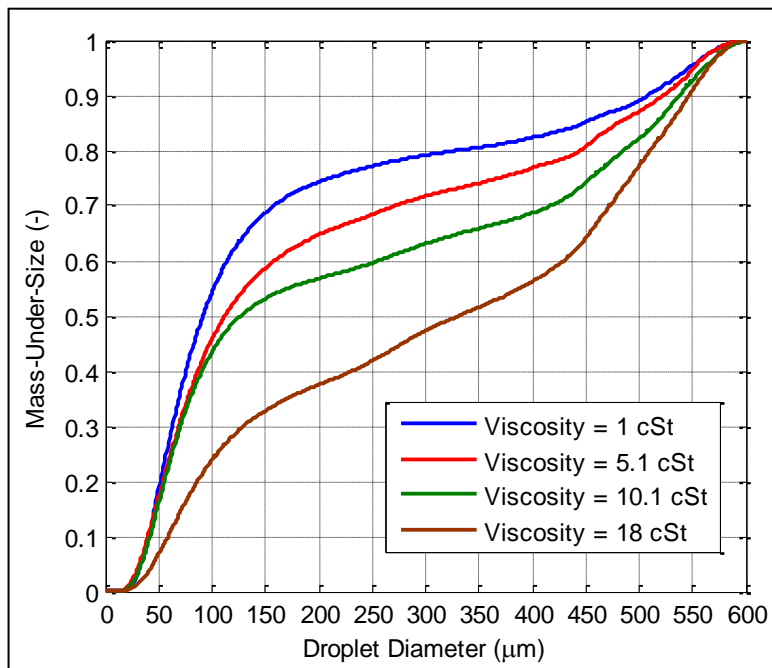


Figure F.6 Cumulative droplet size distribution.

Table F.3 Validated local droplet count varying with kinematic viscosity increases.

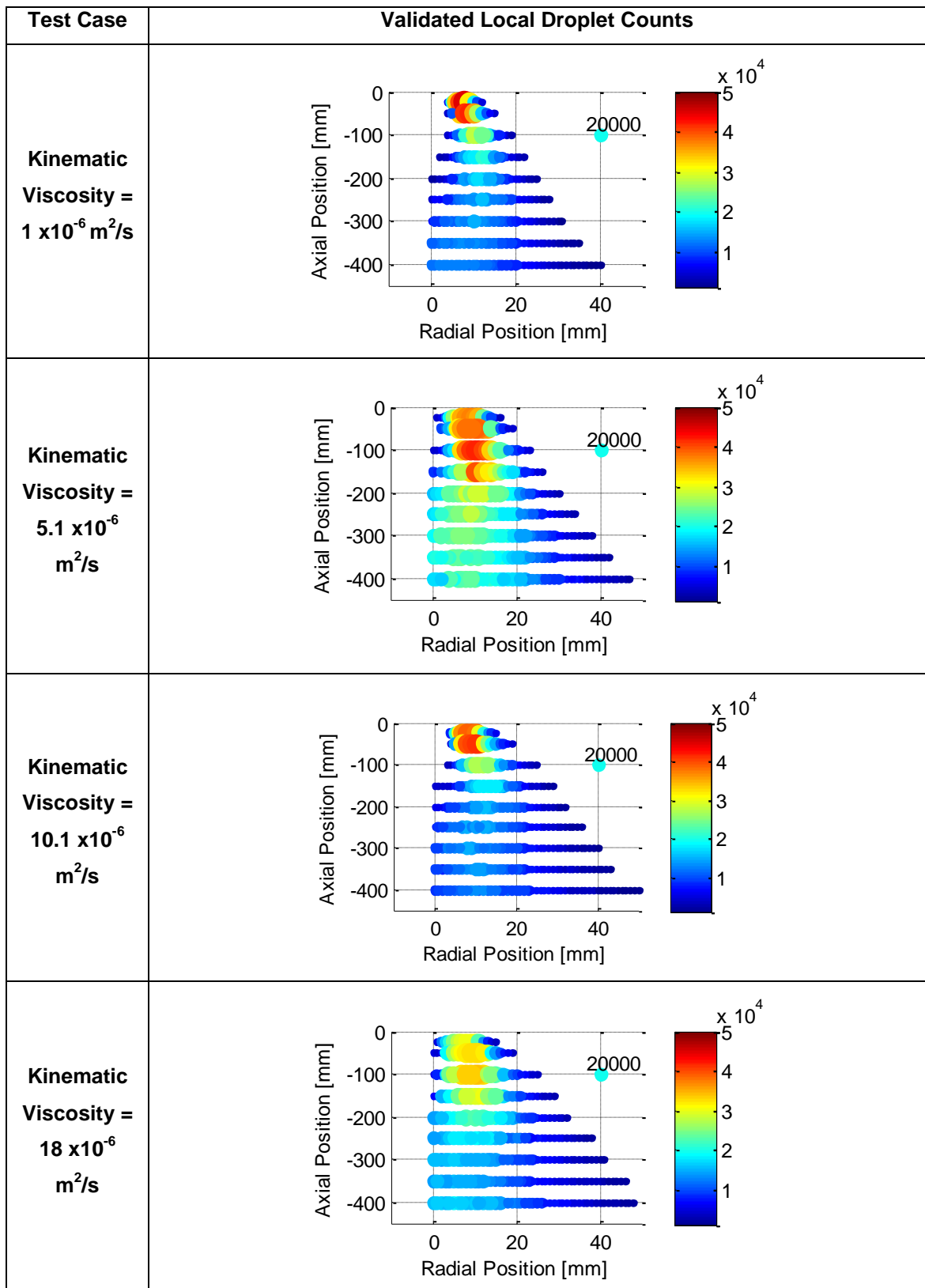


Table F.4 Average local droplet velocity varying with kinematic viscosity increases.

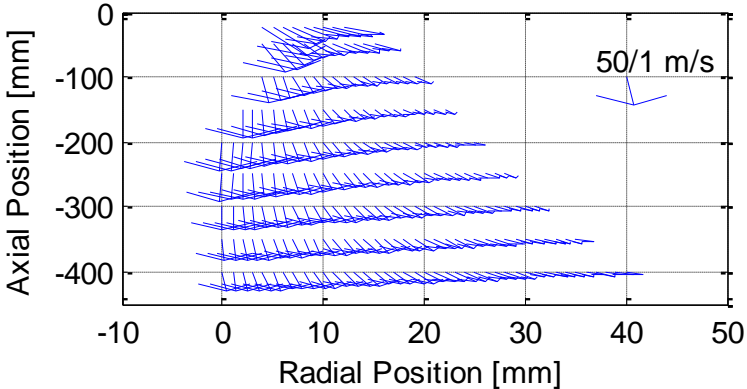
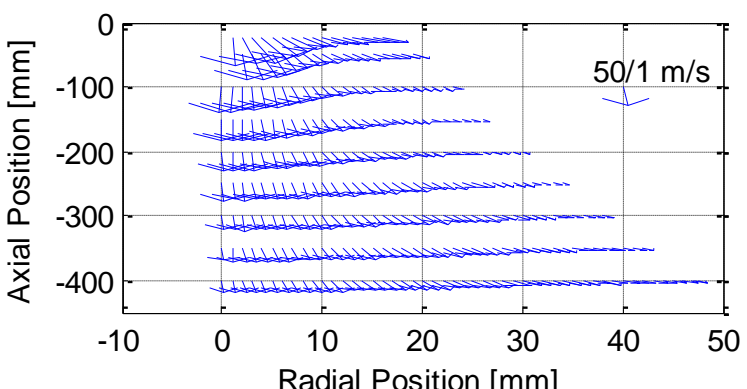
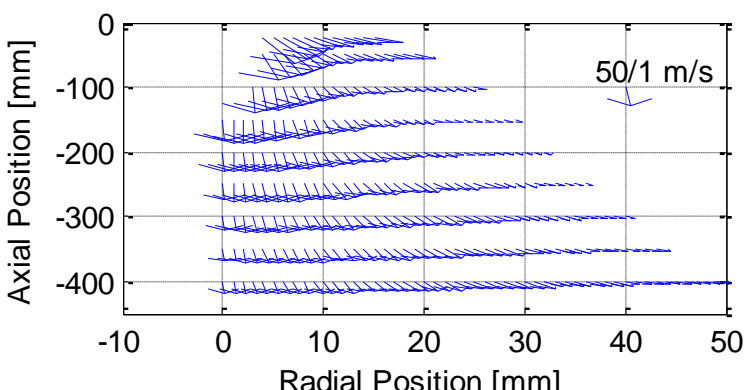
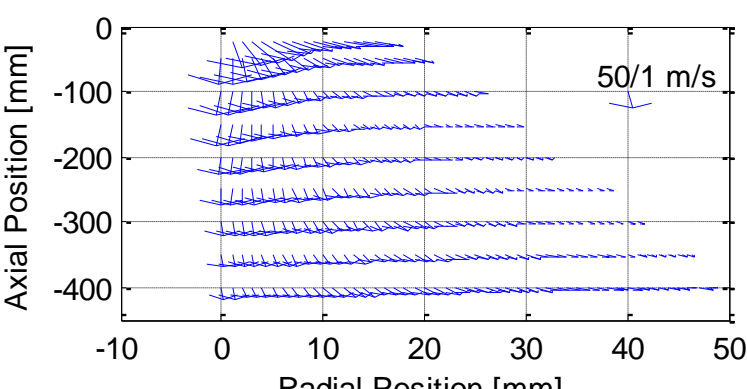
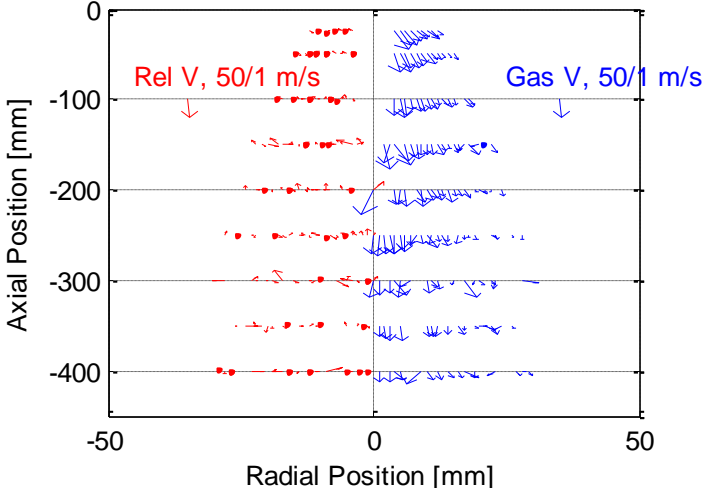
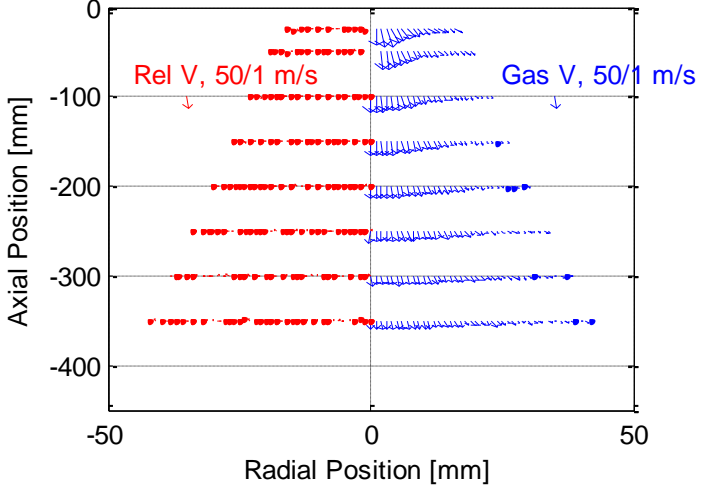
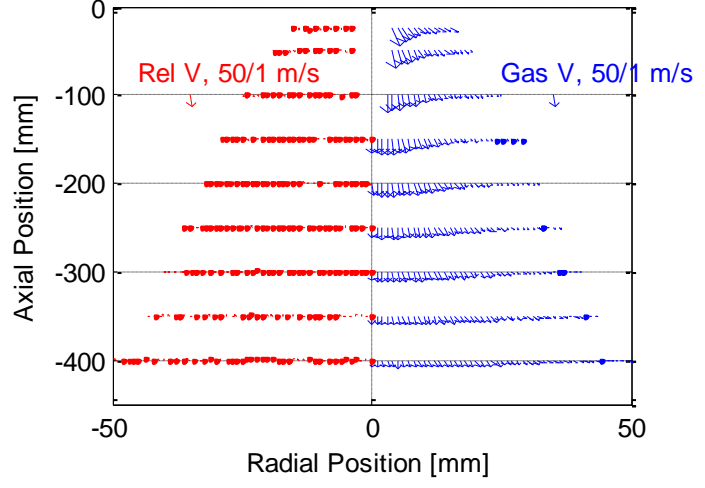
Test Case	Local Droplet Velocity
<p><b>Kinematic Viscosity</b>  <math>= 1 \times 10^{-6} \text{ m}^2/\text{s}</math></p>	
<p><b>Kinematic Viscosity</b>  <math>= 5.1 \times 10^{-6} \text{ m}^2/\text{s}</math></p>	
<p><b>Kinematic Viscosity</b>  <math>= 10.1 \times 10^{-6} \text{ m}^2/\text{s}</math></p>	
<p><b>Kinematic Viscosity</b>  <math>= 18 \times 10^{-6} \text{ m}^2/\text{s}</math></p>	



Table F.5 Inferred local gas and relative velocity varying with kinematic viscosity increases.

Test Case	Inferred Local Gas and Relative Velocity
<p><b>Kinematic Viscosity</b>  <math>= 1 \times 10^{-6} \text{ m}^2/\text{s}</math></p>	
<p><b>Kinematic Viscosity</b>  <math>= 5.1 \times 10^{-6} \text{ m}^2/\text{s}</math></p>	
<p><b>Kinematic Viscosity</b>  <math>= 10.1 \times 10^{-6} \text{ m}^2/\text{s}</math></p>	

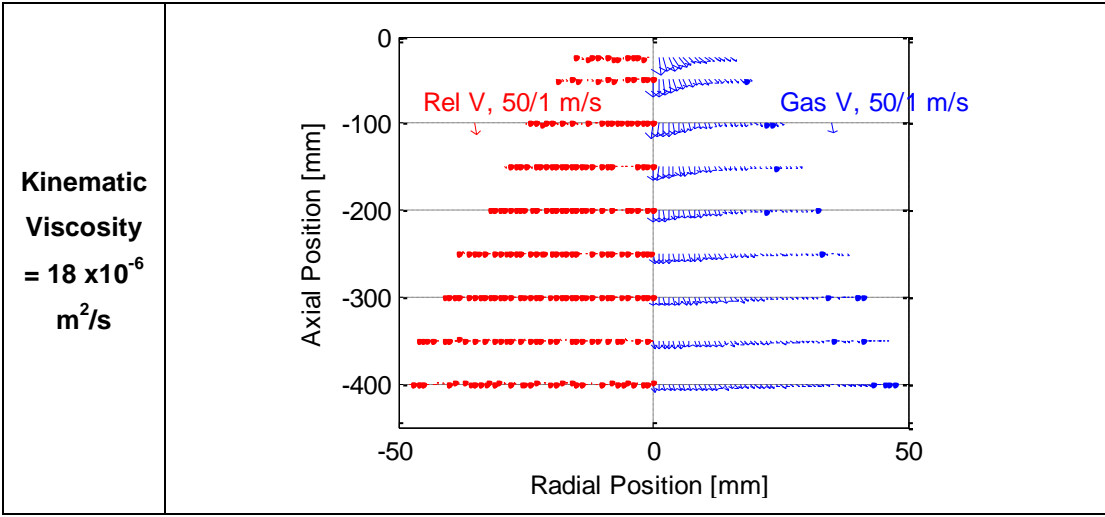


Table F.6 Average local droplet AMD and SMD varying with kinematic viscosity increases.

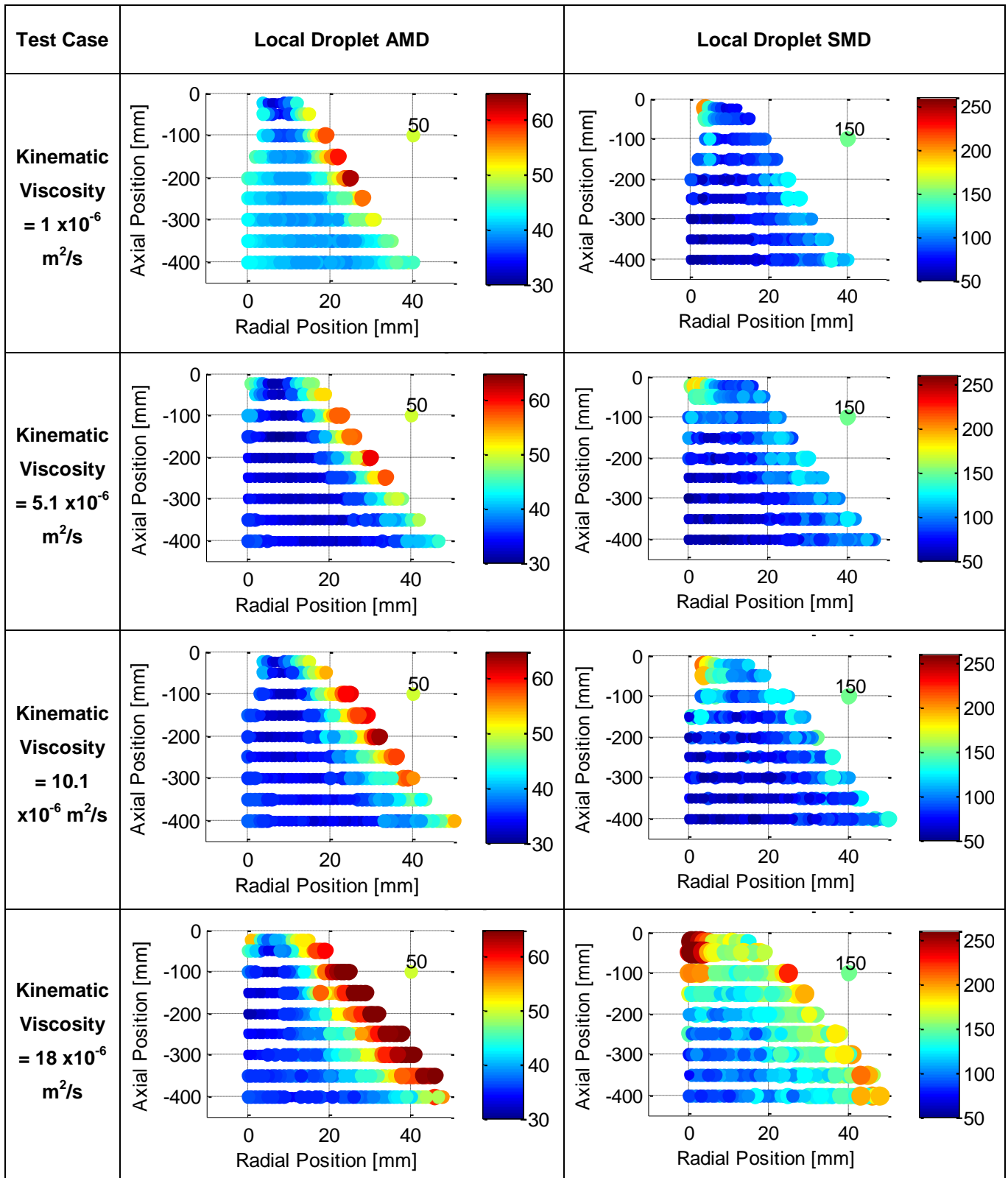
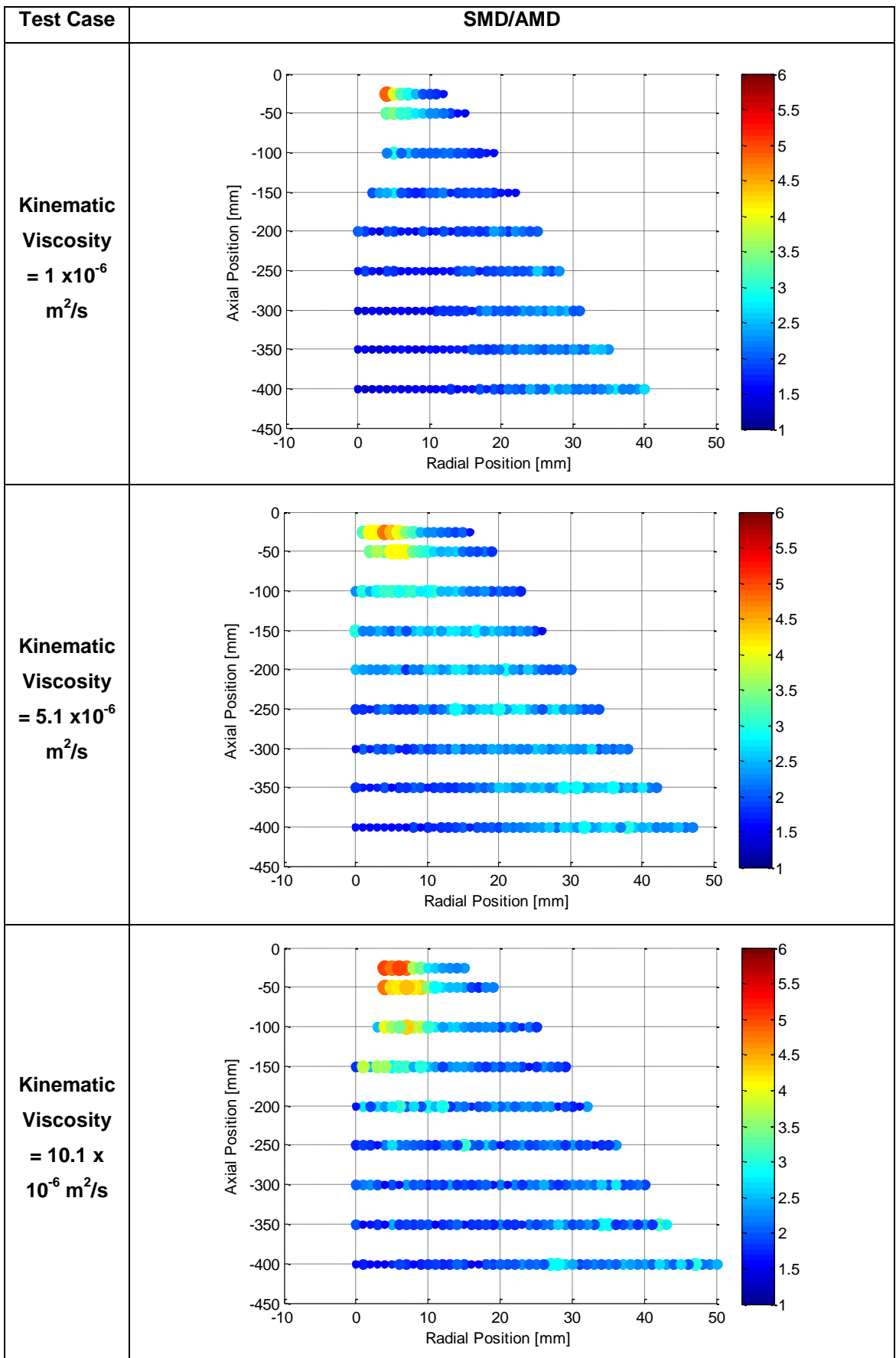


Table F.7 Local droplet SMD/AMD ratio varying with kinematic viscosity increases.



**Kinematic  
Viscosity**  
 $= 18 \times 10^{-6}$   
 $\text{m}^2/\text{s}$

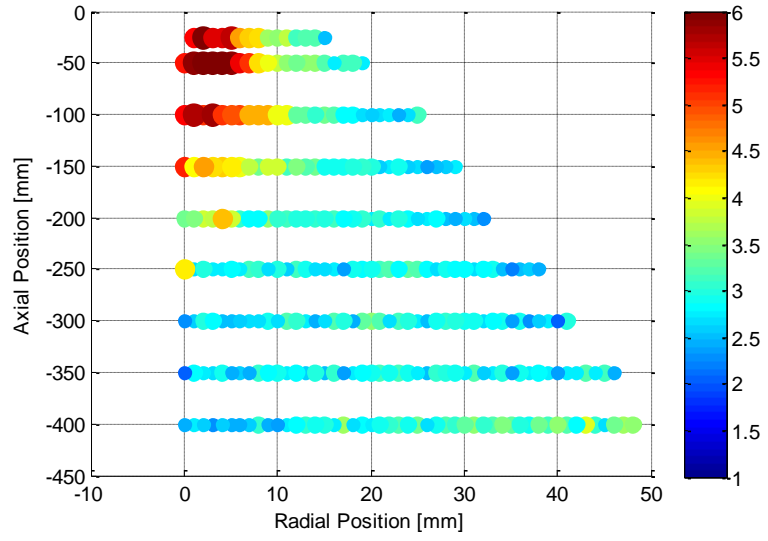


Table F.8 Local average droplet Weber number varying with kinematic viscosity increases.

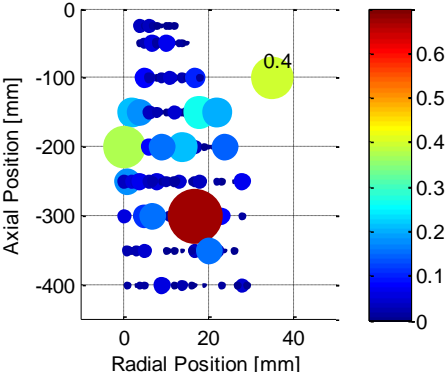
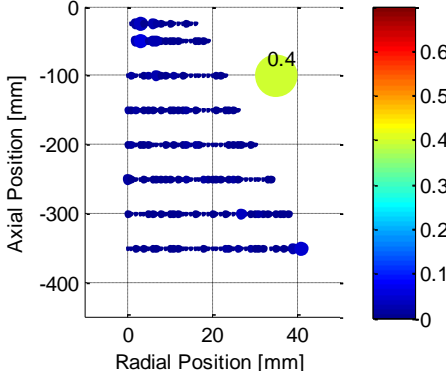
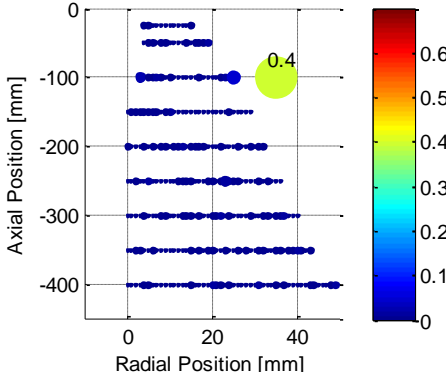
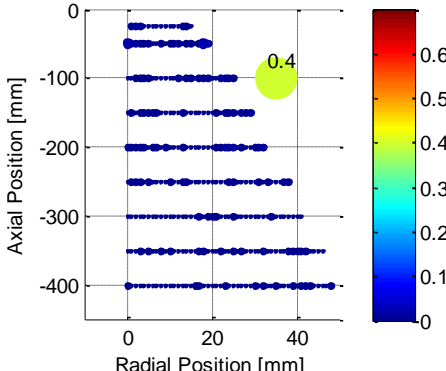
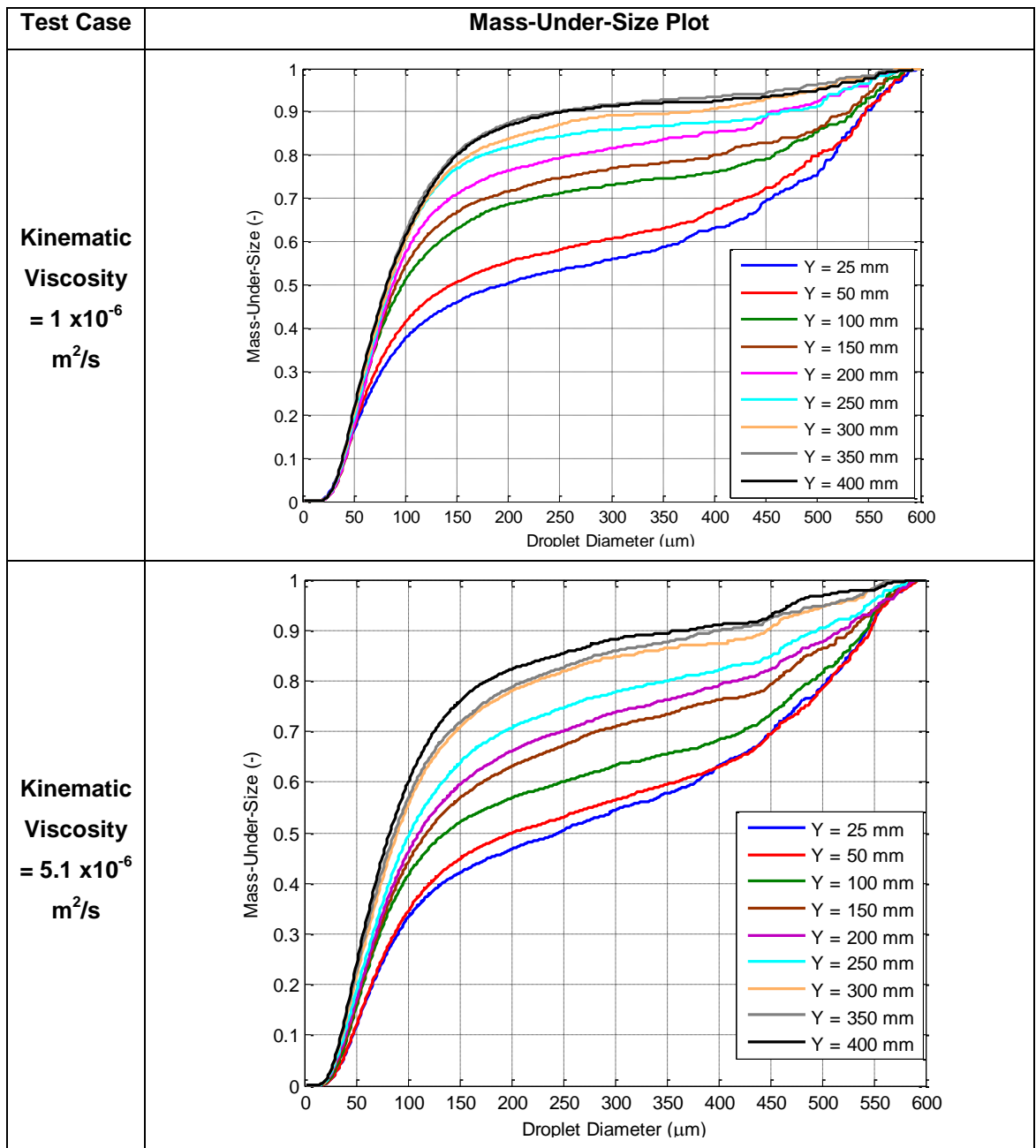
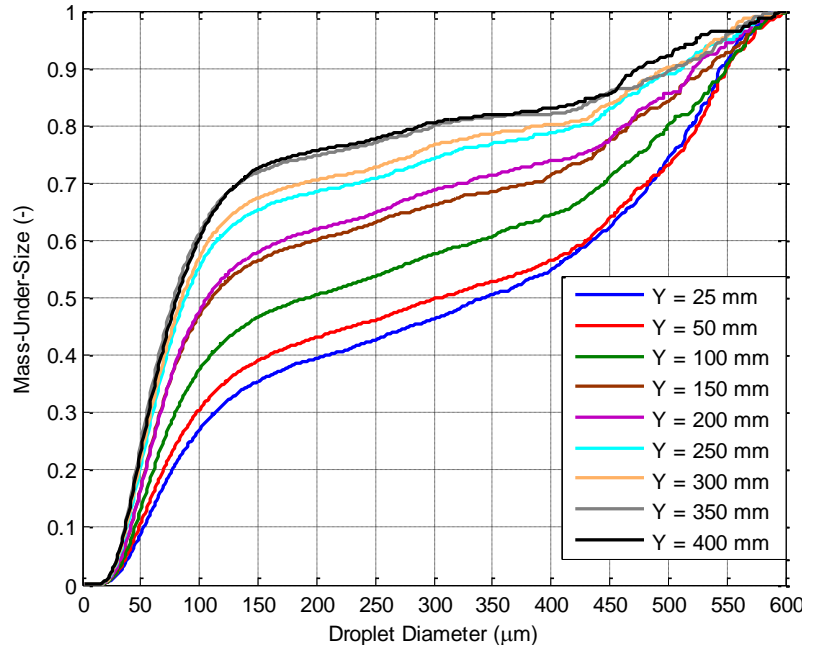
Test Case	Local Average Weber Number, $We$
<p><b>Kinematic Viscosity</b>  <math>= 1 \times 10^{-6} \text{ m}^2/\text{s}</math></p>	
<p><b>Kinematic Viscosity</b>  <math>= 5.1 \times 10^{-6} \text{ m}^2/\text{s}</math></p>	
<p><b>Kinematic Viscosity</b>  <math>= 10.1 \times 10^{-6} \text{ m}^2/\text{s}</math></p>	
<p><b>Kinematic Viscosity</b>  <math>= 18 \times 10^{-6} \text{ m}^2/\text{s}</math></p>	

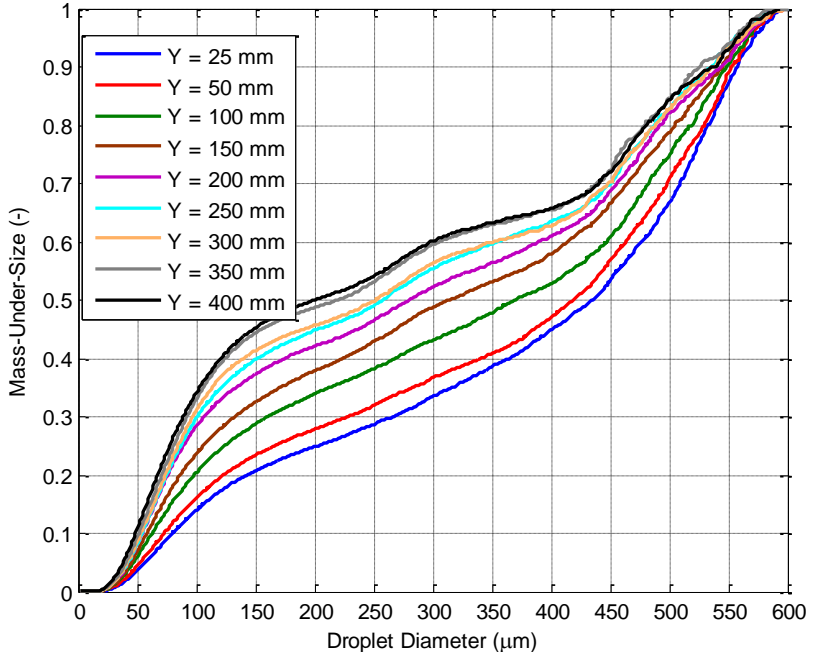
Table F.9 Cumulative mass-under-size plots for entire downstream locations.



**Kinematic  
Viscosity  
= 10.1  
 $\times 10^{-6}$  m<sup>2</sup>/s**



**Kinematic  
Viscosity  
= 18 x10<sup>-6</sup>  
m<sup>2</sup>/s**





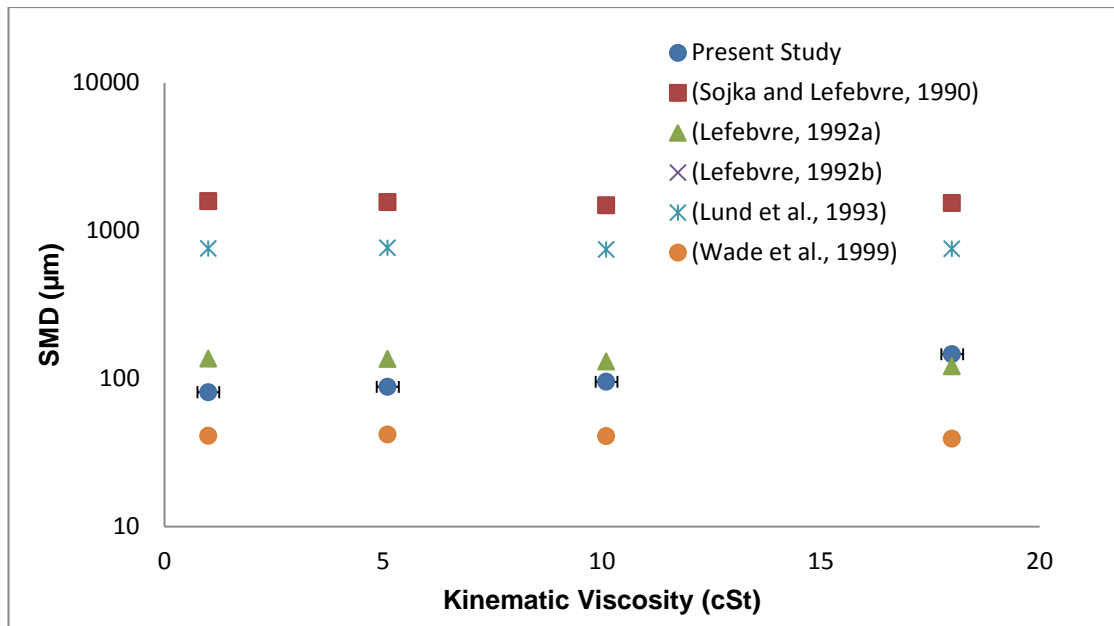


Figure F.7 Comparison of global spray SMD from PDA experiments with that predicted by correlations in the literature.

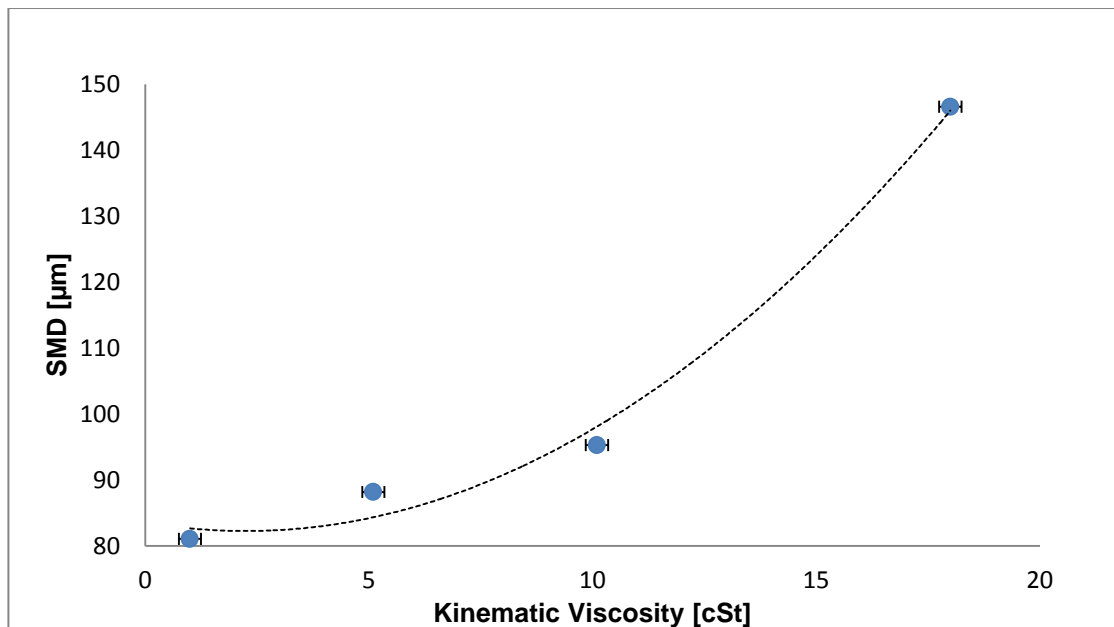


Figure F.8 The relationship between kinematic viscosity and global spray SMD as calculated using PDA.